Advanced Technologies in Earth Sciences

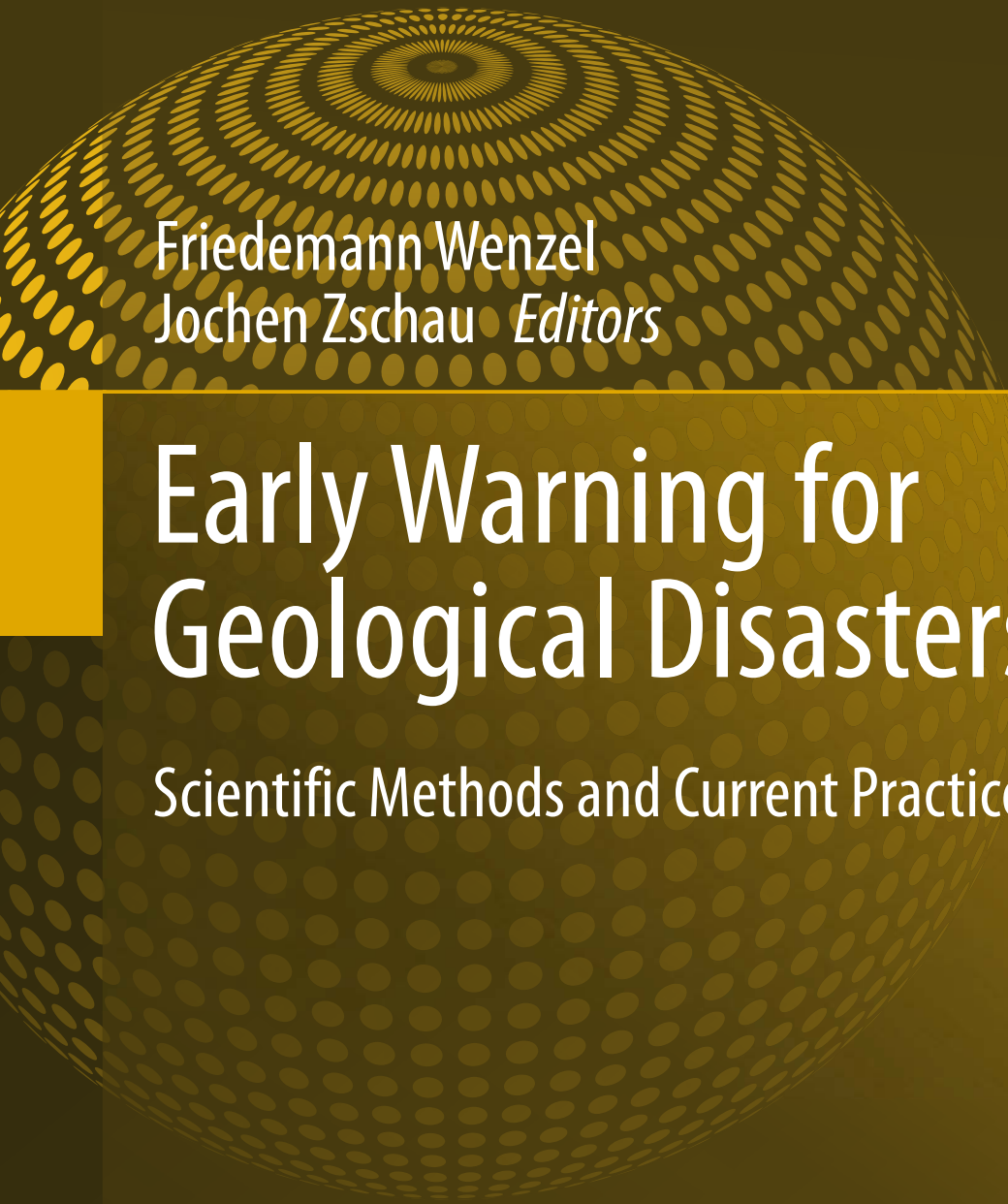

Friedemann Wenzel
Jochen Zschau *Editors*

Early Warning for Geological Disasters

Scientific Methods and Current Practice

GEOTECHNOLOGIEN

Springer

Advanced Technologies in Earth Sciences

For further volumes:
http://www.springer.com/series/8384

Friedemann Wenzel · Jochen Zschau
Editors

Early Warning for Geological Disasters

Scientific Methods and Current Practice

Springer

Editors
Friedemann Wenzel
Geophysical Institute
Karlsruhe Institute of Technology
Karlsruhe
Germany

Jochen Zschau
Section 2.1 Earthquake Risk and Early Warning
Deutsches GeoForschungsZentrum
Potsdam
Germany

ISSN 2190-1635 ISSN 2190-1643 (electronic)
ISBN 978-3-642-12232-3 ISBN 978-3-642-12233-0 (eBook)
DOI 10.1007/978-3-642-12233-0
Springer Heidelberg New York Dordrecht London

Library of Congress Control Number: 2013936972

Printed on acid-free paper

Springer is part of Springer Science+Business Media (www.springer.com)

Preface

Research into early warning for geological disasters covers all geological phenomena: volcanic crises, landslides, earthquakes and tsunamis. The past few years have seen new technologies developed that could be utilised in these fields for early warning, real-time loss estimations and rapid disaster response. They include self-organising sensor networks, new satellite imagery with high resolution, multi-sensor observational capacities and crowd sourcing for rapid information provision. From these and improved physical models, data processing and communication methodologies, a significant step towards better early warning capabilities has been achieved. At the same time, early warning systems have started to become part of the disaster risk management practice. For example, the Japanese earthquake early warning system was made public in 2007 by the Japanese Meteorological Agency (JMA). The efforts to establish a tsunami warning system for the Indian Ocean following the tragic mega-tsunami of 2004 are being coordinated by the UNESCO Intergovernmental Oceanographic Commission—and have resulted so far in three national systems (Australia, India and Indonesia) that provide warnings. Thus, apart from new research, more experience was built up in the application of early warning methodologies and the integration of its recipients ('last mile') in the early warning process. This book therefore marks an important point where (1) research activities continue to grow—supported by a number of national and trans-national research programmes such as the European Commission FP7 program and (2) experience with applications is expanding so that more feedback from experience and practice to the research community is becoming available. Therefore, for this stage in the development of early warning systems for geological disasters it is timely to produce a volume that documents the state of the art, provides an overview on recent developments and serves as a knowledge resource for researchers and practitioners.

We utilise the UNISDR definition of early warning (UNISDR 2009). This definition encompasses the range of factors necessary to achieve effective responses to warnings. A people-centred early warning system by necessity comprises four key elements: Knowledge of the risks; monitoring, analysis and forecasting of the hazards; communication or dissemination of alerts and warnings; and local capabilities to respond to the warnings received.

The chapters contained in this book on Early Warning Systems (EWS) cover all geological disasters, however, with a focus on earthquakes and tsunamis, as these have caused significant death tolls and losses to property, infrastructure and the environment in recent years. They cover many aspects of early warning, beginning with scientific and technological issues (instrumentation, algorithms, data management) but also addressing issues related to the dissemination of warnings and decision making.

The most advanced and best tested earthquake early warning system that also includes tsunami warnings has been operated by the Japanese Meteorological Agency (JMA) since 2007. A critical performance test of the system is involved in the Tohoku earthquake of March 11, 2011 with a magnitude of 9.0 that cost the lives of almost 20,000 people, nearly 100 % of them due to the tsunami waves. The chapter of Hoshiba and Ozaki outlines the performance of the system in detail and reports on the quality of the earthquake and the tsunami warnings and advisories, including lessons learned and a discussion on how to improve the system. One deficiency of the system turned out to be the inherent assumption that an earthquakes rupture can be treated as a point source for seismic waves. This is an acceptable assumption for many earthquakes below magnitude 7, but is no longer valid for large earthquakes with magnitudes in the range of 8 and greater, where fault lengths are in the range of hundreds of kilometres. The chapter of Yamada discusses a methodology that allows for the estimation of the fault rupture extent in real-time. It naturally relies on a dense seismic network, which is available in Japan, and allows the identification of a fault rupture by classifying stations in near source and far source.

A successful early warning system that has experienced several tests is the Mexican one, discussed and described in the chapter of Cuéllar et al. The early warning for the recent earthquake on March 20, 2012, with a magnitude of 7.4 (Ometepec earthquake) was able to demonstrate the value of the system to the general public.

Another promising development is the Californian early warning system which is currently being tested. It combines three different methodologies: Onsite early warning with one or at the utmost two stations, which is very fast but exhibits a high error range, ELARMS which relies on four stations and allows a higher precision but reduced speed, and the virtual seismologist approach with an increasing number of stations being used during the earthquake, which is rather slow in terms of early warning but shows very good performance in determining the magnitude and location of the event. The chapter of Böse et al. presents details of the system and demonstrates its performance in a number of examples. A large number of scientists, also end users from industry, emergency response and infrastructure operators are involved in its testing, and stakeholders provide valuable knowledge to improve the performance of the system.

Utilisation of earthquake early warning systems in Europe is lacking significantly behind the pioneer applications in Japan, California, Taiwan and Mexico. However, efforts have been made over more than a decade to protect the cities of

Istanbul and Bucharest, and the territory of Campania in Southern Italy. In addition to these regional advances, two European research projects (FP6 SAFER—Seismic Early Warning for Europe and FP7 REAKT—Strategies and Tools for Real Time Earthquake Reduction) have advanced our knowledge and the level of application in Europe significantly. The chapter of Gasparini and Manfredi outlines the history of earthquake early warning in Europe, its current status and its future prospects.

Some applications in Europe—without being comprehensive—are discussed in three chapters. The chapter of Wenzel et al. presents results from a project focusing on a warning system for Istanbul. Which involves a broader approach than earthquake early warning in a strict sense, with modern information technologies being combined with seismology and instrumental methodologies to develop an earthquake disaster information system for the Marmara region. The chapter by Zollo et al. presents an approach to early warning for Southern Italy that integrates regional and on-site systems. The system is described and demonstrated by several cases, which show the benefits of a robust methodology with respect to the early warning performance. The chapter of Bonn et al. focuses on earthquake early warning for transport lines. The aim is to enable the issuing of alert maps before the strong motion phase of seismic waves can endanger trains. Although the system has so far only been developed as a concept, it could demonstrate that a service-oriented system architecture can provide various users with rapid information, relevant for warning, rescue and repair.

Another set of chapters is dedicated to earthquake and tsunami early warning for the Indian Ocean, with an emphasis on warnings for Sumatra. This work is based on the significant effort made by German funding agencies and scientific institutions to develop the German-Indonesian Tsunami Early Warning System (GITEWS), which was established after the devastating tsunami in the Indian Ocean on December 26, 2004. The value of this set of chapters is particularly in the combination of technological issues of an early warning system with the communication of warning information, as well as in the aspects of evacuation and early warning implementation in the emergency response structures of the country. Lauterjung et al. discuss the system concept as an ‘end-to-end’ approach aiming at the complete coverage of the warning chain from rapid hazard detection through to decision support to capacity development in communities, and the implementation of disaster risk reduction measures. Spahn et al. focus on the implementation of the system in the day-to-day operations of communities and emergency response agencies. The focus is very much on tsunami preparedness. The time period for the development of sustainable tsunami preparedness at all levels, ranging from the community to the provincial and central government, is significantly longer than the scientific development and technical implementation stages of the system and thus provides major challenges in making the system useful. Goseberg et al. also refer to the ‘last mile’ aspects of tsunami early warning although, with a focus on evacuation planning and risk reduction in tsunami threatened coastal areas. It discusses the generation and compilation of a geo-database that includes remote sensing data, information on social vulnerability related to exposure, risk

perception and evacuation behaviour, while also allowing for the simulation of realistic scenarios of inundation. Wächter and Usländer stress the software and hardware aspects of tsunami warning systems in general, based on the experience of the GITEWS project. They show that significant advances in information and communication technology is the basis for making systems such as this workable, provided that protocol interfaces and data exchange are organised in a systematic and standardised way with reference architectures.

The intense seismicity and the dense seismic networks available in Taiwan have promoted work on earthquake early warning for several years. Wu and Lin present a chapter which focuses on the use of MEMS (Micro-Electric Mechanical Systems) types of accelerometer, which are specifically designed for earthquake early warning purposes with the main advantage of being very low cost. An earthquake early warning experiment in the Hualien region (Eastern Taiwan) is discussed in detail. Whereas the chapter of Wu and Lin focuses on MEMS technology for accelerometers Picozzi et al. have developed a system with the same type of accelerometers but as a self-organising seismic early warning information network (SOSEWIN) which allows early warning proper, but can also be used for many other earthquake engineering purposes such as structural health monitoring and aftershock detection. The system in terms of hard- and software is described and analysed, the optimisation procedures explained and test examples with very encouraging results presented.

In addition to earthquakes and tsunamis the book contains one chapter on earthquake early warning for landslides, specifically for instable alpine slopes, by Thuro et al. It discusses a cost-effective landslide monitoring and early warning system based on time domain reflectometry (TDR) for the detection of subsurface displacement in boreholes and reflectorless video tacheometry (VTPS) and GIS information for determining 3D-surface movements.

The chapter by Ferrucci et al. presents the rational and the main achievements of the operational prototype of the first multi-method system for volcanic monitoring in a number of regions. The system was extensively tested in 2011 during major eruptions in Eritrea and the Congo.

Applications of early warning to site-specific engineering systems have not been intensively investigated, thus the chapter of Iervolino is an important contribution that addresses this gap by providing a review of the work done in this field and illustrating a possible performance-based approach for the specific design and application of earthquake early warning systems to engineering structures.

Two more chapters were included as they provide innovative thoughts on early warning which have not been frequently discussed in the literature so far. The chapter of Woo and Marzocchi looks at operational earthquake forecasting and decision making. Operational earthquake forecasting would accommodate the probability of an earthquake's occurrence changing with time, which, although remaining low, according to the authors would still allow a number of appropriate responses. This goes beyond early warning as it does not rely on an already occurred earthquake where seconds or tens of seconds are used for implementing measures, but involves earthquake forecasting in the short term for decision

making. The chapter of Wyss et al. refers to classical earthquake early warning, providing only seconds of warning time until intense ground motion arrives. Its innovative part is the suggestion of so-called earthquake protection units (EPUs) that should be incorporated into buildings and would allow the effective protection of residents. The appeal of the suggestion is that it would increase the survival changes of potentially a large segment of the population.

The novel scientific concepts and current practices of early warning for geological disasters described in this book show the increasing potential of early warning methodologies for serving the needs of disaster management, decision makers and the public. We, therefore, hope that this book will contribute to initiating new activities for an effective exploitation of this potential with the ultimate result of reducing the level of risk in areas prone to geological hazards.

F. Wenzel
J. Zschau

Reference

UNISDR (2009) UNISDR terminology on disaster risk reduction, Geneva, Switzerland.www.preventionweb.net/files/7817_UNISDRTerminologyEnglish.pdf. Accessed May 2009

Acknowledgments

We are indebted to the many authors who devoted their time to writing contributions for this volume. We are also very grateful to Ms. Gaby Bartman at the Karlsruhe Institute for Technology and the Geophysical Institute who did most of the editorial work on the manuscripts; without her the book would not have been compiled and prepared.

We are further thankful to the German Ministry of Education and Research (BMBF) who provided support to the early warning projects in Germany through its program Geotechnologies (Geotechnologien) and the German Research Council (DFG). The initiative to develop this book was born in this framework.

Contents

Chapter 1
Earthquake Early Warning and Tsunami Warning of the Japan Meteorological Agency, and Their Performance in the 2011 off the Pacific Coast of Tohoku Earthquake (M_{W} 9.0)

M. Hoshiba and T. Ozaki

Abstract The 2011 off the Pacific coast of Tohoku Earthquake (M_w 9.0) occurred on March 11, 2011, causing strong ground motion around northeastern Japan, and generating a devastating tsunami, that killed more than 16,000 people. Before the strong ground motion hit the cities, the Japan Meteorological Agency (JMA) issued Earthquake Early Warning (EEW) announcements to the general public of the Tohoku district; the warning then was automatically broadcast through TV, radio and cellular phone messages. JMA also issued the first tsunami warnings/advisories based on hypocentral parameters (i.e., location, focal depth and magnitude) at 14:49 (Japan Standard Time), which was about three minutes after the occurrence of the earthquake, and then upgraded them using sea-level observation data. This paper reports on the performance of the EEW and the tsunami warnings/advisories, the lessons learned from the earthquake, and a direction for improving the warning systems.

1.1 Introduction

The 2011 off the Pacific coast of Tohoku Earthquake (the Tohoku Earthquake, M_{W} 9.0) occurred off the pacific coast of Japan at 14:46 (Japan Standard Time) on March 11, 2011 and generated a huge tsunami that killed at least 16,278 people, and left 2,994 people missing (Fire Disaster Management Agency, Japan, report of March 13, 2012).

Strong ground motion was also recorded across a wide area of northeastern Japan. More than 2900 cm/s^2 (three-component vector amplitude) was observed at

M. Hoshiba (✉)
Meteorological Research Institute, Japan Meteorological Agency, Nagamine 1-1, Tsukuba 305-0052, Japan
e-mail: mhoshiba@mri-jma.go.jp

T. Ozaki
Seismological and Volcanological Department, Japan Meteorological Agency, Ohte-machi 1-3-4, Chiyoda , Tokyo100-8122, Japan

F. Wenzel and J. Zschau (eds.), *Early Warning for Geological Disasters*,
Advanced Technologies in Earth Sciences, DOI: 10.1007/978-3-642-12233-0_1,

the MYG004 station of K-NET of the National Research Institute of Earth Science of Disaster Prevention (NIED), whose epicentral distance is 175 km (Aoi et al. 2011a). A seismic intensity of 7 was observed (on a scale from the Japan Meteorological Agency, JMA; details of the intensity scale will be explained in a later section) at this station for only the second time since JMA introduced instrument-based intensity observations in 1996 (Hoshiba et al. 2010). Even at some stations whose epicentral distance exceeded 300 km, acceleration >1,000 cm/s^2 was recorded. Strong ground motion exceeding 500 cm/s^2 was also widely observed in the Tohoku (northeastern Honshu Island) and Kanto (central eastern Honshu) districts. Just before the strong ground motion hit cities in the Tohoku district, the JMA issued Earthquake Early Warning (EEW) announcements to the general public in the district.

This earthquake generated a devastating tsunami along the Pacific coast of Japan. The greatest tsunami height for this event (9.3 m) was recorded at a tidal gauge site at Soma, Fukushima Prefecture. However, because the heights at many other sites are unknown because of flooding, washout, electrical power failure or wiring disconnection, these tsunami heights might be higher than the maximum observed value of 9.3 m. For many sites, the observed tsunami heights were the greatest in the past 100 years of instrumental observation. JMA issued the first tsunami warnings at 14:49, about three minutes after the occurrence of the earthquake, and then upgraded the warnings and widened the warning area seven times, in accordance with tsunami height observations. All tsunami warnings/advisories were cancelled at 17:58 on March 13, two days and three hours after the first tsunami warning.

This paper explains the background of the JMA EEW and tsunami warnings/advisories, and their performance in the M_w 9.0 Tohoku earthquake (e.g., the timing of issuance and preciseness of the prediction of ground motion and tsunami height), and then reports on the lessons learned from the earthquake and a direction for improving the warning systems, based on previous reports from Hoshiba et al. (2011); Ozaki (2011); Hoshiba and Ozaki (2012).

1.2 Earthquake Early Warning of JMA

In this section, we will provide a general background of the observation of seismic intensity and the operation of JMA EEW. We will then describe the performance of the JMA EEW in the Tohoku earthquake, the lessons learned, and a direction for improving the systems.

1.2.1 Observation of JMA Seismic Intensity

In Japan, the JMA intensity scale is widely used to measure seismic intensity. The JMA intensity had been measured manually based on human sensations and the damage caused by ground motion. In 1996, JMA replaced this with instrumental

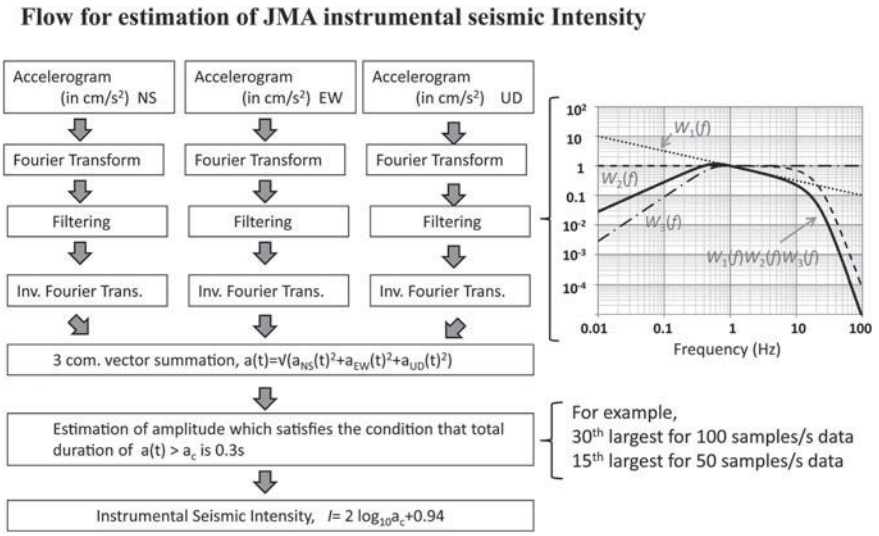

Fig. 1.1 Flow for estimating JMA instrumental seismic intensity from three component accelerograms. The right panel illustrates the frequency dependence of the three weights $W_1(f)$, $W_2(f)$, and $W_3(f)$ and their product $W_1(f)W_2(f)W_3(f)$

measurements, which were defined taking consistency with previous manual measurements into account (JMA 1996). In the instrumental measurements, not only the amplitude but also the frequency and duration of the shaking are considered (JMA 1996; Hoshiba et al. 2010).

The procedure for obtaining JMA instrumental intensity from acceleration waveforms is as follows (Fig. 1.1). Acceleration records (measured in cm/s^2) are Fourier-transformed into the frequency domain and then weighted by the following three factors:

$$W_1(f) = (1/f)^{1/2} \tag{1.1}$$

$$W_2(f) = (1 + 0.694y^2 + 0.241y^4 + 0.0557y^6 + 0.009664y^8 + 0.00134y^{10} + 0.000155y^{12})^{-1/2}, \quad \text{where } y = f/10 \tag{1.2}$$

$$W_3(f) = \{1 - \exp(-(f/0.5)^3)\}^{1/2}, \tag{1.3}$$

where f is the frequency in Hz. Weights (1.2) and (1.3) are a low-pass filter and a high-pass filter, respectively, and (1.1) corresponds to the conversion to create a waveform whose characteristics are between acceleration and velocity. The weight of $1/f$ represents the conversion from acceleration to velocity. The filtered acceleration is obtained by an inverse Fourier transform in which the filter has the characteristics of $W_1(f)W_2(f)W_3(f)$ for amplitude, and no delay for phase. The three components of the filtered accelerations, $a_{\mathrm{ns}}(t)$, $a_{\mathrm{ew}}(t)$, and $a_{\mathrm{ud}}(t)$, are summed to obtain the time series of the vector amplitude, $a(t) = \sqrt{(a_{\mathrm{ns}}(t)^2 + a_{\mathrm{ew}}(t)^2 + a_{\mathrm{ud}}(t)^2)}$. Then, a_c is

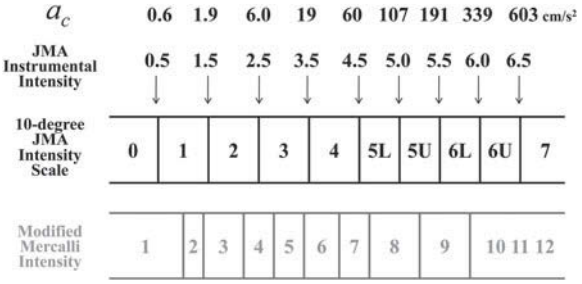

Fig. 1.2 Relation of a_c in (1.4), JMA instrumental seismic intensity and 10-degree JMA intensity scale, as well as approximate relation of JMA intensity scale and the Modified Mercalli scale. Letters of "L" and "U" on levels 5 and 6 of the 10-degree JMA scale represents delineations of "lower" and "upper". (Reprint from Hoshiba et al. 2010)

measured which is defined as the value satisfying the condition that the total duration of $a(t) > a_c$ is 0.3 s, where a_c corresponds to the 30th largest value of $a(t)$ for 100 samples/s data, or the 15th largest for 50 samples/s data. The JMA instrumental intensity, I, is defined as,

$$I = 2\log_{10}(a_c) + 0.94. \tag{1.4}$$

The 10-degree JMA intensity scale rounds off the instrumental intensity to the nearest integer (Fig. 1.2). For example, instrumental intensities in the range of $2.5 \leq I < 3.5$ and $3.5 \leq I < 4.5$ correspond to 3 and 4 on the 10-degree scale, respectively. Intensities of 5 and 6 are divided into two degrees, namely 5-lower ($4.5 \leq I < 5.0$), 5-upper ($5.0 \leq I < 5.5$), 6-lower and 6-upper, respectively. JMA Intensity 1 corresponds to ground motion that people can barely detect (approximately 1 or 2 on the Modified Mercalli Intensity scale, MMI; Fig. 1.2), and 7 is the upper limit (~11 or 12 on the MMI scale). At present, seismic intensity is measured at approximately 4,300 locations throughout Japan by JMA, municipalities, local governments, and NIED. When an earthquake occurs, the intensity data are immediately transmitted to JMA and summarized. The summary is broadcast via TV and radio as well as on the JMA web page beginning within two minutes after the earthquake, and is updated as more data become available.

1.2.2 Operation of JMA's EEW System

EEW aims at mitigating earthquake disasters by giving people enough time to take appropriate safety measures in advance of strong shaking. It has been operational nationwide in Japan by JMA since October, 2007. JMA EEW adopts mainly a network approach in which the hypocenter and magnitude, *M,* are quickly determined using an automatic analysis technique, and the seismic intensities are predicted using an attenuation relation of ground motion and site amplification factors.

The hypocenter is determined by several techniques (Hoshiba et al. 2008), using approximately 1,100 stations from the JMA network and the Hi-net network of NIED; M is determined mainly from the maximum displacement amplitudes, A, using following two relations (Kamigaichi et al. 2009):

$$0.72 \times M = \log_{10} A + 1.2 \times \log_{10} R + 5.0 \times 10^{-4} \times R - 5.0 \times 10^{-3} \times D + 0.46 \quad (1.5)$$

for P wave portions of the recorded wave train, and

$$M = \log_{10} A + \log_{10} \Delta + 1.1 \times 10^{-3} \times \Delta + 7.0 \times 10^{-4} \times D + 1.8, \quad (1.6)$$

for S wave portions, where R, D and Δ are the hypocentral distance, the focal depth and the epicentral distance in km, respectively. Here S waves are used to estimate M for stations where the S wave has already arrived. The P and S wave portions are defined from their theoretical arrival times estimated from R and D. Note that (1.5) and (1.6) are relations for JMA EEW, which is somewhat different from the magnitude estimation for the JMA unified hypocentral catalog. Here displacement waveforms are obtained from acceleration waveforms using a recursive filter that produces characteristics corresponding to the output of a displacement seismometer having an eigenperiod of 6 s and damping factor $h = 0.5$; A is the maximum displacement of the three-component vector amplitude measured in 10 μm. The hypocenter and M are updated as available data increases with elapsed time. Magnitudes determined by (1.5) are called "P wave M", and are applied for P wave portions much earlier than the S wave arrival time predicted from the hypocentral location. "P wave M" remains unchanged around the S wave arrival, and (1.6) is applied for portions later than that. "P wave M" is kept constant around the S wave arrival time in order to prevent overestimating M due to contamination by S waves that arrive earlier than predicted, considering the precision of hypocentral determination. The median value of M obtained for up to five stations is adopted as M of JMA EEW.

Figure 1.3 presents the flow for predicting seismic intensity from the estimated hypocenter and M, in which the attenuation relation of the peak ground velocity (PGV; Si and Midorikawa 1999), site amplification factors derived from topographic data (Matsuoka and Midorikawa 1994), and the empirical relation between PGV and JMA intensity (Midorikawa et al. 1999) are used (Hoshiba et al. 2008; Iwakiri et al. 2011). While many studies of EEW attempt to determine the hypocenter and M from the first several seconds of the P wave, JMA adopts the updating method. This means that the predicted intensity is updated repeatedly in accordance with the updated hypocenter and M. We described the observation of JMA seismic intensity in Sect. 1.2.1. In Fig. 1.3, on the other hand, we describe how the intensity is predicted by JMA EEW based on knowledge of only the location and M. At present, the intensity is predicted at the 4,300 intensity observation sites.

The JMA EEWs are divided into two grades: "forecast" and "warning" (Hoshiba et al. 2008; Kamigaichi et al. 2009; Doi 2011). The JMA EEW "forecast" is issued to advanced users (e.g., railway companies, elevator companies, and others) through provider companies when events are estimated to be M 3.5 or larger, when the

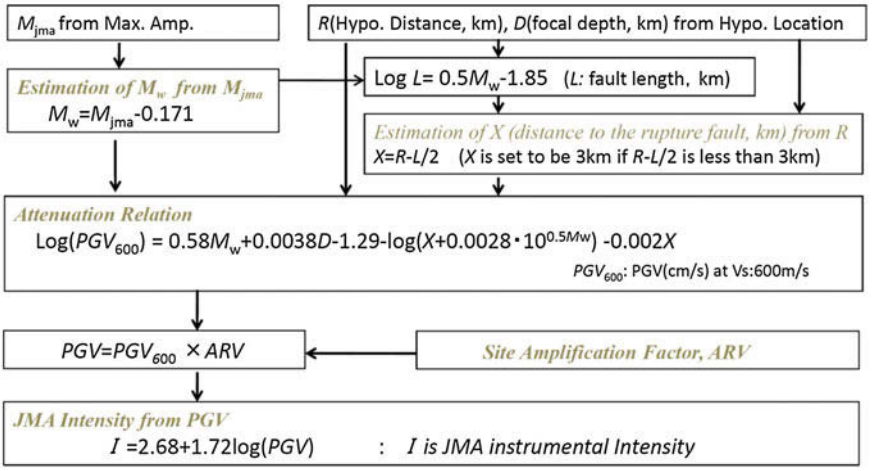

Fig. 1.3 Flow for predicting JMA seismic intensity from estimated hypocenter location, focal depth and *M*. The attenuation relation, site amplification factor and empirical relation between JMA intensity and PGV are based on Si and Midorikawa (1999); Matsuoka and Midorikawa (1994); Midorikawa et al. (1999), respectively. (Reprint from Hoshiba and Ozaki 2012)

predicted seismic intensity is 3 or greater, or when the observed acceleration exceeds 100 cm/s^2. In the "forecast", regions where seismic intensity 4 or greater is predicted are particularly specified. When the intensity is predicted to be 5-lower or greater at any observation station in the seismic intensity network, a "warning" is issued to the general public in regions where intensity 4 or greater is predicted. The "warning" is broadcast in various ways, such as by TV, radio, and cellular phone messages. As mentioned above, JMA EEWs are updated as available data increases with elapsed time. Accordingly JMA EEWs are issued repeatedly with improving accuracy. The "warning" is updated when the seismic intensity is predicted to be 5-lower or greater in regions where the intensity was estimated to be less than 4 in the first "warning" (i.e., where new regions are subject to shaking above the threshold). Even when the update causes the predicted intensity to fall below 5-lower at any stations, the "warning" is not canceled so as to avoid confusion if the predicted intensity rises again. The updated "warning" describes the newly added regions. In the current operation, the warning update is given within 60 s after the first trigger, to avoid too late a warning due to fluctuation in the gradually increasing displacement amplitude of later phases. This cutoff time was introduced into JMA EEW after an experience with a too-late warning during the *M* 7.0 event of May 8, 2008 (JMA 2008).

1.2.3 JMA EEW During the M_w 9.0 Tohoku Earthquake

The JMA EEW system was triggered for the M_w 9.0 earthquake when station OURI detected the initial *P* wave at 14:46:40.2, Japan Standard Time, on March 11

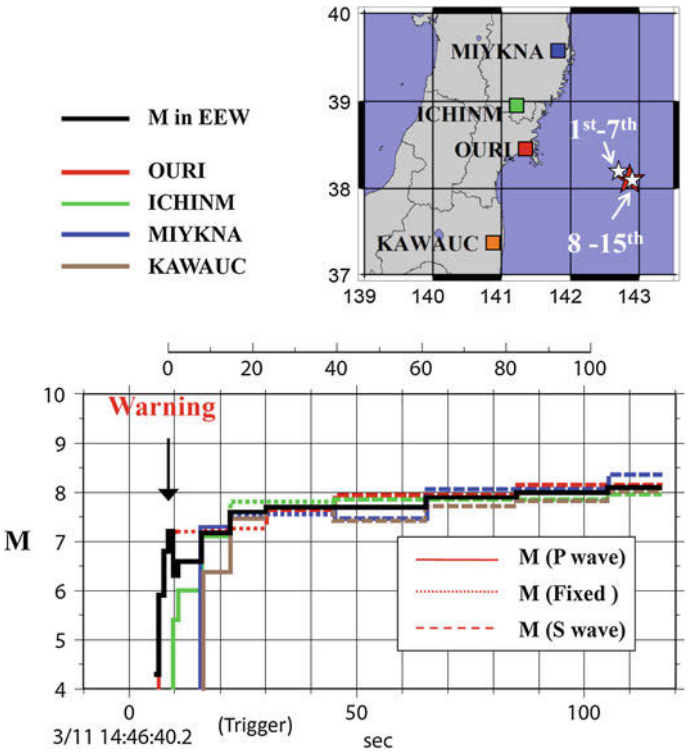

Fig. 1.4 Sequence of determining epicenter and magnitude in JMA EEW for the M_w9.0 Tohoku Earthquake. Upper right panel: Epicenters determined by the JMA EEW system are denoted as a white star for the first to seventh "forecasts" (5.4–11.0 s after the first trigger) and another for the next eight (15.9–116.8 s). The focal depth was estimated to be 10 km for all 15 announcements. The red star indicates the epicenter location from the unified JMA catalog (focal depth is 24 km). The resolution of the JMA EEW system is 0.1° for latitude and longitude, and 10 km for focal depth for hypocenter determination. Lower panel: Magnitudes estimated from maximum displacement amplitude at four stations. Colored lines represent the different stations; the black line is the median value, which is used for JMA EEW. The bottom axis indicates the elapsed time from the first trigger, and the offset axis at the top represents elapsed time from the EEW "warning" (the fourth "forecast"). The solid line indicates the magnitude of the *P* wave, the broken line is that of the *S* wave, and the dotted line shows the period during which the magnitude remained unchanged around the *S* wave arrival. (Reprint from Hoshiba et al. 2011)

(JMA 2011a, b). Figure 1.4 presents the sequence of hypocenter and magnitude updates for the earthquake, and Fig. 1.5 indicates the region of JMA EEW "warning" and "forecast", and the distribution of JMA seismic intensity. Figure 1.6 depicts the waveforms observed at the four stations in Fig. 1.5-I. The first EEW "forecast", the first of 15 announcements, was issued 5.4 s after the trigger (Fig. 1.5-a). The time sequence of the magnitude estimation is indicated in Table 1.1. The magnitude in the first EEW "forecast" was estimated to be 4.3 because the waveform started with a small amplitude. For the Tohoku Earthquake, the hypocenter

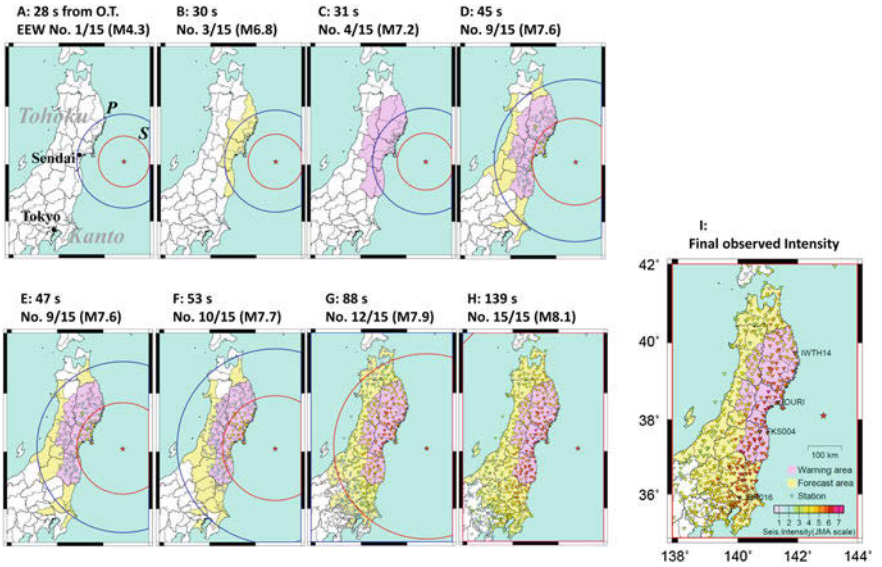

Fig. 1.5 Regions of JMA EEW "warning" and "forecast", and distribution of observed seismic intensities at several timings from the origin time. The pink area indicates the regions where the "warning" was issued, and the *yellow* areas are those specified in the "forecast". The wave fronts of the *P* and *S* waves are indicated by *blue* and *red circles*, respectively. The seismic intensities (*colored triangles*) were measured using waveforms from the K-NET, KiK-net (NIED), and JMA networks. An animation of this figure was presented at the Meteorological Research Institute (2011). (Reprint from Hoshiba and Ozaki 2012)

of Horiuchi et al. (2005)'s technique was adopted using data from Hi-net in several techniques for hypocentral determination, and the magnitude was estimated from the four stations in Fig. 1.4. By the fourth "forecast", 8.6 s after the first trigger (Fig. 1.5-c), the magnitude was estimated to be 7.2 and the seismic intensity was predicted to be 5-lower for central Miyagi Prefecture (around Sendai City). Thus, the fourth "forecast" was a "warning" to the general public in the Tohoku district. Then it was automatically broadcast through TV, radios, and cellular phone broadcasting e-mail messages. NHK, a non-profit broadcasting company, broadcast it nationwide, and other TV and radio companies did so locally. The "warning" was earlier than the *S* wave arrival (the observed intensity was at most 2) and also 15 s earlier than the time that strong ground motion (intensity 5-lower) hit the station closest to the epicenter (Fig. 1.5-e). An animation of this sequence is presented at the Meteorological Research Institute (2011). The reason the magnitude decreased between the fifth and the seventh "forecast" (from 9.6 to 15.9 s after the first trigger) was the small magnitude estimated at the second station, ICHINM, which in turn was due to the small amplitude of the initial part of the event. By the time of the fifteenth "forecast", 116.8 s after the first trigger (Fig. 1.5-h), the magnitude was estimated to be 8.1. This estimated magnitude is almost the upper

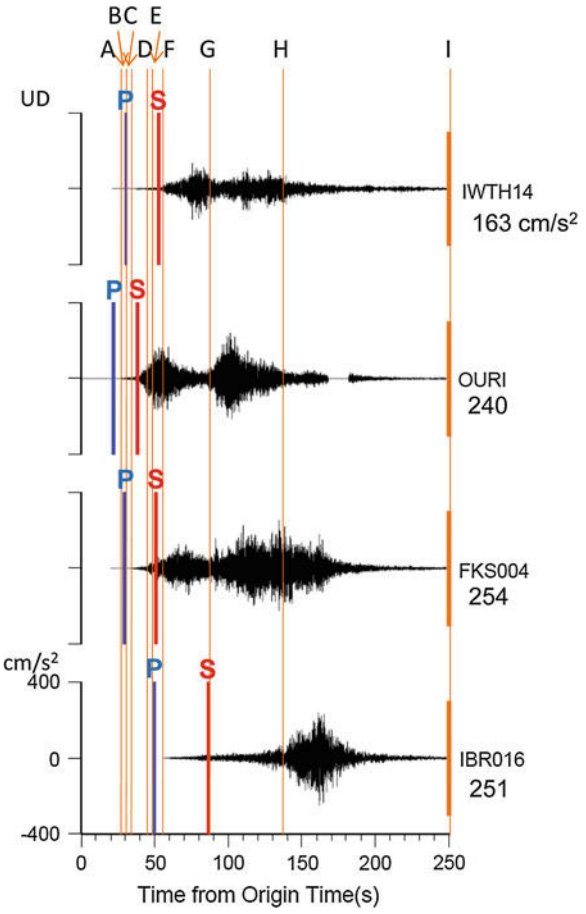

Fig. 1.6 Acceleration waveforms at the four stations in the Tohoku and Kanto districts seen in Fig. 1.5-I. Lapsed time is measured from the origin time (14:46:18.1). P and S wave arrival times are indicated by *blue* and *red* lines. The peak ground acceleration of the vertical component is indicated under the station names. Labels, A to I, indicate timings corresponding to the panels in Fig. 1.5. The data stream was disrupted between 170 and 180 s at OURI. (Reprint from Hoshiba and Ozaki 2012)

limit of JMA displacement magnitude because of amplitude-magnitude saturation for events of $M_{\mathrm{w}} > 8$. The displacement magnitude is estimated from the maximum displacement amplitude corresponding to the output of seismometers having an eigenperiod of 6 s. The displacement magnitude is 8.4 in the unified hypocenter catalog of JMA (Hirose et al. 2011).

Table 1.1 Issuance of JMA Earthquake Early Warning for the 2011 off the Pacific coast of Tohoku Earthquake (M_w9.0; JMA 2011a). For this event, 15 "forecasts" were issued. The fourth one was a "warning". The last column indicates the timings corresponding to the panels in Figs. 1.5 and 1.6. (Reprint from Hoshiba and Ozaki 2012)

No.	Hour:Min:Sec HH:MM:SS.S[a1]	Lapse time(s)[b2]	Mag.	Label in Figs. 1.5 and 1.6
	March 11, 2011			
1	14:46:45.6	5.4	4.3	A
2	14:46:46.7	6.5	5.9	
3	14:46:47.7	7.5	6.8	B
4	14:46:48.8	8.6	7.2	C
5	14:46:49.8	9.6	6.3	
6	14:46:50.9	10.7	6.6	
7	14:46:51.2	11.0	6.6	
8	14:46:56.1	15.9	7.2	
9	14:47:02.4	22.2	7.6	D
10	14:47:10.2	30.0	7.7	F
11	14:47:25.2	45.0	7.7	
12	14:47:45.3	65.1	7.9	G
13	14:48:05.2	85.0	8.0	
14	14:48:25.2	105.0	8.1	
15	14:48:37.0	116.8	8.1	H

[a1] Japan Standard Time
[b2] Measured from first trigger

1.2.4 Observed Waveforms and Seismic Intensity

Figure 1.7 indicates the acceleration and displacement (vertical component) of the M_w 9.0 mainshock and the M_w 6.0 foreshock (O.T. 03:16, March 10) and the same traces shown magnified from around the time of the P wave arrival, in which the displacement was obtained after passing a 0.075 Hz high-pass filter. As described in Sect. 1.2.3, the waveform of the M_w 9.0 mainshock started with small amplitude, comparable to the noise level for displacement (Hoshiba and Iwakiri 2011). For several seconds after the P wave onset, amplitudes of the M_w 9.0 mainshock were much smaller than those of the M_w 6.0 foreshock. The small amplitude does not indicate that the initial rupture of the M_w 9.0 event is large, and does not suggest a large magnitude event. Because the waveforms started with quite small amplitude and the rupture duration was more than 150 s (Yoshida et al. 2011) which was much longer than S-P time at the Tohoku district, many on-site EEW techniques for single-station did not work well (Motosaka 2011) in cases where analysis was performed for only the first several seconds and the system provided no updates.

To investigate in detail the initial portion of the waveforms, the behavior of the peak amplitude and the frequency content is evaluated. Figure 1.8 summarizes the maximum vertical displacement (P_d), velocity (P_v), acceleration (P_a), and τ_c in the

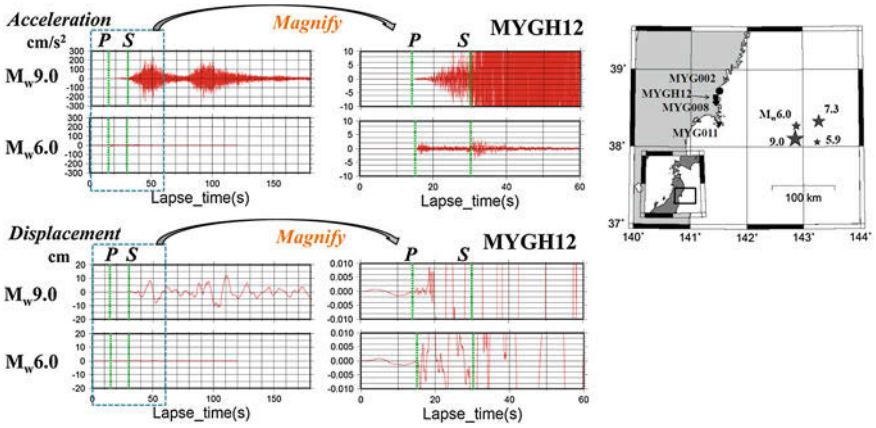

Fig. 1.7 Acceleration (*top*) and displacement (*bottom*) of the vertical component of the M_w9.0 mainshock and M_w6.0 foreshock (the origin time is 3:16 on March 10) at MYGH12 (KiK-net, ground surface). Magnified traces are also presented. The arrival times of the P and S phases are denoted by *dotted lines*. Waveforms (*left*) of the M_w6.0 foreshock are too small to be visible on the same scale as that of the M_w9.0 mainshock. The M_w5.9 and 7.3 foreshocks and stations MYG002, MYG008 and MYG011 are referred to in later figures

time windows of t_p to $t_p + t_N$ for various values of t_N for four events (M_w 9.0 mainshock and its three foreshocks of M_w 5.9 on March 9, 13:37, M_w 6.0 on March 10, 03:16 and M_w 7.3 on March 9, 11:45, respectively; see Fig. 1.7) observed at the four stations in Fig. 1.7 (right) (Hoshiba and Iwakiri 2011), where t_p is the P wave arrival time. Here τ_c is estimated from,

$$\tau_c = 2\pi \sqrt{\int_{t_p}^{t_p+t_N} u_d^2(t)dt \Big/ \int_{t_p}^{t_p+t_N} u_v^2(t)dt} \tag{1.7}$$

where $u_d(t)$ and $u_v(t)$ are time series of vertical displacement, and its differential, respectively. τ_c corresponds to the average period of $u_d(t)$ weighted by the displacement spectrum (Kanamori 2005), and is expected to increase with increasing earthquake magnitude. Empirical relations between τ_c and M were proposed to estimate the magnitude. The τ_c method has been investigated by many researchers (e.g., Kanamori 2005; Wu and Kanamori 2005), and most of them have claimed that it is possible to determine the eventual M of the events from the initial several seconds. The τ_c method was proposed for onsite techniques to estimate the magnitude using a single station (Wu and Kanamori 2005); it has also been tested for some network systems around the world (e.g., Zollo et al. 2010), but it is not used in the operation of JMA EEW.

We will examine whether it is possible to discriminate the M_w 9.0 mainshock from the three small events in the initial portion of the waveforms. For $t_N = 3 - 5$s, the peak amplitudes of the M_w 9.0 event are comparable to, or even smaller than, those

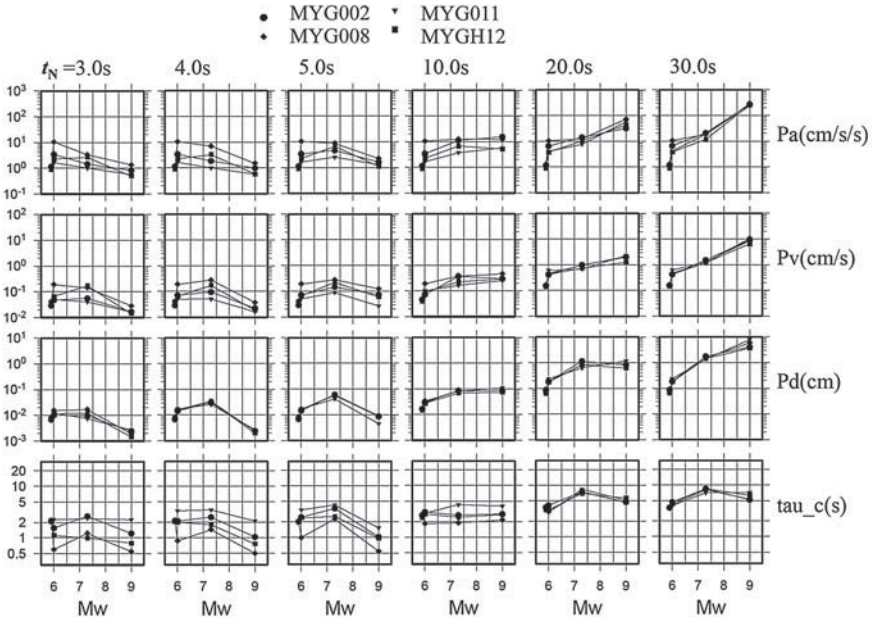

Fig. 1.8 Peak amplitudes P_a, P_v and P_d and parameter τ_c versus M_w for the four events (M_w9.0 mainshock and its three foreshocks, M_w5.9, 6.0 and 7.3) for various values of t_N. The locations of the four stations (K-net and KiK-net) and the four events are indicated in Fig. 1.7. (Reprint from Hoshiba and Iwakiri 2011)

of not only the M_w 7.3 event but also the two smaller foreshocks. In addition, τ_c does not show a clear tendency because of the large variation among the different sites. For t_N = 20 s, P_a of the M_w 9.0 event is larger than that of the M_w 7.3 event beyond the variation among sites, which indicates that P_a discriminates the M_w 9.0 from the M_w 7.3 event. For t_N = 30 s, P_v and P_d also effectively discriminate. However, although τ_c of the M_w 9.0 event is larger than that of the two smallest events, it is slightly smaller than that of the M_w 7.3 event. Thus, it is difficult to recognize the event as being larger than the M_w 7.3 from only τ_c at t_N = 30 s when accelerations exceeding 100 cm/s^2 are recorded at all four stations. Hoshiba and Iwakiri (2011) reported that the τ_p^{max} method (e.g., Nakamura 1988; Allen and Kanamori 2003) did not estimate the magnitude of the M_w 9.0 event well either.

Figure 1.9 presents the frequency spectra of waveforms of the M_w 9.0 and M_w 7.3 events at MYGH12 (KiK-net). The spectrum of the M_w 9.0 event is flat to the frequency of the anti-alias filter, around 30 Hz, for the time window of t_p to $t_p + 30$ s. The spectral ratio indicates that high frequencies are richer for the M_w 9.0 event than for the M_w 7.3 event as compared with low frequencies. This high-frequency content is not apparent for the time window of t_p to $t_p + 10$ s; therefore it is thought that the high-frequency waves arrived after $t_p + 10$ s. The high-frequency content is the reason that a smaller τ_c and τ_p^{max} were obtained for the M_w 9.0 event even for a large value of t_N. The waveforms of rich high frequency from the M_w 9.0 event contradict the

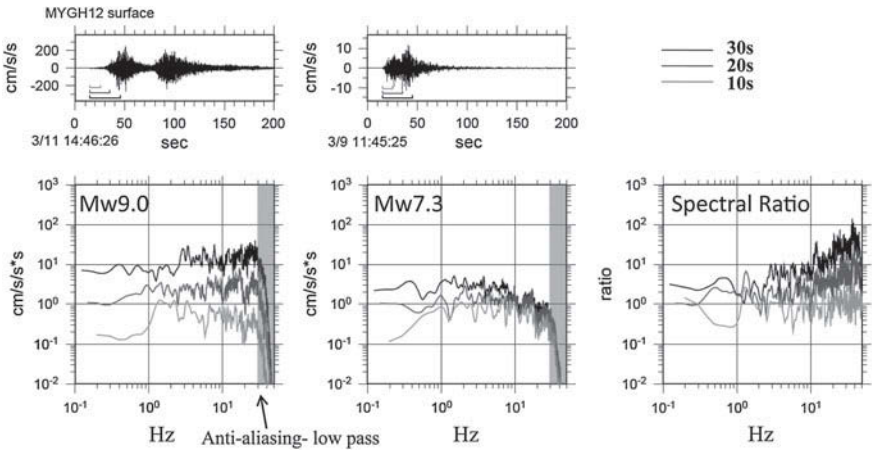

Fig. 1.9 Frequency spectra of the vertical acceleration recorded at MYGH12 for the M_w 9.0 mainshock (*left*), and M_w7.3 foreshock (*center*; O.T. 11:45, March 9), and the ratio of the two spectra (*right*) derived from time windows corresponding to $t_N = 10$ s (*light gray*), 20 s (*dark gray*) and 30 s (*black*). Waveforms are depicted at the *top*. (Modified after Hoshiba and Iwakiri 2011)

expectation that τ_c (and τ_p^{max}) would increase with increasing magnitude. The above results suggest that it would be difficult to estimate the eventual size of the huge earthquake from the first several seconds; thus an updating procedure is necessary using ongoing waveforms for EEW purposes, for both network techniques and single-station onsite methods.

Figure 1.10 indicates the distribution of the observed seismic intensities of the M_w 9.0 event and the 2003 Tokachi Oki earthquake (M_w 8.0). The intensity contours are based on the observed intensities from the dense seismic intensity networks after taking into account the site amplification factors, similar to the idea of ShakeMap (Wald et al. 2006). The observation indicates that the area of strong ground motion (6-upper and 6-lower) for the Tohoku earthquake extends from the Tohoku district to the Kanto district, over an area of approximately 400 km × 100 km, which is much larger than the corresponding area of the 2003 Tokachi Oki earthquake. The huge area of strong ground motion can be attributed to the extent of the fault rupture. The K-NET station MYG004 in Kurihara City, at which intensity 7 was recorded, is 175 km from the epicenter, and some stations at which intensity 6-lower was observed in the Kanto district are more than 350 km from the epicenter.

In addition to the wide area of strong ground motion, the event was characterized by its long duration (Aoi et al. 2011a). Figure 1.6 indicates the acceleration (UD) at the four stations in Fig. 1.5-I. At OURI, two peaks are apparent in the acceleration envelope, due to the complicated source process (e.g., Yoshida et al. 2011; Kurahashi and Irikura 2011; Nakahara et al. 2011). The second peak was 50 s after the first peak. At FKS004 and IBR016, strong ground motion was apparent from later phases, well after the direct *S* phase, and it took approximately 120 s from *P* wave arrival to peak

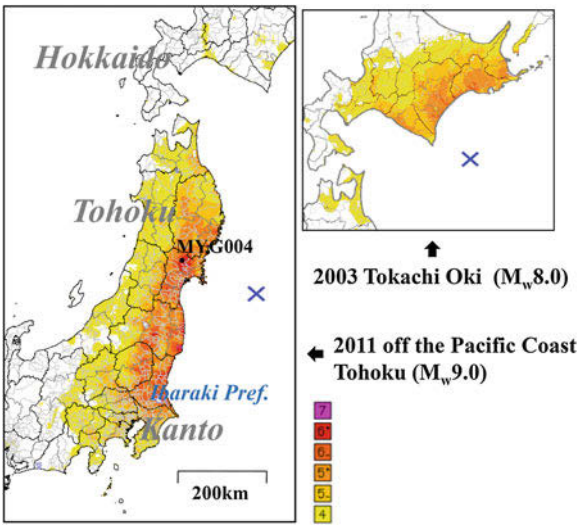

Fig. 1.10 Seismic intensity distribution of the Tohoku earthquake and the 2003 Tokachi Oki earthquake (M_w8.0). (Modified after Hoshiba et al. 2011)

acceleration. Ground motions corresponding to intensity 4, or greater, continued for 120–190 s at many observation stations in the Tohoku and Kanto districts (JMA 2011c).

1.2.5 Under-Prediction of Intensity in Kanto

The JMA EEW system predicted an intensity of 4 in Tokyo in the Kanto district in the fifteenth (final) issue. The timing, 139 s from the origin time, is at H in Figs. 1.5 and 1.6, which was before the start of strong ground motion in the Kanto district (e.g., IBR016). At this time, the magnitude was estimated to be 8.1 (No.15 in Table 1.1). Actual observations, however, eventually reached 5-upper in Tokyo, and 6-upper and 6-lower at many observation stations in the Kanto district (Fig. 1.5-I), which exceeds the criterion of the JMA EEW "warning"; thus it was under-predicted. The under-prediction can be attributed to the greater extent of the later fault rupture of the M_w 9.0 event than that expected based on the M 8.1. Inversion analysis of the source process revealed that the rupture of the M_w 9.0 event extended to off Kanto (Kurahashi and Irikura 2011; Yoshida et al. 2011). The greater extent of the fault rupture reduces the distance to the rupture fault (X in Fig. 1.3), and causes stronger ground motion.

For the northern part of Ibaraki Prefecture in the Kanto district, where the intensity predicted in the first warning (i.e., the fourth "forecast") was less than 4, the predicted intensity rose to 5-lower by the fourteenth "forecast"; however, it was too late to

update the "warning", because it was issued 105 s after the trigger, which is later than the 60 s criterion at which upgrades are stopped.

1.2.6 Performance for Many Aftershocks

After the M_w9.0 main shock, the JMA EEW system did not work well for several hours because of high background noise from the coda waves of the mainshock and active aftershocks, and because of power failures and wiring disconnections.

For several weeks, aftershock activity and induced seismic activity were quite high (Hirose et al. 2011). When multiple aftershocks occurred simultaneously over the wide source region, the system became confused, and did not always determine the location and magnitude correctly. In the 49 days from the mainshock to April 28, 2011, JMA appropriately issued EEW "warnings" for 26 of the 46 events for which seismic intensity 5-lower or greater was actually observed. In contrast, during the same time, 70 EEW "warnings" were issued, but actual observed intensities did not exceed 2 at any observation stations in 17 of the 70 events (JMA 2011d). This ratio is much higher than that of the 41 months between October 2007 (the start of JMA EEW operation) and February 2011 (just before the M_w9.0 Tohoku earthquake): 1 of 17 events did not exceed intensity 2 at any stations (due to a software bug in the amplitude parameters (JMA 2009)).

The number of JMA EEW "warnings" decreased with time: 45 for March, 26 for April, 5 for May, 5 for June, 5 for July and 3 for August. During this period, JMA reduced the distance within which observations are identified as being caused by a common event when multiple observation stations detect seismic waves. JMA also modified their procedure to stop analysis as soon as possible when the event is much smaller than the criteria for a "forecast" described in Sect. 1.2.1. The main reason for the decreased number of "warnings", however, is the decrease in aftershock activity itself.

1.2.7 Improvement for Extent of Rupture and Simultaneous Events

The technical limits of JMA EEW have already been pointed out (e.g., Hoshiba et al. 2008): (1) when two or more earthquakes occur sequentially at short intervals, it is difficult to separate them automatically, thus the hypocenter and magnitude are not estimated appropriately and error in the anticipation of seismic intensity becomes large; (2) for large earthquakes (M>7), the magnitude and seismic intensity may be underestimated because the rupture usually continues for more than 10 s, with the first EEW possibly being disseminated in the middle of the rupture, and (3) for huge earthquakes (M>8), the seismic intensity may be inappropriately estimated because it is difficult to properly take into account the large extent of the fault rupture. For the M_w9.0 Tohoku earthquake, the under-prediction of the seismic intensity in

the Kanto district described in Sect. 1.2.5 is just an example of (3). While quite active aftershocks indicate a case of (1), the aftershock region was much larger than expected.

JMA is seeking methods to address the above problems. In this section, we will describe the techniques that researchers are considering for resolving these issues.

For rapidly estimating the extent of a fault rupture, Yamada et al. (2007), Irikura and Kurahashi (2011) proposed methods using the maximum amplitude (PGA or PGV) to classify stations close to or far from the fault. Böse, Wenzel and Erdik (2008), Yamamoto (2011), Horiuchi (2011) attempted to estimate the source region by inversely applying the attenuation relation of the maximum amplitude or seismic intensity. Yamada and Heaton (2008) used envelopes for estimating the source extent.

For simultaneous multiple events, Yamada and Mori (2011) propose a new method for hypocentral determination in which the source parameters (latitude, longitude, focal depth, magnitude, and origin time) are determined using the Monte Carlo technique.

Instead of rapidly estimating the source location (or source region) and magnitude, a front detection method was proposed in which waveforms of halfway (e.g., Nagashima et al. 2008; Kuyuk and Motosaka 2009) or neighboring stations (e.g., Kanjo 2011; Aoi et al. 2011b) are used to predict ground motion. Hoshiba (2011) proposed a new technique extending the front detection method based on wave propagation theory, using a boundary integral equation method such as the Kirchhoff-Fresnel integral. With these methods, future wave fields can be predicted based on the current wave field of actual observation; that is, through a time evolutional prediction. Because the source location and M are not required, the effects of source extent and simultaneous multiple events are substantially included in these methods. The technique used for predicting ground motion is common for both small and large events, thus application may be possible without switching procedures from normal cases to special cases of a huge earthquake or simultaneous events.

Real-time observation of current ground motion is important in all the methods listed above. JMA is enhancing its seismic intensity observation by introducing real-time transmission, as the first stage in addressing the above problems.

1.3 Tsunami Warning/Advisories of JMA

In this section, we will explain the background of JMA's tsunami warnings/advisories, the performance of the warnings during the Tohoku Earthquake, the lessons learned, and a direction for improving the system.

1.3.1 JMA's Tsunami Warning Systems

JMA started a nationwide legal tsunami-warning operation for local earthquakes in 1952. At that time, tsunamis were predicted manually using tsunami back-propagation charts, and it required approximately 20 min to issue the first warning. Since then, the operation has been improved by enhancing seismic and tidal-gauge observation networks, concentrating analyses, and introducing automatic analysis using a computer system. The required time has gradually decreased over the past 60 years. JMA introduced a quantitative prediction method for both tsunami arrival time and height in 1999 (Tatehata 1998; Kamigaichi 2009), and the present system is based on this method. For this method, more than 100,000 scenarios were calculated using tsunami forward propagation simulation in advance varying the hypocenter location, focal depth and magnitude; the results were then archived as a database. When an earthquake occurs, the arrival times of P and S phases and maximum amplitude are measured automatically by the computer system, and they are then quickly reviewed and corrected, if necessary, by the operational staff on duty. The hypocenter, focal depth and magnitude are determined from the arrival time and the maximum amplitude. The arrival time and height of the tsunami are then predicted using the database. It takes about three minutes after the first detection of an earthquake for a warning to be issued. Since 2006, JMA EEW output (hypocenter location, focal depth, and magnitude determined automatically without reviews by operational staff) has been used to speed up the procedure when the hypocenter is precisely determined in EEW (i.e., estimated to be in or near the seismic observation networks); thus the time has been reduced to as little as 2 min.

JMA has two categories for tsunami warnings and one for advisories (total of 3 categories; see Table 1.2), determined by the predicted tsunami height ("Major tsunami" for a height of 3m or more; "Tsunami" 1–2 m; "Tsunami advisory" 0.5 m). These tsunami warnings/advisories are provided to the 66 areas into which the coast line of the Islands of Japan is divided. These categories are immediately broadcast by TV, radio, sirens and loud-speakers in municipalities along the coast line. In addition to the categories, the predicted tsunami arrival time and height are announced. When a tsunami is actually observed, information about the observation is also disseminated.

Tsunamis are monitored by JMA in real time at 173 tide gauges (as of January 2012) from not only the JMA network but also those of other organizations (e.g., the Cabinet Office, the Ports and Harbours Bureau of the Ministry of Land, Infrastructure, Transport and Tourism (MLIT), the Japan Coast Guard, the Geospatial Information Authority of Japan (GSI), and local governments) (Fig. 1.11). In addition to the tide gauges, 15 GPS buoys (as of January 2012) from the Ports and Harbours Bureau, located 10–20 km off the coast, are used for monitoring. Observed tsunami heights are used for both supplementary tsunami information and changing categories or areas of tsunami warnings/advisories.

Table 1.2 Categories and criteria of tsunami warning and tsunami height estimations

Category		Present (as of Feb. 2012)	Improvement Plan		
		Expression of Tsunami height	Expression of Tsunami height		Estimated height
			Numerical	Qualitative	
Tsunami Warning			Over 10 m		10 m +
	Major Tsunami	10 m or more, 8 m, 6 m, 4 m, 3 m	10 m	Gigantic [a]	5–10 m
			5 m		3–5 m
	Tsunami	2 m, 1 m	3 m	High [a]	1–3 m
Tsunami Advisory		0.5 m	1 m	(Blank)	0.2–1 m

[a] English expressions are being considered

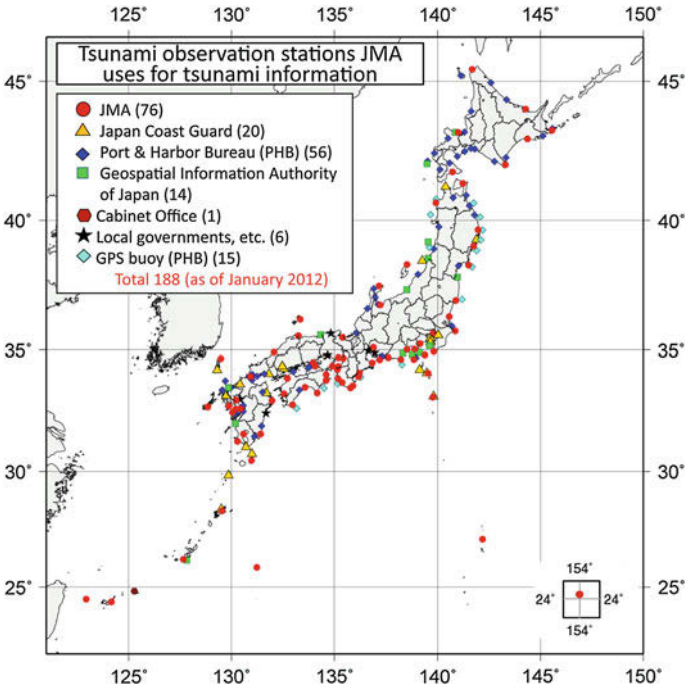

Fig. 1.11 Tsunami observation stations that JMA uses for Tsunami information. (Reprint from Hoshiba and Ozaki 2012)

1.3.2 Performance of JMA Tsunami Warning During M_w 9.0 Tohoku Earthquake

Just after the detection of the earthquake, the JMA EEW procedure was triggered at 14:46, and it estimated *M* to be 8.1 at the fifteenth "forecast" as described in Sect. 1.2.3. However, because the hypocenter was located far from the seismic

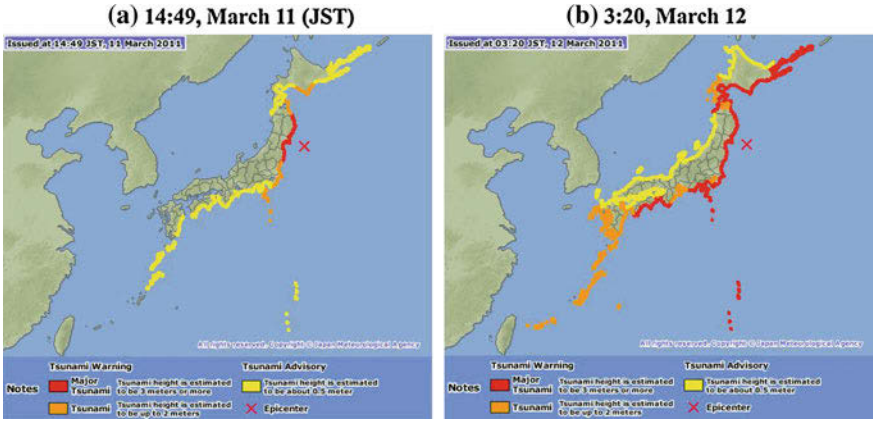

Fig. 1.12 **a** First tsunami warning bulletin (14:49, March 11) and **b** eighth tsunami warning bulletin (03:12, March 12) for the Tohoku Earthquake. (Reprint from Ozaki 2011)

networks, the automatically estimated hypocenter and *M* of EEW were not used. The hypocenter and magnitude (*M* 7.9) were promptly estimated from the P and S phase arrival times and the maximum amplitude provided by the computer and reviewed by the operational staff. Using this hypocenter and *M*, JMA predicted the tsunami arrival time and height, and then issued tsunami warnings/advisories concerning the destructive tsunami along the Pacific coasts of the Japan islands, within about three minutes after the earthquake. The initial warnings were issued at 14:49 on March 11, with "Major Tsunami" warnings for the areas of Iwate Prefecture (predicted height of 3 m), Miyagi Prefecture (6 m), and Fukushima Prefecture (3 m). At the same time, "Tsunami" warnings and "Tsunami advisories" were issued for many other areas from Hokkaido (northern Japan) to Kyushu (southern Japan) (JMA 2011e, Fig. 1.12a). TVs and radios immediately broadcast the warnings/ advisories. Municipalities used sirens and loudspeakers along the coast, and police and fire fighters used police cars and fire engines, respectively, to disseminate these warnings.

After the first warnings, the GPS buoys located 10–20 km off Iwate and Miyagi prefectures observed a steep rise in sea level at around 15:10 (Figs. 1.13 and 1.14), and at 15:14 JMA raised the predicted tsunami height from 3 to 6 m for Iwate and Fukushima prefectures, and from 6 to 10 m or more for Miyagi Prefecture. GPS buoy data indicated this rise about 5–10 min before the arrival of significant tsunami waves on the coast (Fig. 1.13). Other upgrades were conducted for regions where the ongoing predictions were considered to be underestimated in view of the trend of the sea-level variation up to that time. The tsunami warnings/advisories were upgraded a total of seven times (at 15:14, 15:30, 16:08, 18:47, 21:35, and 22:53 on March 11, and at 03:20 on March 12). In the upgrade at 03:20 on March 12, JMA issued tsunami warnings or advisories for Japan's entire coastline (Fig. 1.12b). All tsunami warnings/advisories were cancelled at 17:58 on March 13. This was 2 days and 3 hours after the tsunami warning was issued.

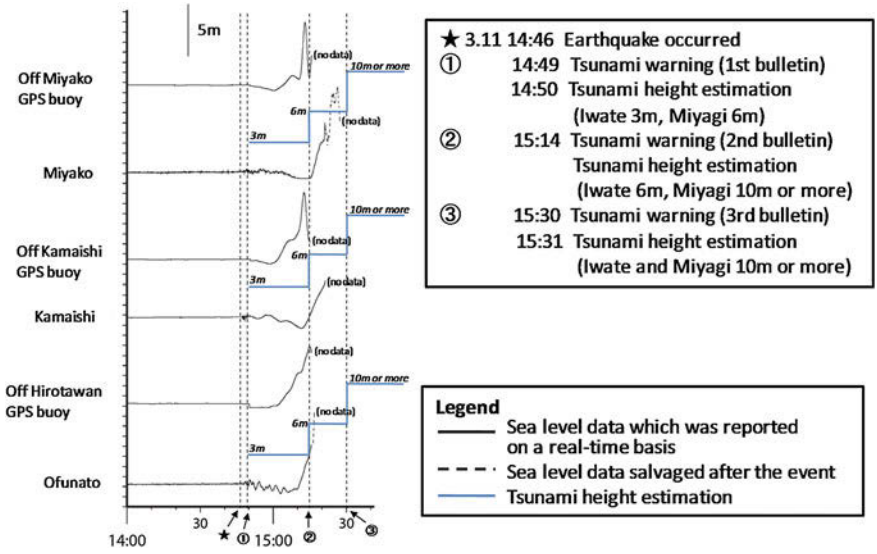

Fig. 1.13 Tsunami records at GPS buoys and tide gauges close to the buoys. *Blue* lines indicate tsunami height estimates for the areas in which the tide gauges and buoys are located. The locations of the buoys and tide gauges are indicated in Fig. 1.14. (Reprint from Hoshiba and Ozaki 2012)

The promptly-estimated magnitude, M 7.9, was based on the displacement magnitude determined from the maximum amplitude. The displacement magnitude can be calculated within a few minutes, but it may be oversaturated for $M_{\mathrm{w}} > 8$, as described in Sect. 1.2.3. JMA updated M to 8.4 (displacement magnitude) at 16:00 and determined the moment magnitude (M_{w}) to be 8.8 by CMT analysis at 17:30, which was calculated from overseas broadband seismic data. On March 13, M_{w} was revised to 9.0 by CMT analysis using a longer-range filter (Hirose et al. 2011). These revised values were not used to update the tsunami warnings because updates based on sea-level observations had provided substantially greater tsunami-height estimates before these larger-magnitude values were obtained.

1.3.3 Observed Tsunami

On the Pacific coast of Tohoku, the first large tsunami wave heights were considered to have arrived at around 15:15 (see Figs. 1.13 and 1.15, and the measurements in Table 1.3) in the earliest areas. After that, quite large amplitudes were recorded at many tidal gauge sites (Fig. 1.16), and most were the largest in the past 100 years of instrumental observation (JMA 2011e). During this huge tsunami, many sea-level station data streams were disrupted for various reasons (e.g., flooding or washout, electric power failure and/or wiring disconnection). As a result, downgrading and

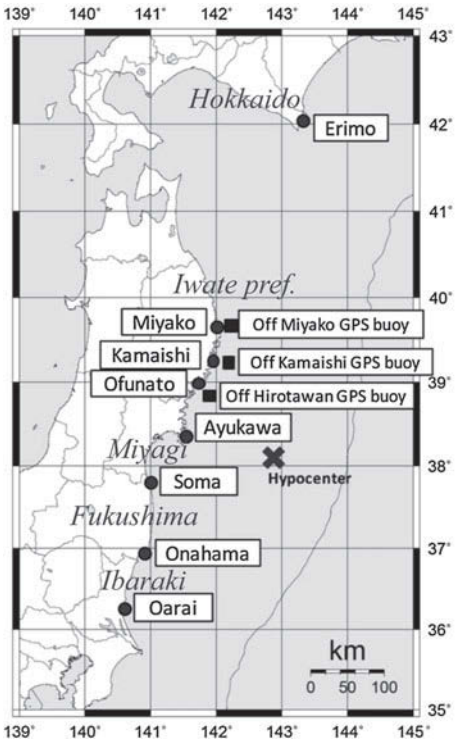

Fig. 1.14 Locations of tide gauges and GPS buoys in Table 1.2 and Figs. 1.13 and 1.14. (Modified after Ozaki 2011)

cancellation of tsunami warnings were based mainly on data from sea-level stations that survived. For some stations, the recording media and tsunami records were retrieved after the event as part of JMA's post-tsunami field surveys (Ofunato in Iwate Prefecture, Miyako in Iwate Prefecture, and Ayukawa in Miyagi Prefecture). While these media preserved a slightly longer data record after online transmission ceased, even these time series were disrupted, implying that tsunami heights might be greater than the data observed at these stations (JMA 2011f, g, h, i). Other tsunami records are available in the March 2011 issue of the Monthly Report on Earthquakes and Volcanoes in Japan (JMA 2011e).

1.3.4 Lessons Learned from the M_w 9.0 Tohoku Earthquake Tsunami and Future Plans

After the devastation caused by the Tohoku Earthquake, JMA held advisory meetings involving tsunami experts and disaster management organizations to consider a plan to improve JMA's tsunami warnings. Based on the discussions in these meetings, the JMA Tsunami Warning Improvement Plan was crafted in September 2011, and

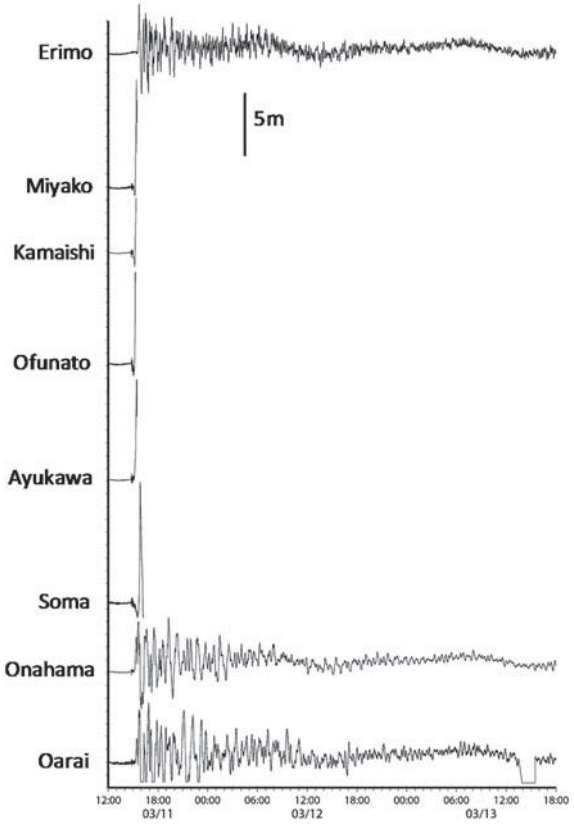

Fig. 1.15 Tsunami records at tide gauges in Table 1.3. The locations of the buoys and tide gauges are indicated in Fig. 1.14 (Reprint from Ozaki 2011)

the Recommendation on Tsunami Warning Criteria and Expression of Warning Messages was crafted in February 2012. The lessons learned from the Tohoku Earthquake and the future plan summarized in these papers are described below.

The major issue regarding JMA's tsunami warnings for the Tohoku Earthquake was that the first tsunami warning issued three minutes after the quake was based on an underestimated M of 7.9; thus, underestimation of the tsunami height of 3 m or 6 m may have resulted in a delay of evacuation. JMA's magnitude, which is equivalent to the surface wave magnitude (M_s) for shallow events, has the advantage of fast availability, but inherently saturates for $M_w > 8$. To deal with this problem, JMA will introduce tools with which the validity of a promptly estimated magnitude can be evaluated before the first tsunami warning issuance. If these tools detect the possibility of a much larger magnitude than the prompt estimation, JMA will issue a tsunami warning, replacing the magnitude with the maximum credible magnitude in the region close to the epicenter. Because of the large uncertainty of magnitude

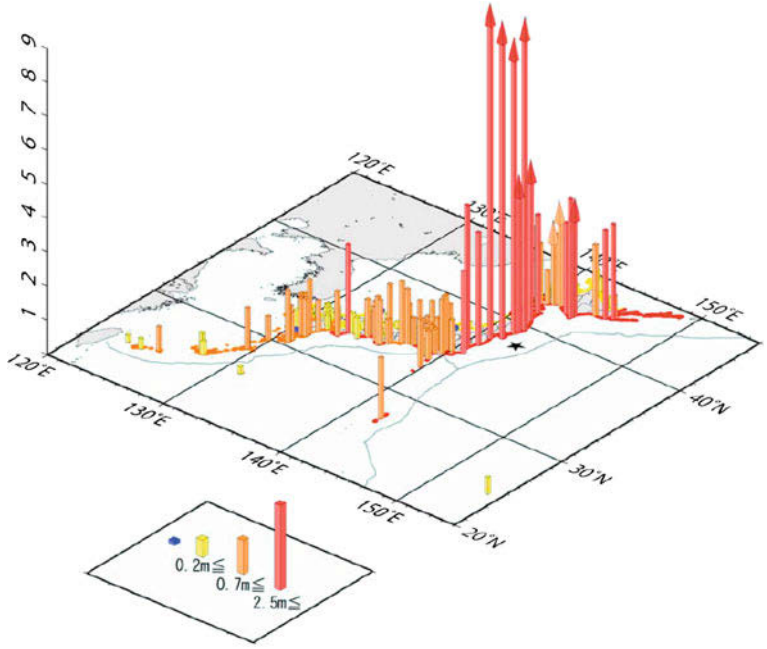

Fig. 1.16 Observed maximum tsunami heights at tide gauges. The *arrow* indicates that data transmutation was interrupted at the site because of flooding, washout, power failure or wiring disconnection; the maximum height is unknown. (Reprint from Ozaki 2011)

and tsunami-height estimation, JMA will issue tsunami height estimates qualitatively rather than numerically in an effort to convey the emergency situation to the public.

For the Tohoku Earthquake, JMA could not calculate M_w within 15 min as with JMA's normal operation, because the very large seismic waves went off the scale of most of JMA's broadband seismographs. Furthermore, offshore tsunami observation data from cabled ocean-bottom pressure gauges deployed around Japan could not be applied for a tsunami warning update. These issues led to a delay of the tsunami warning upgrade for the Tohoku Earthquake. In order to deal with these matters, JMA is planning to deploy 80 new broad-band seismographs with greater measuring ranges to calculate M_w within 15 min even for an earthquake as huge as the Tohoku Earthquake. To utilize ocean-bottom pressure gauges, JMA is developing an analysis method for initial tsunami source inversion to estimate the coastal tsunami height (Tsushima et al. 2011), and plans to deploy three buoy-type pressure sensors far off eastern Japan. Furthermore, the Ministry of Education, Culture, Sports, Science and Technology in Japan is planning to deploy networks of ocean-bottom pressure gauges and ocean-bottom seismometers off eastern Japan using very long cables. An updated tsunami warning based on M_w and ocean-bottom pressure gauges has less uncertainty than the initial warning, and in this case JMA will issue tsunami height estimates numerically.

Table 1.3 Maximum tsunami heights for stations located from north (*top*) to south (*bottom*)

Tide gauge station	Maximum tsunami height	Observed or disrupted time
Erimo, Hokkaido Pref.	3.5 m	15:44
Miyako, Iwate Pref.	8.5 m *	15:26
Kamaishi, Iwate Pref.	4.2 m *	15:21
Ofunato, Iwate Pref.	8.0 m *	15:18
Ayukawa, Miyagi Pref.	8.6 m *	15:26
Soma, Fukushima Pref.	9.3 m *	15:51
Onahama, Fukushima Pref.	3.3 m	15:39
Oarai, Ibaraki Pref.	4.0 m	16:52

The locations of the stations are indicated in Fig. 1.14. An asterisk (*) indicates stations at which data was disrupted; higher tsunamis might have hit these stations afterward

As for tsunami height categorization, it will be decreased from eight levels (0.5 m, 1 m, 2 m, 3 m, 4 m, 6 m, 8 m, and $\geq$10 m) to five (1 m, 3 m, 5 m, 10 m, and $>$10 m), taking into account the realistic variety of countermeasures in a time of emergency and the forecast error range. The estimated tsunami height indicated in the bulletin is the upper bound of estimated heights for the area.

Table 1.2 summarizes the numerical and qualitative expression of tsunami heights and the criteria for tsunami warning and tsunami height estimations described in the improvement plan.

1.4 Summary and Remarks

For the M_w9.0 Tohoku Earthquake, though both EEW and the tsunami warnings from JMA were issued as rapidly as designed, there were problems with their precision. We should learn lessons from this devastating disaster and endeavor to improve the warning systems.

Regarding EEW, JMA issued a “warning” to the Tohoku region despite the fact that the initial part of the waveforms was very small because JMA has adopted an updating method using both P waves and S waves. The frequency content of the waveforms deviated greatly from the empirical τ_c-M and τ_p^{max}-M relations. These results indicate that an updating procedure is important using ongoing waveforms for EEW purposes for both a network technique and the single-station onsite methods, especially for large earthquakes whose rupture duration is much longer than the S-P time. On the other hand, JMA EEW system under-predicted the seismic intensity in the Kanto region because of the large extent of the fault rupture, and the system issued some false alarms because of confusion when multiple aftershocks occurred simultaneously. These results suggest that, in addition to the hypocenter and M, real-time observation of current ground motions is important for correcting the predictions of future ground motion.

Regarding the tsunami, JMA issued a timely initial warning of a "Major Tsunami" about 3 min after the occurrence of the earthquake using seismological analysis. This confirms that the seismological approach is useful for rapid warnings. JMA upgraded the warning based on off-shore tsunami observations, which indicates that observation of the tsunami itself off the coast is useful and that having an updating procedure based on real observations is important. However, the tsunami height predictions in the first warning were greatly underestimated because of the underestimated magnitude. In Japan, where many tsunamis hit the coasts within a short time, a prompt tsunami warning is essential. Yet, it is technically difficult to estimate a magnitude above 8 within several minutes. Considering these conditions, JMA will take the approach of issuing an initial tsunami warning for a huge event applying maximum credible magnitude around the epicenter, if a possibility of saturation of the promptly estimated magnitude is detected. In this case, tsunami height predictions are announced qualitatively not numerically because of the large uncertainty in the magnitude. This initial warning should later be updated as appropriate. To accomplish this, we will enhance the utilization of M_w and ocean-bottom pressure gauges, which give us a more precise estimation of tsunami heights than initial warnings. These methods will enable us to issue more effective tsunami warnings, especially for gigantic events.

One of the items on a survey conducted by Dentsu Research asked respondents which services they regard as useful in cell phones. Results indicated that 24.8 % of 1200 respondents in the Kanto district regard the EEW service as a useful function of cell phone (article in Asahi Shinbun (newspaper), June 4, 2011). This percentage is the second largest response. The first is an e-mail function (58.4 %), the third is a cell-phone TV (22.5 %), and the fourth is Twitter and blogs (17.0 %). This result is notable in the following two ways. One is the increase in the number of people who are aware of the EEW service. Before the M_w9.0 Tohoku Earthquake, few people knew about EEW. The other is that people are starting to recognize EEW as a measure for their safety. This survey was conducted March 23 through 25, 2011, when the JMA EEW system sometimes worked inappropriately (as described in Sect. 1.2.6), yet many people regard JMA EEW as useful despite some false alarms. Although it is necessary to improve the system to reduce false alarms, this result is encouraging to the community of EEW researchers.

As for the tsunami warning, the improvement measures described in Sect. 1.3.4 will be implemented by the end of 2012, subject to the schedule for system modification of JMA and other organizations responsible for transmitting and using tsunami warning bulletins.

Acknowledgments The authors thank the anonymous reviewer whose comments were useful in revising the manuscript. The authors also thank K. Iwakiri, N. Hayashimoto, H. Kikuta, K. Hirano, Y. Yamada, Y. Ishigaki, T. Kuwayama, K. Nakata, and T. Shimoyama for their help in completing the figures. Seismic intensity data were provided by JMA as well as NIED and local governments and municipalities. Waveform data were obtained from the JMA network, K-NET and KiK-net of NIED. The unified hypocenter catalog and CMT catalog of JMA were used in this analysis. JMA EEW uses a combination of several techniques developed by joint research with the Japan Railway Technical Research Institute, and also by NIED. It also uses real-time data from Hi-net of

NIED in addition to JMA's own network for hypocenter determination. Sea-level data are not only from JMA, but also from the Cabinet Office, the Ports and Harbours Bureau of MLTI, the Japan Coast Guard, GSI, and local governments. We thank all of these organizations for their efforts in maintaining these observations and providing the data. Figures were made using Generic Mapping Tools (Wessel and Smith 1995). This work is partially supported by JSPS KAKENHI Grant Number 24310132 "Establishment of tsunami decay forecasting model".

References

Allen RM, Kanamori H (2003) The potential for earthquake early warning in southern California. Science 300:786–789

Aoi S, Kunugi T, Suzuki W, Morikawa M, Nakamura H, Fujiwara H (2011) Strong ground motions from the 2011 off the Pacific coast of Tohoku Earthquake (in Japanese). Bull JAEE 15:25–28

Aoi S, Kunugi T, Nakamura H, Suzuki W, Fujiwara H (2011b) Real time monitoring of strong ground motion, ERI Meeting of "Rapid analysis and prediction of seismic ground motion", http://wwweic.eri.u-tokyo.ac.jp/viewdoc (in Japanese). Accessed 11 Jan 2012

Böse M, Wenzel F, Erdik M (2008) PreSEIS: a neural network-based approach to earthquake early warning for finite fault. Bull Seis Soc Am 98:366–382

Doi K (2011) The operation and performance of Earthquake Early Warnings by the Japan Meteorological Agency. Soil Dyn Earthq Eng 31:119–126

Hirose F, Miyaoka K, Hayashimoto N, Yamazaki T, Nakamura M (2011) Outline of the 2011 off the Pacific Coast Tohoku Earthquake (M_w9.0)–Seismicity: Foreshock, Mainshock, Aftershock, and Induced Earthquake. Earth Planets Space 63:513–518

Horiuchi S, Negishi H, Abe K, Kaminuma A, Fujinawa Y (2005) An automatic processing system for broadcasting earthquake alarms. Bull Seism Soc Am 95:708–718

Horiuchi S (2011). Development of EEW system for huge earthquakes, ERI Meeting of "Rapid analysis and prediction of seismic ground motion", http://wwweic.eri.u-tokyo.ac.jp/viewdoc/yure2011/11_horiuchi.pdf (in Japanese). Accessed 11 Jan 2012

Hoshiba M, Kamigaichi O, Saito M, Tsukada S, Hamada N (2008) Earthquake early warning starts nationwide in Japan. EOS Trans Am Geophys Union 89:73–74

Hoshiba M, Ohtake K, Iwakiri K, Aketagawa T, Nakamura H, Yamamoto S (2010) How precisely can we anticipate seismic intensities? A study of uncertainty of anticipated seismic intensities for the Earthquake Early Warning method in Japan. Earth Planets Space 62:611–620

Hoshiba M, Iwakiri K (2011) Initial 30 seconds of the 2011 off the Pacific coast Tohoku earthquake (M_w9.0) amplitude and τ_c for magnitude estimation for Earthquake Early Warning. Earth Plants Spaces 63:553–557

Hoshiba M, Iwakiri K, Hayashimoto N, Shimoyama T, Hirano K, Yamada Y, Ishigaki Y, Kikuta H (2011) Outline of the 2011 off the Pacific coast of Tohoku Earthquake (M_w 9.0) –Earthquake Early Warning and observed seismic intensity. Earth Planets Space 63:547–551

Hoshiba M (2011). Expectation of ground motion in Earthquake Early Warning using real time monitoring of wavefield: a method based on Kirchhoff-Fresnel integral without information of hypocenter and magnitude, AGU fall meeting, S51F–05

Hoshiba M, Ozaki T (2012) Earthquake Early Warning and Tsunami warning of JMA of the 2011 off the Pacific coast of Tohoku Earthquake (in Japanese). Zisin 2(64):155–168

Irikura K, Kurahashi S (2011) Improvement of Earthquake Early Warning considering rupture extent. ERI Meeting of Rapid analysis and prediction of seismic ground motion, http://wwweic.eri.u-tokyo.ac.jp/viewdoc/yure2011/12_irikura.pdf (in Japanese). Accessed 11 Jan 2012

Iwakiri K, Hoshiba M, Nakamura K, Morikawa N (2011) Improvement in the accuracy of expected seismic intensities for earthquake early warning in Japan by using empirically estimated site amplification factors. Earth Planets Space 63:57–69

Japan Meteorological Agency (1996) Seismic Intensity. Gyosei (in Japanese), Tokyo 238
Japan Meteorological Agency (2008) On the earthquake occurring off Ibaraki Prefecture on 8 May 2008 (press release), http://www.jma.go.jp/jma/press/0805/08a/200805080330.html (in Japanese). Accessed 8 Aug 2012
Japan Meteorological Agency (2009) On the false alarm of JMA EEW (2^{nd} issue of press release), http://www.jma.go.jp/jma/press/0908/25b/200908251700.html (in Japanese). Accessed 8 Aug 2012
Japan Meteorological Agency (2011a) On the 2011 off the Pacific coast of Tohoku earthquake (1^{st} issue of press release), http://www.jma.go.jp/jma/press/1103/11b/201103111600.html (in Japanese). Accessed 8 Aug 2012
Japan Meteorological Agency (2011b) Report of Earthquake Early Warning, http://www.seisvol.kishou.go.jp/eq/EEW/kaisetsu/joho/joho.html (in Japanese). Accessed 8 Aug 2012
Japan Meteorological Agency (2011c) On the ground motions observed by seismic intensity meters at the 2011 off the Pacific coast of Tohoku earthquake, (press release) http://www.jma.go.jp/jma/press/1103/25a/201103251030.html (in Japanese). Accessed 8 Aug 2012
Japan Meteorological Agency (2011d) Report of the Earthquake Early Warning after the 2011 off the Pacific coast of Tohoku earthquake, (press release) http://www.jma.go.jp/jma/press/1104/28b/eew_hyouka2.html (in Japanese). Accessed 8 Aug 2012
Japan Meteorological Agency (2011e) Monthly Report on Earthquakes and Volcanoes in Japan, March 2011. http://www.seisvol.kishou.go.jp/eq/gaikyo/monthly201103 /201103index.html (in Japanese). Accessed 8 Aug 2012
Japan Meteorological Agency (2011f) Tsunami observation data at Miyako and Ofunato (press release), http://www.jma.go.jp/jma/press/1103/23b/tsunami_miyako_ofunato.html (in Japanese). Accessed 8 Aug 2012
Japan Meteorological Agency (2011g) Tsunami observation data at Ishinomaki-Ayukawa (press release), http://www.jma.go.jp/jma/press/1103/29c/201103291900.html (in Japanese) Accessed 8 Aug 2012
Japan Meteorological Agency (2011h) Tsunami observation data at Soma (press release), http://www.jma.go.jp/jma/press/1104/13a/201104131600.html (in Japanese). Accessed 8 Aug 2012
Japan Meteorological Agency (2011i) Tsunami observation data at Ishinomaki-Ayukawa (update) (press release), http://www.jma.go.jp/jma/press/1106/03b/tsunami_ayukawa2.html (in Japanese). Accessed 8 Aug 2012
Kamigaichi O (2009) Tsunami forecasting and warning. Encyclopedia of complexity and system science, Springer, pp 9592–9618
Kamigaichi O, Saito M, Doi K, Matsumori T, Tsukada S, Takeda K, Shimoyama T, Nakamura K, Kiyomoto M, Watanabe Y (2009) Earthquake early warning in Japan—warning the general public and future prospect. Seismol Res Let 80:717–726
Kanamori H (2005) Real-time seismology and earthquake damage mitigation. Annu Rev Earth Planet Sci 33:195–214
Kanjo K (2011) Improvement of the accuracy and speed of the Earthquake Early Warning which adapted the real-time data. ERI meeting of Rapid analysis and prediction of seismic ground motion, http://wwweic.eri.u-tokyo.ac.jp/viewdoc/yure2011/14_kanjyo.pdf (in Japanese). Accessed 7 Feb 2012
Kurahashi S, Irikura K (2011) Source model for generating strong ground motions during the 2011 off the Pacific coast of Tohoku Earthquake. Earth Plants Spaces 63:571–576
Kuyuk HS, Motosaka M (2009) Real-time ground motion forecasting using front-site waveform data based on artificial neural network. J Disaster Res 4:260–266
Matsuoka M, Midorikawa S (1994) The digital national land information and seismic microzoning (in Japanese). Proceeding of the 22nd symposium of earthquake ground motion, AIJ, pp 23–34
Meteorological Research Institute (2011) Report of the 2011 off the Pacific coast of Tohoku earthquake, http://www.mri-jma.go.jp/Dep/sv/2011tohokutaiheiyo/index.html#earthquake-early-warning (in Japanese with English explanation). Accessed 8 Aug 2012

Midorikawa S, Fujimoto K, Muramatsu I (1999) Correlation of new J.M.A. instrumental seismic intensity with former J.M.A. seismic intensity and ground motion parameters, (in Japanese). J Inst Soc Saf Sci 51–56

Motosaka M (2011) Lessons learned from the Pacific coast of Tohoku Earthquake—current status and problems of EEW systems. ERI Meeting of Rapid analysis and prediction of seismic ground motion, http://wwweic.eri.u-tokyo.ac.jp/viewdoc/yure2011/05_motosaka.pdf (in Japanese). Accessed 7 Feb 2012

Nakahara H, Sato H, Nishimura T, Fujiwara H (2011) Direct observation of rupture propagation during the 2011 off the Pacific coast of Tohoku Earthquake (M_w 9.0) using a small seismic array. Earth Planets Space 63:589–594

Nakamura Y (1988) On the urgent earthquake detection and alarm system (UrEDAS). Proc Ninth World Conf Earthq Eng 7:673–678

Nagashima I, Yoshimura C, Uchiyama Y, Maseki R, Itoi T (2008) Real-time prediction of earthquake ground motion using empirical transfer function. Proceedings of 14^{th} world conference on, earthquake engineering, S02–023

Ozaki T (2011) Outline of the 2011 off the Pacific coast of Tohoku Earthquake (M_w 9.0) Tsunami warnings/advisories and observations. Earth Planets Space 63:827–830

Si H, Midorikawa S (1999) Attenuation relationships of peak ground acceleration and velocity considering effects of fault type and site condition. (in Japanese). J Struct Constr Eng AIJ 523: 63–70

Tatehata H (1998) Application of tsunami numerical simulation technique to Tsunami warning (in Japanese). Kaiyo Monthly Special Issue 15:23–30

Tsushima H, Hirata K, Hayashi Y, Tanioka Y, Kimura K, Sakai S, Shinohara M, Kanazawa T, Hino R, Maeda K (2011) Near-field tsunami forecasting using offshore tsunami data from the 2011 off the Pacific coast of Tohoku Earthquake. Earth Planets Space 63:821–826

Yamada M, Heaton T, Beck J (2007) Real-time estimation of fault rupture extent using near-source versus far-source classification. Bull Seis Soc Am 97:1890–1910

Yamada M, Heaton T (2008) Real-time estimation of fault rupture extent using envelopes of acceleration. Bull Seis Soc Am 98:607–619

Yamada M, Mori J (2011) Future developments for the earthquake early warning system following the 2011 off the Pacific Coast of Tohoku Earthquake. AGU fall Meeting, S51F–02

Yamamoto S (2011) Successive estimation of the rupture extent of the Pacific coast of Tohoku Earthquake. ERI meeting of Rapid analysis and prediction of seismic ground motion, http://wwweic.eri.u-tokyo.ac.jp/viewdoc/yure2011/10_yamamoto.pdf (in Japanese). Accessed 7 Feb 2012

Yoshida Y, Ueno H, Muto D, Aoki S (2011) Source process of the 2011 off the Pacific coast of Tohoku Earthquake with the combination of teleseismic and strong motion data. Earth Planets Space 63:565–569

Wald DJ, Worden BC, Quitoriano V, Pankow KL (2006) ShakeMap manual, technical manual, user guide and software guide, http://pubs.usgs.gov/tm/2005/12A01/pdf/508TM12-A1.pdf. Accessed 8 Aug 2012

Wessel P, Smith WHF (1995) New version of the generic mapping tool released. EOS Trans AGU 76:329

Wu YM, Kanamori H (2005) Experiment on an onsite early warning method for the Taiwan early warning systems. Bull Seis Soc Am 95:347–353

Zollo A, Amoroso O, Lancieri M, Wu YM, Kanamori H (2010) A threshold-based earthquake early warning using dense accelerometer networks. Geophys J Int 183:963–974

Chapter 2
Estimation of Fault Rupture Extent Using Near-Source Records for Earthquake Early Warning

M. Yamada

Abstract This chapter presents a methodology to estimate fault rupture extent in real time for the earthquake early warning. This approach identifies the fault rupture geometry by classifying stations into near source and far source. Suppose there is a sufficiently dense seismic network, the distribution of the near-source station can be used for identifying the fault geometry. In this chapter, we improved a discriminant function to classify seismic records into near-source or far-source records proposed in the previous work. We added the earthquake dataset obtained after 2007, and updated the discriminant function. Furthermore, we integrate the information on each station and proposed a methodology to display the fault rupture surface from the distribution of near-source stations. The probability that a station is near-source obtained from this optimal discriminant function shows the extent of the near-source area reasonably well, suggesting that the approach provides a good indicator of near-source and far-source stations for real-time analyses. After applying interpolation, we successfully displayed the fault rupture surface from the distribution of near-source stations.

2.1 Introduction

Earthquake Early Warning provided for public people in Japan by Japan Meteorological Agency (JMA) is one of the most advanced real-time warning systems in the world. The earthquake early warning system, which provides information about strong shaking within seconds of a quake, has been in place since October 2007 and has provided more than 10 warnings of strong earthquakes—by cellular phone, television, radio and local-community speaker system.

On March 11 2011, the earthquake early warning system detected the earthquake off the Pacific coast of Tohoku (hereafter the 2011 Tohoku earthquake), and about

M. Yamada (✉)
Disaster Prevention Research Institute, Kyoto University, Kyoto, Japan
e-mail: masumi@eqh.dpri.kyoto-u.ac.jp

F. Wenzel and J. Zschau (eds.), *Early Warning for Geological Disasters*,
Advanced Technologies in Earth Sciences, DOI: 10.1007/978-3-642-12233-0_2,

8 s after the first P-wave detection at the closest seismic station, issued a warning to the public in the Tohoku region close to the epicenter (Japan 2011). However, the overall performance of the system was not satisfactory, mainly because of the complex character and relatively small amplitude of the beginning of the rupture. The system underestimated ground motion because current JMA system assumes a point source, and does not consider fault finiteness. However, the rupture of the 2011 Tohoku earthquake extended as far as 500 km away, so the large population in the greater Tokyo region, where many areas experienced strong and damaging shaking, received no warning. That said, updates did improve as more information became available (Sagiya et al. 2011).

For the accurate ground motion estimation, it is important to estimate fault rupture extent in real time. Izutani and Hirasawa (2003) presented a method to determine fault parameters of large shallow earthquake from azimuthal dependence of strong motion duration due to directivity. Yamada et al. (2007) proposed a methodology to identify the fault rupture geometry by classifying stations into near source and far source. Recently, the estimation of rupture dimension attracts research attention and several new approaches were proposed (Horiuchi and Horiuchi 2011; Yamada and Heaton 2008; Yamamoto et al. 2008).

In order to estimate the fault rupture extent in real time, we use the same approach with Yamada et al. (2007). Suppose there is a sufficiently dense seismic network, the distribution of the near-source station can be used for identifying the fault geometry. Yamada et al. (2007) proposed a discriminant function to classify seismic records into near-source or far-source records. In this chapter, we added the earthquake dataset obtained after the work of Yamada et al. (2007), and updated the discriminant function. Furthermore, we integrate the information on each station and proposed a methodology to display the fault rupture surface from the distribution of near-source stations.

2.2 Data

We used strong-motion records of seventeen shallow crustal earthquakes with magnitude greater than 6.0 and containing records of near-source stations. The selected earthquakes are shown in Table 2.1. Here, we define a near-source station as a station whose fault distance is less than 10 km. In this chapter, the definition of the fault distance is the shortest distance between the station and the surface projection of the fault rupture surface (Joyner-Boore distance) (Joyner and Boore 1981). 1319 three-component strong-motion data are used for the classification analysis, and 11 % (142 records) are from near-source stations. The source of new records, not included in Yamada et al. (2007), were the K-net, KiK-net, and JMA strong motion network. The classification as near source or far source in the dataset is based on rupture area models used for waveform inversions. Fault models used for classifying stations are also shown in Table 2.1. If the Joyner-Boore distance is less than 10 km, we define the station as a near source. This dataset is used as a training dataset of the classification problem.

Table 2.1 List of the earthquake dataset used for the classification analysis

Earthquake	Year	Date	Mw	NS	FS	Total	ARV	Reference
Imperial Valley	1979	10/15	6.5	14	20	34		Hartzell and Heaton (1983)
Loma Prieta	1989	10/17	6.9	8	38	46		Wald et al. (1991)
Landers	1992	6/28	7.3	1	35	36		Wald and Heaton (1994)
Northridge	1994	1/17	6.6	17	133	150		Wald et al. (1996)
Kobe	1995	1/17	6.9	4	14	18		Wald (1996)
Izmit	1999	8/17	7.6	4	10	14		Sekiguchi and Iwata (2002)
Chi-Chi	1999	9/20	7.6	42	169	211		Ji et al. (2003)
Western Tottori*	2000	10/6	6.7	5	96	101	X	Semmane et al. (2005)
Denali	2002	11/3	7.8	1	3	4		Tsuboi et al. (2003)
Niigataken-Chuetsu	2004	10/23	6.6	13	95	108	X	Honda et al. (2005)
Noto-Hanto*	2007	3/25	6.7	3	46	49	X	Shiba (2008)
Niigataken-Chuetsuoki*	2007	7/16	6.6	7	76	83	X	Aoi et al. (2008)
Wenchuan*	2008	5/12	7.9	6	34	40		Koketsu et al. (2008)
Iwate-Miyagi*	2008	6/14	6.9	6	115	121	X	Suzuki et al. (2010)
Surugawan*	2009	8/11	*6.4	3	121	124	X	Aoi et al. (2010)
Northern Nagano*	2011	3/12	6.3	4	95	99	X	Hata et al. (2012)
Fukushima-Hamadori*	2011	4/11	6.7	4	77	81	X	Somei et al. (2011)
Total				142	1177	1319		

Asterisks after the earthquake name indicate that the data was not used in Yamada et al. (2007) and new in this article. Moment magnitude (Mw) is cited from the Harvard Centroid Moment Tensor solution and USGS for the Surugawan earthquake. The numbers of near-source (NS) and far-source (FS) data for each earthquake are also shown. Availability of site amplification factors is shown in the column of ARV. The fault models in the reference are used as selection criteria to classify near-source and far-source stations

2.2.1 Data Processing

We processed the accelerograms obtained from the seventeen earthquakes according to the following method. A bias is removed from the accelerograms by subtracting the pre-event mean. The peak amplitudes of the horizontal components are calculated by the square root of the sum of squared maxima of north-south and east-west components. The peak amplitude of the up-down component is used directly for the peak vertical component. The following processes are completed for all the data.

- Jerk: The three-component accelerograms are differentiated in the time domain, using a simple finite-difference approximation. The peak value of each component is selected.
- Acceleration: Original accelerograms are used to select the peak value.
- Velocity: The acceleration records are integrated once in the time domain and are high-pass filtered using a fourth-order Butterworth filter with a corner frequency of 0.075 Hz.
- Displacement: The filtered velocity records are integrated once in the time domain and used as a displacement record.

The peak features used for the classification analysis are these four measurements and vertical and horizontal components in each measurement. Several combinations of these eight features are used to find the best performance of the classification.

2.2.2 Data Distribution

We compute the base 10 log of the ground motion amplitudes and find the means and standard deviations for the near-source and far-source records. Figure 2.1 shows the histograms and Gaussian densities given by the sample means and standard deviations of ground motion measures for the near-source and far-source records. The Gaussian densities are good approximations of the histograms of the log of the ground motion data. Figure 2.1 also shows that the distance between means for the near-source and far-source datasets is larger in high-frequency than low-frequency motions. Therefore, we expect that the high-frequency motion is a good measure to classify near-source and far-source records.

High-frequency near-source ground motions have long been researched by engineers and seismologists. High-frequency ground motions depend weakly on magnitude in the near-source (Hanks and Johnson 1976; Hanks and McGuire 1981; Joyner and Boore 1981). This helps to analyze ground motions with a wide range of magnitude. On the other hand, low-frequency motion has a strong correlation with magnitude and its amplitude increases as the magnitude becomes large. High-frequency ground motion decays in amplitude more rapidly with distance than low-frequency motion (Hanks and McGuire 1981). Therefore, high-frequency motion (e.g. acceleration, jerk) has high correlations with the fault distance (Campbell 1981) and is a good proxy to classify near-source and far-source records.

2.2.3 Soil Amplification Factors

In order to consider amplification of the subsurface soil, site amplification factors (ARV) are computed for the strong motion data recorded in Japan. ARV stands for amplitude ratio of PGV at the ground surface relative to engineering bedrock with average S-wave velocity 700 m/s. K-NET and KiK-net provide velocity structures obtained from logging data, so the average S-wave velocity (m/s) from surface to 30 m depth (Vs30) can be computed from the velocity structures. The site amplification factor between surface and engineering bedrock (Vs = 600 m/s) has a following relationship with Vs30 (Midorikawa et al. 1992).

$$\mathrm{ARV} = 10^{(1.83-0.66(\log_{10}(\mathrm{Vs30})))} \tag{2.1}$$

For stations without logging data, ARV is computed by the method proposed by Matsuoka et al. (2005). This approach uses microtopography to estimate ARV.

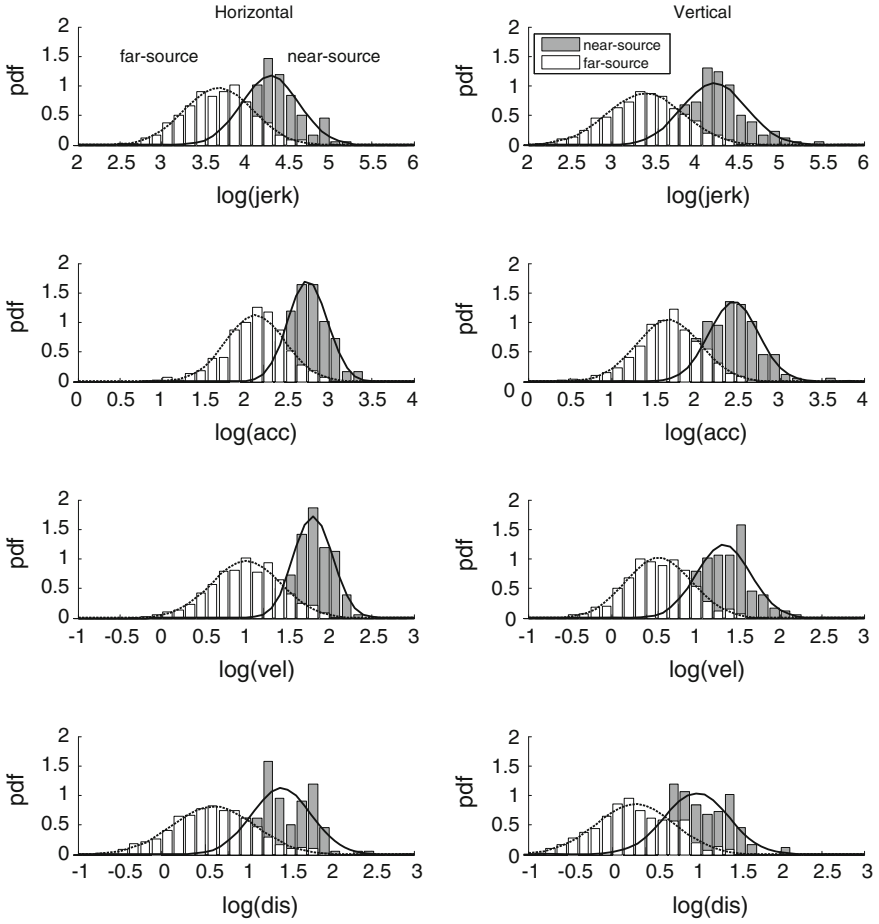

Fig. 2.1 Histograms and Gaussian densities based on the sample means and standard deviations of the log of ground motions for the near-source and far-source records. These are distributions for jerk, acceleration, velocity, and displacement from the *top*

Because the ARV is the amplification from the engineering bedrock to the surface, the velocity records at the engineering bedrock are estimated as ground velocity records divided by ARV. The ARV-corrected velocity records are used in Sect. 2.4.3.

2.3 Method

In order to estimate the fault rupture extent in real time, we use the same approach with Yamada et al. (2007). Suppose there is a sufficiently dense seismic network, the distribution of the near-source station can be used for identifying the fault geometry.

Adding the earthquake dataset obtained after the work of Yamada et al. (2007), we update the discriminant function to classify seismic records into near-source or far-source records. To estimate the fault rupture extent in real time, we take the following three steps:

(1) Prepare a training dataset. Collect strong motion data from earthquake strong motion archives and discover a discriminant function which provides the best performance in terms of near-source/far-source classification.
(2) Allocate new observations when they are obtained to one of the two groups based on the discriminant function.
(3) Integrate this near-source information and display the 2D fault rupture surface by interpolation technique.

We developed a new approach to estimate 2D fault rupture dimension from the discriminant function (see Sect. 2.3.2). We also examined the effect of dataset, discriminant boundary, and the correction of site amplification factor, which are not included in the previous work.

2.3.1 Near-Source and Far-Source Discriminant Function

We assume the discriminant function to classify records into near source and far source is expressed as a linear combination of the log of ground-motion amplitudes:

$$f(X_i|\theta) = c_1 x_{i1} + c_2 x_{i2} + \ldots + c_m x_{im} + d = \sum_{k=1}^{m} c_k x_{ik} + d \qquad (2.2)$$

where x_{ik} is the kth feature parameter of the ground motion at the ith station, m is the number of feature parameters, $X_i = [x_{i1}, x_{i2}, \ldots, x_{im}] = [\log_{10}(\text{component 1}); \log_{10}(\text{component 2}); \ldots; \log_{10}(\text{component } m)]$, $c_1, \ldots, c_m$ is the regression coefficients, d is the decision boundary constant, and $\theta = [c_1, c_2, \ldots, c_m, d]^{\mathrm{T}}$. We may use m components out of the eight ground-motion components. The coefficients $c_1, \ldots, c_m$ and d are determined from the training dataset by Bayesian analysis. This discriminant function is used to allocate new observations to one of the near-source or far-source groups, where $f(X_i|\theta) = 0$ is the boundary between the two groups in the feature parameter space. The station with observation X_i is classified as near source if $f(X_i|\theta)$ is positive. If $f(X_i|\theta)$ is negative, the station is classified as a far-source station.

We define the predictive probability that the ith station is near source by applying the logistic sigmoid function;

$$P(X_i, \theta) = 1/(1 + e^{-f(X_i|\theta)}) \qquad (2.3)$$

As $f(X_i|\theta)$ becomes larger, the station is more likely to be near source, and the probability that the station is near-source becomes closer to one. The predictive probability that the station is far-source is then $1 - P(X_i, \theta)$.

The probability density function (pdf) of parameter θ conditioned on data *Dn* and model class *M* can be expressed using Bayes's theorem (Yamada et al. 2007):

$$P(\theta|D_n, M) \propto 1/(\sqrt{2\pi}\sigma)^{m+1} \exp(-1/(2\sigma^2)\theta^T\theta \times \prod_{i=1}^{n} 1/(1 + e^{-f(X_i|\theta)}) \quad (2.4)$$

where σ is a standard deviation of the prior of each model parameter. Here, we select the prior of each model parameter to be a Gaussian PDF with zero mean and standard deviation $\sigma = 100$. We need to find the optimal parameter θ that maximizes this posterior pdf. Note that the model class *M* defines the combination of ground motion measures. This multidimensional optimization problem is solved by a numerical optimization algorithm provided by Matlab (Yamada et al. 2007).

Yamada et al. (2007) performed Bayesian model class selection and found the best combination of ground motion measures to provide the best performance of classification is the vertical acceleration and horizontal velocity. We performed this analysis with the new dataset, and the same combination was selected. Therefore, we use the following equation as a discriminant function.

$$f(X_i|\theta) = c_1 \log_{10} Za_i + c_2 \log_{10} Hv_i + d \quad (2.5)$$

where Za_i is the vertical acceleration and Hv_i is the horizontal velocity at the station *i*.

2.3.2 Estimating 2D Fault Rupture Dimension

The rupture estimation approach proposed in the previous section depends on the station density, and denser station distribution can provide more accurate estimation. The predictive probability that a station is near-source is assigned to a location of the station, so it would be useful if we can transfer this information at a point to information on the surface. Here, we apply an interpolation and try to obtain the fault rupture surface from probability at each station. The probability *P(Y)* that a site *Y* is near-source is expressed as a sum of weighted probability of station *i*:

$$P(Y) = \sum_{i=1}^{n} [2P(X_i, \theta) - 1]w(R_i), \quad (2.6)$$

where *n* is the number of stations, R_i is Joyner-Boore distance between station *i* and site *Y*, $w(R_i)$ is a weighting as a function of distance and density parameter ρ.

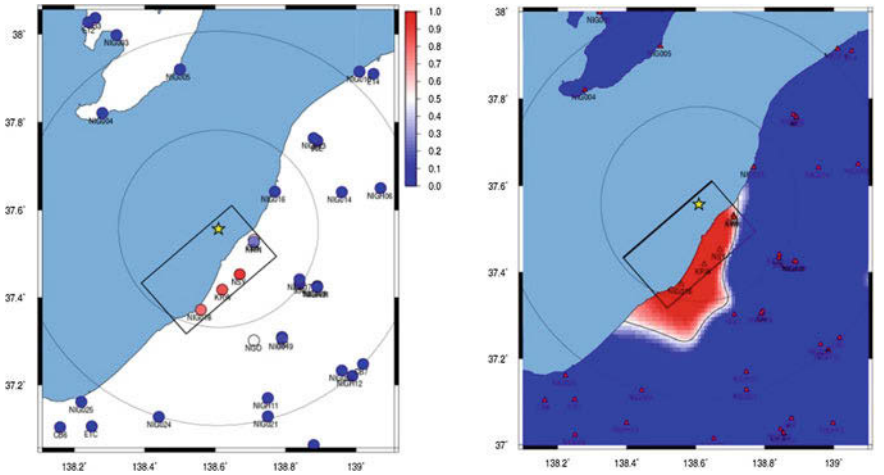

Fig. 2.2 The probability that the station is near source at each station (*left*) and estimated fault rupture surface by interpolation technique (*right*). The *red color* has higher probability that the station is located at near source, and the *blue color* has higher probability that the station is located at far source. The fault projections are shown in the *solid lines*. The *star symbol* denotes the epicenter of the earthquake

$$w(R_i) = \begin{cases} 1 & if \quad R_i < 10[km] \\ 0.5(\cos\ [180(R_i - 10)/(\rho - 10)] + 1) & if \quad 10 \leq R_i < \rho[km] \\ 0 & if \quad R_i \geq \rho[km] \end{cases} \quad (2.7)$$

The density parameter ρ is determined based on the station spacing. The interpolation efficiency can be maximized if you use average station spacing for ρ. If ρ is too large against the station spacing, the probability at a site is affected by a station far away. If ρ is too small, there are many sites who cannot obtain the probability since all $w(R_i)$ becomes zero. As for Japanese seismic network, the average station spacing is about 20 km, so $\rho = 20$ is used as a proper density parameter. We assumed the location of an epicenter is given and used the epicenter as a single 'near-source' station with probability $P(X_i, \theta) = 1$. The performance is shown in Fig. 2.2.

The rupture surface can be approximately estimated even the station density is not dense enough by applying this interpolation technique. For example, the station spacing of 2008 Wenchuan earthquake is about 50 km. However, the fault rupture extends as far as a couple of hundred km, the rupture dimension can be estimated by setting $\rho = 50$. Ideally, the station spacing for accurate fault rupture estimation is 10–20 km.

2.4 Results

We obtained a discriminant function classifying near-source and far-source stations that maximizes the posterior pdf. We used two different dataset: All dataset (Japanese + outside of Japan) and Japanese dataset. We also examined the effect of fault distance considering dip angle in the Sect. 2.4.2, and effect of site amplification factor (ARV) in the Sect. 2.4.3.

2.4.1 Classification Function with All Datasets

Table 2.2 shows the optimal parameters for the classification function obtained from Yamada et al. (2007) and all dataset in this chapter. Evidence is an index to select the optimal model class if the same dataset was used (Yamada et al. 2007). Note that the evidence is log-scaled, and the larger value of the evidence indicates a better fit to the dataset. The evidence of the previous work shows the smaller value, but we cannot compare the evidence of the different datasets. The ratios of the parameters are very similar, meaning both discriminate functions provide very similar result to classify near-source and far-source stations. The optimal discriminant function with all dataset is expressed as:

$$f(X_i|\theta) = 4.40 \log_{10} Za_i + 5.17 \log_{10} Hv_i - 19.12. \tag{2.8}$$

where Za_i is the vertical acceleration and Hv_i is the horizontal velocity at the station i.

The classification performance of the discriminant function obtained from all dataset is shown in Fig. 2.3 and confusion matrix is shown in Table 2.3. Circle symbols show the near-source records and cross symbols show the far-source records. Suppose the 50 % of the probability is a boundary of near source and far source, black symbols are correctly classified, and red symbols are incorrectly classified. This figure shows most of the misclassified records are located at the boundary of the near source and far source (about 10 km of the fault). We found that the near-source data with very low probability of near-source were located at the edge of the fault, which indicates that the fault models used here are those from the source inversion and not necessarily the best indicator of near-source and far-source stations.

Table 2.2 The optimal parameters for the discriminant functions based on the all dataset in this chapter and dataset of Yamada et al. (2007)

	c_1	c_2	d	Evidence
Yamada et al. (2007)	6.05	7.89	−27.09	−96
All dataset in this chapter	4.40	5.17	−19.12	−179

The values for the evidence of each model class are log-scaled

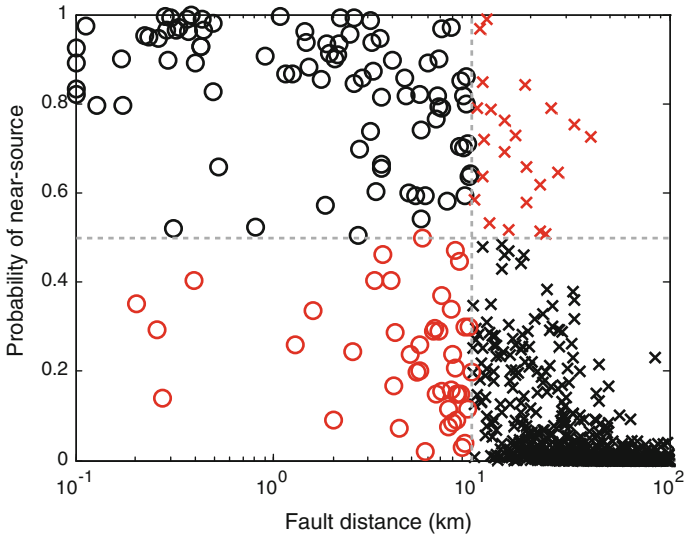

Fig. 2.3 The classification performance of the discriminant function from all dataset in this chapter. *Circle symbols* show the near-source records and *cross symbols* show the far-source records. Suppose the 50 % of the probability is a boundary of near source and far source, *black symbols* are correctly classified, and *red symbols* are incorrectly classified

We performed the leave-one-out cross validation to check the robustness of the discriminant function. The idea of this method is to predict the probability of a station from the discriminant function constructed from the dataset from which that station is excluded. This process is repeated for all 1319 data, and the accuracy of prediction is computed. The percentage of misclassified data is only 5 % (68/1319). Therefore, we conclude that the discriminant function is stable enough for a new dataset which is not included in the training dataset (Figs. 2.4 and 2.5).

2.4.2 Effect of Dip Angle of the Fault

As a boundary of near-source and far-source, we use the Joyner-Boore distance. In this section, we consider dip angle of the fault and use shortest distance between a station and the fault rupture surface (i.e. fault distance). We compared the classification performance with the boundary of 10 km of these distance definitions. Table 2.4

Table 2.3 Confusion matrix for near-source versus far-source classification by the discriminant function from all dataset in this chapter

Dataset	NS	FS
Classified as NS	88 (66 %)	23 (2 %)
Classified as FS	45 (34 %)	1163 (98 %)

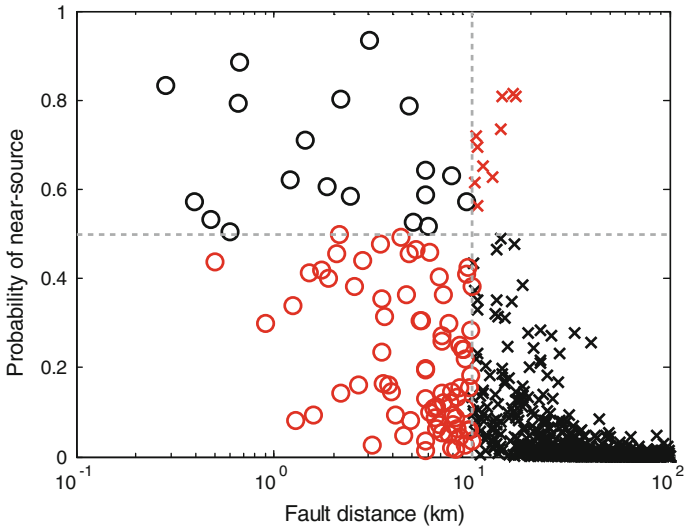

Fig. 2.4 The classification performance of the discriminant function from all dataset with rupture distance. *Circle symbols* show the near-source records and *cross symbols* show the far-source records. Suppose the 50 % of the probability is a boundary of near source and far source, *black symbols* are correctly classified, and *red symbols* are incorrectly classified

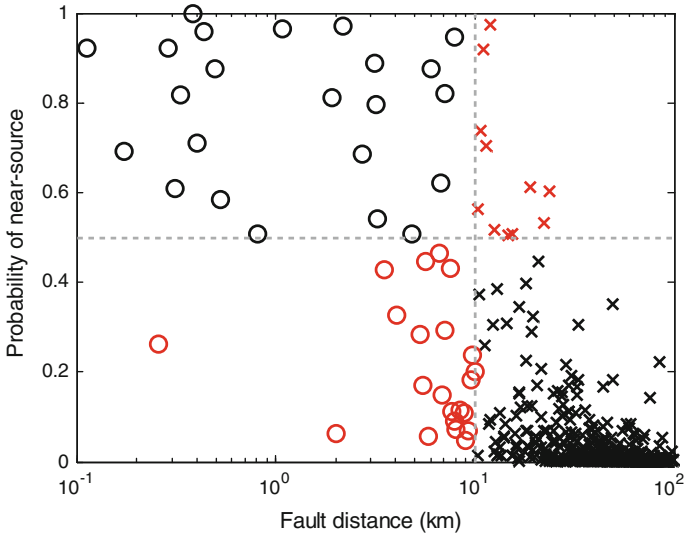

Fig. 2.5 The classification performance of the discriminant function from Japanese dataset with ARV correction. *Circle symbols* show the near-source records and *cross symbols* show the far-source records. Suppose the 50 % of the probability is a boundary of near source and far source, *black symbols* are correctly classified, and *red symbols* are incorrectly classified

Table 2.4 The optimal parameters for the discriminant functions based on the all dataset with Joyner-Boore distance and rupture distance as a boundary of near source and far source

	c_1	c_2	d	Evidence
Joyner-Boore distance	4.40	5.17	−19.12	−179
Rupture distance	2.18	4.61	−13.89	−196

The values for the evidence of each model class are log-scaled

shows the optimal parameters for the discriminant function and evidence of each model. The model with Joyner-Boore distance is better than the model with rupture distance. This implies that the amplitudes of ground motion have better correlation with Joyner-Boore distance. Although Joyner-Boore distance and rupture distance are exactly the same for the strike-slip fault mechanism, the Joyner-Boore distance is shorter than rupture distance for the thrust fault event. If the station is located on the hanging-wall, the amplitude tends to be large. In such a case, Joyner-Boore distance is a constant but rupture distance becomes longer depending on the dip angle. Therefore, to classify near-source and far-source records, Joyner-Boore distance shows the better classification performance and that means it is difficult to estimate the dip angle of the fault from this approach.

The evidence of the ARV corrected discriminant function is slightly smaller than the discriminant function with no ARV correction. However, the ARV corrected discriminant function can provide smaller variance on the probability if two stations are close each other. Therefore, if the ARV at a site is available, it is better to use Eq. 2.9.

2.4.3 Effect of Soil Amplification

Ground motions are amplified by the subsurface soil, so the amplitude depends on the subsurface soil structure. Especially velocity records are strongly affected by the site amplification factor (ARV) between surface and engineering bedrock (Midorikawa et al. 1992). We used Japanese dataset whose ARV at the station is available and compared the results of corrected velocity records by ARV with the results of uncorrected velocity records. Although acceleration records are also affected by the subsurface soil structure, the amplification characteristics are more complicated and difficult to evaluate (Si and Midorikawa 2000). Therefore, we consider only the effect of ARV on velocity records (Tables 2.5, 2.6 and 2.7).

The optimal discriminant function with ARV correction is:

$$f(X_i|\theta) = 4.35 \log_{10} Za_i + 2.82 \log_{10}(Hv_i/ARV_i) - 14.89. \qquad (2.9)$$

where ARV_i is site amplification factor at the station i.

Table 2.5 Confusion matrix for near-source versus far-source classification by the discriminant function from all dataset with rupture distance

Dataset	NS	FS
Classified as NS	19 (19 %)	10 (1 %)
Classified as FS	79 (81 %)	1211 (99 %)

Table 2.6 The optimal parameters for the discriminant functions based on the Japanese dataset with and without ARV correction

	c_1	c_2	d	Evidence
No ARV	3.98	3.47	−15.50	−89
ARV corrected	4.35	2.82	−14.89	−93

The values for the evidence of each model class are log-scaled

Table 2.7 Confusion matrix for near-source versus far-source classification by the discriminant function from Japanese dataset with ARV correction

Dataset	NS	FS
Classified as NS	23 (51 %)	22 (2 %)
Classified as FS	11 (49 %)	710 (98 %)

2.4.4 Estimated Rupture Dimension

We apply the optimal discriminant function (in Eq. 2.9) to all the stations in the Japanese dataset and estimated the fault rupture extent by applying the interpolation. Figure 2.6 shows the results of estimation. The regions with a high probability of being in the near-source are consistent with the area within 10 km from fault geometry in the most cases. As mentioned before, the fault models that are used here are those from the source inversion, and they are not necessarily the best indicator of near-source and far-source stations.

This approach also works for dataset whose ARV is not available. We apply the optimal discriminant function (in Eq. 2.9) to dataset whose site condition is unknown, and estimated the fault rupture extent by applying the smoothing filter. Figure 2.7 shows the results of estimation. If the number of near-source station is too small against the size of earthquake, the result is very poor. The 1992 Landers, 1999 Izmit, and 2002 Denali earthquakes show poor estimation of the fault rupture extent. However, the number of near-source station is greater than five, the estimated near-source region is in general consistent with the fault rupture surface. 1999 Chi-Chi and 2008 Wenchuan earthquakes have larger magnitude than Japanese earthquakes shown in Fig. 2.6, but the results shows reasonably good performance to estimate fault rupture dimension.

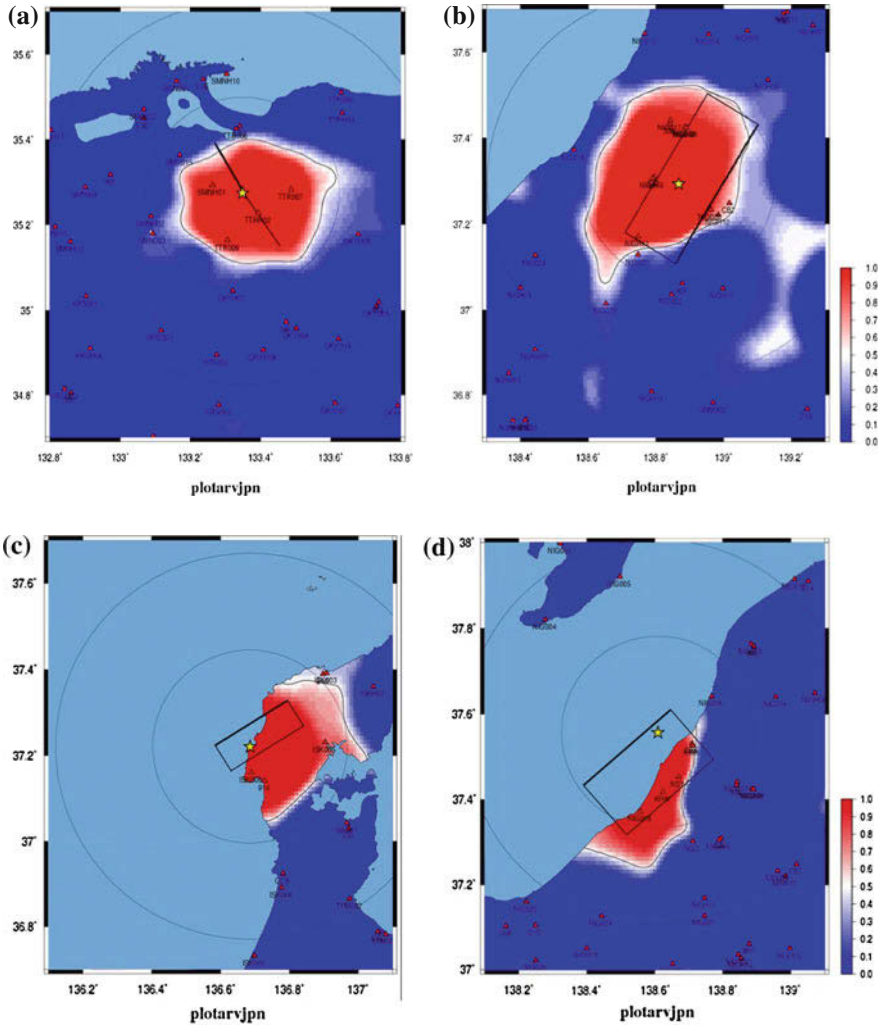

Fig. 2.6 Estimated fault rupture surface for Japanese earthquakes. The *red color* has higher probability that the region is located at near source, and the *blue color* has higher probability that the region is located at far source. The symbols for the fault and epicenter are the same as in Fig. 2.2. **a** 2000 Western Tottori **b** 2004 Niigataken-Chuetsu **c** 2007 Noto-Hanto **d** 2007 Niigataken-Chuetsuoki **e** 2008 Iwate-Miyagi **f** 2009 Surugawan **g** 2011 Northern Nagano **h** 2011 Fukushima-Hamadori

2.5 Conclusion

In this chapter, extending the concept of Yamada et al., we proposed a new discriminant function to classify seismic records into near-source or far-source records. Furthermore, we integrate the information on each station and proposed a methodol-

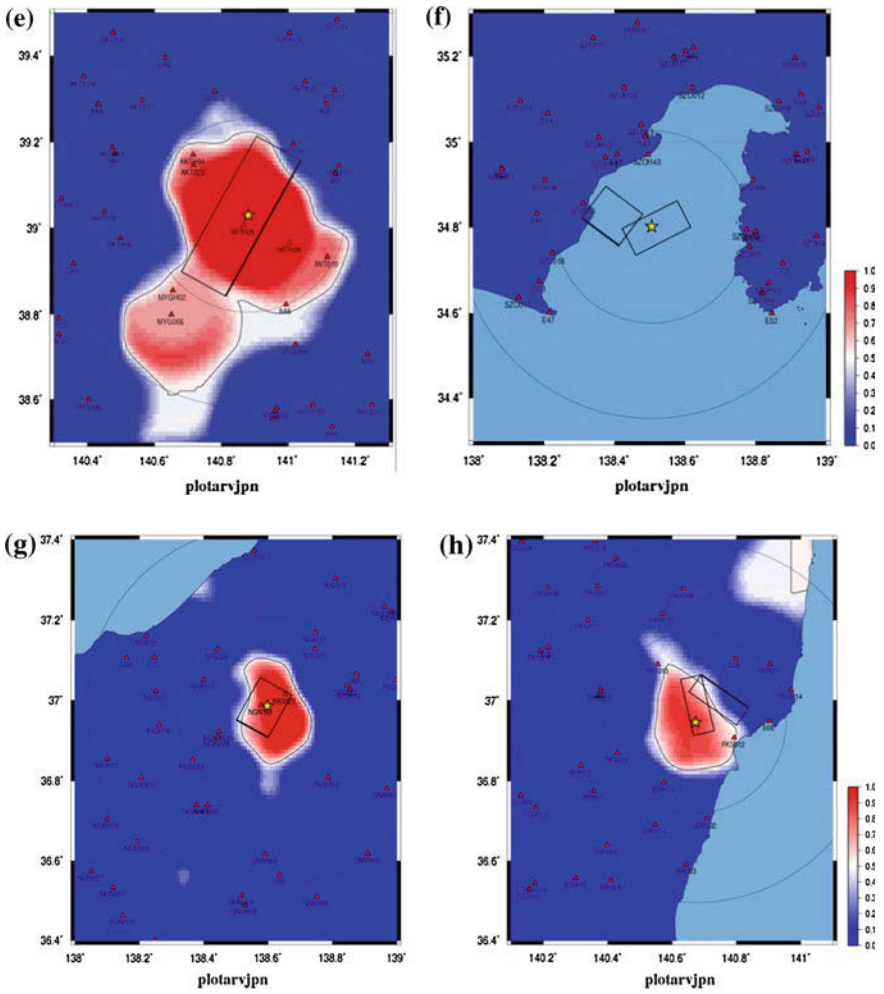

Fig. 2.6 Continued

ogy to display the fault rupture surface from the distribution of near-source stations. We constructed a new dataset of the latest large earthquakes and analyzed them to find a linear function that best discriminates near-source and far-source records. The best discriminant function is:

$$
\begin{aligned}
f(X_i|\theta) &= 4.30\log_{10} Za_i + 5.09\log_{10} Hv_i - 18.77, && \text{if ARV is unknown} \\
f(X_i|\theta) &= 4.26\log_{10} Za_i + 2.63\log_{10}(Hv_i/ARV_i) - 14.50, && \text{if ARV is available} \\
P(X_i,\theta) &= 1/(1+e^{-f(X_i|\theta)}) &&
\end{aligned}
\tag{2.10}
$$

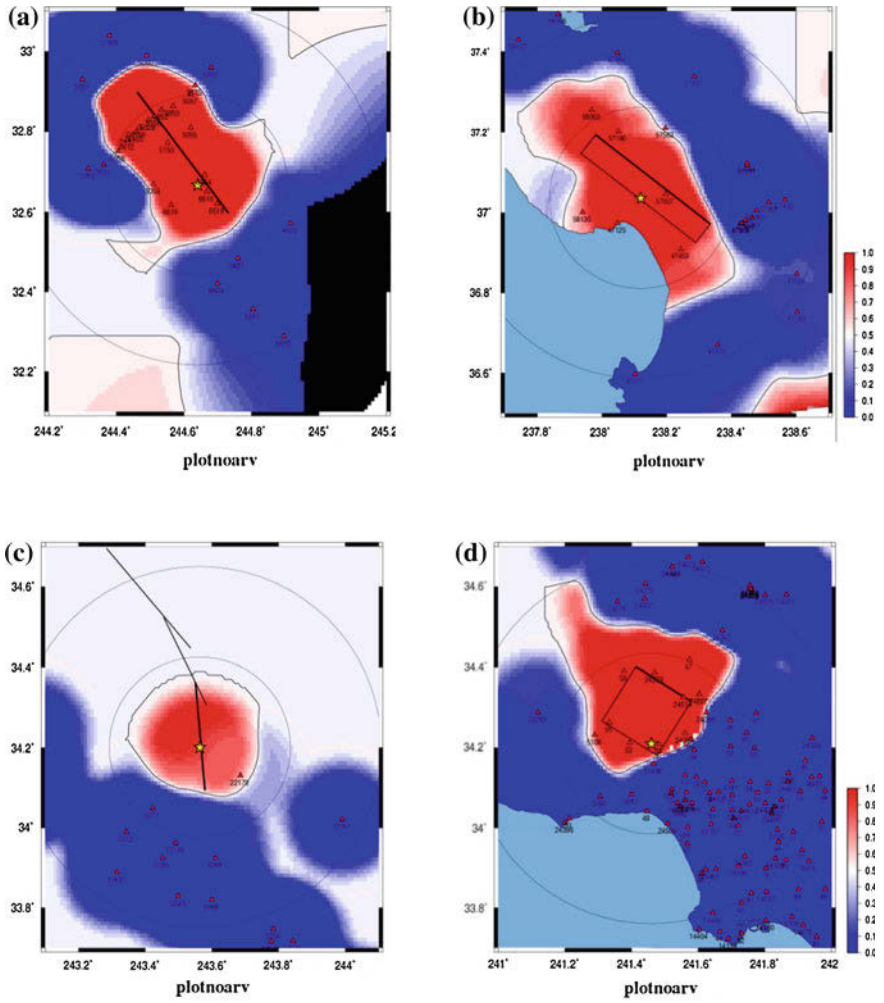

Fig. 2.7 Estimated fault rupture surface for earthquakes whose site condition is unknown. The *red color* has higher probability that the region is located at near source, and the *blue color* has higher probability that the region is located at far source. The symbols for the fault and epicenter are the same as in Fig. 2.2. **a** 1979 Imperial Valley **b** 1989 Landers **c** 1992 Landers **d** 1994 Northridge **e** 1995 Kobe **f** 1999 Izmit **g** 2002 Denali **h** 1999 Chi-Chi **i** 2008 Wenchuan

where Za_i and Hv_i denote the peak values of the vertical acceleration and horizontal velocity, respectively, and $P(X_i, \theta)$ is the probability that a station is near-source. This function indicates that the amplitude of high-frequency components is effective in classifying near-source and far-source stations.

The probability that a station is near-source obtained from this optimal discriminant function for all the earthquakes shows the extent of the near-source area quite

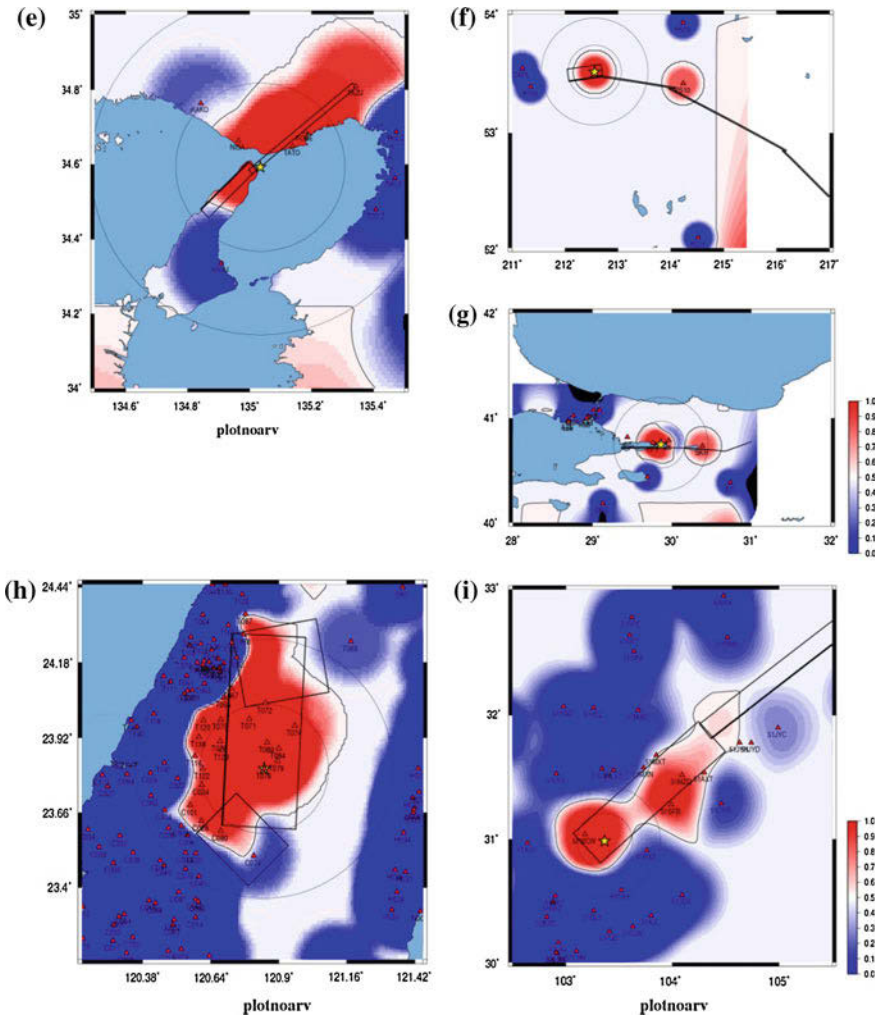

Fig. 2.7 continued

well, suggesting that the approach provides a good indicator of near-source and far-source stations for real-time analyses. After applying interpolation, we successfully displayed the fault rupture surface from the distribution of near-source stations. The regions with a high probability of being in the near-source are consistent with the area within 10 km from fault geometry in the most cases. Note that this function is constructed by the training dataset with magnitude greater than 6.2, so it only works for large earthquakes.

Acknowledgments The authors acknowledge the National Research Institute for Earth Science and Disaster Prevention (NIED) and Japan Meteorological Agency (JMA) for the use of the seismic data. Some of the figures are generated by Generic Mapping Tools (Wessel and Smith 1991).

References

Aoi S, Enescu B, Suzuki W, Asano Y, Obara K, Kunugi T, Shiomi K (2010) Stress transfer in the Tokai subduction zone from the 2009 Suruga Bay earthquake in Japan. Nat Geosci 3(7):496–500

Aoi S, Sekiguchi H, Morikawa N, Kunugi T (2008) Source process of the 2007 Niigata-ken Chuetsu-oki earthquake derived from near-fault strong motion data. Earth Planets and Space (EPS) 60(11):1131

Campbell KW (1981) Near-source attenuation of peak horizontal acceleration. Bull Seismol Soc Am 71(6):2039–2070

Hanks TC, Johnson DA (1976) Geophysical assessment of peak accelerations. Bull Seismol Soc Am 66(3):959–968

Hanks TC, McGuire RK (1981) The character of high-frequency strong ground motion. Bull Seismol Soc Am 71(6):2071–2095

Hartzell SH, Heaton TH (1983) Inversion of strong ground motion and teleseismic waveform data for the fault rupture history of the 1979 Imperial Valley, California, earthquake. Bull Seismol Soc Am 73(6A):1553–1583

Hata Y, Murata A, Nozu A, Miyajima M (2012) Ground motion evaluation at Yokokura village for the 2011 Nagano—Niigata border earthquake based on the site effects substitution method. J Jpn Assoc Earthq Eng

Honda R, Aoi S, Morikawa N, Sekiguchi H, Kunugi T, Fujiwara H (2005) Ground motion and rupture process of the 2004 Mid Niigata prefecture earthquake obtained from strong motion data of K-NET and KiK-net. Earth Planets and Space 57(6):527–532

Horiuchi S, Horiuchi Y (2011) Real-time location of fault area distribution for the Tsunami warning and shaking intensity estimation of a massive scale earthquake. Seismological Society of Japan, Shizuoka

Izutani Y, Hirasawa T (1987) Use of strong motion duration for rapid evaluation of fault parameters. J Phys Earth 35(2):171–190

JapanMeteorologicalAgency Earthquake early warning for the 2011 off the Pacific coast of Tohoku Earthquake (2011) [cited 2012 June 27]. http://www.seisvol.kishou.go.jp/eq/EEW/kaisetsu/joho/20110311144640/content/contentout.html

Ji C, Helmberger DV, Wald DJ, Ma KF (2003) Slip history and dynamic implications of the 1999 Chi-Chi, Taiwan, earthquake. J Geophys Res 108(B9):2412

Joyner WB, Boore DM (1981) Peak horizontal acceleration and velocity from strong-motion records including records from the 1979 Imperial Valley, California, earthquake. Bull Seismol Soc Am 71(6):2011–2038

Koketsu K, Yokota Y, Ghasemi H, Hikima K, Miyake H, Wang Z (2008) Source process and ground motions of the 2008 Wenchuan Earthquake, China, grant-in-aid for special purposes of 2008, MEXT, No. 20900002

Matsuoka M, Wakamatsu K, Fujimoto K, Midorikawa S (2005) Nationwide site amplification zoning using GIS-based Japan engineering geomorphologic classification map. In: 9th International conference on structural safety and reliability, Rome

Midorikawa S, Matsuoka M, Sakugawa K (1992) Evaluation of site effects on peak ground acceleration and velocity observed during the 1987 Chiba-ken-toho-oki earthquake. J Struct Constr Eng, AIJ 442:71–78

Sagiya T, Kanamori H, Yagi Y, Yamada Y, Mori J (2011) Rebuilding seismology. Nature 473:146–148

Sekiguchi H, Iwata T (2002) Rupture process of the 1999 Kocaeli, Turkey, earthquake estimated from strong-motion waveforms. Bull Seismol Soc Am 92(1):300–311

Semmane F, Cotton F, Campillo M (2005) The 2000 Tottori earthquake: a shallow earthquake with no surface rupture and slip properties controlled by depth. J Geophys Res 110(B3):B03306

Shiba Y (2008) Rupture process during the 2007 Noto Hanto earthquake (MJMA 6.9) and strong-motion simulation in the source region. Earth Planets and Space (EPS), 60(10):1023–1028

Si H, Midorikawa S(2000) New attenuation relations for peak ground acceleration and velocity considering effects of fault type and site condition. In: 12th World conference on earthquake engineering

Somei K, Miyakoshi K, Irikura K (2011) Estimation of source model and strong motion simulation for the 2011 East Fukushima prefecture earthquake using the empirical Green's function method. Seismological Society of Japan, Shizuoka

Suzuki W, Aoi S, Sekiguchi H (2010) Rupture process of the 2008 Iwate-Miyagi Nairiku, Japan, earthquake derived from near-source strong-motion records. Bull Seismol Soc Am 100(1):256–266

Tsuboi S, Komatitsch D, Ji C, Tromp J (2003) Broadband modeling of the 2002 Denali fault earthquake on the earth simulator. Phys Earth Planet Inter 139(3–4):305–313

Wald DJ (1996) Slip history of the 1995 Kobe, Japan, earthquake determined from strong motion, teleseismic, and geodetic data. J Phys Earth 44(5):489–504

Wald DJ, Heaton TH (1994) Spatial and temporal distribution of slip for the 1992 Landers, California, earthquake. Bull Seismol Soc Am 84(3):668–691

Wald DJ, Heaton TH, Hudnut KW (1996) The slip history of the 1994 Northridge, California, earthquake determined from strong-motion, teleseismic, GPS, and leveling data. Bull Seismol Soc Am 86(1B):S49–S70

Wald DJ, Helmberger DV, Heaton TH (1991) Rupture model of the 1989 Loma Prieta earthquake from the inversion of strong-motion and broadband teleseismic data. Bull Seismol Soc Am 81(5):1540–1572

Wessel P, Smith WHF (1991) Free software helps map and display data. EOS 72(441):445–446

Yamada M, Heaton TH (2008) Real-time estimation of fault rupture extent using envelopes of acceleration. Bull Seismol Soc Am 98(2):607–619

Yamada M, Heaton TH, Beck J (2007) Real-time estimation of fault rupture extent using near-source versus far-source classification. Bull Seismol Soc Am 97(6):1890–1910

Yamamoto S, Horiuchi S, Nakamura H, Wu C, Irikura K, Fukushima Y (2008) Seismic intensity estimation taking into account fault finiteness for earthquake early warning. In: Japan Geoscience Union meeting, Chiba

Chapter 3
CISN ShakeAlert: An Earthquake Early Warning Demonstration System for California

M. Böse, R. Allen, H. Brown, G. Gua, M. Fischer, E. Hauksson, T. Heaten, M. Hellweg, M. Liukis, D. Neuhauser, P. Maechling, K. Solanki*, M. Vinci*, I. Henson*, O. Khainovski*, S. Kuyuk*, M. Carpio*, M.-A. Meier* and T. Jordan*

Abstract To demonstrate the feasibility of earthquake early warning (EEW) in California, we have developed and implemented the CISN ShakeAlert demonstration system. A Decision Module combines estimates and uncertainties determined by three algorithms implemented in parallel, $\tau_c - P_d$ Onsite, Virtual Seismologist, and ElarmS, to calculate and report at a given time the most probable earthquake magnitude and location, as well as the likelihood of correct alarm. A User Display receives the alert messages in real-time, calculates the expected local shaking intensity, and displays the information on a map. Currently, CISN ShakeAlert is being tested by ~70 individuals and test users from industries and emergency response organizations in California. During the next 3 years we plan to expand this demonstration warning system to the entire US West Coast.

3.1 Introduction

Scientists and engineers at the California Institute of Technology (Caltech), UC Berkeley, the Swiss Federal Institute of Technology (ETH), and the University of Southern California (USC) started in 2007 to develop and implement an earthquake

*CISN EEW Group.

M. Böse (✉) · E. Hauksson · T. Heaton · K. Solanki · M. Vinci
California Institute of Technology (Caltech), Pasadena, USA
e-mail: mboese@caltech.edu

R. Allen · H. Brown · M. Hellweg · D. Neuhauser · I. Henson · O. Khainovski · S. Kuyuk
UC Berkeley (UCB), Berkeley, USA

G. Cua · M. Fischer · M. Carpio · M.-A. Meier
Swiss Federal Institute of Technology (ETH), Zurich, Switzerland

M. Liukis · P. Maechling · T. Jordan
University of Southern California (USC), Los Angeles, USA

F. Wenzel and J. Zschau (eds.), *Early Warning for Geological Disasters*,
Advanced Technologies in Earth Sciences, DOI: 10.1007/978-3-642-12233-0_3,

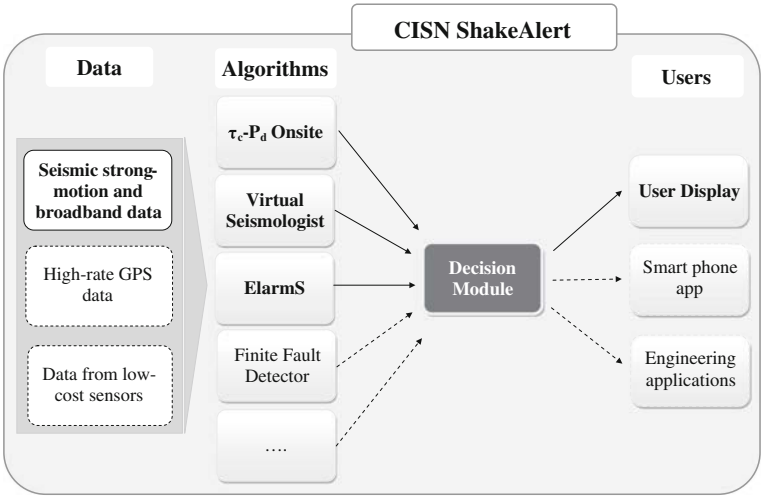

Fig. 3.1 The current CISN ShakeAlert system receives real-time estimates of earthquake source and ground-motion parameters determined by three algorithms, $\tau_c - P_d$ Onsite, Virtual Seismologist, and ElarmS, that run in parallel in California. The Decision Module combines these estimates and provides a unified 'ShakeAlert' view of the earthquake in progress. The ShakeAlert information includes rapid estimates of magnitudes, locations, expected seismic intensities, and probabilities of correct alarm (called 'likelihood' parameter). A User Display that runs on a user's computer receives and displays the alert messages in real-time. Dashed lines show components under development, including, for instance, the usage of high-rate GPS-data and a finite fault detector for the rapid detection of large earthquakes

early warning (EEW) demonstration system for California, called CISN ShakeAlert. The project is funded by the US Geological Survey (USGS), as well as participating partners. The USGS has the formal responsibility of issuing earthquake alerts in California. ShakeAlert makes use of the existing infrastructure of the California Integrated Seismic Network (CISN), including real-time waveform data streams from ~380 broadband and strong-motion stations throughout California.

The USGS/ANSS/ARRA program provided Government Furnished Equipment and funding to upgrade the CISN during the past 2 years. ARRA funds were used to upgrade around 210 CISN stations with faster Q330 s dataloggers, upgrade telemetry hubs, and build a state-of-the-art microwave telemetry backbone (Romanowicz et al. 2011; Thomas et al. 2011). These improvements have reduced data latencies in the CISN data acquisition systems. Waveform data thus arrive within seconds at the three processing facilities at Caltech/USGS Pasadena, UC Berkeley, and USGS Menlo Park, providing the basis for EEW in California.

CISN ShakeAlert is a distributed system, which enables the independent development of individual system components (Fig. 3.1). An associator, called Decision Module, combines the outputs from three EEW algorithms implemented in parallel, $\tau_c - P_d$ Onsite (Böse et al. 2009a, b; Kanamori 2005; Wu et al. 2007), Virtual Seismologist (Cua et al. 2009; Cua and Heaton 2007), and ElarmS (Allen 2007; Allen

et al. 2009; Allen and Kanamori 2003). Each algorithm is capable of detecting and characterizing earthquakes within seconds from event initiation. The Decision Module uses estimates of source parameters and uncertainties determined by the three algorithms to calculate, update, and report the most probable solutions at a given time. The earthquake alert information includes rapid estimates of magnitudes, locations, expected seismic intensities, and probabilities of correct alarm (called 'likelihood' parameter). A User Display that runs on a user's computer receives and displays the alert messages in real-time (Fig. 3.1).

3.2 Early Warning Algorithms

The following subsections give a brief description of the three EEW algorithms used in CISN ShakeAlert.

3.2.1 $\tau_c - P_d$ Onsite Algorithm

The $\tau_c - P_d$ Onsite algorithm belongs to the group of single-sensor approaches to EEW (Kanamori 2005). In principle, this type of warning approach can be quicker at detecting and processing of earthquakes, but is expected to be less reliable compared to regional warning algorithms that are based on observations at multiple seismic sensors.

The $\tau_c - P_d$ Onsite algorithm—developed by Kanamori (2005) as an extension of earlier methods proposed by Nakamura (1988) and Allen and Kanamori (2003)—uses the period τ_c and amplitude P_d of initial shaking to estimate the size and forthcoming shaking in an earthquake. The period parameter τ_c is defined as $\tau_c = 2\pi/\sqrt{r}$, with

$$r = \left[\int_0^{\tau_o} \dot{u}^2(t)dt\right] / \left[\int_0^{\tau_o} u^2(t)dt\right], \tag{3.1}$$

where u(t) and $\dot{u}(t)$ are the ground-motion displacement and velocity time series, and τ_0 is the duration of the time window used. Usually, τ_0 is set to 3.0 [s]. Wu et al. (2007) systematically studied the archived records from earthquakes in southern California to determine a $\log_{10}(\tau_c)$-Mw scaling relationship for EEW. The second parameter, P_d, which is the maximum amplitude of the high-pass filtered (>0.075 Hz) vertical displacement during the initial 3.0 [s] of the P wave, is used to estimate the peak ground velocity (PGV) at the recording site (Wu et al. 2007).

Our real-time tests of the $\tau_c - P_d$ Onsite algorithm in California over the past 5 years (Böse et al. 2009b) have shown that some modifications are necessary to decrease the number of false triggers and thus to increase the robustness of the algorithm. In particular in real-time mode during small to moderate-sized earthquakes there may be too many false alarms, as well as too much scatter in the source parameter

estimates. The main modifications, which we have implemented, are the $\tau_c - P_d$ Trigger—Criterion (Böse et al. 2009a) and the Two-Station-Method.

The $\tau_c - P_d$ Trigger—Criterion is based on τ_c-dependent and implicit magnitude-dependent P_d thresholds. For a local earthquake with period τ_c and rupture-to-site distance r, $r_{min} \leq r \leq r_{max}$, we expect $P_{d,min} \leq P_d \leq P_{d,max}$. Böse et al. (2009a) determined displacement amplitudes $P_{d,min}$ and $P_{d,max}$ from empirical attenuation relations for earthquakes in southern California with $r_{min} = 1\,km$ to $r_{max} = 100\,km$. The application of the $\tau_c - P_d$ Trigger—Criterion removed 97 % of previous false triggers throughout California and led to a significant reduction of the scatter in magnitude estimates for small earthquakes (Böse et al. 2009a).

The second modification that we have implemented is the Two-Station-Method. A 'trigger' at a station, i.e. τ_c and P_d values that have passed the $\tau_c - P_d$ Trigger-Criterion, needs to be confirmed by one or more 'picks' of the seismic P-wave at neighbored stations, before being reported to the ShakeAlert system. Whenever one or more close-by stations detect the P-wave within a certain time window, the trigger is confirmed and reported. The earthquake location is updated, assuming that the epicenter is in between the two stations taking into account travel time differences.

If two or more reports are associated with each other, i.e. are expected to refer to the same earthquake, we start calculating and reporting the median values of the magnitude. On-line and off-lines tests with waveform data from California, Taiwan and Japan, have shown, that the magnitude errors are normally distributed with $\sigma_{M,\,single} \approx 0.55$, if estimated at single stations. As can be shown from Monte Carlo simulations, the errors should decrease with $\sigma_{M,\,multiple} = (\text{number of stations})^{-0.4}$, if magnitudes are estimated from median values from multiple stations. However, the errors observed for earthquakes in California are larger than these estimates suggest. A possible explanation is that the uncertainties at different stations (for the same event) are correlated with each other. Thus we need to consider inter- and intra-event errors caused by the variability from earthquake to earthquake (e.g. caused by different stress drops) and the variability from station to station (during the same event). In a preliminary error analysis, we find $\sigma_{M,\,inter} = 0.55$ and $\sigma_{M,\,intra} = 0.37$ (Barba et al. 2010), and obtain

$$\sigma_{M,\,multiple}(\sigma_{M,\,inter},\ \sigma_{M,\,intra}) \approx 0.4 + 0.3\,\exp(-\text{number of stations}/3.6). \quad (3.2)$$

The uncertainties in epicenter location for earthquakes within CISN are 0.14° (≈15 km), and for PGV $\sigma\sigma_{log(PGV),\,single} = 0.326$ (Wu et al. 2007). For the current telemetry and processing delays in the CISN first reports from $\tau_c - P_d$ Onsite usually become available 5 s after event origin or later, depending on the distance between the earthquake and the reporting station, as well as station equipment.

To quantify the probability of correct alert, we calculate a preliminary likelihood parameter, which depends on the number of reporting stations and the time in between these reports. If the number of reporting stations does not increase with time as expected for a moderate or large earthquake, a 'Cancel' message is sent to

the CISN ShakeAlert Decision Module and User Display for event deletion and user notification.

We are also developing new algorithms for more rapid and more robust onsite warning, such as PreSEIS Onsite, which is based on Artificial Neural Networks (Böse et al. 2012a). PreSEIS Onsite uses the acceleration, velocity and displacement waveforms from a single three-component broadband or strong-motion sensor to perform real-time earthquake/noise discrimination and near/far source classification. When a local earthquake is detected, the algorithm estimates the moment magnitude, epicentral distance Δ, and peak ground velocity (PGV) at the site of observation. Our training and test datasets consist of 2,431 records of 161 crustal earthquakes in California, Japan and Taiwan with $3.1 \leq M \leq 7.6$ at $\Delta \leq 115$ km. First estimates become available at 0.25 s after the P-pick and are regularly updated with progressing time. We find that the prediction errors of this new approach are around 60 % smaller compared to the $\tau_c - P_d$ Onsite algorithm (Böse et al. 2012a).

3.2.2 Virtual Seismologist Algorithm

The Virtual Seismologist (VS) method is a Bayesian approach to earthquake early warning (EEW) that estimates earthquake magnitude, location, and the distribution of peak ground motion using observed ground motion amplitudes, predefined prior information, and envelope attenuation relationships (Cua 2005; Cua et al. 2009; Cua and Heaton 2007). The application of Bayes' theorem in EEW (Cua 2005) states that the most probable source estimate at any given time is a combination of contributions from prior information (possibilities include network topology or station health status, regional hazard maps, earthquake forecasts, the Gutenberg-Richter magnitude-frequency relationship) and constraints from the available ground motion observations. VS is envisioned as an intelligent, automated system capable of mimicking how human seismologists can make quick, relatively accurate, "back-of-the-envelope" interpretations of real-time (and at times, incomplete) earthquake information, using a mix of experience and available data.

The formulation of the VS Bayesian methodology, the development of the underlying relationships describing the dependence of various channels of ground motion envelopes on magnitude and distance, and how these pieces come together for early warning estimation, was the result of the work of Cua and Heaton (2007) at Caltech. Implementation of the VS algorithm into real-time codes is an on-going effort of the Swiss Seismological Service at ETH Zürich, with support from ETH, the US Geological Survey, and from European projects SAFER (Seismic Early Warning for Europe), NERA (Network of European Research Infrastructures for Earthquake Risk Assessment and Mitigation), and REAKT (Strategies and Tools for Real-Time Earthquake Risk Reduction). Since the contribution of prior information can be considered relatively static over the timescale of a given earthquake rupture, VS implementation efforts have thus far focused on real-time processing of incoming waveform data. The VS code implementation currently running in real-time

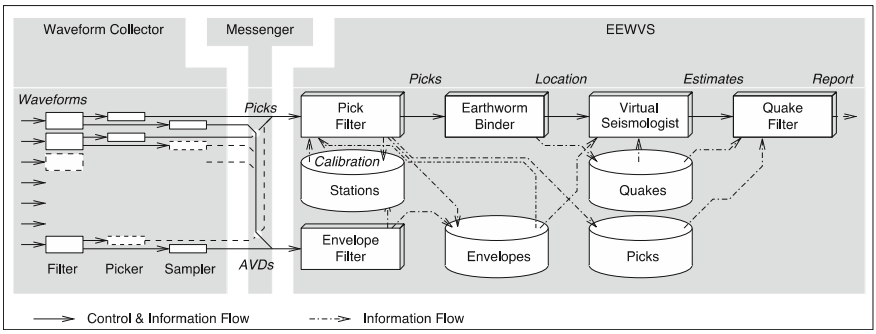

Fig. 3.2 System architecture of Virtual Seismologist codes (from Cua et al. 2009). What we refer to as the VS codes consists of 3 subsystems (collection of modules). The Waveform Collector subsystem performs basic waveform processing such as picking, gain correction, baseline removal, filtering, down-sampling, and the calculation of the ground motion envelopes used by VS. The Messenger subsystem sends information (picks and ground motion envelopes) to the EEWVS (Earthquake Early Warning Virtual Seismologist) subsystem. The EEWVS subsystem includes the Binder module for providing location estimates, which is then passed to the magnitude estimation module. The QuakeFilter module (within the EEWVS subsystem) compares the consistency of the candidate location and magnitude estimate with the available pick and envelope data

in California and Europe was designed and developed by Dr. Michael Fischer during his term at the Swiss Seismological Service at ETH Zürich.

Conceptually, VS maps incoming phase arrival and ground motion envelope amplitude information into continuously updated estimates of earthquake magnitude, location, depth, origin time, and likelihood. Within the context of the ShakeAlert effort, the likelihood parameter expresses a degree of belief that the incoming data come from a real earthquake (as opposed to noise). The higher the likelihood value, the more consistent the incoming data are with a regional earthquake. Figure 3.2 (Cua et al. 2009) shows the system architecture of the VS codes. Phase picks from a short-term average/long-term average picker based on Allen (1978) are first sent to a Pick Filter. If the picks satisfy certain thresholds, they are sent to the Binder Earthworm phase associator module (Dietz 2002), which provides estimates of event origin time, latitude, longitude, and depth. The location estimate is passed to the Virtual Seismologist module in Fig. 3.2, which provides a magnitude estimate, given the Binder location estimate, and the available ground motion envelope values. The QuakeFilter module then takes the candidate event information (location estimate from the Binder module, magnitude estimate from Virtual Seismologist module), checks the consistency of these estimates with the observed phase picks and ground motion envelope values, and outputs a likelihood value. We refer the reader to (Cua et al. 2009), for a more detailed discussion of the VS system architecture and real-time processing.

The use of ShakeMap-style site corrections (Wald et al. 1999) using shear wave velocity in the upper 30 m (Vs30) and the Borcherdt (1994) approach is currently implemented in the real-time codes. Caprio et al. (2011) are comparing the

effectiveness of empirical station corrections and Vs30-based corrections in improving VS magnitude estimation.

Within the CISN ShakeAlert system, the VS algorithm is configured to require a minimum of four stations to initiate an initial event declaration (origin time, latitude, longitude, depth, magnitude, likelihood). Estimates and their updates are sent to the Decision Module, which combines the VS estimates with available estimates from $\tau_c - P_d$ Onsite and ElarmS, to produce the ShakeAlert estimate. VS can also predict peak ground motions at specified locations. However, this particular feature is suppressed within the ShakeAlert system, since the prediction of peak motions at the user sites is done by the User Display.

VS is currently running as three separate installations at the three processing facilities at Caltech/USGS Pasadena, UC Berkeley, and USGS Menlo Park. From the last 5 years of real-time testing, we find that, in general, the quality of the location estimate drives the quality of the magnitude estimate. If the location estimate is correct (or reasonably close to the true location), the VS magnitude estimate is quite good. Figure 3.3 shows the magnitude error (VS magnitude estimate – catalogue magni-

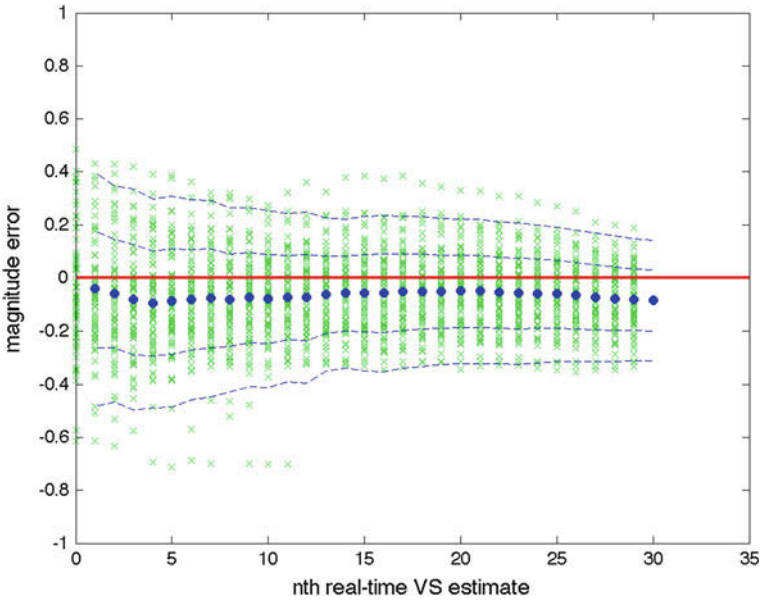

Fig. 3.3 VS magnitude error (VS magnitude – catalogue magnitude) for 80 southern California events from January through October 2011 with initial location estimates within 15 km of the catalogue location. The *green crosses* denote the temporal evolution of VS magnitude errors for individual events. The *blue dots* indicate the average VS magnitude error for 30 s following the initial VS estimate. The real-time envelope values are corrected to bedrock using the Borcherdt (1994) Vs30-based approach, similar to how the ShakeMap (Wald et al. 1999) codes correct for site amplification using Vs30, before the magnitude estimation step. This Vs30-based correction appears to over-correct for site amplification, as is indicated by the systematic offset of the average VS magnitude error by about 0.1 magnitude units

tude) for real-time VS detections with initial epicentral location estimates within 15 km of the catalogue epicenter for 80 M >= 3.0 southern California events from January through October 2011. On average, if the location is reasonable (i.e., within 15 km of the true location), the VS magnitude estimate is within 0.1 magnitude units of the catalogue magnitude. (The systematic 0.1 magnitude unit underestimation is due to an over-correction of site amplification effects.) This indicates that, if provided a reasonable location estimate, the underlying ground motion envelope relationships from Cua and Heaton (2007) coupled with the Vs30-based correction provides reasonable magnitude estimates. However, the Binder earthworm module was not designed as an EEW associator, and, when operating on 4 picks, simply supplies a hypocenter that fits the arrival times, without being able to recognize whether a particular pick is erroneous or not. Thus, whether the early location estimates are reasonable or not, is determined by how effective the Pick Filter module is at distinguishing between earthquake- or non-earthquake-related picks.

The minimum requirement of 4 picks for an initial event declaration corresponds to initial VS estimates becoming available, on average, around 20 s after the earthquake origin time (the expected initial VS estimate time is a function of station density in a given region), corresponding to an average blind zone of about 70 km. While VS can calculate a magnitude estimate with as little as 2 s of P-wave information from a single station, using less than 4 stations for a location estimate results in too many false detections. An experimental version of VS, called VS-MTED (Virtual Seismologist Multiple Threshold Event Detection) was developed by Fischer et al. (2009) to enable single-station event declarations when amplitudes are high enough, potentially allowing for larger warning times for large events, while requiring a larger number of stations for picks with low amplitudes to minimize false alerts from small earthquakes. Meier et al. (2011) are exploring ways of using the concept of not-yet-arrived data (Horiuchi et al. 2005; Satriano et al. 2007) to improve the discrimination of earthquake and non-earthquake signals with sparse observations. Faster, more robust discrimination between earthquake and noise signals would allow VS (or any other network-based EEW approach, for that matter) to provide faster, more reliable EEW estimates.

3.2.3 ElarmS Algorithm

ElarmS is a network-based early warning algorithm. P-wave detections and subsequent parameters (frequency, amplitude) are combined from several proximal stations to collectively characterize an event (Allen 2007; Allen et al. 2009; Allen and Kanamori 2003; Brown et al. 2010a, b). Network-based algorithms are generally more accurate than single-station algorithms, but are not as fast.

ElarmS consists of two processing modules. The Waveform Processing module, or WP, runs in parallel at three locations (UC Berkeley, USGS Menlo Park, Caltech/USGS Pasadena) and receives the constantly streaming waveforms from seismic sensors throughout California. The WP scans the waveforms looking for

P-wave arrivals, detected by a short-term/long-term average method (Allen 1978). When a P-wave is detected the WP records peak amplitudes (displacement, velocity and acceleration), maximum predominant period, and signal to noise ratios every tenth of a second for 4 s following the P-wave pick. Every second it sends these parameters, along with the original P-wave arrival time, to the ElarmS Event Monitor module.

The Event Monitor module, or EVM, runs in a single installation at UC Berkeley. It receives the P-wave detections and parameters from the three WP modules, and identifies earthquakes in progress, by associating triggers (P-wave detections), estimating event location and estimating event magnitude. Finally the EVM sends an alert message to the ShakeAlert Decision Module if appropriate.

ElarmS associates triggers together using a space/time window based on expected travel times. If P-wave detections occur near each other in space and time, ElarmS will associate those triggers together into a single event. Later triggers are added to the event using the space/time window and the estimated event epicenter.

The event hypocenter is estimated using a grid search. The grid extends 50 km in each horizontal direction from the mean trigger location, at a fixed depth of 8 km, and with 1 km resolution. Imagining that an earthquake begins at each grid point, ElarmS predicts the P-wave arrival time at each triggered station. The predicted travel times are compared to the actual observed arrival times, and the grid point with the lowest residuals is used as the event hypocenter.

ElarmS calculates magnitude twice, using two separate scaling relations, and then averages the two magnitudes into a single event magnitude. The first scaling relations are based on the maximum predominant period, τ_p^{max}, of the first 4 s of P-wave. The vertical waveforms are integrated to velocity if necessary (for accelerometer data) and low-pass filtered at 3 Hz. Then τ_p is defined by the iterative equation:

$$\tau_{p,i} = 2\pi \left(X_i / D_i\right)^{1/2} \tag{3.3}$$

where $X_i = \alpha X_{i-1} + x_i^2$, x_i is the ground velocity of the previous sample, $D_i = \alpha D_{i-1} + (dx/dt)_i^2$, and α is a smoothing constant (Wurman et al. 2007). τ_p^{max} is the maximum observed τ_p, and the period-based magnitude for each triggered station is then:

$$M_{\tau p} = 5.22 + 6.66 \log_{10}(\tau_p^{max}) \tag{3.4}$$

The $M_{\tau p}$values from all triggered stations are averaged together to get a single $M_{\tau p}$for the event.

For the amplitude-based scaling relations, ElarmS uses the peak displacement, P_d, observed at velocity instruments and the peak velocity, P_v, observed at accelerometers. Again, the waveforms are low-pass filtered at 3 Hz and only vertical instruments are used. The amplitude-based magnitude is:

$$M_p = 1.04 \log_{10}(P_d) + 1.27 \log_{10}(R) + 5.16 \quad \text{[HHZ channels]} \tag{3.5}$$

$$M_p = 1.37 \log_{10}(P_v) + 1.57 \log_{10}(R) + 4.25 \quad \text{[HHZ channels]} \tag{3.6}$$

$$M_p = 1.63 \log_{10}(P_v) + 1.65 \log_{10}(R) + 4.40 \quad \text{[HHZ channels]} \tag{3.7}$$

where R is the distance (in kilometers) to the estimated event epicenter (Wurman et al. 2007). The $M_p$values from all triggered stations are averaged together to get a single M_p value for the event. Finally, the M_p and $M_{\tau p}$ are averaged together into a single event magnitude, M, which is sent in any alert messages to the Decision Module.

ElarmS has been sending alert messages to the Decision Module since March 2011 for Northern California events. Between March 18, 2011 and December 6, 2011, there were 138 real events $M \geq 3.0$ in this region (according to the ANSS catalog). ElarmS successfully sent alert messages for 106 of the events, corresponding to a 77 % success rate. For events $M \geq 3.5$, ElarmS sent alerts for 37 out of 45 events, for an 82 % success rate. ElarmS also had a 25 % false alert rate. False alerts are alerts for which there is no corresponding event in the ANSS catalog.

In 2011 we developed a second generation ElarmS code. ElarmS-2 consists of an upgraded Waveform Processing module for faster performance, and a redesigned Event Monitor module for improved accuracy. The new WP module processes smaller packets of waveform data and sends the resulting parameters more promptly. Changes to the EVM module include a more modern coding language (C++), a revised trigger associator, and a new alert filter which verifies each event before sending an alert to the Decision Module. ElarmS-2 is in the final stages of testing and will replace ElarmS-1 in early 2012.

3.3 Decision Module

The Decision Module (DM) of CISN ShakeAlert (Fig. 3.1) combines earthquake information feeds from the three algorithms ($\tau_c - P_d$ Onsite, Virtual Seismologist, and ElarmS) to provide a unified 'ShakeAlert' view of earthquakes in progress. The DM publishes this information in an xml-formatted message for use by any number of users, including the User Display application. The DM has been operational since February 2011 (Neuhauser et al. 2010).

ShakeAlert uses the Java-based publish/subscribe ActiveMQ Messaging Broker with C++ Messaging Service extension for all communication between the ShakeAlert modules, and all messages are in XML format. The Decision Module subscribes to the earthquake message topics that are published by the $\tau_c - P_d$ Onsite, Virtual Seismologist and ElarmS algorithms. When the DM receives a message of a possible earthquake, it tries to associate the event message with any current event messages that it has stored using a location and time metric (Fig. 3.4). If DM cannot associate the message, it assumes that the newly received message is describing a new earthquake in progress and publishes the earthquake in XML format. If DM does

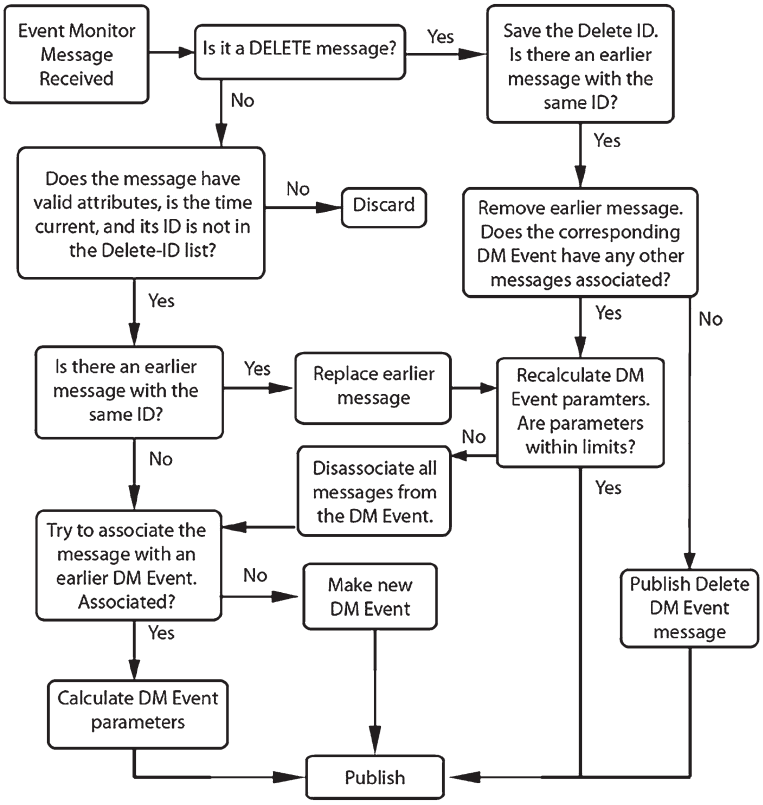

Fig. 3.4 Flow chart for DM logic

manage to associate the message with another earthquake in its memory, it updates the earthquake parameters and republishes the earthquake message (Neuhauser et al. 2010).

Earthquake source parameters from different algorithms are currently combined using a weighted average based on parameter uncertainties. In the future it is intended to include other types of information including prior information using a Bayesian scheme (Neuhauser et al. 2010). When provided by the algorithms, the DM will also output combined uncertainty information for earthquake location and magnitude, and likelihood estimates in its output message to allow end user applications to customize their actions based on these values. In addition, the DM can include both observed and predicted ground motions provided by the algorithms.

The DM receives periodic heartbeat messages from the algorithms, and forwards these messages in addition to its own heartbeat message to the ActiveMQ broker. A separate Health Aggregator module receives these heartbeat messages, determines the overall state of the ShakeAlert modules, and publishes a summary State-of-Health message through ActiveMQ to the User Display and any other user applications interested in monitoring the status of the ShakeAlert system.

3.4 User Display

The User Display (UD) receives XML messages from the Decision Module (DM) and displays their content in a simple and easily understandable way (Böse et al. 2010; Solanki et al. 2011). The app is written in Java and is thus platform-independent. The current version 2.3 has the following features:

- calculation and display of remaining warning time for a given user
- calculation and display of expected MMI intensity at this site (the user can specify a Vs30 value for site characterization if desired)
- description of expected MMI intensity at user site (e.g., "Moderate Shaking expected")
- display of estimated magnitude
- display of the probability of correct alarm ('likelihood' parameter)
- calculation and display of P/S-wavefronts
- display of user site
- display of a 30-km radius blind-zone around the user for education purpose
- siren and audio announcement

The User Display pops up automatically whenever a DM message is received (Fig. 3.5). The user can set thresholds for intensities, magnitudes and probability

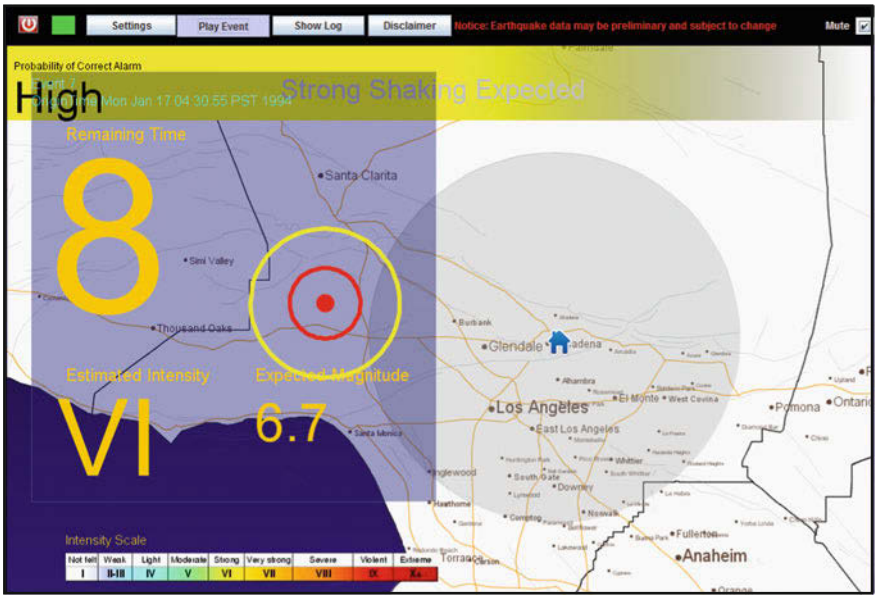

Fig. 3.5 Simulated performance of the User Display for the 1994 M6.7 Northridge earthquake in southern California with a user at Caltech (*blue house*). *Yellow* and *red circles* show P- and S-wavefronts. The *shaded area* around the user gives an approximation of the current blindzone of CISN ShakeAlert

values to reduce the number of reports. Like the 'CISN Display' (www.cisn.org) UD uses Openmap. Multiple map layers showing, e.g., fault lines or infrastructure can be added. XML messages received by the UD are stored locally in a history folder and can be replayed. A log-file summarizes the key information for each received DM report. Network Time Protocol (NTP) is used for time synchronization. Further features include password-protection, encrypted communication with the DM, and the capability to receive and display heartbeats from the three algorithms and DM to ensure robust communication.

3.5 Performance of CISN ShakeAlert

The CISN Testing Center (CTC) is a standalone computational system that runs routine evaluations of the CISN ShakeAlert system by comparing ShakeAlert earthquake forecast parameters, including magnitude and location, against observed earthquake parameters from the ANSS catalog. The intended users of CTC performance evaluations include the scientists and engineers developing the ShakeAlert system, and scientists working to improve earthquake early warning algorithms. The CTC is designed to provide reliable ShakeAlert system forecast evaluations and to provide open performance evaluations that can easily be repeated. To support tracking of ShakeAlert performance over time, the CTC is designed to be inexpensive to build and operate. These testing goals were used to establish the design and operation of the CISN Testing Center.

We have implemented the CTC at the Southern California Earthquake Center (SCEC) headquarters using computer resources that are separate from CISN ShakeAlert computer systems. The CTC software running at SCEC is based on the Collaboratory for the Study of Earthquake Predictability (CSEP) automated testing framework (Zechar et al. 2010) developed for the CSEP Project at SCEC (Jordan 2006). The CSEP software (CSEP 2012) is designed to perform validation testing of short-term earthquake forecasts and it is currently in use in earthquake forecast testing centers in the US (Jordan 2006), Switzerland (Marzocchi et al. 2010), Japan (Nanjo et al. 2011), and New Zealand (Gerstenberger and Rhoades 2010). The CSEP software provides utility programs that can retrieve observational earthquake catalogs from ANSS and other seismological data centers, and other programs that support evaluation of seismic forecasts. SCEC developers have written specialized evaluation modules to evaluate operational performance of the ShakeAlert EEW system (Maechling et al. 2011).

CTC testing is one part of a larger ShakeAlert system testing approach that includes software unit tests, system regression tests, and performance evaluation testing. CTC evaluations focus on ShakeAlert end-to-end system performance and ShakeAlert earthquake parameter forecast validation. An overview of the CISN ShakeAlert System and the CTC components are shown in Fig. 3.6.

The CTC automates ShakeAlert evaluations and provides routine feedback on system performance to ShakeAlert developers. Each night, or on request, the CTC

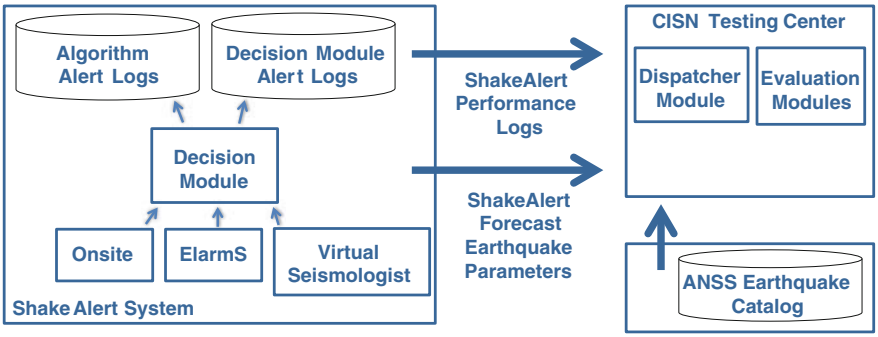

Fig. 3.6 The CISN Testing Center (CTC) (*right*) collects earthquake early warnings from ShakeAlert algorithms and from the ShakeAlert Decision Module (*left*) and evaluates ShakeAlert performance by comparing ShakeAlert forecast parameters against observed parameters in the ANSS earthquake catalog (*bottom right*)

server at SCEC initiates retrieval of ShakeAlert forecast logs and retrieval of the current ANSS catalog. Then, using both the forecast and observational information, the CTC software runs performance metrics and posts the evaluation results online for review by scientists and engineers. Example forecast evaluation summaries from the operational ShakeAlert system are shown in Fig. 3.7.

The CTC performance metrics (Maechling et al. 2009) developed by the scientific and engineering groups during ShakeAlert development can be put into three general categories; speed of operation, event performance, and cumulative event performance.

The CTC speed of operation summary measures how long it took the ShakeAlert system to produce the first alert for an earthquake. We measure this as time in seconds between an event origin time and the time the ShakeAlert Decision Modules publishes the first alert for the event. This measurement varies depending on the location of the earthquake, performance of the CISN real-time seismic network, and performance of the ShakeAlert algorithms and Decision Module.

The CTC event summaries show the earthquake forecast parameters produced by the real-time ShakeAlert algorithms and Decision Module as a time series showing how the forecast parameters change with time. To generate event summaries, the ShakeAlert system logs the performance of the seismological algorithms within ShakeAlert, as well as the processing of the Decision Module, which sends alerts to ShakeAlert end-users.

The CTC cumulative event summaries show performance measures for the ShakeAlert system for a given catalog of earthquakes. Cumulative performance summaries are useful in detecting systematic bias in performance such as consistent over-, or under-prediction of final magnitudes. CTC cumulative plots show performance of first report, and final report, showing how ShakeAlert forecast parameter estimates change during course of an alert.

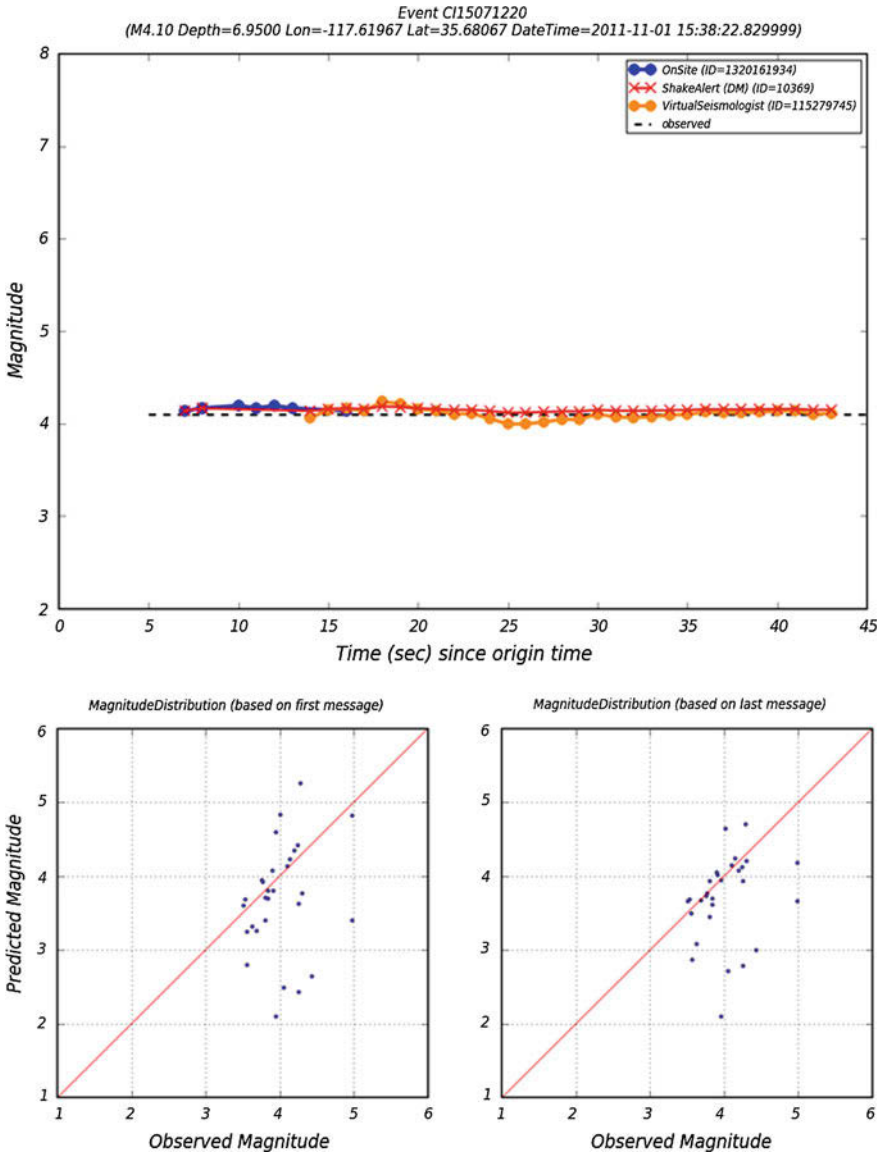

Fig. 3.7 Preliminary CISN testing results from ShakeAlert system show (*top*) time series of magnitude forecasts produced by the $\tau_c - P_d$ OnSite algorithm (*blue*), Virtual Seismologist algorithm (*orange*), and ShakeAlert Decision Module (*red*) for a central California M4.1 earthquake, with time scale showing seconds after origin time that ShakeAlert information is produced. The two graphs (*bottom*) compare ANSS final magnitude values to ShakeAlert Decision Module forecasts for approximately 4 months of M3.5+ California earthquakes based on ShakeAlert first report (*bottom left*), and ShakeAlert final report (*bottom right*)

We believe that the automated testing capability of the CTC software will provide consistent and inexpensive evaluations of ShakeAlert system performance over time. The CISN Testing Center measurements establish ShakeAlert system performance baseline against which we can measure future system performance as EEW algorithms and ShakeAlert Decision Modules software are updated and the CISN network is changed.

We have also developed software to replay the waveform records of historic and simulated earthquakes as simulated real-time data streams. The streams are processed by the same codes as used in the real-time ShakeAlert system. This way we can study the possible performance of the system and assess uncertainties for a much larger dataset of possible earthquake scenarios.

3.6 Outreach

Warnings of imminent shaking are of little use if the recipients are not prepared to act on them. In principle, two classes of use are possible, those based on automated procedures and those based on individual actions. For both cases, preparatory work is necessary to make use of rapidly received alerts. The latter case must be based on broad-based education of the recipients, which is well beyond the scope of our project. In Japan, for example, the public issuance of earthquake early warnings was preceded by a broad information campaign. We are focusing our outreach efforts on prospective users of early warning information who may be able to implement automatic responses that will save lives and property, and improve the possibility and speed of recovery from damaging earthquakes.

Currently, about 70 scientists and engineers receive ShakeAlert information through the User Display. In spring 2012, we have started to add new users to test the ShakeAlert output, which were chosen from industries and institutions throughout California. These users provide critical services to the State of California or its agencies, or operate critical infrastructure. Two examples are the California Emergency Management Agency (CalEMA) which is the state-wide coordinator of emergency response activities, and the Bay Area Rapid Transit District (BART) which provides transportation services in the San Francisco Bay Area.

The goal of the test with prospective users of EEW is twofold. First, as the producers of the early warning information and alerts, we need information from the users. Exactly what types of information are useful to the users? We also need to evaluate delivery mechanisms, procedures, and possible user products (Hellweg et al. 2010; Hellweg and Vinci 2011; Vinci et al. 2009). Secondly, we want the alert recipients to evaluate the effectiveness of possible uses within their organization, as well as the benefits of having alert information available to themselves and to society. To support both these aspects of our project, interaction with and education of the users is very important. A detailed introduction to the CISN ShakeAlert system is an integral part of our interaction with the users, as are regular opportunities for feedback and support. We will support their efforts to determine and implement appropriate

responses. In future workshops, users will be surveyed to document how EEW was used in their organizations as well as how it is expected improve their earthquake response, as well as documenting the expected savings in terms of lives, damage, and improved resilience.

3.7 Research on Finite Fault Ruptures

Seismic ground motions can be underestimated when predicted from epicentral rather than rupture-to-site distances. This can result in warnings not being issued because shaking intensities do not exceed pre-defined thresholds. A prominent example is from the recent 2011 M9.0 Tohoku-Oki earthquake in Japan: while ground motion predictions by the Japanese Meteorological Agency (JMA) were fairly accurate in the Sendai area, close to the point of rupture nucleation, a warning was not transmitted to people and users in the Kanto district around Tokyo. Shaking in this region was strong, but underrated by the JMA EEW system that relies on point source approximations of earthquakes.

As part of the ongoing methodological development, we have been investigating the use of real-time GPS displacement data streams for rapid earthquake detection and source parameter estimation for large earthquakes (Allen and Ziv 2011). Using the example of the 2010, Mw7.2 El Mayor-Cucapah earthquake in Baja California, we have developed a simple algorithm to extract the permanent displacement at GPS sites starting one oscillation after triggering on the dynamic long-period signal. The estimate is continually improved with time. These permanent displacements can then be inverted for source characteristics given an approximate estimate of the fault plane. Estimates of fault plane parameters are available from existing fault catalogs and the appropriate region of fault rupture could be selected based on the seismic epicenter (Allen and Ziv 2011).

To take into account source finiteness for large earthquakes, we have also developed the Finite Fault Rupture Detector, FinDer (Böse et al. 2012b). FinDer uses image recognition techniques to automatically detect and map finite faults in real-time. The approach is based on a rapid (high-frequency) near/far-source classification of ground motion amplitudes in a dense seismic network (<50 km), and comparison with a set of pre-calculated templates using 'Matching by Correlation'. The knowledge on source dimensions as provided by FinDer will make predicted shaking intensities more accurate and thus more useful for EEW, ShakeMaps, and related real-time products in the future, because it will allow the usage of rupture-to-site distances in empirical ground-motion prediction equations.

Predicting the shaking from large earthquakes requires some estimate of the likelihood of the future evolution of an ongoing rupture. It seems reasonable to assume that large slip amplitudes increase the probability for evolving into a large earthquake. From simulated sets of 1-D rupture series from stochastic models of spatially heterogeneous slip, we found that while large slip amplitudes increase the probability for the continuation of a rupture and the possible evolution into a large earthquake,

the recognition that rupture is occurring on a spatially smooth fault, such as the San Andreas Fault, has an even stronger effect (Böse and Heaton 2010). We conclude that an EEW system for large earthquakes will benefit from a rapid recognition of the causative fault and consideration of its smoothness. FinDer is suited for such rapid fault association (Böse et al. 2012b). If the predicted location and azimuth of the rupture agrees well with the parameters of a known fault, the probability that rupture is occurring along this fault is high. If rupture is occurring along a smooth (mature) fault, a warning should be issued immediately, because the probability for a large earthquake is high.

3.8 Conclusions and Outlook

Around 145 years after Dr. Cooper (1868) proposed the implementation of earthquake early warning (EEW) for San Francisco, and 25 years after Heaton (1985) envisioned a seismic computerized alert network for California, scientists and engineers from several institutions in- and outside of California have developed an EEW demonstration system. This system is based on the infrastructure of the California Integrated Seismic Network (CISN). CISN ShakeAlert combines the outputs of three independently running algorithms for EEW ($\tau_c - P_d$ Onsite, Virtual Seismologist, and ElarmS) to calculate and report a unified view of the ongoing earthquake. The ShakeAlert structure is open and flexible to allow the integration of additional algorithms and tools in the future (Fig. 3.1).

Within the next 3 years, we plan to expand the coverage of the current ShakeAlert system to the entire Pacific Westcoast, including the Cascadia subduction-zone, where great earthquakes with high tsunami-potential can occur. We also plan to integrate ShakeAlert into the daily routine operations of CISN (AQMS system). Our future research and development will mainly focus on the rapid detection and processing of ground motions from large earthquakes, possibly with the integration of real-time GPS data streams and development of new algorithms for finite-fault rupture detection (Allen and Ziv 2011; Böse and Heaton 2010; Böse et al. 2012b).

We are also working on methodologies that will make it possible to automatically detect and process complex fore-, main- and aftershocks sequences. One approach will be to predict the envelope of seismic ground motions for a proposed foreshock magnitude and location (Karakus and Heaton 2011). If there is significant disagreement between the predicted and observed amplitudes as recorded and calculated for a nearby station, it is likely that the waveforms from two or more earthquakes overlap in time.

In collaboration with the Computer Science Department at Caltech, we have started to implement the User Display and additional apps on the Android smart phone (Faulkner et al. 2011). In addition, an automated decision-making system framework for EEW applications is being developed to perform real-time cost-benefit analyses of actions controlled by EEW (Wu and Beck 2011).

CISN ShakeAlert is an EEW demonstration system. It is not robust enough to provide reliable and timely EEW throughout California. To design and build an EEW system that was robust enough to support the economy of California, much more resources would be needed than what is available today.

Acknowledgments This work is funded through contracts G09AC00258, G09AC00259, G09AC00255, and G09AC00256 from USGS/ANSS to the California Institute of Technology (Caltech), UC Berkeley, USC/SCEC, and ETH. It is also funded by grants from the Gordon and Betty Moore Foundation to Caltech and UC Berkeley. USC/SCEC received additional funding through SCEC3 (NSF Cooperative Agreement EAR-0529922 and USGS Cooperative Agreement 07HQAG0008). This is SCEC contribution #1641 and contribution #10072 of the Seismological Laboratory, Geological and Planetary Sciences at Caltech.

References

Allen RV (1978) Automatic earthquake recognition and timing from single traces. Bull Seismol Soc Am 68(5):1521–1532

Allen RM (2007) The ElarmS earthquake warning methodology and application across California. In: Gasparini P, Zschau J (eds) Seismic early warning. Springer, New York, pp 21–44

Allen RM, Brown H, Hellweg M, Khainovski O, Lombard P, Neuhauser D (2009) Real-time earthquake detection and hazard assessment by ElarmS across California. Geophys Res Lett 36 L00B08. doi:10.1029/2008GL036766

Allen RM, Kanamori H (2003) The potential for earthquake early warning in southern California. Science 300:786–789

Allen RM, Ziv A (2011) Application of real-time GPS to earthquake early warning. Geophys Res Lett 38 L16310. doi:10.1029/2011GL047947

Barba M, Böse M, Hauksson E (2010) In: The earthquake early warning demonstration tool (EEWDT) Southern California Earthquake Center (SCEC) Meeting, Palm Springs, California, 11–15 Sept 2010

Böse M, Heaton TH (2010) Probabilistic prediction of rupture length, slip and seismic ground motions for an ongoing rupture: implications for early warning for large earthquakes. Geophys J Int 183(2):1014–1030. doi:10.1111/j.1365-246X.2010.04774.x

Böse M, Heaton TH, Hauksson E (2012a) Rapid estimation of earthquake source and ground-motion parameters for earthquake early warning using data from single three-component broadband or strong-motion sensor. Bull Seismol Soc Am 102(2). doi:10.1785/0120110152

Böse M, Heaton TH, Hauksson E (2012b) Real-time finite fault rupture detector (FinDer) for large earthquakes. Geophys J Int 191:803–812

Böse M, Hauksson E, Solanki K, Kanamori H, Wu Y-M, Heaton T H (2009a) A new trigger criterion for improved real-time performance of on-site earthquake early warning in southern California, Bull Seism Soc Am 99(2-A): 897–905. doi:10.1785/0120080034

Böse M, Hauksson E, Solanki K, Kanamori H, Heaton TH (2009b) Real-time testing of the on-site warning algorithm in southern California and its performance during the July 29 2008 Mw5.4 Chino Hills earthquake. Geophys Res Lett 36, L00B03. doi:10.1029/2008GL036366

Böse M, Solanki K, Allen RM, Brown H, Cua GB, Given D, Hauksson E, Heaton TH, CISN Earthquake Early Warning Project Team (2010) CISN ShakeAlert: development of a prototype user display for providing earthquake alerts to end users, American Geophysical Union, Fall meeting 2010, abstract #NH33A-1369

Borcherdt RD (1994) Estimates of site-dependent response spectra for design (methodology and justification). Earthq Spectr 10:617–654

Brown HM, Allen RM, Hellweg M, Khainovski O, Neuhauser D, Souf A (2010) Development of the ElarmS methodology for earthquake early warning: realtime application in California and offline testing in Japan. Soil Dyn Earthq Eng 31:188–200. doi:10.1016/j.soildyn.2010.03.008

Brown HM, Lim I, Allen RM, Neuhauser D, Khainovski O, Hellweg M (2010b) CISN earthquake early warning: ElarmS, NH33A-1372, 2010 fall meeting AGU. San Francisco, Dec 2010

Caprio M, Cua GB, Fischer M, Wiemer S, Heaton TH (2011) CISN ShakeAlert: accounting for site amplification and quantifying time and spatial dependence of uncertainty estimates in the virtual seismologist earthquake early warning algorithm. American Geophysical Union Fall meeting, San Francisco, pp S53A–2251

Cooper M (1868) Editorial in: San Francisco Daily Evening. Bulletin, 3 Nov 1868

CSEP (2012) CSEP Testing Center Software and documentation. http://www.cseptesting.org

Cua GB (2005) Creating the virtual seismologist: developments in ground motion characterization and seismic early warning. California Institute of Technology, Pasadena, California

Cua G, Fischer M, Heaton T, Wiemer S, Giardini D (2009) Real-time performance of the virtual seismologist method in southern California. Seismol Res Lett 80:740–748. doi:710.1785/gssrl.1780.1785.1740

Cua G, Heaton T (2007) The virtual seismologist (VS) method: a bayesian approach to earthquake early warning. In: Gasparini P, Manfredi G, Zschau J (eds) Earthquake early warning systems. Springer, Berlin, pp 97–132

Dietz L (2002) Notes on configuring BINDER_EW: earthworm's phase associator. From http://www.isti2.com/ew/ovr/binder_setup.html

Faulkner M, Olson M, Chandy R, Krause J, Chandy KM, Krause A (2011) The next big one: detecting earthquakes and other rare events from community-based sensors. In: Proceedings of the 10th ACM/IEEE international conference on information processing in sensor networks, ACM

Fischer M, Caprio M, Cua GB, Heaton TH, Clinton JF, Wiemer S (2009) Multiple-threshold event detection and other enhancements to the virtual seismologist earthquake early warning algorithm. Amercian Geophysical Union Fall meeting, San Francisco, pp S22A–02

Gerstenberger MC, Rhoades DA (2010) New Zealand earthquake forecast testing centre. Pure Appl Geophys 167:877–892

Heaton T (1985) A model for a seismic computerized alert network. Science 228(4702):987–990

Hellweg, M, Allen RM, Brown H, Neuhauser DS, Khainovsky O (2010) CISN ShakeAlert: progress toward using early warnings for earthquakes in California, Abstract NH33A-1368 presented at 2010 fall meeting, AGU, San Francisco, California, 13–17 Dec 2010

Hellweg M, Vinci M (2011) CISN shakealert: using early warnings for earthquakes in California, Abstract S53A–2254 presented at 2011 Fall Meeting, AGU, San Francisco, California, 5–9 Dec 2011

Horiuchi S, Negishi H, Abe K, Kamimura A, Fujinawa Y (2005) An automatic processing system for broadcasting earthquake alarms. Bull Seismol Soc Am 95(2):708–718

Jordan TH (2006) Earthquake predictability, brick by brick. Seismol Res Lett 77:3–6

Kanamori H (2005) Real-time seismology and earthquake damage mitigation. Annu Rev Earth Planet Sci 33:195–214. doi:10.1146/annurev.earth.33.092203.122626

Karakus G, Heaton T (2011) Methodologies to automatically recognize foreshock/mainshock pairs. S53A–2268, AGU Fall Meeting, San Francisco, Dec 2011

Maechling PJ, Jordan TH, Liukis M, Callaghan S (2009) Developing performance measures for the CISN earthquake early warning testing center. Eos Trans AGU, 90(52), Fall Meeting Supplement, Abstract S13A–1717

Maechling PJ, Liukis M, Jordan TH, CISN EEW Team (2011) Development of ShakeAlert performance evaluation software. Abstract S53A–2255 presented at 2011 Fall Meeting, AGU, San Francisco, California, 5–9 Dec 2011

Marzocchi W, Schorlemmer D, Wiemer S (eds) (2010) An earthquake forecast experiment in Italy. Special volume, Ann Geofisica 53(3):163

Meier M-A, Cua GB, Fischer M, Wiemer S (2011) CISN ShakeAlert: improving the virtual seismologist earthquake early warning framework to provide faster, more robust warning information. S53A–2252, AGU Fall Meeting, San Francisco, Dec 2011

Nakamura Y (1988) On the urgent earthquake detection and alarm system (UrEDAS). In: Proceedings of the 9th world conference on earthquake engineering. Tokyo-Kyoto, Japan

Nanjo KZ, Tsuruoka H, Hirata N, Jordan TH (2011) Overview of the first earthquake forecast testing experiment in Japan. Earth Planets Space 63:159–169. doi:10.5047/eps.2010.10.003

Neuhauser DS, Khainovsky O, Böse M, Solanki K, Cua G, Heaton TH, Allen R (2010) CISN ShakeAlert: the decision module for earthquake alerts. AGU Fall Meeting, NH33A-1370. San Francisco, Dec 2010

Romanowicz B, Dreger D, Hellweg M (2011) Upgrading the broadband and borehole seismic networks operated by the Berkeley seismological laboratory at the university of California, Berkeley, USGS Award Number G09AC00487, Final technical report

Satriano C, Lomax A, and Zollo A (2007) Optimal, real-time earthquake location for early warning. In: Gasparini P, Manfredi G, Zschau J (eds) Earthquake early warning systems. Springer, Berlin Heidelberg

Solanki K, Böse M, Hauksson E, Heaton TH, CISN EEW Group (2011) CISN ShakeAlert: protoype user display for providing earthquake early warnings to test users. AGU Fall Meeting, S53A–2250, San Francisco, Dec 2011

Thomas V, Bhadha R, Crummey J, Curtis W, Devora A, Flores I, Given D, Hauksson E, Johnson D, Koesterer C, Lydeen S, Sutton D, Watkins M, Yu E (2011) Modernization of the caltech/USGS southern California seismic network—ARRA and beyond. AGU Fall Meeting, S51A–2194, San Francisco, Dec 2011

Vinci M, Hellweg M, Jones LM, Khainovski O, Schwartz K, Lehrer D, Allen RM, Neuhauser DS (2009) CISN ShakeAlert: using early warnings for earthquakes in California. Eos, 90(52), Fall Meeting Supplement, S13A–1720

Wald DJ, Quitoriano V, Heaton T, Kanamori H, Scrivner CW, Worden BC (1999) TriNet "ShakeMaps": rapid generation of peak ground motion and intensity maps for earthquakes in southern California. Earthquake Spectra 15(3):537–556

Wu S, Beck JL (2011) An automated decision-making system framework for earthquake early warning system applications. In: Conference proceedings of the 8th international conference on urban earthquake engineering (CUEE): 1737–1740, Tokyo, Japan, Mar 2011

Wu Y-M, Kanamori H, Allen RM, Hauksson E (2007) Determination of earthquake early warning parameters, τc and Pd, for southern California. Geophys J Int 170:711–717. doi:10.1111/j.1365-246X.3732007.03430.x

Wurman G, Allen RM, Lombard P (2007) Toward earthquake early warning in northern California. J Geophys Res 112 B08311

Zechar JD, Schorlemmer D, Liukis M, Yu J, Euchner F, Maechling PJ, Jordan TH (2010) The collaboratory for the study of earthquake predictability perspective on computational earthquake science. Concurr Comput-Pract Exp 22:1836–1847. doi:10.1002/cpe.1519

Chapter 4
The Mexican Seismic Alert System (SASMEX): Its Alert Signals, Broadcast Results and Performance During the M 7.4 Punta Maldonado Earthquake of March 20th, 2012

A. Cuéllar, J. M. Espinosa-Aranda, R. Suárez, G. Ibarrola, A. Uribe, F. H. Rodríguez, R. Islas, G. M. Rodríguez, A. García and B. Frontana

Abstract The Mexican Seismic Alert System (SASMEX) comprises the Seismic Alert System of Mexico City (SAS), in continuous operation since 1991, and the Seismic Alert System of Oaxaca City (SASO) that started its services in 2003. The SAS generates automatic broadcasts of Public and Preventive Alert Signals to the cities of Mexico, Toluca, Acapulco and Chilpancingo, and SASO by now only to Oaxaca City. Historically in Mexico City, due to their great distance to the coast of Guerrero, the SAS has issued its Alert Signals with an opportunity average of 60 s. In Oaxaca City the SASO gives 30 s time opportunity, if the earthquake detected is occurring in the Oaxaca coast region, or less time, if the seismic event hits near this town. The paper reviews both systems, its performance characteristics and its recent test by the Ometepec M 7.4 earthquake of March 20, 2012.

4.1 Introduction

The Seismic Alert System of Mexico City (SAS) generates automatic broadcast of Public and Preventive Alert Signals to the cities of Mexico, Toluca, Acapulco and Chilpancingo, and the Seismic Alert System of Oaxaca City (SASO) by now only to Oaxaca City. Two types of SASMEX Seismic Alert Signals ranges were determined in accordance with each local Civil Protection Authorities: Public Alert if they

A. Cuéllar (✉) · J. M. Espinosa-Aranda · G. Ibarrola · A. Uribe · R. Islas · A. García
Centro de Instrumentación y Registro Sísmico, A. C., Anaxágoras 814 Narvarte,
03020 Mexico, D. F., Mexico
e-mail: acutellarmtz@yahoo.com.mx

F. H. Rodríguez · G. M. Rodríguez · B. Frontana
Facultad de Ingeniería, Universidad Nacional Autónoma de México,
Mexico, D. F., Mexico

A. Cuéllar · R. Suárez
Instituto de Geofísica, Universidad Nacional Autónoma de México,
Mexico, D. F., Mexico

F. Wenzel and J. Zschau (eds.), *Early Warning for Geological Disasters*,
Advanced Technologies in Earth Sciences, DOI: 10.1007/978-3-642-12233-0_4,

expect strong earthquake effects and Preventive Alert Signal, for moderated ones. SAS originally had 12 field sensor stations covering partial segment of the Guerrero coast, nowadays covers additionally Michoacan, Jalisco Colima and Guerrero coast completely with 36 field sensor stations supported by the Mexico City Government; the SASO has 37 field sensor stations operating in the coast, central and north of the Oaxaca, covering their seismic danger territory. Since 1993, the SAS is pioneer in the automatic public alerts broadcast services, thanks to the support of the *Asociación de Radiodifusores del Valle de México, A.C.* (ARVM). Historically in Mexico City, due to their great distance to the coast of Guerrero, the SAS has issued its Alert Signals with an opportunity average of 60 s. In Oaxaca City the SASO gives 30 s time opportunity, if the earthquake detected is occurring in the Oaxaca coast region, or less time, if the seismic event hits near this town. Also the SASO has been supported since its implementation for local commercial radio stations. To this day the SAS and SASO have generated respectively 14 and 20 Public Alert Signals, also 59 and 13 Preventive Alerts of more than 2200 earthquakes detected by their sensing field stations. Additionally the federal government is promoting to increase the observation capacity of the seismic danger in Mexico City and the other cities located in seismic regions, to detect and warn any strong seismic effect.

To reach better efficiency in the seismic warning delivery, the Government of the Federal District through the Authority of the Historical Center in 2008, to innovate the SAS, installing VHF radio transmitters, similar to the communication technology like the National Weather Radio (NWR) and Specific Area Message Encoding (SAME) called NWR-SAME, following the code standards of the National Oceanographic and Atmospheric Administration (NOAA) and the Emergency Alert Systems (EAS) of United States; adding a new code (SARMEX) with the capabilities like fast response (2 s or less) to emit the earthquake early warning signal in order to enhance the effectiveness in the Seismic Alert Signals required. This technology also will be implemented in the SASO, and recently the federal authorities have decided to support the coverage with NWR-SAME-SARMEX receivers in other populated cities or urban areas located in seismic regions of Mexico.

On March 20, 2012, during the occurrence of earthquake M 7.4 Ometepec Gro., close to Punta Maldonado, the SASMEX warned Public Alert in the cities of Acapulco and Chilpancingo, Gro., and Oaxaca, Oax., and warned Preventive Alert in the metropolitan area of the valley of Mexico. The time of opportunity was between 80 and 40 s, due to the distance between 175 and 360 km from epicenter to cities where the SASMEX broadcasted their public earthquake early warnings.

After experiencing the serious seismic disaster generated by the "Caleta de Campos" M8.1 Michoacán earthquake in 1985, Mexico City Authorities have been promoting since 1989 the design and evolution of *Sistema de Alerta Sísmica* (*SAS*), with the aim to mitigate possible future earthquake damage produced by such as the latent "Guerrero Gap" seismic danger (Espinosa-Aranda et al. 1992).

The original *SAS* idea was developed by *Centro de Instrumentación y Registro Sísmico* (CIRES) Civil Association. This technological resource started its experimental operation in August 1991 and has been available and evaluated as a public service since 1993. To date it is applied and evaluated in more than 80 elementary

schools, both private and public, located in urban regions prone to seismic risk and where early warning of seismic alert signals from *SAS* has been useful, as well as in the Mexico City subway rail transport (METRO). Recently has started the installation of more than 40,000 NWR-SAME-SARMEX receivers for elementary public schools of Mexico City.

SAS disseminates public seismic alert in the valleys of Mexico and Toluca, this one located about 50 km NW of Mexico City. In addition, it also alerts on a contract basis to more than 280 miscellaneous institutions comprising schools, public buildings and emergency organizations. The implementation of *SAS* in the Mexico Valley has made possible to anticipate the arrival of the effects of S-waves with an average of 60 s, time enough to allow execution of safety of automatic system procedures for the protection of equipment or systems susceptible to undergo damage, such as power plants, computer systems and telecommunication networks (Kanamori 2003). On May 14, 1993, after *SAS* identified an earthquake M6.0 and anticipated with 65 s the imminent arrival of its effect in Mexico City, the local authorities decided to disclose early warning notices publicly. The alert signal broadcast was possible thanks to the support from most of the commercial radio and television networks grouped in the *Asociación de Radiodifusores del Valle de Mexico* (ARVM), Civil Association, which agreed to contribute as a social service for their audience since August 1993. *SAS*, has high availability and reliability of their four basic sub-systems: Seismic Detection, Communication, Warning Dissemination and Central Control and Recording, to guarantee the effective earthquake alert public service (Espinosa-Aranda et al. 1995).

On September 14, 1995 at 8:04 AM in Mexico City, having elapsed almost ten years after the tragic earthquake of 1985 (Espinosa-Aranda et al. 1995), *SAS* anticipated with 72 s the arrival of the effect of an M 7.3 earthquake occurred near the town of Copala, Guerrero, This earthquake proved the adequacy of the processes of response and evacuation of schools, where the *SAS* early warnings were received, since the population performed these activities successfully (Goltz and Flores 1997).

On June 15th 1999, a damaging M6.7 earthquake induced the Department of Civil Protection of Oaxaca to request CIRES the design, construction and installation of the *Sistema de Alerta Sísmica de Oaxaca* (*SASO*). A better time-efficiency criteria to define the seismic range of the *SASO* warnings emerged in a technological evolution from the original algorithm used by *SAS*, designed back in 1989 (Espinosa-Aranda et al. 1992), to fulfill the requirements demanded by this application.

Thanks to the Oaxaca Authorities initiative, the Mexico City Mayor, with the participation of the Mexican Secretariat of the Interior, it has been agreed a *SASO* and *SAS* function integration to constitute them as a single entity, the so-called *Sistema de Alerta Sísmica Mexicano* (*SASMEX*). And recently has been decided to increase as necessary the number of seismic sensors to provide an effective warning of impending regional seismic risk disseminating notices of seismic alert in vulnerable cities (Fig. 4.1). With the service rendered by EA*SAS* systems in each sensible region, it will be possible to prevent in advance the seismic effects on the site as well as define the most suitable alert warning for each particular risk condition, and to review these factors systematically (Espinosa-Aranda et al. 2009).

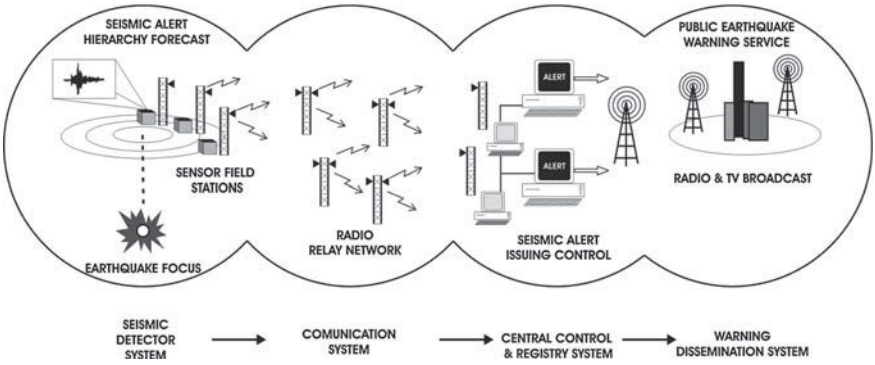

Fig. 4.1 The Mexican Seismic Alert System

In 2007, to support the activities of Civil Protection of the coastal state of Guerrero, Mexico City Authorities authorized the installation of Alternate Emitters for the warning issued by the *SAS* (EA*SAS*) in the cities of Acapulco and Chilpancingo. The EA*SAS* of Guerrero provide public automatic alert services controlling the transmissions of the local commercial broadcasting stations covering the demand of private seismic alert services offered to 102 institutional users.

In order to improve the efficiency in the dissemination of the warning provided by *SAS* initially in schools, recently *La Autoridad del Centro Histórico* in Mexico City sponsored the installation of three dedicated VHF radio transmitters, thus benefiting by the use of commercially available low-cost receivers carrying the Public Alert^{TM} logo, that meet technical standards of NOAA Weather Radio (NWR) Specific Area Message Encoding (SAME) protocols and the Emergency Alert System (EAS) event codes, such as those in use to warn against diverse natural hazards in the USA. The Mexico City application require the NOAA-SAME-EAS protocols, an enhancement in order to include a new code to operate earthquake early warning signals, without delay, omitting the normal two tones previous to signal advise (Espinosa-Aranda et al. 2009).

The Consumer Electronics Association Standards of United States (CEA), approved the Mexican Risks Advisory System (SARMEX) standard that uses all characteristics of the NWR-SAME protocols in March 2011, but enhances the response time when the Earthquake Early Warning codes are emitted, additionally, the Mexican earthquake early warning sound is included to distinguish it from others messages.

4.2 SASMEX Achievements

The SASMEX part for the Mexico City (called SAS) has been regarded as the first system in the world for earthquake early warning that disseminates its notices to the public (Lee and Espinosa-Aranda 1998). The Prevention Time is close to 60 s. This is because the major seismic effects threatening the Valley of Mexico are originated at

the coastal region of the Pacific Ocean at a distance of at least 320 km and since their strongest components travel at 4 km per second, taking 80 s to arrive, whereas notices broadcasted by radio from the epicenter area can be transmitted instantaneously anticipating the seismic effects.

The SASMEX forecast begins calculating parameters measured in the Field Stations, FS, when an earthquake is detected, SASMEX in the Mexican Pacific Coast from Colima to Oaxaca, uses the acceleration data of the vertical, longitudinal and transversal components to calculate the Acceleration Quadratic Integration and the rate of this integration, both measured during the 2*(S-P) lapse, that is, the first P wave arrives until the S wave begins. In north and center of Oaxaca it uses the dominant period, measured in the vertical component during the first three seconds after de P wave begins; in case of the S-P is less than 3 s, then the FS uses two additional parameters: the Maximum Acceleration and the Acceleration Quadratic Integration, from the vertical component too (Espinosa-Aranda et al. 2010).

The parameters are sent automatically to determine the alert range, this forecast is used to define the seismic warning range of the impending occurrence of a dangerous earthquake detected by the first two FS (Espinosa-Aranda and Rodriguez 2003). The first FS message defines the warning range, either strong or moderate, and with the second one, triggers the Type of Warning process respectively as "Public Alert" or "Preventive Alert". However the range of Public and Preventive in Oaxaca, Chilpancingo and Acapulco is less than Mexico City, in order to be more sensible due to minor distance from these cities to the danger seismic area in contrast with Mexico City. The Prevention Time is defined as the time elapsed between the beginning of the warning signal and the beginning of the S phase, related to the region where it is intended to mitigate the risk (Espinosa-Aranda et al. 2009).

SASMEX for Mexico City (SAS) since its experimental operational stage in 1991, *SAS* has detected more than 2300 seismic events with magnitudes from M3.0 to M 7.4 and it has emitted 14 earthquakes warnings as "Public Alerts" and 59 as "Preventive Alerts (Table 4.1). The *SAS* performance showed in the Table 4.1 is accounted by the number of FS's that registered each warned earthquake (# SENS. OP.), the Forecast (MAGNITUDE), the Type of Warning emitted (ALERT RANGE) and Prevention Time. The DISTANCE in Table 4.1 is measured from the epicenter to the first FS which detected the earthquake.

SASMEX for Oaxaca (called *SASO)* constitutes a technological development evolved from *SAS*; *SASO* has 36 FS and 11 radio relay stations to link its coastal, central, and northern included isthmus regions (Fig. 4.2). Since its commissioning, *SASO* has issued 20 Public Alert and 13 Preventive Alert warnings from the detection and analysis of more than 230 sensed earthquakes (Table 4.2 similar to Table 4.1).

From April 2012, *SASMEX* identifies the strong earthquakes along the coast of the State of Guerrero, Michoacán, Jalisco and Colima with a linear layout of 36 of SAS and 11 of SASO FS spaced approximately every 25 km to be able to perform an efficient survey because many seismic foci of this region occur at similar depths (Fig. 4.2).

Table 4.1 SAS Performance of earthquake early warnings since 1991–2012

		NACIONAL SEISMIC SERVICE (SSN), UNAM				SAS FORECAST RESULT		
#	Region	Local date-time	Latitude	Longitude	Depth (km)	Sens. Op.	Alert range	Prevention time (s)
72	Oaxaca	02/04/2012 12:36	16.27	−98.47	10	6	Preventive	80
71	Oaxaca	20/03/2012 12:03	16.42	−498.36	15	7	Preventive	80
70	Guerrero	10/12/2011 19:48	17.84	−99.98	58	10	Preventive	16
69	Guerrero Coast	18/06/2011 17:55	16.92	−99.60	26	5	Preventive	
68	Guerrero Coast	05/05/2011 08:24	16.61	−98.91	11	6	Public	65
67	Guerrero Coast	25/05/2010 18:36	17.11	−101.2	15	8	Preventive	63
66	Guerrero Coast	27/04/2009 16:46	16.90	−99.58	7	4	Preventive	57
65	Guerrero	27/03/2009 02:48	17.35	−100.82	30	7	Preventive	58
64	Guerrero	11/11/2008 05:02	16.62	−100.8	15	4	Preventive	
63	Guerrero	06/11/2007 00:35	17.08	−100.14	9	9	Public	68
62	Guerrero	28/04/2007 08:56	16.94	−99.82	9	6	Preventive	
61	Guerrero	13/04/2007 03:43	17.27	−100.27	51	8	Preventive	56
60	Guerrero	13/04/2007 00:42	17.09	−100.44	41	6	Public	58
59	Guerrero	31/03/2007 00:18	17.00	−99.79	34	5	Preventive	
58	Guerrero	18/09/2005 06:25	17.05	−100.02	8	3	Preventive	
57	Guerrero Coast	09/01/2003 20:08	16.97	−100.3	30	7	Preventive	58
56	Guerrero	27/09/2002 02:04	17.16	−100.59	37	4	Preventive	58
55	Guerrero Coast	25/09/2002 13:14	16.86	−100.12	5	4	Preventive	57
C	Guerrero Coast	18/04/2002 12:02	16.42	−101.1	15	0	Fail	
54	Guerrero Coast	16/02/2002 22:10	16.94	−99.93	37	6	Preventive	
53	Guerrero Coast	07/10/2001 22:39	16.94	−100.14	4	8	Public	65
52	Guerrero	06/03/2001 15:57	17.14	−100.1	32	9	Preventive	63
51	Guerrero Coast	05/03/2001 04:17	17.13	−100.06	32	8	Preventive	66
50	Guerrero Coast	14/04/2000 20:45	16.88	−100.35	9	5	Preventive	66

(continued)

Table 4.1 Continued

#	Region	NACIONAL SEISMIC SERVICE (SSN), UNAM				SAS FORECAST RESULT		
		Local date-time	Latitude	Longitude	Depth (km)	Sens. Op.	Alert range	Prevention time (s)
49	Guerrero	17/03/2000 18:50	17.08	−99.31	31	7	Preventive	68
48	Puebla-Oaxaca Border	15/06/1999 15:42	18.18	−97.51	69	9	Preventive	15
47	Guerrero	30/05/1999 04:58	17.26	−100.79	53	5	Preventive	68
46	Guerrero	24/04/1999 22:08	17.28	−100.8	27	4	Preventive	68
45	Guerrero Coast	07/09/1998 01:53	16.77	−99.67	12	3	Preventive	
44	Guerrero Coast	09/08/1998 11:18	16.87	−100.25	3	3	Preventive	
43	Guerrero Coast	17/07/1998 06:18	16.98	−100.16	27	7	Public	74
42	Guerrero Coast	05/07/1998 14:55	16.83	−100.12	5	6	Public	66
41	Guerrero Coast	09/05/1998 12:03	17.34	−101.41	18	4	Preventive	60
40	Guerrero	11/03/1998 08:13	17.01	−100.11	40	4	Preventive	
39	Guerrero Coast	21/12/1997 23:22	17.14	−101.24	5	5	Public	69
38	Guerrero Coast	26/08/1997 19:13	16.76	−99.00	28	6	Preventive	45
37	Guerrero	19/07/1997 02:34	17.22	−100.56	51	6	Preventive	56
36	Oaxaca-Guerrero Coast	14/07/1997 20:26	16.39	−98.74	11	3	Preventive	
35	Guerrero Coast	11/07/1997 17:23	16.76	−99.7	10	3	Preventive	
34	Low Balsas River	22/05/1997 02:50	18.41	−101.81	59	4	Preventive	
33	Guerrero	08/05/1997 10:58	17.32	−100.44	12	5	Preventive	55
32	Guerrero	23/03/1997 14:23	17.39	−100.88	31	4	Preventive	
31	Guerrero	21/03/1997 21:49	17.04	−99.76	30	7	Preventive	55
30	Michoacan Coast	11/01/1997 14:28	17.91	−103.04	16	7	Preventive	42
29	Guerrero	27/10/1996 03:15	17.11	−100.9	27	3	Preventive	
28	Guerrero	19/07/1996 04:00	17.35	−100.29	20	6	Preventive	
27	Guerrero Coast	15/07/1996 16:23	17.45	−101.16	20	6	Preventive	65
26	Guerrero Coast	13/03/1996 15:04	16.52	−99.08	18	6	Public	74
25	Guerrero Coast	16/09/1995 10:09	16.4	−98.69	10	2	Preventive	
24	Guerrero Coast	15/09/1995 21:20	16.3	−98.62	10	4	Public	

(continued)

Table 4.1 Continued

		NACIONAL SEISMIC SERVICE (SSN), UNAM				SAS FORECAST RESULT		
#	Region	Local date-time	Latitude	Longitude	Depth (km)	Sens. Op.	Alert range	Prevention time (s)
23	Oaxaca-Guerrero Coast	14/09/1995 08:09				5	Preventive	
22	Oaxaca-Guerrero Coast	14/09/1995 08:04	16.31	−98.88	22	9	Public	72
21	Oaxaca Coast	31/05/1995 06:49	15.97	−98.77	14	2	Preventive	
20	Guerrero Coast	14/04/1995 00:01	16.44	−99.09	15	6	Preventive	
19	Low Balsas River	10/12/1994 10:17	18.02	−101.56	78	6	Preventive	34
18	Guerrero Coast	29/10/1994 10:44	16.97	−99.89	24	9	Preventive	58
17	High Balsas River	22/05/1994 19:41	18.03	−100.57	23	8	Preventive	30
B		16/11/1993 19:11				1	Public (Fail)	
A	Guerrero Coast	24/10/1993 01:52				9	(Fail)	
16	Guerrero Coast	10/09/1993 04:50	16.57	−98.94	20	4	Preventive	70
15	Guerrero	29/07/1993 14:17	17.38	−100.65	43	4	Preventive	
14	Oaxaca-Guerrero Coast	15/05/1993 02:26	16.54	−98.65	20	4	Public	
13	Oaxaca-Guerrero Coast	14/05/1993 21:12	16.47	98.72	15	6	Public	73
12	Oaxaca-Guerrero Coast	14/05/1993 21:09	16.43	−98.74	20	6	Public	65
11	Guerrero Coast	31/03/1993 04:18	17.18	−101.02	8	4	Preventive	
10	Guerrero Coast	09/11/1992 20:13	16.89	−100.1	6	3	Public	
9	Guerrero Coast	04/11/1992 22:33	16.83	−99.66	8	2	Preventive	
8	Guerrero Coast	30/10/1992 02:16	17.14	−100.79	21	3	Preventive	
7	Guerrero Coast	16/10/1992 11:28	16.51	−99.17	17.4	5	Preventive	
6	Guerrero	02/08/1992 06:54	17.13	−100.3	25	6	Preventive	
5	Oaxaca-Guerrero Coast	07/06/1992 11:41	16.22	−98.87	5.2	3	Preventive	
4	Oaxaca-Guerrero Coast	07/06/1992 03:01	16.17	−98.9	2	3	Preventive	
3	Guerrero Coast	15/05/1992 02:35	16.83	−99.98	23	3	Preventive	
2	Guerrero Coast	26/04/1992 14:53	16.78	−100.09	15	4	Preventive	
1	Oaxaca-Guerrero Coast	16/10/1991 12:36	16.83	−100.24	5	1	Preventive	

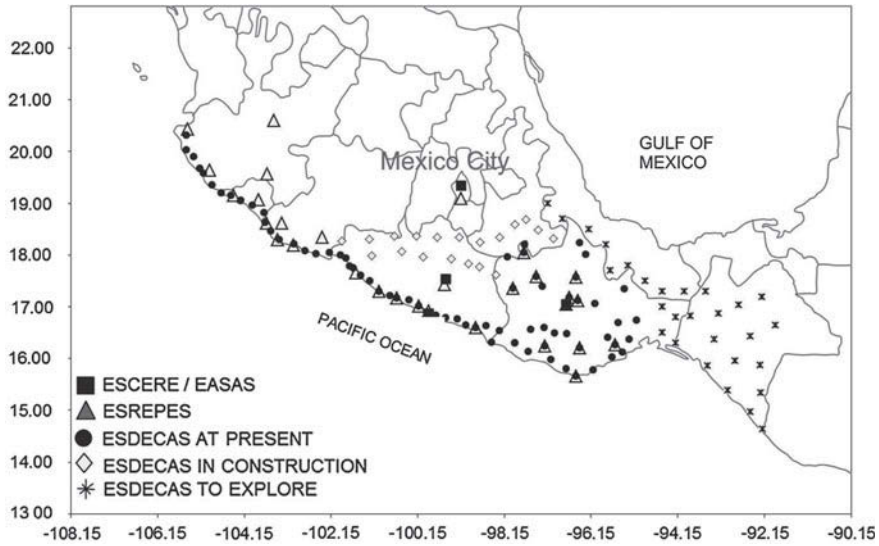

Fig. 4.2 Current topology of SASMEX

4.3 SASMEX Warning Broadcast

After the damages suffered in Mexico City during the 1985 earthquake, the law for Civil Protection and its bylaw were established. Among other requirements, it states that individuals and corporations must design action plans and emergency drills to mitigate vulnerability conditions and reduce the severity of disasters. Each action plan must be registered and certified in presence of municipal or local authorities that also supervise and enforce the regular practice of emergency response procedures (Suárez et al. 2009). The safety and security procedures, as well as the activity of each group in a certain facility, are established accordingly to the display of every building. Distribution of spaces and the identification of the risk and safety zones are considered (Official Gazette of the Federation, 2006; Mexico City Official Gazette 1996).

SASMEX for Mexico City (SAS) has been able to recognize a great number of seismic events, encode their range, and spread warnings as Public or Preventive Alerts. This service operates through three alternative technologies: remotely controlled audio switches installed in radio and TV stations operated by *SAS* that broadcast Public Alert warnings for strong earthquakes; radio receivers that radiate warnings when *SASMEX* emits Preventive and Public Alert signals of strong and moderate earthquakes; and beginning in December of 2008, receivers that include NWR-SAME technology capable of disseminating the Preventive and Public *SAS*'s alerts, as well as other natural disasters' warnings. These warning messages represent a useful service to reduce the vulnerability against a variety of risk conditions. During 2009, in accordance to the Civil Protection of Mexico City Officials

Table 4.2 SASO performance of earthquake early warnings since 2003–2012

		NACIONAL SEISMIC SERVICE (SSN), UNAM				SASO FORECAST RESULT		
#	Region	Local date-time	Latitude	Longitude	Depth (km)	Sens. Op.	Alert range	Prevention time (s)
33	Oaxaca	13/04/2012 08:07	16.22	−98.15	16	12	Public	38
32	Oaxaca	13/04/2012 05:10	16.11	−98.34	14	12	Public	40
31	Oaxaca	02/04/2012 12:36	16.27	−98.47	0	15	Public	40
30	Oaxaca	23/03/2012 19:58	16.26	−98.29	10	5	Preventive	
29	Oaxaca	22/03/2012 17:47	16.48	−98.29	24	13	Public	40
28	Oaxaca	22/03/2012 16:14	16.22	−98.47	9	8	Preventive	
27	Oaxaca	21/03/2012 05:36	16.51	−98.5	20	5	Preventive	
26	Oaxaca	20/03/2012 14:14	16.34	−98.28	15	12	Preventive	
25	Oaxaca	20/03/2012 12:36	16.21	−98.58	14	9	Public	
24	Oaxaca	20/03/2012 12:23	—	—	—	10	Public	
23	Oaxaca	20/03/2012 12:02	16.42	−98.36	15	22	Public	40
22	Oaxaca	04/03/2012 03:58	16.68	−94.4	108	3	Preventive	
21	Oaxaca	11/02/2012 23:56	17.36	−96.51	96	6	Preventive	
20	Oaxaca	15/01/2012 16:49	16.35	−97.83	5	10	Preventive	
19	Oaxaca	30/12/2011 09:47	16.91	−95.37	90	4	Preventive	
18	Oaxaca	16/12/2011 07:02	16.22	−98.3	5	8	Public	
17	Oaxaca	09/07/2011 07:43	15.87	−96.42	22	18	Public	
16	Guerrero	05/05/2011 08:25	16.61	−98.91	11	15	Public	
15	Oaxaca	14/04/2011 11:34	16.7	−95.09	102	5	Public	
14	Veracruz	07/04/2011 08:12	17.2	−94.34	167	23	Public	
13	Oaxaca	05/04/2011 15:18	16.32	−96.15	15	4	Public	
12	Oaxaca	04/02/2011 11:32	17.25	−96.56	76	3	Public	
11	Oaxaca	30/06/2010 02:22	16.22	−98.03	8	22	Public	
10	Oaxaca	16/04/2010 05:01	16.14	−98.41	10	4	Public	

(continued)

Table 4.2 Continued

#	Region	NACIONAL SEISMIC SERVICE (SSN), UNAM				SASO FORECAST RESULT		
		Local date-time	Latitude	Longitude	Depth (km)	Sens. Op.	Alert range	Prevention time (s)
9	Oaxaca	08/02/2010 18:48	15.9	−96.86	37	14	Public	
8	Chiapas	05/07/2007 20:09	16.35	−93.99	113	5	Preventive	40
7	Oaxaca	15/03/2007 07:13	16.08	−97.26	15	6	Preventive	
6	Oaxaca	24/01/2007 22:23	16.21	−97.14	6	2	Preventive	
5	Oaxaca	19/08/2006 00:41	15.91	−97.3	52	8	Public	
4	Oaxaca	15/12/2004 02:05	16.05	−95.43	10	4	Preventive	
B	Oaxaca	18/08/2004 04:03	16.3	−95.12	63	9	(Comx Fail)	
A	Veracruz-Oaxaca	07/08/2004 06:49	17.06	−95.44	112	10	(Fail)	
3	Oaxaca-Guerrero Coast	14/06/2004 17:54	16.31	−98.06	10	6	Public	30
2	Oaxaca Coast	13/01/2004 15:28	16	−97.16	14	10	Public	
1	Oaxaca	13/01/2004 13:50	16.01	−97.16	14	6	Preventive	

(*Secretaría de Protección Civil del GDF*), access to the use of the radio receiver makes mandatory to have an Internal Civil Protection Plan and practice emergency response procedures frequently.

Mexico City since 1992, have pioneered in the use of the *SAS* (Espinosa-Aranda, et al., 1998) beginning with twenty six Elementary Schools of the Ministry of Education of Mexico City (*Secretaría de Educación Pública de la Ciudad de México*). Each facility has an internal plan for civil protection that is systematically practiced and executed whenever *SAS* sends a warning signal to the radio receiver. From 1993 to the date, as stated before, more than 80 elementary, middle, and higher education institutions have been furnished with this equipment.

The Public Electric Transportation System and the METRO have used the *SAS* warnings by means of radio receivers in their control center since 1992, but they do not share the signals with the passengers. In case of a seismic warning, the manager of the control center gives proper instructions for the train operators to stop in the nearest station, or delay their start and keep the doors open for passengers' safety. This is an internal security and emergency procedure that has given great use to the 60 s that *SAS* can offer.

In Mexico, the transmission of radio and TV seismic alert signals began in 1993, through most of the partners of the Association of Broadcasters of the Mexico Valley (*Asociación de Radiodifusores del Valle de México A.C.*) and TV channels 11, 22, 13, and channel 34 in Toluca Valley. To be able of properly disseminate the signals, the broadcasters accepted the use of a remotely controlled switch operated by *SAS*, which substitutes the regular signal for the official alert signal during 60 s in case of a strong earthquake warning. The effectiveness of this resource is optimal in top rating periods because a greater part of the population is warned and can start predefined preventive actions. To date, twenty eight AM, FM and TV channels spread the warnings in Mexico City and Toluca Valley as well as nine radio and two TV stations in Oaxaca City. Also, Emergency Response and Civil Protection Institutions use the radio receiver to prepare emergency vehicles and start the evacuation of their parking lots. There are 13 institutions that use this equipment, including the Red Cross and Firefighters.

Nowadays, *SASMEX for Mexico City (SAS)* serves more than 240 public and private buildings in Mexico City; they receive seismic alert signals through the radio receiver. To guarantee the dissemination of the warning sound, some buildings have displayed loudspeakers arrays where their correct performance should be verified.

In addition to start preventive measures, *SASMEX* signals are used to trigger structural health recording procedures to identify possible damage in buildings.

Since March 27, 2009 at 02:48:32 (local time), when *SAS* emitted a "Preventive Alert" signal, anticipating the effects of the M5.3 earthquake from the coast of Guerrero. Then for the first time *SAS* used the NOAA-SAME technology validating the effective use of this resource. At that time eight monitoring NOAA receivers successfully reacted and provided 58 s of Prevention Time. Nowadays with a technical enhancement to expedite reaction, by reducing receiver's response time, the NWR-SAME with SARMEX protocol helps to mitigate the seismic vulnerability in Mexico.

On April 27, 2009 at 11:46:45 (local time), *SAS* emitted a signal of "Preventive Alert", anticipating the effects of the M5.7 earthquake from the coast of Guerrero. *SAS* confirmed the adequacy to use the NOAA-SAME technology in the city for this purpose. *SASMEX* in Oaxaca has a similar range of users to the one of Mexico City, with the exception of automatic powerful loudspeakers installed in public spaces, which can be heard in the public squares of Oaxaca City. As in Mexico City, Oaxaca and Toluca, in Chilpancingo and Acapulco both Guerrero State cities, received *SAS* warnings in more than 100 users, among radio, TV stations, schools, emergency response institutions and others in 2007. On 20th March 2012, for the earthquake M 7.4 of Oaxaca, SASMEX broadcasted Public Alert Warning to Oaxaca, and Acapulco cities, Chilpancingo and Mexico City, were activated with Preventive Alert Warning range, due to communication issues. On April 13th 2012 SASMEX activated two earthquake early warnings at 05:10:03 08:07:23 (Local Time) for the seismic event M5.2 and 5.1 respectively; with that seismic events, SASMEX for Mexico City worked for first time as an interconnected system.

4.4 The Punta Maldonado Earthquake

The earthquake was located between SAS and SASO seismic station arrays in the Punta Maldonado region with Mw = 7.4, it is noteworthy that on the date of this event, these systems had not yet achieved sensor interface through the link between Mexico City and Oaxaca therefor SAS and SASO's seismic sensor arrays operated in separately way.

The earthquake was detected by 32 seismic stations in Oaxaca and seven in Guerrero. During the first 48 h more than 100 seismic events were recorded under the Llano Grande LG01 seismic station which was closest to the epicenter (Fig. 4.3).

Llano Grande seismic station was the first to detect the earthquake, it is located within 25 km of the hypocenter, the SP time observed was of about 2.6 s. Llano

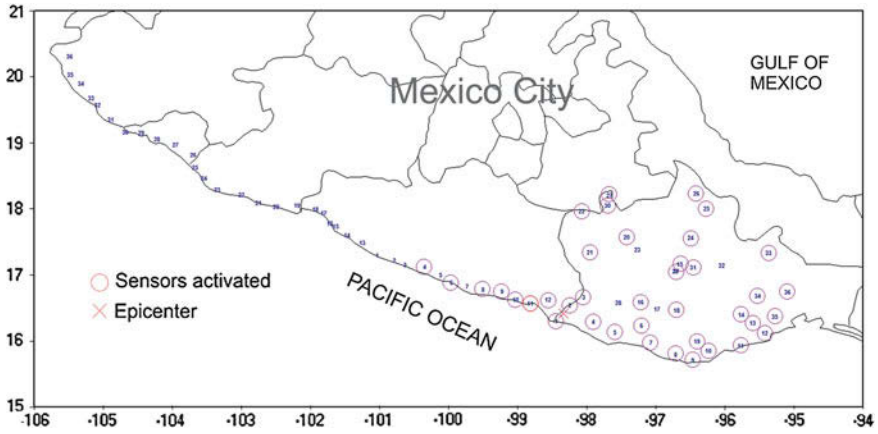

Fig. 4.3 Sensors Activated (*circles*) during the $Mw = 7.4$ earthquake on March 20th, 2012

Table 4.3 Main sequences of SASMEX seismic sensors performance during the Mw = 7.4 earthquake on March 20th, 2012

Local time	Station	Network	Forecast result
12:02:56	LG01	SASO	Strong
12:02:58	MT02	SASO	Strong
12:02:58	Easas Oaxaca	SASO	Public
12:02:59	HU12	SAS	Strong
12:03:03	MA12	SAS	Strong
12:03:03	Easas Acapulco	SAS	Strong
12:03:09	CR10	SAS	Moderate
12:03:09	Easas Chilpancingo	SAS	Preventive
12:03:09	Easas Mexico City	SAS	Preventive
12:03:14	MA11	SAS	Strong
12:03:14	Easas Chilpancingo	SAS	Public

Grande transmitted its power and slope parameters calculated for 2*(S-P) to the city of Oaxaca at 12:02:56, a little more than 5 s after detecting the onset of the P wave, and estimated the event developing as a strong earthquake. The above information began the process of activation of Alert for the city of Oaxaca. MT02-station "Mártires de Tacubaya" confirmed the process, at 12:02:58, 2 s after the previous one, and calculating the parameters of slope and amplitude in the period 2*(S-P) approximately 12 s, conveyed them to the City of Oaxaca, it also predicted strong earthquake, which was the confirmation of the process and prognosis Public Alert activated in Oaxaca.

In Acapulco, the field station HU12-Huehuetán transmitted its parameters with a strong earthquake forecast to 12:02:59. The station was confirmed MA11-Marquelia at 12:03:03 and after calculating the parameters at time 2*(S-P) as HU12, transmitted its parameters a second after the event detected at the beginning of the wave packet P (Table 4.3, Fig. 4.4). This led to the city of Acapulco earthquake also will predict and deliver Strong Public Warning.

Risk parameters and HU12-MA11-Marquelia Huehuetán must be received in Chilpancingo and Mexico City, but due to interference in the stretch of Acapulco and Chilpancingo caused the MA11 data were not recognized. HU12 data were received at 12:02:59 and CR10-"El Carrizo" seismic station transmitted at 12:03:09 parameters once estimated slope parameters and energy in the period 2*(SP) of approximately 16 s (Table 4.2). The station CR10 predicted the earthquake as Moderate. Although, combining strong and moderate earthquake determinations to activate the alert as Preventive, which was issued at Chilpancingo and Mexico City at 12:09:09? During the earthquake, the seismic station Marquelia aired a second time hazard signal, Chilpancingo changed the forecast to Public alert at 12:03:14. The time of opportunity for the city of Acapulco was 25 s, to Oaxaca City 45, to Chilpancingo was estimated to 45 s and finally in Mexico City was of 80 s.

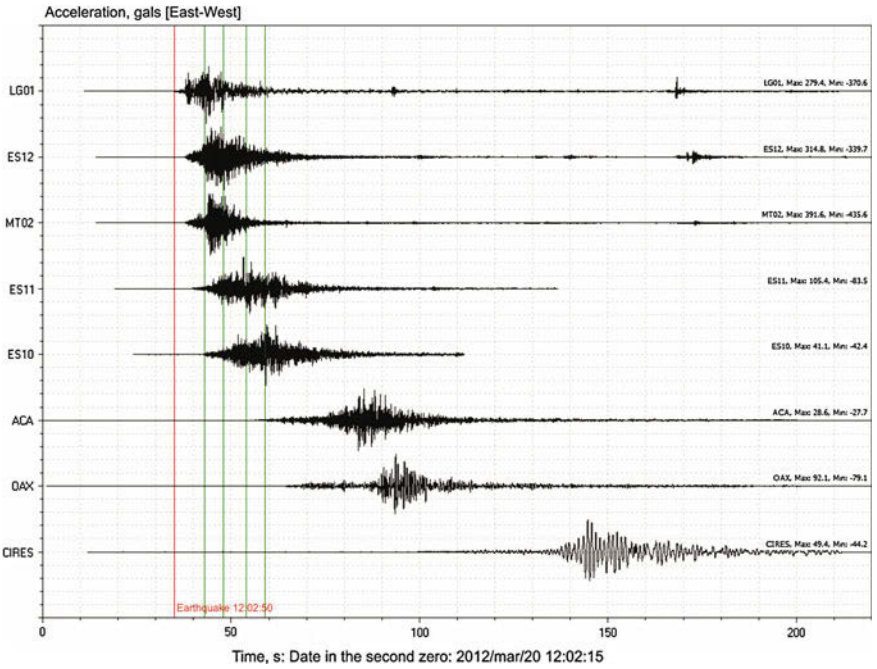

Fig. 4.4 SASMEX performance during the Mw = 7.4 earthquake on March 20th, 2012

4.4.1 Human Response After Activation of the Seismic Alert in Mexico City

During the Preventive Alert warning in Mexico City and given the opportunity time of 80 s civil protection were instrumented procedures and additionally it served to check the effectiveness of the NWR radio receiver SARMEX that had been installed in 640 public schools. Several radio and television broadcasting companies warned their audiences that the alert had been activated and warned with 80 s of opportunity that an earthquake was coming.

In government offices, especially at the House of Representatives, the Federal Electoral Institute documented the reaction of civil defense personnel as well as of the people who were in those buildings; they made use of the seismic alert drills carried out every few months for the case of occurrence of an earthquake.

4.5 Discussion

Since damaging earthquakes are rare, the development of this technological resource has deemed necessary to optimize the reliability and availability indexes of their basic elements in order to guarantee the effective dissemination of alert warnings in the

occurrence of damaging events including forecasting criteria of seismic risk. The *SASMEX* system has its own designs and self-evaluation procedures as well as a continuing technological improvement program aimed to have an assurance of its services. In the design, development and operation of *SAS* and *SASO*, now SASMEX, it is acquired the compromise to improve continuously their subsystems that conform them as well as the processes of detection, computation, communication, forecast and effective broadcast of the warnings in case of earthquake as such as the low-cost NWR-SAME radio receivers with Public alert protocols, SARMEX that includes protocol which improve the activation of NWR receiver for immediately to respond in case of earthquake in order to have the longest time of opportunity possible.

The SASMEX in the process of enlargement and integration envisions a future with federal government support extended to the cities of Chiapas and Veracruz. While Mexico City by soil characteristics and demographics are considered a risk seismic region, there are neighboring cities of seismic hazard zones, which must have notices Seismic Alert System of Mexico. The SASMEX during the earthquake of March 20, 2012, M 7.4 generated earthquake early warnings to Mexico City, Toluca, Acapulco, Chilpancingo and Oaxaca City, giving a time of opportunity at least 25 s in the city of Acapulco, and more than 80 s in Mexico City which warning was disseminated SASPER receptors and SARMEX radio receivers.

Public-oriented discussions together with the proper detection of the earthquake, the reliability of message transmission and the risk evaluation constitute necessary elements in the systems of early warning systems. However, if dissemination and training campaigns launched among the population exposed to natural hazards continue to be insufficiently funded, any early warning system will be exposed to failure to comply with its main objective for which it was designed (United Nations 2006). The technological development of early warning systems applicable to earthquakes is continuously improving and it is convenient to analyze the full spectrum of earthquake early warning. Nevertheless, other high-priority tasks must be reinforced by the authorities, like the diffusion and knowledge of the seismic danger around the city, the continuous program of prevention when the signal of seismic alert is emitted.

Acknowledgments The authors deeply acknowledge the support received from the Mexico City Government Authorities since 1989, originally through its *Secretaría de Obras y Servicios, Comité Directivo del Sistema de Alerta Sísmica,* the *Coordinación General, Secetaría de Educación, Instituto Local de Infraestructura Física Educativa and Secretaría de Protección Civil de la Ciudad de México,* who have decided to apply this technological development, proposed after our 1985 earthquake disaster experience, with the aim to mitigate the seismic vulnerability in the metropolitan population of the Mexico City valley. We are also grateful to *Autoridad del Centro Histórico de la Ciudad de México,* by its valuable sponsorship required to install the radio transmitters system used to disclose via low-cost receivers of the EAS-SAME-Public Alert system the warnings issued by the *SAS* system. We would also like to thank the *Secretaría de Educación Publica* (Public Education Ministry), that supported the *SAS* experimental program since 1992 in some schools of Mexico City; the valuable support from the *Asociación de Radiodifusores del Valle de México*, that since 1993 broadcasts the automatic warnings issued by the *SAS* to the general public; and, the government of Oaxaca, that in 2002, through its *Unidad Estatal de Proteccion Civil*, promoted the *SASO* design and development. Finally but not less, to *Teléfonos de México* (TELMEX) and of *Comisión Federal de Electricidad* (CFE) for their valuable infrastructure support that has expedited the installation

and exploitation of these *SAS* and *SASO* resources. Finally we thank the *Coordinadora Nacional de Protecćión Civil*, *Centro Nacional de Prevención de Desastres (CENAPRED)* and *Secretaría de Seguridad Pública* for its decision and support to coordinate several activities such as to use their telecommunications infrastructure as redundant via to guarantee the SASMEX critical information.

References

Espinosa-Aranda JM, Jimenez A, Contreras O, Ibarrola G, Ortega R (1992) Mexico city seismic alert system. International symposium on earthquake disaster prevention, proceedings CENAPRED-JICA, vol I. Mexico, pp 315–321

Espinosa-Aranda JM, Jimenez A, Ibarrola G, Alcantar F, Aguilar A, Inostroza M, Maldonado S (1995) Mexico city Seismic Alert System. Seismol Res Lett 66(6):42–53

Espinosa-Aranda JM, Rodriguez FH (2003) The Seismic Alert System of Mexico city. International handbook of earthquake and engineering Seismology 81B, International association of Seismology & physics of the earth's interior, committee on education

Espinosa-Aranda JM, Cuellar A, Ibarrola G, Garcia A, Islas R, Maldonado S, Rodriguez FH (2009) Evolution of the Mexican Seismic Alert System (SASMEX). Seismol Res Lett 80(5):694–706

Espinosa-Aranda JM, Cuellar A, Rodríguez FH, Frontana B, Ibarrola G, Islas R, García A (2010) The Seismic Alert System of Mexico (SASMEX): progress and its current applications. Soil Dyn Earthq Eng 31:154–162

Goltz JD, Flores PJ (1997) Real-time earthquake early warning and public policy: a report on Mexico city's Sistema de Alerta Sismica. Seismol Res Lett 68(5):727–733

Kanamori H (2003) Earthquake prediction: an overview. International handbook of earthquake and engineering Seismology 81B, International association of Seismology & physics of the earth's interior, committee on education

Lee WHK, Espinosa-Aranda JM (1998) Earthquake early warning systems: current status and perspectives. International IDNDR-conference on early warning systems for the reduction of natural disasters, Potsdam, Federal Republic of Germany, 7–11 Sept 1998

Mexico City Official Gazette (1996) Reglamento de la Ley de Protección Civil para el Distrito Federal (1996), Gaceta Oficial del Distrito Federal Mexico, 21 Oct 1996

Official Gazette of the Federation (2006) Ley General de Protección Civil (2006) Diario Oficial de la Federación, Mexico, 24 April 2006

Suárez G, Novelo D, Mansilla E (2009) Performance evaluation of the Seismic Alert System (SAS) in Mexico city: a seismological and social perspective. Seismol Res Lett 80(5): 717–726

United Nations (2006). Global Survey of Early Warning Systems An assessment of capacities, gaps and opportunities towards building a comprehensive global early warning system for all natural hazards. United Nations Inter-Agency Secretariat of the International Strategy for Disaster Reduction (UN/ISDR)) Final Version

Chapter 5
Development of Earthquake Early Warning Systems in the European Union

P. Gasparini and G. Manfredi

Abstract Utilization of Earthquake Early Warning Systems (EEWS) in Europe is lagging significantly in respect of pioneer applications in Japan and Mexico. The first reported implementation of a EEWS in Europe is the on-site system designed to protect the Ignalina nuclear power plant in Lithuania. At the beginning of this century, some research groups in Europe started to develop EEW to protect the cities of Istanbul and Bucharest and the territory of Campania, in Southern Italy. Coordinate research effort involving all the groups interested in earthquake early warning started EU FP6 SAFER (Seismic eArly warning For EuRope) project and is continuing with the activities of the EU FP7 REAKT (Strategies and tools for Real Time EArthquake RisK ReducTion) project.

5.1 Introduction

Utilization of Earthquake Early Warning Systems (EEWS) in Europe is lagging significantly in respect of pioneer applications in Japan and Mexico. The first system designed to protect a specific infrastructure, the Shinkansen railway fast transport system, was deployed in Japan in the late sixties. This system evolved into the UrEDAS (Urgent Earthquake Detection and Alarm System) in 1984. It uses the first 3 s of a P-wave to estimate earthquake parameters and to give an alarm. The 1995 Kobe earthquake, which caused extensive and severe damages to viaducts and other structures, prompted the implementation of an improved version called Compact UrEDAS which became operational for railways and metro in 1998. The 2004

P. Gasparini (✉) · G. Manfredi
Universitá di Napoli 'Federico II', Napoli, Italy
e-mail: paolo.gasparini@na.infn.it

P. Gasparini · G. Manfredi
AMRA Scarl, Via Nuova Agnano 11, Napoli, Italy
e-mail: gamanfre@unina.it

F. Wenzel and J. Zschau (eds.), *Early Warning for Geological Disasters*,
Advanced Technologies in Earth Sciences, DOI: 10.1007/978-3-642-12233-0_5,

M6.6 Niigata-Chuetsu earthquake was the first to require the activation of Compact-UrEDAS. It issued a warning 1 s after P-wavedetection, which resulted in electric power shut down and emergency brakes activation on 4 trains moving at the speed of 200 km/h in the epicentral area. Only one carriage of one train derailed with no victim because its speed had been sufficiently reduced (Kanamori 2007; Nakamura et al. 2011).

After the Kobe earthquake the Japanese Government launched the development of a national EEW system. More than 2,000 seismic and strong motion stations were installed with a constant density all over Japan. The Japan Meteorological Agency (JMA) started to test EEW methods extensively in 2004. JMA began EEW national service for advanced users in August 2006 and to the public in October 2007. Mandate and responsibility are clearly defined by the Meteorological Service Law approved in 2009. The EEWS performed efficiently for general public, industries and railways in several cases (Kanamori 2007; Nakamura et al. 2011; Hoshiba et al. 2008).

A seismic alert system (SAS) was implemented in 1991 for Mexico, where damages are produced by large earthquakes occurring in the subduction zone off the Pacific coast at a distance of about 300 km from the capital. The earthquake detector system was aligned parallel to the Pacific, allowing for a warning time of 58–74 s. The warning is used to alert schools, governmental agencies, and some industries (Espinosa-Aranda et al. 1995, 2011).

In Taiwan a network consisting of about 100 accelerometers covers the island with sensors' density similar to that of Japan (1 sensor every 20 km). A virtual sub-network algorithm was developed to locate earthquakes and to calculate their magnitudes using P- and S- wave energy. The system is still in an experimental stage, and a promotion plan aiming at implementing several applications between 2013 and 2016 was developed (Wu and Teng 2002; Hsiao et al. 2009).

An Earthquake Alarm System (ElarmS) was developed and tested in California. It uses the frequency content of the P-waves first detected at any station of a seismic network to estimate earthquake magnitude and arrival times to estimate location. Radial attenuation relations are utilized to predict ground shaking at a given site. The potentiality of the system for several cities of California was estimated (Allen and Kanamori 2003; Allen 2007; Allen et al. 2009).

5.2 EEW in Europe at the Dawn of XXI Century

The first reported implementation of a EEWS in Europe was designed to protect a nuclear power plant. International regulations on the security of nuclear power plant in seismic areas demand that on site accelerometers must be used to monitor Peak Ground Acceleration (PGA). When PGA is higher than a threshold, a system halting the reactor is activated. Systems of this type exist in many nuclear power plants around the world. However they are not EEWS "sensu stricto" as the alert occurs when the PGA exceeds a given threshold value and not before. The on-site system designed to protect the Ignalina nuclear power plant in Lithuania (Wieland et al. 2000) is a

real EEW system. It consisted of six stations encircling the power plant at a radius of 30 km plus a seventh station installed within the plant. The ground motion was measured continuously at each station by three accelerometers and a seismometer. The system generated an alert when the ground acceleration at one station exceeded a threshold value of 0.025 g. The alarm was meant to be used to stop nuclear reactions by the insertion of control rods. The operation required 2.5 s, whereas the alarm arrived at least 4 s before peak ground oscillation if the distance to the earthquake focus was more than 30 km. The Ignalina power plant was completely dismantled on December 31, 2009. No report is available on the performance of the EEWS.

Europe has the potentiality to develop and apply extensively EEW methods. In fact the European territory is covered by many high quality seismic networks, managed by national and European agencies, including local networks specifically designed for seismic early warning. Real time analysis of signals from these networks offers the possibility of implementing EEW for issuing alerts and for giving information useful for after event crisis management, such as real time shake maps and information on expected damage and rapid loss estimation. They can provide emergency managers with a better capability of planning rescue actions based on reliably described scenarios.

The timely information provided by earthquake early warning systems can also be used to forecast the time evolution of an earthquake sequence as well as triggered events, such as landslides and tsunami. This is a relevant feature as a large percentage of the casualties and economic losses resulting from strong earthquakes occurred in the European territory in the last few centuries are due to triggered industrial accidents (such as at Izmit in 1999), tsunamis (e.g. the Messina earthquake in 1908 and the Lisbon earthquake in 1755), fires (e.g. Messina 1908), and landslides (e.g. South Italy earthquakes in 1857). A thoughtful application of EEW systems can be very efficient in reducing such effects. No EEW for the protection of lifelines, transport systems, strategic buildings (hospitals, schools, etc.) is active up to now in Europe.

At the beginning of this century, some research groups in Europe started to develop EEW to protect the cities of Istanbul and Bucharest and the territory of Campania, in Southern Italy.

The EEW system developed for Bucharest takes advantage of the highly localized source of large earthquakes in the Romanian Vrancea zone of the south-eastern Carpathians. The four strong events (M 6.9–7.7) observed during the last century all occurred in the same region at hypocentral distances of ∼160 km. A regional network in the Vrancea region is used to detect earthquakes and issue a warning to industrial facilities in Bucharest, providing 20–25 s warning time (Wenzel et al. 1999; Böse et al. 2007; Marmureanu et al. 2011).

After the north Anatolian fault ruptured close to the Marmara Sea in 1999 generating two catastrophic M 7+ earthquakes and a westward migration of earthquakes along the fault toward Istanbul was forecasted, plans and preparations for the installation of the Istanbul earthquake rapid response and early warning system (IERREWS) for the city were initiated. The system used a dense strong motion network. It was aimed at giving a fast loss estimate (rapid response) and a 8–10 s warning to industrial users in the city (Alcik et al. 2009, 2011; Sesetyan et al. 2011).

The system in Naples (ISNET) was originally designed to give an alert to the Napoli Civil Defence Office within a few seconds or tens of seconds after an earthquake occurrence in the neighbouring Irpinia region, the same area where a disastrous earthquake was generated on the 23rd of November 1980. At present, real time accelerometric data are telemetered to the national Department of Civil Protection in Rome. Information can be used to generate real-time shake maps and damage scenarios to help emergency actions. The whole system is meant to be utilized by other end users (authorities managing fast trains, life lines, hospitals, etc.) to trigger active protection control systems (Weber et al. 2007; Zollo et al. 2009).

The Virtual Seismologist (VS) algorithm was a further approach being developed in Europe and USA (Cua and Heaton 2007). It is a Bayesian approach to regional, network-based earthquake early warning (EEW). Earthquake magnitude, location, and peak ground motion distribution are estimated from observed ground motion amplitudes and triggers, predefined prior information, and appropriate ground motion prediction equations. In the Bayesian approach, incoming observations contribute to continuously updated estimates of EEW information; prior information constrains the EEW estimates at an early stage of the event when not enough observations are available. The VS estimates (magnitude, location, peak ground shaking) are updated each second until no more new picks are reported (Cua and Heaton 2007).

In September 2004, in the framework of the EC FP6 SSA NaRaS (Natural Risk Assessment) Project, a Workshop was organized in Naples, Italy on "Seismic Early Warning of European Cities: toward a coordinated effort to raise the level of basic knowledge". Researchers attending the meeting from eight European countries (France, Germany, Greece, Iceland, Italy, Portugal, Switzerland, Turkey), United States, Taiwan and Japan unanimously approved a recommendation submitted to the European Commission, stressing the still unresolved basic questions for full application of early warning to society's need and asking for future calls to contain specific reference to seismic early warning methods (Gasparini et al. 2007).

The following year a collaboration call focussed specifically on Earthquake Early Warning was issued in the frame of FP6, which was awarded to the SAFER Project.

5.3 The SAFER Project

The SAFER Project (www.saferproject.eu) was carried out between July 2006 and June 2009 by a Consortium including all the European institutions active on EEW and many others with perspective interest in the methodologies. The Consortium was formed by 20 institutes from 11 European and Mediterranean countries (Germany, Italy, Greece, Romania, Switzerland, Norway, France, the Netherlands, Iceland, Turkey and Egypt), and one each from three of the extra European countries most active in this field: i.e. Japan, Taiwan and U.S.A. (Fig. 5.1). The Consortium included universities, governmental and non-governmental research institutes and private companies. It was lead by Jochen Zschau, GFZ German Research Centre for Geosciences, Potsdam, Germany.

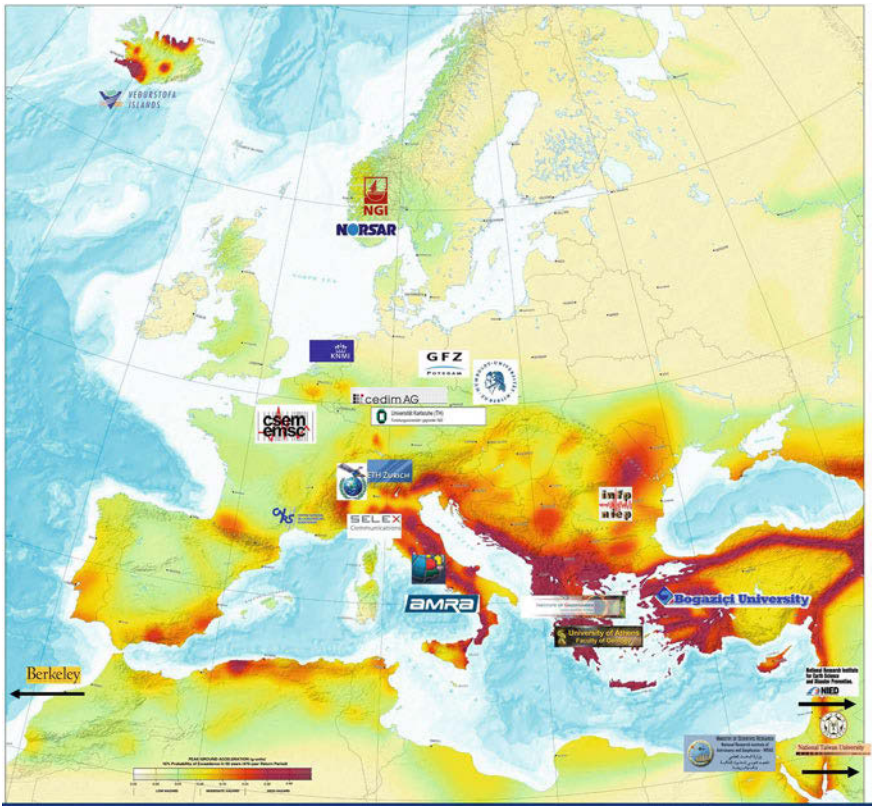

Fig. 5.1 Partnership of the SAFER project

SAFER was strongly multi-disciplinary, calling upon expertise in seismology, structural and geotechnical engineering, informatics, and statistics. Coherently with call requirements SAFER faced only the scientific and technical aspects. Communication, social science and economy issues were not considered. SAFER was strongly linked with pure (e.g. fundamental physics of the Earth's crust under stress) and applied (e.g. response of structures to ground shaking) research.

From the scientific point of view one of the main problems still matter of debate was the forecasting of the magnitude of an earthquake based on the information given by the first 3 s of P-waves. The most used parameters were the dominant frequency (τcmax), the average frequency (τc) or the peak displacement (Pd). The application to M $>$ 6 earthquakes was of major concern as the rock fracturing will still be in progress when the forecasting is done (Allen and Kanamori 2003; Kanamori 2005; Wu and Kanamori 2005).

Once the magnitude and location of an earthquake have been determined, the expected peak ground shaking at a given location must be rapidly determined to trigger early warning actions. Preliminary alert maps should be generated and near

real time shake maps should be produced for rapid response. Methodologies for the implementation of these procedures were under way in Japan and California.

The implementation of automated actions for engineering applications required the development of automatic decision making tools for each application based on estimates of uncertainties, and of the expected consequences of false and missed alarms. Facing of all these problems was just starting at the beginning of SAFER.

The general objective of SAFER was to develop tools for effective earthquake early warning that can be used for disaster management in Europe and, particularly, in Europe's densely populated cities.

SAFER meant to achieve the general objective through:

(a) the development and implementation of improved algorithms for the fast determination of earthquake source parameters (event location, as well as new approaches for fast magnitude/moment determinations based on strong motion data, modern seismic array technology and the concept of energy magnitude) combining the conflicting demands of rapidity and reliability;
(b) further elaboration of innovative concepts for providing in an evolutionary process real-time alert maps and predicted shake maps within seconds and minutes;
(c) the development of fast algorithms for damage scenario simulations, including forecasting of aftershock time evolution and of earthquake triggered effects (such as tsunamis and landslides);
(d) deployment of decision making procedures for engineering applications of EEW to the real time protection of endangered structures and devices;
(e) applications to selected test cities (Athens, Bucharest, Cairo, Istanbul Napoli).
(f) a selection of the main achievements of the project is here reported.

(a) Earthquake Size and Damage Potential Now Available Within a Few Seconds

Knowing the size (magnitude) of an earthquake in real-time is essential for rapidly estimating the damage potential, deciding whether an alarm needs to be issued, and initiating appropriate response measures. SAFER has explored the information on this parameter that can be extracted from the first few seconds of the fastest seismic wave, the P-wave. In particular, it has provided a novel method that does not only estimate the magnitude of an event within a few seconds, but for the first time also offers the related probabilities which tell the users how reliable the estimate really is. In addition, the method follows an evolutionary approach meaning that as more data become available (longer time series, more triggered seismic stations), the reliability of the inferred earthquake size information improves. PRESTo (Probabilistic and Evolutionary Early Warning System), a tool developed within SAFER, has these features. It is rapid, reliable and provides the related uncertainties allowing appropriate decisions to be made for mitigating actions (Zollo et al. 2009; Satriano et al. 2010).

Related to the determination of the earthquake size, SAFER has also been successfully testing a new method for obtaining the first rough estimate of the damage potential of an earthquake in near real-time, i.e. even before the earthquake hits or

immediately after, when generally there is no other information available on the extent of the damage to be expected. The quantities necessary for estimating the damage potential can be obtained from the first 3 s of the P-wave (Convertito et al. 2009).

(b) The Real-time "Shake Map" Technology is Now Implemented in Large Cities of Europe

"Shake Map" is a method that allows to produce maps of peak earthquake ground shaking in real time from information available within seismic networks. If this information comes from the first P-wave arrival before the real ground shaking has reached its peak level, scientists will talk about "alert maps". In this case the peak ground shaking is predicted and not measured. Both "alert maps" (predicted) and "shake maps" (measured) are important components of the seismic early warning- and rapid response chain because they can contribute to activate disaster mitigation actions within seconds to minutes after the onset of an earthquake.

In Europe the capability of deriving "alert maps" and "shake maps" from seismic data in real-time did not exist before the start of the SAFER-project in 2006. SAFER in close co-operation with the EU-project Network of Research Infrastructures for European Seismology (NERIES) has now implemented this technology in the test cities Istanbul, Bucharest, Naples and Cairo, and by this and after having carefully applied appropriate regional calibrations, has considerably improved the seismic early warning capability in these metropolitan areas (Erdik et al. 2011; Köhler et al. 2009).

(c) Towards a People Centred Early Warning System

The success of EEW systems is very much dependent on how accurately the ground shaking due to an earthquake can be determined in real-time. Serious limitations for this come from the spacing between seismometers in a classical set up of seismic networks which requires interpolation of ground shaking and by this may introduce large uncertainties. The spacing between seismometers cannot easily be reduced mainly due to economical reasons.

SAFER, therefore, proposes a completely new generation of early warning systems, based on low-cost sensors (taken from the air-bag system of the car industry) that are connected and wireless communicating with each other in a decentralized people- centered and self-organizing observation- and warning network.. "Decentralized" means that the total information available in the network will not only be transmitted to a warning centre but will also be available at every node of the network. "People centered" means that people can afford to buy their own sensor and by installing it in their home may not only gain from, but also contribute to the warning network. This would ensure the dense coverage of an urban area with early warning sensors, not tens or hundreds, but thousands or ten thousands, which is necessary to gather accurate warning information. The system has to be "self-organizing" in order to automatically adapt to changes in the network configuration if, for instance, the number of users will increase, or some of the network sensors will fail as a consequence of a strong earthquake.

The prototype of such a low-cost and self-organizing system has been developed in the frame of SAFER and has been successfully tested in the city of Istanbul. It has also been applied to monitoring the health state of critical infrastructures such as the Fatih Sultan Mehmet Suspension bridge across the Bospouros or certain buildings in L'Aquila (Italy) after the strong earthquake of April 6th, 2009. Although the number of nodes for which the network has been configurated at present is still conventional, Self-Organizing Seismic Early Warning Information Network (SOSEWIN) as the system is called, has opened a novel avenue for seismic early warning that is extremely promising (Fleming et al. 2009; Picozzi et al. 2008).

(d) When an Early Warning Should be Issued?

Engineering applications of EEW need to be designed in a way to minimize the cost of false alarms. The design is specific for each application and location.

For example, the economic consequences from stopping a train can be different in different countries, and they are certainly different from those of shutting down a gas line. The level of acceptance of a false alarm is the leading decisional parameter for every action to be taken on the basis of early warning. SAFER developed a fully probabilistic framework for applications of earthquake early warning based on cost-benefit analysis. The procedure starts from the real-time prediction of ground motion parameters, including the check of the sensitivity of the EW information to uncertainties in estimations of magnitude and distance. The decision whether to issue an alarm or not is made automatically at each site and for each application using a decisional rule.

For example, assuming that the predicted ground motion intensity measure is the PGA, a simple rule may consist of issuing the alarm if the probability that a critical peak ground motion value will be exceeded is larger than a pre-fixed threshold. The critical peak ground motion and the probability threshold may be established on the basis of cost/benefits and the analysis of the consequences so that the risk reduction provided by the alarm will be higher that the consequences of a false alarm (Iervolino et al. 2009; Iervolino 2011).

A decisional methodology was developed and applied to the Campania region, but the concepts and algorithms are of general use. Using a simple model of earthquake source, and the available warning times, an estimate was made of the possible risk reduction actions on the Campania territory.

AMRA produced EaRly warninG demO (ERGO), a visual terminal installed at the Faculty of engineering of the University of Naples Federico II on July 25 2008 and has continuously operated since then. ERGO processes in real-time the accelerometric data and it is able to issue an alarm in the case of events occurring with magnitude larger than 3 in the southern Apennines region. The terminal includes a panel showing the time evolution of the Probability Density Functions of PGA at the site, computed from the information on magnitude and distance by the Irpinia EEW network. The terminal also indicates, during the lead time, the time variations of the probability that the critical PGA value will be exceeded, along with the residual warning time and the probability of false alarms.

(e) Improving the Earthquake Early Warning Capabilities in Five Euro- Mediterranean Cities

Five major earthquake-prone cities have been identified as test areas; Athens, Bucharest, Cairo, Istanbul, Naples. All these cities in recent years have experienced severe earthquakes. These cities either have acquired, or are in the process of acquiring earthquake early warning systems. They offer a range of different challenges to the SAFER project, as they are threatened by earthquakes generated in different tectonic environment and at different distances. For example, Bucharest is severely affected by earthquakes occurring in a subducting slab underneath the Vrancea region, 150 km north of the city. They occur in a restricted area and depth range, and the involved distances allow warning times in the order of 30 s. In contrast, Istanbul is only a few tens of kilometres off the Marmara Sea segments of the North Anatolian strike-slip fault, and warning times may be less than 10 s. Both of these cities are expected to experience the effects of events of $M > 7$. Naples is located close to another seismotectonic setting. It is about 80 km away from the nearest crustal dip-slip faults of the Apennine range. The seismic early warning network can provide the city of Naples with about 20 s alert time.

Cairo, on the other hand, is expected to experience earthquakes generally less than M6. However, due to the extreme seismic vulnerability its earthquake risk is high. In 1992 a moderate earthquake of magnitude 5.8 caused 561 deaths, 9832 injured and left a direct economic damage of more than 35 million US$. This earthquake had happened on the Dahshour zone, one of two seismic zones directly covering parts of Greater Cairo. The other zone is the Cairo Suez district that is as well able to generate earthquakes above magnitude 5.5.

SAFER contributed to the advancement of EEW and real-time risk reduction for each test city in a different way, given the great differences in the tectonic and geological situation, the characteristics of available seismic/accelerometric networks and the existing level of information on vulnerability.

5.4 The REAKT Project

The REAKT (Strategies and Tools for Real Time Earthquake Risk Reduction) (www.reaktproject.eu) is a follow up and an enlargement of SAFER. In fact it conveys the experience gained and the results of former FP6 and running FP7 project on seismic risk (SAFER, NERIES, NERA, SHARE, SYNER-g) to establish the best practice on how to use jointly all the information coming from earthquake forecast, early warning and real time vulnerability assessment for real time risk mitigation (Fig. 5.2).

The REAKT project started on September 1, 2011 and has a duration of 36 months. REAKT consortium is formed by 23 partners, 18 coming from ten European countries and one each from Barbados, Jamaica, Japan, Taiwan and United States. Many of them had participated to SAFER and the other above mentioned project. The Consortium is lead by Paolo Gasparini, AMRA Scarl, Napoli.

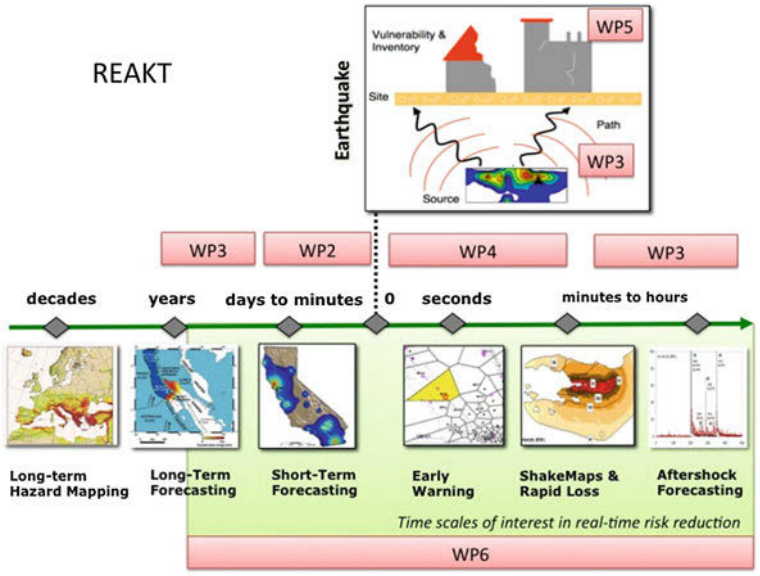

Fig. 5.2 Sketch of the different components and different time scale to be integrated in the used system level approach

REAKT aims to address the issues of real-time earthquake hazard estimation and emergency response from end-to-end, with work packages focused on operational earthquake forecasting, earthquake early warning (EEW), real-time vulnerability systems, and optimized end-user decision-making with uncertain information. This will be pursued through the following specific objectives:

- a better understanding of physical processes underlying seismicity changes on a time scale from minutes to months;
- the development, calibration and testing of models of probabilistic earthquake forecasting and the investigation of its potential for operational earthquake forecasting;
- the development of time-dependent fragility functions for buildings, selected infrastructures, and utility systems;
- the development of real time loss estimation models over the lifetime of structures and systems due to foreshocks, main shocks and their subsequent aftershock sequences;
- the construction of a detailed methodology for optimal decision making associated with an earthquake early warning system (EEWS), with operational earthquake forecasting (OEF) and with real time vulnerability and loss assessment in order to facilitate the selection of risk reduction measures by end users;
- the study of the content and way of delivering public communication, recognizing the value of a degree of self-organization in community decision making;
- the application of real time risk reduction systems to different situations.

REAKT will use a system-level earthquake science approach that requires that the various temporal scales of relevance for hazard and risk mitigation in the various WPs are integrated through common tools, databases and methods (as sketched in Fig. 5.2).

- the development of off-line testing and implementation of a new approach for early warning where the network-based and on-site methods are integrated and used in the very first seconds after a moderate to large earthquake to map the most probable damaged zones;
- a new threshold-based approach representing a step forward in respect of the presently developed EEW methodologies. It allows to by-pass the problems and uncertainties related to the real-time magnitude and peak motion predictions through empirical ground motion equations;
- the real-time Virtual Seismologist (VS) and PRESTo algorithms, developed in the FP6 SAFER Project, will be extended from an EEW approach to a more generalized earthquake information system with continuous characterization of uncertainty as a function of time from the earthquake origin;
- new functionalities of the real-time VS codes, with a focus on real-time;
- test installations in Switzerland and other European test sites, and the PRESTo algorithm will be developed to include the threshold based approach, with application in southern Italy and Turkey;
- the possibility of predicting the frequency content by an EEW (also integrating the on-site and regional/hybrid EEW) will be investigated;
- a life cycle-cost approach will be developed to evaluate the performance of semi-active EEW driven control systems vs. passive control systems (e.g. seismic isolation);
- study of feasibility, design and off line testing of a mobile early warning system to be rapidly implemented during seismic crises;
- SOSEWIN system will be adapted to monitor on going damages within buildings during seismic crises, with the integration of a digital video camera.

The ten industrial facilities selected as test sites include the SINES industrial complex in Portugal, nuclear plants in Switzerland, power plants and power transmission systems in Iceland, natural gas distribution networks and the Fatih Sultan Mehmet bridge in Istanbul, a section of the Circumvesuviana railway in Campania, Italy, the Rion-Antirion bridge in Patras, and the port and AHEPA hospital in Thessaloniki. The feasibility of a regional EEW system to protect industrial facilities in the Eastern Caribbean is also being investigated. Some end-users are interested in in-depth feasibility studies for use of real-time information and development of rapid response plans, while others intend to install real-time instrumentation and develop customized automated control systems to initiate damage-mitigating actions in the event of strong shaking. From the onset, REAKT scientists and end-users will work together on concept development and initial implementation efforts using the data products and decision-making methodologies developed in the various work packages, with the goal of improving end-user risk mitigation. The aim of this scientific/end-user partnership is to ensure that scientific efforts are applicable to operational, real-world

problems. The close collaboration between scientific and end-user partners, from the beginning of the project, is among the innovative aspects of REAKT.

SAFER and REAKT created a core community of top European seismologists and engineers working in the field of EEW. The requests that the SAFER research group is continuously receiving to organize meetings or to present the results to international meetings, shows that SAFER and REAKT are quite visible and well considered even in countries, like Japan, who are the traditional leaders in this field.

Both projects prompted the exchange of information and methodologies amongst most of the European institutions running local seismic networks for early warning and amongst the research groups active in this field. The projects attracted more than 40 young researchers, an European young community able to continue and forward the research in this field.

Acknowledgments This paper is a contribution from the EC FP7 REAKT project.

References

Kanamori H (2007) Real time earthquake damage mitigation measures. In: Gasparini P, Manfredi G, Zschau J (eds) Earthquake early warning systems. Springer, Berlin, pp 1–8. ISBN-13 978–3-540-72240-3

Nakamura Y, Saita J, Sato T (2011) On an earthquake early warning system (EEWS) and its applications. Soil Dyn Earthq Eng 31:127–136. doi:10.1016/j.soildyn.2010.04.012

Hoshiba M, Kamigaichi O, Saito M, Tsukada S, Hamada N (2008) Earthquake early warning starts nationwide in Japan. EOS 89:73–80

Kamigaichi O, Saito M, Doi K, Matsumori T, Takeda K, Shimoyama T, Nakamura K, Kiyokoto M, Watanabe Y (2009) Earthquake early warning in Japan: warning the general public and future prospects. Seismol Res Lett 80:717–726

Doi K (2011) The operation and performance of earthquake early warnings by the Japan meteorological agency. Soil Dyn Earthq Eng 31:119–126 doi:10.1016/j.soildyn. 2010.04.012

Espinosa-Aranda JM, Jimenez A, Ibarrola G, Alcantar F, Aguilar A, Inostroza M, Maldonado S (1995) Mexico city seismic alert system. Seismol Res Lett 66:42–52

Espinosa-Aranda JM, Cuellar A, Rodriguez FH, Frontana B, Ibarrola G, Isals R, Garcia A (2011) The seismic alert System of Mexico (SASMEX): progress and its current applications. Soil Dyn Earthq Eng 31(2):154–162

Wu YM, Teng TL (2002) A VSN approach to earthquake early warning. Bull Seismol Soc Am 92:2008–2018

Hsiao NC, Wu YM, Shin TC, Zhao L, Teng TL (2009) Development of earthquake early warning system in Taiwan, Geophys. Res. Lett 36:L00B02. doi:10.1029/2008GL036596

Allen RM, Kanamori H (2003) The potential for earthquake early warning in southern California. Science 300:786–789

Allen RM (2007) The ElarmS earthquake early warning methodology and its application across California. In: Gasparini P, Manfredi G , Zschau J (eds) Earthquake early warning systems. Springer, pp 21–44. ISBN-13 978–3-540-72240-3

Allen RM, Gasparini P, Kamigaichi O, Böse M (2009) The status of earthquake early warning around the world: an introductory overview. Seismol Res Lett 80(5):682–693. doi:10.1785/gssrl.80.5.682

Wieland M, Griesser L, Kuendig C (2000) Seismic early warning system for a nuclear power plant. In: Proceedings of 12th world conference on earthquake engineering. Auckland, New Zealand

Wenzel F, Oncescu M, Baur M, Fiedrich F, Ionescu C (1999) An early warning system for Bucharest. Seismol Res Lett 70(2):161–169

Böse M, Ionescu C, Wenzel F (2007) Earthquake early warning for Bucharest, Romania: novel and revised scaling relations. Geophys Res Lett 34:L07302. doi:10.1029/2007GL029396

Marmureanu A, Ionescu C, Cioflan CO (2011) Advanced real-time acquisition of the Vrancea earthquake early warning system. Soil Dyn Earthq Eng 31(2):163–169

Alcik H, Ozel O, Apaydin N, Erdik M (2009) A study on warning algorithms for Istanbul earthquake early warning system. Geophys Res Lett 36:L00B05. doi:10.1029/ 2008GL036659

Alcik H, Ozel O, Wu YM, Ozel NM, Erdik M (2011) An alternative approach for the Istanbul earthquake early warning system. Soil Dyn Earthq Eng (Special Issue Earthquake Early Warning) 31:181–187

Sesetyan K, Zulfikar C, Demircioglu MB, Hancilar U, Kamer Y, Erdik M (2011) Istanbul earthquake rapid response system: methods and practices. Soil Dyn Earthq Eng (Special Issue Earthquake Early Warning) 31:170–180

Weber E, Convertito V, Iannaccone G, Zollo A, Bobbio A, Cantore L, Corciulo M, Di Crosta M, Elia L, Martino C, Romeo A, Satriano C (2007) An advanced seismic network in southern apennines (Italy) for seismicity investigations and experimentation with earthquake early warning. Seismol Res Lett 78(6):622–634. doi: 10.1785/gssrl.78.6.622

Zollo A, Iannaccone G, Lancieri M, Cantore L, Convertito V, Emolo A, Festa G, Gallovic F, Vassallo M, Martino C, Satriano C, Gasparini P (2009) Earthquake early warning system in southern Italy: methodologies and performance evaluation. J Geophys Res 36:L00B07. doi:10.1029/2008GL036689

Cua G, Heaton T (2007) The virtual Seismologist (VS) method: a Bayesian approach to earthquake early-warning. In: Gasparini P, Manfredi G, Zschau J (eds) Earthquake early warning systems. Springer, Berlin. pp 97–132. ISBN-13 978–3-540-72240-3

Gasparini P, Manfredi G, Zschau J (eds) (2007) Earthquakes early warning systems. Springer, Berlin, 350 pp. ISBN: 978-3-540-72240-3

Kanamori H (2005) Real-time seismology and earthquake damage mitigation. Annu Rev Earth Planet Sci 33:195–214

Wu YM, Kanamori H (2005) Experiment on an onsite early warning method for the Taiwan early warning system. Bull Seismol Soc Am 95:347–353

Satriano C, Elia L, Martino C, Lancieri M, Zollo A, Iannaccone G (2010) PRESTo the earthquake early warning system for Southern Italy : concepts, capabilities and future perspective. Soil Dyn Earthq Eng doi:10.1016/j.sildyn.2012.06.008

Convertito V, De Matteis R, Cantore L, Zollo A, Iannaccone G, Caccavale M (2009) Rapid estimation of ground-shaking maps for seismic emergency management in the Campania region of southern Italy. Nat Hazards. doi:10.1007/s11069-009-9359-2

Erdik M, Sesetyan K, Demircioglu MB, Hancilar U, Zulficar C (2011) Rapid assessment after damaging eartquakes. Soil Dyn Earthq Eng (Special Issue Earthquake Early Warning) 31: 247–266

Köhler N, Cua G, Wenzel F, Böse M (2009) Rapid source parameter estimations of Southern California earthquakes using PreSEIS. Seismol Res Lett. doi:10.1785/gssrl.80.5.743

Fleming K, Picozzi M, Milkereit C, Kuehnlenz F, Lichtblau B, Fischer J, Zulfikar C, Ozel O, the SAFER and EDIM working groups (2009) The Self-organising seismic early warning information system (SOSEWIN). Seismol Res Lett 80(5):755–771

Picozzi M, SAFER and EDIM work groups (2008) Seismological and early warning activities of the SOSEWIN, Geophysical Research Abstracts, Vol. 10, EGU2008-A-07001, EGU General Assembly

Iervolino I, Giorgio M, Galasso G, Manfredi G (2009) Uncertainty in early warning predictions of engineering ground motion parameters: what really matters? Geophys Res Lett 36:L00B06. doi:10.1029/2008GL036644

Iervolino I (2011) Performance-based earthquake early warning. Soil Dyn Earthq Eng 31(2):209–222

Chapter 6
EDIM: Earthquake Disaster Information System for the Marmara Region, Turkey

F. Wenzel, M. Erdik, N. Köhler, J. Zschau, C. Milkereit, M. Picozzi, J. Fischer, J. P. Redlich, F. Kühnlenz, B. Lichtblau, I. Eveslage, I. Christ, R. Lessing and C. Kiehle

Abstract The Istanbul Earthquake Early Warning and Rapid Response System has been established in the aftermath of the 1999 Kocaeli earthquake, and represents one of the few examples of operational earthquake warning systems in Europe. Several new methodologies and technologies have been developed in the 'environment' of this existing system in order to improve early warning but also validate methods and compare progress with the existing technology. Main improvements refer to testing and optimizing the existing system with a realistic catalogue of accelerograms, development of a self-organizing and distributed observational system in terms of hardware and communication software, and utilization of information technology. We thus improved the three relevant pillars of the early warning methodologies: Monitoring, warning, and communication.

F. Wenzel (✉) · N. Köhler
Geophysical Institute, Karlsruhe Institute for Technology (KIT), Hertzstr. 16,
76187 Karlsruhe, Germany
e-mail: friedemann.wenzel@kit.edu

J. Zschau · C. Milkereit · M. Picozzi
Deutsches GeoForschungsZentrum Postdam, Telegrafenberg, 14473 Potsdam, Germany

J. Fischer · J. P. Redlich · F. Kühnlenz · B. Lichtblau · I. Eveslage
Computer Science Department, Humboldt University Berlin, Rudower Chaussee 25,
12489 Berlin, Germany

I. Christ · R. Lessing
DELPHI IMM Gmbh, Friedrich-Ebert-Str. 8, 14467 Potsdam, Germany

C. Kiehle
lat/lon GmbH, Aennchenstr. 19, 53177 Bonn, Germany

M. Erdik
Kandilli Observatory and Earthquake Research Institute (KOERI), Bogazici University,
81220 Istanbul, Turkey

F. Wenzel and J. Zschau (eds.), *Early Warning for Geological Disasters*,
Advanced Technologies in Earth Sciences, DOI: 10.1007/978-3-642-12233-0_6,

6.1 Introduction

The main objectives of EDIM were the enhancement of the existing Istanbul Earthquake Early Warning System (IEEWS) with a number of scientific and technological developments, which establish a transferable methodology and technology for early warning systems in general. The project focused on three topics: (1) analysis of and options for the improvement of the current IEEWS; (2) development of a self-organising sensor system and the exploration of its application potential to early warning and other items; (3) development of a geo-information infrastructure tuned to early warning purposes. These developments took place in the frame of the Istanbul system which allows testing the novel methodologies and studying their options for operational use. A critical condition for this was the close partnership with the Kandilli Observatory and Earthquake Research Institute (KOERI, Professor Mustafa Erdik).

EDIM is structured in three work packages dealing with real-time information from regional accelerometer networks (Work package A), the self-organising sensor system (Work package B); the geo-information infrastructure (Work package C). Project partners are the Karlsruhe Institute for Technology (KIT), Deutsches GeoForschungsZentrum Potsdam (GFZ), Humboldt Universität zu Berlin, Institut für Informatik, DELPHI Informationsmuster und Management GmbH, Potsdam, und lat/lon GmbH, Bonn.

6.2 Enhancement of the Current Early Warning System (KIT)

In order to study the performance of the current system and its expansion to the Marmara Sea region an accelerometric data set had to be generated. As the available strong motion data base in Western Turkey contains mostly events of the 1999 Kocaeli earthquake and subsequent aftershocks, and only few small magnitude events in the Marmara Sea appropriate data had to be synthesized. This data set consists of accelerograms for 280 earthquakes with magnitudes between 4.5 and 7.5 that are distributed in the Marmara Sea and the adjacent areas in a way that is compatible with historical seismicity. The accelerograms are simulated with FINSIM, which allows stochastic simulation of finite sources (Beresnev and Atkinson 1997). The program has been modified in order to include P-waves with special emphasis on the first few seconds which are relevant for early warning. A major effort has been made to make the synthesized data compatible with the observational data base. In addition we assured that the synthetic data fit the most recently developed attenuation relations for Western Turkey. Figure 6.1 shows the distribution of epicenters for the synthetic data set and also the location of the existing early warning stations (black triangles), as well as locations of early warning stations to be used in the future.

With this data base different options for warning systems could be evaluated. In a first step we studied the performance of the existing threshold based warning

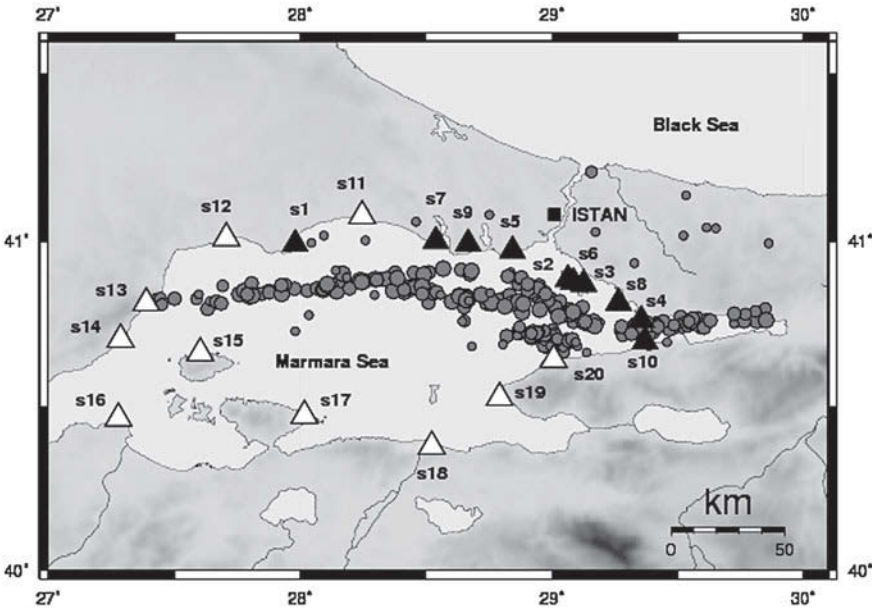

Fig. 6.1 Distributions of epicenters for the synthetic data set and location of the existing early warning stations (*black triangles*), as well as foreseen station locations (*white triangles*)

system. The IEEWS comprises 10 real-time three-component accelerometric sensors distributed along the shoreline of the Sea of Marmara (Fig. 6.1). The current system is based on three trigger thresholds that need to be exceeded at three or more sensors within 5 s before a warning is declared. The current thresholds are 0.02, 0.05 and 0.1 g, corresponding to warning class I, II, and III (Erdik et al. 2003). The current values have been chosen based on expert judgement without a clear quantitative relationship to the expected ground motion in Istanbul. In a first step we optimized these thresholds with the given station locations. For evaluation we used the criteria of properly classifying the events in three classes of ground motion in Istanbul and of the possibly shortest early warning time, with emphasis on the large events. For optimization a Genetic Algorithm has been used. The procedure is described in detail in Oth et al. (2010). It turns out that the trigger thresholds should be modified from the values given above to 0.03, 0.12 and 0.16 g. With this selection it is assured that all earthquakes which exceed a ground motion in Istanbul in excess of 0.12 g are classified as III and all smaller events are properly identified. The average warning time ranges between 5–6 s, but can as large as 20 s in certain cases. Another attempt has been made to optimize station locations and find optimum sites for ocean-based recording systems (ocean-bottom seismometer—OBS).

The early warning algorithm preSEIS, developed by Böse et al. (2008) had not been thoroughly tested before so that this became an important step in terms of evaluating its operational capacity. preSEIS is a neural network-based approach for early

warning and has been compared with the 'virtual seismologist' approach to Southern Californian data (Köhler et al. 2009a). In addition preSEIS has been tested with data of the Japanese K-NET network where 69 earthquakes in the magnitude range of 3.8–7.2 have been selected; 66 of those were used for training and 3 were tested for early warning. This real-date example provides very good performance values for preSEIS (Köhler 2010). preSEIS is used in the context of the IEEWS as a benchmark system, which is assumed to provide the best possible performance of an early warning system, against which different installations of instruments or other warning types such as the actual used threshold based method can be compared. With this approach the added value of the installation of additional stations could be studied. The additional foreseen installation would improve the early warning time by second to seconds. However, it requires a change in threshold values (Köhler et al. 2009b).

The availability of a high quality synthetic data set allows simulating scenario earthquakes such as the 1509 earthquake. This earthquake had a magnitude of 7.3 and caused severe damage in the Istanbul area. Presumably a 70 km long segment ruptured. Using the damage estimation service developed by DELPHI in the context of EDIM the damage that would occur on the nowadays building structure in Istanbul could be estimated for the scenarios.

6.3 The Self-Organizing Seismic Early Warning Information System (GFZ Potsdam)

The Helmholtz Centre Potsdam GFZ German Research Centre for Geosciences, as part of its commitment to the EDIM project and in cooperation with the Humboldt Universität zu Berlin (HUB), developed the Self-Organising Seismic Early Warning Information Network (SOSEWIN). SOSEWIN is a completely new generation of early warning systems, based on low-cost sensors (taken originally from the air-bag system of the car industry) that are connected and wireless communicating with each other in a decentralized people- centred and self-organizing observation- and warning network. The vision for the future is to integrate SOSEWIN into existing standard seismic early warning (EW) and seismological monitoring systems (Fig. 6.2).

Furthermore, dedicated software was developed with the primary goal of performing real-time seismological analysis for seismic EW (Fig. 6.3). Considering the early warning requirement of issuing ground-motion estimates as quickly as possible, the general scheme designed for real-time processing involves local, relatively simple, rapid, and robust analysis of data (Fig. 6.3). The SOSEWIN's analyses of the earthquake's initial *P* waves allow the event detection, as well as the estimation of parameters that allow some indication of the severity of the ground motion, and the epicentral area localization. Moreover, in cooperation with the HUB, a decentralized decision-making approach, which is termed 'Alarming Protocol' and where the information obtained by the single SOSEWIN nodes are combined and used for seismic early warning purposes, was developed (Fig. 6.3).

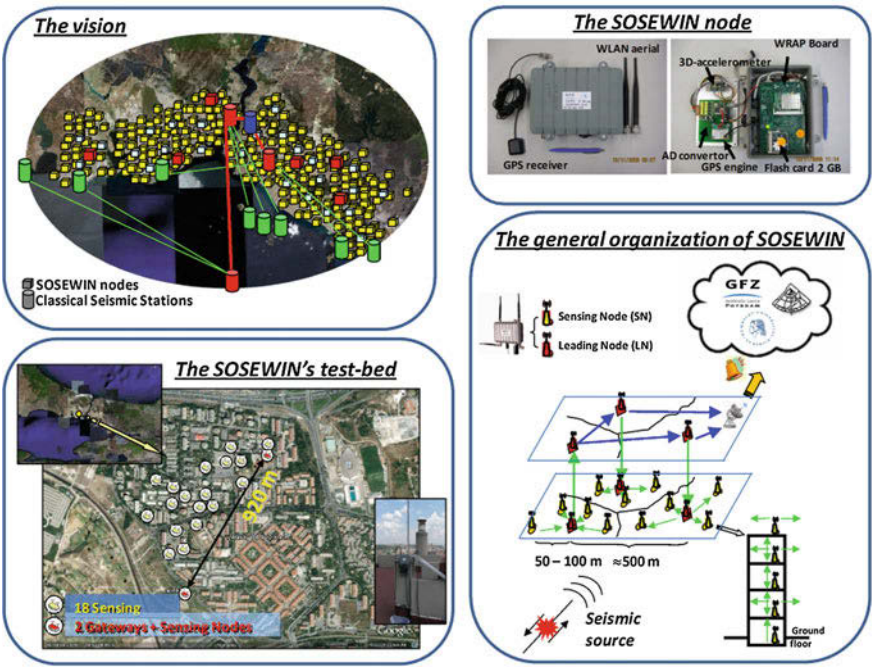

Fig. 6.2 Overview of the self-organizing seismic early warning information network (SOSEWIN)

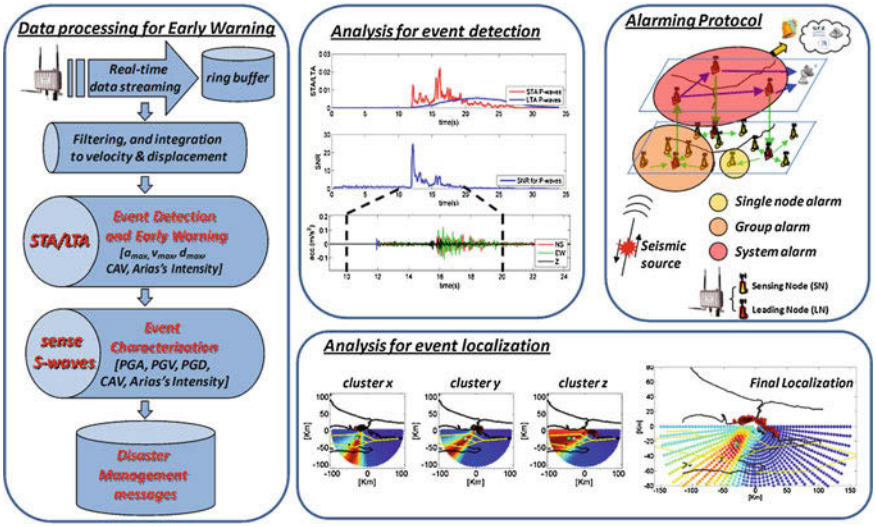

Fig. 6.3 Summary of the SOSEWIN's analyses

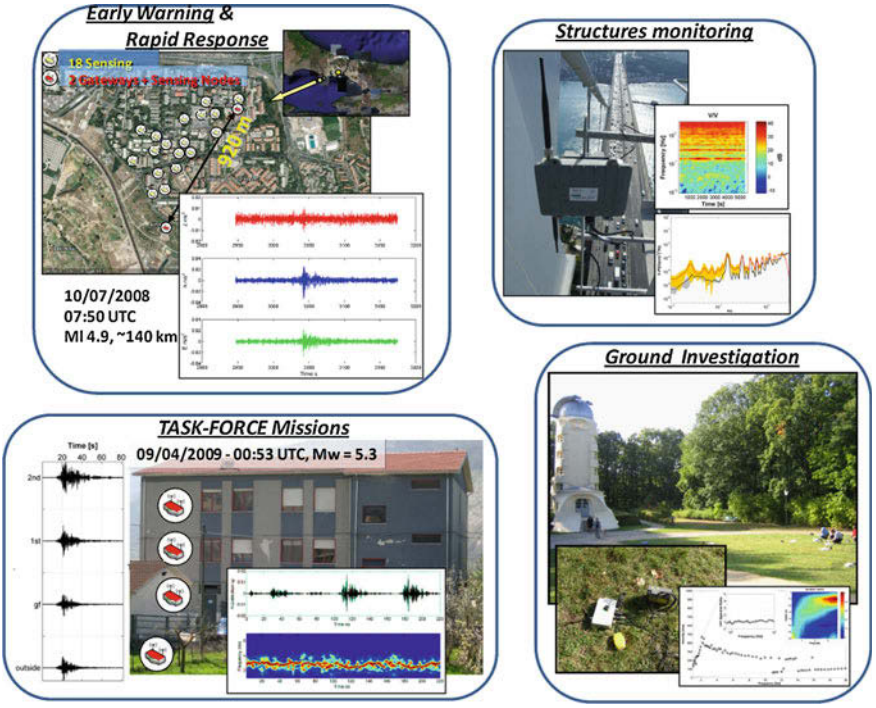

Fig. 6.4 Overview of the SOSEWIN applications

Besides the seismic early warning, the SOSEWIN system was successfully tested in the framework of: an Earthquake Task Force Mission following the L'Aquila (Italy) seismic sequence 2009 (Picozzi et al. 2009a), the monitoring of the vibration characteristics of the Fatih Sultan Mehmet Bridge in Istanbul (Turkey) (Picozzi et al. 2010), and the study of the subsoil characteristics which affect the ground motion during earthquakes (Picozzi et al. 2009b), (Fig. 6.4).

Finally, it is worth to mention that the SOSEWIN system already attracted the attention of both the scientific community and the industry. In fact, we were contacted both by a company of the oil-industry whether a commercial product is available which can be used in site early warning (e.g. refinery), and by international colleagues for future cooperation on this approach in seismic early warning for Megacities (e.g. China). Hence, this was the trigger that the GFZ Potsdam and the HU Berlin agreed to develop a concept for a commercial SOSEWIN-product with focus on seismological early warning. Indeed, in cooperation with a company we are planning to further develop the hardware and software as technology transfer from within the GEOTECHNOLOGIEN program to a commercial application.

6.4 Infrastructure of Self-Organizing Sensor Systems (HU, Computer Science Department)

The Self-Organizing Seismic Early Warning Information Network (SOSEWIN), which has been developed within the EDIM project, is technically a decentralised, wireless mesh sensor network, made up of low-cost components, with a special seismological application that supports earthquake early warning and rapid response tasks. The contribution of HUB was the development of the system software for the sensor nodes and the Alarming Protocol responsible for cooperatively detecting and distributing alarms throughout the network (Fig. 6.5).

- The basic operating system with self-organising routing software. A Linux operating system Pen WRT (OpenWRT 2010) was configured and for wireless communication capabilities a self-organising mesh network routing protocol (olsrd 2010) was identified.
- The integration of the acceleration sensors (coupled with GPS) into the system. A self-written data-provider is able to deliver the sensor's data to a Seedlink server, the Alarming Protocol or with its plug-in architecture to any other conceivable processing software.
- The developed Alarming Protocol, which is responsible for a collaborative decision within the network about an earthquake event and the distribution of an alarm message. Following a model-based development approach, the Alarming Protocol is based on common structure and behavioural models. The Alarming Protocol is defined using a formal description language (SDL in addition with ASN.1/UML/C++) (Ahrens et al. 2009). Using such a formal model, code for

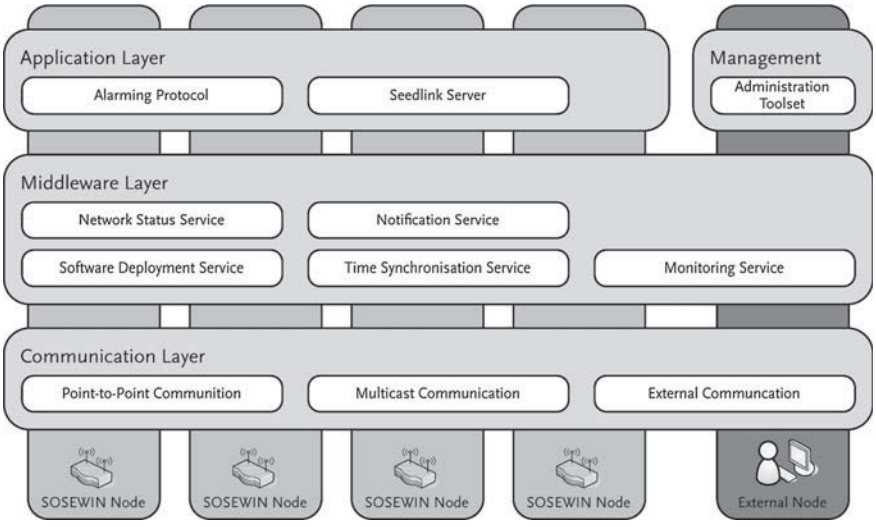

Fig. 6.5 An overview of the current SOSEWIN layer architecture with several services

the target hardware platform (sensor nodes) and for different kinds of simulators supporting different experiment scenarios (including the system's environment) is generated.
- Self-written components realizing the several network middleware services. The Network Status Service allows external users to access the network topology with link qualities for management purposes. An administrator can update the software easily via the Software Deployment Service remotely. The Notification Service allows external users to register for receiving earthquake or other imaginable alarms. For example, such a user is the web service infrastructure developed by lat/lon in WP C2. The Time Synchronisation Service allows nodes without receiving a GPS signal to synchronize their clocks to other nodes having a GPS connection.

In cooperation with the Helmholtz Centre Potsdam, GFZ German Research Centre for Geosciences and the kind support by our Turkish partner, KOERI, 20 SOSEWIN nodes were deployed in 2008 in the Ataköy area of Istanbul as a real-world installation. 18 nodes were deployed at the rooftops of 13-story buildings. Additionally two nodes have the role of internet gateways (DSL connections) at different places. Till the end of the project, this installation has been running for nearly two years. After learning the first lessons, this period was nearly without outage for one and a half year. During the last winter some nodes broke down and may need on-site-maintenance now (most likely due to the problems of a long-time outdoor deployment of such hardware). Nevertheless, the remaining network is still operable and providing data, which proofs the robustness and self-organizing idea of such a network.

Our model-based development and experimentation approach (Fischer et al. 2009) allows us to observe the behaviour of the Alarming Protocol model in different execution environments (several simulators, a virtual network or the Ataköy installation) and improve the same model by these different observations. For that, a complex toolchain was set up, managed by a self-developed Experiment Management System (EMS) in addition to a Geographic Information System (GIS). All tools are integrated in our GIS-based Development and Administration Framework for Wireless Sensor Networks GAFA4WSN (GAF4WSN Framework 2010). With this infrastructure, large networks with thousands of nodes can be simulated in their behaviour, visualized and evaluated. It allows also monitoring and administrating the prototype SOSEWIN installed in Istanbul.

Together with the development of the Alarming Protocol, different types of simulators have been developed, which focus on different aspects of the system, completely integrated into the EMS:

- A simulator based on the ODEMx framework (ODEMx 2011). Simulations with this simulator mainly focus on the validation and evaluation of the alarming protocol. For simplification, it abstracts just to the application level and contains only a very simplified network-stack model.
- A simulator based on the ns-3 framework (The ns-3 network simulator 2010). This simulator focuses on the wireless networking part with its challenges and yields results about warning times in a more realistic network model. Results

obtained from experiments done with increasing network size (up to 255 nodes) show that the difference between system alarm and first p-wave detection time does not depend on the size of the network. Thus, increasing the number of nodes will lead to a better coverage of an area without having a substantial effect on the performance of the alarming protocol.
- An emulation of a SOSEWIN network with virtualized nodes that runs exactly the same software as it is deployed on the real sensor nodes, but allows larger number of nodes and faster testing than deploying software on the real nodes.

Several experiments with different synthetic earthquakes and different distances to the sensor network were done with 8 nodes of the SOSEWIN prototype in Istanbul. The mean alarming delay (the time between the first P-wave arriving at the network and the emerged system alarm) averages 1.9 s (min: 0.56 s, max: 4.8 s). The evaluation has shown that the most time was consumed for the communication between the nodes, which was quite slow due to the fact that, as already mentioned, several nodes broke down. This caused several weak links between the nodes. Another reason was the small number of only three cluster heads in the Alarming Protocol, which means that all cluster heads have to emerge a group alarm in order to generate a system alarm. But several experiments with alarming delays around and in less than 1.0 s proof the potential of the SOSEWIN early warning system, especially for large and denser network installations.

6.5 Development of a Dynamic Geoinformation-Infrastructure (DELPHI IMM GmbH, Potsdam)

The aim of the project is to improve and enhance the existing Istanbul Earthquake Early Warning System (IEEWS) in different ways. As part of the EDIM project our working package deals with the provision of earthquake information to users. In the field of disaster management a lot of earthquake information must be collected, analyzed and published long before (planning period), short time before (early warning) and short time after an earthquake happened (rapid response). For every period it is necessary to provide all important information to planning authorities as well as to decision-makers. We decide for a mediation system (web portal) to provide quickly earthquake information to many special user groups. We focus on information about building damage due to earthquake which could be a serious problem for the rapidly growing Megacity Istanbul which is less than 10 km away from the Marmara Fault. Therefore, it is an interface to working packages A and B by using for example the geophysical result as input for calculating the impact on population (Fig. 6.6).

The mediation system consists basically of a MapClient with typical MapClient functions for navigation and layer configuration. Beyond these functions, the EDIM mediation system offers special useful tools improving the earthquake interpretation.

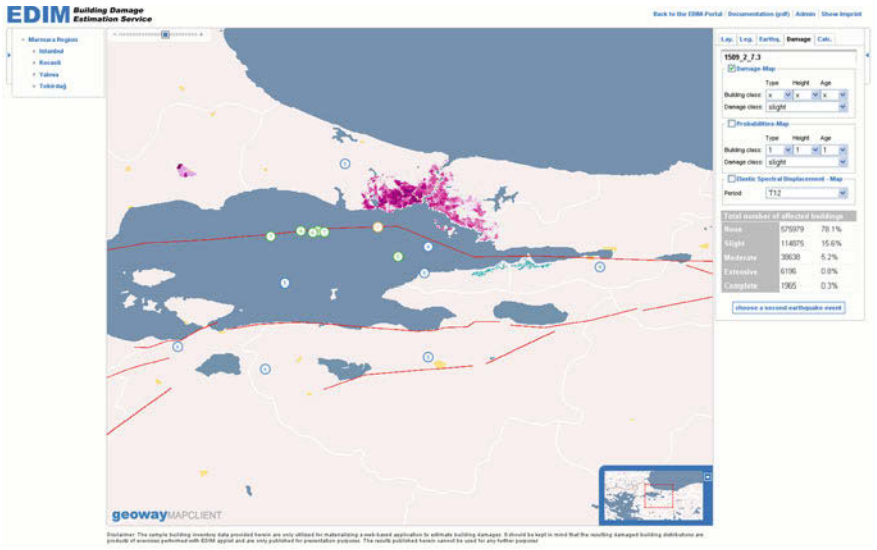

Fig. 6.6 EDIM mediation system

For example, visualized earthquakes can be filtered according to date or magnitude. Building damage information can represent each building class, damage class and moreover it can be filtered according to particular building properties, i.e. only multi-story buildings were taken into account. Two earthquake events can then be compared regarding visual and statistical differentiations.

In addition to this map representation, the mediation system integrates an online service for estimating building damage in order to produce very quickly new information layer. Consequently, a rapid assessment of damage distribution or cost estimations of past earthquakes can be done. Another field of application having emerged during the project term is the use of the system as a validation tool for synthetically computed earthquake scenarios. A performance-based procedure (FEMA356) is used, which was adopted to Istanbul by KOERI (Kandilli Observatory and Earthquake Research Institute, Bogazici University, Istanbul, Turkey). KOERI gave input for software requirements by providing and validating the implemented calculation method. Results were presented several times to KOERI and AKOM (Centre of Disaster Management) in Istanbul during the project term.

Earthquake information and building inventory are required as input for the service DES (Building Damage Estimation Service). A checking verifies the technical and structural input data quality since DES needs a special kind of data quality like data format, cell size and associating index. On the one hand DES has been required to be transferable to other regions, at least for the greater Marmara region. On the other hand, the building damage estimation service can only be performed for the Istanbul building classification as only the behaviour of all these building types is known.

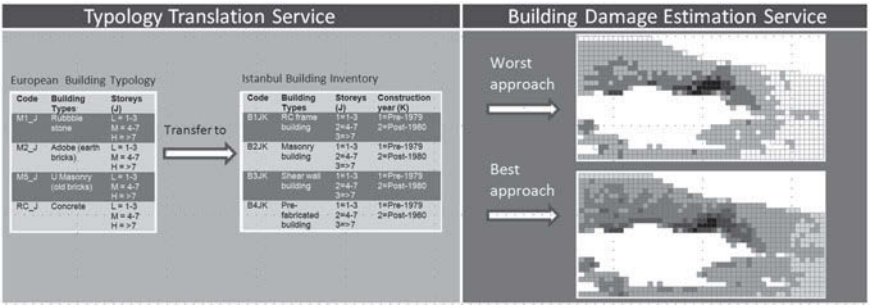

Fig. 6.7 Using semantic interoperability for classification mapping

For this aspect of reuse data or services, a 'typology translation service' has to be interconnected between input and DES in order to establish semantic interoperability. The typology translation service' matches a source data classification to a target data classification. Figure 6.7 shows the European Building Typology in contrast to the Istanbul Building Inventory.

Some object types of the source data classification have an ambiguous matching to the target data classification compared to others which have not. For this reason we propose a best and worst approach. This approach is based on a vulnerability matrix for all combinations of building class and damage class. The most vulnerable adequate object type—taking only similar object types into account—serves as matching point for the worst method and in contrast to the least vulnerable object type for the best method. Heterogeneous earthquake data is supported as input as well. In conclusion, the building damage estimation service (plus further services) gives not only an assessment of the impact on buildings due to earthquakes but also handles heterogeneous input datasets from different data sources, different authorities or collected by different measurements. Therefore, it is a precondition that a defined minimum of information in the dataset is available.

As Istanbul is a rapid growing metropolitan area it could be very interesting to get a new collection of its building inventory. The last data collection refers to 2000. Our idea to tackle this problem was to acquire geographic datasets on our own by classifying earth observation data which provide rapid mapping and topical information. We opt for TerraSAR-X sensor regarding independency of sunlight and cloud cover as well as providing high-resolution radar images maximum in two days. A TerraSAR-X scene for the centre of Istanbul was offered from the company Infoterra Germany, thanks to them, as basis for the extraction of input parameters for DES and a land cover classification according to MOLAND (Fig. 6.8). Reflection of radar data are dominated by surface roughness and surface material. Reflection could be a hint of the building material. The radar phenomenon of the reflection shade can be used to extract building heights. The phenomena of foreshortening and layover have to be considered by interpretation of radar shades.

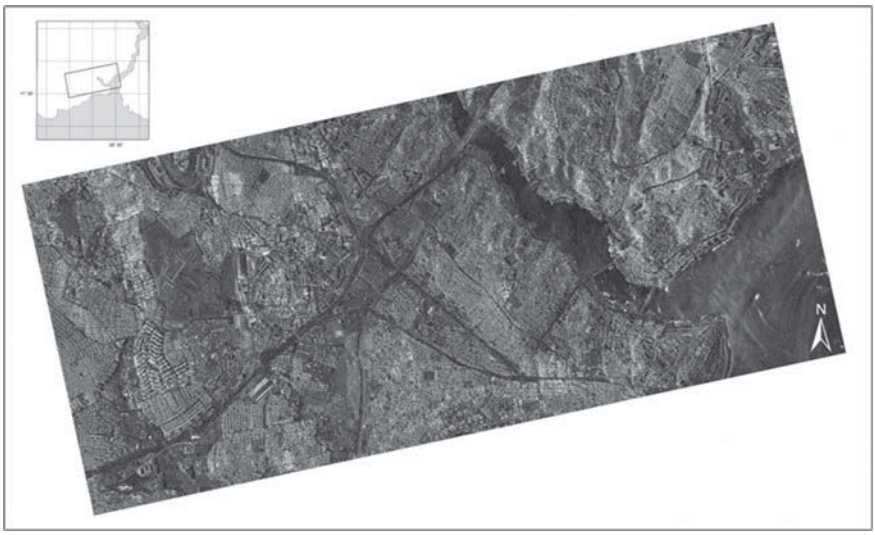

Fig. 6.8 TerraSAR-X sensor data for the centre of Istanbul; © 2008 Astrium Services / Inforterra GmbH

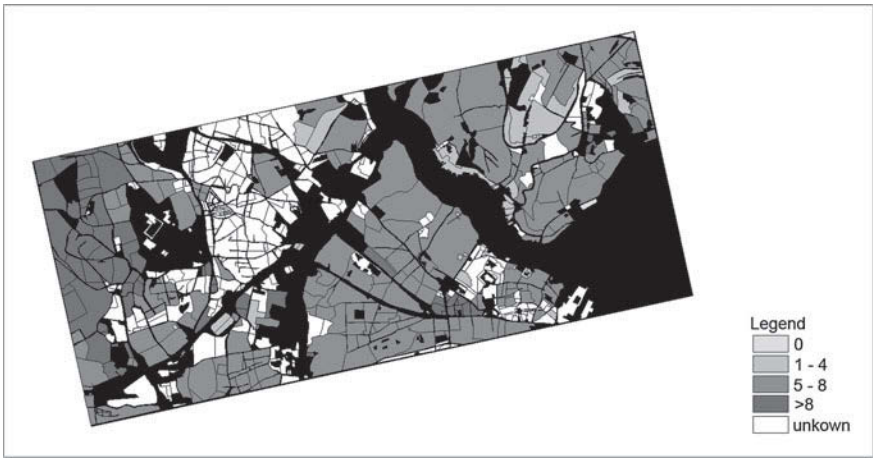

Fig. 6.9 Derivation of building heights (storeys) based on TerraSAR-X sensor data

The height derivation for the city of Istanbul was limited because of high-density area, hilly terrain and a lack of homogenous buildings (Fig. 6.9). The problem of hilly terrains could be solved with satellite TanDEM-X. Together with the almost identical radar satellite TerraSAR-X it will form a high-precision radar interferometer.

6.6 Conclusions

The integration of strong motion seismology, sensor system hard- and software development, and geoinformation real-time management tools prove a successful concept in making seismic early warning a novel technology with high potential for scientific and technological innovation, disaster mitigation, and many spin-offs for other fields. EDIM can serve as a model for further developments in the field of early warning on a global scale.

Acknowledgments The project EDIM is part of the R&D-Programme GEOTECHNOLOGIEN. GEOTECHNOLOGIEN is funded by the German Ministry of Education and Research (BMBF) and the German Research Council (DFG).

References

Ahrens K, Eveslage I, Fischer J, Kuehnlenz F, Weber D (2009) The challenges of using SDL for the development of wireless sensor networks. In: Proceedings 14th system design languages forum, Bochum

Beresnev I, Atkinson G (1997) Modeling finite-fault radiation from the w^n spectrum. Bull Seismol Soc Am 87(1):67–84

Böse M, Wenzel F, Erdik M (2008) PreSEIS: a neural network-based approach to earthquake early warning for finite faults. Bull Seismol Soc Am 98(1):366–382

Erdik M, Fahjan Y, Ozel O, Alcik H, Mert A, Gul M (2003) Istanbul earthquake rapid response and the early warning system. Bull Earthq Eng 1:157–163

Fischer J, Kühnlenz F, Ahrens K, Eveslage I (2009) Model-based development of self-organizing earthquake early warning systems. In: Proceedings MATHMOD 09 Vienna

GAF4WSN Framework. http://www.informatik.hu-berlin.de/sam/gaf4wsn/GAF4WSN/Welcome.html. Accessed 2010

Köhler N (2010) Real-time information from seismic networks. Dissertation, Karlsruhe Institute of Technology (KIT)

Köhler N, Cua G, Wenzel F, Böse M (2009a) Rapid source parameter estimations of southern California earthquakes using PreSEIS. Seismol Res Lett 80(5):748–754

Köhler N, Wenzel F, Erdik M, Alcik H, Mert A, Böse M (2009b) Expansion of the Istanbul earthquake early warning system—performance tests. In: Workshop Proceedings "Seismicity patterns in the Euro-Med region", Luxembourg, November 17–19, pp 83–87

ODEMx. http://odemx.sourceforge.net/. Accessed 2011

olsrd—an adhoc wireless mesh routing daemon. http://www.olsr.org/. Accessed 2010

OpenWRT. http://www.openwrt.org. Accessed 2010

Oth A, Böse M, Wenzel F, Köhler N, Erdik M (2010) Evaluation and optimization of seismic networks and algorithms for earthquake early warning—the case of Istanbul (Turkey). J Geophys Res. doi:10.1029/2010JB007447

Picozzi M, Ditommaso R, Parolai S, Mucciarelli M, Milkereit C, Sobiesiak M, Di Giacomo D, Gallipoli MR, Pilz M, Vona M, Zschau J (2009a) Real time monitoring of structures in task-force missions: the example of the Mw = 6.3 Central Italy Earthquake. Nat Hazards. doi:10.1007/s11069-009-9481-1

Picozzi M, Milkereit C, Zulfikar C, Fleming K, Ditommaso R, Erdik M, Zschau J, Fischer J, Safak E, Özel O, Apaydin N (2009b) Wireless technologies for the monitoring of strategic civil

infrastructures: an ambient vibration test on the Fatih Sultan Mehmet Suspension Bridge in Istanbul. Turkey. Bull Earthq Eng. doi:10.1007/s10518-009-9132-7

Picozzi M, Milkereit C, Parolai S, Jaeckel K-H, Veit I, Fischer J, Zschau J (2010) GFZ wireless seismic array (GFZ-WISE), a wireless mesh network of seismic sensors: New perspectives for seismic noise Array investigations and site monitoring. Sensors 10:3280–3304

The ns-3 network simulator. http://www.nsnam.org/. Accessed 2010

Chapter 7
An Integrated Regional and On-Site Earthquake Early Warning System for Southern Italy: Concepts, Methodologies and Performances

A. Zollo, S. Colombelli, L. Elia, A. Emolo, G. Festa, G. Iannaccone, C. Martino and P. Gasparini

Abstract We present an approach to Earthquake Early Warning for Southern Italy that integrates regional and on-site systems. The regional approach is based on the PRobabilistic and Evolutionary early warning SysTem (PRESTo) software platform. PRESTo processes 3-components acceleration data streams and provides a peak ground-motion prediction at target sites based on earthquake location and magnitude computed from P-wave analysis at few stations in the source vicinity. On the other hand, the on-site system is based on the real-time measurement of peak displacement and dominant period, on a 3 s P-wave time-window. These values are compared to thresholds, set for a minimum magnitude 6 and instrumental intensity VII, derived from empirical regression analyses on strong-motion data. Here we present an overview of the system and describe the algorithms implemented in the PRESTo platform. We also show some case-studies and propose a robust methodology to evaluate the performance of this Early Warning System.

7.1 Introduction

The concept of Earthquake Early Warning System (EEWS) today is becoming more and more popular in the seismological community, especially in the most active seismic regions of the world. EEW means the rapid detection of an ongoing earthquake and the broadcasting of a warning in a target area, before the arrival of the destructive waves. Earthquake Early Warning Systems experienced a sudden improvement

A. Zollo (✉), S. Colombelli, L. Elia, A. Emolo, G. Festa, C. Martino, P. Gasparini
Department of Physics, University of Naples Federico II, Naples, Italy
e-mail: aldo.zollo@unina.it

G. Iannaccone
Osservatorio Vesuviano, INGV, Naples, Italy

L. Elia, C. Martino, P. Gasparini
AMRA Scarl, Naples, Italy

F. Wenzel and J. Zschau (eds.), *Early Warning for Geological Disasters*,
Advanced Technologies in Earth Sciences, DOI: 10.1007/978-3-642-12233-0_7,

and a wide diffusion in many active seismic regions of the world in the last three decades. They are currently operating in Japan (Nakamura 1984, 1988; Odaka et al. 2003; Horiuchi et al. 2005), Taiwan (Wu and Teng 2002; Wu and Zhao 2006), and Mexico (Espinosa-Aranda et al. 2009). Many other systems are under development and testing in other regions of the world such as California (Allen and Kanamori 2003; Allen et al. 2009a, b; Böse et al. 2009), Turkey (Alcik et al. 2009), Romania (Böse et al. 2007), and China (Peng et al. 2011). In southern Italy the early warning system PRESTo (Probabilistic and Evolutionary early warning SysTem) (Satriano et al. 2010) is under testing since December 2009. It is currently used to monitor the Apenninic fault system and to detect small-to-moderate size events in the area where the M_W 6.9, 1980 Irpinia earthquake occurred (Zollo et al. 2009a; Zollo 2009b; Iannaccone 2010).

Most of existing EEWS essentially operate in two different configurations, the "regional" (or network-based) and the "on-site" (or station-based), depending on the source-to-site distance and on the geometry of the considered network with respect to the source area. The regional configuration is generally adopted when the network is deployed in the source area, while the targets to be protected are far away from it. In this approach, the early portion of recorded signals is used to rapidly evaluate the source parameters (essentially, event location and magnitude) and to predict a ground-motion intensity measure (e.g., Peak Ground Velocity, PGV, and/or Peak Ground Acceleration, PGA) at distant sites, through empirical Ground Motion Prediction Equations (GMPE). As data are acquired by the network, the initial estimations are updated, providing a continuously refined information about the earthquake parameters and ground shaking prediction at target sites. Given the source-to-site distance, the "lead-time" (i.e., the time between the alert issue and the arrival of damaging waves at the target site) can be relatively long in a regional configuration, although the prediction of the shaking at distant sites may be affected by large uncertainties due to the use of empirical predictive relationships.

The on-site approach, instead, is generally used when the sites to be protected are close to the source area. In this configuration the early portion of recorded P-wave signals is used to predict the ensuing peak ground-motion at the same site and to provide a local alert level, based on the combination of Early Warning (EW) parameters (such as P-wave peak displacement and/or predominant period). The main advantage of such an approach is that the alert for an impending earthquake at the target site is issued based on a local measurement of P-wave ground motion, avoiding the use of empirical predictive laws and bypassing the estimation of earthquake location and magnitude, which might be affected by large uncertainties in a real-time analysis.

The new idea for EEWS is the integration of the two approaches, which allows to get accurate estimations of earthquake parameters, reliable prediction of the expected ground motion and quite large lead times. The integrated approach, recently proposed by Zollo et al. (2010), is essentially based on three key-elements: (i) the definition of a local alert level from the combination of the initial Peak Displacement (P_d) and the average dominant period (τ_c); (ii) the use of the initial peak displacement as a proxy for the Peak Ground Velocity; (iii) the real-time mapping of a Potential Damage Zone (PDZ). The integrated approach has been off-line tested for the 2009,

M_W 6.3 L'Aquila (Central Italy) earthquake and ten Japanese large earthquakes Colombelli et al. (2012). Recently, the method has been also implemented in the PRESTo software platform, and is currently under testing in southern Italy using data streaming of small-to-moderate events from the Irpinia Seismic Network (ISNet).

In the present paper we describe the PRESTo software platform, with a special focus on the methodologies and on the performance evaluation for the system.

7.2 The PRESTo Software Platform

PRobabilistic and Evolutionary early warning SysTem (PRESTo) (Satriano et al. 2010) is a software platform for EEW that integrates recently developed algorithms for real-time earthquake location, magnitude estimation and damage assessment into a highly configurable and easily portable package. The system is under active experimentation in southern Italy on the Irpinia Seismic Network (ISNet) (Iannaccone 2010), which is deployed around the seismogenic area where the 1980, M_W 6.9 Irpinia earthquake occurred, and that is expected to produce a large earthquake within the next 20 years.

PRESTo continuously processes the live streams of 3-components acceleration data from the stations for P-waves arrival detection and, while an earthquake is occurring, promptly performs the event detection, location, magnitude estimation, damage zone assessment and peak ground-motion prediction at target sites. The earthquake location uses an evolutionary real-time technique based on an Equal Differential Time (EDT) formulation, and a probabilistic approach for defining the hypocenter (Satriano et al. 2008). This algorithm, at each time step, relies on both the information from triggered arrivals and not-yet-triggered stations. The latter information enable the algorithm to rapidly constrain the most likely location area in the first few seconds of the P-wave propagation. Magnitude estimation exploits an empirical relationship that correlates the final event magnitude with the logarithm of the filtered peak ground-displacements, measured over the first $2 \div 4$ s of signal starting at the detected P-wave arrival and the estimated S-wave arrival (Lancieri and Zollo 2008). The peak ground-motion parameters (PGA, PGV) at a given distance can be estimated from location and magnitude using region specific Ground Motion Prediction Equations (e.g., Emolo et al. 2011 for low-magnitude earthquakes; Akkar and Bommer 2007 for moderate-to-large magnitude events). The evolutionary estimates of source parameters and ground shaking at target sites, and their respective uncertainties, are sent as alarm messages to vulnerable structures and can reach them before the destructive waves arrive, enabling the recipients to initiate automatic safety procedures. PRESTo is designed to handle both low-magnitude and moderate-to-large earthquakes, by using two different sets of parameters for its algorithms at the same time (e.g., signal filters, regression laws, thresholds). This allows to test the real-time behavior of the system both for the low-magnitude seismicity, currently occurring in the Irpinia region, that is recorded by the ISNet network, and, at the same time, to perform Early Warning for eventual energetic earthquakes. PRESTo

has been under continuous real-time testing during the past two years (2010–2011) using data streaming from the ISNet stations, and has produced a bulletin of more than a hundred low-magnitude events (http://isnet.fisica.unina.it). Meanwhile, due to the unavailability of large magnitude events recorded at ISNet, PRESTo has been tested off-line, by playing-back in the system both real and synthetic seismograms for moderate-to-large events occurred in Italy and elsewhere (Satriano et al. 2010).

When a dense seismic network is deployed in the fault area, PRESTo can produce reliable estimates of earthquake location and size within 5–6 s from the event origin time, and a stable solution is generally reached within 10 s from it.

After analyzing strong motion data from modern accelerometric networks deployed in Japan, Taiwan and Italy, we recently integrated the regional approach with a threshold-based EW method that allows, in the very first seconds after the occurrence of a moderate-to-large seismic event, to map the most probable damaged zone which is a relevant information for the efficient planning of the rescue operations in the immediate post-event emergency phase. The method is based on the real-time measurement, at near-source stations located at increasing distances from the earthquake epicenter, of two parameters evaluated over a three-seconds window after the P-wave arrival: the peak displacement (P_d) and the predominant period (τ_c) given by

$$\tau_c = 2n \sqrt{\frac{\int_0^{t_o} [u(t)]^2 dt}{\int_0^{t_o} [v(t)]^2 dt}} \tag{7.1}$$

where u is ground displacement and v is velocity on a short 3 s time-window of P-waves signal on the vertical component. The measured values are compared to threshold values, set for a minimum magnitude of 6 and instrumental intensity VII, based on the empirical regression analysis of strong motion data (Colombelli et al. 2012). At each recording site, an alert level is assigned based on a decision table with four alert levels according to the P_d and τ_c values. Given the real-time, evolutionary estimation of earthquake location from first-P arrivals, the method provides an estimation of the extent of the potential damage zone as inferred from continuously updated averages of the period parameter and from mapping of the alert levels determined at the near-source accelerometer stations.

Concerning implementation details, PRESTo is a stand-alone executable written in C++, a programming language that provides optimal speed performance (a key element for an early-warning system) without sacrificing the code expressiveness, thanks to its object-oriented nature. The code is easily portable to different operating systems (Windows, Linux and Mac OS X), thanks to the SDL library (Simple Direct-Media Layer), used for abstracting low-level operations, and the OpenGL libraries, a de facto standard for scientific and interactive visualization. The software is organized into a main thread that implements the core processing procedures activated during an earthquake, and some additional processing threads that handle the continuous tasks, such as waveforms acquisition and their processing. A block diagram of the system and its inputs and outputs is reported in Fig. 7.1. The main tasks performed by the system are described hereinafter.

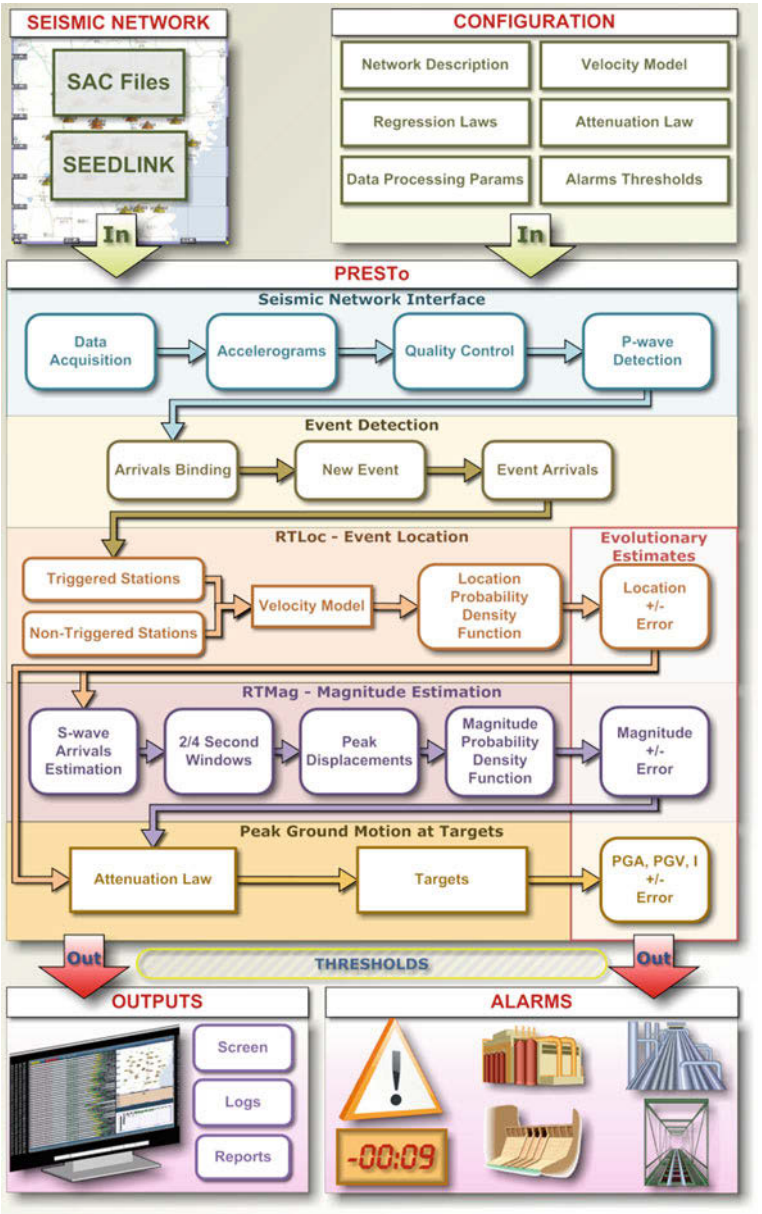

Fig. 7.1 Block diagram of the PRESTo early warning system (*middle*) showing its inner components and the data exchange among them. The data-flow starts with inputs to the system (*top*) and ends with its outputs (*bottom*)

In real-time mode, ground acceleration from three components (or optionally from just the vertical component) is acquired from the stations via the SeedLink protocol. This is a robust and widely used protocol for waveform data transmission in seismology, and is implemented using the official libSlink library. Conversely, in simulation mode the waveforms recorded during a past earthquake (or synthetic waveforms produced for historical events), can be played-back in the system reading files in SAC format (Goldstein et al. 2003). In the latter case the streams of 1 s SeedLink packets are simulated, with the optional feature of also producing random communication delays and data gaps for a more realistic test. For each station, a thread running concurrently with the rest of the program performs the acquisition and automatic phase picking.

Incoming acceleration packets are processed for automatic phases picking by the Filter Picker (FP) algorithm developed by Lomax et al. (2012), which is based on the same basic concepts used in the Baer and Kradolfer's picker (Baer and Kradolfer 1987) and the Allen's picker (Allen 1978, 1982). FP is designed so that it operates stably on continuous, real-time, broad-band signals, and avoiding excessive picking during large events. It is able to analyze only the new packets of data, as it retains memory of past computations, rather than having to re-process a larger waveform buffer every time. Picks are produced as soon as the arrival waveform is available, making it especially suitable for an EW application. Furthermore, the picker is easily configurable with only five parameters (three of which can use defaults based on the sampling rate only if needed).

For all detected P-waves arrivals an on-site (i.e., local to the station) threshold based alert level is computed, telling whether to expect local and/or remote damage. The alert level (0–3) is computed by measuring the peak displacement P_d and predominant period τ_c (Eq. 7.1), and comparing their values with threshold values. The default thresholds have been chosen in order to have the maximum alert level (level 3) for an earthquake characterized by a predicted magnitude M larger than 6 and an Instrumental Intensity (I_{MM}) larger than VII. The alert level at each station is based solely on data recorded at that site, and is independent of the information provided by other stations and/or from the earthquake detection performed by the regional EW algorithms. In an integrated regional/on-site approach, an instrumental intensity map can be computed starting from a region-wide grid of expected PGVs. This parameter is predicted at stations using a correlation between the on-site P_d measured on a short time window and PGV, while elsewhere it is provided by the regional system through the estimation of the earthquake source parameters and using a GMPE. PGV is correlated to I_{MM} that in turn is correlated to the expected damage so that, through interpolation, a region-wide Potential Damaged Zone can be provided in a few seconds after the earthquake origin time.

The main thread, which runs in parallel with the acquisition threads, keeps a list of the last P-waves picks as well as detected earthquakes, in order to perform the Early Warning on more than one earthquake. A new event is declared when arrivals at a fixed number of stations are detected in a short coincidence time window. Subsequent picks at further stations are associated to the latest quake if they fall within the

association time window, or they are kept in a list of non-associated picks for the possible declaration of new earthquakes.

The probabilistic earthquake location of recent earthquakes is updated using the RTLoc algorithm (Satriano et al. 2008), if either new picks have been associated to the event, or more than a second has passed from the previous location estimate. The most probable hypocenter, origin time and covariance matrix (uncertainty ellipsoid) are computed based on the velocity model of the geographic area, P-waves arrival times at stations, non-triggered stations and current time. The velocity model is provided in two 3D grids per station, holding the travel times from each point of the location grid to the station (one grid for P-waves and one for S-waves).

Magnitude is continually estimated for still live earthquakes that were successfully located. The peak displacements are measured at each station associated to the event, as soon as waveform data are available in a short time window ($2 \div 4$ s) after the detected P-waves arrival and theoretical S-waves arrival. Each time window provides a Gaussian-like magnitude Probability Density Function for the station, with mean value given by

$$\frac{\log P_d - A - C \log\left(\frac{R}{10}\right)}{B} \tag{7.2}$$

where R is the hypocentral distance in km, P_d is the filtered peak displacement in meters and A, B and C are coefficients that depend on the signal window. The earthquake magnitude probability distribution is obtained, assuming a Bayesian approach, by multiplying together the distributions for all time windows and stations, with an *a priori* distribution corresponding to the Gutenberg-Richter law. This provides both a most likely magnitude (peak of the distribution) and uncertainty (magnitude range where the integral of the distribution rises from 5 to 95 %). If the resulting magnitude is below a threshold (i.e., a low-magnitude event was detected) the magnitude is recomputed using different filters to obtain the displacement. For this reason it is possible to test the behavior of the system on low-magnitude events, while at the same time performing Early Warning for moderate-to-large earthquakes.

Using magnitude and location from the previous steps, the peak velocity and acceleration are estimated at stations (to compare with measured values) and targets, through attenuation laws whose coefficients can be user-specified. The lead-time at each target site, i.e., the seconds remaining before the estimated S-waves arrival there, is also computed. However, the actual lead-time available to perform automatic safety procedures at targets is expected to be larger than that estimated by the system, considering that the peak ground-motion due to S-waves is expected to occur later than the S-waves arrival time.

Alarm messages are sent over the internet to remote target sites. These are short User Datagram Protocol (UDP) packets that contain the most up-to-date estimated source parameters and uncertainties, the peak ground shaking expected at the recipient target, and the remaining seconds before the arrival of destructive waves (S-waves). The average measured P_d and τ_c at the stations are also provided. The UDP transport layer has been chosen since alarms are short, stream-like (e.g., the most recent message supersedes previous ones) and need to be delivered as fast as

possible, that is what UDP is designed for. In addition to "earthquake" messages, "heart-beat" messages are also continuously sent to targets (e.g., every few seconds) to signal the working condition of the EWS and communication lines. As a last step, the final estimates of the earthquake source parameters are sent as cell phone text message to a distribution list, as well as via e-mail (in this case also attaching a short log and a screenshot), and the PRESTo bulletin is updated.

7.3 Methodology

With the purpose to build a powerful tool for end-users, the PRESTo software platform has been conceived to be a fully adaptable system. The large number of configuration parameters and the different accepted input/output data format make it suitable to various seismogenic regions and network configurations. At present PRESTo is running in two different configurations. On the one hand it runs as a standard regional system, providing earthquake location, magnitude and regional alert notification; on the other hand it works as a On-site/Threshold-based approach, providing the local alert levels as a common single-station system. Both configurations are currently under testing at ISNet network; the next step will be the integration of the two approaches for the construction of a complete system, capable of providing several outputs and information about the earthquake underway.

In its original development, the PRESTo software platform has been conceived to be a regional system using the stations of ISNet network. The system is aimed at the real-time monitoring of the Campania Lucania Apennine (Southern Italy) and at providing a warning in specific target area of the Campania region (e.g., the city of Naples, about 100 km away from the source area). We have described in the previous section how both modalities are implemented in the PRESTo system. Hereinafter we are going to describe with some detail the theory that underlies the threshold-based configuration, referring to the articles by Zollo et al. (2010) and Colombelli et al. (2012) for further information.

The "threshold-based" method is essentially based on the real-time, joint measurement of initial peak displacement (P_d) and average period (τ_c) (Wu and Kanamori 2005, 2008) in a 3 s window after the P-wave arrival time. In this approach, the initial peak displacement is used as a proxy for the Peak Ground Velocity in order to get a real-time estimation of the Potential Damage Area.

Based on the analysis of strong-motion data from different seismic regions of the world, (Zollo et al. 2010) derived the regression relationship between the initial peak displacement P_d and the Peak Ground Velocity. Measuring P_d in centimeters and PGV in centimeters per seconds they found:

$$\log(PGV) = 0.73(\pm 0.01) \cdot \log(P_d) + 1.30(\pm 0.02). \tag{7.3}$$

The period parameter, (τ_c, Eq. 7.1), is instead used to estimate the earthquake magnitude M. Measuring τ_c in seconds and through a best-fit weighted regression

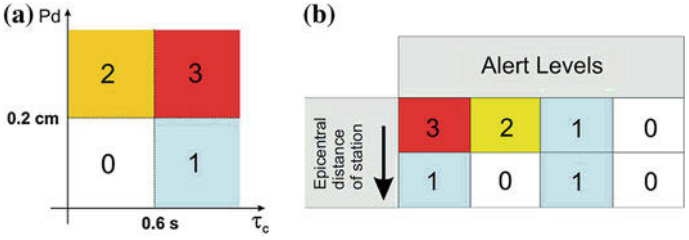

Fig. 7.2 Alert levels and threshold values for observed early warning parameters (after Zollo et al. 2010). **a** P_d versus τ_c diagram showing the chosen threshold values and the regions delimiting the different alert levels: level 3 means damage expected nearby and far away from the station; level 2 means damage expected only nearby the station; level 1 means damage expected only far away from the station; level 0 means no expected damage. **b** Expected variation of alert levels as a function of the epicentral distance: the allowed transitions between alert levels are from 3 to 1 and from 2 to 0

line on average binned data (Δ M = 0.3) with the same data set used before, (Zollo et al. 2010) found:

$$\log(\tau_c) = 0.21(\pm 0.01) \cdot M - 1.19(\pm 0.08). \tag{7.4}$$

In a standard attenuation relationship, the peak amplitude depends, at the first order, on the hypocentral distance (R) and on the earthquake magnitude, thus, given the dependency of average period on the earthquake magnitude, Eqs. 7.3 and 7.4 have been combined in order to derive an empirical relationship among P_d, τ_c and hypocentral distance R. A multivariate linear regression analysis provided the following equation:

$$\log(P_d) = 1.93(\pm 0.03) \cdot \log(\tau_c) - 1.23(\pm 0.09) \cdot \log(R) + 0.6(\pm 0.1) \tag{7.5}$$

where R is measured in kilometers, τ_c in seconds, P_d in centimeters.

As usual in a common on-site system, the two EW parameters are measured along the first 3 s of signal after the P-wave arrival time. The measured values of P_d and τ_c are then compared to threshold values and a local alert level is assigned at each recording site, based on a decision table. Four alert levels (0, 1, 2 and 3) have been defined based on the combination of P_d and τ_c at a given site; the threshold values have been set according to Eqs. 7.3 and 7.4 and correspond to a minimum magnitude M = 6 (from the τ_c versus M equation) and to an instrumental intensity I_{MM} = VII from the P_d versus PGV equation, assuming that the peak ground velocity could provide the instrumental intensity through the relationship of (Wald et al. 1999).

The alert level scheme comes from an original idea of (Wu and Kanamori 2005) and can be interpreted in terms of potential damaging effects nearby the recording station and far away from it. For example, following the scheme of Fig. 7.2, the maximum alert level (level 3, i.e. $\tau_c \geq 0.6$ s and $P_d \geq 0.2$ cm) corresponds to an earthquake with predicted magnitude M $\geq$ 6 and with an expected instrumental

intensity $I_{MM} \geq$ VII. This means that the earthquake is likely to have a large size and to be located close to the recording site. Thus, we expect a high level of damage either nearby and far away from the recording station. On the contrary, in case of a recorded alert level equal to 0 (i.e., $\tau_c < 0.6$ s and $P_d < 0.2$ cm), the event is likely to be small and far from the site, thus no damage is expected either close or far away from the station. Analogous considerations can be done for the alert levels 1 and 2.

The "threshold-based" integrated method combines the use of a regional network with the single-station approach, using the scheme discussed in the following.

As soon as a station has been triggered by an earthquake, a preliminary location is obtained by using the real-time location technique implemented in the RTLoc code of (Satriano et al. 2008). As soon as 3 s of P-wave signal are available, P_d and τ_c are measured at the triggered station and a local alert level is assigned based in their combination. The whole area of interest (i.e., the area covered by stations and the target area) is then dived into cells and Eq. 7.5 is used to predict peak displacement values at each node of the grid so to fill the gaps where the measurements are not yet available (Colombelli et al. 2012). Then, measured and predicted P_d values are interpolated and the Potential Damage Zone is delimited by the isoline corresponding to $P_d = 0.2$ cm, which represents the threshold level on the initial peak displacement.

This routine is repeated every second so to update the PDZ. As other stations are triggered and 3 s of P-wave signal are available, P_d and τ_c are measured and further local alert levels are assigned. Meanwhile, the event location is refined by using all the available P-pickings and more data are used for the interpolation procedure.

7.4 Application and Performances

In this section we describe and discuss two different strategies for a quantitative assessment of the system performances: the former is relative to the regional configuration while the latter refers to the on-site methodology.

7.4.1 Regional Configuration

PRESTo is continuously running on real-time data streaming from 31 stations of the Irpinia Seismic Network. The performance of the regional approach to EEW implemented in PRESTo was evaluated by comparing the real magnitude and origin time of each event from the manually revised ISNet Bulletin (http://isnet.fisica.unina.it) to the final estimates obtained in real time by PRESTo.

We evaluated the performance by counting the total number of detected events and the missed and false alarms, using 162 microevents ($0.5 \leq M \leq 3.7$) recorded from 2009/12/21 to 2011/11/15. Successful, missed and false alarms are defined according to the criteria provided in the Table 7.1.

Table 7.1 Criteria adopted to distinguish among successful, missed and false alarms in testing the performance of the PRESTo system in the regional configuration

Successful alarm	An event for which the differences in magnitude (ΔM) and origin time (ΔOT) with respect to the real values are small: $\Delta M \leq 1$ and $\Delta OT \leq 15$ s
Missed alarm	An event with M $\geq$ 2.5 that is not automatically detected
False alarm	A false event (for instance, a storm) that is declared by PRESTo

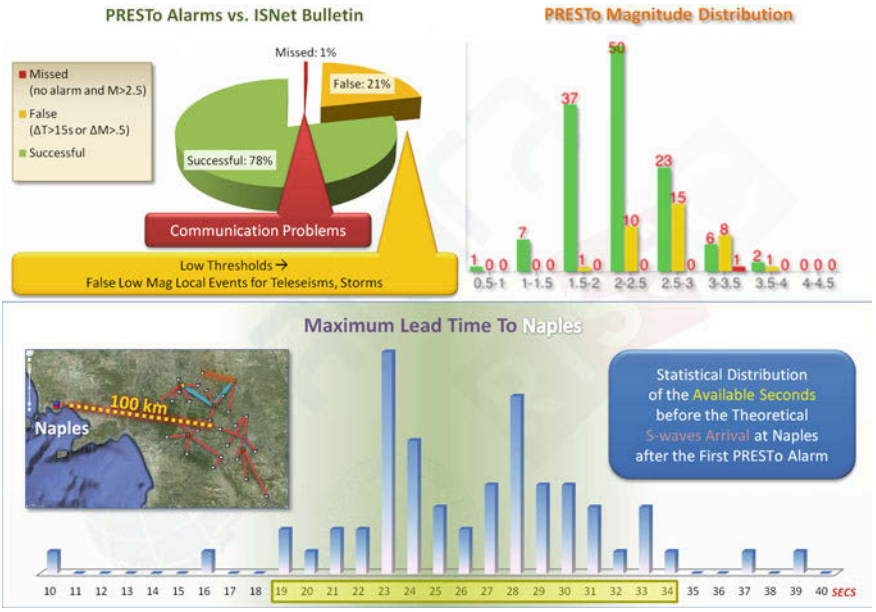

Fig. 7.3 Statistics for the real-time performance of PRESTo in the regional configuration, performed on the low-magnitude seismicity recorded by the ISNet network (0.5 $\leq$ M $\leq$ 3.7). *Top-left* percentages of successful, missed and false alarm based on the discrepancy with the manually revised ISNet Bulletin. *Top-right* distribution of magnitude estimates for each class of alarm. *Bottom* distribution of the seconds available to the city of Naples for events detected by PRESTo: interval from the very first PRESTo alarm to the arrival of S-waves

The statistics derived from the analysis are shown in Fig. 7.3. We have to stress that the (small number of) missed alarms are caused by communication problems among stations. False alarms (about one fifth of the analyzed events) are essentially associated with storms, that in case of adverse weather conditions may be declared as seismic events, and with regional events that are incorrectly declared as local events since the hypocentral searching is restricted to the region covered by the location grid encompassing ISNet. In the same figure we also represented the Maximum Lead Times for the city of Naples (located about 100 km far from the network) i.e.,

the difference between the time at which the first alert is issued and the theoretical S-waves arrival time at the city center.

As a further application, we studied off-line the performance of PRESTo for the L'Aquila earthquake that occurred in central Italy on 6th April 2009 (M_L 5.9, M_W 6.3). The seismic event was caused by a rupture produced along a fault of about 17 km in length, oriented along the Apenninic direction, and had an hypocentral depth of about 8 km (Cirella et al. 2009; Maercklin et al. 2011). It caused hundreds of victims and considerable damage to buildings, with the city of L'Aquila, at about 6 km away from the epicenter being particularly struck. We simulated this earthquake in PRESTo by playing-back three-component accelerograms recorded by the 18 stations of the National Accelerometric Network (RAN) closest to the epicenter. The employed velocity model can be found in Bagh et al. (2007). It is characterized by a V_P/V_S ratio equal to 1.83.

Figure 7.4 shows two screenshots of PRESTo during the simulation: in the top panel is reported the second alarm sent by the system that is the first alarm issued characterized by low uncertainties, while in the bottom panel the final estimates are shown.

A detailed study of the temporal evolution of inputs and outputs is shown in Fig. 7.5. The first estimate of location and magnitude was available 5.6 s after the actual origin time, which is just 2.1 s after the first P-waves arrival at station AQV. It is a very short interval, considering that before being able to estimate the earthquake magnitude, it is necessary to wait for the triggering of few stations in a short time frame in order to locate the hypocenter, and that at least 2 s of signal of either S-or P-waves is needed to be available. The promptness of PRESTo to send the first alert is then to be attributed to the high density of stations in near proximity of the epicenter (AQV, AQG, AQK, GSA, MTR, ANT and FMG). The very first magnitude estimate is affected by a large uncertainty as it basically relies on a single station, GSA. The other stations are in fact too close to the epicenter so that even the shortest 2 s P-waves window can't be used due to overlapping with the S-waves window. Therefore, 2 further seconds after the S-waves arrival at these stations need to elapse before they can contribute to improve the magnitude estimation. After just one second from the first alarm a good estimate of the source parameters is already available, i.e. it is in good agreement with the actual values and affected by a small uncertainty.

The maximum lead-times, i.e. relative to the very first estimate that is provided, for two remote sites to protect are: 10.5 s for the city of Teramo, and 22.6 s for Rome, minus 1 s in a more reasonable scenario whereby the recipients wait for a smaller uncertainty, which is indeed provided by the second alert. These are the best possible results given the requisites of the employed methodology. Figure 7.6 contains a plot of measured peak ground velocities at the stations (PGV) as a function of the estimated lead-times. The lead-times are conservative as they were calculated from the second alarm issued by PRESTo. Finally, the PGV estimates provided by PRESTo at the RAN stations are almost always consistent with the measured values, or with a discrepancy that does not exceed 0.5 logarithmic units.

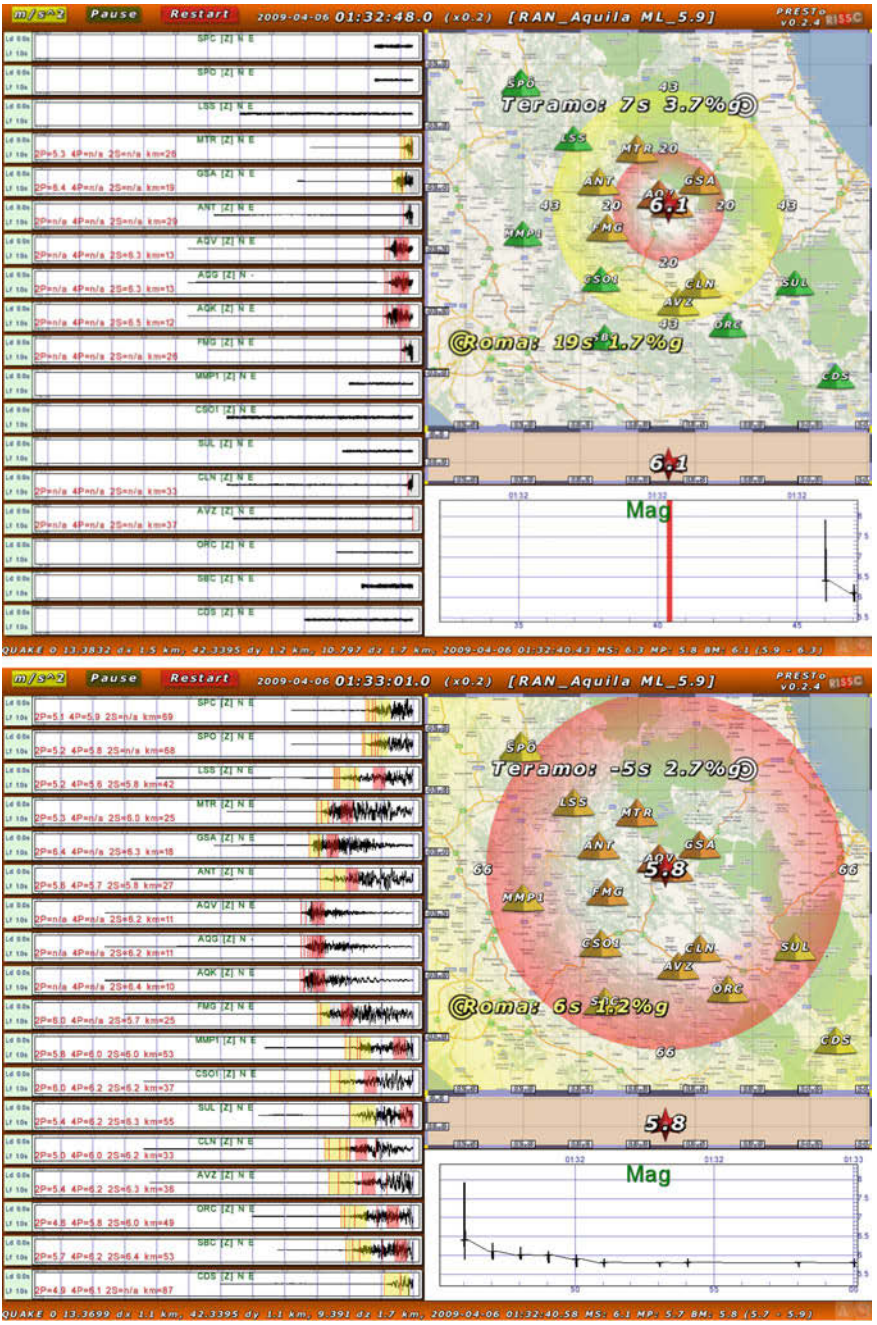

Fig. 7.4 Screen shots of PRESTo during the simulation of the 2009, ML 5.9, L'Aquila earthquake. *Top* the first estimates of the earthquake source parameters that are affected by a low uncertainty are provided about 7 s after the origin time. *Bottom* the earthquake has been processed for some seconds and the estimates have converged to the final values. This screen shot shows the complete picture of inputs and outputs

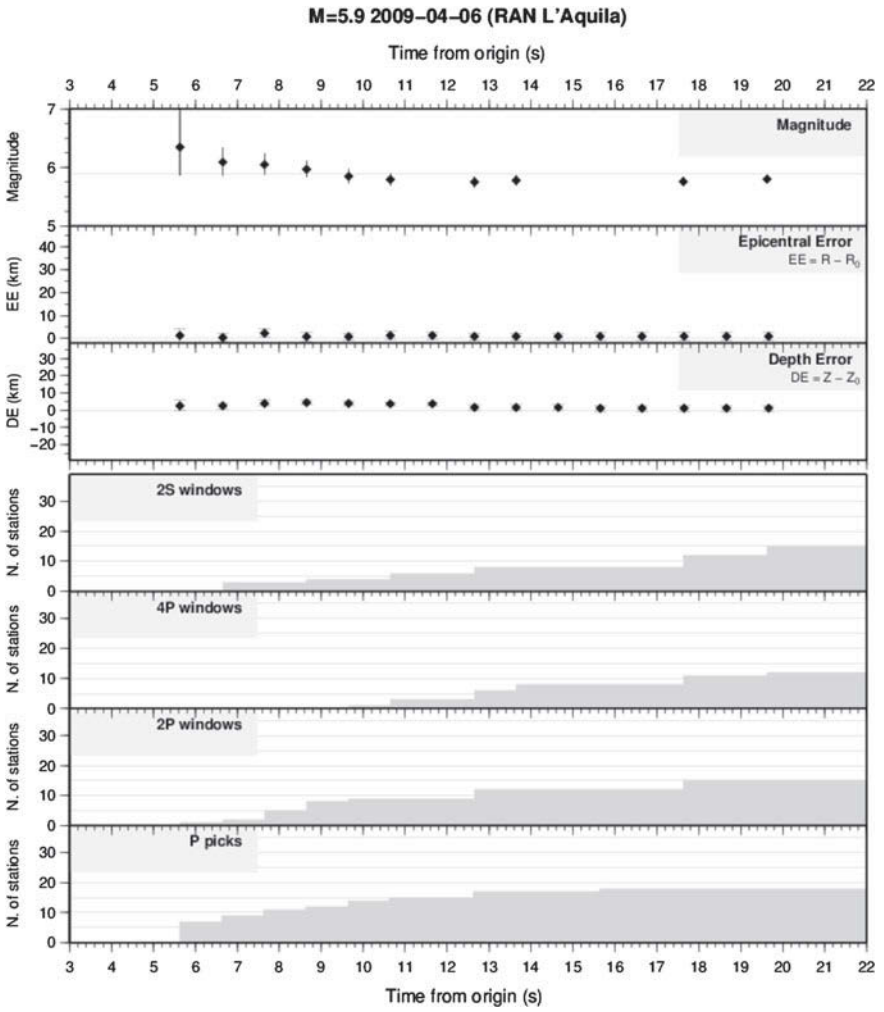

Fig. 7.5 Play-back in PRESTo of the 2009 L'Aquila earthquake: temporal evolution of input data (*bottom* cumulative number of signal time windows and arrival times) and of PRESTo estimates (*top* magnitude, epicenter, depth). The latter are compared with the reference values (from the INGV Bulletin available at http://cnt.rm.ingv.it)

7.4.2 On-Site Methodology

The "threshold-based" on-site methodology has been tested off-line on ten Japanese strong earthquakes ($M > 6$) for a total number of 1,341 records.

A first qualitative analysis of results can be obtained from the visual comparison of the rapidly predicted potential damage zone and the observed ground shaking (or intensity) distribution. The real-time PDZ (i.e., the area delimited by the isoline

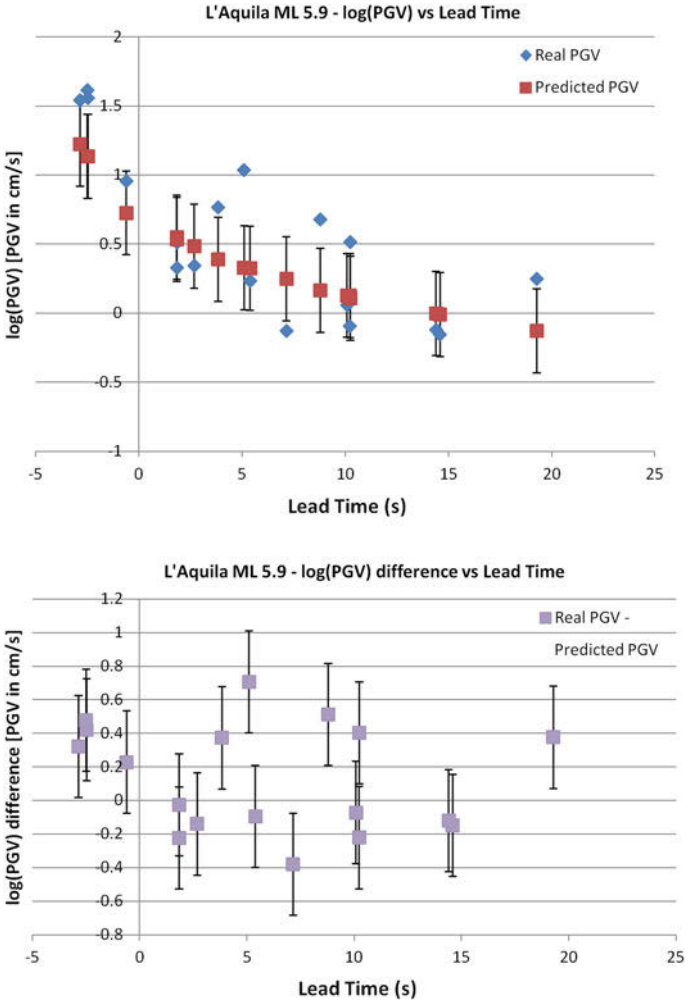

Fig. 7.6 Play-back in PRESTo of the 2009 L'Aquila earthquake. *Top* distribution of measured (*blue diamonds*) and predicted (*red squares*) Peak Ground Velocities at RAN stations, as a function of lead-time. PGVs were predicted by PRESTo using the Akkar and Bommer (2007) GMPE. *Bottom* difference between measured and predicted PGVs. Error bars on the PRESTo estimates correspond to the standard deviation of the adopted GMPE

corresponding to $P_d = 0.2$ cm) is expected to reproduce with a good approximation the area within which the highest intensity values are observed. For each of the analyzed earthquakes we compared the PDZ map with the instrumental intensity (I_{MM}) and the Japanese intensity (I_{JMA}) maps. Some examples of the results obtained are shown in Fig. 7.7. The simple visual comparison among the three maps shows that the real-time

Table 7.2 Definition of successful, missed and false alarms

Recorded alert level	Successful alarm	Missed alarm	False alarm
3	$I_{MM} \geq$ VII	n.d.[a]	$I_{MM} <$ VII
2	$I_{MM} \geq$ VII	n.d.[a]	$I_{MM} <$ VII
1	$I_{MM} <$ VII	$I_{MM} \geq$ VII	n.d.[a]
0	$I_{MM} <$ VII	$I_{MM} \geq$ VII	n.d.[a]

Each recorded alert level corresponds to a successful, missed or false alarm, based on the observed values of intensity at the recording site. For example, a recorded alert level 3 corresponds to a successful alarm if the observed intensity is $\geq$ VII and to a false alarm if the observed intensity is $\leq$ VII. In the same way, the recorded alert level 1 can be a successful alarm if the observed intensity is $<$ VII and a missed alarms if the observed intensity is $\geq$ VII. The alert levels 3 or 2 cannot be missed alarms, as well as 1 and 0 cannot be false alarms

[a] *n.d.* not defined

PDZ is very consistent with the area in which the highest level of damage is reported, both on the I_{JMA} and I_{MM} maps.

A more robust strategy for a quantitative assessment of the system performance consists in evaluating the correspondence between the alert level issued at each station and the macroseismic intensity really experimented during the earthquake. To this end, we defined "successful", "missed" and "false" alarms, based on the criteria listed in the Table 7.2. For example, according to the definition of alert level 3 (i.e., $P_d > 0.2$ cm), the instrumental intensity is expected to be greater than VII. Thus, a recorded alert level 3 corresponds to a successful alarm if the real observed intensity is larger than VII. On the other hand, it is considered a false alarm if the observed intensity is $\leq$ VII. Similarly, the recorded alert level 1 corresponds to successful alarm if the observed intensity is less than VII, and to a missed alarms if the observed intensity is $\geq$ VII.

To evaluate the system performance we then counted the total number of successful, missed and false alarms, according to the definitions given before. The main results are shown in Fig. 7.8: the 87.4 % of alert levels was correctly assigned, false alarms were the 11.9 % and missed alarms the 0.7 %. Despite the very high percentage of successful alarms, the percentage of false alarms turned out to be relatively high. In order to understand the relevance of this result we computed the difference between the predicted intensity (I_{MM} = VII) and the real observed intensity value. The variance distribution represented in the left panel of Fig. 7.8 shows that the 52 % of the false alarms correspond to a real observed intensity equal to V. In this case the alert levels are obviously overestimated even if it should be noted that a value of V on the intensity scale is synonymous of an earthquake that can produce some damage. Thus, the 52 % of the false alarms were, in any case, not completely wrong.

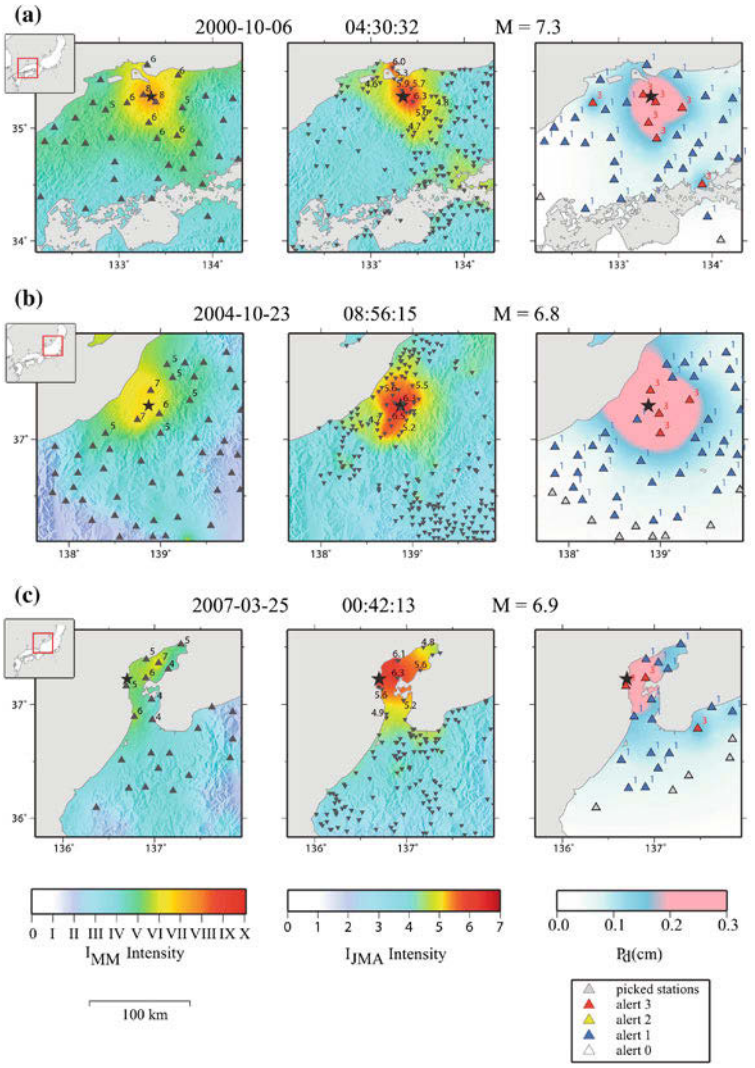

Fig. 7.7 Examples of results for the threshold-based method for **a** M 7.3, 2007, Western Tottori earthquake, **b** M 6.8, 2004, Chuetsu earthquake and **c** M 6.9, 2007, Noto-Hanto earthquake. In each panel, the black star represents the epicenter and the triangles indicate the stations used for the analysis. Left panels. I_{MM} maps obtained from the observed PGV values at K-Net and Kik-Net stations. Values of measured PGV are reported for some stations in the epicentral area, as a reference. Center panels. The instrumental intensity, I_{JMA} maps, as measured at JMA sites are represented by the same color palette than the I_{MM} map, but adapted from 0 to 7. Values of instrumental intensity are reported for some stations in the epicentral area, as a reference. Right panels. the "operative early-warning map" resulting from the interpolation of measured and predicted Pd values. Triggered stations are represented by grey triangles, while red and blue triangles show the alert level recorded at each station, as soon as 3 seconds of signal after the P–picking are available. The PDZ is delimited by the color transition from light blue to red

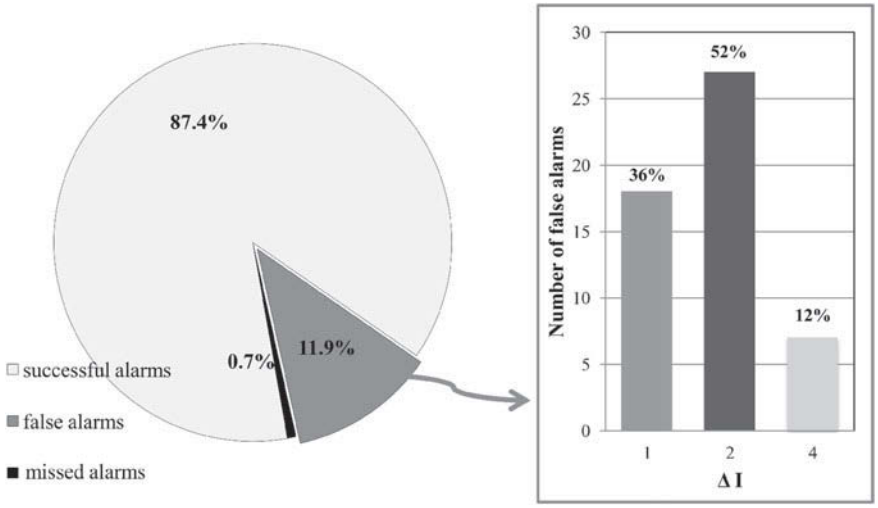

Fig. 7.8 Cumulative statistic of successes/failures of the threshold-based system. *Left-side* relative percentage of successful, false and missed alarms, which are about 87, 11 and 0.7 %, respectively. *Right-side* histogram for the false alarms. ΔI represents the difference between predicted (I_{MM} = VII) and observed intensity values. 36 % of false alert levels 3 corresponds to an intensity value of VI; 52 % corresponds to intensity V and 12 % to intensity III

7.5 Conclusions

Most of the existing earthquake early-warning systems are either "regional" or "on-site". A new concept is the integration of these approaches through the definition of alert levels and the real-time estimation of the earthquake Potential Damage Zone. In the regional approach the ground-motion parameters are computed only using earthquake location and magnitude; on the other hand, in a classical on-site approach the alert notification is based only on local ground-motion measurements. The integrated approach, instead, is based on the combined use of measured and predicted ground-motion parameters. Thus, it is likely to provide a more robust prediction of the potential earthquake damage effects.

The integrated approach is under development and testing in Southern Italy, using data streaming from the Irpinia Seismic Network. Here we presented the preliminary results of performance tests for the on-site and the regional method separately. The integrated approach will be tested off-line using moderate-to-strong earthquakes from worldwide catalogues.

7.5.1 Data and Resources

Waveforms used in this study have been extracted from ISNet database managed by AMRA Scarl (Analisi e Monitoraggio del Rischio Ambientale) and are available on-line at http://seismnet.na.infn.it/index.jsp after registration. Most of the analysis and figures were produced using GNUPLOT (http://www.gnuplot.info/ last accessed January 2012), SAC (Goldstein et al. 2003) which can be requested from the Incorporated Research Institutions for Seismology (http://www.iris.edu last accessed January 2012), and GMT Generic Mapping Tools (Wessel and Smith 1995) (http://gmt.soest.hawaii.edu/ last accessed January 2012). Details about the real-time seismological data transmission protocol SeedLink are available on-line at http://www.iris.edu/data/dmc-seedlink.htm (last accessed March 2012).

Acknowledgments This work was financially supported by Dipartimento della Protezione Civile (DPC) through Analisi e Monitoraggio del Rischio Ambientale (AMRA Scarl).

References

Akkar S, Bommer JJ (2007) Empirical prediction equations for peak ground velocity derived from strong-motions records from europe and the middle east. Bull Seism Soc Am 97:511–530

Alcik H, Ozel O, Apaydin N, Erdik M (2009) A study on warning algorithms for Istanbul earthquake early warning system, Geophys Res Lett 36: L00B05. doi:10.1029/2008GL036659

Allen RM, Kanamori H (2003) The potential for earthquake early warning in southern California. Science 300:685–848

Allen RM, Brown H, Hellweg M, Khainovski O, Lombard P, Neuhauser D (2009a) Real-time earthquake detection and hazard assessment by ElarmS across California. Geophys Res Lett 36: L00B08. doi:10.1029/2008GL036766

Allen RM, Gasparini P, Kamigaichi O, Böse M (2009b) The status of earthquake early warning around the world: an introductory overview. Seism Res Lett 80:682–693

Allen RV (1978) Automatic earthquake recognition and timing from single traces. Bull Seism Soc Am 68:521–532

Allen RV (1982) Automatic phase pickers: their present use and future prospects. Bull Seism Soc Am 72:225–242

Baer M, Kradolfer U (1987) An automatic phase picker for local and teleseismic events. Bull Seism Soc Am 77:1437–1445

Bagh S, Chiaraluce L, De Gori P, Moretti M, Govoni A, Chiarabba C, Di Bartolomeo P, Romanelli M (2007) Background seismicity in the central apennines of Italy: the Abruzzo region case study. Tectonophysics 444:80–92. doi:10.1016/j.tecto.2007.08.009

Böse M, Ionescu C, Wenzel F (2007) Earthquake early warning for Bucharest, Romania: novel and revised scaling relations, Geophys Res Lett 34. doi:10.1029/2007GL029396

Böse M, Hauksson E, Solanki K, Kanamori H, Heaton TH (2009) Real-time testing of the on-site warning algorithm in Southern California and its performance during the July 29, 2008 Mw 5.4 Chino Hills earthquake. Geophys Res Lett 36. doi:10.1029/2008GL036366

Cirella A, Piatanesi A, Cocco M, Tinti E, Scognamiglio L, Michelini A, Lomax A, Boschi E (2009) Rupture history of the 2009 L'Aquila (Italy) earthquake from non-linear joint inversion of strong motion and GPS data. Geophys Res Lett 36: L19304. doi:10.1029/2009GL039795

Colombelli S, Amoroso O, Zollo A, Kanamori H (2012) Test of a threshold-based earthquake early-warning method using Japanese data. Bull Seism Soc Am 102. doi:10.1785/0120110149

Emolo A, Convertito V, Cantore L (2011) Ground-motion predictive equations for low-magnitude earthquakes in the Campania-Lucania area, southern Italy. J Geophys Eng 8:46–60. doi:10.1088/1742-2132/8/1/007

Espinosa-Aranda JM, Cuellar A, Garcia A, Ibarrola G, Islas R, Maldonado S, Rodriguez FH (2009) Evolution of the Mexican Seismic Alert System. Seism Res Lett 80:694–706

Goldstein P, Dodge D, Firpoand M, Minner L (2003) SAC2000: Signal processing and analysis tools for seismologists and engineers. In: IASPEI international handbook of earthquake and engineering seismology

Horiuchi S, Negishi N, Abe K, Kamimura K, Fujinawa Y (2005) An automatic processing system for broadcasting system earthquake alarms. Bull Seism Soc Am 95:347–353

Iannaccone G, Zollo A, Elia L, Convertito V, Satriano C, Festa G, Martino C, Lancieri M, Bobbio A, Stabile TA, Vassallo M, Emolo A (2010) A prototype system for earthquake early-warning and alert management in southern Italy. Bull Earthq Eng 8:1105–1129. doi:10.1007/s10518-009-9131-8

Lancieri M, Zollo A (2008) A Bayesian approach to the real time estimation of magnitude from the early P-and S-wave displacement peaks. J Geophys Res 113(B12302). doi:10.1029/2007JB005386

Lomax A, Satriano C, Vassallo M (2012) Automatic picker developments and optimization: FilterPicker—a robust, broadband picker for real-time seismic monitoring and earthquake early-warning. Seism Res Lett 83(3):531–540. doi:101785/gssrl.83.3.531

Maercklin N, Zollo A, Orefice A, Festa G, Emolo A, De Matteis R, Delouis B, Bobbio A (2011) The effectiveness of a distant accelerometer array to compute seismic source parameters: the April 2009 L'Aquila earthquake case history. Bull Seism Soc Am 101:354–365. doi:10.1785/0120100124

Nakamura Y (1984) Development of earthquake early-warning system for the Shinkansen, some recent earthquake engineering research and practical in Japan. In: The Japanese national committee of the international association for earthquake engineering, pp 224–238

Nakamura Y (1988) On the urgent earthquake detection and alarm system (UrEDAS). In: Proceedings of the 9th world conference earthquake engineering, vol 7, pp 673–678

Odaka T, Ashiya K, Tsukada S, Sato S, Ohtake K, Nozaka D (2003) A new method of quickly estimating epicentral distance and magnitude from a single seismic record. Bull Seism Soc Am 93:526–532

Peng HS, Wu ZL, Wu YM, Yu SM, Zhang DN, Huang WH (2011) Developing a prototype earthquake early warning system in the Beijing capital region. Seism Res Lett 82:394–403

Satriano C, Lomax A, Zollo A (2008) Real-time evolutionary earthquake location for seismic early warning. Bull Seism Soc Am 98:1482–1494

Satriano C, Elia L, Martino C, Lancieri M, Zollo A, Iannaccone G (2010) PRESTo, the earthquake early warning system for southern Italy: concepts, capabilities and future perspectives. Soil Dyn Earthq Eng. doi:10.1016/j.soildyn.2010.06.008

Wald DJ, Quitoriano V, Heaton TH, Kanamori H (1999) Relationships between peak ground acceleration, peak ground velocity and modified mercalli intensity in California. Earthq Spectra 15:557–564

Wessel P, Smith WHF (1995) New version of the generic mapping tools released. EOS Trans AGU 76:329

Wu YM, Kanamori H (2005) Rapid assessment of damage potential of earthquake in Taiwan from beginning of P waves. Bull Seism Soc Am 95:1181–1185. doi:10.1785/0120040193

Wu YM, Kanamori H (2008) Development of an earthquake early warning system using real-time strong motion signals. Sensors 8:1–9

Wu YM, Teng LT (2002) A virtual sub-network approach to earthquake early warning. Bull Seism Soc Am 92:2008–2018

Wu YM, Zhao L (2006) Magnitude estimation using the first three seconds P-wave amplitude in earthquake early warning. Geophys Res Lett 33:L16312. doi:10.1029/2006GL026871

Zollo A, Amoroso O, Lancieri M, Wu YM, Kanamori H (2010) A threshold-based earthquake early warning using dense accelerometer networks. Geophys J Int 183:963–974

Zollo A, Iannaccone G, Convertito V, Elia L, Iervolino I, Lancieri M, Lomax A, Martino C, Satriano C, Weber E, Gasparini P (2009a) The earthquake early warning system in southern Italy. Encyc Complex Syst Sci 5:2395–2421. doi:10.1007/978-0-387-30440-3

Zollo A, Iannaccone G, Lancieri M, Cantore L, Convertito V, Emolo A, Festa G, Gallovič F, Vassallo M, Martino C, Satriano C, Gasparini P (2009b) Earthquake early warning system in southern Italy: methodologies and performance evaluation. Geophys Res Lett 36: L00B07. doi:10.1029/2008GL03668

Chapter 8
Earthquake Early Warning for Transport Lines

G. Bonn, A. Buchmann, D. Hilbring, E. Hohnecker, T. Titzschkau and F. Wenzel

Abstract This paper discusses an earthquake early warning system for transport lines. The focus lies on first producing an alert map before the strong motion phase to warn endangered trains and on then providing a damage map of the railway infrastructure immediately after the strong motion phase. We find that an efficient framework for earthquake early warning is provided by combining the information from a neural network algorithm for predicting ground motion in real-time, by railway track integrated sensors, and by risk analyses for railway operation and infrastructure via a service-oriented system architecture. In particular, we demonstrate that by consistently employing standardized and end user adapted services throughout the entire early warning chain, pertinent early warning information required for efficient rescue and repair measures can be made instantly available to end users in the form of alert and damage maps.

8.1 Introduction

Natural disasters have led to a rising number of human losses, destruction of infrastructure and consequently economic damage in recent years (Topics Geo 2008). There is a need and a large potential for early warning systems in a world where population and economic strength are continuously increasing and depend significantly

G. Bonn · D. Hilbring (✉)
Fraunhofer IOSB, Karlsruhe, Fraunhoferstr. 1,76131 Karlsruhe, Germany
e-mail: desiree.hilbring@iosb.fraunhofer.de

A. Buchmann · E. Hohnecker
Department of Railway Systems, Karlsruhe Institute of Technology (KIT), Otto-Ammann-Platz 9, 76131 Karlsruhe, Germany

T. Titzschkau · F. Wenzel
Geophysical Institute, Karlsruhe Institute of Technology (KIT), Hertzstr. 16, 76187 Karlsruhe, Germany

F. Wenzel and J. Zschau (eds.), *Early Warning for Geological Disasters*, Advanced Technologies in Earth Sciences, DOI: 10.1007/978-3-642-12233-0_8,

on the functionality of the infrastructure. As recent events have shown, the world community is no longer willing to accept catastrophes caused by major earthquakes as mere fate. The motivations for the research project 'Earthquake Early Warning for Transport Lines (EWS Transport)' are based on the knowledge gained from recent advances in the fields of sensor, computer, and information and communication technologies. This opens up new possibilities for reducing the risk through the use of an early warning system in connection with support systems for decision making.

The project EWS Transport was funded by Geotechnologien, a geoscientific research and development programme supported by the German Federal Ministry for Education and Research (BMBF) and the German Research Foundation (DFG). It analyses the potential of earthquake early warning systems for railway lines. The interdisciplinary project consortium consists of geophysicists, civil engineers, and computer scientists and works on end-user oriented questions. The Geophysical Institute (GPI) of the Karlsruhe Institute of Technology (KIT) was responsible for the real-time seismology. The Department of Railway Systems (ISE) of the KIT worked on the identification and reduction of risks for train operations before and during an earthquake, as well as on railway infrastructure damage assessment after an earthquake. The Fraunhofer Institute of Optronics, System Technologies and Image Exploitation (IOSB) worked on the specification and implementation of an appropriate system architecture, because early detection of an earthquake in combination with alert creation, the possible manipulation of rail traffic and finally the damage estimation is a complex task. The main goal of the system architecture is portability. The system should not only be applicable to other regions, but also to other types of natural disasters or to the protection of other types of infrastructure systems. Therefore, a flexible service architecture based on geospatial standards was chosen.

A range of sophisticated earthquake early warning systems have been proposed in recent years (e.g. Allen and Kanamori 2003; Horiuchi et al. 2005; Cua and Heaton 2007; Weber et al. 2007; Böse et al. 2008) resulting from extensive research on suitable sensors, system configurations and early warning algorithms. However, feared consequences of possible false alarms, liability issues as well as a general lack of interested end users have prevented the widespread use of earthquake early warning systems. They are often implemented for research purposes only. Fully operational systems that actually trigger actions and/or emit public warnings include the 'Seismic Alert System' for Mexico City (Espinosa-Aranda et al. 1995; Suárez et al. 2009), the Taiwanese 'Early Warning System' and 'Rapid Reporting System' (Wu and Teng 2002), the Japan Meteorological Agency earthquake early warning system (Kamigaichi et al. 2009) and the Japanese 'Urgent Earthquake Detection and Alarm System UrEDAS' (Nakamura 2004; Nakamura and Saita 2007). Recently, the usefulness of early warning for saving human lives in metropolitan areas even for lead times less than 10 s has been emphasized (Wyss 2012).

Currently, no earthquake early warning system application in operation focuses on the special requirements of transport lines, with the exception of the Japanese UrEDAS for railways. It was developed in the 1980 s and has been continuously updated. In recent years, UrEDAS has been repeatedly activated. When an earthquake occurs, single stations equipped with 3D accelerometers detect the P waves,

calculate the earthquake magnitude and within 4 s transmit a radio warning signal to endangered sites within a range of about 200 km. A standard emergency measure is then, for example, the deceleration and stopping of a fast Shinkansen train. Each single UrEDAS station is able to measure, calculate, and transmit corresponding warning signals. A higher level network organization is not used.

Possible disadvantages of the system are the low network density, e.g. 14 sensors distributed along 515 km of railway tracks in the case of Tokaido Shinkansen line, and the lack of information relevant for risk estimation and damage prevention, such as hypocenter location, wave propagation direction, and shake maps. A higher density network of P wave detectors could help in saving valuable seconds and could provide a more detailed and more reliable damage prognosis. Further information concerning the propagation direction and amplitudes of seismic waves in the three spatial dimensions could be used for assessing the impact of an earthquake on train operations and various infrastructure elements with higher accuracy and for choosing the most suitable emergency measures.

In the project EWS Transport an earthquake early warning system for transport lines was developed and tested. It comprises new ideas ranging from neural networks for earthquake detection and dense networks of sensors integrated into the railway infrastructure up to powerful information systems. An in-depth description of the system has been published as online first article (Hilbring et al. 2010).

8.2 Open Architecture for Early Warning Systems

The "Reference Model of Open Distributed Processing" of the International Organization for Standardization (ISO) defines a standardized way to describe system architectures (RM-ODP 2009). The European Project ORCHESTRA adopted this approach and applied it to the design of an open service-oriented architecture for risk management. The outcomes were published by the Open Geospatial Consortium (OGC) as best practices paper (Usländer 2007). A follow-on European Project called Sensors Anywhere (SANY) analyzed the principles of ORCHESTRA and extended them to include the sensor domain. The result is the Sensor Service Architecture published as OGC discussion paper (Usländer 2009).

This research work from the fields of risk management and the sensor domain provides a good basis for the development of architectures for early warning systems. Therefore, the principles developed by ORCHESTRA and SANY were taken into account for the development of the early warning system architecture for transport lines.

8.2.1 Application Scenarios

The first step in the development of the EWS Transport architecture was the definition of the system requirements. They were identified by defining several application

scenarios, so called use cases, for the early warning system. Each use case describes a step by step workflow which needs to be processed to reach the desired results. The following three use cases reflect the main requirements of an earthquake early warning system for transport lines:

- The use case "Earthquake Early Warning" defines the early warning task starting with the detection of an earthquake based on its fast P wave, continues with the risk estimation for the train operation and ends with the notification of the concerned railway operating company.
- The use case "Structural Health Monitoring" starts with the compilation of the shake map based on the measured slower, but damaging S wave PGA values. It continues with the damage estimation for railway infrastructure elements such as railway tracks and bridges.
- The use case "Permanent Infrastructure Monitoring" addresses the potential use of sensors integrated in the system for permanent monitoring of infrastructure elements.

8.2.2 Functional Blocks

Looking at the application scenarios, one can see that the requirements for the early warning system are quite complex and concern different institutions. Therefore, several functional blocks are defined in the early warning architecture to clearly distinguish between the different scopes of the early warning system (see Fig. 8.1).

The block "Sensor System & Early Detection" realizes the early detection of the hazard. This block encapsulates the sensor network from the early warning system. The block "Assessment & Decision" combines the hazard information delivered by the first block and the infrastructure in danger (which is the railway infrastructure for the case of EWS Transport) to identify potential hazards and damage. The block "Action Execution" is responsible for the execution of actions proposed by the block "Assessment & Decision". This block represents the interface to the institutions requiring the early warning information. The final block "Visualization & Analysis" visualizes the results and provides the means for adequate analysis functionality in the previous blocks.

8.2.3 Services

In the next step, the necessary components that are required to fulfill the tasks described by the application scenarios are identified. The respective components and their allocation to the corresponding functional blocks are shown in Fig. 8.1. Firstly, the figure shows the components needed for the realization of the early detection and alert creation of an earthquake. Secondly, it shows components which are necessary for the creation of appropriate decisions regarding the infrastructure in

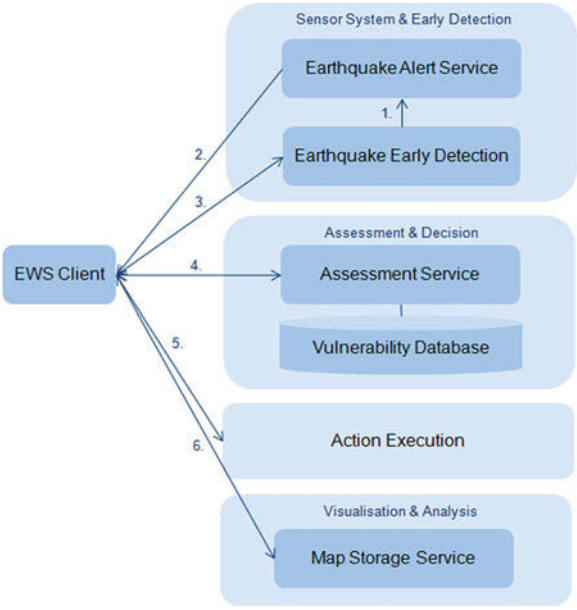

Fig. 8.1 Functional blocks of early warning architecture and their components

danger. Information about this infrastructure is stored in the vulnerability database. Finally it shows a map service which is needed to visualize the results, such as the actions that have been triggered by the decisions.

At this stage the principles of building an open service architecture come into play. To ensure flexibility and exchangeability the use of standard based interfaces is needed. ORCHESTRA and SANY analyzed existing standardized services from the OGC, provided recommendations for their use and defined missing extensions (OGC 2009). The following sections describe different aspects addressed by ORCHESTRA and SANY which play important roles for the development of early warning systems and which therefore have been considered by EWS Transport for the definition of an early warning system architecture.

8.2.3.1 Event Handling

A central aspect of an early warning architecture is an event-based interaction model. For an earthquake early warning system the timely alert notification is crucial in order to ensure the possibility of taking appropriate measures before the earth-quake hits, since the available timeframe will only be a few seconds to minutes, at the most. Flexibility and adaptability are among the key characteristics of the event-based interaction model because event generators do not call any specific type of event receivers. Indeed, they do not even need to know them.

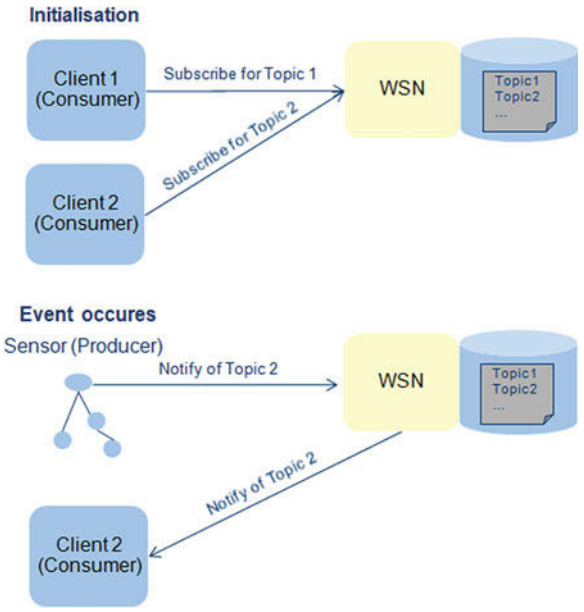

Fig. 8.2 Event based interaction model

The event-driven model consists of at least of two components: (1) a component (e.g. a sensor) sensing the event and emitting the notification and (2) a consumer receiving this notification.

SANY analyzed the OASIS Web Service Notification (WSN) standard for the applicability of event-driven workflows in sensor service architectures (see Fig. 8.2) (Graham et al. 2006). In the initialization phase a consumer subscribes to specific topics of the WSN, according to his interests. When an event occurs the producer notifies the WSN, which then filters the received event and notifies only interested consumers. This event based interaction model has been re-used by EWS Transport.

8.2.3.2 Alerts

An early warning system can produce different alerts to inform interested institutions. Depending on the duties of the institution and the receiving component of the alert message (software or human being), more or less technical messages are needed. An earthquake early warning system requires machine readable messages, since the critical time frame to execute actions is typically only between 10 and 60 s. However, the information must also be comprehensible for humans to serve as basis for the planning in the response phase of the risk management cycle. Therefore, EWS Transport chose to use the XML-based Common Alerting Protocol (CAP) for the alert notification messages (Jones and Bottere 2005) (see Fig. 8.3). The following notifications were defined in the earthquake early warning architecture:

```
<cap:alert xmlns:cap="urn:oasis:names:tc:emergency:cap:1.1"
xmlns:xsi="http://www.w3.org/2001/XMLSchema-instance"
xsi:schemaLocation="urn:oasis:names:tc:emergency:cap:1.1 cap.xsd ">
  <cap:identifier/>
  <cap:sender>PreSEIS</cap:sender>
  <cap:sent>2009-08-06T08:31:28Z</cap:sent>
  <cap:status>Actual</cap:status>
  <cap:msgType>Alert</cap:msgType>
  <cap:scope>Public</cap:scope>
  <cap:info>
    <cap:category>Geo</cap:category>
    <cap:event>Earthquake</cap:event>
    <cap:urgency>Past</cap:urgency>
    <cap:severity>Unknown</cap:severity>
    <cap:certainty>Observed</cap:certainty>
    <cap:senderName>PreSEIS</cap:senderName>
    <cap:headline>ShakpeMap</cap:headline>
    <cap:description>An earthquake S-Wave has been detected. An shake map has been calculated.
    This is a computer generated message and has not yet been reviewed by a human.</cap:description>
    <cap:parameter>
      <cap:valueName>SOS</cap:valueName>
      <cap:value>http://ews-transport.iitb.fraunhofer.de/servlet/is/Entry..SOSRequest/</cap:value>
    </cap:parameter>
    <cap:parameter>
      <cap:valueName>Offering</cap:valueName>
      <cap:value>EWSTDemo</cap:value>
    </cap:parameter>
    <cap:parameter>
      <cap:valueName>ObservedProperty</cap:valueName>
      <cap:value>http://sweet.jpl.nasa.gov/ontology/phenomena.owl#Earthquake</cap:value>
    </cap:parameter>
    <cap:parameter>
    <cap:parameter>
    <cap:parameter>
      <cap:valueName>Magnitude</cap:valueName>
      <cap:value>7.9</cap:value>
    </cap:parameter>
    <cap:parameter>
      <cap:valueName>Lat</cap:valueName>
      <cap:value>8.983</cap:value>
    </cap:parameter>
    <cap:parameter>
      <cap:valueName>Long</cap:valueName>
      <cap:value>48.27</cap:value>
    </cap:parameter>
    <cap:parameter>
      <cap:valueName>Depth</cap:valueName>
      <cap:value>9</cap:value>
    </cap:parameter>
    <cap:area>
      <cap:areaDesc>Feature of interest Baden-Wuerttemberg</cap:areaDesc>
      <cap:polygon>47.4,7.4 47.4,10.7 49.9,10.7 49.9,7.4 47.4,7.4</cap:polygon>
    </cap:area>
  </cap:info>
</cap:alert>
```

Fig. 8.3 Common alerting protocol (CAP) with shake map alert

- The "AlertMap" notification informs the consumer that an earthquake P wave has been detected and that parameters (magnitude, hypocenter, affected region) for the expected earthquake could be estimated.
- The "ShakeMap" notification informs the consumer that an earthquake has occurred and that the corresponding earthquake parameters have been measured and are available.
- The "DamageMap" notification informs the consumer that potential damage caused by the earthquake has been calculated and is available.

8.2.3.3 SOS and Coverages

OGC defined a Sensor Observation Service (SOS) (Nah and Priest 2007), which provides means for accessing data from the sensor domain. The SOS uses the Observation & Measurement Model (O&M) (Cox 2007) to define the accessible data. Typical datasets accessible by an SOS are time series datasets. SANY used the O&M to define a new observation type, a coverage, which provides a number of values structured in a rectified grid.

This principle has been re-used by EWS Transport and extended to define an additional observation type representing an earthquake. This earthquake observation type consists of two data arrays. The first array describes the earthquake parameters hypocenter, magnitude. The second data array describes a coverage holding PGA (peak ground acceleration) values for the area of interest. The newly defined earthquake observation type can be used to describe earthquake data representing the alert map, which contains estimated earthquake parameters for the upcoming earthquake, as well as earthquake data representing the shake map, which contains measured earthquake parameters after the strong-motion phase of the earthquake.

8.2.3.4 Information Retrieval Model

The goal of the early warning system is not only to provide data for the institution wanting to protect its infrastructure, but also to provide data for other institutions concerned with the management of the catastrophe. For this reason SANY utilized service oriented methods along with OGC services to make information available via several standardized service interfaces. This ensures that different clients of several institutions can access data corresponding to their interests. The employed service oriented method used to achieve this goal is called information retrieval model. The model consists of several steps:

- Step 1: Information retrieval via Sensor Observation Service (SOS) [SOS: Nah and Priest (2007) and Sensor Model Language used inside SOS: Botts (2007)]. Usually "raw" data are provided, which need further processing to derive the information of interest to the user.

- Step 2: Configuration via Sensor Planning Service (SPS) (Simonis 2007) or Web Processing Service (WPS) (Schut 2007). This step processes the data according to the needs of the user.
- Step 3: Access to results via SOS or Web Feature Service (WFS) (Vretanos 2005).

8.2.3.5 Coverage Visualization

The early warning system requires an appropriately standardized solution for visualizing the alert and shake maps provided as coverages by the SOS. For this purpose, the Map and Diagram Service (MDS) developed by ORCHESTRA, which is an extension of the well known Web Map Service (WMS) standard, can be used (Iosifescu-Enesu 2007; Beaujardière 2002). It offers possibilities for the visualization of coverages in the ASCII Grid format, which can be easily created from the acceleration field provided by the SOS. The use of the MDS can be recommended for the visualization of alert maps and shake maps.

8.3 Earthquake Early Warning Demonstrator

An important goal of EWS Transport was the implementation and testing of the specified early warning system architecture. The most important parts of the architecture have been described in the previous section for the case of earthquake early warning for transport lines. This section describes the earthquake early warning demonstrator, which has been implemented to test the architecture, and also explains how the principles from Sects. 8.2.2 and 8.2.3 have been applied. The application of standard-based interfaces for the implementation of an early warning system is especially of interest.

Several reasons motivated the decision to implement the early warning demonstrator based on Web Services. Firstly, this implementation architecture provides the possibility to create a distributed architecture and helps testing the exchangeability and interoperability of components. Secondly, many OGC services are available as open source components and their applicability could be tested for early warning systems. Thirdly, the Earthquake Early Warning Demonstrator is online accessible for demonstrations: http://ews-transport.iosb.fraunhofer.de/servlet/is/394/.

8.3.1 Example: Test Area Baden-Württemberg

To test and demonstrate the functionalities of EWS Transport, a specific area (test area) was selected for which the implementation of the early warning system could be simulated. The test area is simply one application example for EWS Transport. The system can easily be transferred to other regions due to the service oriented design of the system architecture which ensures portability.

The federal state of Baden-Württemberg (BW), located in the south-west of Germany, was chosen as an exemplary test area for EWS Transport because of the availability of GIS railway data (see Sect. 8.3.4), knowledge of the railway operational system and information on the local geology. BW is the state in Germany with the highest seismic activity which, however, from a global viewpoint is low but not negligible. The maximum magnitudes range between 6.0 and 6.5 and in terms of European Macroseismic Scale intensities, the non-exceedance probability of 90 % in 50 years ranges between V and VIII (Grünthal and Bosse 1996; Grünthal 1998). Due to the rare occurrence of earthquakes and the lack of large magnitude events, there is a shortage of observed data that are suitable for this study. Synthetic seismograms of earthquakes in and around BW thus have been generated and provide the basis for the simulation of EWS Transport options.

8.3.2 Synthetic Data

Within the scope of this study, Sokolov and Wenzel (2008) developed the first stochastic ground motion model customized to BW. It is based on regional earthquake ground motion data and site amplification parameters. With this model, ground motion records can be created at any point in the test area and for any given hypocenter and magnitude. In order to generate scenarios that are as realistic as possible and as hazardous as necessary for EWS Transport testing purposes, the historic earthquake catalog of Germany was consulted (Leydecker 2008). The distribution of earthquakes was obtained from hypocenter coordinates of historic events with an intensity $\geq$5 in a radius of 250 km around the center of BW. A Gutenberg-Richter relationship of $log_{10}N = 4.9 - 0.72M_L$, where N is the number of earthquakes with a local magnitude M_L or greater, was determined from all earthquakes in the catalog with $M_L \geq 2.5$. As input for the generation of synthetic ground motion, 290 earthquakes with a magnitude distribution between 4.5 and 6.5 following the Gutenberg-Richter relationship were randomly distributed over the hypocenters. For the sake of testing the system, 15 additional earthquakes with magnitudes between 6.6 and 8.0, which are considered as impossible in this area, were added at the locations of historically greatest earthquake intensity. The distribution of all 305 earthquakes is shown in Fig. 8.4.

For the current version of the online simulation synthetic ground motion was generated at the location of the 13 stations of the federal earthquake service of BW (LED) that have direct data transfer (http://www.lgrb.uni-freiburg.de) (Fig. 8.4, white squares) and at 50 additional virtual stations that are randomly distributed along railway lines in the test area (Fig. 8.4, black triangles). This scenario was chosen because measurements along railway lines have shown that low-cost instruments implemented in the track will not be able to detect P waves due to the low sensitivity of the instruments and the high noise level of the environment (Hilbring et al. 2010). At the LED stations, sensitive instruments record ground motion in a quiet environment and thus are very well suited for the detection of P waves

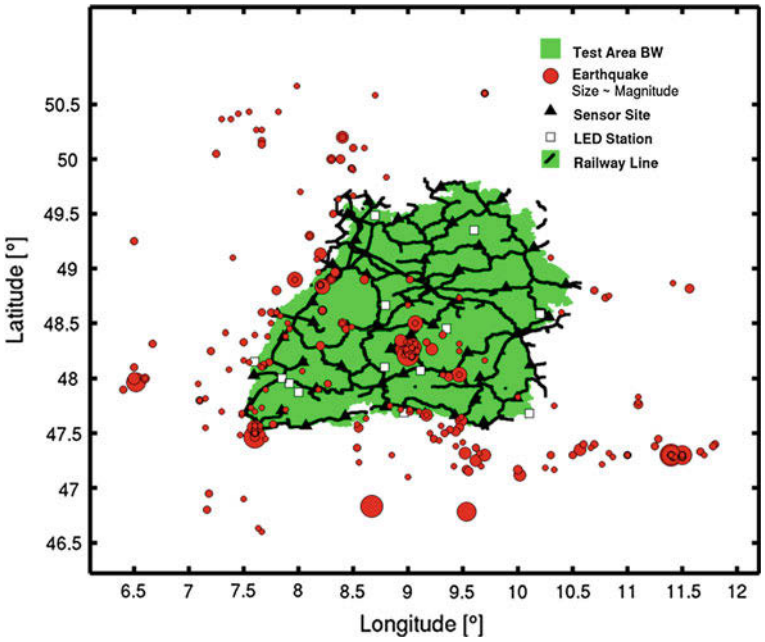

Fig. 8.4 Map of the test area BW showing the distribution of 305 synthetic earthquakes, the sensor sites and the railway lines

(use case "Earthquake Early Warning"). The instruments along the railway lines, however, are able to register the PGA amplitude caused by an earthquake directly at the track which is important for accurate damage assessment of the infrastructure (use case "Structural Health Monitoring"). Furthermore, continuous ground acceleration measurements along train tracks may be used for infrastructure monitoring. With a combination of such sensor systems one could make use of the given infrastructure, power lines and communication options to provide comprehensive information directly for and directly at the object of interest.

P and S waves were simulated separately with different input parameters for the average radiation pattern, the wave velocity and the attenuation model. The waveforms were then combined to obtain a complete seismogram, using travel times respective to an average P wave velocity $v_p = 6$ km/s (Stange and Brüstle 2005) and an S wave velocity $v_s = 3.5$ km/s ($v_s = (1/\sqrt{3})\, v_p$; Lay and Wallace 1995). A waveform example is given in Fig. 8.5.

The synthetic data used in this analysis are very basic and source and path effects have not been optimized. However, the purpose of the demonstrator is to test and prove the research outcomes of EWS Transport and the implemented components could easily be changed to support regions with higher seismic activity for which real ground motion data are available.

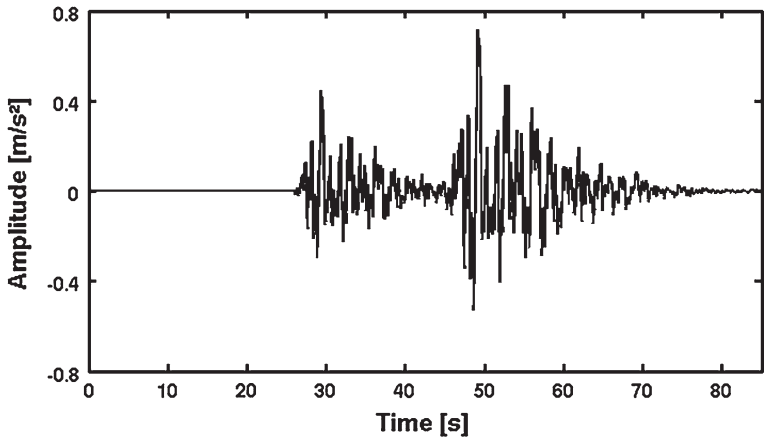

Fig. 8.5 Synthetic waveform Example of a magnitude 6.5 earthquake in a hypocenter to station distance of 63.3 km

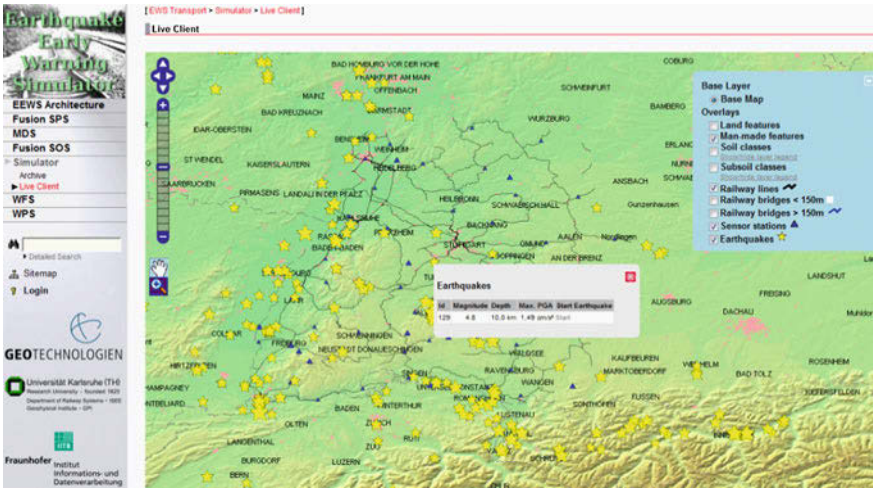

Fig. 8.6 Screen shot of web based earthquake early warning simulation program (Live Client)

In the so called "Live Client" of the demonstrator (see Fig. 8.6) users can select any one of the 305 test datasets for earthquakes in BW to start the simulation. The triggered workflow involves two major application scenarios: "Earthquake Early Warning" and "Structural Health Monitoring". The application scenario "Earthquake Early Warning" is mapped to the component structure of the early warning architecture and appropriate standardized services are identified (see Fig. 8.7).

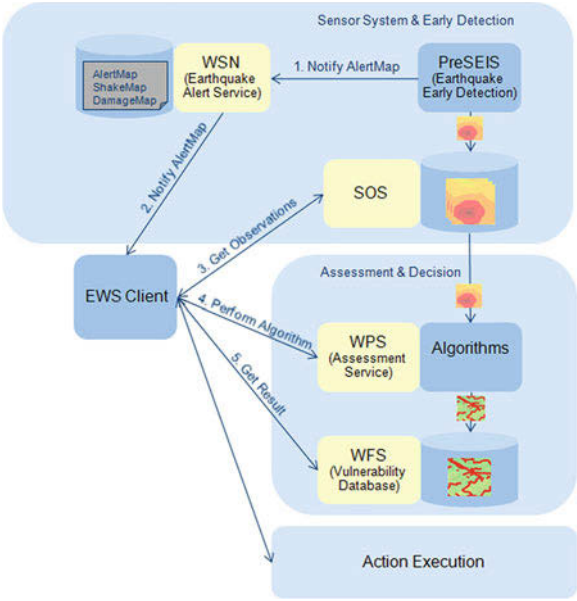

Fig. 8.7 Workflow of application scenario "Earthquake Early Warning"

8.3.3 Earthquake Early Detection Using PreSEIS and Alert Map Creation

EWS Transport implements a modified version of the earthquake early warning method PreSEIS (Böse et al. 2008) for earthquake detection and analysis. In PreSEIS, earthquake parameters are extracted from the sensor network via artificial neural net technology (see Fig. 8.8).

This early warning method combines the advantages of regional and on-site early warning approaches (Böse et al. 2008; Köhler et al. 2009): PreSEIS is quick and reliable because it is not required that seismic waves have arrived at all stations before parameter estimations can be issued and the parameters are continuously updated using the incoming information from all triggered and not yet triggered stations. The synthetic data used in this analysis are very basic, however, PreSEIS has already been proven to work successfully with real data (Köhler et al. 2009) and this study has its focus on the special requirements of an earthquake early warning system for railway lines.

Two layer feed forward neural networks with an input, a hidden and an output layer (see Fig. 8.8) are trained with a subset of the synthetic dataset to extract information from P waves at the 13 LED stations and issue parameter estimations, which are updated every 0.5 s. Generally, the errors on the parameter estimates decrease with increasing time because more information becomes available for the analysis, but as a trade-off the early warning time decreases. The networks are trained to estimate

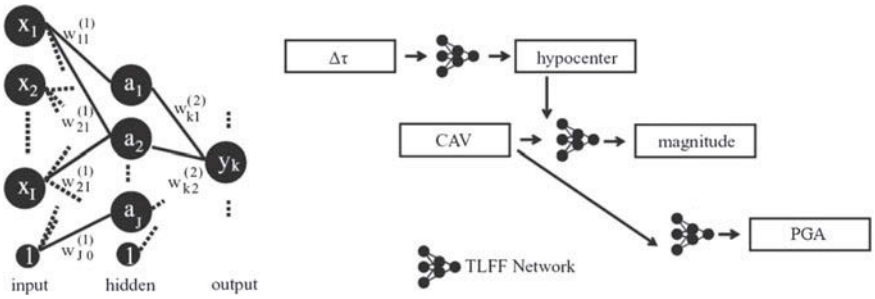

Fig. 8.8 Two layer feed-forward (TLFF) network and parameter estimation in PreSEIS (modified from Böse et al. 2008)

(i) hypocenter coordinates from the onset time differences Δt and (ii) magnitude from the hypocenter estimate and the cumulated absolute velocity (CAV) of the data, as well as (iii) the expected horizontal PGA from the CAV only (see Fig. 8.8). The PGA estimates are made for each of the 50 virtual sites along the railway lines, i.e. directly at user sites. The ability of the network to estimate correct parameters from 'unknown' earthquakes (not included in the training dataset) is tested with the remainder of the dataset.

Based on the 50 PGA estimates, alert maps for BW with a resolution of 1 km^2 are calculated by interpolation. Alert maps are a crucial component of EWS Transport as they provide the basis for risk assessment along the railway lines in the test area (see Sect. 8.3.4). In the current version of the demonstrator only one alert map, calculated 3 s after the detection of the first P wave at one station, is used for further analysis. For decision makers, a continuously updated alert map is not helpful because the warning time for earthquakes is very short and emergency measures cannot be changed every 0.5 s depending on new information. Therefore, one has to select a certain time after which the estimated alert map is deemed good enough yet the warning time remains large enough to take appropriate measures.

The earthquake event triggered by PreSEIS is structured as CAP "AlertMap" notification to the WSN once an earthquake has been detected. The WSN notifies the EWS client. The EWS client accesses the earthquake observations via the Sensor Observation Service (SOS) and receives the newly defined earthquake observation type (see Sect. 8.2.3.3) as shown in Fig. 8.7. In the application scenario "Earthquake Early Warning" the PGA values are estimated values of the ground acceleration in the upcoming earthquake based on which an alert map with a resolution of 1 km^2 is created for the whole region by interpolation.

8.3.4 Risk Estimation

The Alert Map is combined with railway infrastructure data for risk estimation. Concerning the early warning phase, the horizontal PGA at the track site (abbreviated

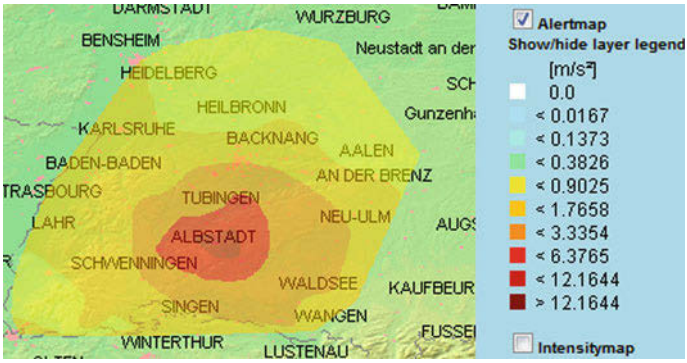

Fig. 8.9 Visualization of predicted ground acceleration (alert map) in test area for a simulated magnitude 7.9 earthquake near Albstadt

as a) is identified as the crucial parameter that characterizes the risk in train operation. In particular, acceleration thresholds above which train derailment is likely to occur and pertinent emergency measures have been defined as a function of train velocity.

According to current practice for high speed trains in Japan (Shinkansen) the local acceleration threshold is defined as $a = 0.4\ \mathrm{m/s^2}$. If accelerations above this value are recorded, the local power supply at the train position is switched off and an emergency braking of the train is initiated (Nakamura 1996). These measures are applied directly, i.e. without the intermediary of a train control center.

As a first step, EWS Transport thus adopts the local PGA at the track site as the relevant risk parameter and $a_1 = 0.4\ \mathrm{m/s^2}$ as the critical threshold above which train operation must be considered unsafe and emergency train control measures are initiated.

Emergency measures (see Fig. 8.10) depend on the estimated ground acceleration a along the track (see Fig. 8.9) and, in the second step, on the type of railway system, e.g. high speed or low speed lines. Instead of the actual train velocities the known maximum line speeds are used to define appropriate measures. Two measures are employed in EWS Transport for the use case "Earthquake Early Warning":

(a) for high speed lines with $v > 80$ km/h trains are stopped and the corresponding lines are closed if $a \geq a_1 = 0.4\ \mathrm{m/s^2}$ (red lines in Fig. 8.10);
(b) for low speed lines with $v < 80$ km/h, the train speed is reduced to $v < 20$ km/h if $0.4\ \mathrm{m/s^2} \leq a < 1.0\ \mathrm{m/s^2}$ (brown lines in Fig. 8.10). For $a \geq 1\ \mathrm{m/s^2}$ low speed trains are stopped and the lines are closed. These acceleration thresholds and the corresponding emergency measures are compiled in Table 8.1.

This classification is motivated by the fact that high speed trains are more vulnerable to derailment than low speed trains. When a train moves along a straight track segment the wheels exert dynamical vertical and horizontal forces on the track. These dynamical forces increase with train speed. As an example, we mention the sinusoidal motion of the wheelset that occurs as a result of conical wheel profiles first

Fig. 8.10 Map of closed (*red*) and speed-reduced (*brown*) railway lines in test area for the simulated earthquake

Table 8.1 Ground acceleration thresholds and emergency measures for different train speeds

	Reduce train speed to v $<$ 20 km/h	Stop train, close line
High speed line v $>$ 80 km/h	Not applicable	a $\geq$ 0.4 m/s^2
Low speed line v $\leq$ 80 km/h	0.4 m/s^2 $\leq$ a $<$ 1.0 m/s^2	a $\geq$ 1.0 m/s^2

described by Klingel (Esveld 2001). Associated with this so called Klingel motion are dynamical horizontal forces that increase quadratically with train speed.

Derailment takes place when dynamical horizontal track forces Y exceed a certain critical value beyond which track stability is no longer guaranteed (Prud'homme 1978). Numerous tests have shown that track stability and hence safety against derailment requires that horizontal forces on the track be below $Y < \alpha \left(10 + 2\frac{Q}{3}\right)$, where Q is the static vertical wheel load and α is an empirical parameter. Typical values for alpha range between 0.85 and 1.4 depending on the type of railway superstructure (Lichtberger 2004). For a vertical wheel load Q = 110 kN and α = 1, one obtains as the critical ratio of horizontal to vertical track forces $Y/Q < 0.76$.

Ground shaking and seismically induced track irregularities cause additional train velocity dependent horizontal forces so that fast trains reach these critical Y/Q values

earlier than slow trains. It should be clear that the acceleration thresholds in Table 8.1 are not calculated from the derailment criteria but are based on experience.

The catalogue of emergency measures can be extended and refined as more detailed information about the positions and velocities of individual trains on the network becomes available. For example, if the train positions and velocities are known certain potentially hazardous situations, such as trains coming to a halt on a damaged bridge, or freight and passenger trains meeting on a bridge in danger can be avoided via the measure "controlled braking".

The "Deutsche Bahn AG" supplied the EWS Transport research partners with data of its infrastructure in BW. EWS Transport decided to define processing algorithms for the risk and damage estimations based on the Web Processing Service (WPS) of the OGC. The algorithm described above has been implemented as risk estimation process in the WPS. The results are recommended actions for the railway company to be executed for trains at risk (e.g. close a specific line segment). This information is combined with the line-based railway track geometry. The resulting spatial data is included into a Web Feature Service (see Fig. 8.7). This ensures that the results can also be accessed from outside the system. Additionally, the data can easily be accessed and visualized by components speaking WFS. This concludes the "Earthquake Early Warning" workflow, which applies the principles described in Sects. 8.2.3.1–8.2.3.3 (see Sect. 8.2.3).

8.3.5 Application Scenario "Structural Health Monitoring"

The demonstrator continues with the application of the "Structural Health Monitoring" workflow. Figure 8.11 shows the respective architecture.

8.3.5.1 Shake Map

Immediately after an earthquake, a shake map with a resolution of 1 km^2 is calculated by interpolation of the 50 true PGA values obtained from the seismograms of each station along the railway lines (see Fig. 8.12). Shake maps allow the identification of areas that have been affected by very high ground shaking and the assessment of potential damage to the railway infrastructure (see Sect. 8.3.5.2). The implementation of a large number of sensors, e.g. every 1 km, in the railway track would provide a highly resolved shake map which consequently can be used for very accurate damage estimation. PreSEIS triggers a CAP-based "ShakeMap" event once the strong-motion phase of the earthquake has finished.

As in the application scenario "Earthquake Early Warning", the EWS Client notified by the WSN accesses the earthquake observation data via the Sensor Observation Service. The difference is that now the values provided in the PGA coverage, which define the shake map, are measured values from the S wave and not estimates. The information contained in the shake map is then combined with railway

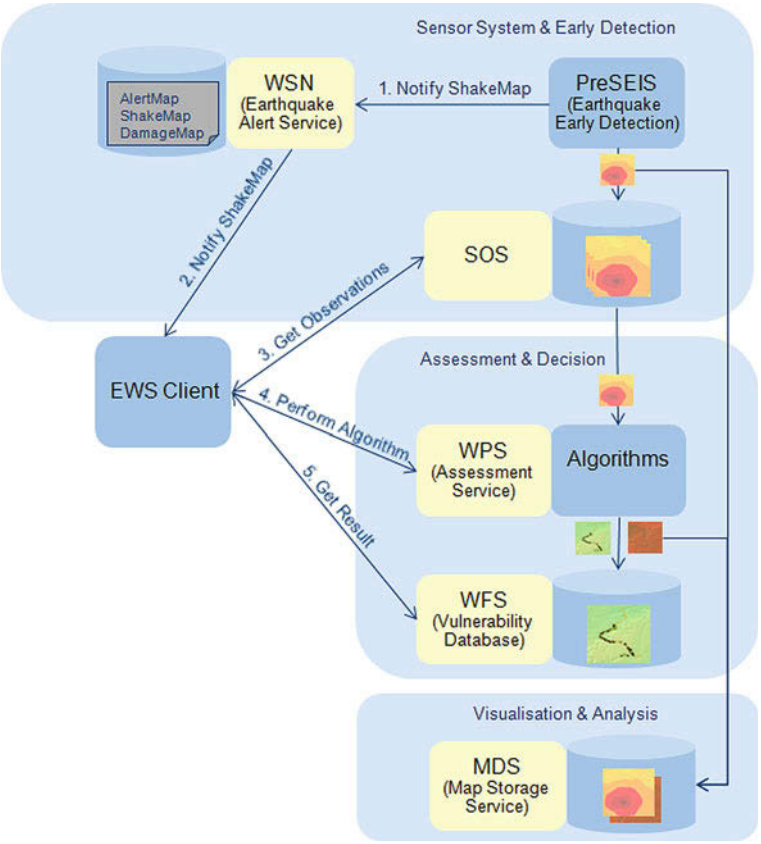

Fig. 8.11 Application scenario "Structural Health Monitoring"

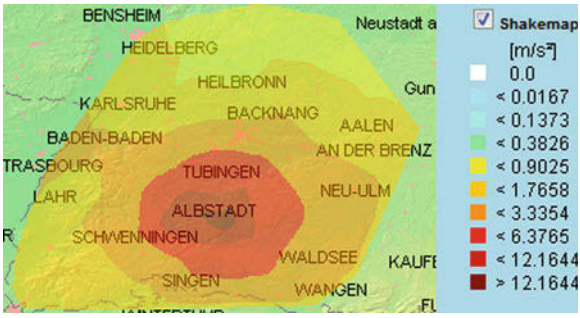

Fig. 8.12 Visualization of measured ground motion (shake map) in test area for a simulated magnitude 7.9 earthquake near Albstadt

infrastructure information. This time the goal is to estimate potential damage to the railway infrastructure since, after the occurrence of an earthquake, the railway operating company requires information on the condition of its railway infrastructure to initiate inspections and repairs so that train operation can be resumed as quickly as possible.

8.3.5.2 Damage Estimation

A damage catalogue is constructed for a specific railway network and geographical region. For this purpose, infrastructure data of the "Deutsche Bahn AG" (GIS ArcView shape files), which contain the entire railway network including information on the geographic location of stations, bridges, tunnels, as well as route number, electrification, etc. are used. These data have been supplemented with additional information relevant for seismic damage assessment, such as railway superstructure type and line bearing capacity. The damage catalogue is organized in the form of a matrix where the rows contain the various railway infrastructure elements (e.g. track, bridges, tunnels, buildings) and their main attributes (e.g. for bridges these are: length, number of spans, width, construction type, construction year, etc.) and the columns describe various damage classes together with the ground acceleration thresholds underlying the definition of these damage classes. The following section concentrates on assessing the seismic vulnerability of two railway infrastructure elements, namely bridges and straight tracks.

Bridges

A seismic damage analysis is available for highway bridges (Meskouris et al. 2007; Basöz and Mander 1999). Five bridge damage classes (none, minor, moderate, major, complete) and the corresponding median PGA values are defined for various generic bridge construction types. Basöz and Mander (1999) identify six bridge construction categories: (i) multi-column bents simply supported, (ii) single-column bents box girders, (iii) continuous concrete, (iv) continuous steel, (v) single span, (vi) long bridges ($l > 150$ m).

Presently, the EWS Transport database for the test area BW includes only two bridge classes, short bridges with a length $l < 150$ m and long bridges with $l > 150$ m. For both bridge types and the five damage classes the corresponding acceleration thresholds a_i for $i = 2 \ldots 5$ (medians) are taken from Basöz and Mander (1999) for "single span" and "long bridges" (see Table 8.2) and are integrated in the EWS Transport database. A lower ($a_1 = 0$) and an upper ($a_6 = \infty$) value for the PGA are also introduced. The five damage classes 1–5 are then defined as a function of median ground acceleration thresholds $a_1 \ldots a_6$ and bridge type as follows: a bridge is in damage class i if the local PGA a satisfies the following condition $a_i \leq a < a_{i+1}$. For example, a "long bridge" is estimated to be in damage class 3 if the local ground acceleration is equal to or exceeds 4.9 m/s^2 but remains below 5.9 m/s^2. These

Table 8.2 Acceleration thresholds for two bridge types and damage classes 1–5 (see text)

a (m/s^2)	a_1	a_2	a_3	a_4	a_5	a_6
Short bridges	0	7.8	8.8	10.8	15.7	∞
Long bridges	0	3.9	4.9	5.9	7.8	∞
Damage class	No(1)	Minor(2)	Moderate(3)	Major(4)	Complete(5)	

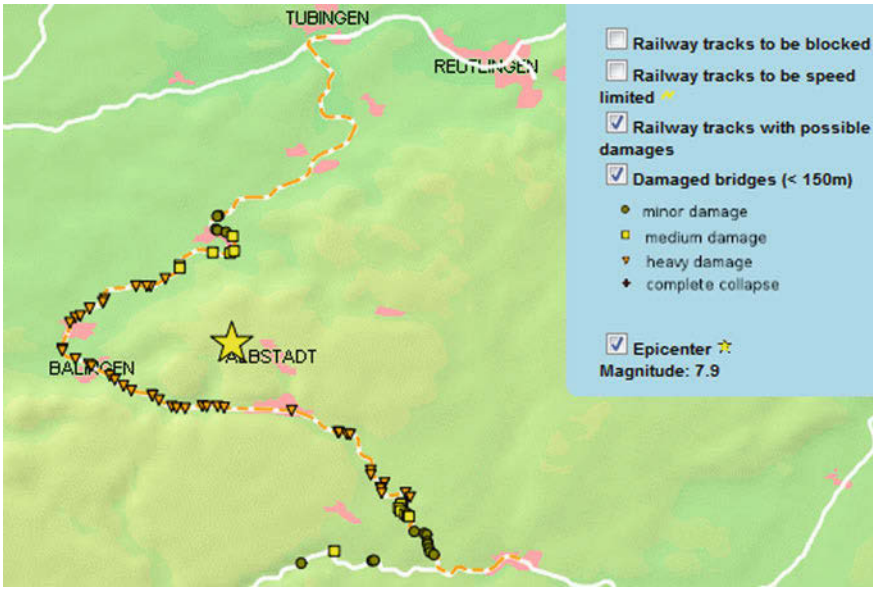

Fig. 8.13 Visualization of estimated damage of railway bridges and tracks for the simulated earthquake (damage map) based on the PGA thresholds in Tables 8.2 and 8.3

acceleration thresholds are used as input values for the damage assessment and damage map generation in the demonstrator (see Fig. 8.13).

Straight Track

The seismic vulnerability of a straight track segment is mainly characterized by the lateral track resistance w (N/m). The latter is defined as the critical horizontal force which leads to a lateral sleeper displacement of 2 mm, beyond which the static Coulomb friction goes over into sliding friction. The lateral track resistance depends on the type of track superstructure (ballast track or slab track), the type of sleepers (wooden or concrete sleepers) as well as the density and granular composition of the ballast bed. If the lateral forces due to ground acceleration exceed the critical horizontal force, permanent track deformation (buckling) will result. In Table 8.3

Table 8.3 Lateral track resistance w (Fendrich 2007; Lichtberger 2004) and corresponding acceleration thresholds a_{thresh} for various railway track systems

	Lateral track resistance w (kN/m)	a_{thresh} (m/s^2)
Ballast (wooden sleepers)	5.0	4.0
Ballast (concrete sleepers B70)	17.0	10.0
No ballast (wooden sleepers)	1.0	3.0
Slab track	$\gg$17	$\gg$10

critical horizontal ground acceleration thresholds a_{thresh} are defined for different railway superstructures.

For demonstration purposes, only two damage classes (no damage and major damage) and a single ground acceleration threshold are currently employed. The value of $a_{thresh} = 4\ m/s^2$ defines the threshold above which major track damage results. It should be emphasized that the acceleration thresholds compiled in Table 8.3 are crude estimates based on the lateral resistance and mass per unit length of track. Further research is required to substantiate or, if necessary, to modify the above thresholds for a straight track segment. In addition, if railway tracks are laid on an embankment or in a cut, the seismic vulnerability of these earth structures has to be taken into account. Railway embankments are more vulnerable than railway tracks themselves and require a separate analysis. Clearly, for tracks laid on an embankment ground acceleration thresholds can be significantly lower than the values listed in Table 8.3 (Nakamura 1997).

The damage catalogue described above is integrated into the demonstrator via GeoServer (2009). The Web Feature Service (WFS) interface of GeoServer provides access to the static railway infrastructure data. The damage catalogue is accessed by a damage algorithm implemented as a process via the WPS interface. The damage algorithm combines the shake map with the railway track and bridge geometries. As a result, the infrastructure geometry (railway tracks and long bridges are represented by line strings; short bridges by points) as well as the pertinent damage classes are available for access and visualization via the Web Feature Service.

8.3.6 Access from Outside the System

The information created by the application scenario "Structural Health Monitoring" provides the basis for further actions. For this purpose, the EWS Client sends another event, the "DamageMap" notification to the WSN, once all damage estimation calculations have been finished. Interested components from outside the system can register for this event to be informed when an earthquake occurs.

8.3.7 *Application Scenario "Permanent Infrastructure Monitoring"*

The same dense network of track integrated acceleration sensors that has been used for fast damage map generation as described in application scenario "structural health monitoring" can also be used for permanent infrastructure monitoring. An accelerometer network can detect critical deviations from regular track geometry and rail head irregularities. When a train passes over these defects, it will generate characteristic traces in the vibration spectra. In addition, also irregularities of the rolling stock, such as wheel flats, polygonized wheels and broken axles cause typical track vibration signals that can be detected (Müller-Borrutau et al. 2009).

Currently, railway infrastructure is inspected in regular intervals with rail measuring vehicles. For example, rail measuring cars equipped with georadar, laser, and camera systems measure the condition of track substructure, track geometry, and rail geometry roughly every 6–12 months. Irregularities in the railway infrastructure occurring in between two inspections may gradually increase with time, but might remain undetected. A permanent and continuous infrastructure monitoring network may help in avoiding extensive repairs by detecting deviations in an early stage. Furthermore, continuous monitoring could be more cost efficient than inspections with measuring cars for which manpower has to be paid and tracks have to be closed temporarily (economic loss).

Aside from standard piezoelectric accelerometers, modern laser and fiber optic sensor techniques avoiding electromagnetic interferences with existing track based train control equipment are nowadays available and may be employed to the benefit of both: the railway infrastructure and rolling stock operators. The various aspects of track integrated sensors and their use for permanent infrastructure monitoring are described in more detail elsewhere (Quante and Schnellbögl 2009; Eisenmann 2009).

8.4 Summary

Recent advances in real-time seismology, geospatial and infrastructure data processing, as well as information and communication technologies were combined to develop a novel, web-based earthquake early warning system for railways. A major result of this work is the modeling and visualization of the entire early warning chain ranging from P wave detection to infrastructure damage estimation and risk reducing measures in the form of a web-based simulation program. It is accessible for demonstrations under the URL: http://ews-transport.iosb.fraunhofer.de/servlet/is/394/. We demonstrated that a service-oriented system architecture based on geospatial standards is very well suited to integrate the various aspects of earthquake early warning in a coherent end-user oriented framework. In particular, ground motion data as well as results from risk analyses for train operation and railway infrastructure are instantly

visualized in the form of alert, shake, and damage maps to assist the planning of rescue and repair measures.

The service-oriented design of the system architecture ensures portability so that it can be transferred to other natural hazards, e.g. landslides and to other infrastructures at risk, e.g. roads. Furthermore, the open standard-based system architecture allows the integration of other open services and thus ensures easy access to system results from outside of the early warning system. EWS Transport thus offers innovative system functionalities beyond those of the Japanese UrEDAS, the currently only existing early warning system for railway lines.

Acknowledgments We thank the BMBF/DFG Geotechnologien programme for financial support of project BMBF 03G0656A

References

Allen R, Kanamori H (2003) The potential for earthquake early warning in Southern California. Science 300:786–789

Beaujardière J (ed) (2002) Web map service implementation specification, OGC 01-068r3

Basöz N, Mander J (1999) Enhancement of highway transportation lifeline module in HAZUS, Draft 7. Federal Emergency Management Agency (FEMA) and National Institute for Building Sciences

Böse M, Wenzel F, Erdik M (2008) PreSEIS: a neural network-based approach to earthquake early warning for finite faults. Bull Seism Soc Am 98(1):366–382

Botts M (ed) (2007) OpenGIS sensor model language (SensorML) implementation specification, OGC 07-000

Cox S (ed) (2007) Observations and measurements—Part 1—Observation schema, OGC 07–022r1

Cua G, Heaton T (2007) The Virtual Seismologist (VS) method: a Bayesian approach to earthquake early warning. In: Gasparini P, Manfredi G, Zschau J (eds) Earthquake early warning systems. Springer, Berlin, pp 97–132. ISBN: 978-3-540-72240-3

Eisenmann Th (2009) Fiber optical sensing with fiber Bragg gratings. BMBF Geotechnologien Science Report 15

Esveld C (2001) Modern railway track. MRT Productions, Zaltbommel

Espinosa-Aranda J, Jimenez A, Ibarolla G, Alcantar F, Aguilar A, Inostroza M, Maldonado S (1995) Mexico City seismic alert system. Seismol Res Lett 66(6):42–53

Fendrich L (2007) Handbuch Eisenbahninfrastruktur. Springer, Berlin

GeoServer (visited in September 2009) GeoServer. http://geoserver.org

Graham S, Hull D, Murray B (2006) OASIS web services base notification 1.3 (WS-BaseNotification). http://docs.oasis-open.org/wsn/wsn-ws_base_notification-1.3-spec-os.pdf

Grünthal G (1998) Macroseismic Scale 1998 EMS-98, Chairman of the ESC Working Group "Macroseismic Scales". GeoForschungsZentrum Potsdam, Germany

Grünthal G, Bosse Ch (1996) Probabilistische Karte der Erbebengefährdung der Bundesrepublik Deutschland—Erdbebenzonierungskarte für das Nationale Anwendung-sdokument zum Eurocode 8, GeoForschungsZentrum Potsdam, STR 96/10, 24 pp

Hilbring D, Titzschkau T, Buchmann A, Bonn G, Wenzel F, Hohnecker E (2010) Earthquake early warning for transport lines. Nat Hazards. doi:10.1007/s11069-010-9609-3

Horiuchi S, Negishi H, Abe K, Kamimura A, Fujinawa Y (2005) An automatic processing system for broadcasting earthquake alarms. Bull Seism Soc Am 95(2):708–718

Iosifescu-Enesu I (2007) ORCHESTRA, specification of the map and diagram service. http://www.euorchestra.org/docs/OASpecs/Map_and_Diagram_Service_Specification_v3.0-ETHZ.pdf
Jones E, Bottere A (2005) OASIS common alerting protocol, v1.1, OASIS Standard CAP-V1.1, Oct 2005. http://www.oasis-open.org/committees/download.php/15135/emergency-CAPv1.1-Corrected-DOM.pdf
Kamigaichi O, Saito M, Doi K, Matsumori T, Tsukada S, Takeda K, Shimoyama T, Nakamura K, Kiyomoto M, Watanabe Y (2009) Earthquake early warning in Japan: warning the general public and future prospects. Seismol Res Lett 80(5):717–726
Köhler N, Cua G, Wenzel F, Böse M (2009) Rapid source parameter estimations of southern California earthquakes using PreSEIS. Seism Res Lett 80(5):748–754
Lay T, Wallace TC (1995) Modern global seismology. International geophysics series, vol 58. Academic Press, San Diego
Lichtberger B (2004) Handbuch Gleis. Tetzlaff, Hamburg
Leydecker G (2008) Erdbebenkatalog für die Bundesrepublik Deutschland mit Randgebieten ab dem Jahre 800. http://www.bgr.de/quakecat; Bundesanstalt für Geowissenschaften und Rohstoffe (BGR); Version 22.05.2008
Meskouris K, Renault Ph, Butenweg Ch, Hinzen KG, Weber B (2007) Gefährdungsabschätzung von Brücken in Deutschland unter Erdbebenbelastung, Forschung Straßenbau und Straßenverkehrstechnik 952, Bundesministerium für Verkehr, Bau und Stadtentwicklung
Müller-Borrutau F, Breitsamter N, Pieper S (2009) Measuring the effects that flat spots have on the dynamic wheel load and on rail pad forces. Railw Tech Rev 1:24–29
Nah A, Priest M (2007) Sensor observation service, Open Geospatial Consortium, OGC 06-009r6
Nakamura Y (1996) Real-time information systems for seismic hazards mitigation UrEDAS, HERAS and PIC. Q Rev RTRI 37(3):112–127
Nakamura Y (1997) Seismic vulnerability indices for ground structures using microtremor. In: World congress on railway research, Florence, Italy 16–19 Nov 1997
Nakamura Y (2004) UrEDAS, urgent earthquake detection and alarm system, now and future. In: 13th world conference on earthquake engineering, Vancouver, B.C., Canada, 1–6 Aug 2004, Paper No. 908
Nakamura Y, Saita J (2007) UrEDAS, the earthquake warning system: today and tomorrow. In: Gasparini P, Manfredi G, Zschau J (eds) Earthquake early warning systems. Springer, Berlin, pp 249–281. ISBN: 978-3-540-72240-3
OGC (visited in August 2009) OGC, Open Geospatial Consortium, Inc. http://www.opengeospatial.org/
Prud'homme A (1978) Forces and behaviour of railroad tracks at very high train speeds. In: Kerr AD (ed) Railroad track mechanics and technology. Pergamon, Oxford
Quante F, Schnellbögl G (2009) Railway infrastructure and seismic early warning systems. BMBF Geotechnologien Science Report 15
RM-ODP (visited in July 2009) ISO reference model for open distributed processing. http://www.rm-odp.net
Schut P (2007) OpenGIS web processing service. Open Geospatial Inc., OGC 05-007r7
Simonis I (2007) OpenGIS sensor planning service implementation specification, OGC 07-014r3
Sokolov V, Wenzel F (2008) Toward realistic ground motion prediction models for Baden-Württemberg, Germany. In: Proceedings of the 31 general assembly of European seismological commission, Sept 2008, Crete, Greece, CD ROM
Stange S, Brüstle W (2005) The Albstadt/Swabian Jura seismic source zone reviewed through the study of the earthquake of March 22 2003. Jahresberichte und Mitteilungen Oberrheinscher Geologischer Verein, Neue Folge, vol 87, pp 391–414
Suárez G, Novelo D, Mansilla E (2009) Performance evaluation of the seismic alert system (SAS) in Mexico City: a seismological and a social perspective. Seismol Res Lett 80(5):707–716
Topics Geo (2008) Naturkatastrophen 2008 Analysen, Bewertungen, Positionen, Münchener Rückversicherungs-Gesellschaft. http://www.munichre.com/publications/302-06021_de.pdf

Usländer T (2007) Reference model for the ORCHESTRA architecture (RM-OA) V2 (Rev 2.1), OGC 07-097

Usländer T (2009) Specification of the sensor service architecture (SensorSA), OGC 09-132r1

Vretanos PA (2005) Web feature service implementation specification, OGC 04-094

Weber E, Iannaccone G, Zollo A, Bobbio A, Cantore L, Corciulo M, Convertito V, Di Crosta M, Elia L, Emolo A, Martino C, Romeo A, Satriano C (2007) Development and testing of an advanced monitoring infrastructure (ISNet) for seismic early-warning applications in the Campania region of Southern Italy. In: Gasparini P, Manfredi G, Zschau J (eds) Earthquake early warning systems. Springer, Berlin, pp 325–341

Wyss M (2012) The earthquake closet: rendering early warning useful. Nat Hazards. doi:10.1007/s11069-012-0177-6

Wu YM, Teng T (2002) A virtual subnetwork approach to earthquake early warning. Bull Seism Soc Am 92(5):2008–2018

Chapter 9
The Earthquake and Tsunami Early Warning System for the Indian Ocean (GITEWS)

Joern Lauterjung, Alexander Rudloff, Ute Münch and Daniel J. Acksel

Abstract The German-Indonesian Tsunami Early Warning System (GITEWS) has been established after the devasting Tsunami in the Indian Ocean on December 26, 2004. The system follows an "end-to-end" approach to cover the complete warning chain from rapid hazard detection over decision support to capacity development of communities at risk and the implementation of disaster reduction measures. The paper discusses the specific challenges of Tsunami early warning in Indonesia, describes recent developments in instrumentation and data analysis and summarizes the system performance over the past 5 years.

9.1 Introduction

Indonesia is located along the most prominent active continental margin in the Indian Ocean, the so-called Sunda Arc making it one of the world's most threatened areas in terms of events such as earthquakes, volcanoes, and tsunamis associated with tectonic activity. On 26 December 2004 an earthquake of magnitude 9.3 (Stein and Okal 2005) occurred off the northern shores of Sumatra, causing the tsunami great enough to affect the whole Indian Ocean, with almost a quarter of a million people losing their lives. The affected areas were neither prepared in terms of early-warning nor disaster response.

In quick response Germany offered—during the UN World Conference on Disaster Reduction in Kobe, Hyogo/Japan in January 2005—to aid the development of a fast and reliable warning procedure for the Indonesian population so that a catastrophe of such scale could be avoided in the future. This aid would be provided in the form of technical support for the development and installation of a tsunami early warning system for the Indian Ocean and further to assist capacity building

J. Lauterjung (✉) · A. Rudloff · U. Münch · D.J. Acksel
Deutsches GeoForschungsZentrum GFZ, 14473Potsdam, Telegrafenberg, Germany
e-mail: lau@gfz-potsdam.de

F. Wenzel and J. Zschau (eds.), *Early Warning for Geological Disasters*,
Advanced Technologies in Earth Sciences, DOI: 10.1007/978-3-642-12233-0_9,

amongst the local communities. The Indonesian government accepted this offer as well as affected countries such as Sri Lanka, the Maldives and even East-African countries. The major part of our work targeted Indonesia, the area being the main source of tsunami risk for the surrounding Indian Ocean. The technical concept of such a warning system would have to deal with the extremely brief alarm periods for Indonesia, due to its close proximity to the Sunda Arc. For this reason the *German Indonesian Tsunami Early Warning System* (*GITEWS*) integrates various state of the art monitoring technologies and analysis methods (Münch et al. 2011).

Indonesia has a unique geotectonic position with its associated consequences in terms of natural hazards. The Sunda Arc lies on an active convergent plate boundary, where the Indo-Australian Plate is subducted at a speed of ~7 cm/y under the Eurasian Plate (Tregoning et al. 1994). The subduction zone comprises some 6,000 km from the north of Sumatra to the island of Sumbawa, running between 100 and 200 km parallel to the Indonesian coastline (Fig. 9.1). As a result of the subduction process, this region is regularly devastated by shallow megathrust earthquakes (McCloskey et al. 2008; Nalbant et al. 2005; Natawidjaja et al. 2006; Sibuet et al. 2007). Although the destruction resulting from energy released in a sudden slip or rupture is often devastating, far worse consequences arise through the tsunami triggered. The earthquake on 26 December 2004 ruptured the ocean floor over a distance of some 1,200 km (Krüger and Ohrnberger 2005) generating an ocean floor uplift of up to 10 m. This jolt from beneath generated waves on the Indian Ocean causing a tsunami of up to 30 m (northern Sumatra) (Borrero et al. 2006), leading to over 200 thousand casualties, as far away the east African coastline 7,000 km from its origin. The specific geodynamic situation of Indonesia requires a Tsunami Early Warning System which can provide extremely short early warning times but also produce reliable tsunami warnings after an earthquake based on highly uncertain data. The

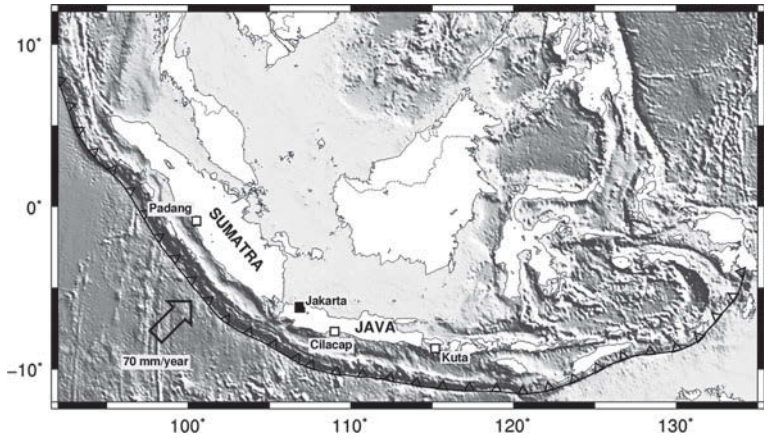

Fig. 9.1 The Sunda Arc is a major active plate boundary, where the Indo-Australian Plate is subducted at a speed of ~7 cm/y under the Eurasian Plate. The subduction zone (Sunda Arc) extends from the north of Sumatra to the island of Sumbawa

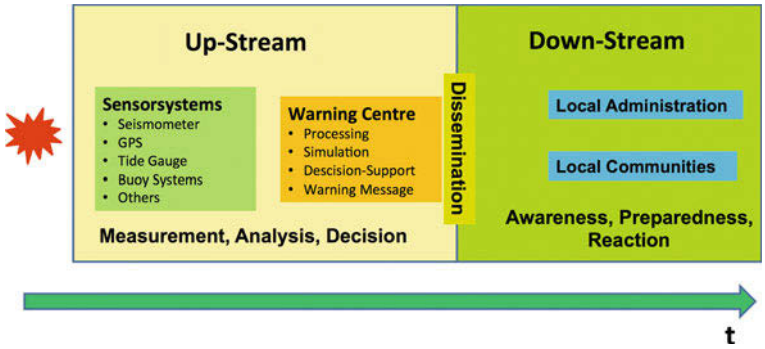

Fig. 9.2 Schematic End-to-End approach of GITEWS. The *up-stream* part is characterized by the measurement of the hazard and decision making while the *down-stream* part deals with the preparedness and reaction of the communities at risk

scientific development and technical support for the realisation of such a system has been provided by a consortium of nine German research institutions led by the GFZ German Research Centre for Geosciences in close cooperation with partners from Indonesia, China, Japan and the US (Rudloff et al. 2009).

Indonesia also faces tsunami risk in its North-Eastern territory (Sulawesi, Banda Sea, Molucca Sea). Various sensor systems such as seismic and GPS stations as well as tide gauges were installed here by Indonesian institutes. The data is merged and integrated into the central warning centre in Jakarta (Fleischer et al. 2010).

The system was planned and implemented as an "End-to-End" system (see Fig. 9.2). This includes:

- the necessary sensor instrumentation in Indonesia and elsewhere in the Indian Ocean to assess and identify the hazard as quickly as possible,
- a tsunami modelling and simulation system including tsunami excitation, propagation and inundation on the coast,
- a scenario and risk information-based decision support system (DSS),
- a communication system to disseminate warnings and other information.

Lastly but most importantly a dedicated program for capacity development for system operation and maintenance as well as for preparedness and response in local communities at risk ("Last Mile") has been carried out within the GITEWS project (Lauterjung et al. 2010).

9.2 Technical Concept

Of the tsunamis recorded to date, most were caused by substantial earthquakes on the ocean floor. Earthquake parameters i.e. location and magnitude are therefore commonly used as input parameters for tsunami simulation or the selection

of pre-calculated scenarios from scenario databases. Usually earthquake parameters are the initial information available for tsunami early warning. Strong earthquakes however are not confined to a single location but occur as ruptures of several hundred kilometres in length with a complex slip distribution along the fault plane(s). Strategies for tsunami early warning, therefore, have to distinguish between two cases:

- Far-field tsunami: A long travel distance for the tsunami compared to the earthquake rupture length. In this case the rupture orientation (given by the fault orientation) is essential but details such as the exact position of the rupture or slip distribution are not critical for tsunami forecast at a given coastal point.
- Near-field tsunami: Tsunami travel distances of a similar order (of magnitude) to the earthquake rupture length. The exact position and parameters of the rupture plane as well as the slip distribution are essential for tsunami forecast at a given coastal point.

Indonesia is invariably faced with near-field tsunamis (travel times from the source to the coastline between 20–40 min) so that the system was technically designed with a focus on high speed, incorporating early input parameters with high uncertainties. As already mentioned, near-field tsunami forecasting is challenging due to the necessity for precise characterisation of the earthquake rupture including details of the slip distribution. In order to provide an early warning, this has to be achieved as quickly as possible (5–10 min after the earthquake). Seismological observations can only provide the primary earthquake parameters such as location, depth and magnitude within 2–4 min (Hanka et al. 2010). Thus, the epicentre and magnitude are poorly defined immediately after the earthquake, and errors in both depth and location of up to 50 km can occur. Therefore, an assessment of tsunami potential and—if positive—propagation models have to be made on the basis of highly uncertain parameters and a reliable local early warning still depends largely on additional information of the rupture characteristics. A completely new approach in tackling the problem of rupture characterisation, especially the slip distribution of an earthquake is the monitoring of co-seismic crustal deformation by real-time or near real-time GPS deformation monitoring (Hoechner et al. 2008; Sobolev et al. 2007). Other investigations (Konca et al. 2008; Vigny et al. 2005) show that GPS is suitable for detecting deformations of several centimetres to metres over a distance of several hundred kilometres from the earthquake. This information is available 5–10 min (depending on the distance to the earthquake) after the event and can be used immediately to determine the rupture's direction. Therefore GPS is a striking and cost effective tool for the characterisation of an earthquake's source geometry. Within the project a GPS network consisting of a nation-wide reference network and GPS stations along the Indian Ocean coastline (combined with tide gauges following GLOSS[1] standards) was established in Indonesia. Near real-time processing (solutions for the network every 2 min, Falck et al. 2010) is performed at the early warning centre.

[1] Global Sea Level Observation System.

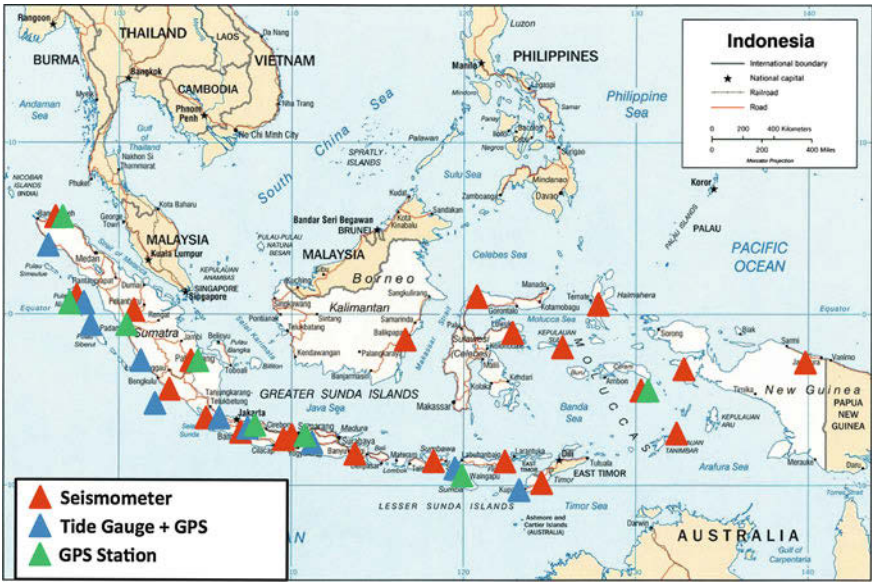

Fig. 9.3 Actual distribution of sensor instrumentation in Indonesia (German contribution to the warning system only)

The Indonesian tsunami early warning system consists of terrestrial networks such as seismological and geodetic stations as well as oceanographic instruments (see also Fig. 9.3). To minimize false alarms and to ensure redundancy, the application of different sensor technology is extremly important. All data are transmitted via satellite to the Warning Centre at BMKG (Badan Meteorologi, Klimatologi dan Geofisika) in Jakarta and are evaluated immediately.

The core of the early warning system is a network of seismic broadband stations (150 Stations, thereof 105 from Indonesia, 20 from Germany, 15 from Japan and 10 from China) as it gives the first important information on a possible tsunamogenic event. Data is transmitted in real time via VSAT[2] to the warning centre in Jakarta and analysed with the newly developed seismic processing software SeisComP3 (Hanka et al. 2010). The warning centre has access to about 230 seismic stations in the region and also includes data from seismic stations around the Indian Ocean. This system has been in operation at the BMKG since 2007 and successfully provides rapid nationwide earthquake information for Indonesia and all Indian Ocean neighbours including the ASEAN countries. Nevertheless, based on seismological measurements alone it is mostly impossible to decide in the first minutes after an earthquake whether a tsunami has been generated or not.

Therefore, a plan was drawn-up to detect tsunami signals directly on the ocean using GPS-buoys connected with ocean bottom pressure units and tide gauges at the

[2] Very Small Aperture Terminal.

coastline. The buoys have two functions: (1) they work as a relay station for data from the underwater pressure sensors, using acoustic data transmission from the sea floor to a modem close to the water surface. The buoy forwards all data via a satellite connection directly to the warning centre. (2) The other application and functionality is the GPS technology of the buoy. Although GPS is not as accurate as the pressure data, it delivers valuable information on sea level change with a precision of 5–10 cm within minutes. Applying GPS technology on tsunami buoys is a significant technical improvement compared to other buoy systems (Schöne et al. 2011a).

Again, the requirement of the warning system being as fast as possible made it necessary to position the buoy systems as near to the trench as possible to measure tsunami shortly after their generation. This also implies that the buoys are near to the coastline due to the geographic situation in Indonesia. Therefore, the buoy systems suffer from two drawbacks:

(1) The necessary position of the buoy system and the pressure sensor nearby the earthquake source (the trench) results in a strong aliasing of the tsunami signal by seismic noise (in many cases much larger than the tsunami signal). Due to the measuring characteristic of the pressure sensors currently available (15 sec integration time), filtering the tsunami signal from the seismic background noise is almost impossible (Meinig et al. 2005). This can be overcome, however, by the use of GPS onboard the buoy (Schöne et al. 2011a).
(2) In the case of Indonesia the buoy systems have to be placed near to the coastline. They are, therefore, in the reach of local fisher boats which use the buoys as mooring place for their fishing activities. As a result the buoys regularly become damaged leading in extreme cases to a total loss. Such vandalism is a general problem for buoy systems worldwide (Data Buoy Cooperation Panel, International Tsunameter Partnership 2011) and results in a dramatic decrease of the availability of near coast deployments.

For these reasons it was finally decided to no longer rely on such buoy systems due to the lack of reliability and for cost reasons. Cost calculations showed that the maintenance of the buoy systems—taking into account the aforementioned boundary conditions—would consume almost 50 % of the overall budget for the maintenance and operation of the warning system as a whole.

Tide gauges installed along the Indonesian coastline as well as on islands off the Indonesian mainland are capable of monitoring the instantaneous sea level changes in near real-time. An integrated concept was developed for GITEWS (Schöne et al. 2011b), comprising three different tide gauge sensors and a GPS receiver for vertical movement control (and as part of the GPS network for co-seismic deformation monitoring) at each site.

Tsunami simulations are particularly important, because based on a handful of measured information an overall picture of the situation has to be calculated. Ocean-wide tsunami-simulations are pre-calculated for a dense net of earthquake locations along the Sunda Trench and for a wide variety of magnitudes (7.5–9.0) (Behrens et al. 2010). These pre-calculated simulations are stored in a data base and can be selected accordingly based on the available sensor data. As time plays a crucial role in the

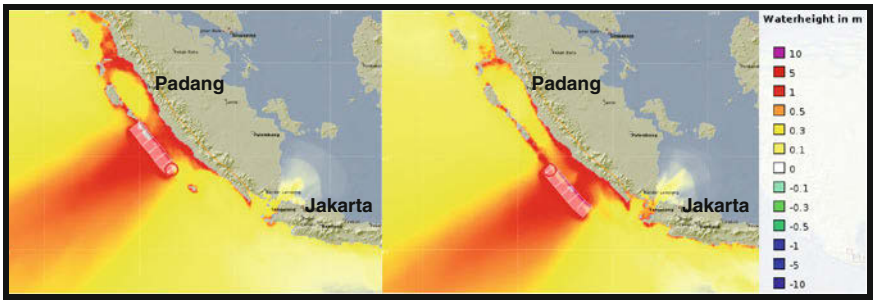

Fig. 9.4 Tsunami simulation based on location and magnitude (8.4) of a hypothetical earthquake off-shore Bengkulu, Sumatra. The figure *left* depicts the situation for the earthquake with a rupture running from the epicentre to the north. Especially the big city Padang is strongly effected, the south of Sumatra is not. The figure on the *right* hand depicts the situation for the earthquake with a rupture running from the epicentre to the south. Now the City of Padang is not affected but the south of Sumatra

warning procedure the selection process is fully automated. To include all available sensor information in this automated process a special approach has been developed. In a first step earthquake parameters (location and magnitude) are used to pre-select a number of scenarios with almost the same probability. All other sensors are treated as individual and non-related sources of information (GPS-stations, tide gauges). For each of these sensors theoretical response functions are calculated for every simulation (theoretical displacement vectors in case of GPS, theoretical tsunami arrival times and wave height for tide gauges). This data can be directly compared to the respective measured values and are used to reduce the list of best-fitting scenarios (for details see Behrens et al. 2010). The inclusion of GPS displacement vectors reflects, in particular, the slip distribution of a larger earthquake and supports the decision of earthquake rupture direction, which is of special importance for near-field tsunami forecasting (Fig. 9.4). Some seconds after the first earthquake evaluation the best fitting scenario resulting from the selection process gives a first impression, including wave heights, arrival times and inundation areas along the coast.

In the Decision Support System (DSS) the different information will be aggregated to quickly draw a detailed picture of the actual situation (Fig. 9.5) (Steinmetz et al. 2010). In combination with additional static geo-information i.e. hazard and/or vulnerability maps (Strunz et al. 2011), settlement structure in the affected coastal areas, this is essential for the decision making process of the authorities and the population. In this way the staff responsible at the warning centre attains a clear picture of the situation and based on this, can disseminate an adequate warning.

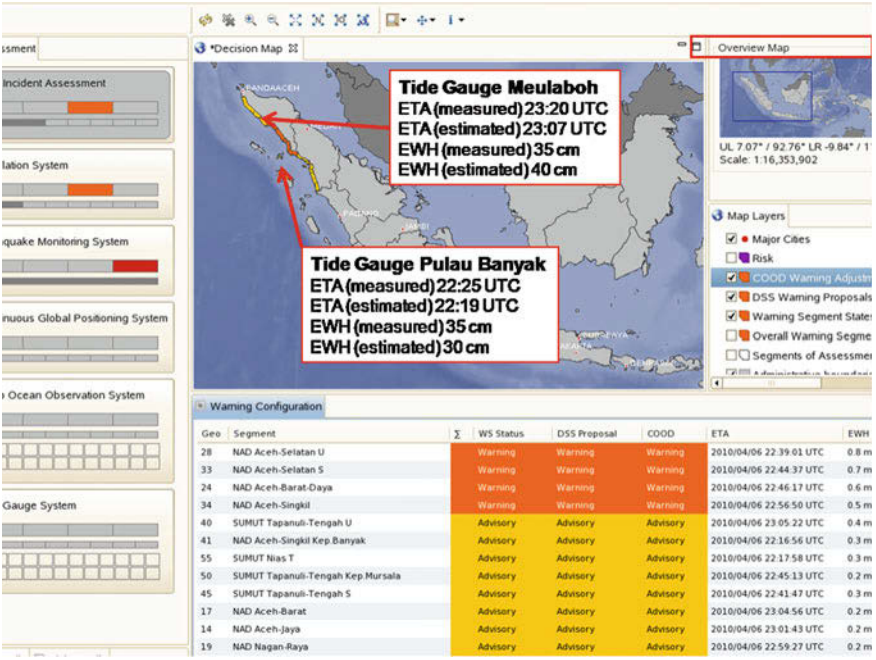

Fig. 9.5 Decision view of the Decision Support System. Shown is a map of the region of interest, the individual warning segments (administrative units) and the respective warning levels (in this case orange for warning and yellow for advisory). Also shown are the readings of two tide gauges in comparison with the predicted values for the tsunami generated by the earth-quake of 6 April 2010 off-shore North Sumatra. This aggregated view of the situation is the basis for the decision to be taken by the so-called Officer-on-Duty in the warning centre

9.3 System Performance

The Tsunami Early Warning System (TEWS) has produced its first tsunami warning on 12. September 2007 following the Bengkulu quake off shore south Sumatra. As the warning system is simulation based it is able to give warning information for single segments along the coastline. For the implementation the administrative districts of Indonesia along the coastline have been chosen as warning segments. In principle a warning can be produced for even smaller segments but as the final responsibility for the reaction lies on district level those entities have been chosen. The warning computed from the scenarios is divided into four warning levels depending on the estimated wave height (EWH) at the coastline (Table 9.1):

Communities at risk need to react very fast in case of a major hazard, therefore the warning messages need to be clear and comprehensible, because the trained reaction schemes of the population (evacuation etc.) can only cover a few cases within the short time available for reaction.

Table 9.1 Different warning levels

EQ (earthquake)	Earthquake information only	No tsunami
Advisory	A minor tsunami might have been generated	EWH < 0.5 m
Warning	A tsunami has been generated	0.5 m < EWH < 3.0 m
Major warning	A major tsunami has been generated	EWH > 3.0 m

Table 9.2 List of tsunami alerts triggered by the warning system from 2007 to 2012

Region	Date	M	Depth (km)	Dec	TH	Comment
Southern Sumatra	12.09.2007	7.9	10	Major	4 m	
Southern Sumatra	12.09.2007	7.7	24	Warn	1 m	
Talaud Islands	13.09.2007	6.4	30	EQ	n.a.	
Southwest of Sumatra	24.10.2007	7.0	10	Adv.	n.a.	
Sumbawa Region	25.11.2007	6.8	45	EQ	n.a.	
Southern Sumatra	25.02.2008	7.2	10	Major	12 cm	Initially overestimated M (final is 7.2)
Southern Sumatra	25.02.2008	7.0	26	Adv	n.a.	
Sunda Strait	26.08.2008	6.6	20	EQ	n.a.	
Halmahera	11.09.2008	7.6	109	EQ	n.a.	Deep earthquake
Irian Jaya Region	03.01.2009	7.2	10	Major	78 cm	
Java	02.09.2009	7.3	30	warn	80 cm	
Banda Sea	24.10.2009	7.3	165	EQ	n.a.	Deep earthquake
Northern Sumatra	06.04.2010	7.2	32	Adv	40 cm	
Northern Sumatra	09.05.2010	7.2	30	Adv	n.a.	
Nicobar Islands	12.06.2010	7.5	21	adv	n.a.	
New Britain Region	18.07.2010	7.1	26	EQ	n.a.	
Southern Sumatra	25.10.2010	7.8	10	Warn	>10 m	Mentawai slow tsunami quake
South of Java	04.03.2011	7.2	24	EQ	n.a.	Normal event off trench
Northern Sumatra	11.04.2012	8.9	10	Major	80 cm	Strike-slip quake, no major tsunami

Keys: *M* = Magnitude, *Dec* = Decision proposal by DSS, *EQ* = only earthquake information, *adv* = Advisory (EWH < 0.5 m), *warn* = Warning (0.5 m < EWH < 3 m), *major* = Major Warning (EWH > 3 m), *TH* = measured tsunami height (at nearest tide gauge), *Color coding*: *green* = predicted warning level ok, *yellow* = predicted warning level is one level wrong, *red* = false warning (for color see online)

Table 9.2 shows the warning information which was published by the warning system for larger earthquakes around Indonesia during the past 5 years of operation from 2007 to 2012. In 15 of 19 events (see Table 9.2) a correct estimation in terms of warning levels has been documented. Only in 3 cases an incorrect estimation of the warning level (always an overestimation) has been recorded where the warning level was one level too high, and in only one case a major overestimation (false alarm) has been published. No tsunami stayed undetected by the system. However it must be mentioned that the direct comparison of estimated wave heights and the measured wave heights (i.e. at tide gauges) may give deviations of up to 50 %, in most cases overestimations by the system. This is due to the worst case scenario approach which is implemented in the system due to the large uncertainties in the input values in the early time after an earthquake. On the other hand the estimated arrival times for the warning segments show much smaller deviations from the measured arrival times as the wave heights.

The recent Indian Ocean Earthquake of April 11, 2012, Mw 8.6, about 450 km west of northern Sumatra, produced only a minor tsunami of about 1 m at the Indonesian coastlines. This is due to the strike-slip character of this intraplate quake and the consequently low co-seismic vertical displacement of the ocean floor. The Earthquake was registered by the warning system after 3.5 min with an overestimated magnitude of 8.9. Due to the Standard Operations Procedures in the warning centre a major tsunami warning was issued after 4 min and 30 s based on a magnitude 8.9. As the region where this quake occured is not covered by precalculated scenarios (too far off the subduction zone) an online tool for tsunami forecasting was used based on a subduction-like source model. Therefore the estimated wave heights (EWH) leading to the major warning level have been much too high (in some parts of the coastline 5 m and more).

9.4 Capacity Development

Not only does the sustainable operation of the system depend on the establishment of the necessary technological bases for hazard detection, modelling and decision support, but the development of the institutional and human capacities necessary for the nationwide implementation and application of the system as well as structures for effective decision making in Indonesia are just as important. In addition to the implementation of its technical components, GITEWS consequently included Capacity Development activities aimed at individuals, decision-makers, administrative bodies, disaster risk management organizations as well as the private sector at local and national levels (Schlurmann and Siebert 2011).

In general, the basic concept of Capacity Development (CD) aims to disseminate a realistic assessment of risks concerning extreme natural hazards with appropriate technical and socio-economic equipment. CD, therefore, incorporates training programmes, aimed at strengthening the capabilities of individuals and institutions to focus on the occurrences and effects of natural hazard-related phenomena and

processes, and their associated risks to prevent or mitigate disasters. Moreover, academic scholars have been integrated into relevant research projects in order to gain useful practical insights and the basic conceptions of project management through continuing education. Governmental agencies and other national and international decision-makers also needed a range of scientific and engineering tools to effectively prevent or mitigate disasters and have been supported by experts and other competencies within the framework of the project by means of capacity development programmes as well as through co-operations and networking.

Based on these objectives, the GITEWS capacity building programme incorporated three levels being integrated in subprojects targeting the scientific audience and technological sphere as well as national institutions and local communities:

1. Academic and technical programmes: development and enhancement of research capabilities and technical skills by means of coordinated PhD and tailor-made Post-doc programmes, with workshops and seminars to expand the abilities and expertise of scientists and technicians in the relevant organizations and institutions in order to meet the scientific and technological needs of GITEWS.
2. Institutional development programmes: development and strengthening of operational institutions and governmental bodies to enable cooperation, management and organizational structure of TEWS at the national level.
3. Local disaster mitigation programmes: generate and bring-on warning and disaster preparedness mechanisms and strategies at local administrative and organisational level in three pilot areas, i.e. Padang, Western Sumatra; Cilacap, South-Java, and Kuta, Bali (Spahn et al. 2010). Strategies and measures to educate the population in coastal areas to respond correctly to warning information transpired to be of utmost importance. This is particularly true due to the extremely short time span (20–40 min) between the earthquake and the tsunami impact. Standard Operation Procedures (SOPs) and evacuation plans have been customised for this specific precondition (Tsunami Kit, Early Warning and Community Preparedness in Indonesia 2010).

9.5 Conclusions and Outlook

New concepts and procedures for the fast and reliable determination of strong earthquakes, the modelling and simulation of tsunamis and the assessment of the situation have been implemented in the warning system. In particular, the direct incorporation of a broad variety of different sensors provides fast information on independent physical parameters, thus, resulting in a stable system and minimizing breakdowns. The operational Early Warning System was handed over to Indonesian authorities on 29 March 2011 and is since then operated in full responsibility of the BMKG.

A newly developed seismic processing software dedicated to rapid evaluation of strong earthquakes (Hanka et al. 2010) has been in operation at the warning centre since 2007. The software has proven its functionality not only in Indonesia, but also

in over 40 data and warning centres world-wide (i.e. India, New Zealand, Maldives, France, and many more).

The various applications of GPS developed within the project show great potential in receiving additional information on earthquake mechanisms or detecting sea level changes at an early stage.

Information from the different sensor systems converge in a Central Early Warning and Mitigation Centre at the BMKG in Jakarta. Using a Decision Support System the sensor data is matched with the pre-calculated tsunami scenarios and additional geospatial data and maps to enable the responsible officer on duty to access the danger and to release warning bulletins or warning cancellations respectively. In this context the education and training of local authorities and the population at risk is an important ongoing task within the capacity development programme.

Recent developments in GPS processing (Real-time Precise Point Positioning, Ge et al. (2011) have made it possible to use co-seismic displacement vectors registered by GPS more efficiently in the early warning process especially in the case of near-field tsunami. Babeyko and coworkers (2012) presented their recent results using a limited number of Japanese GPS stations for the direct inversion of co-seismic displacements into the slip distribution of the 2011 Tohuku Earthquake. They demonstrated how a respective density of GPS stations the slip distribution of an Earth quake can be calculated with sufficient accuracy for early warning within 2–3 min. These findings have also been confirmed by other groups (i.e. Wei et al. 2011). Together with near-real time Tsunami modelling tools this will open a new perspective to switch the early warning process from the static, database oriented approach using pre-calculated Tsunami scenarios to a forecast approach based on directly measured sensor information from seismic and GPS networks in real-time.

Acknowledgments The GITEWS project (German Indonesian Tsunami Early Warning System) was carried out by a large group of scientists and engineers from the GFZ German Research Centre for Geosciences (consortium leader) and its partners from the Alfred Wegener Institute for Polar and Marine Research (AWI), the German Aerospace Center (DLR), the Helmholtz-Zentrum Geesthacht Centre for Materials and Coastal Research (HZG), the German Marine Research Consortium (KDM), the GEOMAR | Helmholtz Centre for Ocean Research Kiel, the United Nations University (UNU), the Federal Institute for Geosciences and Natural Resources (BGR), the German Agency for Technical Cooperation GmbH (GIZ), as well as from Indonesia and other international partners. Particular thank we would like to give to Dr. Sri Woro B. Harijono and Dr. Prih Harjadi (Badan Meteorologi, Klimatologi dan Geophysik, Jakarta), Dr. Idwan Suhardi and Mr. Pariatmono (Indonesian Minsitry for Research RISTEK) and Dr. Cecep Subarya in place of the many Indonesian colleagues who contributed to the development and the success of the GITEWS project. Funding was provided by the German Federal Ministry for Education and Research (BMBF) through the GITEWS project, Grant03TSU01 and still is within the PROTECTS project, Grant03TSU07. The authors would like to thank Phelim Burgess for a language tuning of the original manuscript.

References

Babeyko A, Hoechner A (2012) Accuracy of tsunami source inversion with real-time GPS. Geophys Res Abstr 14:EGU2012-4571

Behrens J, Androsov A, Babeyko AY, Harig S, Klaschka F, Mentrup L (2010) A new multi-sensor approach to simulation assisted tsunami early warning. Nat Hazards Earth Syst Sci 10:1085–1100

Borrero JC, Synolakis CE, Fritz H (2006) Northern Sumatra field survey after the December 2004 great Sumatra earthquake and Indian Ocean tsunami. Earthq Spectra 22(S3):S93–S104

Data Buoy Cooperation Panel, International Tsunameter Partnership (2011) Ocean data buoy vandalism—incidence, impact and responses. DBCP technical document no. 41. http://wo.jcommops.org/cgi-bin/WebObjects/JCOMMOPS.woa/wa/doc?group=DBCP_DOC.. Accessed 2012

Falck C, Ramatschi M, Subarya C, Bartsch M, Merx A, Hoeberechts J, Schmidt G (2010) Near real-time GPS applications for tsunami early warning systems. Nat Hazards Earth Syst Sci 10:181–189

Fleischer J, Häner R, Herrnkind S, Kloth A, Kriegel U, Schwarting H, Wächter J (2010) An integration platform for herterogeneoous snsor systems in GITEWS—tsunami service bus. Nat Hazards Earth Syst Sci 10:1239–1252. doi:10.5194/nhess-10-1239-2010

Ge M, Chen J, Dousa J, Li X, Gendt G, Wickert J (2011) Development of the GFZ real-time precise point positioning service general assembly European geosciences union (Vienna, Austria 2011) 2011. Geophys Res Abstr 13:EGU2011-3865

Hanka W, Saul J, Weber B, Becker J, Harjadi P, Fauzi and GITEWS Seismology Group (2010) Real-time earthquake monitoring for tsunami warning in the Indian Ocean and beyond. Nat Hazards Earth Syst Sci 10:2611–2622

Hoechner A, Babeyko AY, Sobolev SV (2008) Enhanced GPS inversion technique applied to the 2004 Sumatra earthquake and tsunami. Geophys Res Lett 35:L08310. doi:10.1029/2007GL033133

Konca AO, Avouac J-P, Sladen A, Meltzner AJ, Sieh K, Fang P, Li Z, Galetzka J, Genrich J, Chlieh M, Hillmann D, Natawidjaja DH, Bock Y, Fielding EJ, Chen Ji, Helmberger DV (2008) Partial rupture of a locked patch of the Sumatra megathrust during the 2007 earthquake sequence. Nature 456:631–635. doi:10.1038/nature07572

Krüger F, Ohrnberger M (2005) Spatio-temporal source characteristics of the 26 December 2004 Sumatra earthquake as imaged by teleseismic broadband arrays. Geophys Res Lett 32:L24312. doi:10.1029/2005GL023939

Lauterjung J, Münch U, Rudloff A (2010) The challenge of installing a tsunami early warning system in the vicinity of the Sunda Arc, Indonesia. Nat Hazards Earth Syst Sci 10:641–646. doi:10.5194/nhess-10-641-2010

McCloskey J, Antonioli A, Piatanesi A, Sieh K, Steacy S, Nalbant S, Cocco M, Giunchi C, Huang J, Dunlop P (2008) Tsunami threat in the Indian Ocean from a future megathrust earthquake west of Sumatra. EPSL 265:61–81. doi:10.1016/j.epsl.2007.09.034

Meinig C, Stalin SE, Nakamura AI, Gonzalez F, Milburn HB (2005) Technology developments in real-time tsunami measuring, monitoring and forecasting. In: Oceans 2005, MTS (Marine Technology Society)/IEEE proceedings, vol 2, pp 1673–1679

Münch U, Rudloff A, Lauterjung J (2011) Postface "The GITEWS Project—results, summary and outlook". Nat Hazards Earth Syst Sci 11:765–769. doi:10.5194/nhess-11-765-2011

Nalbant SS, Steacy S, Sieh K, Natawidjaja D, McCloskey J (2005) Earthquake risk on the Sunda trench. Nature 435:756–757. doi:10.1038/nature435756a

Natawidjaja DH, Sieh K, Chlieh M, Galetzka J, Suwargadi BW, Cheng H, Edwards RL, Avouac JP, Ward SN (2006) Source parameters of the great Sumatran megathrust earthquakes of 1797 and 1833 inferred from coral microatolls. J Geophys Res 111:B06403. doi:10.1029/2005JB004025

Rudloff A, Lauterjung J, Münch U, Tinti S (2009) Preface "The GITEWS Project (German-Indonesian Tsunami Early Warning System)". Nat Hazards Earth Syst Sci 9:1,381–1,382

Schlurmann T, Siebert M (2011) The capacity building programmes of GITEWS—visions, goals, lessons learned, and re-iterated needs and demands. Nat Hazards Earth Syst Sci 11:293–300

Schöne T, Pandoe W, Mudita I, Roemer S, Illigner J, Zech C, Galas R (2011) GPS water level measurements for Indonesia's tsunami early warning system. Nat Hazards Earth Syst Sci 11:741–749

Schöne T, Illigner J, Manurung P, Subarya C, Khafid Zech C, Galas R (2011) GPS-controlled tide gauges in Indonesia—a German contribution to Indonesia's tsunami early warning system. Nat Hazards Earth Syst Sci 11:731–740

Sibuet J-C, Rangin C, LePichon X, Singh S, Cattaneo A, Graindorge D, Klingelhoefer F, Lin J, Malod J, Maury T, Schneider J-L, Sultan N, Umber M, Yamaguchi H (2007) 26th December 2004 great Sumatra-Andaman earthquake: co-seismic and post-seismic motions in northern Sumatra. EPSL 263:88–103. doi:10.1016/j.epsl.2007.09.005

Sobolev SV, Babeyko AY, Wang R, Hoechner A, Galas R, Rothacher M, Sein DV, Schröter J, Lauterjung J, Subarya C (2007) Tsunami early warning using GPS-shield arrays. J Geophys Res 112:B08415. doi:10.1029/2006JB004640

Spahn H, Hoppe M, Vidiarina HD, Usdianto B (2010) Experience from three years of local capacity development for tsunami early warning in Indonesia: challenges, answers and the way ahead. Nat Hazards Earth Syst Sci 10:1411–1429

Stein S, Okal EA (2005) Speed and size of the Sumatra earthquake. Nature 434:581–582. doi:10.1038/434581a

Steinmetz T, Raape U, Teßmann S, Strobl C, Friedemann M, Kukofka T, Riedlinger T, Mikusch E, Dech S (2010) Tsunami early warning and decision support. Nat Hazards Earth Syst Sci 10:1839–1850

Strunz G, Post J, Zosseder K, Wegscheider S, Mück M, Riedlinger T, Mehl H, Dech S, Birkmann J, Gebert N, Harjono H, Anwar HZ, Sumaryono RMK, Muhari A (2011) Tsunami risk assessment in Indonesia. Nat Hazards Earth Syst Sci 11:67–82

Tregoning PF, Brunner K, Bock Y, Puntodewo SSO, McCaffrey R, Genrich JF, Calais E, Rais J, Subarya C (1994) First geodetic measurement of convergence across the java trench. Geophys Res Lett 21(19):2135–2138

Tsunami Kit, Early Warning and Community Preparedness in Indonesia (2010). http://www.gitews.org/tsunami-kit/index_en.html. Accessed 2012

Vigny C, Simons WJF, Abu S, Bamphenyu R, Saitrapod C, Chooskaul N, Socquet C, Omar K, Abidin HZ, Ambrosius AC (2005) Insight into the 2004 Sumatra-Andaman earthquake from GPS measurements in south east Asia. Nature 436:201–206. doi:10.1038/nature03937

Wei Y, Titov VV, Newman A, Hayes G, Tang L, Chamberlin C (2011) Near-field hazard assessment of March 11, 2011 Japan tsunami sources inferred from different methods. In: OCEANS 2011, IEEE conference publications, pp 1–9

Chapter 10
Walking the Last Mile: Contributions to the Development of an End-to-End Tsunami Early Warning System in Indonesia

H. Spahn, M. Hoppe, A. Kodijat, I. Rafliana, B. Usdianto and H. Dwi Vidiarina

Abstract Establishing the Tsunami Early Warning System in Indonesia (InaTEWS) has been a process of learning and innovation. Three different initiatives, implemented by the German-Indonesian Cooperation for a Tsunami Early Warning System (GITEWS), the Indonesian Institute of Sciences (Lembaga Ilmu Pengetahuan Indonesian—LIPI) and the United Nations Educational, Scientific and Cultural Organization (UNESCO), contributed to the learning and innovation process with a strong focus on tsunami preparedness at the community level during the implementation phase of InaTEWS. The lessons learned as well as the tested and validated procedures resulting from this innovative process have been documented and are currently being extended to make them available nationwide. Experiences from the pilot phase show that there is still a great need to strengthen the capacity of national government insti-

H. Spahn (✉) · H. Dwi Vidiarina
GIZ International Services, Jakarta, Indonesia
e-mail: harald.spahn@giz.de

H. Dwi Vidiarina
e-mail: henny.vidiarina@giz.de

M. Hoppe
GIZ, Eschborn, Germany
e-mail: michael.hoppe@giz.de

A. Kodijat
JTIC, Jakarta, Indonesia
e-mail: ardito.kodijat@gmail.com

I. Rafliana
LIPI, Jakarta, Indonesia
e-mail: irina_rafliana@hotmail.com

B. Usdianto
GIZ International Services, Yogyakarta, Indonesia
e-mail: benny.usdianto@giz.de

F. Wenzel and J. Zschau (eds.), *Early Warning for Geological Disasters*,
Advanced Technologies in Earth Sciences, DOI: 10.1007/978-3-642-12233-0_10,

tutions, local governments and civil society in order to provide the services necessary for sustainable tsunami preparedness. Key points for the way ahead are building a better understanding of the system, the warning service and the contents of warnings, strengthening the role of local disaster-management agencies and governments as well as the institutionalization of early warning at all levels and to systematically scaling up the successful experiences from pilot areas.

Abbreviations

BMKG	Badan Meteorologi Klimatologi dan Geofisika (National Agency for Meteorology, Climatology and Geophysics)
BNPB	Badan Nasional Penanggulangan Bencana (National Disaster Management Agency)
BPBD	Badan Penanggulangan Bencana Daerah (Local Disaster Management Agency)
CBDRM	Community-based disaster-risk management
CD	Compact Disc
CIDA	Canadian International Development Agency
COMPRESS	Community Preparedness
CSO	Civil society organisation
DMO	Disaster management organization
DRR	Disaster risk reduction
GFZ	German Research Centre for Geosciences
GITEWS	German-Indonesian Cooperation for a Tsunami Early Warning System
GIZ/GTZ	German International Cooperation (since 2011) / German Technical Cooperation (prior to 2011)
GPS	Global Positioning System
ICG IOTEWS	Intergovernmental Coordination Group for the Indian Ocean Tsunami Warning System
IFRC	International Federation of Red Cross and Red Crescent Societies
InaTEWS	Indonesian Tsunami Early Warning System
INGO	International non-governmental organisation
IOC	Intergovernmental Oceanographic Commission
ITIC	International Tsunami Information Centre
JTIC	Jakarta Tsunami Information Centre
Kemdiknas	Kementerian Pendidikan Nasional (Ministry of Education)
KOGAMI	Komunitas Siaga Tsunami (a local NGO in Padang)
LIPI	Lembaga Ilmu Pengetahuan Indonesia (Indonesian Institute of Sciences)
NGO	Non-governmental organisation
NTB	West Nusa Tenggara province
NTWC	National Tsunami Warning Centre
PROTECTS	Project for Training, Education and Consulting for a Tsunami Early Warning System
SOP	Standard operating procedure
TDMRC	Tsunami Disaster Management and Research Centre
TEW	Tsunami Early Warning
TIC	Tsunami Information Centre
UN	United Nations
UNESCAP	United Nations Economic and Social Commission for Asia and the Pacific

UNESCO United Nations Educational, Scientific and Cultural Organization
UNISDR United Nations International Strategy for Disaster Reduction

10.1 Introduction

Tsunami early warning is more than just science and technology—it is about people. People who are involved in designing, operating and maintaining the warning system; people who are in charge of providing services related to the system and, last but not least, people who live in at-risk areas, who require quick, clear and reliable information from the system to support them in taking the right decisions during an emergency.

Implementing an effective "end-to-end" tsunami early warning system is a complex task and requires both the contribution and coordination of a wide range of individuals and institutions in different fields, such as science and engineering, governance and public service delivery and disaster risk management, as well as from the private sector and civil society. A sustainable system must be integrated into institutional frameworks and policies at international, national and local levels.

Establishing the Tsunami Early Warning System in Indonesia (InaTEWS) has been a process of learning and innovation. Concepts and mechanisms have been tailored in order to respond to the specific characteristics and requirements of the Indonesian archipelago and to allow communities at risk to benefit from the warning services so that casualties may be reduced during future tsunami events. The lessons learned as well as the tested and validated procedures resulting from this innovative process have been documented and are currently being extended to make them available nationwide.

This paper—based on practical experience—intends to contribute to the discussion about important aspects that should be considered when developing effective national end-to-end tsunami early warning systems. It addresses issues of the so-called "last mile", focusing on the downstream process and follows a people-centred perspective, which looks at the needs of communities at risk. It starts with a discussion of general concepts and the overall framework for the development of a people-centred tsunami early warning system. In the following section, it analyses the specific conditions in Indonesia for designing and operating InaTEWS as an effective end-to-end system. The authors then describe the contributions and lessons learned from the three different initiatives mentioned above, which have supported the learning and innovation process since 2006, as well as the ongoing expansion process to make the experiences available across the country.

10.2 Putting InaTEWS into Perspective: Framework and Related Concepts

The devastating tsunami that hit Indonesia and other Indian Ocean countries in 2004 led to the development of tsunami early warning for the Indian Ocean region. The Intergovernmental Oceanographic Commission (IOC) under the auspices of UNESCO coordinates this initiative. Each country is responsible for establishing its own national warning system. Selected countries are designated as Regional Tsunami Service Providers for the Indian Ocean region. Indonesia started its development of a national tsunami early warning system in 2005 and the system was officially inaugurated in late-2008.

The need to develop and strengthen early warning became a central theme during the World Conference on Disaster Reduction that took place in Kobe only a month after the devastating tsunami on 26 December 2004. The main output of the conference, the Hyogo Framework for Action 2005–2015, put developing and strengthening early warning systems that were people-centred as one of the priorities for action (UNISDR 2009). "People-centred early warning suggests that rather than being vulnerable, people can be capable, resilient and able to protect themselves" (IFRC 2009). The main objective of a people-centred early warning system like InaTEWS is "to enable individuals, communities and organisations threatened by a hazard to prepare and to act appropriately and in sufficient time to reduce the possibility of harm or loss" (UNISDR 2006a). Only if it actively engages institutions as well as the people at risk and is tailored to their needs, will a warning system be able to save lives. Warnings need to be understood by those at risk, taking into account the social and cultural characteristics of the target audience, and need to include guidance on how to act upon them (United Nations 2005).

Developing and running such a system demands the contribution and coordination of a wide range of individuals, institutions and many specialties—science and engineering, governance and public service delivery, disaster risk management, news media and public outreach. Without the involvement of all stakeholders—authorities and government institutions from various sectors and at all levels, communities at risk, NGOs and the private sector—an early warning system will not be effective (Sorensen 2009; UNISDR 2006a).

This means that InaTEWS has to operate end-to-end to trigger the expected reaction along Indonesian shorelines. The monitoring and detection technology of InaTEWS is a combination of earthquake, sea-level and land monitoring. The incoming data feeds into a decision-support system that enables the National Tsunami Warning Centre (NTWC, hosted by the Meteorology, Climatology and Geophysics Agency—BMKG) to disseminate a sequence of warning messages to selected interface institutions, local governments and national media stations. Local authorities need to make sure they can receive the warnings, as they are in charge of disseminating warnings and guidance to their communities. Preparedness and sufficient response capacity are the vital preconditions for an appropriate reaction to warnings

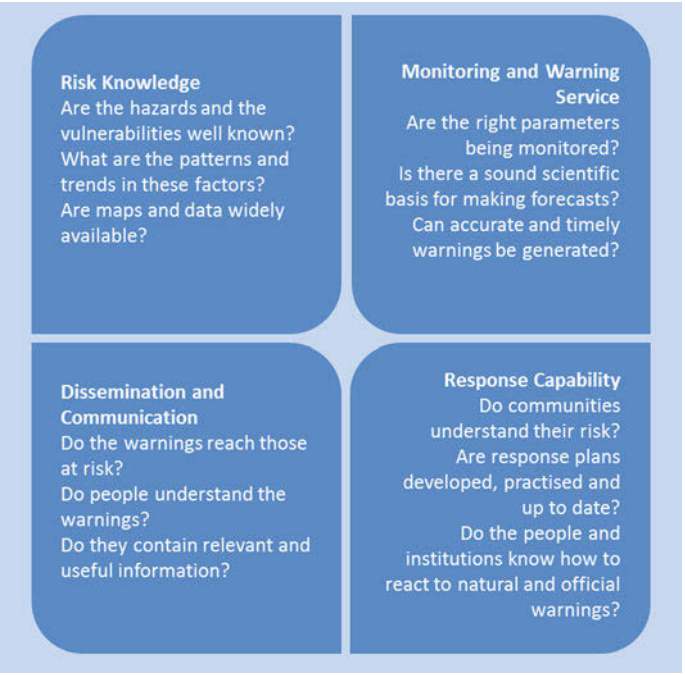

Fig. 10.1 The four elements of a people-centred tsunami early warning system (modified from UNISDR (2006a, b))

and guidance. Shortcomings in any one of these elements can mean the failure of the whole system (Spahn et al. 2010).

The Third International Conference on Early Warning, held in Bonn in 2006, produced a tool for practitioners entitled "Developing Early Warning Systems: A Checklist" (UNISDR 2006a), which assists governments and communities to develop and evaluate their systems in order to ensure that all components work properly. The checklist assesses the sufficiency of the four key components of a warning system: risk knowledge, monitoring and warning services, dissemination and communication and response capability (Fig. 10.1).

The concluding statement at the conference in Bonn highlighted that "effective early warning systems must be an integral part of disaster risk-reduction strategies in national development frameworks", and emphasised the important role of local communities (UNISDR 2006b). Within the overall concept of disaster risk reduction (or management), early warning is part of the preparedness efforts before a disaster (Fig. 10.2). To work effectively, InaTEWS needs to be integrated with disaster-management structures at all levels of government and within the community. This is to ensure its long-term effectiveness.

Community-based disaster risk management (CBDRM) in the context of InaTEWS is related to the people-centred character of early warning. It includes

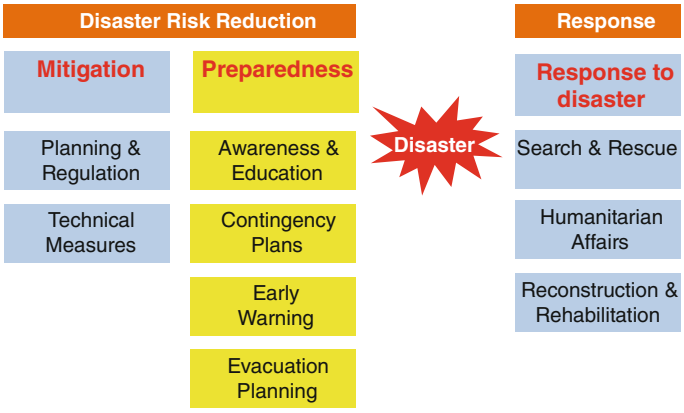

Fig. 10.2 Early warning as part of preparedness and disaster risk reduction

measures in risk analysis and planning, e.g. evacuation planning and the setting up of local warning arrangements as part of a national disaster-risk management system. CBDRM within InaTEWS stresses the special role attached to district or city authorities, particularly in the enforcement of early warning procedures and clear policies that will help people to react consistently in the event of a tsunami threat (Fig. 10.3).

A people-centred early warning system with CBDRM aims to empower local stakeholders by granting them ownership of the system, which should lead to a sustainable reduction in disaster risks. However, people's full potential can only be utilised if government and civil society build partnerships, based not only on local participation and ownership but also on political and economic support from national institutions (UNISDR 2009). These partnerships are particularly important as the development of certain references, such as designing tsunami-hazard maps, cannot be delegated entirely to communities, as it requires expert input. However, communities have to be able to use these references to develop their own preparedness plans. People simply have to be better prepared and trained as the system is considered effective only if warnings can trigger appropriate reactions and people are able to save themselves before the tsunami waves reach the shore (Bollin 2003; Spahn et al. 2010).

10.3 InaTEWS: Context and Challenges

10.3.1 The Challenge of Near-Field Tsunamis

Coastal communities in Indonesia have to cope with the threat of near-field tsunamis. The very short travel time of this kind of tsunami from its source—a nearby epicentre—to the shore generally limits warning and evacuation times to 20–40 min.

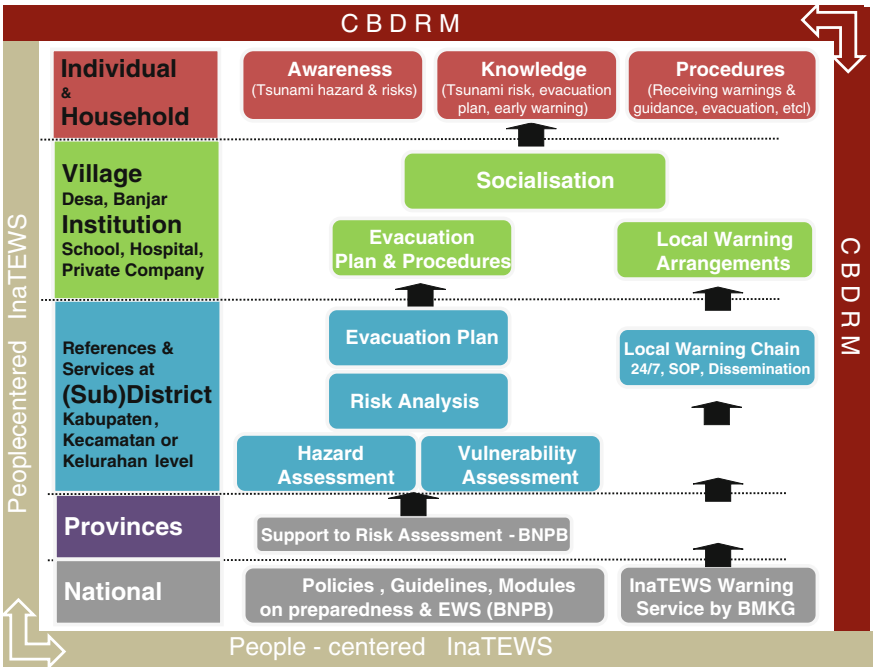

Fig. 10.3 Tasks and responsibilities in tsunami early warning and community-based disaster risk management at various levels

Specific local tectonic, seismic and bathymetric conditions may make warning and evacuation times even shorter in some areas. It was often questioned whether under such circumstances an early warning system could make a difference.

Experiences in Indonesia provide a reference for what a tsunami early warning system can do vis-à-vis near-field tsunamis and what it cannot do (Fig. 10.4). There are certainly scenarios in which the system cannot provide any protection. Following the 2010 Mentawai earthquake, InaTEWS issued a tsunami warning within five minutes, but it didn't reach at-risk communities on time as affected coastal areas, which were located at too short a distance to the tsunami source, were inundated by waves before the warning was received (Yulianto et al. 2011). Similar conditions can be found all across the island chain west of Sumatra and coastlines facing back-arc faults, such as the north coast of Bali, West Nusa Tenggara and East Nusa Tenggara provinces (for example, the Flores tsunami in 1992). People in these areas will have to rely on natural warning signs alone. Self-evacuation after strong ground shaking should be the standard procedure. Nevertheless, these communities can benefit from InaTEWS as the system provides "No Threat" information when a strong earthquake does not have the potential to trigger a tsunami, and "End of Threat" messages once an existing tsunami threat has ended so that people can return to their homes.

Unfortunately, nature does not always provide clear warning signs. Indonesia experienced several “slow earthquakes”, or “tsunami earthquakes”, (Banyuwangi tsunami 1994; Pangandaran tsunami 2006; and Mentawai tsunami 2010), which were strong enough to trigger tsunamis but weren’t felt strongly by those most at risk due to the fact that the seismic energy was released over a longer period of time, resulting in swaying movements rather than the usual strong ground shaking. In all these cases, people were caught by surprise. As the epicentres of the Banyuwangi and Pangandaran tsunamis were located around 200 km off the coast of southern Java, there would have been enough lead time to provide warnings to the communities at risk. In both cases, a functioning early warning system would most probably have saved lives. Although a tsunami warning was generated in the 2006 event, it didn’t reach the communities as the requisite links hadn’t yet been established.

Coastlines around Sumatra, Java and Bali, which are vulnerable to tsunamis caused by megathrust earthquakes, can expect to have lead times of around 20–40 min. Although this is an extremely short time frame, it does allow for the issuing of tsunami warnings and the execution of evacuation processes. Consequently, InaTEWS policy obliges the NTWC to disseminate a first tsunami warning within five minutes after the occurrence of an earthquake with tsunami potential. During these first few minutes, the NTWC relies on seismic and land-based Global Positioning System (GPS) real-time data, as well as on predetermined flooding scenarios for the potentially affected coastal areas, which are processed by a decision-support system. The actual generation of a tsunami is not confirmed when sending out the first warning. Subsequently, data from sea-level monitoring provides updates on the occurrence of tsunami waves (Lauterjung et al. 2010). This means that over time the situation becomes clearer and the NTWC can provide updated warnings.

Decision making in calling for an evacuation and the dissemination of guidance at local levels are important steps during the downstream process and are mandated to local authorities. This remains one of the major challenges as it requires the implementation of local 24/7 services, quick decision-making processes as well as procedures and technologies to disseminate a call for evacuation. This part of the warning chain has been developed and tested successfully in a number of pilot areas but it is far from being implemented nationwide. As the provision of guidance by local authorities is not yet reliable, the role of public media in disseminating warnings from the NTWC, together with the ability of people in affected communities to understand the broadcasted information and to quickly make a decision on how to react, will be decisive factors in making the warning system effective (Thomalla et al. 2009).

Early warning in the context of near-field tsunamis requires dealing with a considerable degree of uncertainty. Due to the limited time for evacuation, officers with the NTWC as well as local authorities need to decide whether to send out a warning and to call for evacuation, even though they cannot be sure that a tsunami was actually generated. It is obvious, therefore, that under such conditions Indonesia will face situations when warnings are issued but in fact no tsunami occurs. Often, people mistakenly tend to interpret this as a “false alarm”. It is necessary, however, to address the issue of “uncertainty” openly in order to maintain public trust in and the credibility of the warning system (Mileti et al. 2004).

The experiences in Indonesia show that it is necessary to combine approaches based on natural warning signs and the early warning system. Understanding and reacting appropriately to natural warning signs should always be the first line of defence, while official tsunami warnings and guidance are important to reinforce or cancel evacuations.

10.3.2 The Institutional Setting

The foundation for the successful development and sustainability of an early warning system relies on well-developed governance and institutional arrangements supported by effective management structures and solid institutional regulations. Whether or not a warning reaches those in an area at risk largely depends on whether all the stakeholders in the warning chain are aware of, and are able to carry out, their roles and responsibilities. Early warning is the responsibility of government and needs adequate planning and funding and political commitment at all levels. However, the complexities of the early warning system require intensive exchange, coordination and collaboration among many sectors and disciplines (UNISDR 2006b).

The devastating disaster caused by the 2004 tsunami was the starting point for a huge effort in tsunami preparedness in Indonesia. Besides the development of InaTEWS, it also triggered the setting up of a new institutional framework for disaster management. Following the issuance of the Disaster Management Law (2007), the National Disaster Management Agency (Badan Nasional Penanggulangan Bencana—BNPB) was founded in 2008.

Despite the fact that most provinces and districts have now established a Local Disaster Management Agency (Badan Penanggulangan Bencana Daerah—BPBD) in their respective areas, local authorities generally still lack an understanding of their role in local preparedness planning and tsunami early warning; particularly in terms of determining how to react and how to disseminate official calls for evacuation to their communities based on warnings from the NTWC. Many of the newly established BPBDs still struggle with a lack of skilled personnel at management and operational levels (Civil Society Organisation 2009; Thomalla et al. 2009).

The Indonesian legal framework regarding tsunami early warning assigns roles to various actors. Law 31/2009 authorises the BMKG to issue tsunami early warnings. Government Regulation 21/2008 and the Decree by the Head of the BNPB, 3/2008, clarify that local governments are responsible for issuing immediate public announcements containing clear guidance and instructions to support the inhabitants and visitors in a threatened area to react quickly and appropriately. The Decree by the Minister of Communications and Information, 20/2006, requires that national and local television and radio stations (commercial and public) immediately interrupt programmes to broadcast tsunami early warnings and advice from the BMKG (GTZ-GITEWS 2010b).

However, developing effective governance is still a major challenge for the Government of Indonesia. While InaTEWS' technology for earthquake monitoring,

ocean observation and forecasting has been declared fully operational since March 2011, the major challenge for the end-to-end early warning system is to define clear institutional arrangements and responsibilities for the long-term development of both institutional and public response capabilities among the end-users of the warning system, namely the local authorities and communities in tsunami-prone regions (Spahn et al. 2010).

10.3.3 Limitations for Preparedness Planning

Although Indonesia had experienced a number of devastating tsunamis in the past, a more comprehensive approach in tackling tsunami hazards was not adopted until the 2004 Indian Ocean tsunami. During InaTEWS' initial development stage, efforts focused more upon the upstream side (monitoring and warning services and warning dissemination) of the system. The development of the downstream side (dissemination and communication as well as response capability), which addresses community preparedness and capacity building, was not as well defined and faced a number of limitations, such as lacking the involvement of the National Disaster Management Agency. Due to the prevailing response and recovery paradigm in disaster management in Indonesia, there had never been a clear and structured programme for capacity building in tsunami preparedness. Only since 2008 has the new disaster management agency, the BNPB, adopted an approach that extends beyond merely coordinating emergency relief efforts to encompassing all phases of pre-disaster prevention and preparedness and post-disaster recovery.

As around 50 % of the 80,000 km of coastline in Indonesia is prone to tsunamis and communities are scattered across vast and often remote areas, it is a real challenge to build preparedness in all of these communities. The BNPB has already identified areas that face higher tsunami risks, which will be prioritized in the National Action Plan (BNBP Regulation 2010).

Tsunami-preparedness planning needs to be based on realistic hazard and risk assessments. In Indonesia, such information is often unavailable, meaning that most of the preparedness activities at a community level are based on assumptions derived from rule of thumb and limited information. Although a minimum standard for tsunami risk assessment has been developed (BNPB Regulation 2012), implementation is still a big challenge due to the limited availability of experts and adequate data to support local processes. Therefore, community evacuation plans are often developed based on rough contour maps without reliable information on tsunami inundations, which in turn results in non-specific, generalised tsunami awareness, preparedness and education materials being used for community trainings.

Preparedness activities at the community level in Indonesia are conducted by various actors. Besides government institutions, many come from the NGO, INGO or civil society sectors. This poses another challenge as each organisation usually follows its own approach, often with limited knowledge and information about tsunami issues, especially regarding early warning arrangements and procedures. This leads

to cases where differing or conflicting information confuses people living in high-risk areas. The assessment following the Mentawai tsunami, for instance, revealed the impact of misleading information about tsunami arrival times on local evacuation behaviour (Yulianto et al. 2011).

10.3.4 Vulnerability in the Context of Tsunami Preparedness

Tsunami preparedness in relation to near-field tsunamis is mainly about survival. As experience shows, the chance of surviving a tsunami are not equally distributed. Many who were killed in the 2004 Indian Ocean tsunami were women and children. In Indonesia, in four villages in the Aceh Besar district only 189 of 676 survivors were female. Male survivors outnumbered female survivors by a ratio of almost 3:1. In other villages, 77–80 % of accounted deaths were female (Oxfam International 2005). During the Japan tsunami in March 2011, the highest death toll was among the elderly.

When designing early warning systems, it is essential to recognise that different groups have different vulnerabilities according to culture, gender or other characteristics that influence their capacity to effectively prepare for, prevent and respond to disasters (UNISDR 2006b). While InaTEWS has made significant progress, approaches to systematically consider the needs of vulnerable groups have not yet been implemented. Although a number of preparedness initiatives address the school sector, the Ministry of Education (Kementerian Pendidikan Nasional—Kemdiknas) hasn't been substantially involved.

Chances of survival are also related to the level of knowledge about tsunamis and how to react. In spite of an increased dissemination of knowledge following a series of recent tsunami disasters in Indonesia and also in Japan by the media and through public education, it is presumed that a large number of coastal residents remain unaware about the nature of this threat and how to mitigate risk. Compared to other hazards, tsunamis are a more complex natural phenomenon that can cause massive destruction. The complexities involved in a tsunami threat may in themselves be factors that discourage many disaster management institutions as well as individual practitioners from becoming proactive motivators to increase knowledge and change attitudes in the community.

10.3.5 Challenges and Strengths Related to Sociocultural Heterogeneity and Religious Perspectives on Disaster Risk Reduction and Tsunami Warning

Indonesia as the fourth most-populated country in the world has followers of at least five major religious faiths. Islam is the majority religion, followed by Christian

Protestantism, Catholicism, Hinduism and Buddhism. The strong belief in God within these faiths has created a set of values that determine how nature is understood and how risks are perceived, which need to be taken into account when developing InaTEWS. Muslims, for example, generally perceive natural disasters as the will of God, which thus generates a certain level of acceptance and resilience regarding a disaster event, even one as catastrophic as the Indian Ocean tsunami in 2004. In some cases, the level of acceptance may also lead to fatalistic beliefs that nothing more can be done once God has commanded a disaster to occur. Hindus practise the Tri Hita Kirana, which emphasises the importance of balancing the relationship between human beings, God and nature. It generates the particular belief, for example, that if human beings destroy nature, disasters will occur.

Faiths and beliefs are also influenced by traditional culture and social settings, and vice versa. A source of strength among some communities, which still persists to this day, is the tradition of *gotong royong*, or voluntary collective action in which all community members assist one another. This idea of self-help was in fact formally adopted as one of Indonesia's guiding ideological principles. The more a community maintains the values of *gotong royong*, the less vulnerable it is to certain disasters because there is a greater interdependency in the community's recovery mechanisms (Hidayati 2011). It is a great challenge to maintain these values in urban or modern communities, which possess more independent and individualistic features.

In traditional cultures, such as on the remote Simeulue Island in Aceh, local knowledge played a decisive role in saving lives in 2004. This particular island became well-known at the time, as 95 % of its population survived the giant tsunami wave, although the community was geographically closest to the epicentre of the earthquake (Yogaswara and Yulianto 2006). Traditional local knowledge, known as *Smong*, recorded experiences from former tsunamis and taught the island's population how to recognise a tsunami threat and to run to higher ground. *Smong* was traditionally passed down through the generations through songs and lullabies. Interestingly, during a recent study, it was found that Simeulue children of primary-school age were no longer familiar with *Smong*. If a large tsunami does not occur until the next generation, this local knowledge may well disappear in the meantime.

10.3.6 Understanding the System

Ultimately, the performance of the end-to-end warning system will be measured by the ability of at-risk communities and local authorities to translate warnings into protective action. This will only work if the end-users of the system, i.e. those people at risk, thoroughly understand the warnings and guidance and know what to do. Raising community awareness, communicating both the benefits of the system and how it can save lives and building trust in the system are still major challenges for InaTEWS.

There is a lack of knowledge not only about the role of the NTWC and the responsibility of local authorities but also about the technical functionality of the

system. Often the "system" is seen as a network of technical devices rather than a system that, in fact, depends greatly on human capacities and skills, systematic local preparedness planning, agreed procedures, decision-making capacity and a common understanding of what to do and how to react (Spahn et al. 2010). To enable local governments to establish the requirements for an end-to-end system and to provide their communities with a clear picture of how it works, official guidelines from the national level on the particularities of tsunami early warning and a dialogue between entities at all levels are needed.

Experience shows that knowledge about tsunami early warning among news media personnel is still limited and their understanding of the system and the risks involved tend to be on a par with the public's understanding rather than that of the NTWC personnel and disaster managers (Spahn et al. 2010). When explaining how the system works, public education activities need to make clear the limitations of the system with regards to the accuracy of initial warnings, given the fact that the first warning is the only information available that can be used to reinforce community response after an earthquake. Overstating what InaTEWS can do or being less than clear about what it cannot do will ultimately decrease people's trust in the system and damage its credibility.

10.4 Developing and Building the System: Learning and Innovation

During the set-up phase of the system, a learning process was required to develop the concepts, tools and processes related to risk knowledge, monitoring and warning services, dissemination and communication of warnings and the response capability and preparedness by authorities and those at risk, in accordance with specific Indonesian conditions. All these processes need to function across multiple levels (Fig. 10.5), involving all the respective stakeholders, and they also need to include clearly-defined governance and institutional arrangements.

This chapter describes the approaches, lessons learned and knowledge management utilised in the three different initiatives implemented by GITEWS, LIPI and UNESCO's Jakarta Tsunami Information Centre (JTIC), which contributed to the learning and innovation process with a strong focus on tsunami preparedness at the community level during the implementation phase of InaTEWS.

10.4.1 The GITEWS Pilot Project

As part of the German-Indonesian Cooperation for a Tsunami Early Warning System (GITEWS), the *Capacity Building in Local Communities* project was implemented from 2006 to 2011 by the German International Cooperation (GIZ) and its Indonesian

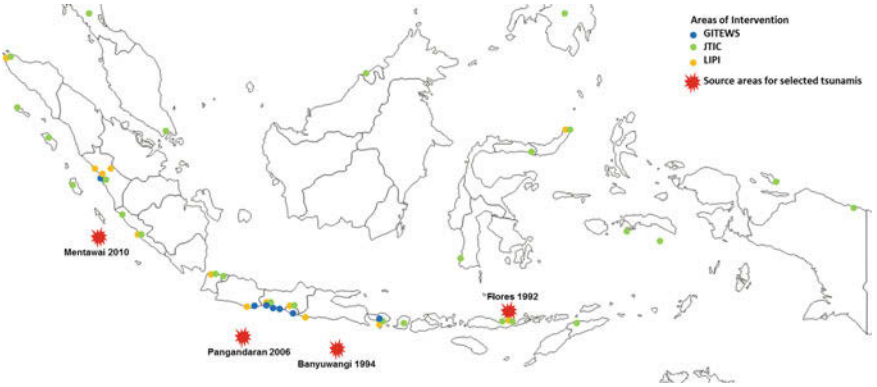

Fig. 10.4 Map showing sources of several selected tsunamis and areas of intervention by GITEWS, LIPI and the JTIC (Base map for Fig. 10.4 was taken from d-maps.com (property of Daniel Dalet). http://d-maps.com/carte.php?lib=indonesia_map\&num_car=301\&lang=en)

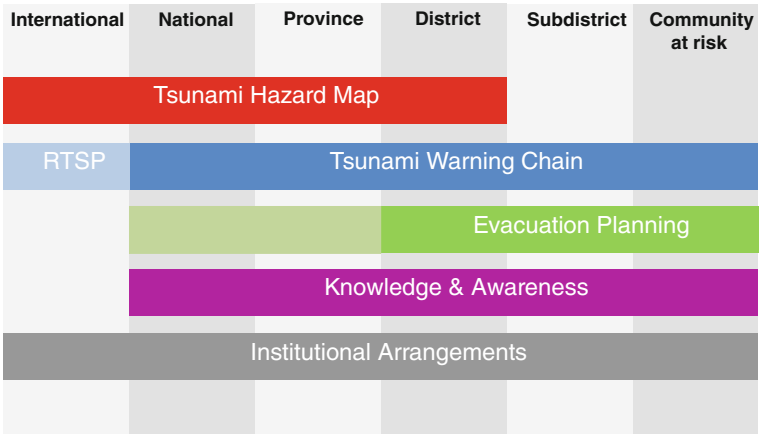

Fig. 10.5 Multiple-level approach

partners at national and local levels. The project aimed to support the development of mechanisms and strategies to enable people in high-risk areas to receive prompt alerts in order to be able to quickly execute adequate life-saving responses. It was designed as a pilot project with pilot locations being the city of Padang in West Sumatra; the province of Bali including selected districts on the island; and five districts in the regions of Yogyakarta and Central Java along the southern coast of Java (Fig. 10.5).

In these pilot areas, the project collaborated with local government institutions from various sectors (disaster response and civil defence as well as local planning boards) and worked together with actors from civil society, such as the Indonesian Red Cross, local non-governmental organisations (NGOs), and the private sector. To strengthen multi-sector and multi-stakeholder coordination for preparedness and

to facilitate cooperation with GIZ, the local government partners in the pilot areas appointed local multi-stakeholder working groups. Through workshops, trainings and exercises as well as learning from others experiences, these groups developed applicable solutions for tsunami early warning and preparedness at local government and community levels. These processes were supported by the provision of technical advice and small funding allowances for local preparedness activities including testing dissemination technology, developing awareness material and supporting outreach and community-awareness programmes. The implementation of the developed solutions lies exclusively with the local partners, primarily local governments, since they are responsible for warning and guiding their people in the event of an emergency.

According to its strategy as a pilot project (Fig. 10.6), the objective of the initiative was threefold (GTZ-GITEWS 2010b). GIZ introduced existing know-how on early warning and preparedness, in line with the overall requirements of InaTEWS as well as the local context of the pilot locations. Based on an assessment of existing local strategies and conditions, the project accompanied its partners during a lengthy working process, providing technical advice on appropriate tools and procedures, helping to clarify roles and responsibilities, and supporting local stakeholders during the implementation process. Experience and good practice information from the pilot areas was validated and translated into concepts, manuals and tools. Thorough documentation of the project's experiences and outputs was recorded in order to make the information available to national institutions mandated with guiding other tsunami-prone regions in their preparedness processes, with the objective of building a reliable end-to-end early warning system throughout Indonesia.

The learning process during the GITEWS pilot project led to the development of a step-by-step approach towards tsunami preparedness across multiple levels (Fig. 10.3). The specific conditions in the context of near-field tsunamis (short lead-times, high level of uncertainty) require that individuals are enabled to quickly take decisions and correct actions based on basic but solid knowledge of local tsunami risks and preparedness plans, even in the absence of guidance from local authorities or the failure of warning services during an emergency. To provide people in communities at risk with more than thumb rules or general instructions on how to react to a tsunami threat, it is necessary to develop local evacuation maps and procedures. Developing such plans at a village level usually requires references regarding hazardous and safe zones and recommended evacuation strategies, as well as the development of local warning services. The responsibility to provide such references, including risk assessments, evacuation plans and the setting up of mechanisms for decision making and disseminating warnings lies with district governments. It is essential, therefore, to develop the required capacities at district level, especially in local disaster-management agencies.

Experiences from the learning and innovation phase resulted in concepts, procedures and products related to the warning chain being provided by the NTWC to the communities at risk. The project played a major role in providing lessons learned as well as facilitating dialogue and an exchange of experiences to adjust the warning system to the needs of the end-users. Many of the experiences from the

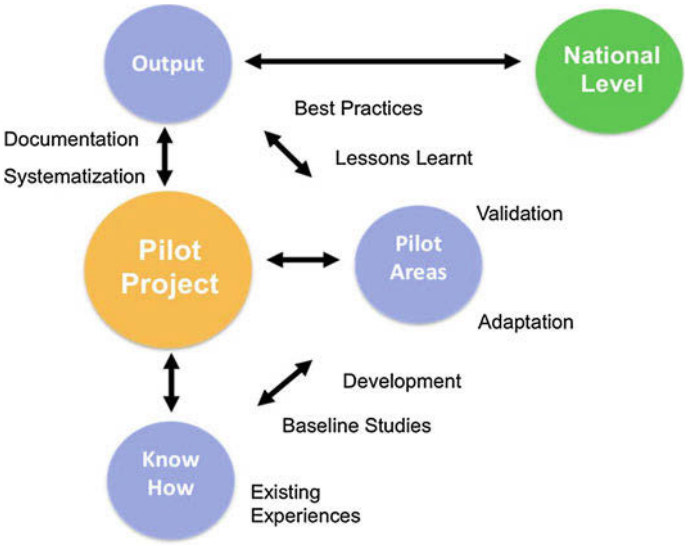

Fig. 10.6 Pilot project strategy

pilot areas were incorporated into the National Warning Service Guidelines (BMKG 2012). Other important outputs developed during the pilot project were manuals and tools to develop basic tsunami-hazard maps and evacuation plans and to set up local warning services and dissemination systems—including 24/7 services—at district levels, to be applied by local actors.

As part of the scheme's knowledge management and in order to make the experiences and results available to other coastal communities and their governments in tsunami-prone areas, the project developed comprehensive documentation—the TSUNAMI*Kit* (Fig. 10.7). The content of the kit is organised according to the key elements of tsunami early warning (Risk Knowledge, Monitoring and Warning Services, Dissemination and Communication, Response Capacity, Knowledge and Awareness, Governance and Institutional Arrangements). For each of these six elements different types of documents were prepared, providing background information (reference and introduction documents, fact sheets) and support for local stakeholders to plan and implement tsunami warning systems and to strengthen preparedness (checklists, manuals, guidebooks and guidelines). Additionally, a collection of materials for public education was included.

10.4.2 Science-Based Preparedness Initiatives by the Indonesian Institute of Sciences (LIPI)

LIPI's role as a governmental research institution takes the form of conducting research, developing innovations and forwarding its findings in the most appro-

Fig. 10.7 Project documentation—TSUNAMI*Kit*—www.gitews.org/tsunami-kit

priate way to influence national policy. Research into natural hazards along with other natural science phenomena was already one of LIPI's strongest competencies a decade before the Indian Ocean tsunami in 2004. Since then, LIPI has gradually shifted its focus towards applied research within a wide array of disciplines, such as geoscience, oceanography, socioeconomics, cultural studies, education and communications.

LIPI believes that the best way to systematically broaden out good practices in disaster risk reduction (DRR) is to establish a collaborative system with dynamic interaction between scientists, practitioners, disaster-management authorities and communities at risk (Fig. 10.8). Indonesia has more than 227 million people who are exposed to earthquake hazards, and more than 5 million exposed to tsunami hazards (BNPB Regulation, 2012). Most communities live in areas with scarce intervention and assistance from local disaster agencies in building preparedness, and some inhabit remote islands with even higher levels of vulnerability but where local populations do not possess an adequate understanding of the underlying risks. The extension of LIPI's role to promote scientific communication and education was therefore an attempt to fill the often wide gap between perceived risks and knowledge.

With its objective being to improve the understanding of risks, disaster-management planning, community preparedness and education, LIPI established the Community Preparedness (COMPRESS) unit to facilitate integration between research and educational efforts. LIPI chose to recruit recent graduates and non-governmental staff to learn and develop skills in providing innovative science-based preparedness interventions and approaches. The programme, which nurtured close collaboration between scientists and educational practitioners, covered many aspects of disaster risk reduction, including risk and community preparedness assessments, school-based preparedness models, the development of standard operating proce-

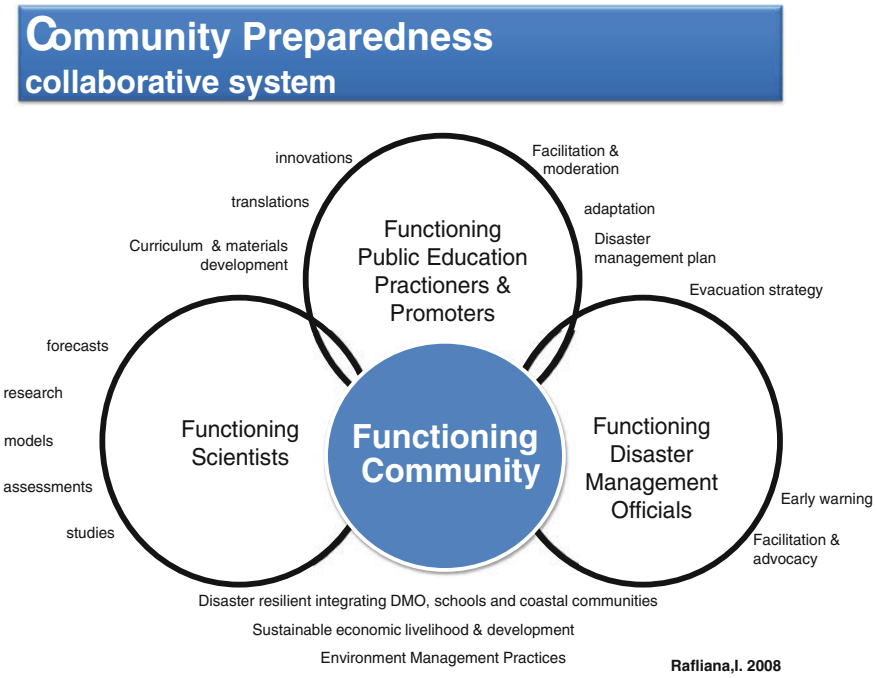

Fig. 10.8 LIPI's four pillars of a collaborative system for community preparedness

dures (SOPs), tsunami exercises, early warning services and community preparedness activities. The results from these efforts enabled the public education unit within COMPRESS to synthesise critical messages that were then made available to the public and the system's users.

The outputs and lesson learned from the programme were documented in the form of guidebooks, minimum requirements and checklists, interactive games and exercises as well as comics for users in schools, communities and local authorities. One highlight was the media guidebook for tsunami warning dissemination, which was the result of a joint collaboration between LIPI, the JTIC, the BMKG, the Ministry of Communications and Information and the BNPB. LIPI has also engaged artists and musicians in preparedness discussions and presentations, helping to organise national exhibitions and the production of songs that emphasise the importance of developing a preparedness culture. A compilation CD entitled *Science in Music* has become one of the tools utilised to encourage people to become more aware and better informed about earthquake and tsunami risks. Overall, COMPRESS worked in more than nine districts and cities in Indonesia, reaching more than 200,000 people including schoolchildren, media personnel, government officials, coastal communities and the general public.

The overriding factor behind LIPI's chosen strategy was the assumption that preparedness should require only limited financial investment as opposed to the

high levels of funding found in most structural-mitigation programmes, which many provinces and districts in Indonesia would not be able to meet. The strategy's main challenges, meanwhile, are the need for sufficient time and providing ongoing assistance to allow the processes to become norms and to build a new culture of preparedness within communities. Meaningful collaboration with organisations that have a similar approach, such as GIZ, the JTIC and UNESCO, is benefitting many districts by assisting them to make the most realistic investment choices concerning preparedness. This collaboration also supports national policies for tsunami preparedness, especially on risk assessments, evacuation planning, early warning and public education.

The evolving processes in developing preparedness capacity in a number of tsunami-prone districts have been noted and some have recorded significant efforts and progress. Nevertheless, the primarily sporadic initiatives throughout Indonesia have for the most part been implemented with significant intervention by external organisations, both national and international, with a marked lack of standardisation by the BNPB.

10.4.3 The Jakarta Tsunami Information Centre

UNESCO's Intergovernmental Oceanographic Commission (IOC), with its vast experience and knowledge regarding the establishment and coordination of the Tsunami Warning System in the Pacific, recognised the important role of a Tsunami Information Centre (TIC) as one of the essential and critical components in supporting the successful operation of a Tsunami Warning System. In 2007, with funding from the Canadian International Development Agency (CIDA), UNESCO-IOC took the initiative to establish the Jakarta Tsunami Information Centre (JTIC), which is housed in the UNESCO office in Jakarta.

The JTIC's mission consists of three fundamental elements: information clearing house, capacity building for preparedness and awareness, and information management and services. As an information resource, the JTIC shared information and publications, and distributed educational and preparedness materials on tsunami and tsunami hazards via its website, www.jtic.org. However, as many of those who needed preparedness and awareness information did not have access to the Internet, the JTIC began to introduce on-site activities.

Between 2007 and 2009, the JTIC implemented a number of initiatives, such as workshops, seminars, trainings, exhibitions and site visits, to strengthen tsunami preparedness within communities in around 20 districts (Fig. 10.4), paying special attention to schools. These initiatives included collaborations with LIPI on a Children's Science Support and Public Education programme in Muko-Muko city, Bengkulu province and a School-Based Preparedness Model (SDPM) training in Maumere, Flores, which also involved a local environmental NGO and local students. In cooperation with a Padang-based NGO, Komunitas Siaga Tsunami (KOGAMI), in West Sumatra, the JTIC implemented a community-based capacity-building programme

for integrated disaster preparedness in two communities and organised 47 SDPM trainings in the province. The results obtained helped form a model for DDR strategy at district and city levels, a training module for earthquake and tsunami evacuation exercises in schools and practical guidelines for communities on how to survive earthquakes and tsunamis. They were also utilised to strengthen school-based disaster preparedness in Banda Aceh in conjunction with the Tsunami Disaster and Mitigation Research Centre (TDMRC) at Syahkuala University.

The main lessons learned from these on-site activities were the importance of actively involving local organisations in order to achieve continuity in preparedness activities and the need to develop locally-adapted educational, awareness, and preparedness materials that reflected and respected particular local cultural contexts.

Furthermore, the JTIC produced a number of information and educational materials to build awareness and strengthen capacities for tsunami preparedness and mitigation at various levels. Several resources from UNESCO-IOC's International Tsunami Information Centre (ITIC) were translated into Indonesian, including the "IOC Tsunami Teacher" DVD and the "Tsunami Glossary". In collaboration with the BMKG, the ITIC's tsunami comic book was adapted to the Indonesian context to provide a highly readable and easy-to-understand booklet on tsunami hazards and warnings.

Flyers, leaflets, stickers and posters were also developed to provide practical information for both the general public and specific target groups, such as boat operators and fishermen. A poster series was published to educate people on how to safeguard and properly maintain tsunami early warning devices, as Indonesia had faced problems of vandalism, thefts and damage to early warning equipment on land and at sea. These posters have been placed in areas where such equipment is installed. The JTIC also published a booklet, "Where the first wave arrives in minutes", which presents survival lessons based on eyewitness accounts of two near-field tsunamis in Indonesia (Aceh 2004 and Java 2006). The booklet is intended for people who live, work or vacation along coastlines where fast-approaching tsunamis may strike.

As part of the joint JTIC—LIPI programme, the JTIC published a lessons-learned booklet derived from the experiences in three schools in Maumere, Flores and Banda Aceh. The booklet provides step-by-step guidelines on how to develop school preparedness based on five parameters: knowledge and attitude; school policy; emergency planning; a school's early warning system; and resource-mobilisation capacity.

In response to the need for locally-adapted materials, the JTIC, supported by the United Nations Economic and Social Commission for Asia and the Pacific (UNESCAP 2009–2011), adapted existing awareness, preparedness and educational materials in terms of context, culture, language and design for the Philippines, Thailand and Timor Leste (Fig. 10.9).

With the establishment of TICs in other tsunami regions (the Caribbean, North-East Atlantic and Mediterranean seas), the Intergovernmental Coordination Group for the Indian Ocean Tsunami Warning System (ICG IOTWS) endorsed the JTIC's 2011 proposal to expand its role to support other Indian Ocean states.

Fig. 10.9 JTIC information materials for tsunami awareness and preparedness

10.5 From Project Work to Service Provision

InaTEWS was designed and set up through the joint efforts of a number of Indonesian institutions and projects by international partners. This initial phase involved a learning and development process, which was mainly project-driven. While the upstream part and the implementation of the NTWC required specialised input from science and technology, the learning and innovation process in the downstream part and at the community level was facilitated by pilot projects in different areas of the archipelago.

Although the system was officially inaugurated in November 2008, further project activities to complete and fine tune the system were still ongoing until 2011. Since then, the character of the activities by the main actors involved in InaTEWS has shifted from time-limited project work to continuous service provision. Core services related to InaTEWS are the provision of tsunami early warnings by the NTWC to interface institutions (the BNPB, the BPBDs and the media), the dissemination of warnings by the national mass media to the general public and the provision of guidance—especially calls for evacuation—by local governments to communities at risk. Other related services include the provision of reference tools for community preparedness, such as tsunami-hazard maps and evacuation plans provided by the BPBDs, as well as information campaigns to raise knowledge and awareness at the grassroots level.

Experiences from the pilot phase show that there is still a great need to strengthen the capacity of national government institutions, local governments and civil society actors in order to provide the services necessary for sustainable tsunami preparedness. The GITEWS review process in 2010 (GITEWS 2010) concluded that integrating the requirements of the warning system (e.g. procedures) within local institutions was a precondition to achieving sustainability. The reviewers also concluded that InaTEWS could not be considered "complete", as the majority of tsunami-prone districts and communities in Indonesia had yet to be linked to the system. Thus, the need for a strategy that would link these districts and communities to InaTEWS and would strengthen local response capabilities to enable communities to react adequately to warnings was also pointed out.

10.5.1 Contributions to the Development of National Standards, Guidelines, Instruments and Procedures for Community-Oriented Tsunami Preparedness

The development of national standards, guidelines, instruments and procedures is a crucial step in expanding upon the successful experiences from the pilot processes in order to provide much-needed references to service providers related to InaTEWS. Developing such standards requires close cooperation and a validation process among the various national stakeholders along with further experience gained by the application of different approaches and products in other tsunami-prone regions of Indonesia.

As prioritised by the BNPB, inter-institutional working groups are addressing quality indicators as a means of measuring public service delivery and impact regarding minimum service standards for tsunami early warning and risk management at local levels. Additional criteria to determine human resource requirements for local tsunami-risk management and to assess human resource development are being discussed to define key competencies, training needs and recruitment in the field of tsunami early warning and tsunami preparedness. Guidelines for minimum standards on tsunami-risk assessments provide guidance for straightforward approaches that can be implemented at the local level.

National guidelines for tsunami warning services, as developed by the NTWC, provide official information regarding InaTEWS and the warning chain from national to local levels, the sequence and content of warning messages—including recommendations on reaction to local authorities—and a clarification on the roles, responsibilities and procedures of all relevant bodies. The purpose of these guidelines is to provide assistance and support to those agencies, both national and regional, that provide a public service in the reception and dissemination of tsunami early warnings, as well as providing assistance to all other stakeholders who are directly responsible for disaster management, especially in regional preparedness and response to emergency situations.

10.5.2 Horizontal and Vertical Knowledge Exchange Across the Country

Coordination and communication between provincial, district, city and national levels are considered prerequisites for both an effective InaTEWS and locally-adapted, sustainable capacity development within tsunami-risk management. Experiences from the GITEWS project showed that a facilitated exchange or dialogue process between local and national levels resulted in a better understanding of the system and contributed to the improvement of procedures, mechanisms and institutional capacities, in particular by addressing the link between the NTWC and local-level actors. The results from these exchange processes produced inputs for the development of national references and guidelines for InaTEWS, drawing on the participation of stakeholders at all levels.

The horizontal and vertical exchange of experience and knowledge plays an important role in the intended expansion process. A peer-to-peer learning approach can facilitate the transfer of knowledge between tsunami-prone regions. Learning from practical experience and case studies not only provides realistic insights into what works and how to overcome obstacles but also increases the motivation for the implementation and replication of processes based on positive examples.

Additionally, visits and discussions with key national actors, such as the BMKG and the BNPB, are held to discuss current state-of-the-art technologies and future plans regarding InaTEWS, and how local communities can link into the system. At the same time, providing an understanding about the expectations among local communities and the challenges they face helps to inform national actors about how to facilitate the implementation of tsunami early warning at the local level.

10.5.3 Capacity-Development Process for Tsunami Preparedness at the Local Level

In order to support Indonesia in strengthening the capacity of local governments and civil society actors so as to provide the services necessary for sustainable tsunami preparedness, the German government launched the "Project for Training, Education and Consulting for a Tsunami Early Warning System" (PROTECTS) as a follow-up project for GITEWS. The new project builds upon the experiences from the former GITEWS pilot areas and supports a horizontal expansion to reach a wider geographical area as well as a vertical expansion to achieve a broader impact by means of institutionalisation.

A capacity-development concept on tsunami preparedness for local communities was designed together with the BNPB and the provincial BPBDs in Bali, Central Java, DI Yogyakarta, East Java, West Java and West Nusa Tenggara. The concept adopts a combination of top-down and bottom-up approaches, along with a multi-level approach, and involves key players at all levels to strengthen the institutional

capacity of the BPBDs in providing services to those at risk. It follows a step-by-step approach towards tsunami preparedness as described in Sect. 10.4.1 (see Fig. 10.3) to build awareness, knowledge and solid procedures within at-risk communities.

Capacity development is practically facilitated through a sequence of workshops, implemented by the provincial BPBDs, involving representatives from local working groups at the district level. During the workshops, participants are introduced to specific topics, such as hazard and risk assessments, evacuation planning, the local warning chain, community awareness and tsunami-simulation exercises. The introduction of national guidelines helps to ensure that local implementation measures are in line with InaTEWS' end-to-end concept. Outside of these workshops, the local working groups are then charged with implementing the required action in their respective regions (Fig. 10.10), making use of existing local knowledge, values and human and material resources.

Additionally, technical trainings on evacuation planning and local warning services, as well as on facilitating preparedness processes and awareness campaigns at grassroots level, are provided to ensure that the necessary skills needed to implement the different components are met. The trainings are designed for specific target groups, such as employees of the BPBDs, community activists and even village residents. Those selected for the trainings are obliged to make a commitment towards supporting the local implementation processes.

10.6 Outlook

10.6.1 Status Quo

The 2011 Japanese tsunami killed about 20,000 people in what is considered the most tsunami-prepared nation in the world. Nevertheless it can be assumed that

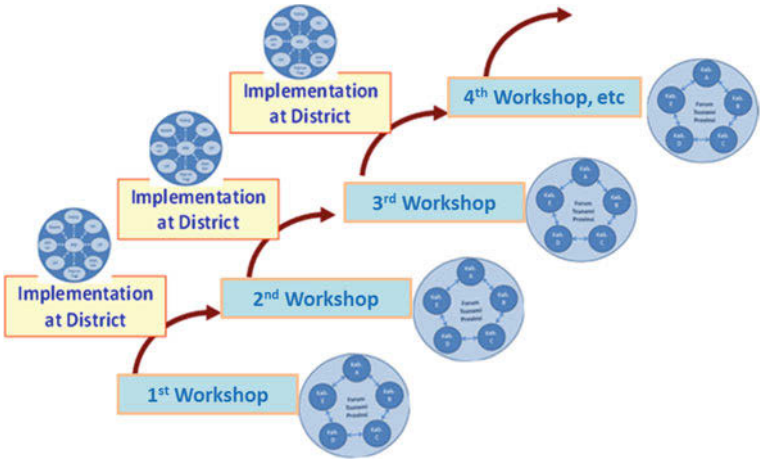

Fig. 10.10 Capacity-development approach

preparedness and early warning efforts in Japan saved many lives during this incident, considering the magnitude of the event and the number of people exposed if compared to the 2004 Indian Ocean tsunami. The assessment of this incident revealed that tsunami inundation in many areas was far more extensive than expected (Koshimura 2011). In the event, even designated evacuation-assembly points were flooded, which caused a loss of life in areas that had been assumed to be safe. This raises the question as to how such rare but extreme events can be properly addressed in hazard assessments and preparedness plans. During the UN University Japan Symposium in Tokyo, held in February 2012, a two-level approach was suggested, to distinguish between frequent tsunamis, (which in Indonesia occur approximately every two years), and extreme events, possessing estimated recurrence intervals of several hundred years. Such an approach may perhaps warrant the introduction of a two-zone concept for evacuation planning. A practical example for such an approach can be found in southern Bali where a two-zone concept was implemented in 2010 (GTZ-GITEWS 2010a). Discussions in Japan also led to the question of whether preparedness and mitigation plans should be based on extreme events with recurrence periods of several hundred years or on the more frequent events with recurrence periods of around 100 years or less. Ultimately, this is a political question, which depends upon how much risk a society is willing to accept or how much risk it can afford to reduce.

Experiences from recent tsunamis, tsunami warnings and tsunami-simulation exercises in Indonesia have been evaluated and documented (Artanti 2011; GIZ-PROTECTS 2011; Usdianto and Juliasman 2011) and provide valuable insights into the current status of the early warning system in Indonesia. The results show that Indonesia has made significant progress, but there is still a long way to go.

With regards to the downstream section, it can be concluded that warning services from the NTWC at the BMKG to interface institutions and national media are, in general, reliable and quick with warnings being sent out within 5 min. The assessments show that currently the general public primarily relies on information disseminated from media sources, as local governments—with a very few exceptions—are not yet ready to forward warnings and provide guidance. This means that people are forced to interpret warnings by themselves and then to decide how to react on them. Unfortunately, the public's understanding of InaTEWS, the national warning services and required reaction is still limited. Efforts are under way to improve understanding about the tsunami early warning system for both the public and institutions. Initiatives include the publication of a media handbook (UNESCO 2011), and a guidebook on the tsunami early warning service by InaTEWS (BMKG 2012).

Local authorities play an important role in the warning chain, as they are responsible for deciding whether to trigger sirens and/or call for an evacuation. In most areas, the required decision-making processes, 24/7 services, and dissemination procedures and technologies at local levels have either not yet been implemented or are not working in a reliable way. Often, even the communication link between the NTWC and the local 24/7 services do not function reliably. There are multiple reasons for this including the breakdown of communication channels during emergency

situations, missing back-up systems, a lack of maintenance of installed equipment as well as disregarding established procedures.

People in risk areas need solid references to determine when, how and to where they should evacuate. Such references include evacuation maps at community (sub-district, village, city quarters) or institutional levels (especially schools, hospitals, hotels and other vulnerable institutions), and local warning arrangements (local sources of information, decision making and calls for evacuation in local areas or institutions). Evacuation plans and local warning arrangements have been developed in some areas with the support of (pilot) projects by various organisations, but most communities still lack such reference information. While national guidelines on tsunami warning services are already available, standards and policies for hazard mapping and evacuation planning are still missing, leading to different approaches in producing community maps, with the consequence that the information produced varies significantly in quality and reliability.

The authors would like to highlight two other issues, which were raised as important points based on the recent experiences in Japan. First of all, it was emphasised that tsunamis are a problem for local communities and that proactive local initiatives are therefore needed to develop locally-adapted mechanisms and measures for tsunami preparedness and mitigation. However, in order to enable local efforts to be effective, such initiatives require substantial support from the national level in the form of policies, resources, references and services, which cater to local needs. Secondly, the experiences in Japan showed that self-protection arrangements played an outstanding role. In a tsunami emergency, survival very much depends on each individual's knowledge and capacity to react in a quick and appropriate way, especially in uncertain conditions. Therefore, it is recommended that preparedness strategies should more widely promote individual, family and community arrangements, which again require solid references provided by local and national disaster-management agencies.

10.6.2 The Way Ahead

Implementing and operating an early warning system involves a continuous learning and improvement process, which ideally contains ongoing improvement cycles of assessment, planning and design, implementation and evaluation. Having completed the initial establishment of InaTEWS and having entered the service-delivery phase, it might be a good moment to conduct a systematic review to obtain a clear understanding of what has been achieved so far and what needs to be improved. Such a review should address all aspects related to the end-to-end system and should include different perspectives from the scientists and practitioners involved in implementing the system, and the communities at risk. For the time being, and based on recent experiences, the following aspects are considered key points.

Building a common understanding of the system: To make the system work, technical and human capacity at all levels must continue to be developed and combined.

To build a common understanding of the system and encourage all actors to assume and play their respective roles, the provision of adequate references and guidelines is necessary. Developing these references is a multi-stakeholder task. Only a joint learning process can produce a tailor-made warning chain that really addresses the needs of communities at risk.

Improving public understanding of the warning service and the contents of warnings: Recently, InaTEWS introduced a new warning scheme based on three different warning levels. It is now necessary to train interface institutions and inform the public as to what reaction is expected according to each level.

Institutionalisation at all levels: During InaTEWS' development process, the system mainly came within the domain of specialised agencies involved with upstream technologies and the setup of the NTWC. In the future, it is envisaged that the National Disaster Management Agency (BNPB) will play a more significant role, especially in the downstream section. For the further development of InaTEWS, a coordination mechanism between all the actors and entities involved, plus a focal point for all issues related to the downstream section, would be extremely valuable.

Creating a sense of ownership at the local level: Strengthening the role of local disaster-management agencies and governments at the local level is crucial in the downstream section. In order to facilitate quick and reliable decision making at local levels, the utilisation of SOPs must be promoted. This will help local governments to deal with uncertainty and to be able to react quickly. As tsunamis will most possibly affect multiple administrative areas, multi-level and multi-sector coordination is required to synchronise SOPs within each of the administrative areas.

Scaling-up: Taking the existing experiences from various pilot areas and applying them to more districts along tsunami-prone coastlines is another challenge in InaTEWS' ongoing development. Now that a solid level of performance has been achieved, the system needs to be promoted proactively. This involves going public, explaining the system, and building relationships with the system's end-users—i.e. communities at risk. This is arguably the most important factor: building people's trust in the system so that it can achieve its ultimate goal—saving lives.

References

Artanti W (2011) The Bali 6.8 earthquake on the 13th October 2011 reaction to the earthquake and related "No Tsunami Threat" message from InaTEWS: a case study. GIZ-PROTECTS, Jakarta

BMKG (2012) Pedoman pelayanan peringatan dini tsunami InaTEWS (Guidebook on Tsunami Early Warning Services by InaTEWS), Jakarta

BNBP Regulation No.3/2010 on national disaster management plan 2010–2014

BNPB Regulation No. 2/2012 on general guidelines for risk assessment

Bollin C (2003) Community-based disaster risk management approach, Experience gained in Central America, GTZ. http://www.gtz.de/de/dokumente/en-community-based-drm.pdf

Civil Society Organisation (2009) The DNA code of risk has two intertwined strands—why vulnerability matters: a civil society response to the draft guidelines for Disaster Risk Assessment in Indonesia

GITEWS (2010) Review of the InaTEWS—framework

GIZ-PROTECTS (2011) IOWave11 in Aceh, Padang and Bantul—an evaluation report
GTZ-GITEWS (2010a) Tsunami evacuation plan for Kelurahan Kuta, Bali: a documentation of the process and results of tsunami evacuation planning. http://www.gitews.org/tsunami-kit/en/id_tsunami_evacuation_map_kuta.html
GTZ-GITEWS (2010b) TSUNAMIKit for local capacity building in InaTEWS. www.gitews.org/tsunami-kit
Hidayati D et al. (2011) Studies on the role of gender in disaster management in Jogjakarta, LIPI National Priority Programme 2012, LIPI
IFRC (2009) World disasters report 2009—focus on early warning, early action. http://www.ifrc.org/Global/WDR2009-full.pdf. Accessed 1 June 2009
Koshimura S (2011) The impact of the 2011 Tohoku earthquake/tsunami disaster—lessons towards tsunami-resilient communities
Lauterjung J, Münch U, Rudloff A (2010) The challenge of installing a tsunami early warning system in the vicinity of the Sunda Arc, Indonesia. Nat Hazards Earth Syst Sci 10:641–646
Mileti D, Nathe S, Gori P, Greene M (2004) Public hazards communication and education: the state of the art. Update of informer issue 2: public education for earthquake hazards (originally published in 1999)
Oxfam International (2005) The tsunami's impact on women, Oxfam Briefing Note
Sorensen H (2009) Hazard warning systems: review of 20 years of progress. Nat Hazards Rev 1(2):119–125
Spahn H, Hoppe M, Vidiarina HD, Usdianto B (2010) Experience from three years of local capacity development for tsunami early warning in Indonesia: challenges, lessons and the way ahead, NHESS 9. www.nat-hazards-earth-syst-sci.net/10/1411/2010/nhess-10-1411-2010.pdf
Thomalla F, Larsen RK, Kanji F, Naruchaikusol S, Tepa C, Ravesloot B, Ahmed AK (2009) From knowledge to action: learning to go the last mile—a participatory assessment of the conditions for strengthening the technology-community linkages of tsunami early warning systems in the Indian Ocean. Stockholm Environment Institute
United Nations (2005) Report of the world conference on disaster reduction Kobe, Hyogo, Japan, 18–22 January 2005 (A/CONF.206/6). www.preventionweb.net/files/17671-finalreportconference1.pdf
UNESCO (2011) Panduan Informasi Peringatan Dini Tsunami bagi Lembaga Penyiaran di Indonesia (Media handbook for tsunami early warning in Indonesia)
UNISDR (2006a) EWC III third international conference on early warning. A checklist, from concept to action, developing early warning systems
UNISDR (2006b) Final statement third international conference on early warning (EWC III). www.unisdr.org/2006/ppew/info-resources/ewc3/FinalStatementfinal.pdf
UNISDR (2009) Global assessment report on disaster risk reduction
Usdianto B, Juliasman J (2011) Tsunami warning on the 4th of April 2011—institutional and community reactions to the earthquake and related tsunami warnings in southern Java. A case study
Yogaswara H, Yulianto E (2006) Smong—local knowledge and strategies on tsunami preparedness in Simeulue island. Nangroe Aceh Darussalam, UNESCO–ISDR, LIPI
Yulianto E, Rafliana I, Aditya V, Febriawati L (2011) Impact of pre-disaster public awareness activity on public readiness: a case study of the 25th October 2010 Mentawai Tsunami, NHESS 11

Chapter 11
The Last-Mile Evacuation Project: A Multi-disciplinary Approach to Evacuation Planning and Risk Reduction in Tsunami-Threatened Coastal Areas

N. Goseberg, G. Lämmel, H. Taubenböck, N. Setiadi, J. Birkmann and T. Schlurmann

Abstract In view of recent tragic and disastrous tsunami events such as the Indian Ocean tsunami in 2004 or the Tohoku-Oki tsunami in 2011 it is still indispensable to aim at deepening our insight into the mechanisms which turn natural disasters into life-changing events for those individuals living at regions at risk. In this context risk mitigation on the basis of well-implemented early warning systems is inevitable to reduce human losses and to pave the way for specific measures on disaster recovery. A possible work chain to assess this complex objective is exemplified by the inter-disciplinary "Last-Mile Evacuation project" which focused on the city of Padang, Indonesia. This city is one of the cities worldwide most imperiled by tsunamis since it is located in the direct neighborhood to the Sunda arc with an average warning time below 30 min. The work chain presented in the present paper comprises the generation and compilation of the underlying geo data basis, the simulation of hydrodynamics, the assessment of physical vulnerability using remote sensing data and techniques, the assessment of social vulnerability related with people's exposure, risk perception, and evacuation behavior, and the modeling of potential evacuation routes. While the main focus of the original project was on city-wide risk assessment,

N. Goseberg (✉) · T. Schlurmann
Franzius-Institute for Hydraulics, Waterways and Coastal Engineering, Leibniz University Hannover, Nienburger Str. 4, 30167 Hannover, Germany
e-mail: goseberg@fi.uni-hannover.de

G. Lämmel
Division Civil Security and Traffic, Jülich Supercomputing Centre Institute for Forschungszentrum Jülich GmbH Institute for Advanced Simulation (IAS) Jülich Supercomputing Centre (JSC), Wilhelm-Johnen-Stra?e, 52425 Jülich, Germany

H.Taubenböck
German Aerospace Center, German Remote Sensing Data Center, Land Surface, Münchner Str. 10, 82234 Wessling, Germany

N. Setiadi and J. Birkmann
Institute for Environment and Human Security (UNU-EHS), United Nations University, Hermann-Ehlers-Str. 10, 53113 Bonn, Germany

F. Wenzel and J. Zschau (eds.), *Early Warning for Geological Disasters*, Advanced Technologies in Earth Sciences, DOI: 10.1007/978-3-642-12233-0_11,

the focal point of this study is a close-up view of the micro-scale dynamics of inundation and evacuation on urban district level. The existing situation and urban setting is subsequently compared with alternative shelter options. Additionally, qualitative information on social aspects to be considered in developing appropriate mitigation options is outlined. It is anticipated to communicate best-practice knowledge on how to approach the assessment of tsunami hazard with potential overlapping areas to other natural disasters.

11.1 Introduction and Motivation

Water-related natural hazards affect communities worldwide on a social, economic and physical level. Those hazards comprise floods and flash floods, storm surges, hurricanes, cyclones, dam breaks and tsunamis amongst others. A temporal distinction is possible by means of quantities such as warning time or propagation speed. On a spatial level, water-related hazards are also classifiable by many quantities, i.e. the total affected area. In this context of water-related hazards, tsunamis represent a severe danger to coastal inhabitants since in many regions warning times are extraordinary short while long sections of a coast could be affected. Hence, Sieh (2006) summarizes what isvital in a chain of measures aiming at saving lives during and after potential megathrust earthquakes worldwide.

Besides basic science, key words such as emergency response, preparedness, warning capabilities, education and infrastructure behavior have to be addressed by ‘at-risk’ communities, local population, emergency managers, stakeholders and politicians. Bernard et al. (2006) further outline how an interconnection of quantitative science and hazard reduction practice allows ameliorating the resilience of tsunami-threatened communities. In this context scientific and educational frontiers are firstly the improvement of tsunami forecast in terms of accuracy, secondly the advance of human response simulation accounting for people’s immediate reaction during catastrophic events and thirdly the application of real-time remote sensing for immediate disaster response and rescue measures.

The city of Padang, Indonesia, is amongst the most threatened cities world-wide. Lauterjung et al. (2010) outline the special hazard to the directly affected coastline of Sumatra as well as Java and demonstrate the urgent demand for early warning measures. Facing the ever growing frequency and magnitude of natural events it emphasizes how crucial disaster preparation has become. Reducing human vulnerability is the only way to minimize the risk of a natural disaster. Besides activities to raise public awareness, the development of early warning systems is indispensable (Bogardi 2004). Attempts to address the high demand for early warning generally rely on seismic data sources which allow for an estimate of the arrival time of the first wave. Ramirez and Perez (2004) report on a local tsunami alert system that informs stakeholders immediately about possible risk sources while supporting them to take necessary measures during and in the aftermath of an event. In the Pacific Ocean an information system has been installed which is capable of detecting long waves in

the deep ocean by means of a distributed network of tsunameter buoys allowing for a rapid assessment of hazard potential due to tsunami (Gonzáles et al. 2005). Some technical progress is achieved for the early warning demand of the Indian Ocean by means of a numerous set of sensors (tsunami buoys, seismometers, real-time GPS measurements) backing up a pre-calculated data base of tsunami incidents and allowing for a reliable source of information to manage any measures during a tsunami in Indonesia and the neighboring countries (Lauterjung et al. 2010).

From a general early warning perspective it is prerequisite to always guarantee that once warnings are issued the message is delivered, received and finally abided by those communities at risk. What is more, early warning systems need not only address a proper warning to the threatened coastal stretches in due time but give information about how severe a single event could impact the coast, i.e. the overall inundation distance. In a warning chain, especially the acceptance of the warning, the dynamics of the hazard evolution at the location at risk, the evacuation procedure and the human behavior is unknown and needs to be adequately addressed by emergency planners and stakeholders.

In this connection the integrated research project "Numerical Last-Mile Tsunami Early Warning and Evacuation Information System" has shown that early warning measures have to be supported by an information framework with a city-wide focus in order to analyze how evacuation procedures could be optimized and how particular regions of high vulnerability could be detected in advance (Setiadi et al. 2010; Setiadi 2011a, b; Taubenböck et al. 2009a, 2012).

11.2 Background

The focal point of this study is a close-up view of the micro-scale dynamics of inundation and evacuation on urban district level. As prerequisite for the land cover and urban structures as well as population distributions have been provided by remote sensing and social science. Additionally physical and social vulnerability is analyzed in detail at the respective quarter of the city of Padang (cp. Fig. 11.1), where high velocities and water levels would occur during a tsunami inundation (Schlurmann et al. 2010). The focus region is chosen because one of the main drainage tributaries, the river Arau, opens the coastline for extra-ordinary penetration of the approaching tsunami wave. The evacuation situation is equally complicated since only one bridge (Siti Nurbaya Bridge, cp. Figs. 11.2, 11.3 or 11.5) is available to allow for an immediate evacuation in the direction of the Padang headland at the river mouth of Arau. Due to probable damage to this bridge in the aftermath of the earthquake-induced tsunami, simulation results suggest that the Siti Nurbaya Bridge should not be used for evacuations (Lämmel et al. 2010). This means the only plausible evacuation direction is to the east (safe hinterland).

It is well documented that Sumatra's third largest urban area (Fig. 11.1) counting more than one million inhabitants is one of the most imperiled cities in the Indian Ocean rim due to potential tsunami hazards originating off the coast of Padang. The

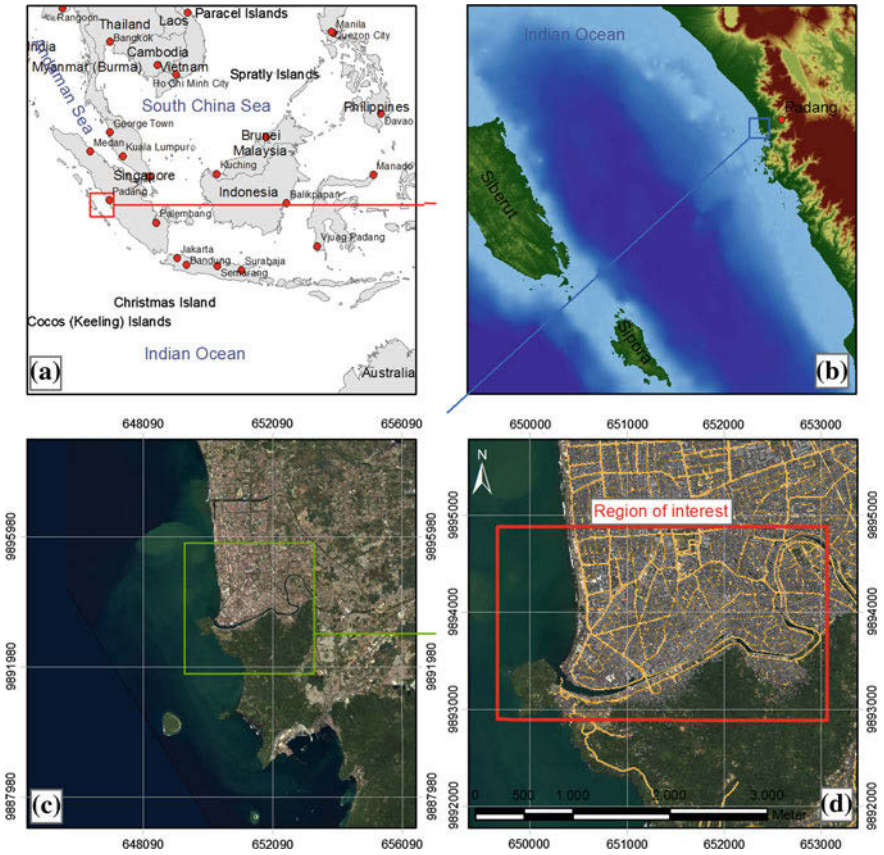

Fig. 11.1 Overview of the region of interest, **a** Indonesia and its surrounding countries, **b** topographic and bathymetric settings of Sumatra, the Mentawai island and the Sunda arc, **c** overview of the city of Padang and the harbor, **d** focus region in Padang around the river mouth of the Arau river, street network and access to the hilly headland

city is located directly on the coast, partially situated beneath the sea level and drained by numerous artificial waterways and rivers. Thus, the city of Padang is located in a zone of extreme risk due to severe earthquakes and tentatively triggered tsunamis. The complex and dynamic urban system of Padang features a high concentration of population, infrastructure and economic values. Padang features supra-regional relevance with an international airport, a port as well as binding to the rail network. Thus, the city illustrated in Fig. 11.1 possesses a central economical role for the coastal region and the mountainous back-country.

Databases of earthquake and tsunami events for the Indian Ocean correlate a high percentage of tsunami to the origin of the Sunda arc directly facing the Pa-dang coastline with an average return period of tsunami events being generated every 3 years (Rastogi and Jaiswal 2006). A study of historic tsunamis in

the Padang region exemplifies the extraordinary risk posed to the local community (Borrero et al. 2006).

11.3 Assessment of Physical and Social Vulnerability

UN/ISDR (United Nations/ISDR 2004) defines vulnerability as "the conditions determined by physical, social, economic and environmental factors or processes, which increase the susceptibility of a community to the impact of hazards; for positive factors, which increase the ability of people to cope with hazards". While the definition seems to be self-explaining, the influencing factors and processes in different dimensions (physical, social, economic, and environmental) need to be specifically identified based on the hazard context and the goal of the vulnerability assessment itself. The vulnerability analysis here follows the BBC-Meta-Framework (Birkmann 2006) that considers exposure, susceptibility, and coping capacity as components of vulnerability and link vulnerability assessment within the feedback loop to inform disaster risk reduction intervention. In our study, we focus on physical and social vulnerability in the context of tsunami early warning and evacuation. It deals with the questions of dynamic exposure of the population and buildings to potential tsunamis shaped by urban land-use setting, building stability to withstand earthquakes prior to tsunami events, as well as preparedness of the community to conduct mass evacuation to safe areas within a short warning time.

For an area-wide coverage and analysis, especially in dynamically growing and changing areas, earth observation serves as an independent and relatively cost-effective data source. We used the combination of optical high resolution satellite data and a highly resolved digital elevation model to classify the urban land cover and the urban morphology in its three dimensions (Taubenböck et al. 2009a). The results are eight classes mapping the urban morphology—houses, streets, sealed areas, grassland, trees, wetland, bare soil, and water. With it, exposed elements are mapped, located and described in a quantitative way with parameters such as building size and height, building density, roof types, floor-space index, vegetation fraction, infrastructure, or undeveloped areas. Figure 11.2 presents the classified 3D city model for the test area in downtown Padang.

However, while for remote sensing there is often a relatively simple and direct relationship between land cover type and detected spectral reflectance, the same is seldom true for land use or further assessments such as on building stability. Nevertheless, the derived physical parameters like building sizes and heights, roof types, etc. often indirectly correlate to the usage or stability of the buildings.

The assessment of physical stability of buildings is an essential step to support risk management and evacuation planning. But with almost 100,000 buildings within the entire city and more than 9,000 buildings in the study area surveying of the complete building stock was out of reach for time and cost reasons.

A combination of civil engineering and remote sensing approach aims at overcoming this problem: On the one hand civil engineering allows a highly detailed

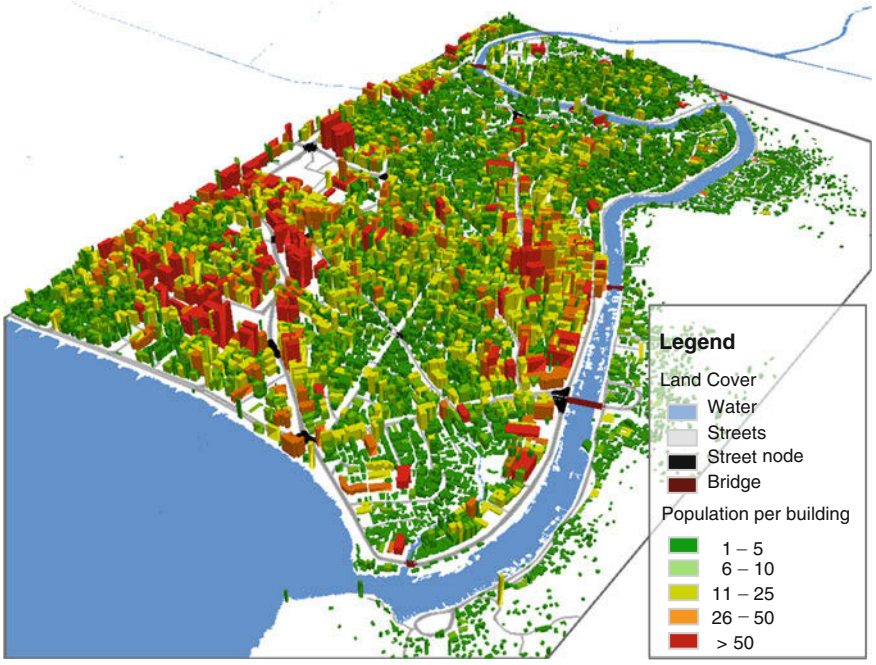

Fig. 11.2 Three dimensional view on the urban morphology and population distribution projected on the buildings exemplified for the afternoon

stability analysis of individual buildings by an extensive house by house inspection. For Padang, 500 buildings have been surveyed gathering data on their physical characteristics like e.g. height, material, existence of columns, foundation of main structures, existence of stirrup or/and main beam or damage due to previous earthquakes. In combination with physical tests, like the hammer test on supporting pillars, the stability of the structures was assessed individually.

An additive approach was applied for the various physical parameters and a normalized vulnerability (stability) index calculated (100 = stable structure; 0 instable structure). The sample selection of the surveyed buildings aimed at a complete coverage of differing housing types—from small, low height shacks to large, high-rise building types, equally distributed within the entire city area of Padang.

The secondary research objective is to correlate the limited amount of physical parameters derived from remote sensing data to the detailed survey on building stability to allow for a mapping and assessment of potentially stable structures.

The result does not show an obvious correlation, but reveals that buildings with a higher stability (vulnerability value) predominantly show a higher building volume (Taubenböck 2011). In our case we identified an 85.71 % probability for a stable structure for buildings with a volume higher than 3500 m^3. The extrapolation on the complete building stock using the 3D city model identified 183 buildings with a high

Table 11.1 Quantification and location of affected buildings, potential shelters and shares of structural types

Name of zone	Probability [%]	Buildings affected	Potential shelters	Semantic classification [%]
No hazard	0.0	889	22	
Low hazard	0.01–5.0	7.261	5	• 13.1 slums
Medium hazard	5.01–15.0	882	–	• 30.4 low class
High hazard	15.01–45.0	157	–	• 55.2 medium class
Extreme hazard	45.01–100.0	40	–	• 1.4 high class
Total		9.238	27	

probability to be appropriate for vertical evacuation. The interdisciplinary analysis thus allows reducing the amount of buildings to be surveyed for a final official designation as vertical evacuation shelter from 100.000 to 183 (or 27 in the study area) which is feasible for surveys. Table 11.1 shows the quantification of potentially affected buildings, potential shelters and the shares of building structure types for the study area with respect to the risk zones based on spatial inundation modeling.

With the combination of in-situ field survey data, the population census (Setiadi et al. 2010) as well as the physical parameters of the building stock an indirect classification to assess the land use has been derived. Thus, spatial knowledge on commercial, industrial, residential and mixed usage has been projected on the 3D city model.

Beyond this a semantic classification has been performed. The idea of semantic classification aims at a first assumed interrelation between physically homogeneous sectors within the complex urban morphology and the socioeconomic characteristics of people residing there. The combination of the area-wide available statistical physical parameters describing the building stock of Padang per sector—built-up density, average house size, average building height, location—enables to identify physically homogeneous areas. As one example, we assume for the semantic class 'slum' highest building densities, lowest building sizes and heights as well as organic building alignment (Taubenböck et al. 2009b).

It is obvious that the physical and semantic information on the urban morphology (building size, height, occupancy, location, semantic class) allows indirect conclusions on the population distribution, even on its spatiotemporal shift within the course of a day.

On the basis of the punctual information of population data (933 households) distributed around the entire city collected through fieldwork by UNU-EHS in 2008 the mathematical concept is based on a bottom-up extrapolation. For the different semantic classes the particular punctual information on individual buildings is averaged to get a characteristic number of inhabitants per m^2 per semantic class. With knowledge on occupancy the population distribution on building level has been assessed at three different times of the day: morning, afternoon and night (Setiadi et al. 2010). Thus, the population flux between day—and night-time reveals a spatial shift of vulnera-

Table 11.2 Time-dependent assessment of affected people and quantity of groups of higher vulnerability with respect to the tsunami inundation map

Name of zone	Number of people affected (of which belong to more vulnerable group: woman, children and elderly)		
	Morning	Afternoon	Night
No hazard	3.261 (2.310)	3.574 (2.510)	4.502 (2.994)
Low hazard	72.802 (46.505)	59.501 (37.208)	46.850 (30.863)
Medium hazard	3.886 (2.569)	3.539 (2.312)	3.531 (2.333)
High hazard	724 (450)	779 (496)	835 (560)
Extreme hazard	170 (109)	160 (100)	156 (96)
Total	80.843 (51.943)	67.553 (42.626)	55.874 (36.846)

bility, e. g. the highly prone market areas at day-time are almost empty and thus less vulnerable at night-time. Table. 11.2 gives an overview on the potentially affected people with respect to time.

Additionally, social vulnerability assessment was conducted using a combination of qualitative and quantitative approaches to provide a further understanding of the (1) daily activity pattern of the population groups (input parameter for the calculation of potentially affected people above), (2) access to early warning and evaluation of evacuation facilities from people's perspectives, and (3) risk perception and evacuation behavior.[1] Data used were collected from existing statistical data of the population census (the last census year during the study was 2000) and sub-district in figures of 2006 obtained from the official statistical office (BPS), as well as household surveys conducted by UNU-EHS in 2008 and 2009, participatory mapping, and additional qualitative information from local actors (Setiadi, short visits in 2008 and field observation in June-August 2009[2]).

The region of interest captures an area shared by 3 *Kecamatan* (sub-districts) and 11 *Kelurahan* (villages under sub-districts). The *Kecamatan* represent areas with significant trading sector activities, close to the central business district of the city of Padang at the northern boundary and including a trading center at the river mouth ("the old town"). Based on the Population Census 2000 the area is occupied by a much less proportion of the *Minang* group, the most dominant tribal group in the city of Padang and West Sumatra, at village level compared to the rest of the area in the city. It is occupied by 40 % of other ethnic or tribal groups, of which about 30 % are ethnic Chinese. This figure implies diverse communities with different cultural norms and belief, which should be considered when communicating tsunami risk and understanding existing behaviors towards warning information.

[1] For further explanation on the analysis methods and findings see Setiadi and Birkmann (2010); Setiadi et al. (2010); Setiadi (2011a); Taubenböck et al. (2012).

[2] Please note that especially the qualitative data represent the situation in the city up to the data collection period. Slight changes in the city may have taken place, especially after the major earthquake event in September 2009 and the latest progress in disaster management of the city.

Concerning people's access to early warning, an index of early warning dissemination media—public (sirens, trained mosques and community groups) and private (radio, TV, mobile and landline phone)—was calculated at the building level based on media availability at home and in workplaces as well as their spatial coverage. In the area of interest, the index values vary from very high to low. It is important to note that the area containing high and extreme hazard at the river mouth have a low access; here, about 8,000 people (in the working hours even 9,000) do not have access to any of the existing public media. Moreover, the existing evacuation infrastructure was still rated as not sufficient by the majority of our survey respondents (this corresponds to the evacuation modeling results in the next chapter).

Another important social aspect to consider in using the evacuation modeling analysis is the evacuation behavior, which relates to the degree of knowledge, existing socialization and preparedness activities, and socio-cultural values of various communities. Our household survey showed that in the city only 34 % evacuated (some still with a considerable delay) after receiving a "potential tsunami" warning in the earthquake event in 2007, however, 75 % intended to conduct evacuation in the future. The evacuation readiness of the people was also assessed based on parameters on people's awareness (basic knowledge of tsunami, perception of tsunami hazard, perception of vulnerability and preparedness, perception of own capability to conduct evacuation) and specific knowledge about evacuation (knowledge of existing evacuation facilities, early warning and participation in the evacuation drill). On average, the majority of the people have sufficient awareness while the evacuation knowledge of more than half of the respondents was still low. It was also found that the level of awareness was correlated to the intention of evacuation, i.e. it may be considered as one influencing factor of evacuation behaviors.

Additionally, various opinions on tsunami risk and necessity to immediately evacuate were identified in the qualitative study, which relate to people's belief in God's fate, discussion on news in the media, of the community/religious leaders or rumors circulated from mouth to mouth. Some of the people also relate the uncertainty of the tsunami occurrence with the risk and costs they have to deal with (income/property losses, traffic accidents, availability of vehicle for elderly, possibility for family evacuation, accommodation in the evacuation place). Also, some people from the ethnic Chinese community who were interviewed perceived that they have not been involved sufficiently or were not fully aware of preparedness activities from the city.

11.4 Tsunami Hazard and Inundation Modeling

The Sunda megathrust is the fault which marks the interface between the convergent plate boundary of the Eurasian and the subducting Indo-Australien plate. The long list of major earthquakes along this fault illustrates the enormous hazard potential posed by the interface locking and accumulated stresses within the earth' crust. This leads to periodical earthquakes and triggered tsunamis, e.g. in the years 1797, 1833, 2004, 2005 (Sieh 2006). Reoccurrence intervals are in the range of 200–300

years prognosticated especially for the part of the fault in the vicinity of Padang (Mentawai patch) which was deduced from the growth pattern of coral microatoll analysis (Natawidjaja et al. 2006). A high probability of a next great rupture with M>8 along the Mentawai patch is also revealed by McCloskey et al. (2007).

Besides the investigations on excitation mechanisms leading to tsunami, currently only few studies deal with the propagation and the inundation of those long waves. Borrero et al. (2006) examines the impact of the 1797 and 1833 earthquake and tsunami to the Sumatra coastline focusing on the city of Padang and Benkulu. This first study allows for an approximate estimation of hazard zones in the Padang area although on a rough geo data basis. A natural step forward was taken by Taubenböck et al. (2009a) by incorporating not only an analysis of flow dynamics but also account for socio-economic and physical vulnerability as well as evacuation dynamics in order to improve the overall disaster preparedness of the Padang community. Most importantly, the transdisciplinary analysis is based on a highly resolved data set for run-up and inundation modeling, census and other data bases. A detailed hazard and inundation map was produced on a city-wide level to assist the effort of developing evacuation routes and disaster preparedness.

A detailed study of different practical approaches to model dense development in residential areas is presented by Muhari et al. (2010), who compared water surface elevations and flow velocities for plain elevation models, for building integrated elevation models and for distributed roughness models. They found that especially in the case of detailed evacuation modeling digital elevation models integrating building footprints are a good choice while for the overall inundation extent distributed roughness models are sufficient. The complex interaction of tsunami run-up and near-shore buildings is investigated experimentally by Goseberg (2011).

In the following a model of the city of Padang is applied that relies on the approach to account for the existence of buildings in the flow field. Details of the numerical model and model setup are described in (Taubenböck et al. 2009a, 2012; Schlurmann et al. 2010). The ANUGA numerical code solves the shallow water wave equations (Nielsen et al. 2005). The model setup accounts for a rupture scenario outlined in detail in Schlurmann et al. (2010) based on a highly-resolved bathymetric and topographical data set which was finally resampled to 3.0 m raster width. Additionally static subsidence of $\Delta z = -1.32\,\mathrm{m}$ was assumed from the rupture scenario as well as an increased sea level of 0.80 m during wave attack. These assumptions were presumed to account for uncertainties related to the interaction of on-land flow and urban infrastructure as well as roughness influence on the energy dissipation during wave run-up. The leading wave front found for this scenario exceeds a wave height of $h_{max,1} = 6.70\,\mathrm{m}$. While the second wave crest is only about $h_{max,2} = 2.00\,\mathrm{m}$ and might presumably, but falsely indicate less heightened tsunami alert, the third wave crest again reaches a wave height of $h_{max,3} = 5.00\,\mathrm{m}$. Arrival time of the first wave crest is about 16 min after the earthquake takes place. A detailed description of the sea bottom deformation leading to the tsunami event is given in Schlurmann et al. (2010). Figure 11.3 depicts the evolution of flow depth in the centre of the old town of Padang. Although the inundation begins at the coastline, it is noticeable that very soon after the wave front arrives, the inundation also propagates north starting from

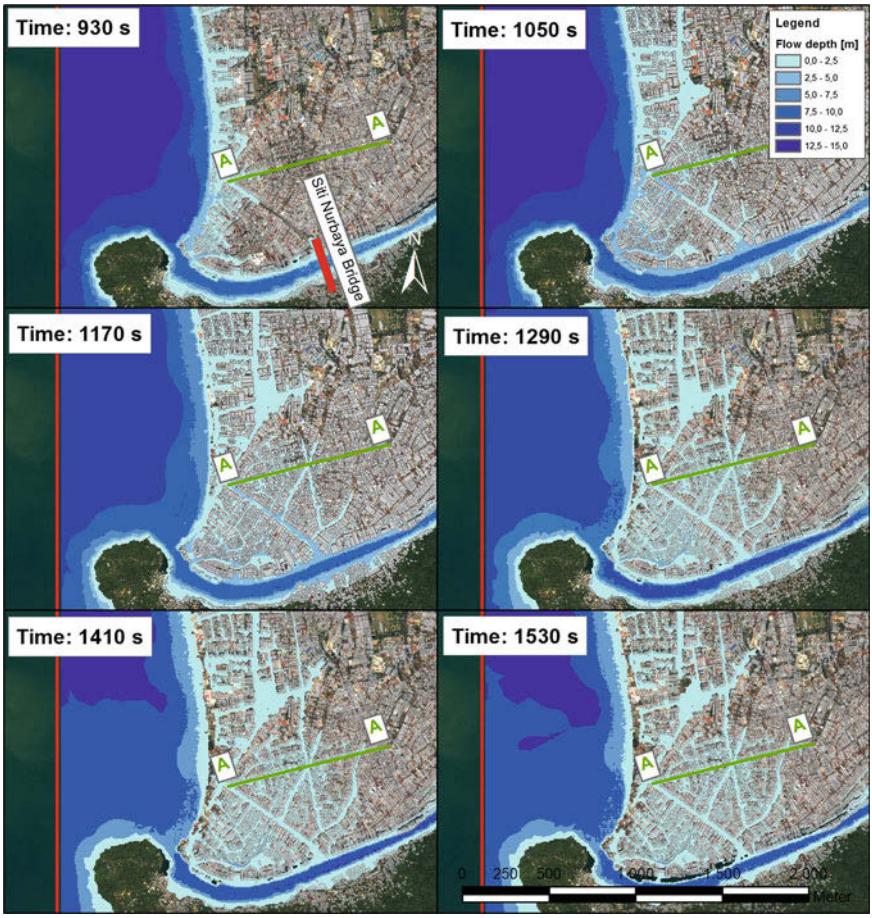

Fig. 11.3 Sequence of flow depth for the old town of Padang, timing is relative with respect to the model boundary, model boundary resides approx. 18 km offshore and the time offset to the earthquake event amounts to 960 s, thus absolute timing is yielded when offset time is added to relative times

the south of the region of interest, where river Arau drains into the sea. The upper left panel of Fig. 11.2 also illustrates that the surrounding of the only bridge leading to higher ground (Siti Nurbaya Bridge) is inundated at an early stage of the inundation process. This is due to the fact that the bridgeheads are close to the river banks and the low lying topography.

Overall water levels start rising first along the river bank, but due to low lying topography of the old town inundation propagates inland rather soon. Maximum flow depth rise in the old town to approximately 3.5 m at relative time 1050 s. Hence a coupling strategy of propagation and high resolution inundation models has been chosen for the simulations timing is given relative to the high resolution model

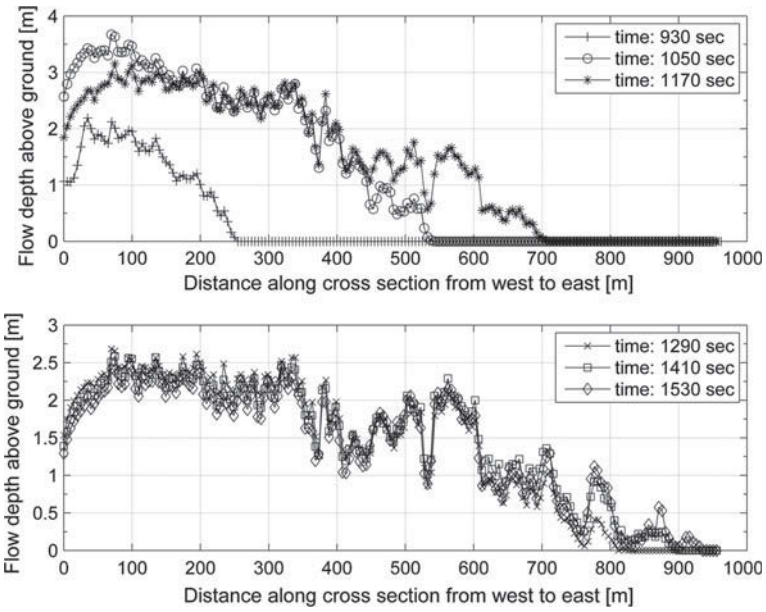

Fig. 11.4 Flow depth over ground over the distance along the cross section at Jl. Cokroaminoto for six specific time steps of the simulation, timing is relative with respect to the model boundary, model boundary resides approx. 18 km offshore and the time offset to the earthquake event amounts to 960 s, thus absolute timing is yielded when offset time is added to relative times

boundary. This offshore boundary taking the input of a coarse propagation model resides approximately 18 km offshore off the Padang coastline. Therefore a time offset of 960 s has to be added to the relative times to yield absolute times. Figure 11.4 displays how flow depths along a cross section positioned at the Jl. Cokroaminoto evolve during the inundation phase of tsunami run-up. The cross section is also marked in Fig. 11.3 as cross section A-A. Flow depth at the chosen position peak 3.5 m but decrease with continuing flooding to 2.5 m along the first 350 m of the flow depth profile. Flooding progresses at an approximate speed of approximately 2.4 m/s at the tip of the wave front taken from time 930–1050 s, while propagation speed reduces successively every next 120 s to 1.36, 0.88, 0.66 and 0.36 m/s. Under congested conditions a typical pedestrian walks with an average speed of 1.34 m/s (see, e.g. Weidmann 1993). However this theoretic value can be much lower for elderly people or people with children.

Thus, even if there would be no congestion the water still propagates much faster (at least in the early stages) than the evacuees could walk. The derivation of the inundation progress velocity explains how inundation analysis and evacuation modeling is interconnected. First detailed inundation dynamics is obtained and subsequently processed by means of blocking inundated parts of the street network in the evacuation analysis. Hence hydrodynamic boundary conditions are fed into the evacuation simulation.

11.5 Evacuation Modeling

The evacuation modeling for a city of Padang's size is a challenging task. Overall more than 300,000 people are at risk in the event of a major tsunami. In addition, a dense net of urban waterways posing barriers that hinder people from reaching the safe hinterland characterizes Padang. One of such barriers is the Arau River shown in Fig. 11.1. The river hinders people from reaching safe hills in the south. This is one reason why a detailed inundation as well as evacuation modeling and analysis are necessary. Therefore a comprehensive simulation framework to test and optimize different evacuation strategies has been proposed (Lämmel et al. 2010, 2009). The focus of this work is less on the evacuation modeling itself but more on a detailed analysis of different evacuation strategies. A broad discussion on the evacuation modeling using the multi-agent simulation toolbox MATSim is given in Lämmel (2011).

When developing evacuation strategies, there are different, sometimes conflicting, objectives. For instance, an evacuation can be modeled from the individual evacuee's perspective. This can be done by choosing a shelter location and an evacuation route for each evacuee that is optimal under the given circumstances. Such a solution would be a (Nash 1951) since no one can gain by unilateral deviation from the assigned route and shelter location. Thus, this solution would be stable, which is indeed a desired characteristic. However, a Nash equilibrium does not necessarily lead to the shortest possible evacuation in terms of average evacuation times. A situation where the average evacuation time (or system travel time) is minimal is called system optimum. However, the system optimum requires cooperative behavior (individual minimization of the social impact of one's behavior) and does, therefore, not follow an intrinsic motivation of the evacuees. For that reason, this kind of behavior has to be enforced externally. Technical details how this can be implemented in a multi-agent simulation are given in Lämmel and Flötteröd (2009). A third important objective is the avoidance of unnecessary risk during an evacuation. There is a relation between risk and uncertainty. For example it could be risky to recommend a bridge as part of a tsunami evacuation route if it is not certain if the bridge withstand the tsunamigenic earthquake. Therefore risky evacuation routes should be avoided as long as non-risky, possibly longer, routes exist. Another uncertain aspect in relation with tsunami evacuations is the amount of advance warning time. If the advance warning time is long a particular evacuation plan may work well. However, if the advance warning time is to short the same evacuation plan will fail. This means if the precise advance warning time is unknown the evacuation plan becomes risky. When looking at Fig. 11.5 it is apparent, that for many people living at the north bank of the Arau River the shortest evacuation route goes over the Siti Nurbaya Bridge to the hills in the south. However, if the advance warning time is unknown then it is risky to cross the river since it could be that the tsunami approaches while evacuees are still on the bridge. The length of the warning time is highly dependent on the given hazard scenario and usually a design scenario is chosen for practical evacuation planning. The evaluation of warning time duration has to be done by local stakeholders on the

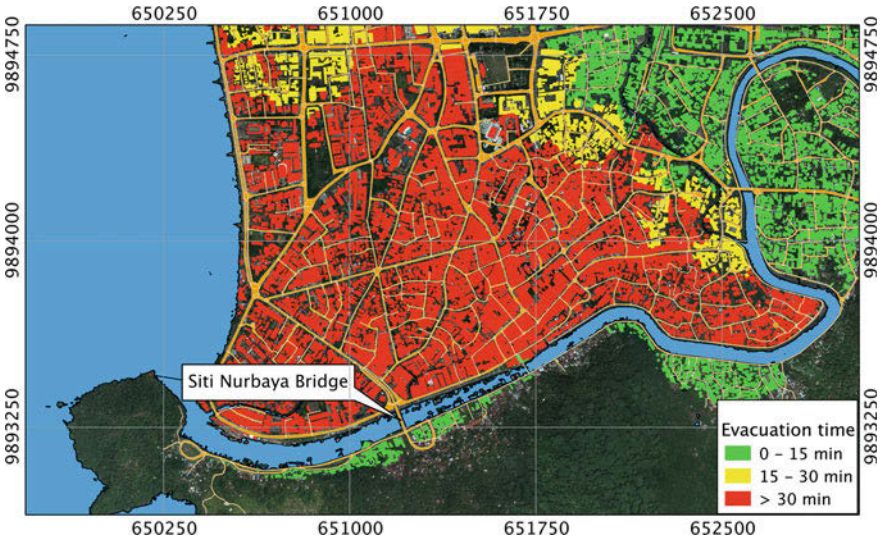

Fig. 11.5 Simulation results for the risk reducing evacuation approach (Run 1)

basis of social and topographical features in the region of interest. For that reason we recommend avoiding risky bridges as long as non-risky possible longer alternative paths exist. A general approach how this can be modeled in a simulation context is the risk reducing evacuation strategy approach (Lämmel et al. 2011). Simulation results for this approach (Run 1) are given in Fig. 11.5. The figure shows average evacuation times on buildings level. People from the green buildings may escape within 15 min; people from the yellow buildings would need between 15 and 30 min, and people starting their evacuation from a red building need more than 30 min to evacuate. This is the outcome of a microscopic evacuation simulation performed with MATSim. In the simulation every evacuee tries to minimize her individual evacuation time. The result is an approximately risk reducing Nash equilibrium (Lämmel 2011).

The simulation assumes a rational and well-behaved population. This means that in reality the result may look much worse. Still, the simulation can be used as a benchmark to see which areas need long evacuation times. The simulation result shows that long evacuation times are expected for large parts of the investigation area. One possible solution to improve the situation is the construction of shelters inside the hazard zone.

For Padang one could build tsunami proof concrete towers or platforms that are high enough and strong enough or, as it is discussed in chapter “Assessment of the Physical and Socio-economic Vulnerability”, draw on existing buildings that seem to be high and strong enough to withstand earthquakes and tsunamis. Some evacuation shelters are going to be built in near future in Padang. However, so far none of the projected shelters is ready for use. To see which impact shelters can have on an evacuation we assume three hypothetical shelters in the area of investigation.

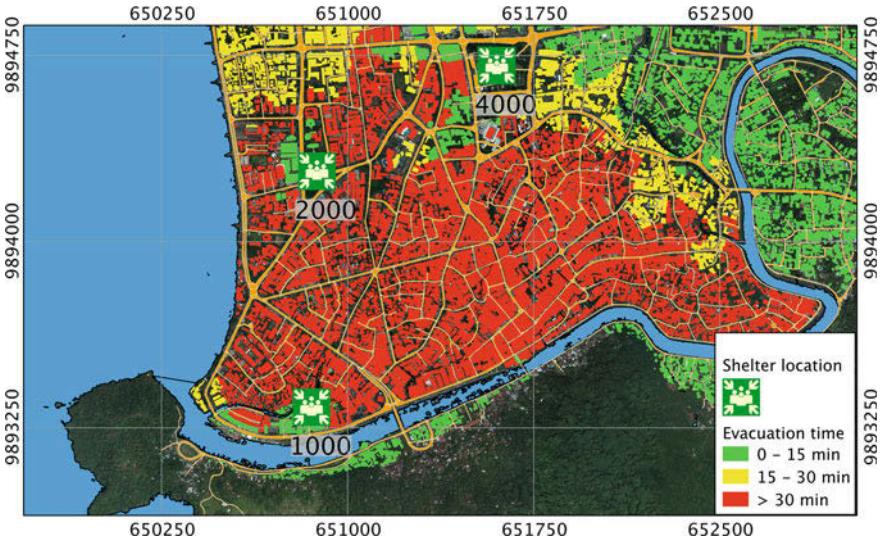

Fig. 11.6 Shelter locations simulation results risk reducing evacuation approach with shelters (Run 2)

The shelter locations are given in Fig. 11.6. In total the shelters have space for 7000 evacuees, which correspond to approx. 10 % of the population in the area of investigation. Technical details of the simulation approach for shelters are discussed in Flötteröd and Lämmel (2010). The result of the simulation run with shelters (Run 2) clearly shows that people living near to a shelter would significantly gain. Up to this point one would conclude that an evacuation with shelter buildings do much better. However this is not always true, even if the majority of the population would gain by the chosen shelter constellation, some of them would also lose. A simple "gains and losses" analysis is given in Fig. 11.7, where it is focused only on the extreme cases. Buildings whose people evacuate in Run 2 (with shelters) more than 10 min faster compared to Run 1 (without shelters) are green, and buildings whose people need more than 10 min longer in Run 2 are red. It is shown that many evacuees are worse-off if the hypothetical shelter constellation is applied.

The reason for this phenomenon is that people that are assigned to shelter buildings cause congestion on the streets in front of the shelters. These congestions delays evacuees further upstream even if they have no intention entering the shelter in question. This is a general problem with shelters. A detailed discussion on this matter is given in Lämmel (2011).

The results of this investigation lead to two conclusion. First, it is expected that the evacuation time for large parts of the investigation area is longer than 30 min. The second conclusion is that arbitrary shelter constellations in the city would improve the situation for people who are living next by, but it is possible that other people are worse-off because of the shelters. Our recommendation is to place shelters near to

Fig. 11.7 Gains and losses in terms of evacuation time: evacuees departing from green buildings gain more than 10 min because of the shelters; evacuees departing from red buildings lose more than 10 min

the coast and build them large enough so that all people living in the area between shelter and coast have access to one of the shelters. In cases where this is not possible shelters should at least not be placed next to major evacuation routes to make sure that people that have to use these routes do not experience congestion because of the shelters.

11.6 From Knowledge to Scientific Policy Advice

A primary objective of this study is to highlight how interdisciplinary research could positively contribute to disaster risk mitigation measures, evacuation planning and awareness raising by means of micro-scale dynamics of inundation and evacuation on urban district level. Following this attempt, interdisciplinary research allows in this special case of the old town of Padang benefiting from a broad range of information and data sources which enables the determination of urgently needed policy actions from a scientific perspective.

Within the "Last-Mile" project a master plan based on the scientific findings has been developed suggesting measures for risk mitigation for the complex urban environment of the coastal city (Taubenböck et al. 2012). General political recommendations and lessons learnt as well as recommendation for urban planning, evacuation and communication strategies have been suggested. The master plan addresses the entire city of Padang, thus does not resolve to direct recommendations at a certain location but gives general ideas and solutions in order to deal with a holistic perspec-

tive on disaster risk reduction that is framed in a set of various Capacity Buildung measures on the whole (Schlurmann and Siebert 2011). The present study focuses on one district of the city and thus allows a detailed suggestion of tangible measures for risk mitigation with respect to location and thematic knowledge.

Firstly, it is important to have a good knowledge of the potentially exposed people at risk. This takes into account knowledge of where hot spots of vulnerability are concentrated at any time of a day. Especially, daytime-dependent information of people at risk is crucial for evacuation planning and—at a later stage of a potential disaster—for emergency planning measures. For instance, assignment of vertical evacuation buildings in hazard-exposed settlements and close to schools is of priority. This determination becomes possible physical, social and transport science methodologies coincide and interact aiming to achieve disaster risk reduction strategies. A clear recommendation for the old town of Padang is hence identified: for the prevention of congestions during an actual tsunami warning, vertical and decentralized evacuation shelters should be planned directly at the coast-line being physically-robust to withstand the anticipated strengths of the quake and impacts of the approaching tsunami.

Secondly, even though the access to tsunami early warning is quite widely distributed in the city, it is to note that not all community groups have the same access to public media as well as been involved in community preparedness activities. Moreover, it has been shown that the individual evacuation behavior also reflects a complex socio-cultural setting and dissemination of information. Thus, an involvement of people's representatives and community or religious leaders is crucial in order to ensure equal distribution of and access to clear information about existing and likeliness of future tsunami hazards and evacuation procedures as well as development of positive attitude of the people towards preparedness activities, including Capacity Building program to enhance readiness as well as willingness to evacuate. In addition, public warning sirens or informative television screens with uninterrupted power supply are.

Thirdly, the analysis of inundation dynamics on a micro-scale level offers the chance to derive physically-sound flow paths, flow velocities and the temporal evolution of the edge of the flood waves (tsunami bore) while propagating through the densely urbanized agglomeration. At the same time, those flow paths are utilized by evacuees while rescue themselves according to their warning perception. As identified the low lying old town bridge head as well as the Siti Nurbaya Bridge itself are not recommended for evacuation purposes since derived risk level predominates over evacuation time. Hence two options are imaginable: (a) the positioning of stiff, reinforced concrete shelters nearby or (b) the raising of the road leading to the bridge head of Siti Nurbaya Bridge. While the first recommendation would allow for a decrease in local evacuation time, the second recommendation additionally functions as a dike-like infrastructure which decelerates propagation speed of the tsunami within the vicinity of the bridge head. Those practical options are developed on the basis of information only available through interlinked transdisciplinary research with the overall purpose of efficient and easy to adopt disaster risk reduction measures.

11.7 Summary and Outlook

A close-up analysis of vulnerability, risk and hazard due to tsunami is carried out for the city of Padang on a micro-scale, district level. Many studies nowadays focus on a city wide determination of hazard impacts and its global assessment with respect to the inhabitants. In this context, it must be re-iterated, that urban agglomerations are not uniformly exposed to the impacts of disasters. Hence it could be of significance to spotlight into special focus regions where either bottlenecks of evacuation are expected or where disproportionally high impacts or vulnerable groups of people are expected. A city district of Padang where both reveals true is the old town and showcases an excellent example of micro-scale disaster risk reduction analysis.

Therefore a work chain of physical and social assessment of vulnerability, the analysis of the hydrodynamic evolution during the inundation process and finally a thorough study of the evacuation has been performed. By means of well defined interfaces between the research outcomes, a set of reasonable and trustworthy recommendations become available at a microscopic district level. Those recommendations may facilitate the development of individually tailored measures and local disaster management schemes for the preparation of the next great earthquake along the Sunda arc. However, beyond any technical preparation measure, it remains true that individual and community training is still the key driver in reducing loss of live during any natural hazard.

Acknowledgments The authors would to thank the DFG/BMBF special Programme "Geotechnologies"—Early Warning Systems in Earth Management. Sponsorship Code: 03G0643A-E. We would also like to thank our partners in Padang Indonesia from Andalas University and the city municipality of Padang.

References

Bernard E, Mofjeld H, Tito V, Synolakis C, Gonzalez F, Purvis M, Sharpe J, Mayberry G, Robertson R (2006) Tsunami: scientific frontiers, mitigation, forecasting and policy implications. Philos Trans R Soc A: Math Phys Eng Sci 364(1845):1989–2007

Birkmann J (2006) Measuring vulnerability to promote disaster resilient societies: conceptual frameworks and definitions. In: Birkmann J (ed) Measuring vulnerability to natural hazards: towards disaster resilient societies. United Nations University, New York, pp 9–54

Bogardi J (2004) Hazards, risks and vulnerabilities in a changing environment. Glob Environ Change 14:361–365

Borrero JC, Sieh K, Chlieh M, Synolakis CE (2006) Tsunami inundation modeling for western Sumatra. Proc Nat Acad Sci USA 103(52):19673–19677

Flötteröd G, Lämmel G (2010) Evacuation simulation with limited capacity sinks. In: Filipe J, Kacprzyk J (eds) Proceedings of the international conference on evolutionary computation. SciTePress, Valencia, pp 249–254

Gonzáles F, Bernard EN, Meinig C, Eble MC, Mofjeld HO, Stalin S (2005) The NTHMP tsunameter network. Nat Hazards 35:25–39

Goseberg N (2011) The run-up of long waves—laboratory-scaled geophysical reproduction and onshore interaction with macro-roughness elements. Ph.D. thesis, University Hannover, Germany. http://edok01.tib.uni-hannover.de/edoks/e01dh11/662627997.pdf

Lämmel G (2011) Escaping the tsunami: evacuation strategies for large urban areas. Concepts and implementation of a multi-agent based approach. Ph.D. thesis, TU Berlin. http://opus.kobv.de/tuberlin/volltexte/2011/3270/

Lämmel G, Grether D, Nagel K (2010) The representation and implementation of time-dependent inundation in large-scale microscopic evacuation simulations. Trans Res Part C: Emerg Technol 18(1):84–98

Lämmel G, Klüpfel H, Nagel K (2011) Risk minimizing evacuation strategies under uncertainty. In: Peacock R, Kuligowski E, Averill J (eds) Pedestrian and evacuation dynamics. New York, Springer, pp 287–296

Lämmel G, Flötteröd G (2009) Towards system optimum: finding optimal routing strategies in time-dependent networks for large-scale evacuation problems. In: Mertsching B, Hund M, Aziz Z (eds) KI 2009: advances in artificial intelligence. LNCS (LNAI), vol 5803. Springer, Heidelberg, pp 532–539

Lämmel G, Klüpfel H, Nagel K (2009) The MATSim network flow model for traffic simulation adapted to large-scale emergency egress and an application to the evacuation of the Indone-sian city of Padang in case of a tsunami warning. In: Timmermans H (ed) Pedestrian behavior, chapter 11. Emerald Group Publishing Limited, Bingley, pp 245–265

Lauterjung J, Münch U, Rudloff A (2010) The challenge of installing a tsunami early warning system in the vicinity of the Sunda Arc. Indonesia Nat Hazards Earth Syst Sci 10:641–646

McCloskey J, Antonioli A, Piatanesi A, Sieh K, Steacy S, Nalbant S, Cocco M, Giunchi C, Huang J, Dunlop P (2007) Tsunami threat in the Indian Ocean from a future megathrust earthquake west of Sumatra. Earth Planet Sci Lett 265:61–81

Muhari A, Imamura F, Natawidjaja DH, Diposaptono S, Latief H, Post J, Ismail FA (2010) Tsunami mitigation efforts with pTA in west Sumatra province, Indonesia. J Earthq Tsunami 4:341–368

Nash J (1951) Non-cooperative games. Ann Math 54(2):286–295

Natawidjaja DH, Sieh K, Chlieh M, Galetzka J, Suwarfadi BW, Cheng H, Edwards RL, Avouac JP, Ward SN (2006) Source parameters of the great Sumatran megathrust earthquake of 1797 and 1833 inferred from coral microatolls. JGR 111:B06403. doi:10.1029/2005JB004025

Nielsen O, Roberts S, Gray D, McPherson A, Hitchman A (2005) Hydrodynamic modeling of coastal inundation. In: MODSIM 2005 International congress on modelling and simulation, pp 518–523

Sieh K (2006) Sumatran megathrust earthquakes: from science to saving lives. Phil Trans R Soc A 364(1845):1947–1963

Ramirez FJ, Perez PC (2004) The local tsunami alert system ["SLAT"]: a computational tool for the integral management of a tsunami emergency. Nat Hazards 31:129–142

Rastogi BK, Jaiswal RK (2006) A catalogue of tsunamis in the indian ocean. Sci Tsunami Hazards 25(3):128–143

Schlurmann T, Siebert M (2011) The capacity building programmes of GITEWS—visions, goals, lessons learned, and re-iterated needs and demands. Nat Hazards Earth Syst Sci 11(2):293–300

Schlurmann T, Kongko W, Goseberg N, Natawidjaja DH, Sieh K (2010) Near-field tsunami hazard Map Padang. Utilizing high resolution geospatial data and reasonable source scenaries. In: Smith J (ed) Proceedings of international conference of coastal engineering, West Sumatra

Setiadi N (2011a) Establishment of an effective people-centered tsunami early warning by understanding people's behavior and needs: Case study of Padang, West Sumatra. In: Anwar HZ, Harjono H (eds) Perspektif terhadap kebencanaan dan lingkungan di Indonesia: Studi kasus dan pengurangan dampak risikonya. Sub-Kegiatan Kompetitif Kebencanaan dan Lingkungan, Lembaga Ilmu Pengetahuan Indonesia, Bandung, pp 35–52

Setiadi N (2011b) Daily mobility—excursus—padang, Indonesia. In: Chang Seng S, Birkmann J (ed) Migration and global environmental change: SR4b: early warning in the context of environmental shocks: demographic change, dynamic exposure to hazards, and the role of EWS in

migration flows and human displacement. UK Government's Foresight Project, Migration and Global Environmental Change, UK

Setiadi N, Birkmann J (2010) Working package 1000: socio-economic vulnerability assessment: final report for the "Last-Mile—Evacuation project", DFG/BMBF special program geotechnologies. United Nations University, Institute for Environment and Human, Security (UNU-EHS) (in German)

Setiadi N, Taubenböck H, Raupp S, & Birkmann J (2010) Integrating socio-economic data in spatial analysis: an exposure analysis method for planning urban risk mitigation. In: Manfred S, Vasily VP, Dirk E, Pietro E (eds) REAL CORP 2010, Vienna, 18–20 May 2010

Taubenböck H, Goseberg N, Lämmel G, Setiadi N, Schlurmann T, Nagel K, Siegert F, Birkmann J, Traub K-P, Dech S, Keuck V, Lehmann F, Strunz G, Klüpfel H (2013) Risk reduction at the "Last-Mile": an attempt to turn science into action by the example of Padang, Indonesia. Nat Hazards 65(1):915–945.

Taubenböck H, Goseberg N, Setiadi N, Lämmel G, Moder F, Oczipka M, Klüpfel H, Wahl R, Schlurmann T, Strunz G, Birkmann G, Nagel K, Siegert F, Lehmann F, Dech F, Gress A, Klein R (2009a) Last-mile preparation to a potential disaster—interdisciplinary approach towards tsunami early warning and an evacuation information system for the coastal city of Padang, Indonesia. Nat Hazards Earth Syst Sci (NHESS) 9(4):1509–1528

Taubenböck H, Goseberg N, Lämmel G, Setiadi N, Schlurmann T, Nagel K et al (2012) Risk reduction at the "Last-Mile": from science to action by the example of Padang, Indonesia. Nat Hazards (accepted)

Taubenböck H, Wurm M, Setiadi N, Gebert N, Roth A, Strunz G, Birkmann J, Dech S (2009b) Integrating remote sensing and social science—the correlation of urban morphology with socioeconomic parameters. In: Urban remote sensing joint event. Shanghai, China, p 7

United Nations/ISDR (International Strategy for Disaster Reduction) (2004) Living with risk: a global review of disaster reduction initiatives, united nations international strategy for disaster reduction. UN Publications, Geneva

Weidmann U (1993) Transporttechnik der Fussgänger, Schriftenreihe des IVT, vol 90, 2nd edn. Institute for Transport Planning and Systems, ETH Zürich, (in German)

Chapter 12
The Role of Information and Communication Technology in the Development of Early Warning Systems for Geological Disasters: The Tsunami Show Case

J. Wächter and T. Usländer

Abstract Tsunami warning systems (TWS) are distributed software and hardware systems supporting the reliable detection of imminent tsunami hazards, the rapid situation assessment and the targeted dissemination of customised warning messages. The conceptual evolution of TWS within the last decades is stimulated by and depending on the development of Information and Communication Technology (ICT). The strong influence of ICT emerged in the 1980s when the availability of microcomputer systems and telecommunication facilities facilitated the development of global sensor networks. Since the 1990 s the growth of the Internet has driven standardisation processes for protocols, interfaces and data exchange, providing the foundations for today's TWS. The ongoing development of global warning infrastructures depends on the capability to integrate national and local TWS into system-of-systems. This requires structured software engineering methodologies guided by a reference architecture for TWS. Trends such as cloud computing, ubiquitous sensing and volunteered geographic information will strongly influence the future development of TWS.

12.1 Introduction

Early warning is a major element of disaster risk reduction. Its overall objective is the prevention of loss of life and the reduction of economic losses to a minimum. Following UN (2006) definitions a complete and effective early warning system comprises four interconnected elements:

J. Wächter (✉)
Helmholtz Centre Potsdam, GFZ German Research Centre for Geosciences, Potsdam, Germany
e-mail: wae@gfz-potsdam.de

T. Usländer
Fraunhofer IOSB, Karlsruhe, Germany
e-mail: thomas.uslaender@iosb.fraunhofer.de

F. Wenzel and J. Zschau (eds.), *Early Warning for Geological Disasters*,
Advanced Technologies in Earth Sciences, DOI: 10.1007/978-3-642-12233-0_12,

(1) Risk awareness: knowledge of the likely risks that communities face.
(2) Monitoring and warning service: monitoring of hazards as well as rapid and reliable decision-making processes for early warning.
(3) Dissemination and communication: transfer of understandable warnings and preparedness information to those at risk.
(4) Response capability: knowledge and preparedness of all partners of the information chain.

Early warning for geological disasters includes crises following volcano eruptions, landslides, earthquakes and tsunamis. In terms of Information and Communication Technology (ICT) geological early warning systems (EWS) are integrated software and hardware systems for data acquisition, decision making, and information dissemination thus supporting the detection and analysis of imminent hazards and the targeted dissemination of related warnings. Hence, EWS typically focus on the elements (2) and (3) of the list above.

The technological concepts and performance capabilities of EWS have significantly evolved over the last decades. On the one hand, this progress is resulting from the advancements in the scientific understanding of geological disasters and related phenomena as well as improved scientific modelling approaches. On the other hand, these advancements are directly linked with and enabled by the rapid development of ICT. The effect of ICT is not only reflected by the availability of high-performance tools for supporting near real-time modelling, decision support or visualisation. Both the upstream and the downstream information flow heavily rely upon and benefit from the capabilities of the underlying ICT infrastructures. ICT innovations have also boosted the performance of sensor systems resulting in an increased resolution and improved availability of time series data. Advances in telecommunication infrastructures in parallel with the growth of the Internet have enhanced the variety and performance of channels for warning purposes. More than that, the next generation of mobile computing systems support smart solutions, e.g. low-cost mobile sensor networks enabling new high-resolution monitoring strategies.

This paper investigates the dualism and mutual interdependence of ICT and EWS for geological disasters looking in particular at tsunami warning systems (TWS). TWS provide a representative show case due to their integrated architecture, distributed nature, and the complexity of decision processes. Additionally, requirements in terms of robustness and reliability are very challenging and result from the relative rarity of tsunami events in relation to the life cycle of ICT-based systems. In Sect. 12.2 we focus on the role of ICT in the past evolution of TWS over the last decades and the resulting architectural concepts. Based upon this historical outline Sect. 12.3 presents the main architectural elements of TWS. Section 12.4 proposes a first step towards a TWS reference architecture including tailored methodologies for the application of this reference architecture for the concrete engineering of individual yet interoperable TWS. Section 12.5 summarises the findings about the role of ICT in the evolution of TWS and concludes with a discussion of major ICT trends that will become important for the future development of TWS.

12.2 Evolution of Tsunami Warning Systems Over Time

12.2.1 ICT Development Phases

In the last decades the rapid development of ICT has significantly transformed business processes in industry, government and science. The increasing potential of ICT revolutionised data and information management, in particular the acquisition, processing, analysis and visualisation of data as well as the integration of computer systems into infrastructures. Following Moore's (Schaller 1997) and Kryder's Law (Walter 2005), the ongoing change processes are driven by the continuous miniaturisation of integrated circuits and the increased performance of processing units, memory chips and graphic processing units but also the availability of large, affordable storage capacities. Other technological key drivers are the availability and performance of telecommunication facilities enabling local and wide area networks. The development of ICT in the last decades shows partly overlapping phases with specific characteristics (adapted from Mutsaers et al. 1998):

I. *Data Processing Era*: From the 1970s mainframes and minicomputers become more frequent. Their application is focused on specific, mostly centralised data processing tasks. The number of computer systems is still limited.
II. *Microcomputer Era*: From the early 1980s the appearance of microcomputers or Personal Computers (PC) extended the application of computers to more general information management but also data acquisition and processing tasks. The era is characterised by an increasing utilisation of Local Area Networks. Key concepts for the data transfer between different networks and the internetworking (Internet) have been developed. Microcomputer systems become widespread for distributed desktop applications in business and science.
III. *Internet Era*: In the 1990s, the Internet developed to a global platform for business processes, information provision, communication and entertainment. This process is enabled by the availability of both common protocols for system communication and data transfer combined with an ever increasing bandwidth available at low cost. Since the beginning of the pervasive development and enormous growth of the Internet a strong convergence process including media, applications, and data is obvious. This resulted in the merging of standardisation processes that were formerly restricted to specific communities. This includes not only communication protocols but also standards for data and metadata specifications as well as service interfaces.
IV. *Ubiquitous Computing Era*: As a result of the continuing miniaturisation of technology a new generation of mobile computer systems is available integrated into powerful mobile communication networks with high bandwidth. This development started with the availability of mobile telephones. Today, regular smartphone systems have a basic set of sensors on board (GPS, accelerometer, gyroscope) and, more than that, provide LAN protocols and routing functions thus supporting the implementation of low cost and volunteered sensor networks.

In the following the evolution of TWS will be considered from the viewpoint of these ICT Eras for three selected examples. The first example will look upon the development of seismic systems. Seismic monitoring is one of the core functions of today's tsunami warning systems. Standard software solutions include basis alerting functionality. The second example considers the TWS development in Japan. Permanently challenged by its specific geotectonical position with extremely high tsunami risks and reduced warning times the Japanese situation requires sophisticated technological solutions and conceptual leadership. The third example analyses the Indonesian TWS and its follow-on evolution. The overall concept and architecture of the system was designed from the scratch without limiting factors e.g. superimposition of legacy systems. These developments therefore deliver relevant contribution for a standards-oriented approach for the design of warning systems thus providing an important input for TWS reference architectures.

12.2.2 Seismic Monitoring Systems

The development and performance of today's TWS is closely related to and depending on the evolution of seismology and earthquake monitoring. The first teleseismic earthquake event was registered 1889 in Potsdam by the scientist Rebeur-Paschwitz who initiated a global network of seismographs to monitor the seismicity of the Earth (Kind 2012). This teleseismic recording can be considered as the start to a systematic observation of seismic activities. The first seismometers were mechanical instruments followed by electrodynamic seismometers improving the accuracy of measurements. Before the 1970s analogue media (usually paper or film) were the sole means of recording seismic data.

Seismologists have used digital recording methods since about 1970. In the late 1970s very broadband digital instrumentation became available. At that time the concept of a global network of digital broadband stations, capable of recording large local earthquakes, became viable. One of the first projects to embrace the new digital technology was Global Seismographic Network (GSN) of the U.S. Geological Survey (USGS). Since the beginning the GSN has allied with other global operators (GEOSCOPE, GEOFON) and regional networks such as the Canadian Digital Seismic Network (CDSN), the China Seismic Network (CSN), and the Mediterranean Network (MEDNET) to enable wide distribution of high-quality stations around the world (IRIS Consortium 2003).

In the last two decades seismic sensor networks have been further developed and extended. In order to optimise the operation of seismic networks, observatories and research institutes integrated their networks to virtual networks. Virtual networks associate with recording stations and seismic networks either indefinitely or for a limited time period. The VSN concept supports large projects by integrating seismic stations from different networks to act as a single, newly formed entity. The virtual network naming system supports the provision of data under the auspices of one

or more of these initiatives. For example, the GEOFON Extended Virtual Network (GEVN) is composed of more than 500 stations worldwide (Hanka et al. 2008).

Already in 2003 the IRIS Consortium envisioned an extension of the seismic network to multi-sensor platforms which, in addition to their primary purpose, is capable of monitoring a variety of environmental and tectonic parameters. Along with land and ocean seismic observatories, additional instruments may be included in global monitoring networks of the future. These instruments are laser strain meters, tilt meters, micro-gravimeters, differential GPS, micro-barographs, high-frequency geophones and temperature sensors in deep boreholes, meteorological and ionosphere monitors, monitors of gaseous emissions at volcanic sites, hydrophones, pressure sensors, ocean bottom temperature, salinity and current monitors.

The seismic community has developed and is maintaining a set of standards and tools for the acquisition of seismic data as well as the exchange and management of large seismic data archives. Digital recording methods used since 1970 have increased data quality but data exchange has been complicated by different data logger formats, by different computer systems and by incompatible exchange media.

In 1985, the International Association for Seismology and Physics of the Earth's Interior (IASPEI), Commission on Practice, formed a Working Group on Digital Data Exchange to propose a standard for international digital seismic data exchange. The Standard for the Exchange of Earthquake Data (SEED) was proposed as a new format by the USGS. After the review of a number of existing formats the Federation of Digital Seismographic Networks (FDSN) formally adopted SEED in 1987 (IRIS 2010). In 2004, the QuakeML schema for seismic data has been proposed by Schorlemmer et al. (2004).

12.2.3 Near- and Far-Field Tsunami Warning Systems

Due to its geotectonical position close to a subduction zone Japan is frequently threatened by earthquakes and tsunami. A first systematic forecast/warning system for tsunami was established in September 1941 for the Sanriku Coastal Area, an area which was already devastated by the Sanriku Tsunami of 1933. It served as a blueprint of the Japanese TWS that started its services on April 1, 1952 (Imamura and Abe 2009). The specific challenge for a Japanese TWS results from the near-field situation with only short forecast times. However Japan is also threatened by far-field tsunamis which can be generated in the subduction zones around the Pacific Ocean. The Japanese Meteorological Agency (JMA) has the legal mandate for tsunami early warning.

In an early stage of TWS development, earthquake parameters were manually determined based on the emergency telegrams received from a geographically distributed network of local observatories. The telegram reported the observed earthquake parameters including magnitudes and observation time to the tsunami forecast centre. Within 15 min the centre estimated the earthquake epicentre. Forecasts were issued based on the distance to the epicentre. In the late 1950s Morse code was

gradually replaced by tele-type machines for data communication purposes. Since the 1970s a new generation of seismographs was introduced providing important improvements concerning the time resolution of recording. After the 1995 Kobe earthquake the seismic observation system in Japan was improved considerably. A large number of strong-motion, high-sensitivity, and broadband seismographs were installed to construct dense and uniform networks covering Japan completely.

A core component of the Japanese warning infrastructure is a decision support system. In 1999 a simulation system for quantitative tsunami forecasting became operational (Imamura and Abe 2009). Forecasts include the expected height at the coastline. Tsunami forecast contains the expected maximum tsunami height and the arrival time of the tsunami. Warnings and/or advices are delivered to the national and local authorities for disaster prevention and the broadcasting media. Mayors of cities, towns or villages are responsible for giving evacuation directions to residents to leave tsunami-prone areas.

When a large earthquake occurs at a distant area from Japan, JMA determines the location and the magnitude using seismic data from global seismological observation network. In case of a possible tsunami occurrence, JMA immediately executes the tsunami forecast operation in the same manner as in the case of a near-field tsunami. JMA uses the database derived from numerical simulation to judge whether the tsunami affects the Japanese coast. Data of tsunami observations from foreign countries are also referred to in order to estimate the tsunami height.

Since 2006 forecasts can be issued within 2 or 3 min (Imamura and Abe 2009). When tsunamis are observed, the JMA issues information about observation points, tsunami heights and expected times of arrival (JMA 2009). The Japanese warning system includes a highly-efficient infrastructure for warning dissemination based on a multi-channel approach. Mobile communication and computer systems are increasingly integrated into warning strategies. For example, cell broadcasts were used in the Tohoku tsunami crisis. Additionally, Japanese warning systems are capable of triggering risk reduction measures. Already in the 1960s, an early warning system for stopping high-speed trains was developed (Nakamura 2004).

12.2.4 Standards-Based TWS Architectures

After the Boxing Day tsunami 2004 and more than 200000 casualties, a series of activities have been started with the overall objective to establish an early warning system in the Indian Ocean. In close collaboration between Indonesia and Germany a TSW was designed and implemented (Lauterjung et al. 2010). The GITEWS project (German Indonesian Tsunami Early Warning System) addressed the specific challenges of early warning in a near-field environment with its limited reaction times. In parallel the DEWS project[1] focussed on both the multi-channel warning dissemination in a multi-lingual environment and the communication between warning centres.

[1] DEWS = Distant Early Warning System, http://www.dews-online.org/.

These projects laid the foundation for the design of collaborative decision-support environment as investigated in the TRIDEC project[2].

These projects seized the opportunity to develop an overall generic architecture for TWS based on best practices and the results of international standardisation activities in the geospatial domain and the ICT community. This approach included service-oriented architectural design principles but also open geospatial and Sensor Web service and data specifications from the Open Geospatial Consortium (OGC) (Percivall 2010). Among others, the resulting system approach covers the following aspects:

- Sensor Integration Platform: Different sensor types are integrated via a sensor service bus based on a plug-in approach. Interfaces to seismic systems, buoys, GPS, and tide gauges have been implemented. Plug-in templates can easily be adapted to other types of sensor systems (Fleischer et al. 2010).
- Warning dissemination: Information logistics processes were implemented especially addressing the multi-channel dissemination of customised warning messages in a multilingual environment. Warning messages can be automatically adapted for different consumer groups using templates (Lendholt and Hammitzsch 2011).
- Decision support: Specific adaptable user interfaces were designed for tsunami detection, analysis of coastal hazards and tasking of warning dissemination. In this context the integration of the simulation system is of high relevance (Hammitzsch et al. 2012; Steinmetz et al. 2010).
- Centre-to-Centre: The DEWS prototype implemented centre-to-centre communication patterns. This approach is addressing the execution of complex collaborative emergency management tasks within loosely coupled system-of-systems (Lendholt et al. 2012).
- Workflow support: An open service-oriented architecture enables that transfer and adaption of the system approach to other regions, e.g. the Mediterranean Sea where the distances between potentially tsunamigenic sources and the coast are rather small. Here, decision makers need a customisable system which may be easily adapted to the individual regional situations. A workflow-based decision support system relying upon rule-based decision tables is proposed to deliver the required flexibility (Riedel and Chaves 2012).

12.3 Components of Tsunami Warning Systems

12.3.1 Main Architectural Elements

The overall evolution of TWS as described in Sect. 12.2 reflects a rapid growth of the complexity resulting from an increase of the collaborating components and

[2] TRIDEC = Collaborative, Complex and Critical Decision Support in Evolving Crises, http://www.tridec-online.eu/.

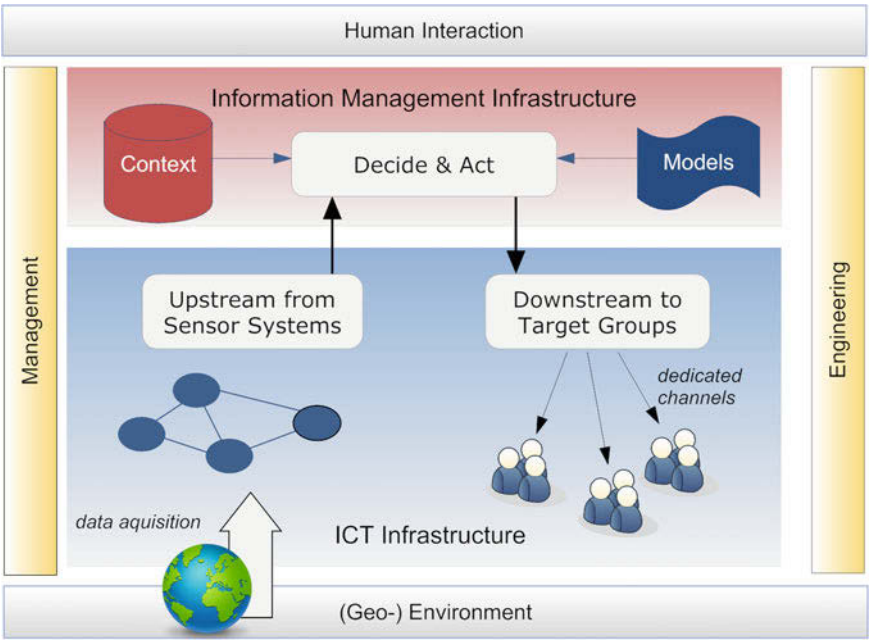

Fig. 12.1 Typical components of tsunami warning systems

implemented functionality. As illustrated in Fig. 12.1 the mapping of TWS functions to main architectural elements reveals three building blocks (Wächter et al. 2012):

- *Data acquisition*: The upstream information flow into the TWS includes earthquake and sea-level monitoring data. In concrete operational warning systems the monitoring task are realised by sensor systems and sensor networks.
- *Decision support*: The decision support included two main tasks. Firstly, the system has to monitor earthquake activities and, once an earthquake has happened, it has to detect if a tsunami was initiated. Secondly, the hazard estimation for affected coastal areas has to be conducted as quickly as possible. As soon as these hazards have been analysed the TWS starts scheduled warning activities.
- *Information dissemination*: The downstream information flow out of the TWS is directed to dedicated customer groups including authorities and the public but also to other warning centres. Warning channels include sirens and radio broadcasting. Messages via E-mail or SMS are used to disseminate customised information.

12.3.2 Upstream Information Flow and Sensor Systems

Sensor systems are responsible for the monitoring of environmental phenomena related to hazards. Sensor systems consist of one or more distributed sensors

transforming real world observations into digital signals that are transmitted to or collected by a central processing and analysis component. Sensor systems process and filter incoming raw time series data into information about specific relevant events, e.g. an earthquake that can be used as a trigger or for validation purposes in decision processes. In addition to seismic monitoring, sea level observation is another important monitoring task of TWS. In this context tide gauges at coast lines play an important role complemented by an increasing number of buoys responsible for sea level monitoring in the open ocean.

The responsibility of seismic systems is the determination of earthquake parameters including location, depth, magnitude and rupture parameters as soon as possible after an earthquake. The data delivered by distributed seismometer network are time series (so called wave forms). In a first step the occurrence of the earthquake is automatically/manually detected ("picked") as a peak in the incoming time series. Based on incoming events from at least three sensors earthquake location and additional parameters like magnitude, depth, or moment tensor will be determined (Hanka et al. 2010). Especially for the assessment of the probability of a tsunami it is becoming increasingly important to identify the earthquake mechanics quite rapidly. Continuous GPS has gained an increasing importance (Falck et al. 2010).

There are two complementary approaches for sea level monitoring. Tide gauges document the effect of tsunami on the coast line. Supported by the WMO a global network of coastal tide gauges has been integrated using the Global Telecommunication System (GTS) operated by WMO for the collection and transfer of tide gauge data to a central facility. For tsunami monitoring in the open ocean the DART real-time tsunami monitoring systems plays a critical role in tsunami forecasting especially for near-field situations. The DART system consists of an ocean bottom unit with pressure sensors capable of detecting tsunami signals form water pressure data. The buoys have to be positioned at strategic locations throughout the ocean.

12.3.3 Decision Support for Tsunami Detection and Hazard Estimation

Within the upstream information flow sensor data streams are processed in a way that only relevant information for decision making is extracted. The resulting high-level event data are the basic input for the decision support in the TWS. The interfaces of individual sensor systems with domain specific protocols and encoding are subject to ongoing standardisation processes.

One key objective of a TWS is the detection of a tsunami as early as possible so that the time available for preparation and response activities is maximised. Frequently, seismic systems delivering earthquake information are the unique input for decision making. In this case warning activities are determined by exceeding predefined thresholds based on the strength of earthquake. However not all earthquakes trigger a tsunami. In regions with strong earthquake activities the verification of the

possible generation of a tsunami is a key issue. Currently sea level observation can provide the necessary input to validate the tsunami generation. Buoys linked with ocean bottom sensors implemented offshore threatened coasts offer reliable option keeping at least a minimum warning time frame for near-field tsunami.

A second key objective of TWS concerns the proper preparation and targeted execution of warning activities. Two aspects are important. Firstly, once a tsunami has been generated the location of the epicentre, the bathymetry and the geometry of the coastline will determine the local tsunami hazard. Tsunami propagation models deliver the input for this process (Babeyko et al. 2010; Behrens et al. 2010). In the Indian Ocean region and also proposed for the Mediterranean a segmentation of the coastal zone in geographically similar units is a way to describe the concrete tsunami threat for defined coastal areas (Lendholt et al. 2012).

Decision support components have to support the continuous interaction of the responsible key personal with the system so that the human/system interface is of particular importance. For instance, there may be very early information provided by the system that point to a major disaster, but information is very unsure. For these reasons decisions about the scheduling and execution of warning activities have to be substantiated based on data resulting from the analyses of comparable events in the past. Based on this input a set of probable earthquake locations is selected. For each of these points, the tsunami propagation is calculated for a defined range of magnitudes. The resulting data sets are stored in a database.

In case of a real alert situation the best fitting simulations are retrieved from the database once the earthquake parameters have been determined thus providing the basis for high resolution coastal hazard determination. The selection of best fitting propagation models is one of the key decision processes of warning centres (Hammitzsch et al. 2012).

TSWs can be linked with other warning centres in regional networks, e.g. in the Indian or the Pacific Ocean region. In this case TWS alerts can not only be initiated by sensor systems but also by other warning centres. The alerts will initiate similar warning dissemination activities to those as described above.

12.3.4 Warning Dissemination and Downstream Information Flow

The management of downstream information flows follows the challenging objective to deliver “the right information, to the right people, in the right time” (GDIN 1997). The situation awareness and warning information dissemination has two addressees, decision makers in crisis management organisations and the public. Decision makers have to be informed about imminent threats and start evacuation procedures. Rescue organisations have to be prepared for the immediate start of rescue activities after the tsunami reached the coast. Warning dissemination to the public helps to reduce the concrete number of potential casualties.

The resulting downstream information flow includes processes that transform alerts into customised warning messages satisfying the information needs of

addressed target groups. Effective targeted warning dissemination depends on a detailed description of the information needs of potential target groups. Finally, this prepared information is disseminated via dedicated channels. A standardised approach for warning dissemination has been proposed by Lendholt (2011).

Tsunami crises do not affect single countries but are a threat to many countries in a specific geographic setting, e.g. the Indian Ocean, the Pacific or the Mediterranean. This specific situation makes coordinated activities of national warning centres necessary based on the effective information exchange between warning centres. The organised reaction of independent systems on common threats is a key challenge for new system-of-system architectures.

12.4 Towards a TWS Reference Architecture

12.4.1 TWS Domain Requirements

In the Pacific Ocean a central tsunami warning centre and core elements of a warning infrastructure have been continuously developed since 1949 when the Pacific Tsunami Warning System (PTWS) was founded (UNESCO 2009). In other regions, e.g. the Indian Ocean and the Mediterranean, no such systems were in place. The Boxing Day Tsunami 2004 triggered various international efforts focused on the establishment of a tsunami early warning infrastructure. These activities were organised under the auspices of the UNESCO/IOC. Despite of significant progress the specification process of warning systems and their general architecture is still on-going (ICG/NEAMTWS 2009, 2011; TOWSWG 2011; UNESCO 2011).

Currently, the main high-level structural elements and components of the tsunami warning infrastructure have been identified including their basic functionality and standard operational procedures. Accordingly, tsunami warning infrastructures consist of national and regional warning centres (NTWC: National Tsunami Warning Centre; RTWC: Regional Tsunami Watch Centre). RTWCs operate as a hub for several NTWCs and coordinate the exchange of regional tsunami related information. NTWCs are responsible on the national level according to respective national legal frameworks and provide warnings, watches, and advisories to their citizens, public and private agencies.

The importance and the need for an adequate and tailored provision of information systems and resource management systems for risk and emergency management is widely recognized (Turoff et al. 2010; Henricksen and Iannella 2010). Starting from stand-alone systems with dedicated tasks there is a trend towards warning systems consisting of loosely-coupled systems. These systems typically have to span organizational, national and/or technological barriers. The distribution of a system-of-systems over a large geographic extent results in an “even greater emphasis on interface design that in traditional system architecting and engineering” (Maier 1998).

12.4.2 Reference Model for TWS

Warning infrastructures have to meet very high domain-specific requirements concerning resilience, robustness, performance and security. Especially in a system-of-systems consisting of independently developed warning systems all interfaces and communication protocols of all participating warning centres have to fulfil these requirements. In order to safeguard a proper and reliable behaviour of the infrastructure the detailed specification of reference architecture for the overall TWS domain is required. On a high level of abstraction this reference model for tsunami warning system (RM-TWS) provides a reference architecture including basis structural elements and relations for the construction of concrete TWS. The specifications typically have to satisfy expectations of readers with different competences and technical backgrounds. The key elements are structured according existing patterns that have been observed in a number of implementations. A sound documentation of its architecture is essential not only in order to guarantee the proper development of TWS that should become elements of a tsunami warning infrastructure but also to support the maintenance and the evolution of an EWS.

The design of a RM-TWS should be based on the existing capabilities of underlying ICT which nowadays encompasses geospatial service platforms. Additionally, the RM-TWS should follow the design principles of service-oriented architectures (SOA) as defined by Erl (2008) in his encyclopedia. These principles include:

- Loose Coupling: "Service contracts impose low consumer coupling requirements and are themselves decoupled from their surrounding environment".
- Service Abstraction: "Service contracts only contain essential information and information about services is limited to what is published in service contracts".
- Service Reusability: "Services contain and express agnostic logic and can be positioned as reusable enterprise resources".

This paper proposes core services and a related information model of a TWS reference architecture based on well-established standards for reference model specifications, e.g. the ISO Reference Model for Open Distributed Processing (ISO/IEC 10746-1). The use of viewpoints is derived from the principle of abstraction as the central idea of architectural specifications. The RM-TWS proposes five viewpoints following the OGC best-practices reference model for environmental risk management applications (Usländer 2007). The main high-level structural elements and components of the tsunami warning infrastructures, as defined in the UNESCO/IOC process, are part of the RM including their basic functionality and standard operational procedures:

- The **Enterprise Viewpoint**: Reflects the analysis phase in terms of the system and the user requirements as well as the technology assessment. Includes rules that govern actors and groups of actors, and their roles.
- The **Information Viewpoint**: Specifies the modelling approach of all categories of information including their thematic, spatial, temporal characteristics as well as their meta-data.

- The Computational Viewpoint: Specifies the interface and service types in a service-oriented TWS, thereby referred to as the **Service Viewpoint**.
- The **Technology Viewpoint**: Specifies the technological choices of the (geospatial) service platform, its characteristics and its operational issues.
- The **Engineering Viewpoint**: Specifies the mapping of the service specifications and information models to the chosen platform obeying its specific characteristics and principles.

The following section describes the current status of the RM-TWS encompassing the information and the service viewpoint. Its mapping to a technological platform such as a Web service environment, i.e. the contents of the Technology and Engineering Viewpoint, is out of scope of this paper and shall be performed by implementation projects, respectively, based on the methodology detailed below.

12.4.3 Service and Information Viewpoint to Foster Interoperability

The interoperability between components in one TWS as well as the interaction between different TWS in a system-of-systems environment is determined by the degree of the standardisation of interfaces, data exchange formats and protocols. TWS shall enable an efficient and flexible exchange of information as well as the remote call and eventually reuse of their embedded functional components across system boundaries. Thus, there must be an agreement on information models and service interfaces—in the best case based on international standards.

An essential element of such an ICT support is an "open geospatial service platform" (see fig. 12.2) which provides seamless access to resources (sensor data, information, services and applications) across organizational, technical, cultural and political borders. "Open" hereby means that service specifications are published and made freely available to interested vendors and users with a view to widespread adoption. Furthermore, an open service platform makes use of existing standards (e.g. International Standardization Organization ISO and the Open Geospatial Consortium OGC) where appropriate and otherwise contributes to the evolution of relevant new standards.

Based on a systematic analysis of user and system requirements, the ORCHESTRA project[3] has specified and implemented a reference model and a series of abstract services that provide the generic and technology-neutral functional grounding of such a platform (Usländer 2007). The SANY project[4] (Havlik et al. 2007) extended it into a Sensor Service Architecture (SensorSA) by the inclusion of sensors and sensor networks (Usländer 2009). This extension is based upon the services and information models of the OGC Sensor Web Enablement (SWE) architecture

[3] ORCHESTRA = Open Architecture and Spatial Data Infrastructure for Risk management, http://www.eu-orchestra.org/.

[4] SANY = Sensors Anywhere, http://www.sany-ip.eu.

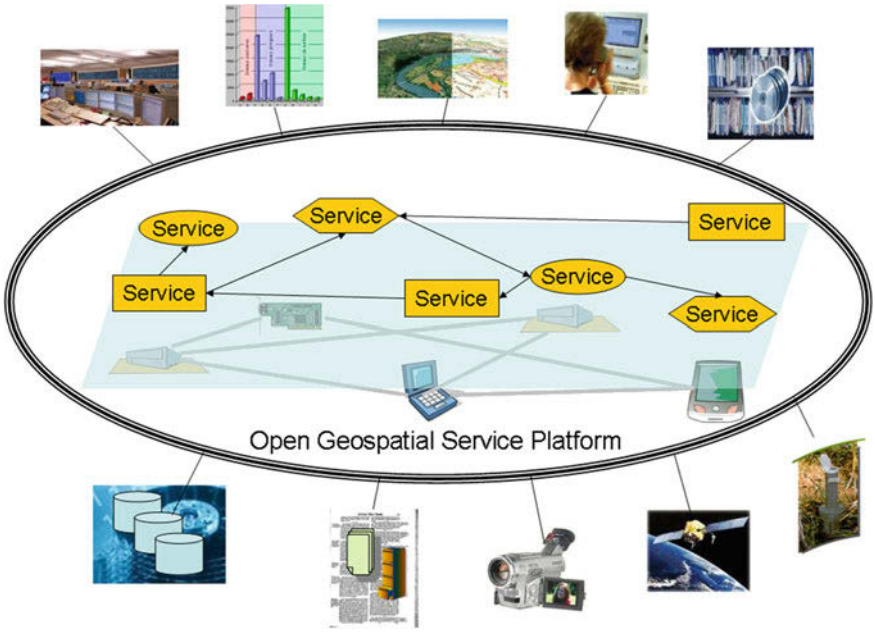

Fig. 12.2 Open geospatial service platform

(Simonis 2008a). The SWE services provide the input data for environmental monitoring as well as for risk management of geo-hazards, whether natural or man-made. They support the upstream part from sensor system according to Fig. 12.1. For the downstream part to target groups standards of OASIS are of high relevance as elaborated and implemented by the European research project DEWS (Distant Early Warning System) (Lendholt et al. 2012).

As a result, a high percentage of the required functionality of the major TWS components as illustrated in Fig. 12.1 is already covered by mapping these proposed abstract services to the given geospatial service platform and tailoring them to the needs, respectively. This design activity results in service profiles that encompass both the Service and the Information Viewpoint of the RM-TWS. Hence, the resulting service profile specifications define the service operations to be supported as well as the models of the data communicated across the network.

The ***Upstream*** from Sensor Systems may use the following services:

- Sensor Observation Service: Provides access to observations from sensors and sensor systems in a standard way that is consistent for all sensor systems including remote, in-situ, fixed and mobile sensors.
- Sensor Alert Service: Provides a means to register for and to receive sensor alert messages.
- Sensor Planning Service: Provides an interface to task any kind of sensor to retrieve collection assets.

- Web Notification Service: Supports asynchronous dialogues (message interchanges) with one or more other services.

These services rely upon data and meta-data specification of the OGC Sensor Web Enablement initiative (Simonis 2008b) such as the Sensor Model Language (SensorML) for the description of sensor characteristics and the Observation and Measurements Model (O&M) for the description of observations of all kinds ranging from sea-level time-series retrieved from buoys up to text entries in social networks (Zielinski et al. 2012).

Decision support processes may benefit from the following information management services:

- Catalogue Service: Ability to publish, query and retrieve descriptive information (meta-information) for resources of any type.
- Coordinate Operation Service: Changes coordinates on features from one coordinate reference system to another.
- Document Access Service: Access to documents of any type (e.g. text and images).
- Feature Access Service: Selection, creation, update and deletion of features available in a service network.
- Map and Diagram Service: Enables geographic clients to interactively visualise geographic and statistical data in maps or diagrams.

These services mainly rely upon the OGC general feature model and catalogue data specifications (Percivall 2010). This Infrastructure may be enhanced by semantic services and interfaces in order to overcome semantic heterogeneity:

- Annotation Service: Relates textual terms to elements of an ontology (e.g. concepts, properties, instances).
- Ontology Access Interface: Supports the storage, retrieval, and deletion of ontologies as well as providing a high-level view on ontologies.

The ***Management*** covers user management and service monitoring as follows:

- Authentication Service: Proves the genuineness of principals (i.e. the identity of a subject) using a set of given credentials.
- Authorisation Service: Provides an authorisation decision for a given interaction context.
- User Management Service: Creates and maintains subjects (users or software components) including groups (of principals) as a special kind of subjects.
- Service Monitoring Service: Provides an overview about service instances currently registered within service network incl. status and load.

These services mainly rely upon data and meta-data specification of the OASIS security information models, in particular the Security Assertion Markup Language (OASIS SAML 2006) and the eXtensible Access Control Markup Language (OASIS XACML 2010).

The ***Downstream*** to target groups may benefit from the series of XML-based messaging standards called Emergency Data Exchange Language (EDXL) provided by the OASIS Emergency Management Technical Committee (EM-TC):

- Common Alert Protocol (CAP): CAP is an XML-based data format for exchanging public warnings and emergencies between alerting technologies. Originally developed by OASIS, the ITU adopted the Common Alerting Protocol as Recommendation X.1303 in 2007 (ITU 2007; Botterell 2006).
- The EDXL Distribution Element (EDXL-DE): An envelope standard for message-distribution among emergency information systems. It serves as container message providing addressing information to route the payload which can be any XML fragment, such as a CAP message (Lendholt et al. 2012).

These two data models may be used in emergency systems in general. In the case of TWS, a dedicated language is required. One candidate is the Tsunami Warning Markup Language (TWML) that is tailored to the communication of tsunami warnings and the edition of tsunami bulletins (Iannella and Robinson 2006). It comprises language elements to describe bulletin contents such as bulletin metadata (issuer, time, frequency of future bulletins, geospatial scope), observations about the seismic activity that triggered the tsunami, observations and predictions about wave activity and expected impacts. TWML may be used in conjunction with EDXL-DE and CAP to represent intended recipients and the category of alerts, respectively.

12.4.4 Engineering of Tsunami Warning Systems

The engineering of TWS requires a sound analysis of user requirements that is fundamental for a successful design and development. Additionally, the engineering methodology should enable a seamless application of the general RM-TWS specifications for the engineering phases of concrete TWS. A combination of the following basic principles is recommended to foster the application of the RM-TWS:

- Step-wise refinement of the design artifacts: It shall be distinguished between an analysis, abstract design, concrete design and engineering step.
- Co-development of requirements and capabilities: An agile analysis and design methodology is recommended following the basic ideas of agility and lean software such as “fix quality—deliver a small increment in a timebox—repeat” (Leffingwell 2011).
- Incremental architecture documentation: It is recommended to incrementally document the resulting TWS architecture according to an established reference model.

These principles require a step-wise refinement of design artefacts. In the ***Analysis*** step the user analyses the problem and expresses the outcome in the form of user requirements, e.g. as use cases. For example, a use case that requests to “get a diagram containing the average sea water gauge values of the last 10 years in the Gulf of Naples, Italy”. In the ***Abstract Design*** step the user requirements are transformed by the system designer into system requirements which then have to be matched with the capabilities of an abstract service platform. Example: Provide a service that enables to “get observation values with a sampling time in the interval [2000-01-01,

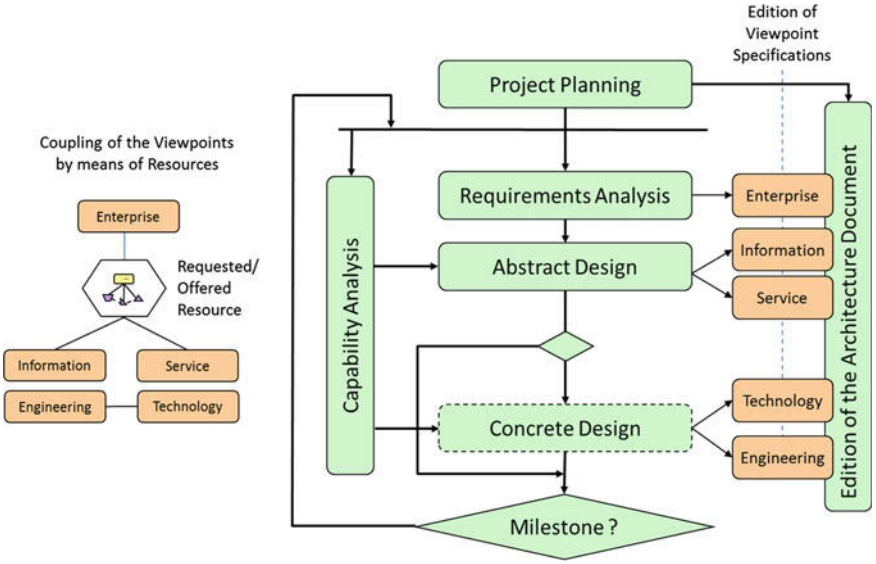

Fig. 12.3 Mapping of design steps to RM-TWS viewpoints

2009-12-31] for the parameter "sea water level" for all water gauge stations located in the Gulf of Naples, Italy". Such services may also be formally specified in the platform-independent modelling language UML (Unified Modeling Language) or its service profile SoaML (OMG 2008).

In the ***Concrete Design*** step the capabilities of the abstract service platform turn into requirements for the design of the concrete service platform and finally result in a specification of its capabilities. Example: The getObservation operation request of the OGC Sensor Observation Service (Na and Priest 2007). In the ***Engineering*** step the specified capabilities of the concrete service platform are implemented as service components and deployed in the context of a service network. Figure 12.3 illustrates the mapping of these design steps to the documentation of a TWS architecture according to the RM-TWS viewpoints. The recommendation for agility is expressed by iteration loops.

In the project planning step the architecture document is being set-up and structured. The Enterprise Viewpoint is being described in the requirements analysis step, mostly in terms of semi-structured use case descriptions (Cockburn 2001; Usländer and Batz 2011), whereas the information and service viewpoint specifications result from the abstract design step. The results of the Concrete Design step, i.e. the platform-specific specifications, are documented in the Technology and Engineering Viewpoint sections. This step may be omitted in a given iteration loop if the focus is first on reaching a milestone by agreeing on the platform-independent level. In parallel to these steps the analysis of the platform capabilities is carried out in order

to judge if requirements may be matched with existing capabilities, or how big the gap (and hence the design and development effort) is.

By applying the prescribed structure of the RM-TWS all relevant architectural aspects are covered. However, readability is a problem as the viewpoints are not enough interrelated. For instance, it is not visible which information model is required by a given service, or vice-versa, which service uses a given information model.

Furthermore, there is a huge gap to the use case descriptions of the Enterprise Viewpoint as these are, by their very nature, independent of the service and information models. In order to better overcome these gaps, a resource-oriented methodology may be used following the resource-oriented architectural style of Fielding (2000). An example is the SERVUS design methodology that is tailored to geospatial service-oriented architectures and relies upon the modeling of both use cases and platform capabilities as resources (Usländer 2010). On the left-hand side of Fig. 12.3 it is illustrated how viewpoints may be better coupled by expressing requirements and capabilities in terms of requested and offered resources.

SERVUS relies upon a resource model as a common modelling language to which both use cases and capabilities may be mapped. Hereby, a resource is an information object that is uniquely identified, may be represented in one or more representational forms (e.g. as a diagram, text document or a map layer) and support resource methods that are taken from a limited set of operations whose semantics are well-known (uniform interface). A resource has own characteristics (attributes) and is linked to other resources forming a resource network. Applying this idea, the abstract design step is then understood to be an iterative discovery and matching activity: requested resources derived from user requirements have to be mapped to fitting offered resources that represent the information objects being accessed and manipulated by geospatial services.

12.5 Conclusions and Perspectives

12.5.1 ICT and Tsunami Warning Systems

The evolution of TWS reflects the development of ICT as motivated in Sect. 12.2.1. In Phase I (Mainframe Era) computer systems were only used for very dedicated TWS functions (Table. 12.1). A first strong influence of ICT on TWS architectures became visible in Phase II (Microcomputer Era) with the availability of microcomputer systems and the digitalisation of sensor data. The architectural foundations for today's sensor networks have been established. Phase III (Internet Era) created the concepts and foundation for the architecture of modern TWS and their basic components which include sensor systems, decision support components, and warning components. The standardisation processes of component interfaces and the encoding of data were fostered by the development and success of the Internet promoted by the work of standardisation organisations such as W3C, OASIS, OGC, and ISO.

Table 12.1 Development phases of tsunami warning systems

Phase/Era	I-Data processing	II-Microcomputer	III-Internet	IV-Ubiquitous computing
<before	1980	1990	2000	today>
TWS				
Architecture	Limited application of computers	Far-field TWS	Near-field TWS	Networks of TWS, system-of-systems
Upstream sensor systems	Analogue registration,first digital seismic recording	Start broadband digital seismic recording	Sea level observation, virtual seismic sensor networks	Multi-sensor platforms, mobile sensors networks
Decision support	Manual evaluation of seismic events	Automatic earthquake detection	Decision tables, tsunami propagation models	Enhanced user interfaces, quantitative tsunami forecasting
Downstream dissemination	Sirens, radio broadcasting	FAX, telephone, TV broadcasting	Mail, web portals, TV narrow casting	Multi-channel warning dissemination, cell broadcasts
ICT				
Computing	Mainframe	Client-server	Internet, Service platforms	Internet of services, cloud computing, internet of things
Communication	Morse telegraphy, teletype, telephone	Proprietary LAN protocols, WAN with limited bandwidth	Internet protocols broadband WAN, satellite links	Broadband mobile communication; ZigBee, PAN, IPv6
Standards	Programming languages	Domain specific protocols: e.g. SEED, RINEX	Global IT standards: OASIS, W3C, open geospatial consortium	Mobile networks, future internet

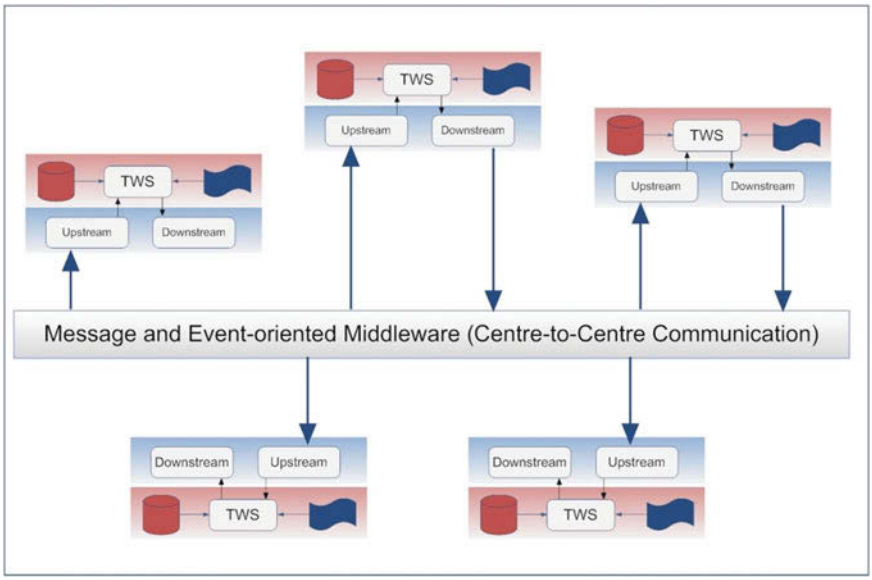

Fig. 12.4 Tsunami warning system of systems

In Phase IV (Ubiquitous Computing Era) the development of ocean-wide warning infrastructures, as discussed in responsible UNESCO/IOC bodies, will become technologically viable. TWS in such environments are systems that are developed and operated independently. In a system-of-systems context of a basin-wide TWS these individual TWS have to collaborate to fulfil common and complex task in crisis management. Core component in such loosely-coupled system-of-systems are message- and event-oriented brokers (fig. 12.4). The RM-TWS outlined above is currently being further developed by the TRIDEC project for such basin-wide warning infrastructures (Moßgraber et al. 2012).

Looking at the domains driving the development of TWS there is a clear shift from domain to ICT experts. In Phase I and II the progress of TWS is mainly driven by development activities within specific scientific communities, e.g. geophysicists, geodesists and geologists. Within Phase III these developments become more and more integrated in and depending on mainstream ICT evolution resulting from both the increasing system complexity and the progress in standardisation. Especially for Phase IV it becomes clearly visible that the potential and strength of ICT is increasingly challenging and pushes the architectural and functional evolution of TWS. Some highly important trends for TWS are cloud computing, ubiquitous sensing, integration of Earth Observation (EO) systems and volunteered geographic information that will be briefly addressed in the following sections.

12.5.2 Cloud Computing

TWS-supporting ICT infrastructures are embedded into the mega-trends of the Internet and the economic domain. **Cloud Computing** provides a new way of thinking about underlying ICT infrastructures for applications. It is not only that data may be "virtually" hosted in a reliable, performing and scalable way on a pay-per-use basis by a cloud provider. For TWS, and for early warning systems in general, it is the even more demanding factor that functions bundled as services will be offered by "the cloud". One of the objectives of the European **Future Internet** Public Private Partnership (FI-PPP) program is to increase the effectiveness of business processes and of the operation of infrastructures supporting applications in application domains such as transport, health, environment or energy (Havlik et al. 2011). The resulting core platform will be defined in terms of so-called "generic enablers" that support the following functions:

- creation, publishing, managing and consuming the Future Internet services;
- deploying the Future Internet services on the cloud, i.e. using cloud computing technologies;
- accessing, processing and analyzing massive data streams, as well as semantically classifying them into valuable knowledge;
- leveraging the ubiquity of heterogeneous, resource-constrained devices in the Internet of Things; and
- accessing the networks and devices through consistent service interfaces.

Using an agile design methodology this core platform will be enhanced and tailored to the application domains by FI-PPP usage area projects running in parallel. There are two usage area projects dealing with geospatial aspects: the ENVIROFI project[5] for environmental applications and the SafeCity project[6] that focuses on public security in cities. These projects are currently developing "specific enablers" that will be highly relevant for TWS-supporting ICT infrastructures of the future. Referring to generic TWS (Fig. 12.1), it is envisioned that in the future both the upstream and the downstream part of the overall TWS architecture may be provided by "cloud services" based upon international standards assuming that the non-functional aspects of trust and dependability of such cloud environments will be solved.

12.5.3 Ubiquitous Sensing

Sensors of various types are indispensable tools in order to feed TWS with data about environmental phenomena and the features of interest that are relevant to assess given geo-hazards. The progress in micro-electronics and the continuing downsizing trend fosters the development and the wide-spread availability of new types of **sensors**.

[5] http://www.envirofi.eu/

[6] http://www.safecity-project.eu

They are getting **ubiquitous** in the sense that sensing capabilities are increasingly embedded in various types of objects, ranging from mobile phones, objects of daily use up to dedicated sensor platforms such as buoys or unmanned aircraft vehicles. They are getting **smart** in the sense that more and more data processing and communication capabilities are embedded in the sensors themselves. These trends have an impact upon the information and communication architecture of TWS. In addition or instead of unprocessed raw data such sensors may deliver already pre-processed information to the higher-level TWS component, accompanied by context information (meta-data) about the conditions at the time of measurement and the associated uncertainty of the transmitted information (e.g. mean water gauge value of the last hour).

The communication capabilities of the sensors may be exploited in two ways:

(1) Sensors with wireless communication and self-description capabilities may connect on local level with other sensors to form **ad-hoc sensor networks** (comprising in-situ and mobile sensors). By exchanging and fusioning their individually observed data, local monitoring results with higher resolution and lower uncertainty may be achieved.
(2) Sensor tasking may be used to request the execution of a "monitoring task" on the sensor level with configurable notification policies towards interested consumers, e.g. notification only when thresholds have been exceeded.

A combination of (1) and (2) enables flexible monitoring strategies with a higher level of dependability. A group of sensors may be requested to execute a "monitoring task" relying upon the self-organization capabilities on the sensor level. The task results may then be linked with the results of process monitoring on a higher level.

12.5.4 Improving Damage Estimation and Situation Awareness

In order to improve the situation picture, two other data sources are getting increasingly important for TWS and for early warning systems in general: remote sensing information and volunteered geographic information. **Remote sensing information** continuously gathered by various EO missions under the auspices of national or cross-national (e.g. European) space agencies is made accessible by means of EO product catalogues and service-oriented infrastructures. Typically, these tasks are provided by ground segment software services which may be called through corresponding interfaces by client applications, e.g. Web portal applications, or other software components such as GIS applications. However, without a coordinated strategy and harmonized development, these ground segment services all have different interfaces following the needs and the business requirements of the individual stakeholders.

While this may not be a problem when accessing EO products just from one mission, it gets difficult and tedious when EO products are required from multiple missions, or even worse, when the EO products from multiple missions shall be

combined or processed together in order to provide higher-level services or to deliver fused EO datasets. In order to solve this problem, service-oriented architectures, also heavily relying upon OGC SWE standard but tailored (profiled) to EO product search and delivery are being defined. Examples are the Heterogeneous Mission Accessibility (HMA) initiative of the European/Canadian Ground Segment Coordination Body (Usländer et al. 2012) and the world-wide initiative to create GEOSS—a Global Earth Observation System of Systems.

The second source of data with an increasing importance is **Volunteered Geographic Information (VGI)** which draws on the concept of citizens as sensors for a next generation digital earth (Craglia et al. 2008). Social media platforms change the way people create and use information during crisis eventsm. It is assumed that the rich information made available by members of the public can contribute to a more effective response to natural disasters (Ostermann and Spinsanti 2011).

12.5.5 ICT and the Human Factor

However, a powerful ICT infrastructure can only solve part of the problem of early warning. The human factor still remains important, too. Coppola (2011) stresses that "Early warning mechanisms must include public education, accurate risk perception, a communications system to relay the message, and an emergency management system to adequately coordinate the response". Public safety from environmental dangers is one of the five key elements in Environmental Security that has to be considered "within and across national borders" (Landholm 1998). According to Coppola (2011) there is a need for further action and the inclusion, training and education of end-users of various disciplines (e.g., geo-scientists, citizens, emergency organizations, environmental and security agencies) including their cultural context and risk perception in order to really exploit the potential of TWS and their underlying ICT capabilities.

Acknowledgments This article is based on the work of the authors in large-scale research and development projects, especially the German Indonesian Tsunami Early Warning System (GITEWS) funded by the German Federal Ministry of Education and Research BMBF, the European FP6 project Distant Early Warning System (DEWS) and the FP6 project Sensors Anywhere (SANY). These research activities are continued by the project Collaborative, Complex, and Critical Decision-support in Evolving Crises (TRIDEC) funded under the European Union's FP7. The authors acknowledge the continuing intensive and fruitful research collaboration within and between these project teams, in particular between IOSB and GFZ.

References

Babeyko AY, Hoechner A, Sobolev SV (2010) Source modelling and inversion with near real-time GPS: a GITEWS perspective for Indonesia. Nat Hazards Earth Syst Sci 10:1617–1627

Behrens J, Androsov A, Babeyko AY, Harig S, Klaschka F, Mentrup L (2010) A new multi-sensor approach to simulation assisted tsunami early warning. Nat Hazards Earth Syst Sci 10: 1085–1100

Botterell A (2006) The common alerting protocol: an open standard for alerting, warning and notification. In: Proceedings of the 3rd international ISCRAM Conference, Netwark, NJ

Cockburn A (2001) Writing effective use cases. Addison-Wesley, Reading, ISBN-13 978–0-201-70225-5

Coppola DP (2011) Introduction to international disaster management. Elsevier Inc., Amsterdam, ISBN 978-0-12-3812174-4

Craglia M, Goodchild MF, Annoni A, Camara G, Gould M, Kuhn W, Mark DM et al (2008) Next-generation digital earth: a position paper from the Vespucci initiative for the advancement of geographic information science. Int J Spat Data Infrastruct Res 3:146–167

Erl T (2008) SOA: principles of service design. Prentice Hall, Boston, ISBN 0-13-234482-3

Falck C, Ramatschi M, Subarya C, Bartsch M, Merx A, Hoeberechts J, Schmidt G (2010) Near real time GPS applications for tsunami early warning systems. Nat Hazards Earth Syst Sci 10:181–189

Fielding RT (2000) Architectural styles and the design of network-based software architectures. Doctoral dissertation, University of California, Irvine. http://www.ics.uci.edu/fielding/pubs/dissertation/top.htm

Fleischer J, Häner R, Herrnkind S, Kloth A, Kriegel U, Schwarting H, Wächter J (2010) An integration platform for heterogeneous sensor systems in GITEWS—tsunami service bus. Nat Hazards Earth Syst Sci 10:1239–1252

GDIN (1997) Harnessing information and technology for disaster management. Disaster Information Task Force Report

Hammitzsch M, Lendholt M, Esbrí MA (2012) User interface prototype for geospatial early warning systems—a tsunami showcase. Nat Hazards Earth Syst Sci 12:555–573

Hanka W, Saul J, Weber B, Becker J, GITEWS Team (2008) Timely regional tsunami warning and rapid global earthquake monitoring. OFREUS Newslett 8:1

Hanka W, Saul J, Weber B, Becker J, Harjadi P, Fauzi, GITEWS Seismology Group (2010) Real-time earthquake monitoring for tsunami warning in the Indian Ocean and beyond. Nat Hazards Earth Syst Sci 10:2611–2622

Havlik D, Schimak G, Denzer R, Stevenot B (2007) SANY (Sensors Anywhere) integrated project. In: Swayne DA, Hrebicek J (eds) Proceedings of the ISESS 2007, Czech Republic, Prague

Havlik D, Schade S, Sabeur Z, Mazzetti P, Watson K, Berre A, Lorenzo J (2011) From Sensor to Observation Web with Environmental Enables in the Future Internet. Sensors Journal 11:3874–3907

Henricksen K, Iannella R (2010) Towards standards-based resource management systems for emergency management. In: van de Walle B, Turoff M, Hiltz SR (eds) Information systems for emergency management, vol 16, Advances in management information systems. M.E. Sharpe, Armonk, pp 327–343 http://www.westerndisastercenter.org/DOCUMENTS/DITF_Report.pdf

Iannella R, Robinson K (2006) Tsunami warning markup language (TWML), NICTA Technical Report. http://xml.coverpages.org/TsunamiWarningML-V10-20060725.pdf

ICG/NEAMTWS (2009) Tsunami early warning and mitigation system in the North Eastern Atlantic, the Mediterranean and Connected Seas, NEAMTWS implementation plan, Version 3.4. Intergovernmental Oceanographic Commission Technical Series 73

Imamura F, Abe I (2009) History and Challenge of Tsunami Warning Systems in Japan. Journal of Disaster Research, Vol.4, No.4

ICG/NEAMTWS (2011) Interim operational users guide for the tsunami early warning and mitigation system in the Northeastern Atlantic, the Mediterranean and Connected Seas (NEAMTWS), Version 1.9

IRIS (2010) SEED reference manual, standard for the exchange of earthquake data. SEED Format Version 2.4

IRIS Consortium (2003) Review of the global seismographic network. http://www.iris.edu/hq/files/programs/gsn/documents/GSN_Review.pdf

ISO/IEC 10746-1 (1998) Information technology—open distributed processing—reference model
ITU—International Telecommunications Union, Series X (2007) Data networks, open system communications and, security, X.1303
JMA (2009) Earthquakes and tsunamis—disaster prevention. Japan Meteorological Agency
Kind R (2012) Foundation of instrumental seismology. The IUGG Electronic Journal 12(2)
Landholm M (1998) Defining environmental security: implications for the U.S. army, Army Environmental Policy Institute, AEPI-IFP-1298
Lauterjung J, Münch U, Rudloff A (2010) The challenge of installing a tsunami early warning system in the vicinity of the Sunda Arc, Indonesia. Nat Hazards Earth Syst Sci 10(4):641–646
Leffingwell D (2011) Agile software requirements—lean requirements practices for teams, programs, and the enterprise. Addison-Wesley, Upper Saddle River, ISBN-13:978–0-321-63584-6
Lendholt M (2011) Tailoring spatial reference in early warning systems to administrative units. Earth Sci Inform 4(1):7–16 (Springer). doi:10.1007/s12145-010-0075-y
Lendholt M, Esbri MA, Hammitzsch M (2012) Interlinking national tsunami early warning systems towards ocean-wide system-of-systems networks. In: Rothkrantz L, Ristvej J, Franco Z (eds) Proceedings of the 9th international ISCRAM conference, Vancouver, Canada
Lendholt M, Hammitzsch M (2011) Generic information logistics for early warning systems. In: Proceedings of the 8th international ISCRAM conference, Lisbon
Maier MW (1998) Architecting principles for systems-of-systems. J Syst Eng 1(4):267–284
Moßgraber J, Middleton S, Hammitzsch M Poslad S (2012) A distributed architecture for tsunami early warning and collaborative decision-support in crises. EGU General Assembly, Geophysical Research Abstracts, 14, EGU 2012–8040-2
Mutsaers EJ, van der Zee H, Giertz H (1998) The evolution of information technology. Inf Manag Comput Secur 6(3):115–126
Nakamura, Y (2004) UrEDAS, urgent earthquake detection and alarm system, now and future. In: 13th world conference on earthquake engineering, Vancouver, August 1–6
Na A, Priest M (2007) Sensor observation service version 1.0. Open-GIS implementation standard, OGC 06–009r6.http://www.opengeospatial.org/standards/sos
OASIS (2006) OASIS, organisation for the advancement of structured information standards. Security Assertion Markup Language (SAML) v2.0, Technical Overview. http://www.oasis-open.org/committees/download.php/20645/sstc-saml-tech-overview-2%200-draft-10.pdf
OASIS (2010) OASIS, Organisation for the advancement of structured information standards. eXtensible Access Control Markup Language (XACML)Version 3.0. Committee Specification 01. http://docs.oasis-open.org/xacml/3.0/xacml-3.0-core-spec-cs-01-en.pdf
OMG (2008) OMG, object management group. Service oriented architecture modeling language (SoaML)—specification for the UML profile and metamodel for services (UPMS). OMG Document ad/08-11-01
Ostermann FO, Spinsanti L (2011) A conceptual workflow for automatically assessing the quality of volunteered geographic information for crisis management. In: Proceedings of the 14th AGILE international conference on geographic information science
Percivall G (2010) The application of open standards to enhance the interoperability of geoscience information. Int J Digital Earth 3(Supplement 1):14–30
Riedel F, Chaves F (2012) Workflows and decision tables for flexible early warning systems. In: Rothkrantz L, Ristvej J, Franco Z (eds) Proceedings of the 9th international ISCRAM conference—Vancouver, Canada
Schaller RR (1997) Moore's law: past, present and future. IEEE Spectr 34(6):52–59. doi:10.1109/6.591665
Schorlemmer D, Wyss A, Maraini S, Wiemer S, Baer M (2004) QuakeML—an XML schema for seismology. Orfeus Newslett 6:2
Simonis I (2008a) OGC sensor web enablement architecture. OGC Best Practices Document 06-021r4, Version 0.4.0
Simonis I (2008b) OGC sensor web enablement architecture. OGC Best Practices Document 06-021r2 Version: 0.1.0

Steinmetz T, Raape U, Teßmann S, Strobl C, Friedemann M, Kukofka T, Riedlinger T, Mikusch E, Dech S (2010) Tsunami early warning and decision support. Nat Hazards Earth Syst Sci 10:1839–1850

TOWS-WG: Working Group on Tsunamis and Other Hazards Related to Sea-Level Warning and Mitigation Systems (TOWSWG) (2011) Fourth meeting, Paris, France 20–21 March, Intergovernmental Oceanographic Commission Reports of Meetings of Experts and Equivalent Bodies

Turoff M, van de Walle B, Hiltz SR (2010) Emergency response information systems—past, present and future. In: van de Walle B, Turoff M, Hiltz SR (eds) Information systems for emergency management, Volume 16, advances in management information systems. M.E. Sharpe, Armonk, pp 369–387

UNESCO (2009) Operational users guide for the pacific tsunami warning and mitigation system (PTWS). IOC Technical Series No. 87

UNESCO (2011) Indian ocean tsunami warning and mitigation system IOTWS. In: Implementation plan eighth session of the intergovernmental coordination group for the Indian ocean tsunami warning and mitigation system (ICG/IOTWS-VIII), Melbourne, Australia, IOC Technical Series No. 71 (Revision 4), 3–6 May 2011

Usländer T (2007) Reference model for the ORCHESTRA architecture. Version 2.1. OGC 07-097 best practices document

Usländer T (2009) Specification of the sensor service architecture, Version 3.0 (Rev. 3.1). OGC Discussion Paper 09-132r1

Usländer T (2010) Service-oriented design of environmental information systems. Ph D thesis of the Karlsruhe Institute of Technology (KIT), Faculty of Computer Science, KIT Scientific Publishing, ISBN 978-3-86644-499-7. http://digbib.ubka.uni-karlsruhe.de/volltexte/1000016721

Usländer T, Batz T (2011) How to analyse user requirements for service-oriented environmental information systems. In: Hřebíček J, Schimak G, Denzer R (eds) ISESS 2011. IFIP AICT, 359, 165–172. Springer, Heidelberg

Usländer T, Coene Y, Marchetti PG (2012) Heterogeneous missions accessibility—design methodology. Architecture and use of geospatial standards for the ground segment support of earth observation missions. European Space Agency (ESA) TM-21. ISBN 978-92-9221-883-6. http://www.spacebooksspsonline.com/product_info.php?cPath=112&products_id=17510

Wächter J, Babeyko A, Fleischer J, Häner R, Hammitzsch M, Kloth A, Lendholt M (2012) Development of tsunami early warning systems and future challenges. Nat Hazards Earth Syst Sci 12:1923–1935

Walter C (2005) Kryder's Law. Sci Am Mag 293:32–33

Zielinski A, Bügel U, Middleton SE, Tokarchuk L, Watson K, Chaves F (2012) Multilingual analysis of twitter news in support of mass emergency events. EGU General Assembly 2012, Geophysical Research Abstracts, 14, EGU2012-8085-5

Chapter 13
A Test of Earthquake Early Warning System Using Low Cost Accelerometer in Hualien, Taiwan

Y.-M. Wu and T.-L. Lin

Abstract The earthquake early warning (EEW) research group at the National Taiwan University (NTU) and one technology company have been developing a Micro Electro Mechanical Systems (MEMS) type of accelerometer (the "*P*alert" EEW sensor) specifically designed for EEW purpose. In addition to the physical properties of the MEMS accelerometer, the main advantage of the MEMS accelerometer comparing to the other seismometers is that it is a relatively very low-cost seismic sensor. We present the performances of the *P*alert EEW network located at the Hualien region during a two-month experiment. The results of the Hualien *P*alert network encourage the further implementations for the MEMS-type of seismometer in the EEW application.

13.1 Introduction

Taiwan has been constantly threatened by large, devastating earthquakes as the consequence of the persistent collision between the Philippine Sea Plate and Eurasian Plate. For Taiwan, the development of earthquake early warning system was first motivated by the Hualien offshore earthquake ($M_w = 7.8$) in November 15, 1986, which caused severe damage in the metropolitan Taipei of about 120 km away from the epicenter. If an EEW system in the Hualien area can provide an earthquake warning within 20 s (i.e. crustal shear-wave travelling time over a distance of 120 km) after the occurrence of the Hualien earthquake, a timely warning can be feasible for the highly populated Taipei area. Since then Taiwan has been developing EEW system and become one of leading countries on EEW practices.

Y.-M. Wu (✉)
Department of Geosciences, National Taiwan University, 10617 Taipei, Taiwan
e-mail: drymwu@ntu.edu.tw

T.-L. Lin
Department of Earth Sciences, National Cheng Kung University, 70101 Tainan, Taiwan

F. Wenzel and J. Zschau (eds.), *Early Warning for Geological Disasters*,
Advanced Technologies in Earth Sciences, DOI: 10.1007/978-3-642-12233-0_13,

The backbone of the present Taiwan EEW system is the Rapid Earthquake Information Release System (RTD; Wu et al. 1997, 2000) operated by the Central Weather Bureau (CWB) since 1995. The RTD network at present consists of 109 telemetered seismic stations covering the entire Taiwan region. Each station is equipped with a three-component, force-balance strong-motion accelerometer with a 16-bit resolution and a ± 2 g full dynamic range recorder.

Although the station density of the RTD network is proven to be rather adequate for repaid reporting and EEW purposes (Hsiao et al. 2009), a higher density of seismic stations is always in great demand (Lin and Wu 2010a, b; Lin et al. 2011) especially for a front-detection type of EEW system, in which the seismograms recorded by closer-to-earthquake seismic sensors are used to estimate the earthquake location, magnitude, and to predict the ground motions at more distant target areas. For example, a short-distance EEW system might be possible with extensive installation of seismometers around seismogenic areas (Wu et al. 2011). However, to increase the number of seismic station equipped with traditional mechanical seismometer will significantly boost the expense of EEW seismic network. Besides, for the other seismogenic zones around the world where only a limited number of seismic stations or even no seismic network is available, a cost-effective seismic network dedicated to EEW or rapid reporting is highly favored.

The MEMS accelerometer that has been introduced in seismic applications (Holland 2003) since 1990s is miniature, cost-saving, and ideal for recording high-frequency, near-field unsaturated ground motions. Consequently, the MEMS accelerometer offers a suitable application for an economical, near-source EEW system. The MEMS accelerometer type of network has been proposed for its potential for EEW using the Quake-Catcher Network (Cochran et al. 2009).

The EEW research group at the NTU and the San Lien Technology Corp. (http://www.sanlien.com.tw) have been developing a MEMS type of accelerometer named the "*P*alert" sensor (Fig. 13.1), specifically designed for EEW purpose. *P*alert can record three-component acceleration and also can perform real-time integration to obtain velocity and displacement. Once an earthquake *P* wave is detected by the triggering algorithms embedded in the sensor, the sensor will compute the average period (τ_c; Kanamori 2005; Wu and Kanamori 2005a, 2008a, b; Wu et al. 2007) and peak amplitude of the filtered vertical displacement (P*d*; Wu and Kanamori 2005b, 2008a, b; Wu et al. 2007) from the first few seconds of the *P*-wave and accordingly send an earthquake alarm signal for on-site EEW purpose. The triggering algorithms include continuous monitoring of acceleration, displacement, and Short-Term-Average (STA)/ Long-Term-Average (LTA) ratio (Allen 1978). *P*alert features with networking capability including streaming real-time data to host, automatically connect to up to 2 servers, and Network Time Protocol (NTP) time calibration.

In this study, we will present the EEW performances of the testing *P*alert EEW network located at the Hualien region (Fig. 13.2), a high seismicity region in eastern Taiwan. The results of the Hualien *P*alert EEW network during its initial phase of operation strongly encourage the further development for the MEMS accelerometer-type of EEW system.

Fig. 13.1 The *P*alert earthquake early warning sensor

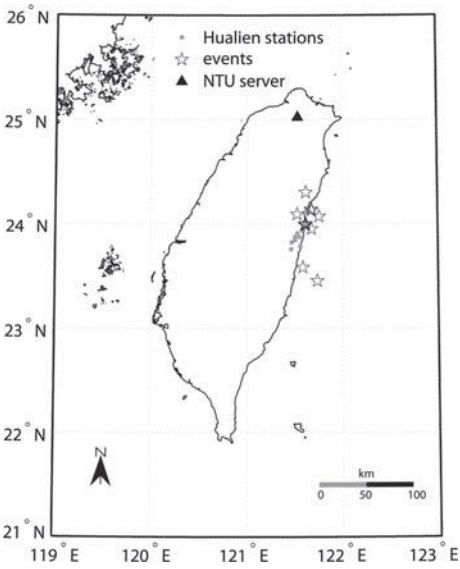

Fig. 13.2 The location map shows the stations (*circles*) of the Hualien EEW network and the epicenters of the 11 study events (*star*). The NTU server of the Hualien EEW network is indicated by the *triangle*

13.2 The Hualien EEW System

The Hualien *P*alert testing EEW network consists of 15 *P*alert stations, and Fig. 13.3 shows the schematic diagram for the field implementation. There are two main structures involved in the network, consisting of local field systems and a central system.

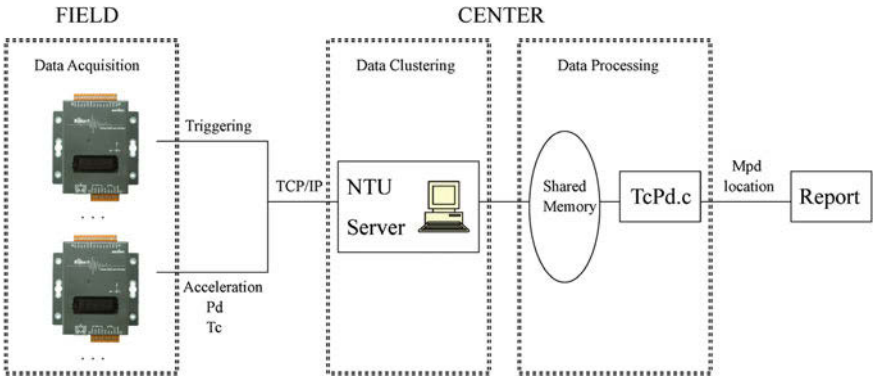

Fig. 13.3 Operation flowchart of the Hualien EEW network

The local system includes signal acquisition and processing by *P*alert and offers onsite early warning when Pd is larger than 0.35 cm (Wu et al. 2011). The central system includes data clustering and analysis by the network server hosted in Taipei, NTU. The information recorded by the *P*alert stations is transmitted to the NTU server ocer the TCP/IP protocol. In case of a power failure due to electrical power tower collapses or disconnected communication lines by strong ground shaking, each station is equipped with an internal battery to provide steady electrical power for at least 4 h. Once more than six *P*alert stations are triggered, an event is declared. The acquired information from the *P*alert stations are then stored in the system-wide shared memory and controlled by the code TcPd.c to generate the EEW/rapid reports with event location and magnitude operated by the NTU server.

The hypocentral location will be determined using the traditional earthquake locating algorithm on a half space linear increasing velocity model. The magnitude determination using the P*d* attenuation relationship with hypocentral distance (*R*) (M_{Pd}; Wu and Zhao 2006), which can be expressed as:

$$M_{Pd} = 4.748 + 1.371 \times \log_{10}(\mathrm{Pd}) + 1.883 \times \log_{10}(R) \tag{13.1}$$

is adopted. As more stations are triggered, the event location and magnitude are continuously updated.

13.3 The Performance of the Hualien EEWS

In this testing, 11 earthquakes in the recording period between June, 2010 and August, 2010 and located near the Hualien EEWS are used (Table 13.1, 13.2). The choices of the events near the Hualien EEW network follow the proposition as using the Hualien network to be the front-detection sensor. Comparisons of the earthquake information

Table 13.1 Source parameters of the 11 earthquakes determined by the Central Weather Bureau (CWB)

	CWB catalog				
Event no.	mm/dd/yy	Origin time	Location (lon, lat)	Depth (km)	Magnitude (M_L)
1	6/18/2010	04:24:06.1	121.68, 24.13	9.6	2.9
2	7/04/2010	02:43:05.0	121.68, 23.95	11.8	4.0
3	7/17/2010	09:04:17.2	121.74, 23.45	40.0	5.2
4	7/24/2010	23:41:10.1	121.62, 24.30	23.5	3.6
5	7/28/2010	22:18:41.2	121.68, 24.14	9.7	3.3
6	7/31/2010	08:13:17.8	121.76, 24.07	46.4	4.6
7	8/10/2010	21:57:51.4	121.53, 24.09	19.4	3.4
8	8/19/2010	07:11:21.3	121.62, 24.00	5.1	3.5
9	8/19/2010	07:45:30.1	121.61, 23.99	7.0	3.8
10	8/20/2010	06:46:23.1	121.62, 23.99	7.7	3.0
11	8/21/2010	16:38:00.0	121.59, 23.58	40.2	5.3

(locations and magnitudes) given by the Hualien EEW system and the CWB published earthquake catalogs are shown in Fig. 13.4. Since a simplified velocity model is used in the code TcPd.c to find the hypocenters and most of the events are located outside the network. So, a large variation of the earthquake locations is indicated in Fig. 13.4. However, for the events with shallow focal depths or located inside the perimeter of the stations the discrepancies of the hypocenters of those between the Hualien EEW system and the CWB catalogs are smaller. The response time as the time difference between the event original time and the first report given by the Hualien EEW system varies between 5 and 25 s with the average time of 9.5 s. Therefore, the Hualien EEW system is capable to issue a timely warning to areas located more than 35 km away from the hypocenter before the arrival of the *S*-wave. The large uncertainty is found in magnitude determination. M_{Pd} estimated with Eq. (13.1) has a 1:1 relationship with M_L with standard deviations of 1.25 and 1.24 for the first and final reports, respectively. However, earthquakes with magnitudes large than 4.0 have a much better correlation between P*d* and the final magnitude.

13.4 Discussion and Conclusions

In addition to the physical properties of the MEMS accelerometer, the main advantage of the MEMS accelerometer comparing to the other seismometers is that it is a relatively very low-cost seismic sensor. For the commercial type of *P*alert the cost is generally less than 1000 US dollar. A seismic network comprising couple tens or even hundreds of the *P*alert sensors can be built by a much lower budget than that with the transitional seismometers.

Table 13.2 Source parameters of the 11 earthquakes determined by the Hualien EEW system

EEW evaluation					
Event* no.	mm/dd/yy	Time	Location (lon, lat)	Depth (km)	Magnitude (M_{pd})
1	6/18/2010	04:24:12.8	121.63, 24.14	4.2	3.4
2	7/04/2010	02:43:10.3	121.72, 23.95	24.9	4.7
2	7/04/2010	02:43:14.3	121.64, 24.02	6.0	4.0
3	7/17/2010	09:04:41.3	121.58, 24.04	9.1	4.4
4	7/24/2010	23:41:20.1	121.61, 24.31	18.5	5.0
5	7/28/2010	22:18:48.2	121.36, 23.76	41.1	5.8
6	7/31/2010	08:13:30.7	121.57, 23.93	12.6	4.6
6	7/31/2010	08:13:31.7	121.56, 23.91	10.6	4.6
7	8/10/2010	21:58:00.3	121.15, 24.31	17.4	5.7
8	8/19/2010	07:11:27.9	121.64, 24.03	2.9	4.0
9	8/19/2010	07:45:35.8	121.57, 24.01	4.2	4.2
9	8/19/2010	07:45:37.8	121.58, 24.01	3.3	4.4
9	8/19/2010	07:45:40.8	121.57, 24.01	4.2	4.4
10	8/20/2010	06:46:29.7	121.69, 24.02	0.7	4.3
11	8/21/2010	16:38:11.1	121.55, 23.61	29.9	5.7
11	8/21/2010	16:38:12.1	121.56, 23.69	21.6	5.6
11	8/21/2010	16:38:13.1	121.56, 23.68	22.9	5.6

*Multiple event numbers indicate that more than one report is made for that event

The differences of the hypocentral locations between the reports by the Hualien EEWS and the CWB catalogs are partly attributed to the simplified velocity model used in the Hualien EEW location algorithm and to the linear station distribution in the N-S direction of the Hualien EEW network. Another source of deviation might be caused by the inaccurate automated first-arrive picking especially for the smaller earthquakes. In the future development of the Hualien EEW system, a 1-D velocity model with more layers might be adopted. Eventually, for the final phase of EEW network development, a low-cost and densely distributed *P*alert-type network over the whole Taiwan region is feasible. Such extensively and densely distributed network is especially useful for a large inland earthquake or with a long rupture length, which is often more capable of causing severe damage than outland ones in Taiwan.

The discrepancies between the predicted M_{Pd} and the catalog M_L might arise from poor earthquake location and consequently incorrect distance term in implementing P*d* attenuation relationship (Fig. 13.4c). Figure 13.5a shows that the standard deviation (1.24) shown in Fig. 13.4c is reduced to 1.06 by replacing the EEW-determined location with the catalog location. The region-depend P*d* attenuation relationship (Wu and Zhao 2006) used in this study (Eq. 13.1) is derived for earthquakes in Southern California and there was no such relationship available during the construction phase of the Hualien EEW network. Figure 13.5b compares M_{Pd} calculated by the newly derived Taiwan P*d* attenuation relationship (Hsiao et al. 2011) with the catalog M_L. The standard deviation (1.24) shown in Fig. 13.4c is significantly reduced to 0.64 without an overestimated bias as shown in Figs. 13.4c and 13.5a. A local P*d* attenuation relationship specifically for the Hualien EEW network might further improve

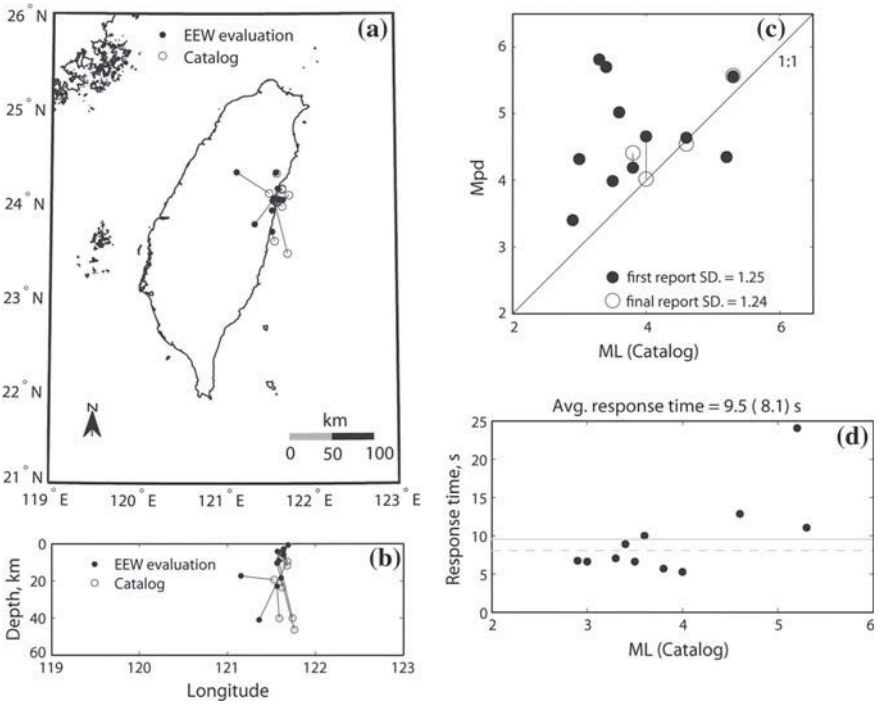

Fig. 13.4 Comparisons of the earthquake information (**a** epicenters, **b** focal depths, **c** magnitudes, **d** response times) given by the real-time, on-line Hualien EEW system and the CWB published earthquake catalogs. In **c**, the *solid* and *open circles* represent the first report with more than six triggered stations and the final report with all available stations, respectively. The response times in (**d**) are those given by the first report. The average response time of 8.1 s indicated by the *dashed line* in (**d**) is the one excluding the maximum response time of 24.1 s

the EEW performance in magnitude determination. Another noticeable feature of the Hualien EEW network is the response time. For the current operating EEW system by CWB the average response time is of about 20 s (Hsiao et al. 2011).

For magnitude determination problem in EEW system, a large event with large rupture dimensions, such as the $M_w = 9.0$, 2011 Tohoku earthquake, likely consists of several strong asperities over the entire rupture volume. Using the first few seconds of the waveform from an initial nucleation rupture for estimating the eventual magnitude, which is the concept behind the EEW system, may be difficult for extremely large earthquakes. However, recently result (Lin and Wu 2012) indicates that the effective shaking method of Wu and Teng (2004) provides excellent magnitude estimation for the 2011 Tohoku earthquake, without a saturation problem. Such approach could be used in *P*alert network for updating magnitude determination. Thus, within few to ten seconds and few minutes P*d* and effective shaking methods could be used for EEW and rapid reporting purposes, respectively.

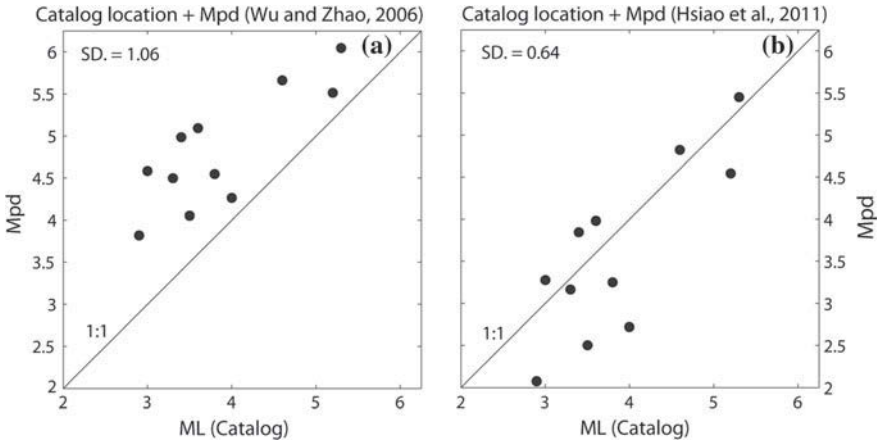

Fig. 13.5 Magnitude (M_{Pd}) determined by the Hualien EEW network by using **a** the Southern California (Wu and Zhao 2006) and **b** the Taiwan P*d* attenuation relationships (Hsiao et al. 2011), respectively, versus M_L in the CWB earthquake catalogs. Both in **a** and **b** the earthquake locations are given by the CWB earthquake catalogs

Our new EEW sensor, *P*alert, using the MEMS sensor has a high commercial potential owing to its low cost. The EEW system could be established in a relatively low budget or *P*alert sensor could be readily added to the existing seismic network to increase the density of the network. The Hualien EEW system belongs to the front-detection type. Nevertheless, our *P*alert sensor also can be used in the on-site type of EEWS, which the initial *P*-wave motion at a target site is used to predict the ground motions of the later *S* and surface waves at the same site.

Acknowledgments Our work was supported by the National Science Council and Central Weather Bureau, Taiwan. We thank Prof. Friedemann Wenzel, Dr. Hanshu Peng and two anonymous reviewers for constructing comments.

References

Allen RV (1978) Automatic earthquake recognition and timing from single traces. Bull Seismol Soc Am 68:1521–1532

Cochran ES, Lawrence JF, Christensen C, Jakka RS (2009) The quake-catcher network: citizen science expanding seismic horizons. Seismol Res Lett 80:26–30

Holland A (2003) Earthquake data recorded by the MEMS accelerometer. Seismol Res Lett 74:20–26

Hsiao NC, Wu YM, Shin TC, Zhao L, Teng TL (2009) Development of earthquake early warning system in Taiwan. Geophys Res Lett. 36:L00B02, doi:10.1029/2008GL036596

Hsiao NC, Wu YM, Zhao L, Chen DY, Huang WT, Kuo KH, Shin TC, Leu PL (2011) A new prototype system for earthquake early warning in Taiwan. Soil Dyn Earthq Eng. 31:201–208, doi:10.1016/j.solidyn.2010.01.008

Kanamori H (2005) Real-time seismology and earthquake damage mitigation. Annu Rev Earth Planet Sci. 33:5.1–5.20, doi:10.1146/annurev.earth.33.092203.122626
Lin TL, Wu YM (2010a) Magnitude determination using strong ground-motion attenuation in earthquake early warning. Geophys Res Lett. 37:L07304, doi:10.1029/2010GL042502
Lin TL, Wu YM (2010b) Magnitude estimation using the covered areas of strong ground motion in earthquake early warning. Geophys Res Lett. 37:L09301, doi:10.1029/2010GL042797
Lin TL, Wu YM, Chen DY (2011) Magnitude estimation using initial P-wave amplitude and its spatial distribution in earthquake early waning in Taiwan. Geophys Res Lett. 38:L09303, doi:10.1029/2011GL047461
Lin TL, Wu YM (2012) A fast magnitude estimation for the M 9.0 2011 Great Tohoku Earthquake. Sismol Res Let. 83:667–671, doi:10.1785/0220110119
Wu YM, Chen CC, Shin TC, Tsai YB, Lee WHK, Teng TL (1997) Taiwan rapid earthquake information release system. Seismol Res Lett 68:931–943
Wu YM, Kanamori H (2005a) Experiment on an onsite early warning method for the Taiwan early warning system. Bull Seismol Soc Am 95:347–353
Wu YM, Kanamori H (2005b) Rapid assessment of damaging potential of earthquakes in Taiwan from the beginning of *P* waves. Bull Seismol Soc Am 95:1181–1185
Wu YM, Kanamori H (2008a) Development of an earthquake early warning system using real-time strong motion signals. Sensors 8:1–9
Wu YM, Kanamori H (2008b) Exploring the feasibility of on-site earthquake early warning using close-in records of the 2007 Noto Hanto earthquake. Earth Planets Space 60:155–160
Wu YM, Kanamori H, Allen R, Hauksson E (2007) Determination of earthquake early warning parameters, τc and Pd, for Southern California. Geophys J Int. 170:711–717, doi:10.1111/j.1365-246X.2007.03430.x
Wu YM, Lee WHK, Chen CC, Shin TC, Teng TL, Tsai YB (2000) Performance of the Taiwan rapid earthquake information release system (RTD) during the 1999 Chi-Chi (Taiwan) earthquake. Seismol Res Lett 71:338–343
Wu YM, Lin TL, Chao WA, Huang HH, Hsiao NC, Chang CH (2011) Faster short-distance earthquake early warning using continued monitoring of filtered vertical displacement: a case study for the 2010 Jiasian earthquake. Taiwan Bull Seism Soc Am. 101:701–709, doi:10.1785/0120100153
Wu YM, Teng TL (2004) Near real-time magnitude determination for large crustal earthquakes. Tectonophysics 390:205–216
Wu YM, Zhao L (2006) Magnitude estimation using the first three seconds *P*-wave amplitude in earthquake early warning. Geophys Res Lett. 33:L16312, doi:10.1029/2006GL026871

Chapter 14
Applications of a Low-Cost, Wireless, Self-Organising System (SOSEWIN) to Earthquake Early Warning and Structural Health Monitoring

M. Picozzi, C. Milkereit, K. Fleming, J. Fischer, K-H. Jaeckel, D. Bindi, S. Parolai and J. Zschau

Abstract The rapid characterization of ground motion during the initial stage of an earthquake is one of the most effective approaches for quantifying the hazard associated with its impact on populated or otherwise sensitive areas. Earthquake early warning (EEW) systems are based on this approach, and aim to mitigate earthquake hazard for a target area by the provision of timely warnings. In addition, during and soon after the occurrence of earthquakes, the necessity for information on the state of health of structures in real-time that permit timely warnings in case of damaging events requires structural health monitoring systems. The Self-Organising Seismic Early Warning Information Network (SOSEWIN) is a new concept in EEW and structural health monitoring (SHM) systems. SOSEWIN employs advances in various technologies to incorporate off-the-shelf sensor, processing and communications components into low-cost sensing units that are linked by advanced, robust and rapid communications routing and network organisational protocols that are appropriate for wireless mesh networks. Significant and innovative aspects of SOSEWIN are that each sensing unit performs on-site, independent analysis of the ground motion, and that the early warning is transmitted throughout the network by means of dedicated alarming processes. In this work, a description of the SOSEWIN philosophy, hardware, and software is provided, as well as an overview of its application within different contexts. In particular, we present the results of tests carried out with SOSEWIN in Istanbul, Turkey, where a first test-bed consisting of 20 instruments is installed, as well as a novel approach for EEW that exploits the SOSEWIN philosophy to obtain, in the event of an earthquake, a real-time structural response assessment fol-

M. Picozzi (✉)
Department of Physics, University of Naples Federico II, Naples, Italy
e-mail: matteo.picozzi@unina.IT

C. Milkereit · K. Fleming · K.-H. Jaeckel · D. Bindi · S. Parolai · J. Zschau
Deutsches GeoForschungsZentrum Postdam, Telegrafenberg, 14473 Potsdam, Germany

J. Fischer
Computer Science Department, Humboldt University Berlin, Rudower Chaussee 25, 12489 Berlin, Germany

F. Wenzel and J. Zschau (eds.), *Early Warning for Geological Disasters*, Advanced Technologies in Earth Sciences, DOI: 10.1007/978-3-642-12233-0_14,

lowing an interferometric approach (Fleming et al. 2009). Finally, the application of SOSEWIN for SHM purposes at a building in L'Aquila (Picozzi et al. 2009a), a suspension bridge in Istanbul (Picozzi et al. 2009b), and a historical arch bridge in Luxembourg City (Oth and Picozzi 2012) are presented.

14.1 Introduction

Rapid urbanisation, the interconnection of economies and increasing dependence on technology makes modern societies ever more vulnerable to natural disasters. This is particularly true when considering the growth of so called mega cities (defined by the United Nations as metropolitan areas with populations exceeding 10 million), the majority of which are in the developing world. This has lead to the recognition of the importance of Early Warning Systems (EWS) and Structure Health Monitoring (SHM) as means of mitigating the potential human and economic losses resulting from natural disasters (e.g., International Strategy for Disaster Reduction International 2005; United Nations 2006).

Earthquake Early Warning (EEW) systems are typically classified as either Regional (REW) or on-Site early warning (SEW) systems. REW are based on the use of a seismic network located near the expected epicentral area, with the aim of detecting, locating, and determining the 'size' of an earthquake in terms of classes considering recorded ground motions, or directly estimating the magnitude, all based on the analysis of the first few seconds of the initial P-waves. This information is then used in appropriate ground motion prediction equations to estimate the shaking at a specific target, with the warning sent by modern communications means, hence exploiting the much greater speed of electromagnetic signals over seismic waves. Such systems are the optimal solution when the seismogenic area is well known and rather far from the site to protect. By contrast, for target sites too close to a seismogenetic area, SEW systems, which are based on the idea of using seismic sensors directly at the target site, are preferable. Again, by exploiting information carried by the faster P-waves, the size of the larger shaking associated with the incoming S and surface waves may be inferred.

On the other hand, SHM is defined as a set of monitoring strategies and analysis methods devoted to assessing the structural integrity of built structures, and especially to obtain insight into their responses in the event of an earthquake. The experience of catastrophic structural failures that have occurred around the globe in recent years has revealed the need for developing new theoretical and technological approaches for improving SHM. With this aim in mind, engineers in both academia and industry have been recently engaged in developing and implementing damage detection systems and methods for monitoring the health of structures such as bridges, buildings, dams, tunnels, and pipelines.

Until few years ago, an extensive implementation of EWS and SHM systems was limited by both the high cost of the necessary instrumentation, and by the constraint of communicating the data to centralised processing and archiving facilities. Only

in recent years have rapid improvements in telemetry technology and the general decrease in communication costs permitted a growing interest in low-cost wireless sensing units. First attempts at exploiting wireless communications technology for SHM were presented by (Straser and Kiremidjian 1996, 1998), who showed that wireless monitoring systems are feasible, reliable and cost-effective. From those pioneering works, several other studies have dealt with the development of such systems, taking advantage of the continuous and rapid improvements in wireless technology (e.g., Lynch 2002, 2003; Grosse et al. 2008; Krüger et al. 2005).

More recently, Fleming et al. (2009) discussed within a seismological context the vision of providing the wider community with EEW systems made up of large numbers of low-cost instruments relying on modern wireless technology, what was termed the *Self-Organising Seismic Early Warning Information Network* (SOSEWIN). SOSEWIN was developed by the *Helmholtz-Zentrum Potsdam Deutsches GeoForschungsZentrum* (GFZ-Potsdam) and the *Humboldt University of Berlin* (HU-Berlin) within the framework of the European projects Seismic eArly warning For EuRope (SAFER)[1] and Earthquake Disaster Information systems for the Marmara Sea region (EDIM, Turkey).[2] The development of the SOSEWIN focused on two points. The first was the design of the low-cost sensing node themselves, while the second was its self-organising, decentralised character. The originality of both of these aspects of the SOSEWIN distinguished this network from more traditional types. Other specific features of SOSEWIN are Fleming et al. (2009):

- Each seismological sensing unit or *Sensing Node* is comprised of low-cost "off-the-shelf" components, with each unit initially costing several hundred Euros, in contrast to 1,000–10,000's for standard seismological stations;
- Each sensor undertakes its own on-site seismological data processing, preliminary analysis, archiving, and communication of data as well as early warning messages. Moreover, each sensor will also have the capacity to measure other environmental parameters (e.g., noise, temperature etc.);
- The reduced sensitivity of the SOSEWIN sensors compared to standard instruments (due to the use of lower-cost components) is compensated by the network's density, which in the future is expected to number 100–1000's of units over areas served currently by the order of 10's of standard stations;
- The SOSEWIN is intended to be a decentralised, self-organising ad-hoc wireless mesh network;
- The early warning decision is carried out within the wireless mesh network of sensing units, taking advantage of their communication capability and the design of a suitable alarming process. Thus, the alarming itself can be done both inside the network (i.e., flooding the alarm to every node), and outside of it, i.e., routing the alarm to the nearest, what is termed gateway node, from which it is sent to some external disaster management/warning centre;
- Its self-organising capability will allow it to adapt continuously to changing circumstances, e.g., the addition/removal/malfunctioning of nodes, interference in

[1] http://www.saferproject.net

[2] http://www.cedim.de/EDIM.php

communications due to local (and possibly time-varying) phenomena, loss of sections of the network following an earthquake etc.;
- Instruments will also be purchasable by the public. Thus, the SOSEWIN will also be able to integrate additional data from private persons to public networks;
- For rapid response purposes in the post-event timeframe, the much higher instrumental density of SOSEWIN means that tools such as ShakeMap (Wald et al. 2006) can rely more on real data, and less on interpolation schemes.

These features make the SOSEWIN system a particularly versatile tool, and for this reason, in the last years, SOSEWIN applications and tests have been presented, considering both EEW and SHM networks. This work presents a summary of these applications and describes the current state of the development of the SOSEWIN.

The first section describes the SOSEWIN sensors. Concerning EEW applications, tests carried out with SOSEWIN in Istanbul, Turkey, where a prototype test-bed consisting of a network of 20 sensors is installed (Oth and Picozzi 2012; Fischer et al. 2009), are presented. Furthermore, Picozzi (2012) presented a novel approach for EEW that exploited the SOSEWIN philosophy for obtaining, in the event of an earthquake, a real-time structural response assessment by an interferometric approach.

Finally, the application of SOSEWIN for SHM purposes is presented for a number of test cases: a building in L'Aquila following the M = 6.3 2009 event (Picozzi et al. 2010), a suspension bridge in Istanbul (Picozzi et al. 2009b), and a historical arch bridge in Luxembourg City (Oth and Picozzi 2012).

14.2 SOSEWIN Sensing Nodes's Hardware, Software and Communication

14.2.1 Hardware

The hardware of a SOSEWIN sensor consists of three main parts: the digitizer board, the Wireless Router Applications Platform (WRAP), and the sensors. In addition, each unit has a GPS for timing and positional information. All components are bought off-the-shelf, with the exception of the digitizer printed circuit board developed within GFZ Potsdam, and all are installed in waterproof outdoor metal cases of reduced dimension and weight. This reduces the cost of the sensors, leading to them being much less expensive than standard seismometers (about 700 € per unit). Figure 14.1 provides a view and schematic overview of the architecture of a SOSEWIN sensor, with some technical details listed in Tables (14.1, 14.2 and 14.3).

The Analog-to-Digital Converter (ADC) board (Fig. 14.1c, Table 14.3) was designed as a low-cost solution, but can still consider special seismic requirements as there are high resolution, anti-alias filtering tools, exact time marks and good time stability included in its design. The board is equipped with either a4- or 8-Channel ADC. These ADCs have a resolution of 24 bits (effectively 19 bits in low-power

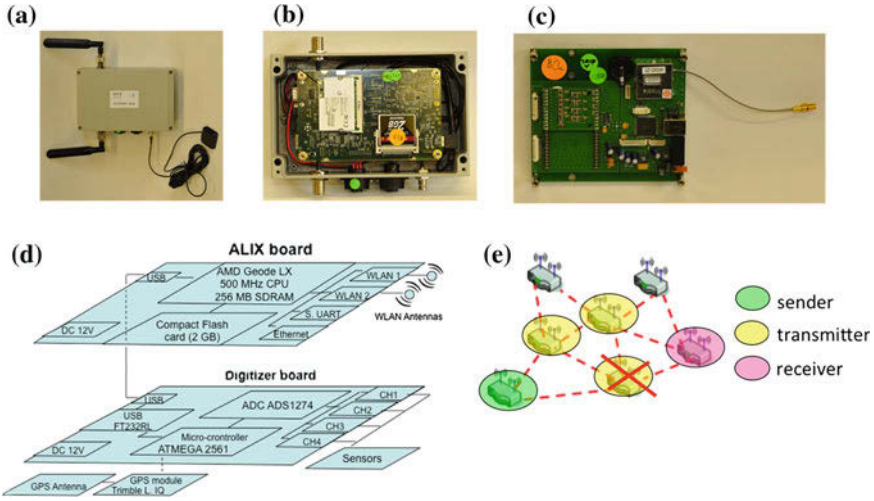

Fig. 14.1 The sensing units employed by the SOSEWIN system. **a** The complete unit. **b** The WRAP board. **c** The ADC board. **d** A schematic overview of the architecture of a sensing unit. Technical details of the various components are listed in Tables (14.1, 14.2 and 14.3). **e** Schematic representation of the routing for communications within the SOSEWIN

Table 14.1 Technical specifications of the SOSEWIN low-cost sensing units

Technical data	
Size	$200 \times 150 \times 80\,\text{mm}^3$
Weight	1.1 kg
Power consumption	~5 W@12 V
2 × WLAN	2.4 GHz / 5.7 GHz /LAN (opt.)
Power supply	10–15 V DC
ADC	4 × ADC (24 bit)
Sensors	Ext. geophones / Internal 3 axis MEMS-accelerometers
GPS receiver	External GPS antenna input

mode, and 20 bits in high-resolution mode), with the sampling rate selectable from 100 to 400 samples per second (sps), although at present 100 sps is being used.

The WRAP board has the three roles: analysis, communications, and storage of data (Fig. 14.1b, Table 14.2). It is made up of an embedded PC that uses a Compact Flash card (currently 2 GBytes, but easily increased) as a hard disk.

The sensor is designed to accommodate different kinds of sensors, since the ADC board has four or eight channels and hence is able to host different modules at the same time, thus leading to the use of instruments considered to be suitable for monitoring different parameters. Accelerometric sensors based on MEMS (Micro Electro Mechanical Systems), originally designed to serve as controllers for air bag safety units, but which have also been successfully incorporated into various seismic

Table 14.2 Technical specifications of the various components that make up the wire router applications platform board as currently used in the SOSEWIN sensing units

ALIX board	
CPU	AMD L × 800 (500 MHz)
Dynamic random access memory (DRAM)	256 MB synchronous dynamic random access memory (SDRAM)
Operating system	OpenWRT
Storage	Compact flash card, currently 2 GB
Power consumption	3–5 W at 12 V DC (excluding miniPCI cards)
Safety features	Watchdog timer built into the CPU, LM77 thermal monitors
User interface	Three front leds, console I/O redirected to serial port
Possible expansions	LPC bus for adding more serial ports, ISA style I/O, GPIO and I^2C bus
Connectivity	One ethernet channel (National DP83816), two miniPCI slots, one serial port
BIOS	tinyBIOS version 1.11
	LAN (10/100)
	2 × USB

networks (Holland 2003), as well as for field acquisition by the exploration sector (Hons et al. 2008), can be incorporated into a sensor and arranged to provide three component data. Furthermore, especially within the framework of SHM activities involving the recording of structures' vibrations, a preamplifier board (Table 14.1), and standard geophones, as well as any other passive sensor, can be connected to the sensing unit.

14.2.2 Software

The main software operating on the SU currently consists of the following:

- OpenWRT: The operating system for the WRAP boards (OpenWRT 2009) with Linux kernel 2.6.22 (Torvalds 2009). OpenWRT is an open-source freely available and highly configurable distribution. By default, it contains only the minimum that is required to run Linux, so that it can run on very size-limited systems. Moreover, it provides an environment for building your own Linux distribution for several platforms, including our x86er target platform for the WRAP boards.
- Data-provider: The program that handles the data streams from the digitizer board, and then archives them via SeedLink (SeisComP).
- SeedLink (SeisComP): The Seismological Communication Processor (SeisComP) is an open-source software package and concept for near real-time seismic data

Table 14.3 Technical specifications of the various components that make up the ADC board as currently used in the SOSEWIN sensingunits

ADC board (GFZ)	
Number of channels	Four (eight Ch. Opt.)
AD convertor resolution/effective resolution	24 bit, effective 19 bit (20 bit in HR Mode)
Input voltage range	+/−2.5 V
Input impedance	10 k Ω
Bit weight	0.3 μ V (30 nV with preamp of gain 10)
Sample rate	Sample Rate:100 sps (200 & 400 sps not yet by software supported)
Signal bandwidth (−3dB)	50 Hz/fs/2
Stop bandwidth attenuation	>100 dB
Analogue anti-alias filter	
Timing	Onboard GPS receiver for timing & Position data
Timing accuracy	Time base better 2.5 ppm
Digital output	USB (1 × virtual com-port, 115 kBaud data/GPS)
Temperature range	−20° to +70°C
Power supply	9–18 V (on board DC/DC converter) or +5 V (USB)
Power consumption	540 mW (low power mode) / 720 mW (high resolution mode)
Different modules available	
MODULES	
MEMS accelerometer	3 axis, +/−1.7 g
	Resolution ∼0.2 mg (rms)
	Tilt Resolution ∼0.01° (Temperature correction required)
Preamplifier	4 Channels
	Gain × 10 (default, set by R)
	Noise ∼ 80 nV(rms) @100 sps
Geophones	3D SM-6/B 4.5 Hz, or any other passive geophone

distribution,[3] developed by the GFZ for a networked seismographic system. In particular, in a seismic network, SeisComP is responsible for the following tasks: data acquisition, data recording, monitoring and controlling, real-time communication, user access, and automatic (near-) real-time data processing (quality control, event detection and location). The SeedLink program is part of SeisComP, and is the system devoted to the near real-time seismic data distribution, that is, a server protocol based on the Transmission Control Protocol (TCP) (Heinloo 2009). In particular, via SeedLink, the data are sent in the form of 512-byte Mini-SEED packets with a 8-byte SeedLink header. In the SOSEWIN sensors, the SeedLink server stores the data in a ring buffer of configurable size on the Compact Flash card. The data in the ring buffer will be kept for the order of 20 days. If more storage is found to be necessary, then it is simply a case of using a larger Compact Flash card.

[3] http://geofon.gfz-potsdam.de/geofon//SeisComP/seedlink.html

- Optimized Link State Routing (OLSR Project 2009): OLSR is a table-driven pro-active routing protocol currently chosen for the wireless mesh network.[4] As a proactive protocol, it periodically assesses and maintains the network topology by flooding information about its direct neighbourhood throughout the whole network. OLSR has proven that it is capable of operating with hundreds of nodes, and it is also widely accepted by several mesh networking communities, i.e., the Freifunk[5] and Funkfeuer[6] projects.

14.2.3 Communications

Each unit has two omni-directional dual-band antennas with opposite vertical polarization. The communication of seismic data and information throughout the network is based on the routing concept. The term routing refers to the procedure of selecting within a network the paths along which data can be sent from a source to a sink. Routing activities within a wireless network are made more complicated by the fact that all nodes act contemporarily as senders, transmitters and receivers of data (Fig. 14.1e).

As stated above, SOSEWIN relies on the OLSR protocols as the routing strategy, and it is these protocols that allow a network of sensors to form a self-organizing ad-hoc wireless mesh network with the ability to adapt to a network's changing state (see above, Fig. 14.1d) in order to maintain optimal communications (Fleming et al. 2009). The main advantages of wireless mesh network for seismic noise array surveys within urban environments are (1) the system is free from cable usage, thus, allowing improved array geometries, and azimuthal coverage, (2) in the case of large arrays, data can also be transferred to a user by multi-hop communications from those instruments that are not in a light-of-sight with the user itself or are too distant (remote stations).

The OLSR that the SOSEWIN employs is a *proactive* routing protocol, where every node has a map of the complete network topology, allowing data to be immediately sent along the optimal path towards the users or the gateways. This leads to each node having a routing table that describes the most efficient way to reach every other node. It makes use of advanced metrics, i.e., measurement methods, for the evaluation of a multi-hop path within the network.

Within SOSEWIN, seismic data are transferred among stations using a multi-hops strategy by means of the SeedLink protocol (i.e., by 512-byte Mini-SEED data packets), with a rate of up to 54 Mbps in both the 2.4 GHz and 5 GHz unlicensed bands. In the case of a low signal-to-noise ratio in the communications, the WLAN cards driver can automatically decrease the rate of transmission. Tests performed within the framework of seismic early-warning activities in Istanbul, Turkey, using

[4] http://www.olsr.org

[5] http://www.freifunk.net

[6] http://www.funkfeuer.at

instruments with the same software and a similar hardware configuration showed that WLAN communications between line-of-sight stations equipped with omni-directional antenna is possible until a distance of ca. 250 m within an urban context (Fleming et al. 2009).

14.3 EEW Applications

14.3.1 Test Deployment in Istanbul, Turkey

The first test-bed deployment of the SOSEWIN was carried out in June, 2008, with a network of 20 stations installed in the Ataköy district of Istanbul (Fig. 14.2). Istanbul is a mega city (population 14 million) that is under significant risk from earthquakes, being located at its nearest point only 10's of kilometres from the North Anatolian Fault, along which there have been a number of large earthquakes over the past century, the most recent being the 1999 Izmit (August 17th, M = 7.4) and 1999 Düzce (November 12th M = 7.2) earthquakes. In response to this seismic threat, there is currently in operation the Istanbul Earthquake Rapid Response and Early Warning System IERREWS (Erdik and Apaydin 2005). IERREWS consists of 100 strong motion recorders in the densely populated areas of metropolitan Istanbul in dial-up mode, and 10 on-line sensors located as close as possible to the Great Marmara Fault, the information obtained being used for emergency action purposes. SOSEWIN would therefore complement the existing network, especially in its ability to "fill in gaps".

The aim of the test-bed installation was to gain experience in establishing wireless networks in an urban environment, and assessing the reliability of the communications between nodes and of the detection algorithms (i.e., setting different thresholds for different sites). Figure 14.2 shows the location of the SOSEWINs, including the two gateways than were connected to the Internet via DSL and allow the data to be transferred in real-time from Istanbul to a Seiscomp Server at GFZ-Potsdam. From there it was distributed to third parties (e.g., the Kandilli Observatory and Earthquake Research Institute, Istanbul, Humboldt-Universität zu Berlin). As said before, the SeisComP performs automatic (near-) real-time data processing (quality control, event detection and location). Thus, centralised early warning activities related to SOSEWIN are being carried out at GFZ-Potsdam. Since the installation of the test bed, no significant seismicity has been observed close to Istanbul that produced strong ground motion at the target sites. For this reason, preliminary tests about the SOSEWIN's performance during strong motion were performed off-line using simulated data (Fig. 14.3).

In particular, earthquake scenarios were produced by means of a synthetic sensor data generator and stored within a model repository. Then, these synthetic data where transferred through the gateways within the SOSEWIN network in Istanbul, where the sensors played the signal analysis and the early warning tasks as if the earthquakes

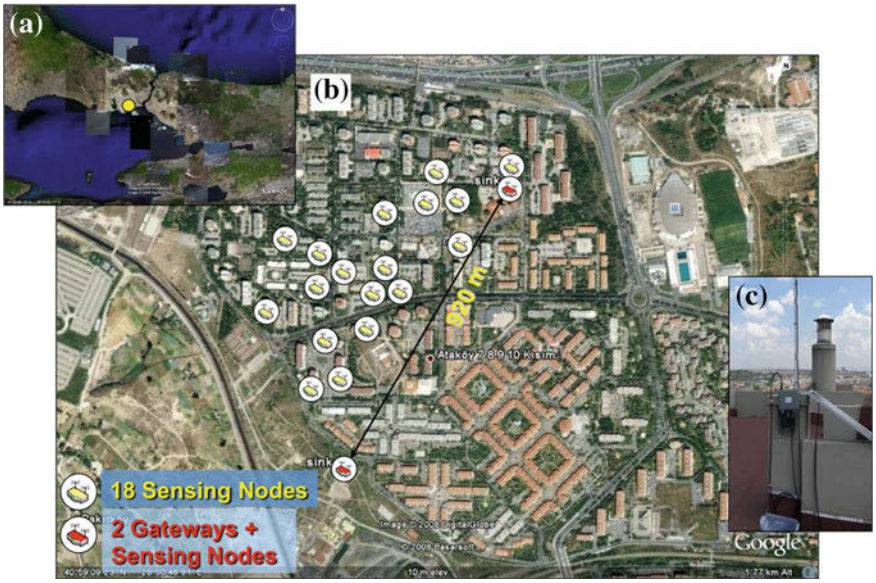

Fig. 14.2 **a** Location map of Istanbul showing the Ataköy district, where the test-bed SOSEWIN is situated. **b** The location of the sensing nodes and gateways for the test SOEWIN in the Ataköy district, Istanbul. **c** A typical SOSEWIN sensing node installation (from, Fleming et al. 2009)

were really occurring. During these tests, the CPU-load was ca. 20 % of the total available, indicating that the sensors are quite capable of performing the real-time processing of strong motion data (personal communication from HU-Berlin). Other tests of the test-bed's performance have focused on the various issues surrounding communications. A first approach for monitoring the network performance quality is the ETX metric (De Couto et al. 2003). This parameter describes the loss rate of a link between sensors, or in other words, the predicted number of data transmissions required to successfully transmit a packet from one sensor to another. When the ETX equals 1, this represents a perfect connection, while increasing ETX values indicate less reliable links. The advantage of the ETX metric over other more basic parameters (e.g., Hop Count Metric) is that when nodes are not in direct contact and communications occurs over a few hops, the ETX metric allows the selection of a route that is optimal with respect to the number of transmissions needed, while also excluding bad quality links from the path. An extensive description of the ETX and other metric parameters can be found in De Couto et al. (2003) and Nachtigall (2005).

In practice, the performance of the mesh network is evaluated by plotting the network topology in terms of the ETX metric. Fig. 14.3b shows an example of such a topology graph for the test-bed SOSEWIN. The quality of the sensors connections is represented using three ranges of values for the ETX metric: from 1 to 3, which is considered a good link, meaning that on average it is necessary for 1 to 3 transmissions

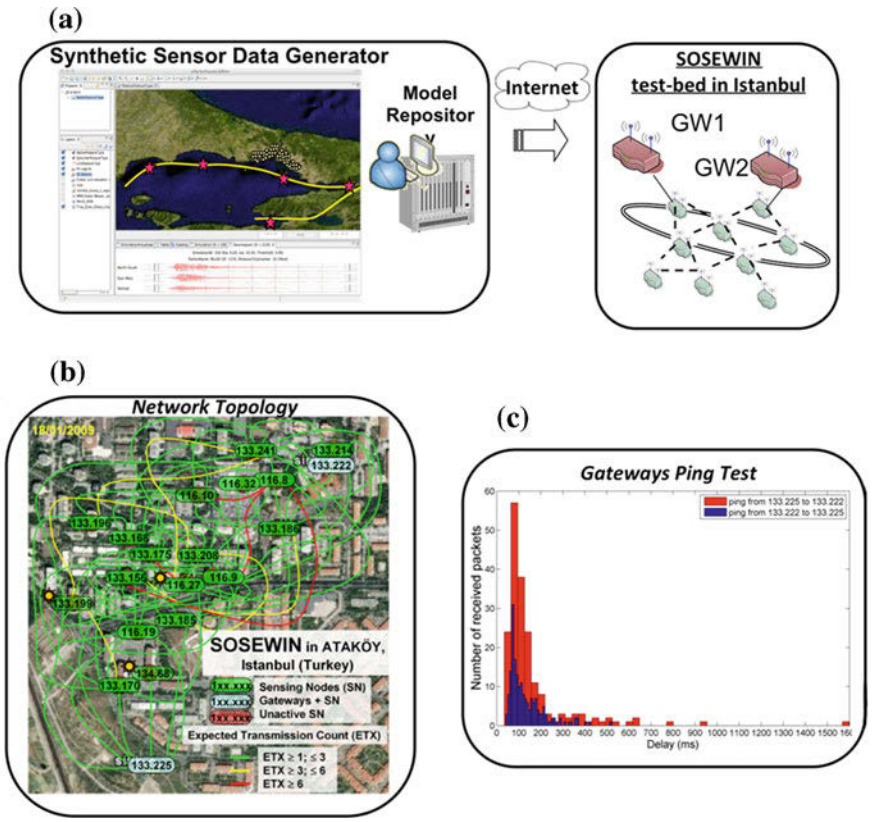

Fig. 14.3 **a** Schematic representation of tests carried out with synthetic data and the SOSEWIN test-bed network in Istanbul, Turkey. **b** Monitoring of the SOSEWIN communication performance by link qualities. **c** Results of the test where 520 byte packages were transmitted 200 times between the two SOSEWIN gateways (in both directions). Note that most packages arrived in less than 100 ms

to ensure a 38 byte packet is successfully transmitted, from 3 to 6, meaning it requires 3–6 attempts for a successful transmission, and higher than 6. It is worth noting that the SOSEWIN test-bed was found to be a high-quality mesh network, with all nodes able to communicate throughout the network, with most connections showing a low ETX value. The next test of the network's performance was to verify the capability of sensors to share warnings about an incoming event in a short time using the multi-hop way. For this purpose, we simulated the transmission of warning between the 2 gateways, which are separated by about 900 m, and we selected the size of the warning-packet to be 520 byte, which is a realistic size for a multi-parameter message. Moreover, the multi-hop transmission of the warning-packet was repeated 200 times in each direction between the sensors. Figure 14.3c shows a histogram that summarises the results of this test. The results for each direction look very

similar, indicating the good quality of communications, hence the independence of the network alarming performance with respect to the direction of the incoming threat. In total, 95 % of the packets reached their target gateway, and the expected time taken for the transmission (found from the mode of the distributions) is 80 and 74 ms from south to north, and north to south, respectively. Considering that the distance between the SOSEWIN gateways is about 900 m, the observed delays indicate that the warning-packets travelled with an effective velocity of about 11.5 and 12.5 km/s, respectively, which is much faster than apparent P-wave velocities (5–7 km/s).

Despite the preliminary character of these tests, the network communication performance of SOSEWIN in Istanbul has given us a great deal of confidence in the development of this new kind of system for earthquake early warning.

14.3.2 Real-Time Early Warning and Structural Response Assessment by an Interferometric Approach and SOSEWIN Sensors

The seismological approaches to EEW have typically been seen as the main application of the real-time characterization of an event's location and size. However, while it is important to note that this information can provide an indication of the expected ground motion at a target site, and specifically, at the base level of a structure, it does not provide any information about the structure's response to the incoming shaking. For this reason, in recent years earthquake engineers have focused their attention on possible strategies to design and exploit EEW systems for real-time structural controls that aim at better preparing structures to respond to earthquakes. For instance, Iervolino et al. (2009) stressed that for the earthquake engineering community, the most advanced EEW application involves structural controls, and, when available, the early warning information should be exploited through active or semi-active control systems.

In the wake of extending EEW to structures Picozzi (2012) presented a method for real-time structural response assessment that combined interferometry and wireless accelerometric sensors such as SOSEWIN units. The key concept of interferometric analyses as applied to structures is the estimation, by the deconvolution of signals recorded at different levels of the structure, of functions termed *impulse response functions* (hereafter IRF) that describe the physical response of a building to an input impulse. Under the assumption that a structure is a linear time-invariant system over the entire duration or a segment of the earthquake shaking, the structure's IRF can be represented in the time domain by the superposition of waves that propagate from the soil through the structure and waves that are reflected at internal impedance contrast boundaries (Kanai 1965). The use of interferometry for assessing the structural response was originally proposed in SHM applications by Snieder and Şafak (2006), who focused their analysis on S-wave earthquake signals recorded at different building levels.

Innovatively Picozzi (2012) extended the application of interferometry to EEW using strong motion data from three moderate events recorded with SOSEWIN sensors installed at different levels of the Navelli city hall (L'Aquila, Italy) during the L'Aquila seismic sequence in 2009. In particular, Picozzi (2012) showed that when deconvolving the P-wave recordings from the horizontal components of the sensor located at top of the structure (Thp), or from any other level, with respect to the signals recorded at the base level (Bhp), the P-wave IRF (i.e., IRFp) presented similar characteristics to the IRF obtained when considering a longer portion of the signals that included the higher amplitude S-waves (i.e., IRFs) (Fig. 14.4). Indeed, the IRFp and IRFs (Fig. 14.4) presented very similar characteristics for the first direct and secondary up- and down-going impulses. Similarly to what was observed by Parolai and Richwalski (2004) from the analysis of ground motion recordings obtained in free-field conditions, the similarities between the IRFp and IRFs were explained by considering the presence within the IRFp of converted P-to-S phases related to a high-impedance contrast, which in the case of a building generally corresponds to the soil/foundations interface. Similarly, Parolai et al. (2009) employed borehole array data and showed that the propagation of upgoing and downgoing waves is consistant with that of S- and P-waves depending on the analysised component of motion, but independent of the chosen signal window. The similarity of IRFp with IRFs confirmed that the IRF computed using the early P-window from the horizontal component of motion could represent for EEW applications a fair first estimate of the structure's response. For this reason, Picozzi (2012) proposed as a first approach to include the estimation of the real-time structural response via the interferometric analysis of the incoming P-wave signals within a EEW schema (Fig. 14.5).

The EEW schema assumed the availability of an early event characterization (i.e., magnitude, *Mw*, and event location. These pieces of information, which allow one to compute the expected ground motion at the base level of the target structure (i.e., Brune-S spectra, Brune (1970), in Fig. 14.5), could be retrieved by an external REW system, or eventually through the inversion of the accelerometer spectra recorded at the base of the structure. At the same time, an early building response estimation could be obtained through the deconvolution of P-wave signals recorded at selected levels of the structure. Therefore, the estimation of the expected shaking at the different levels could be obtained simply by convolving the Brune-S with IRFp. Finally, a simple decisional rule based on the exceedance of a threshold value of the initial estimation of the inter-story drift (ID, i.e., the relative horizontal displacement of two adjacent floors in a building, expressed as a percentage of the story height separating the two adjacent floors) could be exploited to determine whether or not to issue an alarm.

The innovative aspect of the procedure proposed by Picozzi (2012) is that for the first time, the structural response of a specific target is included within an EEW schema. For this reason, the method was named the '*Tailor-made EEW procedure for buildings*' (hereafter TEEW).

Figure 14.6a shows the result of the convolution between the early event characterization (i.e., the Brune-S spectrum representing the shaking that is expected to affect the structure at its base level) and the early structural response estimation

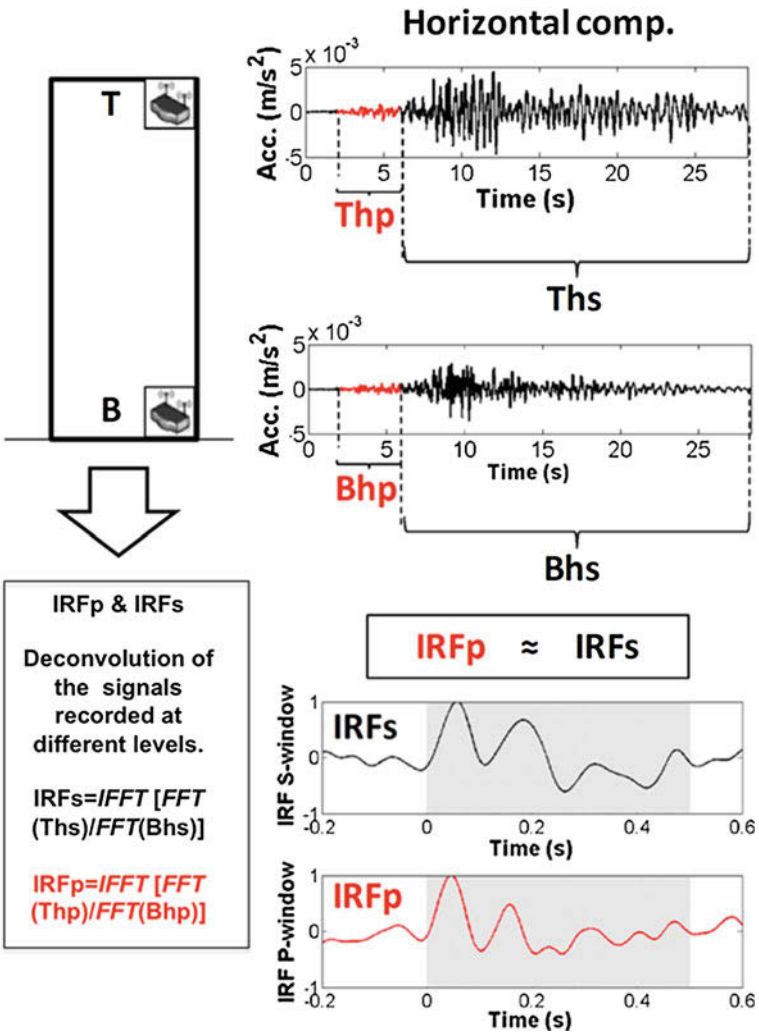

Fig. 14.4 Schematic representation of the target building with accelerometers at the *base* and *top* levels, and earthquake recordings for an aftershock of the L'Aquila seismic sequence 2009 (*see* Picozzi 2012 *for further details*). Recordings for the horizontal component of motion. *Top-level sensor*, 4 s P-window (Thp, in *red*), and S-window (Ths, in *black*). *Base level sensor*, P-window (Bhp), and S-window (Bhs). Impulse response functions for the S-window (IRFs, in *black*), and for the P-window (IRFp, in *red*)

(i.e., IRFp) determined by deconvolving the signals Thp and Bhp, which represent an estimate of the structural response to an impulsive input. The resulting convolution therefore represents the expected structural response at the top level of the structure for the specific event under analysis (i.e., the early warning spectrum at top '*EW Spectra @ Top'*, Fig. 14.6a right panel). Interestingly, the *EW Spectra @ Top* shows,

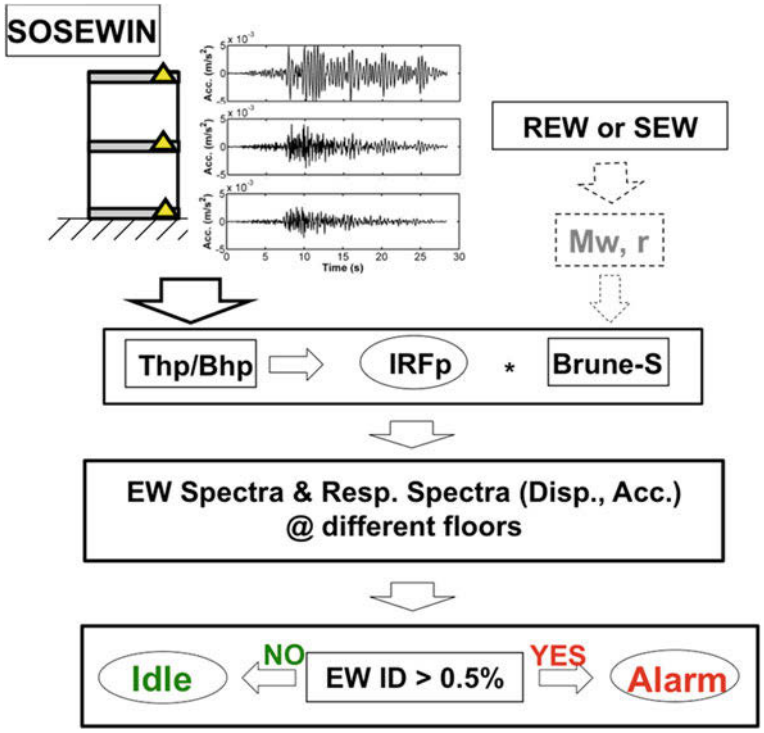

Fig. 14.5 Schematic representation of the TEEW procedure, Picozzi (2012) (See the text for the meaning of the acronyms)

with respect to the theoretical Brune-S spectrum, the presence of peaks and troughs determined by the IRFp characteristics. Figure 14.6b shows in turn the comparison of the *EW Spectra @ Top* obtained using only P-waves with the spectra obtained from the whole event recordings, which also includes S-waves, at the base and top of the structure. Note that differently from the experimental spectrum relevant to the base level, the *EW Spectra @ Top* is able to fairly well reproduce the amplification of the shaking for the same frequencies (i.e., between 2 and 3 Hz) that can be observed in the S-wave spectrum relevant to the sensor on top, and which are clearly related to the structural response (Mucciarelli et al. 2010).

Picozzi (2012) proposed to perform the early assessment of damage for structural and non-structural elements within a building of interest by considering the inter-story drift (ID). In particular, he proposed, as a first example of the decisional rule for the EEW system, that an alarm should be issued in the event that the maximum inter-story drift exceeds at one of the building's levels a threshold value of 0.5 %, which has been observed to represent a reliable threshold of damage for RC buildings (Ponzo et al. 2010). We should comment that usually the maximum inter-story drift is computed in the *post-event time-frame* using time domain displacement time series

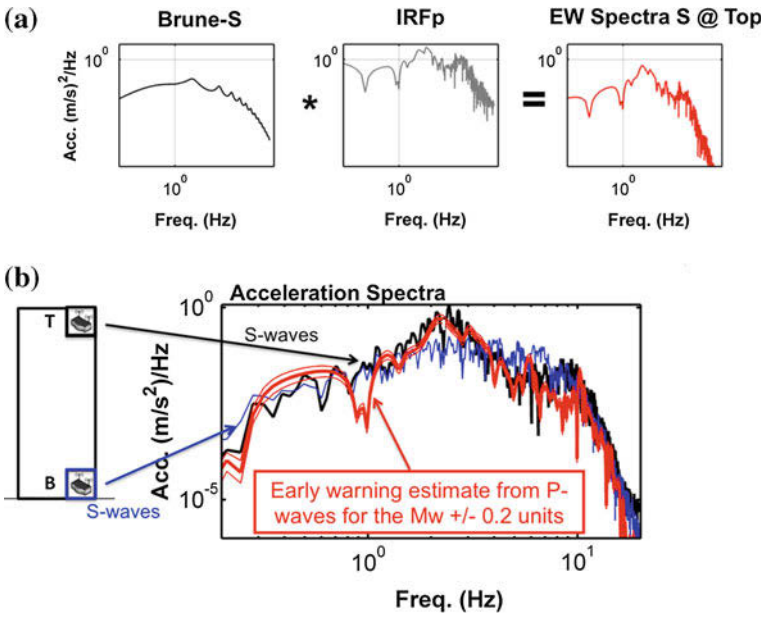

Fig. 14.6 Acceleration spectra for an aftershock of the L'Aquila seismic sequence 2009 (*see* Picozzi 2012 *for further details*). **a** Brune-S spectrum (*black*), IRFp (*gray*), and their convolution named EW Spectra S @ *Top* (*red*). **b** Schematic representation of the target building with accelerometers at the *base* and *top* levels. *Curves* relevant to the sensor at the *base* level (*blue*), the sensor at the *top* level (*black*), the TEEW estimate (*red*), and TEEW estimates for the best-fit Mw +/−0.2 units (*thin red*)

recorded at the different levels of a structure. Clearly, for EEW applications, such an approach cannot be followed. For this reason, the maximum inter-story drift was estimated directly from the EEW estimates of the displacement response spectra (RSD) obtained at the different building levels. In particular, the inter-story drift at the building level '*I*' is computed for different periods as:

$$ID_i(t) = 100 \cdot (\mathrm{RSD}_i(t) - \mathrm{RSD}_{i-1}(t))/\mathrm{Hf}, \tag{14.1}$$

where Hf is the inter-floor height.

Figure 14.7 shows the comparison of the inter-story drift ID(t) computed considering both the whole earthquake's signals, and a EEW estimation. Interestingly, the EEW estimates of inter-story drift for both building levels were in very good agreement with the full record estimates. Moreover, the maximum inter-story drift values were found to be over a range of periods that correspond well to the fundamental resonance period of the structure. Finally, the maximum inter-story drift values that resulted are much smaller than the threshold value of 0.5 % selected to issue the alarm, well in agreement with the macroseismic study presented by Mucciarelli et al. (2010), who indicated that after the damage related to the main

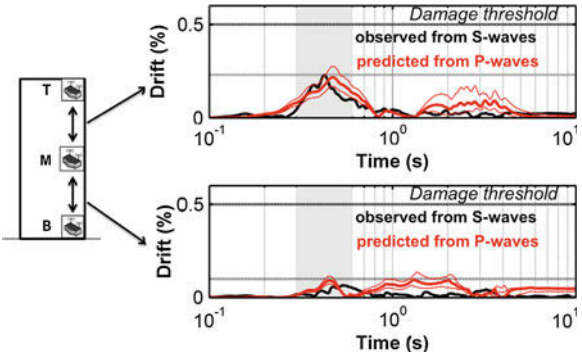

Fig. 14.7 Schematic representation of the target building with accelerometers at the *base*, *middle*, and *top* levels. Inter-story drift estimates for an aftershock of the L'Aquila seismic sequence 2009 (*see* Picozzi 2012 *for further details*). Sensor at the *top* level (*upper panel*), and sensor at the first level (*lower panel*). *Curves* relevant to the ID(*t*) for the whole event recording (*black*), for the TEEW estimate for the best-fit Mw (*thick red*), and for TEEW estimates for the best-fit Mw $+/-0.2$ units (*thin red*). Finally, the maximum inter-story drift (*dashed gray*), and 0.5 % ID threshold (*dashed black*)

shock, the building under study did not show evidence of evolving structural damage during the aftershocks sequence (i.e., which includes the event analysed by Picozzi (2012).

14.4 SHM Applications

14.4.1 Real-Time Monitoring of Structures in Task-Force Missions: the Example of the Mw = 6.3 *Central Italy Earthquake, April 6, 2009*

Soon after the Mw 6.3 Central Italy Earthquake, 6th April 2009, where at least 294 people are known to have died, the German Earthquake Task Force was involved in the installation of a temporary seismological network to support their Italian colleagues (Picozzi et al. 2009a). In particular, under the request and coordination of the Italian Department of Civil Protection (DPC), SOSEWIN accelerometric sensing units were installed within selected strategic infrastructures, both damaged and undamaged, to record aftershocks and undertake the real-time determination of characteristic building parameters (e.g., the Navelli city hall, Fig. 14.8a). This was possible owing to the ease with which SOSEWIN units can be installed and their wireless communication capacity, which allowed safe, remote access to the acquired records. As a result, the SOSEWIN system installed at Navelli provided a large data set of more than fifty

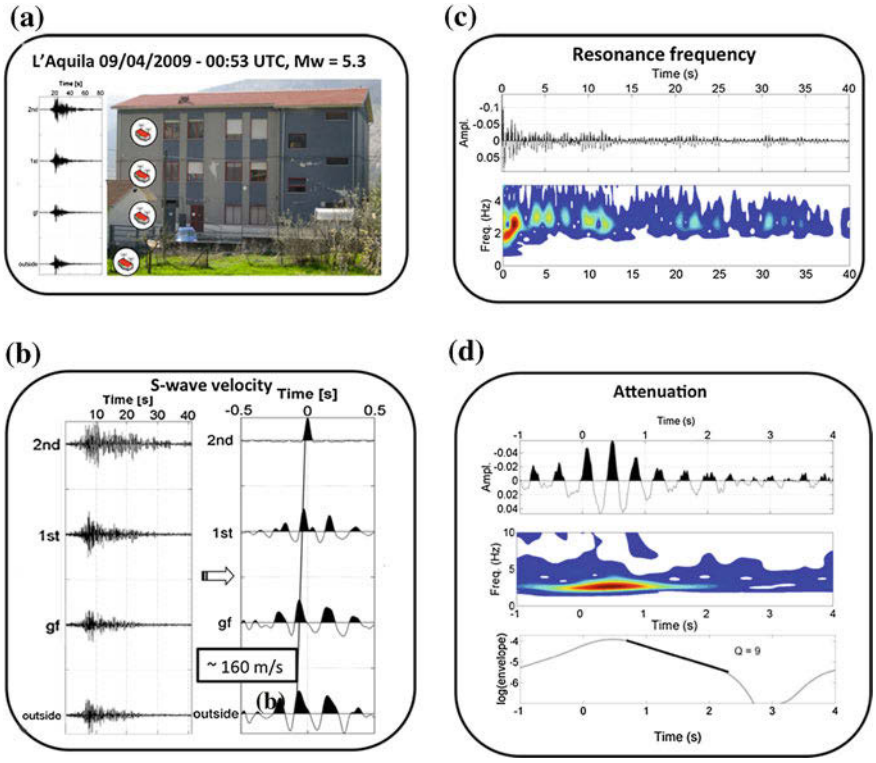

Fig. 14.8 **a** The Navelli's city hall. From the 8th April, 2009, three wireless accelerometric stations were installed on different floors of the Navelli municipality building, with one station deployed outside of it. **b** Signals recorded at the different levels during the strongest aftershock recorded by the SOSEWIN (*left panel*) during the L'Aquila seismic sequence 2009 (*see* Picozzi et al. (2010) *for further details*), and impulse response functions from interferometry (*right panel*) using the sensor at the top of the Navelli city hall as the reference. **c** Impulse response function for the 2nd floor using the signal at the base of the building as the reference (*upper panel*), and its S-transform representation (*lower panel*). **d** Estimation of the quality factor Q. Impulse response functions for the 2nd floor (*upper panel*), its S-transform representations (*middle panel*), and the natural logarithm of the envelopes of the impulse response functions (*lower panel, gray line*). The best-fitting *straight lines* to the linear portion of the envelopes are also indicated (*black line*), as the estimated Q values

aftershocks with Mw higher than 3 (including the third strongest aftershock, Mw 5.4, of the sequence).

Furthermore, taking advantage of the real time accessibility of the four SOSEWIN unit's data soon after each aftershock, it was possible to monitor the behaviour of the building during the aftershock sequence. In particular, applying the interferometric analysis proposed by Snieder and Şafak (2006), Picozzi et al. (2010) showed that a rapid estimation of the velocity of shear waves (Fig. 14.8) within the buildings could be monitored in real-time. Innovatively, Picozzi et al. (2010) proposed to perform time-frequency analyses, in particular, the application of the S-transform

Stockwell et al. (1996), of earthquake signals recorded within the structure and of the empirical IRF estimated from the deconvolution analysis. Hence, in the former case, the time-frequency analysis of earthquake signals allowed for the better monitoring of the variation in the structure's resonance frequency during the aftershock events (Fig. 14.8c). On the other hand, since the S-transform representation of the IRF directly provides the envelope of the different building resonance frequencies, it is straightforward to apply the procedure proposed by Snieder and Şafak (2006) to estimate the attenuation (i.e. Q values in Fig. 14.8d).

Picozzi et al. (2010) showed that the interferometric analysis method combined with recording systems such as SOSEWIN can allow the real-time characterization of a building's response and damage detection to be performed. In particular, the experience gained in Italy showed that the SOSEWIN opens up new possibilities for the real-time structural monitoring of strategic structures, an especially important task after severe earthquakes when the retrieval of critical data for the rapid assessment of possible damage and structural degradation in structures is urgently needed.

14.4.2 SHM Monitoring of Strategic Infrastructures: the Fatih Sultan Mehmet Suspension Bridge in Istanbul, Turkey

The major threats to the structural integrity of bridges primarily consist of the aging of the structural elements, earthquake-induced shaking and standing waves generated by windstorms. The necessity for information on the state of the health of such structures in real-time that allows for timely warnings in the case of damaging events requires structural health monitoring (SHM) systems that contribute to mitigating the risks associated with these threats.

Prototype structural wireless SHM systems have been already validated by tests performed on bridges and other structures (e.g., Lynch 2003; Wang et al. 2006; Loh et al. 2008), where they have been found to be a highly cost-competitive, completely autonomous and very reliable alternative to traditional wired systems. In order to test the performance of the SOSEWIN system for the SHM of bridges, Picozzi et al. (2009b) performed ambient vibration recordings on the Fatih Sultan Mehmet Suspension Bridge in Istanbul, Turkey, the second gravity-anchored suspension bridge spanning the Bosphorus Strait (Fig. 14.9). These suspension bridges represent critical nodes of the transportation system of Istanbul. Hence, their failure during a strong earthquake is a major threat in terms of both the potential for a high number of fatalities and the substantial interruption of emergency response activities (Apaydin and Erdik 2001). For this reason, the Fatih bridge is also equipped with a traditional vibration monitoring system encompassing 5 Guralp Systems CMG-5TD instruments, which are installed on the bridge (Apaydin and Erdik 2001; Apaydin 2002; Stengel 2009). These instruments are located inside at the edges of the bridge's deck and continuously transmit data to the Kandilli Observatory and Earthquake Research Institute (KOERI).

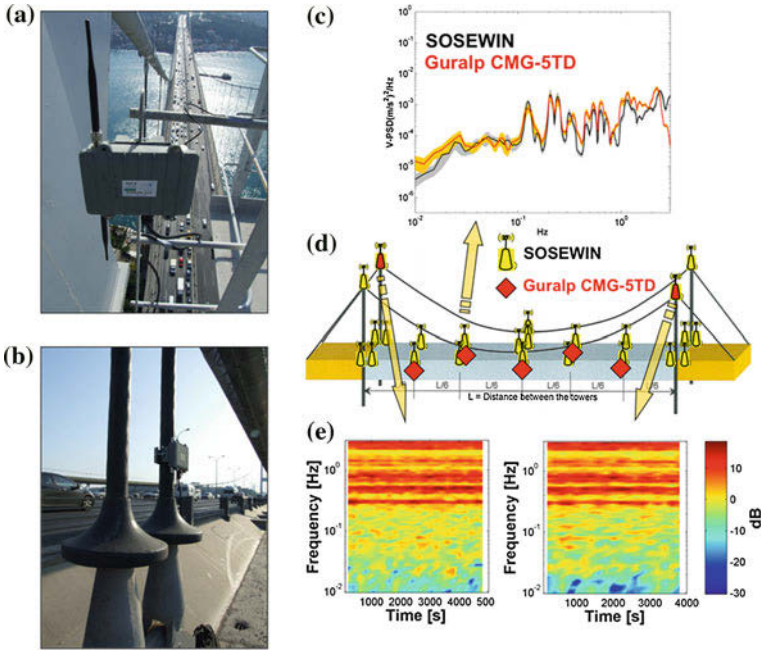

Fig. 14.9 **a** and **b** Examples of sensing node installation during the test measurements carried out with SOSEWIN in June 2008 over the Fatih Sultan Mehmet Bridge in Istanbul, Turkey. **c** Average Power Spectrum Density (PSD) functions plus +/−95 % confidence interval functions for the vertical components of motion for SOSEWIN (*black and grey, respectively*) and Guralp (*red and yellow, respectively*). **d** Measurement positions with SOSEWIN and Guralp instruments. **e** Spectral Ratio (SR) spectrograms for SOSEWIN nodes installed over the bridge's two towers

The measurements with SOSEWIN were performed for a few hours using a network of 24 sensors (Fig. 14.9). This allowed the simultaneous recording of ambient vibrations at different structural elements of the bridge (i.e., with instruments installed along the two sides of the deck, on top of the four towers, and at the base of the two vertical cables in the middle of the bridge). An initial comparison was made between recordings made by SOSEWIN and the Guralp sensors. Figure 14.9c shows the Power Spectrum Density (PSD) functions computed for the vertical components of motion at the sensors located approximately in the middle and one-third of the way along bridge's deck. Despite the SOSEWIN station being located over the bridge's deck while the Guralp sensor was installed inside the deck, the agreement between their PSDs is still strong (Fig. 14.9c). Furthermore, Spectral Ratio (SR) functions were computed using the PSD computed for the 4 reference sensors located outside of the bridge's deck with respect to the other 20 monitored points inside the bridge. Figure (14.9d) shows an example of the SR spectrograms computed for two sensors located at top of the bridge's tower using the transversal component. The SR spectrograms indicate that the ambient vibrations had a stationary character. Picozzi et al. (2009b) showed that the SOSEWIN sensors provided consistent and robust

results, with a clear image of how the various parts of the bridge reacted differently to the ambient vibrations.

Stengel (2009) analyzed the dynamic behaviour of the bridge through the commercial software ARTeMIS Extractor by Structural Vibration Solutions (ARTeMIS 2009) using first a dataset from 7 SOSEWIN instruments, and then an ambient vibration set of 4 of the permanently installed Guralp instruments. The results of the modal analysis of the SOSEWIN recordings were only preliminary, due to the limited time span of the available SOSEWIN data-set, however, it is remarkable that the mode shapes were nonetheless still well estimated. Future modal analysis based on records with longer time periods would benefit from the installation of a denser mesh of monitoring instruments, which could be easily realized using the SOSEWIN system.

14.4.3 SHM Monitoring of strategic infrastructures: the Adolphe Bridge, Luxembourg City.

In areas less exposed to seismic hazard, SHM monitoring still represents an important tool for civil engineers, for instance, if they have to deal with structures exposed to heavy operational demands for extended periods of time and whose structural integrity might be in question or at risk. The continuous monitoring of such structures would allow for the identification of their fundamental response characteristics and any changes of these over time, the latter providing indicators for potential structural degradation. A good example of such a case was represented by the Adolphe Bridge in Luxembourg City. The Adolphe Bridge links the two city quarters on opposite sides of the Vallée de la Pétrusse. This bridge was designed as an open spandrel arch and was officially opened in 1903. Since the bridge connects the Upper City of Luxembourg with the main railway station, it is subject to heavy traffic (in particular, buses), which has considerably weakened the structure over the years since the first renovations that were performed in 1961/62. Moreover, with the LuxTram project[7] which aims to reintroduce tramway traffic to Luxembourg, a major renovation of the bridge is necessary and is expected to be launched in 2012. Following these renovations, the real-time monitoring of the bridge's vibrations could help in assessing the success of these efforts, as well as the bridge's performance on a continuous basis in the future. For these reasons, Oth and Picozzi (2012), as a first step towards proposing a continuous monitoring approach for the Adolphe Bridge and in order to validate the performance of the SOSEWIN system for structural monitoring on such a historical arch bridge (representing a critical infrastructure for the city of Luxembourg), carried out ambient vibration measurements on 11 May 2010, using a dense network composed of 18 wireless sensing units deployed at regular intervals along the bridge deck (Fig. 14.10a). The system was operated for several hours, and it recorded ambient vibrations generated primarily by human activity, that is, by the traffic crossing the bridge. Using these recordings, Oth and Picozzi (2012) analysed the response charac-

[7] www.luxtram.lu

teristics of the Adolphe Bridge and empirically determine the resonance frequencies and modal shapes of the structure, as well as deriving the damping characteristics following the approach proposed by Mucciarelli and Gallipoli (2007). In particular, the modal shapes for the first four modal frequencies of each component of motion were empirically calculated following (Meli et al. 1998). Figure 14.10 shows an example of the normalized modal shapes at two of the investigated modal frequencies on both sides of the deck for the transversal (Fig. 14.10b), vertical (Fig. 14.10c) and longitudinal (Fig. 14.10d) components.

The results of the experiment carried out by Oth and Picozzi (2012) demonstrate the great potential for using the SOSEWIN system as a tool for the permanent monitoring of the Adolphe Bridge following the upcoming renovation works. In fact, SOSEWIN sensors could provide real-time information on the dynamic characteristics of the bridge and their potential modifications that may be of concern, for instance, during heavy storm events.

14.5 Conclusions

In this work, the application of a novel system for earthquake early warning (EEW) and seismic health monitoring (SHM) has been presented. SOSEWIN presents an innovative contribution to such systems, being based on the use of new, low-cost wireless sensing units, specifically designed to form dense wireless mesh networks. These new sensors allow the performance of on-site, independent analysis of the ground motion, and the real-time communication of estimated parameters. Since June, 2008, a test-bed of 20 SOSEWIN sensors has been operating in the Ataköy district of Istanbul. Activities of the network are monitored and data collected in real time by a Seiscomp server installed at GFZ. Until now, no significant seismic activity has been indentified in the area. Preliminary tests of the network communication performance, however, give us confidence in the development of this new kind of system for earthquake early warning. While SOSEWIN is by no means intended to serve as a replacement for existing EEW networks made up of higher quality seismological units, it can nonetheless complement such systems, while also allowing some degree of early warning to be established in areas where more traditional networks are economically prohibitive. We also presented the results of experiments carried out with SOSEWIN during an Earthquake Task Force mission for the structural monitoring of a structure in Italy damaged by the 2009 l'Aquila earthquake in order to present a first off-line application of the building specific EEW procedure. In particular, recording systems like SOSEWIN allow for the real-time characterization of the building's response and damage detection through interferometric analysis. Differently from other EEW approaches, where only the information about the incoming event size is transmitted to the target, the procedure recently proposed by Picozzi (2012) allows a real-time estimation of the effective shaking that a target building has experienced. Finally, several experiments involving the monitoring of a suspension bridge over the Bosphorous in Istanbul, and a historical masonry arch bridge,

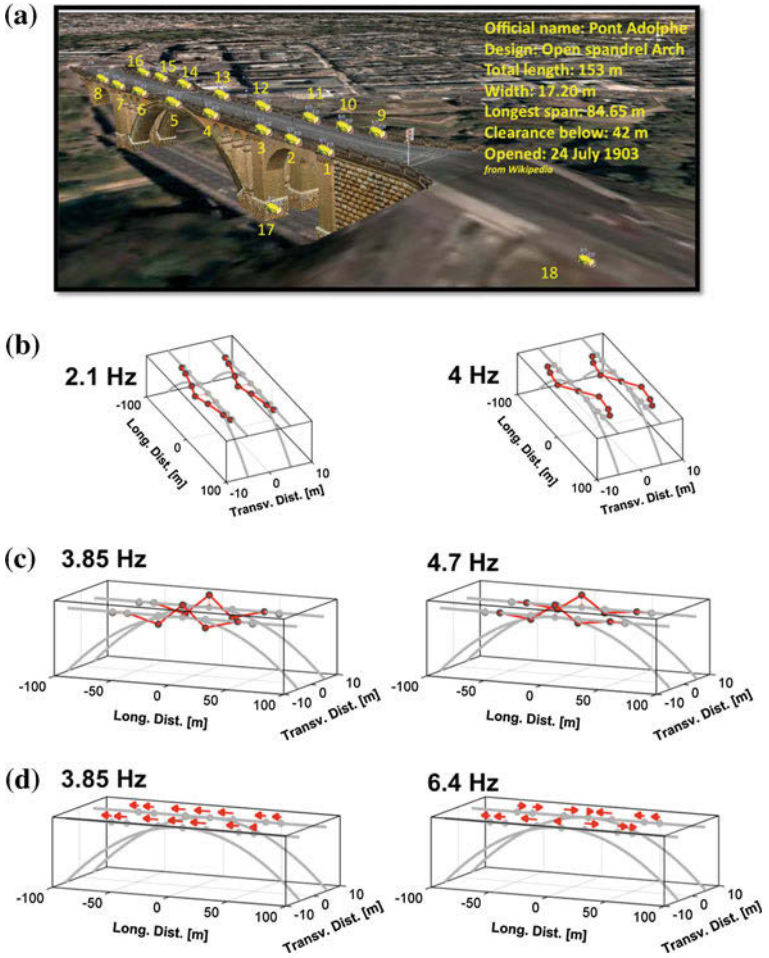

Fig. 14.10 **a** The measurement setup used on the Adolphe bridge, Luxembourg City. **b** Modal shapes (transversal component) illustrating the motion of the entire deck in the transversal direction. Note that the relative amplitude of displacement in the transverse direction is exaggerated. **c** Same as (**b**), but for the vertical component. **d** Same as (**b**), but for the longitudinal component, i.e., compression/dilatation of the bridge deck. Note that the relative direction of motion and amplitude of displacement in the longitudinal direction are represented through the *arrow* direction and length, respectively (see, Oth and Picozzi (2012), for further details)

the Adolphe Bridge, in Luxembourg City, demonstrated that the SOSEWIN system allows new possibilities for the real-time structural monitoring of strategic structures, a fundamental task especially after severe earthquakes, when the retrieval of critical data for the rapid assessment of possible damage and structural degradation in structures is urgently needed. The SOSEWIN system, as seen by the range of applications outlined in this work, shows a great potential for a variety of earthquake

early warning, post-event aftershock recording and structural monitoring under various circumstances. It should again, however, be emphasised that SOSEWIN is not meant to replace existing or higher quality systems, but is intended to complement them.

Acknowledgments The work undertaken in the paper was supported by the Seismic eArly warning For EuRope (SAFER, European Commission proposal no. 036935), Earthquake Data Information system for the Marmara Sea (EDIM, Turkey, German Federal Ministry of Education and Research), PROGRESS (Georisiken im Globalen Wandel) projects, and the German Earthquake Task Force. The establishment of the network in Istanbul was carried out in partnership with Kandilli Observatory and Earthquake Research Institute.
The SAFER and EDIM working groups developing SOSEWIN were: J. Zschau, C. Milkereit, M. Picozzi, K. Fleming, I. Veit, K.-H. Jäckel, J. Nachtigall, and H. Woith (Helmholtz-Zentrum Potsdam Deutsches GeoForschungsZentrum, Germany); J. Fischer, J. P. Redlich, B. Lichtblau, F. Kühnlenz, K. Ahrens, I. Eveslage, and S. Heglmeier (Department of Informatics, Humboldt University (HU) Berlin, Germany). Mike Hönig (Helmholtz-Zentrum Potsdam Deutsches GeoForschungsZentrum, Germany) developed the Analogue-Digital Converters (ADC) board together with one of the authors (K.-H. Jäckel).
We thank M. Erdik, C. Sulfikar, E. Safak·O. Özel and the Bakirköy AKOM staff for their assistance in arranging for and installing the SOSEWIN in Istanbul. We are grateful to M.Mucciarelli, D. Di Giacomo, R. Ditommaso, M. Pilz, and R. Bauz, for the fieldwork during the Task Force mission. The authors wish to thank A. Oth, T. Boxberger, H. Jacob, the *Division des ouvrages d'art* and the *Service géologique* of the *Administration des Ponts et Chaussées*, and in particular Patrick Lenners and Robert Colbach, for their kind support during the planning stage and realization of the experiment on the Adolphe bridge.
The authors wish to thank F. Wenzel and J. Zschau for the invitation to submit our work for this special volume.

References

Apaydin N, Erdik M (2001) Structural vibration monitoring system for the Bosporus suspension bridges. In: Erdik M et al (eds) Strong motion instrumentation for civil engineering structures (NATO Science Series), vol 373. Springer-Verlag, New York

Apaydin N (2002). Seismic analysis of Fatih Sultan Mehmet suspension bridge. Ph.D. thesis, Department of Earthquake Engineering, Bogazici University, Istanbul

ARTeMIS Extractor Pro (2009) Release 4.2, Structural vibrations solutions A/S, Denmark

Brune J (1970) Tectonic stress and the spectra of seismic shear waves from earthquakes. J Geophys Res 75:4997–5009

De Couto DSJ, Aguayo D, Bicket J, Morris R (2003) A high-throughput path metric for multi-hop wireless routing. In: Proceedings of the 9th annual international conference on mobile computing and networking, San Diego, 14–19 Sept 2003

Erdik M, Apaydin N (2005) Earthquake response of suspension bridges. In: Inan E, Kiris A (eds) Vibration problems ICOVP. Springer, pp 181–195

Fischer J, Kühnlenz F, Ahrens K, Eveslage I (2009) Model-based development of self-organizing earthquake early warning systems. In: Proceedings MATHMOD 09 Vienna

Fleming K, Picozzi M, Milkereit C, Kuhnlenz F, Lichtblau B, Fischer J, Zulfikar C, Ozel O (2009) The self-organizing seismic early warning information network (SOSEWIN). Seismol Res Lett 80:755–771. doi:10.1785/gssrl.80.5.755

Grosse CU, Finck F, Kurz JH, Reinhardt HW (2004) Monitoring techniques based on wireless AE sensors for large structures in civil engineering. In: Proceedings of EWGAE 2004 symposium in Berlin, BB90, pp 843–856, 09 Dec 2008

Heinloo A (2009) SeedLink design notes and configuration tips. http://geofon.gfz-potsdam.de/geofon/SeisComP/seedlink.html. Accessed 8 Dec 2009

Holland A (2003) Earthquake data recorded by the MEMS accelerometer. Seismol Res Lett 74:20–26

Hons M, Stewart R, Lawton D, Bertram M (2008) Field data comparisons of MEMS accelerometers and analog geophones. Lead Edge 27:896–902

Iervolino I, Giorgio M, Galasso C, Manfredi G (2009) Uncertainty in early warning predictions of engineering ground motion parameters: what really matters? Geophys Res Lett 6:L00B06. doi:10.1029/2008GL036644

International Strategy for Disaster Reduction (2005) Hyogo framework for action 2005–2015: building the resilience of nations and communities to disasters. In: World conference on disaster reduction, Kobe, 18–22 Jan 2005

Kanai K (1965) Some new problems of seismic vibrations of a structure. In: Proceeding of third world conference on earthquake engineering. Auckland, Wellington, pp II-260–II-275, 22 Jan–Feb 1

Krüger M, Grosse C, Marrón PJ (2005) Wireless structural health monitoring using MEMS. Key Engineering Mat 293–294:625–634

Loh KJ, Lynch JP, Wang Y, Law KH, Fraser M, Elgamal A (2007) Validation of a wireless traffic vibration monitoring system for the Voigt bridge. In: Proceedings of the world forum on smart materials and smart structures technology (SMSST07), Chongqing, Nanjing, 22–27 May 2007. Accessed 09 Dec 2008

Lynch JP (2002) Decentralization of wireless monitoring and control technologies for smart civil structures. Ph.D. thesis, Department of Civil and Environmental Engineering, Stanford University, Stanford. Accessed 09 Dec 2008

Lynch JP, Sundararajan A, Law KH, Kiremidjian AS, Carryer E (2003) Power-efficient wireless structural monitoring with local data processing. In: International conference on structural health monitoring and intelligent infrastructures (SHMII-03), Tokyo, 13–15 Nov. Accessed 09 Dec 2008

Meli R, Faccioli E, Muria-Vila D, Quaas R, Paolucci R (1998) A study of site effects and seismic response of an instrumented building in Mexico City. J Earthq Eng 2(1):89–111. doi:10.1080/13632469809350315

Mucciarelli M, Gallipoli MR (2007) Non-parametric analysis of a single seismometric recording to obtain building dynamic parameters. Ann Geophys 50:259–266. doi:10.4401/ag-3079

Mucciarelli M, Bianca M, Ditommaso R, Gallipoli MR, Masi A, Milkereit C, Picozzi M, Vona M (2010) Far field damage on RC buildings: the case study of Navelli during the L'Aquila (Italy) seismic sequence, 2009. Bull Earthq Eng. doi:10.1007/s10518-010-9201-OnlineFirst

Nachtigall J (2008) Earthquake information system using wireless mesh networks. Magisterarbeit, Humboldt Universität zu Berlin. Geographisches Institut, Berlin, p 138

OLSR Project. http://www.olsr.org/docs/README-Link-Quality.html. Accessed 8 Dec 2009

OpenWRT. http://www.openwrt.org. Accessed 8 Dec 2009

Oth A, Picozzi M (2012) Structural health monitoring using wireless technologies: an ambient vibration test on the Adolphe bridge, Luxembourg City. Adv Civ Eng Hindawi Publishing Corporation 2012(Article ID 876174):17. doi:10.1155/2012/876174

Parolai S, Richwalski S (2004) The importance of converted waves in comparing H/V and RSM site response estimates. Bull Seismol Soc Am 94(1):304–313

Parolai S, Ansal A, Kurtulus A, Strollo A, Wang R, Zschau J (2009) The Atakoy vertical array(Turkey): insights into seismic wave propagation in the shallow-most crustal layers by waveform deconvolution. Geophys J Int. doi:10.1111/j.1365-246X.2009.04257.x

Picozzi M, Ditommaso R, Parolai S, Mucciarelli M, Milkereit C, Sobiesiak M, Di Giacomo D, Gallipoli MR, Pilz M, Vona M, Zschau J (2009a) Real time monitoring of structures in task-force

missions: the example of the Mw = 6.3 Central Italy Earthquake, 6 April 2009, Nat Hazards. doi:10.1007/s11069-009-9481-1

Picozzi M, Milkereit C, Zulfikar C, Fleming K, Ditommaso R, Erdik M, Zschau J, Fischer J, Safak E, Özel O, Apaydin N (2009b) Wireless technologies for the monitoring of strategic civil infrastructures: an ambient vibration test on the Fatih Sultan Mehmet suspension bridge in Istanbul. Bull Earthq Eng 8(3):671–691. doi:10.1007/s10518-009-9132-7

Picozzi M, Parolai S, Mucciarelli M, Milkereit C, Bindi C, Ditommaso R, Vona M, Gallipoli MR, Zschau J (2010) Interferometric analysis of strong ground motion for structural health monitoring: the example of the L'Aquila (Italy) seismic sequence, 2009. Bull Seism Soc Am 101, 2 April 2011. doi: 10.1785/0120100070.

Picozzi M (2012) An attempt of real-time structural response assessment by an interferometric approach: a tailor-made earthquake early warning for buildings. Soil Dyn Earthq Eng 38:109–118. doi:10.1016/j.soildyn.2012.02.003

Ponzo FC, Ditommaso R, Auletta G, Mossucca A (2010) A fast method for structural health monitoring of Italian reinforced concrete strategic buildings. Bull Earthq Eng 8:1421–1434. doi:10.1007/s10518-010-9194-6

Snieder R, Şafak E (2006) Extracting the building response using seismic interferometry: theory and application to the Millikan library in Pasadena. Calif Bull Seism Soc Am 96(2):586–598

Stengel D (2009) System identification for 4 types of structures in Istanbul by frequency domain decomposition and Stochastic subspace identification methods. Diploma thesis, University of Karlsruhe, Karlsruhe

Stockwell RG, Mansinha L, Love RP (1996) Localization of the complex spectrum: the S transform. IEEE Trans Signal Process 44:998–1001

Straser EG, Kiremidjian AS (1996) A modular, visual approach to damage monitoring for civil structures. In: Proceedings of the 2nd international workshop on structural control, Hong Kong

Straser EG, Kiremidjian AS (1998) A modular, wireless damage monitoring system for structures, report no 128. John A. Blume Earthquake Engineering Center, Stanford University, Stanford

Torvalds L (2009) The Linux Kernel. http://www.kernel.org Accessed 8 Dec 2009

United Nations (2006) Global survey of early warning systems. An assessment of capabilities, gaps and opportunities towards building a comprehensive global early warning system for all natural hazards, a report prepared at the request of the secretary-general of the United Nation

Wald DJ, Worden BC, Quitoriano V, Pankow KL (2006) ShakeMap manual; technical manual, users guide, and software guide. http://pubs.usgs.gov/tm/2005/12A01 /pdf/508TM12-A1.pdf

Wang Y, Loh KJ, Lynch JP, Fraser M, Law KH, Elgamal A (2006) Vibration monitoring of the voigt bridge using wired and wireless monitoring systems. In: Proceedings of the 4th China-Japan-US symposium on structural control and monitoring. Hangzhou, China, Oct 16–17 2006. Accessed 09 Dec 2008

Chapter 15
Low Cost 3D Early Warning System for Alpine Instable Slopes: The Aggenalm Landslide Monitoring System

K. Thuro, Th. Wunderlich, O. Heunecke, J. Singer, P. Wasmeier, St. Schuhbäck, J. Festl, Ch. Reith and J. Glabsch

Abstract In course of the alpEWAS (= alpine Early Warning System) research project a cost-effective landslide monitoring and early warning system has been developed between 2007 and 2010. The core of the project has been the development and testing of the three innovative, economically and continuously working measurement systems time domain reflectometry (TDR) for the detection of subsurface displacements in boreholes and reflectorless video tacheometry (VTPS) and low cost global navigation satellite system (GNSS) for the determination of 3D surface movements. These measurement systems are combined together with systems monitoring the trigger factors such as precipitation in a geo sensor network which can be accessed remotely through the internet, thus enabling to forward all data in near real time. The Aggenalm Landslide (Bavarian Alps in the vicinity of Bayrischzell) was chosen as a field laboratory for the alpEWAS project. For more than two years the system has been working continuously except for minor disruptions, acquiring and recording all data.

K. Thuro (✉) · J. Singer · J. Festl
Chair of Engineering Geology, Technische Universität München, Arcisstr. 21,
80333 Munich, Germany
e-mail: thuro@tum.de

Th. Wunderlich · P. Wasmeier · Ch. Reith
Chair of Geodesy, Technische Universität München, Arcisstr. 21,
80333 Munich, Germany
e-mail: th.wunderlich@tum.de

O. Heunecke · St. Schuhbäck · J. Glabsch
Institute of Geodesy, University of Federal Armed Forces Munich,
Werner-Heisenberg-Weg 39, 85577 Neubiberg, Germany
e-mail: otto.heunecke@unibw.de

F. Wenzel and J. Zschau (eds.), *Early Warning for Geological Disasters*,
Advanced Technologies in Earth Sciences, DOI: 10.1007/978-3-642-12233-0_15,

15.1 alpEWAS Project Details

The joint research project alpEWAS—development and testing of an integrative 3D early warning system for alpine instable slopes—aims to combine innovative, efficient and cost-effective measurement techniques for landslide monitoring in a geo sensor network. The project has been funded by the geoscientific research and development program "Geotechnologien" of the German Federal Ministry of Education and Research (BMBF).

Recent events also within the runtime of the research project in the Alps as well as worldwide acknowledge the necessity to design efficient and cost-effective monitoring systems for instable slopes especially for areas that have yet not been monitored or only sporadically due to economic reasons. With the given option of a continuous remote access to the early warning system the stakeholder has the possibility to view and control all information of his scope centrally and to keep the general overview given a situation in which for example due to heavy rainfall several landslides have to be evaluated simultaneously.

The subject of the joint research project is the testing and advancement of three new measurement techniques (Fig. 15.1)

- Time domain reflectometry (TDR)
- Reflectorless video tacheometry (VTPS)
- Low cost GNSS (LCGNSS)

as well as their coaction as an early warning system and their integrative data analysis.

The project alpEWAS (for a closer description see (Singer et al. 2009c; Thuro et al. 2009) and http://www.alpEWAS.de) was outlined in five phases:

1. Selection and investigation of a project area.
2. Design and installation of the early warning system.
3. Learning phase of the early warning system.
4. Testing phase of the early warning system.
5. Automation and optimization of the early warning system.

In the Sudelfeld region—in close reconcilement with the Bavarian Environment Agency (Bayerisches Landesamt für Umwelt, BLfU)—the Aggenalm Landslide has been chosen as a test site since it features very good premises for the testing of new technologies in the field under alpine conditions. During the studies it became obvious that the present movement rates of 1 cm/a are smaller than expected at the initiation of the project and recently only a low hazard potential exists at the Aggenalm. Therefore the assessment of threshold values may be affected or limited (project phase 2 and 3).

Within the scope of the project software applications for the sensor control, data management, complex data processing and integrative data analysis have been developed. After expiry of funding the monitoring of the Aggenalm Landslide is continued by the involved institutes with reduced scope, however.

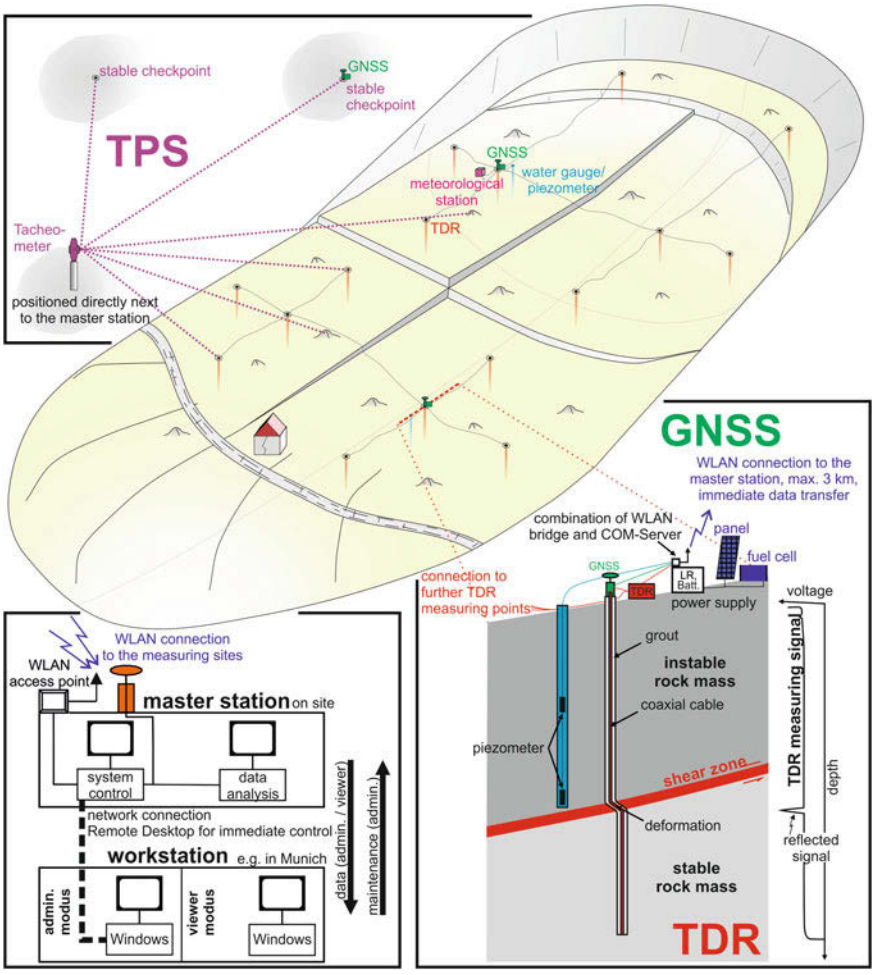

Fig. 15.1 Schematic depiction of the geo sensor network „alpEWAS“ at the aggenalm landslide

A geological review is given by Singer et al. (2009c); the geo sensor network with the technical features is described in Thuro et al. (2010) in detail. Figure 15.2 gives an overview of the different installed sensors of the geo sensor network and their positions at the Aggenalm Landslide.

Consecutively in addition to the aforementioned publications it will be reported on the three measurements techniques, some attained results as well as the combination and analysis of the data.

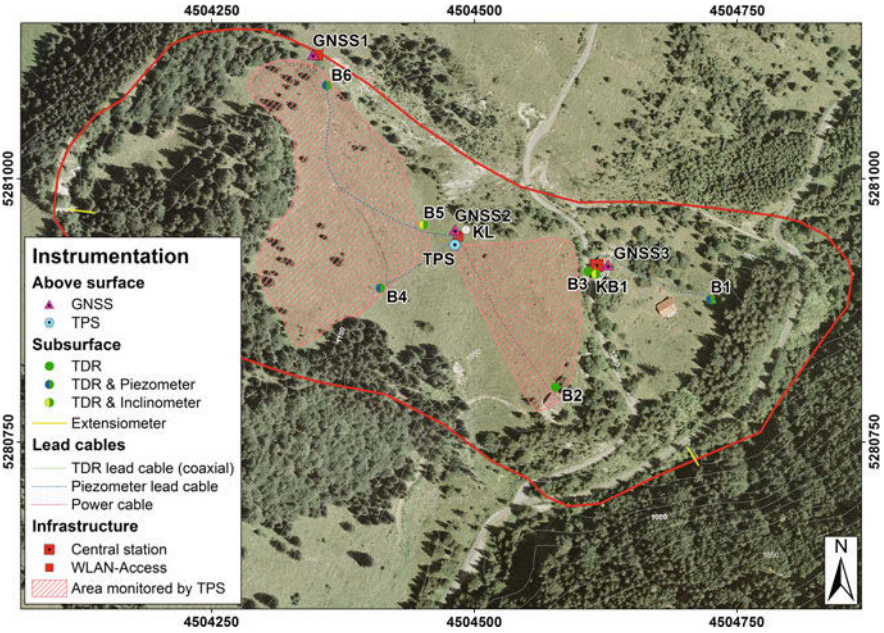

Fig. 15.2 Installation setup of the different sensors installed at the Aggenalm landslide (*red boundary*) depicted in an orthophoto (Singer et al. 2009c)

15.2 Researched Measurement Techniques

15.2.1 Time Domain Reflectometry

Using time domain reflectometry (TDR) to monitor subsurface deformations, a special type of coaxial cable is installed in a borehole. By sending electromagnetic pulses into the cable, changes in the cable's geometry can be detected, thus the amount of deformation is quantified. Several different parameters—the type of cable used (lead and measurement cable) and the grout composition (cement, bentonite, cement additives)—play an important role in the quantification of TDR deformation measurements. These parameters have been determined by means of calibration tests in a comprehensive laboratory program (Singer 2010; Singer et al. 2009b, 2010).

The results of all the laboratory tests combined with experiences from field surveys of the TDR system were incorporated into an installation handbook, which gives standardized installation recommendations consisting of a combination of cable type and grout composition for different geological settings and typical mass movement mechanisms and velocities. Next to the preparation and completion of the installation handbook the TDR deformation analysis software was worked on and refined.

The TDR system, that has been installed at the Aggenalm Landslide, is continuously operating since November 2008 (begin of installation and operation September

2007) and acquires measurements hourly. The TDR system has proven to be a reliable measurement system at large. Over the total period since the beginning of operation, the data loss sums up to about 18 % of the planned measurements mostly because of power shortages and late data retrieval (full data storage before the start of the automatic data acquisition). For the time since the start of the fully automatic data retrieval the data loss adds up to 10 %. Here, a major annoyance in January 2010 accounts for the loss of data. It can be assumed that in future an even higher performance can be achieved due to the automatic data retrieval and data storage as well as the developed Status Monitor Software as the time since February 2010 has already shown.

The field test at the Aggenalm has shown that most of the cables (lead and measuring cables, connectors; mostly installed subsurface) proved to be robust concerning the weather, also during winter. Up to date no significant deformations have been measured with the TDR system at the Aggenalm Landslide, therefore the signal and deformation analysis could only be used and tested for the evaluation of laboratory tests.

Figure 15.3 shows the results of the TDR measurements at the Lampl-Alm (B3) node. Depicted are the reflection coefficient—depth curves as a time series in relation to the reference measurement in October 2008 as well as the results of the inclinometric measurements. The TDR time series shows no measureable deformations, the reflection coefficient doesn't change at all during the depicted time period, only the characteristic noise can be seen. The results of the inclinometric measurements (Fig. 15.3) show slight movements (max. 1–2 mm for KB1). The difference between

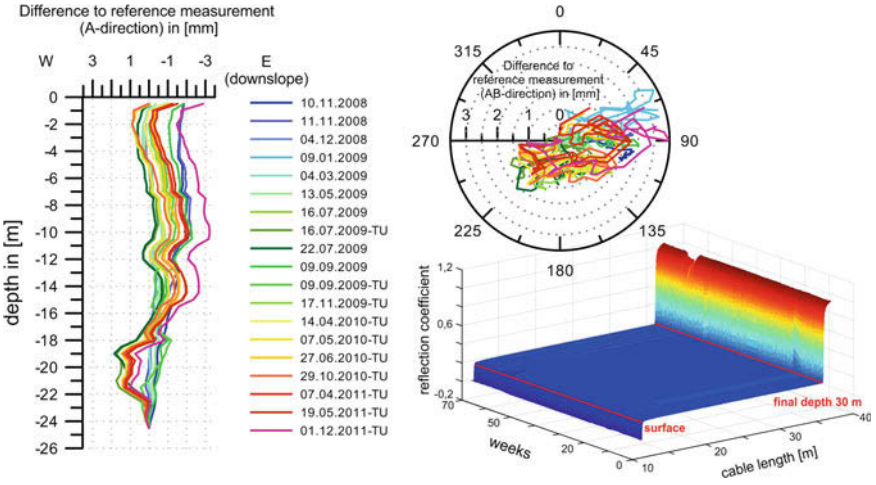

Fig. 15.3 Time series of the inclinometric measurements (*left*) and the TDR measurements (*bottom right*) at the sensor node KB1 and B3 (lower Lampl-Alm). The inclinometric measurements show compared to the reference measurements some small insignificant variations of about 1–2 mm. Over a time span of 70 weeks no deformations (variation of reflection coefficient) can be detected in the TDR measurements

the inclinometric results and the movements measured by the GNSS component (GNSS 3 is located right next to KB1—the inclinometric measurement site) is due to the fact that technical problems arose while establishing KB1; with a depth of about 24.5 m the probable shear zone wasn't reached. The TDR system, which has been installed at a greater depth parallel to KB1 in B3, still does not show any significant deformations, which can be explained by the small amount of deformation which has not yet been able to fracture the grout surrounding the coaxial cable—a prerequisite for a deformation analysis with TDR.

15.2.2 Reflectorless Video Tacheometry

One of the goals of the alpEWAS project was to gain first practical experience in field using an innovative instrument type which is not commonly used for displacement monitoring yet: a video tacheometer (VTPS—video tacheometric positioning system). At this stage the Topcon Imaging Station is the only instrument available on the market which in principle has a video functionality with the necessary precision (Topcon Positioning Systems, Inc. 2008). Other instruments—the Trimble Spatial Station VX and the Leica Viva TS15—could be used only with major cutbacks due to their image resolution and field of view (Leica Geosystems AG 2010; Trimble Navigation Limited 2010). All the instruments mentioned cannot be used scientifically, as the cameras cannot be read out by external devices. External camera control is only possible so far using a Leica Geosystems prototype, which has been coopered in a small batch of only five instruments. It consists of a TPS1200 tacheometer (Leica Geosystems AG 2007) with access to all instrument subsystems, which has been modified with an internal camera (now called IATS2—Image Assisted Total Station 2nd edition). Various limitations by design, especially regarding practical handling, need still to be accepted and have to be abolished by the manufacturer for later marketability. Among others, this includes the tentative cable guiding and the tarring of the modified telescope layout. The prototype is explained in Wasmeier (2009b) and, together with its extensive calibration, in Wasmeier (2009a). Also the obtainable accuracies were examined which in the field are approx. $\sigma < 1$ mgon on average, but under bad conditions up to $\sigma > 2$ mgon. Under laboratory conditions, a repeatable accuracy capability of < 0.15 mgon has been proved.

At the Aggenalm project site the method was used to capture object points distributed on the slope from a central setup point by means of polar measurements and check for displacements. Beforehand, this is quite similar to the conventional setup of a permanent or temporarily tacheometric monitoring system without net measurement. But in contrary to that, in the alpEWAS approach only natural targets and no retroreflecting prisms were used. This goal, on the other hand, also implicates, that permanent measurements will not be possible due to slope exposition and the long-lasting snow coverage in the Sudelfeld area. Especially in wintertime long gaps have to be accepted, as the built-in camera is not specified for temperatures below 0 °C

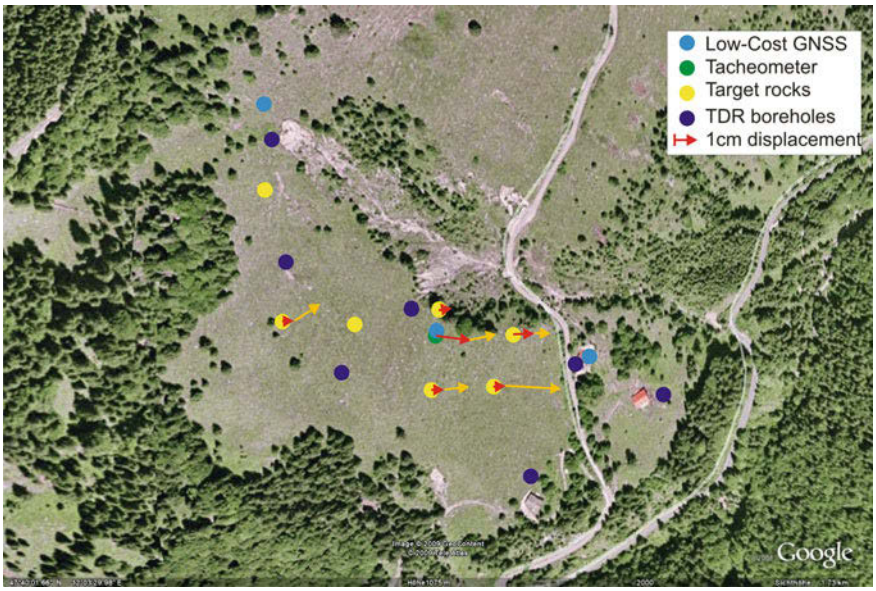

Fig. 15.4 Measurement points at the Aggenalm landslide. The arrows mark the displacement vectors of VTPS between fall 2008 and summer 2010. Target points without vector have not been measured in all epochs due to some failures

In Fig. 15.4 the measurement points in the Aggenalm Landslide are shown. The arrows mark the planar displacement vectors between fall 2008 and fall 2009 (red) and between fall 2009 and summer 2010 (orange). Tacheometric target points without vectors haven't been measured in all epochs due to single measurement failures in target detection or range measurement. The displacements are between 3 and 12 mm, which are not significant due to the necessary setup of the measurement pillar position using stable reference points in big distances, but regarding orientation and absolute value they are highly feasible, also compared to GNSS results.

The advantage of video tacheometry compared to conventional and approved methods lies in the variability of possible target structures which can be both artificial (target marks or reflectors) and natural. Here, depending on the target type, a more or less complex detection algorithm is necessary, which, as a rule, has to be individually designed for the single case. Basically, a big pool of operators and procedures from digital and industrial image analysis is available. The standard chain of work of a target detection using VTPS is shown in Fig. 15.5. At the Aggenalm, surface rocks have been used for natural targeting; but for monitoring purposes in the field also e.g. debris tear-off edges, (parts of) buildings and other natural targets are possible. The measurement principle is an edge-based matching relying on a teaching-phase during the installation of the system. If real deformation detection is the goal, other methods can be used, which e.g. have been evaluated at the TU Wien using the same prototype instrument (Reiterer et al. 2010). Further application possibilities can be found in (Thuro et al. 2010).

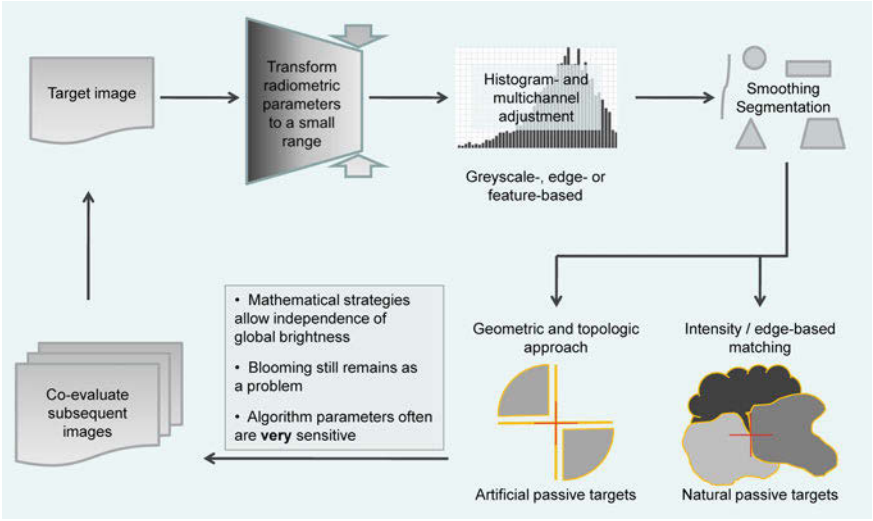

Fig. 15.5 Flow chart of a target point detection

For every image-based analysis the complexity of the algorithms and therefore the reliability of the result have to be questioned critically. Especially in industrial image-driven applications, illumination and other environmental parameters get optimized by default. This is not possible with video tacheometry, especially when working outdoors. Reliability rates of more than 90 % are achievable in exceptional cases only. This was the same in the alpEWAS project; so the goal of an autonomous video tacheometric measurement system had to be abandoned in favor of a semi-automatic, user-controlled measurement process.

Figure 15.5 shows the flowchart of target point detection. Measurement images first become homogenized to be able to use uniform operators and parameters for the deduction of attributes and objects. Final target point detection itself is mainly done using descriptive rules (geometric, topologic and/or radiometric) or matching algorithms. Evaluation of consecutive images imitates integration by time of some normally distributed measurement deviations in the images and therefore raises the accuracy statistically.

Video tacheometry, which was used for displacement monitoring of non-signaled objects in geodesy for the first time, has proven functionality especially under controllable conditions (e.g. indoors). When using in the field, distinct limitations became apparent in the course of the project—mostly because of refraction effects and chaotic short-term atmospheric turbulences. These influences of course also affect traditional tacheometric targeting, but are particularly critical with video tacheometric image processing due to its time-consuming detection algorithms and sensible parameterization. Further developments in this field therefore need to be threefold, while results in one branch will also be input information to the others:

- Advances in hardware to overcome the prototype status. This is primarily the task of the instrument manufacturers, but therefore dependent on economic factors. This makes it a challenge for scientific research to point out appropriate fields of use as well as to evaluate advantages and drawbacks.
- Further enhancements of convenient algorithms. Reliability and scope of application of the usable algorithms have to be improved and accordingly adopted to the special tasks of video tacheometry. To this, also additional fields of usage need to be found and handled in pilot schemes. An example for that could be video tacheometric vibration determination.
- Modeling of atmospheric influences. The main problem of derogation of video tacheometric measurements—refraction and air flickering—has to be analyzed with a special view to the new instrument type and, if it proves possible, to be minimized by empirical or modeled corrections. An according research project is currently in progress (DE-MONTES, http://www.de-montes.eu, 2011–2012) at the Chair of Geodesy (TUM).

15.2.3 Low Cost Global Navigation Satellite System (LC GNSS)

The satellite supported monitoring component of the geo sensor network at the Aggenalm Landslide consists of an all-weather proofed low cost GNSS measurement system based on simple, cheap and robust navigation receivers produced for the mass market. The applied receivers allow a phase tracking of the American GPS as well as the Russian Glonass satellites. Using such receivers permanently, monitoring of discrete points at the surface of the slide is possible with sub centimeter accuracy. In context of a geo sensor network the GNSS stations are just called sensor nodes in the following.

In order to achieve the aspired accuracy with the mentioned equipment, only L1 code and carrier phase receivers are used in combination with a high sophisticated near real time processing. This means that over a predefined period of time—usually 15 min—carrier phase raw data is recorded continuously. By wireless communication techniques (WLAN) all raw data is transmitted “on the fly” to a central computing station. As soon as the data from the different sensor nodes—at least one station should be on stable ground (reference station) and the others are spread on the slope (there are three such stations at the Aggenalm)—is available the baseline processing can start immediately. If there are more reference stations disposable the possibility of a geodetic network adjustment is given. In contrast to ordinary real time kinematic applications the whole evaluation with the developed approach can be designed and controlled individually. In the alpEWAS project it could be shown that accuracies can be achieved which normally can only be obtained by geodetic high-end receivers.

Beside design and construction of the GNSS sensor nodes (Fig. 15.6, right side) focus was laid on the software component called Central Control Application (CCA), which is developed by using LabView®, National Instruments. All steps in the workflow (Fig. 15.6, left side) from the configuration and initialization (1) to the

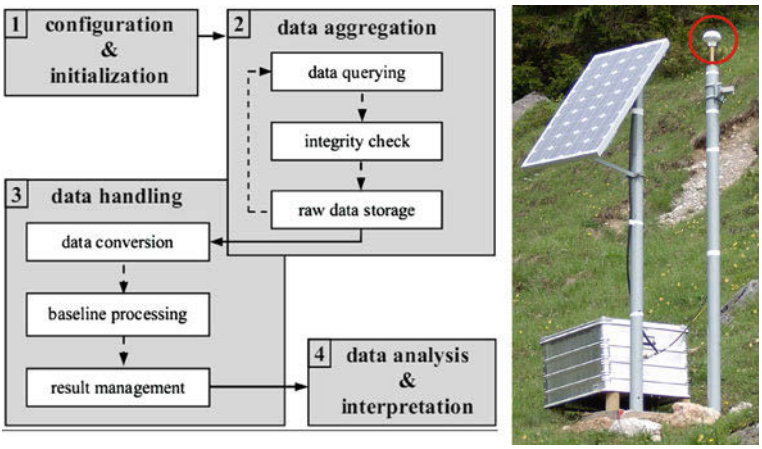

Fig. 15.6 Work flow of the central control application and design of a complete GNSS node with marked antenna in *red* (Glabsch et al. 2010a)

continuous data recording (2) and the parallel operating near real time processing (3) to the transmission of results (4) is controlled and executed. A modular, prospective design offers the option to integrate a diversity of GNSS sensors. Only the corresponding program implementation has to be realized because all receivers deliver binary data only. Individual design of the evaluation is given by the steps 3 and 4 starting with the carrier phase raw data conversion. The processed information obtained from the GNSS nodes (coordinates of the points, quality parameters, and GNSS status information) is stored in a MySQL database and updated every 15 min. All data collected by the geo sensor network is promptly available in a central data sink for an enclosed integrated evaluation, see Sect. 15.3. For further technical details of the developed measuring system please see Glabsch et al. (2009; 2010a; 2010b).

With the current state of the software and the designed sensor nodes a continuous and robust operation of the low cost GNSS monitoring component is realized. Currently, only rare malfunctions occur which are mainly caused by energy shortages. In particular at the central station and the multi-function node in the middle of the slope longer power outages in the 230 V electricity supply system lead to some failures. Only short power black outs can be bridged by an uninterrupted power supply (UPS). Beside these energy shortages a secure GNSS system operation of the autonomous stations is a challenge especially at alpine winters (partial complete snow cover of the antennas and solar panels for days or weeks). An appropriate choice of reliable equipment and the dimensioning of the devices lead to a reliable year-round operation.

Some results of the GNSS monitoring component at the Aggenalm are presented in Figs. 15.7 and 15.8. A more complete look at the picture is given in Sect. 15.3.2.1. In the following the position components (easting Y, northing X, where Y is approximately downhill) are depicted for the period March 2009—December 2010 by a

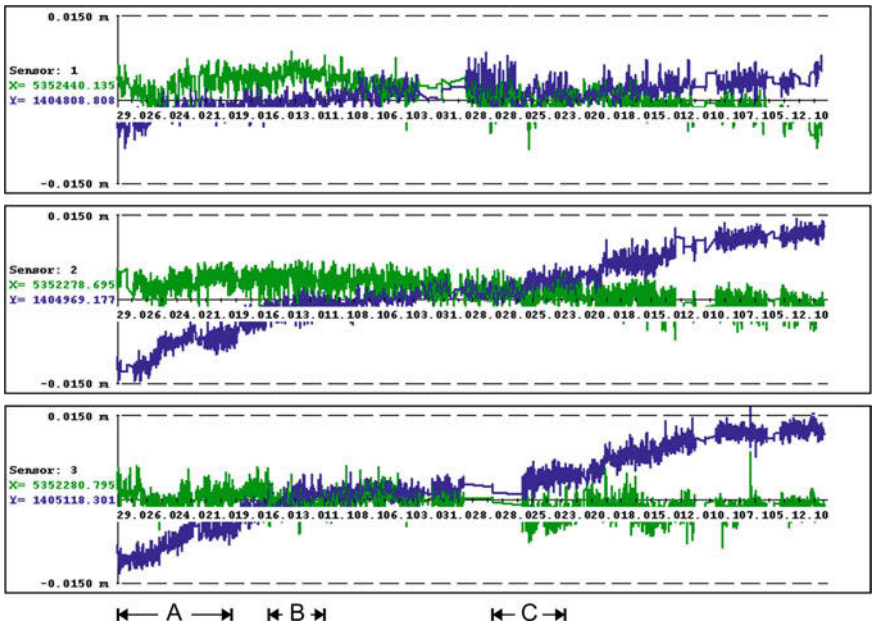

Fig. 15.7 Variations of the sensor nodes 1–3, time period March 2009 to December 2010, moving average (node 1: 12, node 2 and 3: 6 h)

moving average filtering based on a robust estimator. The filter extends over 24 epochs (nodes 2 and 3) and 48 epochs (node 1). Using a time interval of 15 min to acquire the carrier phase measurements the filter length corresponds to 6–12 h. The choice of this filter type and length is the consequence of partially bad obstructions (due to surrounding mountain ridges, trees) at the sensor nodes that lead to temporarily incorrect processing results—even in some cases a successful solution can't be computed at all. Despite some technical problems and the resulting data gaps (Fig. 15.7) long-term trends of the movement can be captured satisfactorily. The time series at node 2 and 3 show slide acceleration phases during springtime (snow melt) in slope direction Y (blue charts).

Presumably due to the low snow coverage in spring 2010 (C) a comparable behavior as in spring 2009 (A) cannot be seen. The effect of a heavy rainfall event in June 2009 (B) is also detectable. An enlarged view for the period 15.03.−15.08.2009 shows the impact of snow melt (end of March to end of April) and the intense rainfall in June 2009 (last two weeks) exemplary at sensor node 2 at Fig. 15.8 especially in slope direction.

The used GNSS monitoring component is based on standard components for sensors, power supply (batteries with solar panels) and WLAN communication. In the actual configuration a complete autarkic GNSS sensor node (Fig. 15.6, right side) requires an investment of about € 3,000. The developed Central Control Application allows a reliable system operation. Although the achieved accuracies with filter

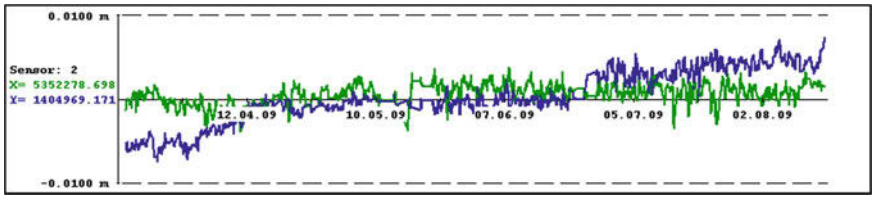

Fig. 15.8 Sensor node 2, variations during 15.03. – 15.08.10, moving average (12 h)

lengths of about 6 h already permit to evaluate long-term behavior of a slope even with only small changes during the year, the full potential of simple navigation receivers for surveillance tasks has not been tapped yet. For an improved early warning a (significant) shortening of the filter length is an essential challenge. Overall, it was possible to examine the use of low cost GNSS sensor technology intensively. The gained results demonstrate that the low cost monitoring approach can successfully be used alternatively to precise tacheometric geodetic surveys or expensive high-end GNSS receivers.

15.3 Data Management and Integrative Data Analysis

15.3.1 Data Management

The alpEWAS Control software package (Fig. 15.9) was developed as a modular software package to control the entire data management within the project. The flexible layout offers an ideal adjustment of the software's sub-programs to the underlying measurement system.

A central component is the open source MySQL database. The link between the geo sensor network, respectively the sensors installed at the field site, and the database is established by sensor plugins. Besides the sensor control, status monitoring and readout of pre-processed data as well as the communication of information via a standardized communication protocol a first analysis is conducted. This provides next to pre-processed data also prompt usable information (1st level results) for further integrative analysis. Various monitoring tools permanently check the current status of the system in order to detect the exceedance of critical system parameters (such as thresholds) as well as failures of individual sensors or subprograms. If one of these malfunctions is detected the system administrator is informed immediately, thus long-time data loss can be avoided. The alpEWAS Live Viewer (Fig. 15.10) is another helpful tool for system maintenance. The interface informs the user about the current system status. Furthermore data can be displayed as time series using different filter options and combinations.

An important interface is the link between the onsite computer center and the end user being interested in information about the current status. The data management

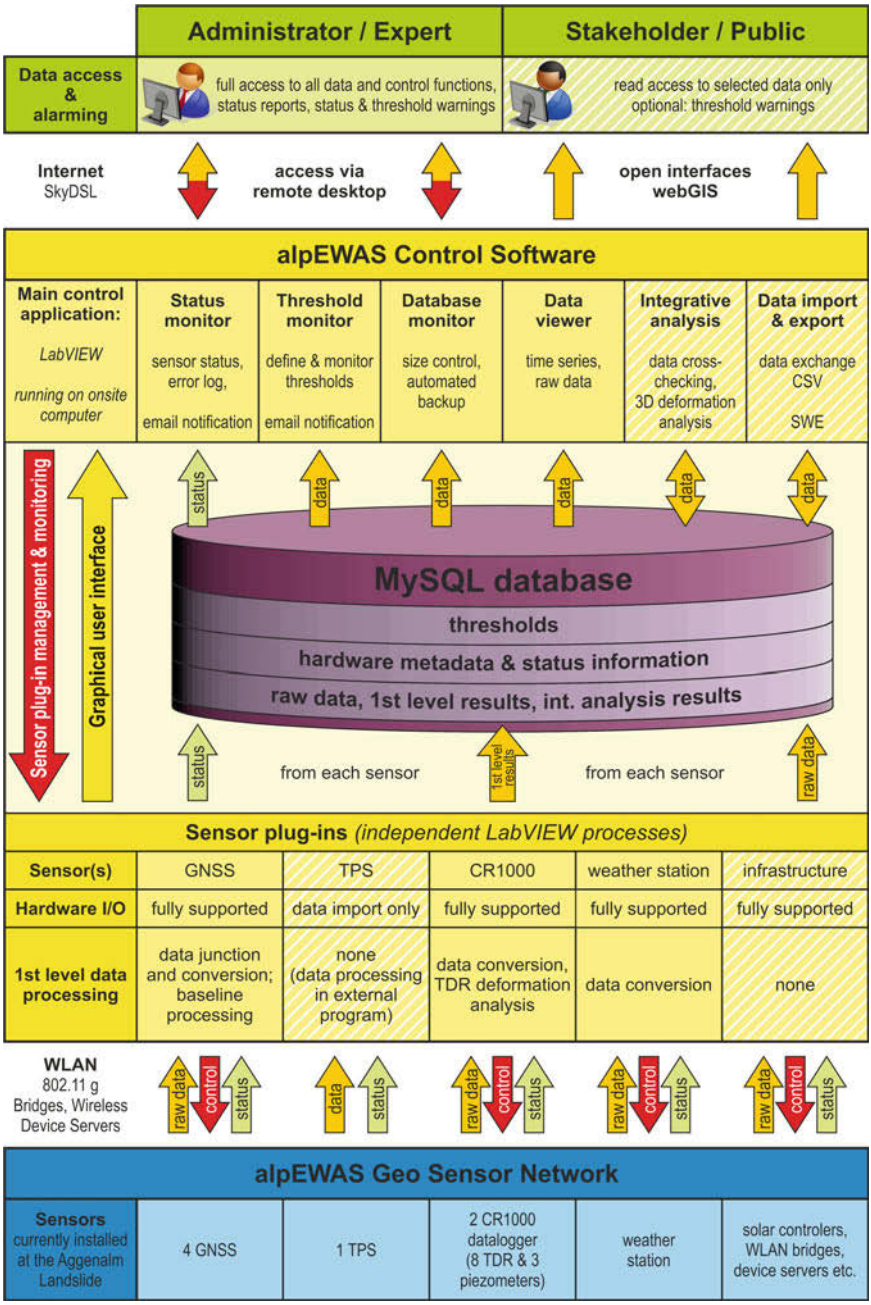

Fig. 15.9 Schema of alpEWAS control, management and data analysis software

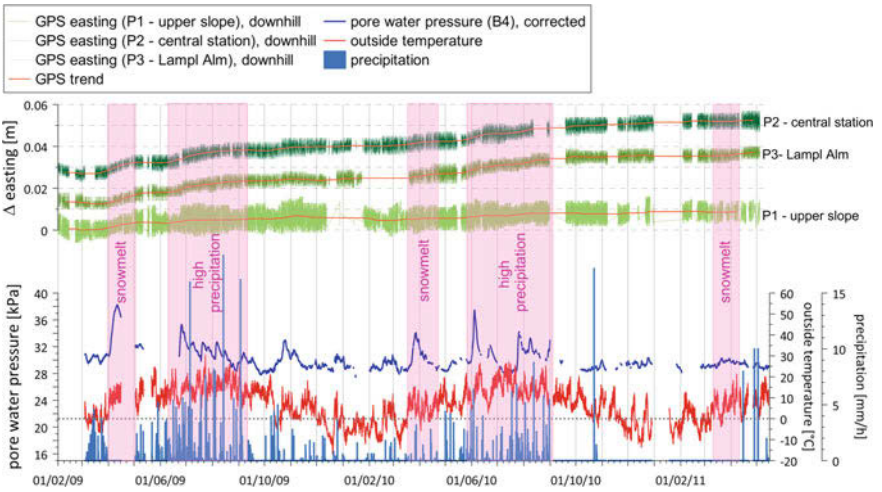

Fig. 15.10 Precipitation and temperature at the central station node and pore water pressure at node B4 as well as GNSS (GPS) deformation measurements of all 3 GNSS nodes for a time span starting February 2009 to May 2011. The gray dotted line marks 0 °C to better show the beginning of the snow melting periods every year

concept is as follows: By reflecting the database constantly from the master computer to a second data server (slave) possessing a broadband connection at the project office high data integrity and almost unlimited parallel data access from several users can be achieved. Complex and computationally intensive analysis can be split to several machines this way if necessary.

For data exchange between heterogeneous systems (interoperability) it is possible to query all results by means of access authorizations via standardized interfaces. Standards such as the worldwide standard of handling space-orientated data for an interoperable benefit being developed by the Sensor Web Enablement (SWE) initiative of the Open Geospatial Consortium (OGC®) are currently being integrated.

The main functions of the Live Viewer are the permanent status information of the systems' state and the possibility to graphically display first results. It can be freely chosen which data base (master or slave) the Live Viewer accesses.

15.3.2 Data Analysis

Since the beginning of February 2009, a continuous monitoring of all sensors with the possibility of remote access and control has been realized, thus permitting to perform time series analysis on the collected data. From prior landslide events in the years 1935 and 1997 and first results of the geomechanical model it has been fancied that one of the major influencing factors on the movements of the Aggenalm

Landslide is the precipitation partly in combination with the snow melt. Aim of the data analysis is to validate the slope's movement characteristics using the data at hand and to identify and quantify the correlations between precipitation, pore water pressure (piezometer) and deformation measurements using time series analysis.

15.3.2.1 Time Series Filtering

Figure 15.10 shows plots of the potential triggering factors, precipitation and pore water pressure (plus temperature) for a time span of almost 2.5 years. The GNSS measurements are more or less continuously recorded since February 2009 and are depicted for all 3 sensor nodes at the Aggenalm Landslide as well. A limiting factor for the analysis are the relatively small deformation rates of about 1 cm/a at the maximum (Fig. 15.10, GNSS P1 about 1 cm and GNSS P2 and P3 about 2.0–2.5 cm in the last 2.5 years). With the VTPS technique comparable results were attained whereas the TDR system couldn't detect subsurface displacements yet, since the clamping process seems still to be in progress (see Sect. 15.2.1).

A small increase of the displacement rate can be observed several times in the time series from February 2009 to May 2011 (Fig. 15.10) after periods of high precipitation and/or snow melt. In spring 2009 and 2010 after the onset of the snow melting period the pore water pressure exceeded 33 kPa (pink shaded areas in Fig. 15.10), whereas in spring 2011 hardly any influence on the pore water pressure by the snow melting can be observed. In spring 2009 the rise in pore water pressure caused by the snow melting from about 30 to 38 kPa equals a water table rise of about 0.8 m. But also after extreme precipitation events, e.g. in July and August 2009 and June 2010, the pore water pressure exceeded 33 kPa. Exemplarily this can be shown on a section of 60 days from June 22nd to August 22nd 2009, where only rare losses of data occurred. Herewith first optical interpretations and comparisons are possible.

For the preparation of the precipitation data a 6 and a 12 h cumulative has been calculated, respectively. This smoothing provides a better comparability with the piezometer and GNSS data. The pore water pressure data set shows a smooth gradient and had to be corrected by the influences of the barometric pressure. To improve the GNSS data furthermore an additional low-pass filter can be applied (Fig. 15.10). Due to different sampling intervals in the data acquisition—the pore water pressure and precipitation are acquired in a five minute interval whereas the GNSS positions are processed for every 15 min—all data has been resampled with the same time interval. Finally, because of minor data losses a 6 h resampling was chosen for Fig. 15.11, where the filtered and resampled time series of precipitation and pore water pressure for the above mentioned 60 day interval are depicted.

One can see that a few days after a major rainfall event (>20 mm in 2 days) the pore water pressure begins to rise (from 30 to 35 kPa, equal 0.5 m). Because of the relatively short time span of identical time series and only few days of heavy precipitation the system (rainfall, increase in pore water pressure, change in GNSS coordinates) can yet not be described by more sophisticated models.

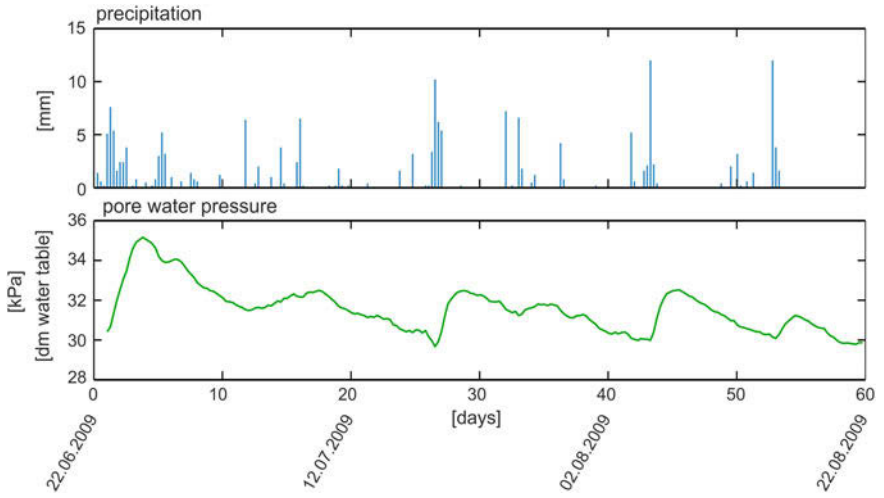

Fig. 15.11 Precipitation and pore water pressure for the period June 22nd to August 22nd 2009 (filtered, 6 h intervals) (Thuro et al. 2010)

15.3.2.2 Time Series: Cross Correlation Analysis

In this first attempt the quantification of the time gap between rainfall and an according rise in pore water pressure was the major objective. To show the temporal dependency cross correlations from the filtered and resampled data were calculated. The analysis of the time span of 60 days shows a correlation between precipitation and the pore water pressure with a delay of 2–3 days, but cross correlation of the piezometric time series with GNSS results did not confirm a significant temporal dependency even though similar characteristics can visually be identified. The numerical analysis (Tadayonfar 2011) of the Aggenalm Landslide may explain why: A rise in pore water pressure of about 6 m (more than 5 times of the hitherto maximum of 1.2 m) would be necessary to get a stronger increase in movement rate. Therefore with the present events the GNSS results in particular are still within its noise making it difficult to get a significant correlation.

Figure 15.12 shows two time series for a shorter span of only 10 days, starting June 23rd 2009. The first two days a strong continuous rainfall (∼25 mm in 2 days) can be observed. The cross correlation of the time series shows a time delay of about 2.5 days. Similar results have been calculated for comparable events—the time delay between precipitation and rise in pore water pressure varies depending on the amount of rainfall as well as system's prerequisites and is about 2–5 days. The time offset after the onset of the snow melt seems to be greater. Here the analysis showed results of about 4–5 days.

The correlation of the presented time series gives a first view on a possible analysis method. Longer time series as well as a greater number of significant precipitation events should allow a further and more detailed interpretation of the cause-and-effect

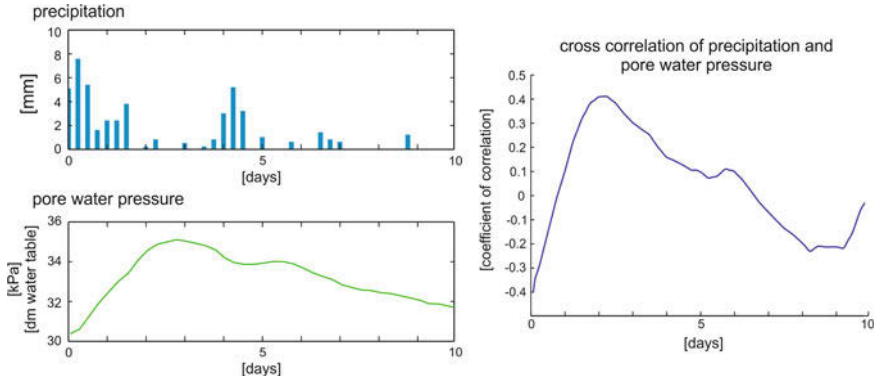

Fig. 15.12 Precipitation and pore water pressure for the 10 day period June 23rd to July 3rd 2009 including a cross correlation (Festl et al. 2011; Thuro et al. 2010)

chain. In particular greater point movements in the GNSS data should make it possible to integrate these in the analysis and also detect dependencies between trigger events and deformation, however.

15.4 Conclusion and Perspective

The developed measurement techniques TDR and low cost GNSS are more or less based on already existing hardware components, while the video tacheometer hasn't been introduced to the market yet, and is still available as a prototype from Leica Geosystems only. New developments in the video tacheometry were mostly accomplished in the fields of the adaption of the system layout for the measuring task "slope monitoring" and in signal analysis and sensor control. The efficiency of TDR and low cost GNSS for continuous monitoring could be proved. Decisive are the developed software components for the data management and complex data analysis. These measurement techniques are now on the cusp of marketability, whereas the range of application isn't limited to mass movements but can be extended to other monitoring tasks such as the monitoring of structural elements (Singer et al. 2009a).

References

Festl J, Singer J, Thuro K (2011) The Aggenalm landslide—first findings of the acquired monitoring data. In: Proceedings of the international symposium on rock slope stability in open pit mining and civil engineering. Vancouver, Canada, 18–21 Sept: 7 p

Glabsch J, Heunecke O, Schuhbäck S (2009) Monitoring the Hornbergl landslide using a recently developed low cost GNSS sensor network. JAG 3: 179–192

Glabsch J, Heunecke O, Schuhbäck S (2010a) Development and testing of a low cost sensor PDGNSS landslide monitoring system using the example of the aggenalm landslide in the bavarian alps. In: Altan O, Backhaus R, Boccardo P, Zlatanova S (eds) Geoinformation for disaster and risk management. JB GIS, Copenhagen, 63–70

Glabsch J, Heunecke O, Schuhbäck S (2010b) Überwachung von Rutschhängenmittels low-cost GNSS Empfängern im near real time processing. In: Wunderlich T (ed) Ingenieurvermessung 10. Wichmann, Berlin, 275–288

Leica Geosystems AG (2007) Leica TPS1200+ Series. XI.07 738600de, Herbrugg, 16 p

Leica Geosystems AG (2010) Leica Viva TS15. Data sheet, Herbrugg, 1 p

Reiterer A, Huber N, Bauer A (2010) Bildbasiertes Erfassen und Matching homologer Punkte mittels Feature-Vektoren—Funktionsweise und Evaluierung beim Einsatz in einem Deformationsmesssystem. In: Wunderlich T (ed) Ingenieurvermessung 10. Wichmann, Berlin, 241–254

Singer J (2010) Development of a continuous monitoring system for instable slopes using time domain reflectometry (TDR). Dissertation, Chair of Engineering Geology, Technische Universität München

Singer J, Grafinger H, Thuro K (2009a) Monitoring the deformation of a temporary top heading invert using time domain reflectometry. Geomech Tunn 2: 238–249

Singer J, Festl J, Thuro K (2009b) Computergestütze Auswertung von time domain reflectometry Messdaten zur Überwachung von Hangbewegungen. In: Marschallinger R, Wanker W (eds) Geomonitoring, FE-Modellierung. Sturzprozesse und Massenbewegungen, Heidelberg, Wichmann, 19–34

Singer J, Schuhbäck S, Wasmeier P, Thuro K, Heunecke O, Wunderlich T, Glabsch J, Festl J (2009c) Monitoring the Aggenalm landslide using economic deformation measurement techniques. Austrian J Earth Sci 102: 20–34

Singer J, Thuro K, Festl J (2010) Development and testing of a time domain reflectometry (TDR) monitoring system for subsurface deformations. In: Zhao J, Labiouse V, Dudt JP, Mathier JF (eds) Rock mechanics in civil and environmental engineering. Taylor and Francis Group, London, 613–616

Tadayonfar G (2011) Numerische Modellierung der Großhangbewegung Aggenalm mit FLAC. Dissertation, Chair of Engineering Geology, Technische Universität München

Thuro K, Wunderlich T, Heunecke O, Singer J, Schuhbäck S, Wasmeier P, Glabsch J, Festl J (2009) Low cost 3D early warning system for alpine instable slopes—the Aggenalm landslide monitoring system. Geomech Tunn 2: 221–237

Thuro K, Singer J, Festl J, Wunderlich T, Wasmeier P, Reith C, Heunecke O, Glabsch J, Schuhbäck S (2010) New landslide monitoring techniques—developments and experiences of the alpEWAS project. JAG 4: 69–90

Topcon Positioning Systems Inc (2008) Topcon imaging station—long-range scanning, imaging and robotic total station. Revision A 7010–0876, Livermore, 4 p

Trimble Navigation Limited (2010) Trimble VX spatial station—Datasheet. 022543-261F, Singapore, 4 p

Wasmeier P (2009a) Grundlagen der Deformationsbestimmung mit Messdaten bildgebender Tachymeter. Dissertation, Chair of Geodesy, Technische Universität München

Wasmeier P (2009b) Videotachymetrie—Sensorfusion mit Potential. AVN, vol 7. Wichmann Verlag, Heidelberg, 261–267

Chapter 16
Operational Integration of Spaceborne Measurements of Lava Discharge Rates and Sulfur Dioxide Concentrations for Global Volcano Monitoring

F. Ferrucci, N. Theys, B. Hirn, L. Clarisse, P. Valks, G. Laneve, R. van der A, S. Tait, C. Di Bartola and H. Brenot

Abstract We present the rationale and the main initial achievements of the operational prototype of the first multi-method system for the real-time, unsupervised, quantitative monitoring of erupted masses simultaneously at all active volcanoes in Europe, Africa, the Eastern Antilles and the ocean islands. The system is structured as a multi-pole, geographically distributed system, where raw datasets from space payloads SEVIRI, MODIS, GOME-2, IASI and OMI are acquired at four downlink stations, distributed to, and automatically processed at six locations in four European nations, then returned to a central post-processor for real-time alert and Wide Area Network display. This architecture is aimed at optimizing quality and timeliness of the advanced methods run within it, and to let the inherent technical knowledge

F. Ferrucci (✉) · S. Tait
Institut de Physique du Globe de Paris, 1 rue Jussieu, 75238 Paris Cedex05, France
e-mail: ferrucci@ipgp.fr

N. Theys · H. Brenot
Institut d'Aéronomie Spatiale de Belgique, 3 Avenue Circulaire, 1180 Bruxelles, Belgium

B. Hirn · C. Di Bartola
Intelligence for Environment and Security—IES Consulting, 34 via di San Valentino, 00197 Roma, Italy

L. Clarisse
Université Libre de Bruxelles, 50 Avenue F.D. Roosevelt, 1050 Bruxelles, Belgium

G. Laneve
Università di Roma "La Sapienza", Sezione Progetto San Marco, 851 via Salaria, 00138 Roma, Italy

P. Valks
Deutsches Zentrum für Luft und Raumfahrt, 82234 Oberpfaffenhofen, Weßling, Germany

R. van der A
Koninklijk Nederlands Meteorologisch Instituut, 10 Wilhelminalaan, NL-3732 GKDe Bilt, The Netherlands

F. Ferrucci
Università della Calabria, Ponte Bucci 15B, 87036 Rende (Cosenza), Italy

F. Wenzel and J. Zschau (eds.), *Early Warning for Geological Disasters*,
Advanced Technologies in Earth Sciences, DOI: 10.1007/978-3-642-12233-0_16,

remain with inventors without concern for individual intellectual property. Before entering operations early in 2012, the system underwent extensive testing in 2011 during the major eruptions of Nabro (Eritrea) and Nyamulagira (DR Congo), which are presented here.

Abbreviation

AIRS	Atmospheric Infrared Sounder
ATBD	Algorithm Theoretical Basis Document
AVHRR	Advanced Very High Resolution Radiometer
DLR	Deutschen Zentrums für Lüft und Raumfarth
EO	Earth Observation
ERS	European Remote Sensing satellite
ESA	European Space Agency
EUMETSAT	European Organization for the Exploitation of Meteorological Satellites
EVOSS	European Volcano Observatory Space Services
GMES	Global Monitoring for Environment and Security
GOES	Geostationary Operational Environmental Satellites
GOME	Global Ozone Monitoring Experiment
IASI	Infrared Atmospheric Sounding Interferometer
IR	InfraRed
JAMI	JApanese Advanced Meteorological Imager
LEO	Low Earth Orbit
METOP	METeorological OPerational satellite
MIR	Mid-InfraRed
MODIS	MODerate resolution Infrared Spectroradiometer
MSG	Meteosat Second Generation
MTSAT	Multifunctional Transport SATellite
NOAA	National Oceanic and Atmospheric Administration
OMI	Ozone Monitoring Instrument
PROMOTE	PROtocol MOniToring for the GMES Service Element
SACS	Support to Aviation Control Service
SCIAMACHY	SCanning Imaging Absorption spectroMeter for Atmospheric ChartograpHY
SEVIRI	Spinning Enhanced Visible and InfraRed Imager
SWIR	Short-Wavelength Infrared
TEMIS	Tropospheric Emission Monitoring Internet Service
TIR	Thermal InfraRed
TOMS	Total Ozone Mapping Spectrometer
UTC	Coordinated Universal Time
UV	Ultraviolet
VAAC	Volcanic Ash Advisory Center
WMO	World Meteorological Organisation

16.1 Introduction

Volcanic eruptions, as is generally the case for major natural hazards, can occur on vastly different scales. Probably the very simplest quantitative expression of this reality is to be found in the volume of magma erupted in any given event, which is known to vary from several thousand cubic kilometres in the greatest events that have been yet identified, down to comparatively trivial fractions of one cubic kilometre that can be ejected in small explosions. This variation of perhaps seven to eight orders of magnitude is naturally accompanied by a frequency magnitude relationship analogous to the well-known Gutenberg-Richter law of global seismology, whereby the bigger the event, the greater the inter-event recurrence time. Nevertheless this kind of after-the-fact measurement is not helpful for the management of a volcanic crisis, for which the requirements are above all those of obtaining real-time information, and quickly identifying changes or variations in the level of activity.

Although a number of eruption regimes have been defined and given different names as volcanology has developed, the coarsest, essentially ≪ binary ≫ classification of eruptive regimes is that of "Explosive" and "Effusive". Though not exclusively, explosive eruptions typically involve magmas that are both more viscous and volatile-rich varieties. The key physical phenomenon is that of magma fragmentation which takes place in the conduit through which magma reaches the surface. This process generates at the vent a powerful gas jet bearing magma fragments ranging from tiny ash particles to much larger pumices, whose maximum attained altitude depends on the difference in temperature between the jet and the surrounding atmosphere, and the fourth root of the actual mass eruption rate. As gas and melt eruption rates can be measured by Remote-Sensing, it is possible to put theoretical and measured constraints on explosive phenomena such as the disruptive, though mild eruption of Eyjafjallajökull, mid-March to early-May 2010 (Kaminski et al. 2011).

Effusive eruptions typically involve less viscous and volatile-poor varieties of magma. The fundamental regime here is that of lava flow whereby magma flows out of a vent to feed a flow that spreads over the ground as a liquid layer whose areal extent and thickness change with time depending mainly on the rate of feeding. One important dynamic feature which is quite often present, notably in the early stages of effusive lava eruptions is that of ≪ fire-fountains ≫ also sometimes called ≪ lava-fountains ≫. It has been plausibly argued, mainly from examples of well-studied Hawaiian eruptions that these fountains are driven by a so-called separated flow regime in which gas and liquid phases move up the conduit at different velocities with a central gas flow surrounded by an annulus of liquid (Vergniolle and Jaupart 1986, 1990).

The key point here is that of separated flow with differential velocities of gas and liquid as opposed to homogeneous flow when the two velocities are equal—this means in practical terms that it is important to have independent proxies for the fluxes of gas and of magmatic liquid. Because magma undergoes a strong decompression as it rises up the conduit to the vent, and because the magmatic volatile phase is highly compressible whereas the liquid phase is essentially incompressible, the volumetric

flux at the vent in most eruption regimes is typically dominated by gas volumetrically speaking, whereas the mass flux is dominated by that of the liquid phase.

Hitherto the use of satellite-based observations to solve this important problem has not been achieved, mainly because the focus has been either that of demonstrating that a specific parameter could be observed, or that of using images that provide high spatial resolution to show the potential of volcano EO. High spatial resolution imagery is typically only acquired rarely at any given site and therefore it is not possible to follow adequately the unfolding of pre-eruptive and eruptive events in time. Nevertheless instruments or payloads which make very regular measurements do exist, albeit with lower spatial resolution, and these can be used to form the basis of a space-based virtual volcano observatory that can follow events with a time resolution allowing to describe the unrests with little or nil temporal aliasing.

A few brilliant experiences in volcano remote sensing provided with global vocation, such as the MODVOLC volcanic Hot-Spot service (Wright et al. 2004), run typically one day behind real-time (http://modis.higp.hawaii.edu/), the GOES 9/10/12 very-low spectral and spatial resolution Hot-Spot service (http://goes.higp.hawaii.edu/goes.shtml), and the NOAA's SO_2 exceptional concentration alert system based on the daily observations by UV payload OMI (http://satepsanone.nesdis.noaa.gov/pub/OMI/OMISO2/), have not achieved the transversal impact they would deserve because of the lack of multi-payload integration able to overcome the limits of single-parameter techniques in volcano assessment. In all cases, they did not focus on fluxes, nor the synergetic merging of fluxes, and the prevailing information is 'when' and 'where' (at different levels of resolution) rather than on 'how much' and 'what rate'.

We may conclude that a "global" monitoring system suited to bring to a satisfactory, generalized level the detection-and-measurement thresholds of activity at unmonitored volcanoes, and to present a minimal backup solution in major emergencies even at well monitored volcanoes, should (i) focus on fluxes and incorporate (ii) multi-parameter capacity, (iii) high-to-very high refresh rate, and (iv) supra-continental synoptic vision. The first two requirements are meant to allow quantitative observation, when applicable; the third and the fourth, to maximize the capacity of detecting and observing, while avoiding temporal aliasing and the inherent risks of misinterpreting short lasting events, or the effects of scattered or infrequent visibility of eruptive locations. These concepts were developed, tested, refined and put into operation in a series of consecutive projects between 2002 and 2013: TEMIS, PROMOTE, SACS, GLOBVOLCANO and SACS+ of the European Space Agency, and EVOSS (European Volcano Observatory Space Services), of the European Commission's GMES—Global Monitoring for Environment and Security.

GLOBVOLCANO, a precursor of EVOSS, demonstrated the feasibility of delivering volcano monitoring services worldwide, based in particular on high spatial resolution sensors for volcanic features on ground, and the use of SO_2 concentrations as a proxy of ash concentrations. Conversely, EVOSS—conceived to act in supra-regional operation theatres, so as to encompass at once several, spatially scattered, long lasting crises (months to years)—gave priority to the analytic measurement of mass fluxes at very-high temporal resolution over high spatial resolution, a methodological breakthrough in real-time monitoring operations and also a solu-

tion to sustainability issues because of the exploitation of geostationary meteorological payloads. EVOSS—which includes also a monitoring line for mapping volume changes with ad-hoc Synthetic Aperture Radar interferometry Radar interferometry (SqueeSAR^{TM}, Ferretti et al. 2011) not dealt with here—includes the near-realtime SO_2 products of SACS derived from multispectral UV/Visible and Infrared, polar-orbiting platforms with daily or half-daily revisit.

Here, we show how the advanced multi-technique integration in EVOSS, allowed monitoring two major volcanic unrests that occurred a few months apart in 2011: the strong reawakening of oversleeping volcano Nabro, Eritrea, occurred in an uninhabited, unmonitored area—and the relevant phases of the great, 2011–2012 eruption of Nyamuragira, DR Congo, a multi-risk prone area presenting significant anthropic complexities.

16.2 Exploited IR and UV Payloads

Satellite payloads satisfying the pre-requisites of high-to-very high temporal resolution stated above, are either geostationary, or wide-swath on platforms in Low Earth Orbit (LEO).

In the first case, they present refresh times ranging between 15 min (SEVIRI onboard MSG) and 30 min (JAMI onboard MTSAT, and Imager onboard GOES).

In the second, efficient revisit intervals at Equator grow to twice daily for Infrared (IR) payloads, which measure day and night, and to once daily for UV payloads which exploit daylight. Much higher revisit frequencies (e.g., up to 6 daily for IR payloads on Iceland) are obtained at high latitudes thanks to track convergence and frame overlap.

16.2.1 Infra-Red Radiometers

The belt of geostationary platforms (see Fig. 16.1) with the above radiometers, theoretically allows going ‘global’, although the technical performance of the three sensors is uneven. GOES’ Imager and MTSAT’s JAMI have only two exploitable IR channels for quantitative assessment of high-temperature ground volcanic features, instead of the four nominally useable in SEVIRI, their image rate is twice lower (30 min against 15) and the IR pixel footprints at Nadir are 16 km^2 for Imager and JAMI, and 9 km^2 for SEVIRI.

SEVIRI, designed for “nowcasting” digital applications and Numerical Weather Prediction, is hosted onboard the MSG geostationary platforms at 0° longitude. It is the key-contribution of EUMETSAT to the Global Observing System of WMO, and constitutes the primary European source of observations over Europe and Africa. The MSG system brought major improvements in the quality of spaceborne meteorological services thanks to its 12 spectral bands and a 10-bit quantification level.

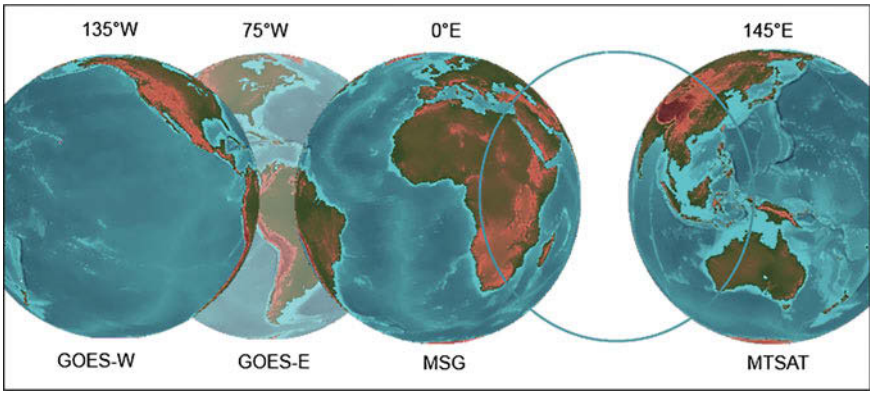

Fig. 16.1 The union of the 'full disks' of MSG-1, -2, -3 (payload SEVIRI), GOES-13, -14, -15 (Imager) and MTSAT-1R and -2 (JAMI), allows observing ∼90 % active volcanoes of the world. As of 2012, coverage of the central Indian Ocean—left blank intentionally—is ensured by the first-generation Meteosat-7 equipped with the 3-channel MVIRI (Meteosat Visible and InfraRed Imager). This payload is unsuited to quantitative EO with the techniques described here: a new-generation payload at ∼60°E would allow filling the gap and duplicating, with different view angles, the observation of volcanic areas of Africa and southeast Asia

As stated earlier, a full disc view image rate of 15 min is still unrivalled in enabling the monitoring of rapidly evolving events.

All polar payloads are acceptable for quantitative volcano monitoring worldwide at daily revisit rates, with the exception of radiometers AVHRR onboard platforms METOP and NOAA, whose major limitation is principally due to the early MIR channel saturation (∼325 K° in average) which impels analytical computing of radiant fluxes at pixel sub-resolutions.

In terms of spectral resolution, the IR satellites we exploit present at least one channel in the MIR window (3–5 μm) and at least two in the TIR window (8–14 μm). Together with SWIR (1.5–2.4 μm), when available, such multispectral data can be analysed for volcanic hot-spot detection and calculation of physical parameters (radiant flux and effusion rate, see Sect. 16.3.1). In particular, MODIS (onboard the Aqua and Terra platforms of NASA) regularly operates in the same classes of ground resolutions and revisiting intervals as AVHRR, but is much better suited to Solid Earth EO. MODIS acquires daytime data in 36 observation channels between Visible and TIR with spatial resolution from 250 m to 1 km, and nighttime data in 16 channels MIR to TIR with a spatial resolution of 1 km and a 12-bit quantification level.

A significant difference is found with the Infrared Atmospheric Sounding Interferometer (IASI), a hyperspectral payload developed by the French CNES and the European consortium EUMETSAT, orbiting onboard METOP-A and exploited here for detection and monitoring of SO_2 and ash. IASI measures the Earth's outgoing thermal radiation for weather forecasting and scientific applications (atmospheric chemistry and climate; Clerbaux et al. 2009). Its large swath guarantees global cov-

erage circa twice daily, with about 1,280,000 acquisitions per day. The instrument has a good spatial resolution, ranging from 12 km circular footprint at nadir, to 20 by 39 km elliptical footprint at full swath. The radiance is measured with three detectors, each covering part of the wide spectral range 645–2760 cm^{-1}. The spectral resolution varies between 0.35 and 0.5 cm^{-1}, apodized at 0.5 cm^{-1} and sampled at 0.25 cm^{-1}, and the radiometric noise is smaller than 0.3 K below 2,000 cm^{-1}.

According to Clarisse et al. (2012), IASI proved effective in retrieving a host of trace gases, some on global daily scale (e.g., CO_2, H_2O, CO, O_3, HCOOH, CH_3OH, NH_3, CH_4) and others sporadically (e.g., HONO, C_2H_4, SO_2, H_2S). Its spectral range covers three SO_2 absorption bands, the $\nu 1$ in the ~8.5 μm atmospheric window; the strong $\nu 3$ band at ~7.3 μm and the combination band $\nu 1 + \nu 3$ at ~4 μm. The larger atmospheric window 8–12 μm is also suitable for measuring coarse aerosols of volcanological interest (ash, ice crystals: Clarisse et al. 2010b).

16.2.2 Ultra-Violet Radiometers

At the time of writing, two UV radiometers onboard LEO platforms can be exploited for SO_2 monitoring: the Global Ozone Monitoring Experiment (GOME-2) onboard METOP-A, and the Ozone Monitoring Instrument (OMI) onboard Aura.

GOME-2 is the successor of the GOME instrument onboard ESA's ERS-2. It is a nadir-scanning UV-Visible spectrometer that measures the back-scattered radiation from the earth-atmosphere system with a spectral coverage of 0.24–0.79 μm, at a resolution ranging between 0.002–0.004 μm. A direct Sun spectrum is recorded once a day. The default ground pixel size is 80 × 40 km^2 (across-track × along-track) covering a swath width of 1920 km, which allows global coverage at the equator in about 1.5 days. Owing to an optimized movement of the scan mirror, the ground pixel size remains nearly constant over the full scan.

The basic GOME-2 SO_2 column products we incorporate for operational monitoring of volcanic activity are provided by the German Aerospace Center (DLR) in the framework of EUMETSAT's Satellite Application Facility on Ozone and Atmospheric Chemistry Monitoring (O3M-SAF). The operational retrieval of the SO_2 column products is performed with the UPAS (Universal Processor for Atmospheric Spectrometers) system, a new generation system for the processing of operational trace gas and cloud property products in near-real time and off-line. The resulting GOME-2 products are disseminated via EUMETCast, WMO/GTS and the Internet in less than two hours after sensing, through a committed, 24 h service.

OMI is a Dutch–Finnish instrument flying on the Sun-synchronous AURA platform of NASA, launched in July 2004. It is a nadir-viewing imaging spectrograph measuring atmosphere-backscattered sunlight in the ultraviolet-visible (UV-VIS) range from 270 to 500 nm (Levelt et al. 2006). In contrast to its forerunners GOME and SCIAMACHY, operating with scanning mirrors and one-dimensional photo diode array detectors, OMI was equipped with two two-dimensional CCD detectors. The CCDs record the complete 270–500 nm spectrum in one direction, then

observe the Earth's atmosphere with a 114° field of view, distributed over 60 discrete viewing angles, perpendicular to the flight direction.

The field of view of OMI corresponds to a 2600 km wide spatial swath, to complete global coverage in one day. Across the track, the size of an OMI pixel varies with viewing zenith angle from 24 km in the nadir to approximately 128 km for the extreme viewing angles of 57° at the edges of the swath.

OMI has three spectral channels; UV1 (270–310 nm) and UV2 (310–365 nm), covered by the first CCD. The second CCD covers the VIS-channel from 365–500 nm with a spectral sampling of 0.21 nm and a spectral resolution of 0.63 nm. SO_2 concentration and the Aerosol Index are retrieved from the UV2 channel (Krotkov et al. 2006). Unfortunately, due to a row anomaly in the CCD array of detectors the radiance data of OMI are altered at all wavelengths for a particular viewing direction of the sensor. This anomaly changes with time and can affect the quality of the products, thus reducing the effective spatial coverage.

A third sensor—the SCanning Imaging Absorption spectroMeter for Atmospheric ChartograpHY (SCIAMACHY; Bovensmann et al. 1999)—was also exploited until April 8, 2012, when it ceased operations together with its platform ENVISAT.

Based on alternated limb-nadir viewing for the vertical profiling of detected gases, it was well-suited for the mapping of aerosols clouds, and the third best sensor in SO_2 monitoring. Its large spectral range (between 240–1700 nm and 1900–2400 nm, with a resolution between 0.2 and 1.5 nm) has allowed observing main atmospheric gases (H_2O, CH_4, CO and CO_2) and many trace gases (O_3, NO_2, BrO, HCHO, CHOCHO, OClO) during its 10-year uninterrupted service.

16.3 Methods

16.3.1 Computation of High-Temperature Ground Features

Four main physical parameters can be determined by passive remote sensing: Integrated temperature (T_i in K), Effective temperature (T_e in K), Radiant flux (Q_{Rad} in W), and—where appropriate—Effusion rate (E_r in m^3/s)

Integrated temperature T_i—The "at-satellite" spectral radiance (R_λ) is composed of three terms: the surface reflected radiance ($R_{\lambda,D}$), the upwelling path radiance ($R_{\lambda,U}$) and the surface thermal radiance $L(\lambda, T)$ given in

$$R_\lambda = R_{\lambda,\text{Thermal}} + \tau_\lambda \rho_\lambda R_{\lambda,D} + R_{\lambda,U}, \tag{16.1}$$

with

$$R_{\lambda,\text{Thermal}} = \tau_\lambda L(\lambda, T), \tag{16.2}$$

τ_λ the atmospheric spectral transmission coefficient and ρ_λ the spectral reflectivity of the target at wavelength λ. According to Planck's distribution law, the spectral radiance of a surface is a function of its integrated temperature T_i (K).

In case of daytime images in NIR (0.78–1.4 μm) and SWIR (1.4–3.0 μm), reflected sunlight may swamp lesser radiant anomalies. In the TIR wavelengths range (8–15 μm) the reflected radiance is negligible: conversely, the background radiates significantly and over long integration times because of solar heating, lava cooling, e.g., eventually leading to error in the radiance assessment for analytical computing. In night-time data, the suppression of the contribution of direct, atmosphere-backscattered and surface-reflected Sun radiation leads to simplified and robust temperature determination (no reflected radiance) and more accurate results (larger S/N ratios). This may provide for radiation in shorter NIR wavelengths (ca. 0.9 μm) to be used in the blackbody curve determination (Flynn and Mouginis-Mark 1992).

In SWIR, the upwelling path radiance contribution is low and the radiation reflected by the surface ($R_{\lambda,\ D}$) can be estimated considering the mean (R_λ) of non-thermally-anomalous pixels surrounding a hot-spot pixel (Flynn et al. 1994; Oppenheimer et al. 1993a).

The sub-pixel thermal structure of remote sensed multi-spectral data can be investigated by means of the so-called 'Dual-band' method, as in Dozier (1981), Matson and Dozier (1981), and Rothery et al. (1988). This physical method is based on the following assumptions:

- If a radiant picture element is composed of two or more distinct temperature components (at least one hot, say T_h, and one much cooler, say T_c) the radiometer's pixel will display a temperature T_i which is the weighted average of the radiance from each component.
- If radiances associated to T_c and T_h respectively, are measured at two distinct wavelengths in two channels λ_1 and λ_2 of the radiometer (Hirn et al. 2008; Glaze et al. 1989; Oppenheimer et al. 1993b; Pieri et al. 1990; Rothery et al. 1988) the fraction (f) of the pixel occupied by the temperature T_h, or the fraction $(1-f)$ of the pixel occupied by T_c, can be solved simultaneously in the equation system (16.3) below.

$$\begin{aligned} R_{1,\text{Thermal}} &= \tau_1 * [f * L(\lambda_1, T_c) + (1 - f) * L(\lambda_1, T_h)] \\ R_{2,\text{Thermal}} &= \tau_2 * [f * L(\lambda_2, T_c) + (1 - f) * L(\lambda_2, T_h)] \end{aligned} \tag{16.3}$$

The above, 'dual-band' method may apply to three temperature components ('three-endmember'; Oppenheimer 1991) when the volcanic feature is smaller, or much smaller than the pixel. This is typical of large pixels as in SEVIRI, JAMI or Imager, where small volcanic features may occupy negligible fractions of individual pixels, the most of which will present a 'background' temperature T_b. In this case, the spectral radiance equation system reads (with $n = 1, 3$):

$$R_{n,\text{Thermal}} = \tau_n * [f_c * L(\lambda_n, T_c) + f_h * L(\lambda_n, T_h) + (1 - f_c - f_h) * L(\lambda_n, T_b)] \quad (16.4)$$

When solving any of the above systems for $R_{n,\text{Thermal}}$, a term called "effective temperature",

$$T_e = \tau_1 * \left[f_c * T_c^4 + f_h * T_h^4 \right]^{1/4} \quad (16.5)$$

can be isolated (Crisp and Baloga 1990; Hirn et al. 2009; Pieri and Baloga 1986). Once the temperature distribution is determined, T_e intervenes in the computation of the total radiant energy flux

$$\text{Q}_{\text{rad}} = \sigma \varepsilon \text{ST}_{\text{e}}^4 \quad (16.6)$$

(Glaze et al. 1989; Rothery et al. 1988).

In (16.6), σ is the Stephan-Boltzmann constant, with S the area of the pixel. Flux density is a good marker of the level of volcanic activity: areas with low flux density are associated to cooling flows or fumarole fields, whereas high flux densities are usually associated to areas of intense, local energy output such as skylights, ephemeral boccas or active domes.

If appropriate, radiant fluxes Q_{rad} (W) can be converted to mass effusion rates E_{r} (m^3/s) with cooling models if petro-physical properties of materials are known and, in particular, the temperature at which lavas don't flow anymore (T_{stop}) is known. One of the approaches to E_{r} computation is (Hirn et al. 2008, 2009; Pieri et al. 1990):

$$E_r = \frac{Q_{\text{rad}}}{\rho_{\text{lava}} \left(C p_{\text{lava}} \Delta T_{\text{stop}} + C_L \Delta \phi \right)} \quad (16.7)$$

Above, $\Delta\text{T}_{\text{stop}}$ equals $\text{T}_h - \text{T}_{\text{stop}}$, and ρ_{lava}, Cp_{lava}, $\Delta\phi$, C_{L} respectively are: the density, the specific heat capacity, the mass fraction of crystals grown and the latent heat of crystallization of involved lavas.

16.4 Measurement of Volcanic Emissions in the Atmosphere

16.4.1 Computation of SO_2 *Concentrations*

The standard output of satellite SO_2 retrievals is the vertical column (VC), which represents the amount of SO_2 molecules in a column overhead per surface unit, at a given location. It is generally expressed in Dobson Units, in use for columnar density of trace gases in the Earth's atmosphere ($1\,\text{DU} = 2.69 \times 10^{16} \text{molecules/cm}^2$).

SO_2 VCs are routinely retrieved from UV backscatter measurements of sunlight from the satellite instruments, using either the Differential Optical Absorption Spectroscopy (DOAS) technique (GOME-2 and SCIAMACHY) or the Linear Fit algo-

rithm (OMI). Although the techniques differ in the details, observation principles are similar. The basis is the Beer-Lambert law that describes the relation between the incident light intensity I_0 (solar spectrum) and the transmitted light intensity I (measured backscattered spectrum) through an absorbing and diffusing medium:

$$I(\lambda) = I_0(\lambda) \exp\left[-\int_0^L \left(\sum_{j=1}^{n} \sigma_{a,i}(\lambda) n_i + diffus(\lambda) \right) ds \right] \tag{16.8}$$

with λ the wavelength. In Eq. (16.8), the light is attenuated along its path L from the Sun by the n different atmospheric absorbers (with absorption cross-section $\sigma_{a,i}$ and density n_i) and by the diffusing molecules and aerosols.

The wavelength window for ultraviolet SO_2 retrievals lies between 310 and 330 nm, where strong SO_2 absorption occurs. Retrievals are obtained in a three-step process, based on the separation of the spectral fitting of absorption signals, and the determination of light path length.

The spectral evaluation that follows, consists of a non-linear fit where atmospheric cross-sections are adjusted to the log-ratio of a measured calibrated earthshine spectrum I_λ and an absorption-free solar spectrum $I_{o,\lambda}$, within a selected wavelength interval. Assuming the light path to be independent of wavelength over small λ intervals, the synthetic equation (Valks et al. 2009) is written:

$$\ln\left[\frac{I_\lambda(s)}{I_{0,\lambda}^{(}s)} \right] = -\sum_g E_g(s) \cdot \sigma_g(\lambda) - \sum_{j=0}^{3} \alpha_j \left(\lambda - \lambda^*\right)^j - \alpha_R R(\lambda) \tag{16.9}$$

Here, I_λ is the earthshine spectrum at wavelength λ, and $I_{0,\lambda}$ the solar spectrum. On the right hand, E_g(s) is the 'Slant Column Density' of the gas g, defined as the total amount of absorbers per unit area integrated along the light path s, with $\sigma_g(\lambda)$ the associated absorption cross-section. The second term in the equation is the closure polynomial for a reference wavelength λ^*, and the third accounts for the rotational Raman scattering, with R(λ) the Ring reference spectrum and α_R its scaling parameters. The fitting minimizes the weighted least squares difference between measured and simulated optical densities.

In a second step, data undergo a background correction aimed to avoid non-zero columns over regions showing very low SO_2 levels, and to ensure a geophysical consistency of results at high solar zenith angles, where there is a strong interference of SO_2 and O_3 absorption signals.

In a third and final step, the SO_2 signal is converted into a SO_2 vertical column using simulated radiation transfers in the atmosphere. Parameters influencing the photons path are: the solar zenith angle and the instrument viewing angles, the surface albedo, the atmospheric absorption, and scattering on molecules and clouds.

As a rule, the information on the height of SO_2 plumes is not available at the time of observations although the measurement sensitivity to SO_2 is altitude-dependent. Consequently, the estimate of vertical columns implies parameterizing the plume

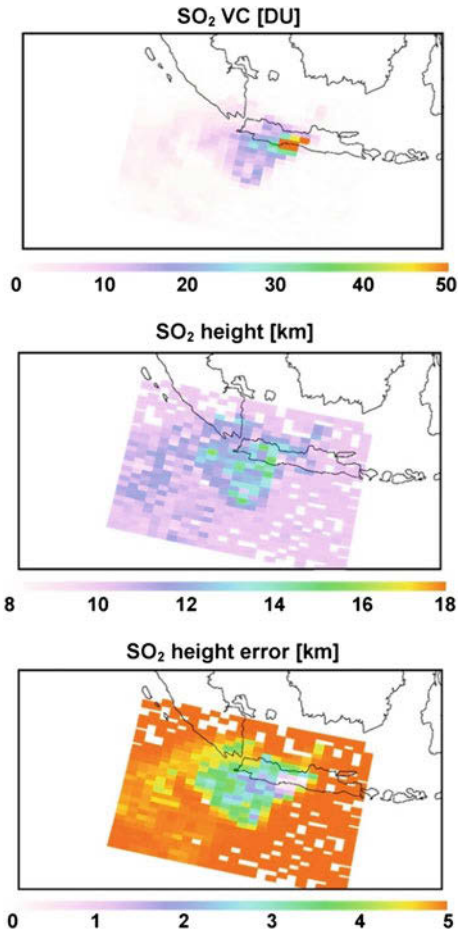

Fig. 16.2 SO_2 vertical columns, plume height estimate and map of errors in height for the eruption of Merapi (Java, Indonesia) on November 5, 2010, observed with the UV payload GOME-2 onboard METOP-A

height, which is usually done at three or four different levels. The lowest level (typically less than 4–5 km, as a function of the troposphere model in latitude and season) signifies SO_2 originating from anthropogenic activities or low-to-mild volcano degassing at low altitudes. The middle tropospheric level is representative of conditions where SO_2 is emitted from effusive volcanic eruptions or quiet degassing from the top of high volcanic edifices. Finally, stratospheric levels are consistent with SO_2 released from explosive volcanic eruptions.

For high SO_2 column amounts (>25 DU), the eventual saturation of SO_2 absorption may lead to underestimate VCs. Hence, it is preferable to retrieve SO_2 using an optimal estimation method based on full radiative transfer modelling. For these conditions, the height of the plume can also be retrieved from spectral UV measurements, taking advantage of the different response of earthshine UV spectra at different plume altitudes. In the peculiar case of the 2010 eruption of Merapi, Java

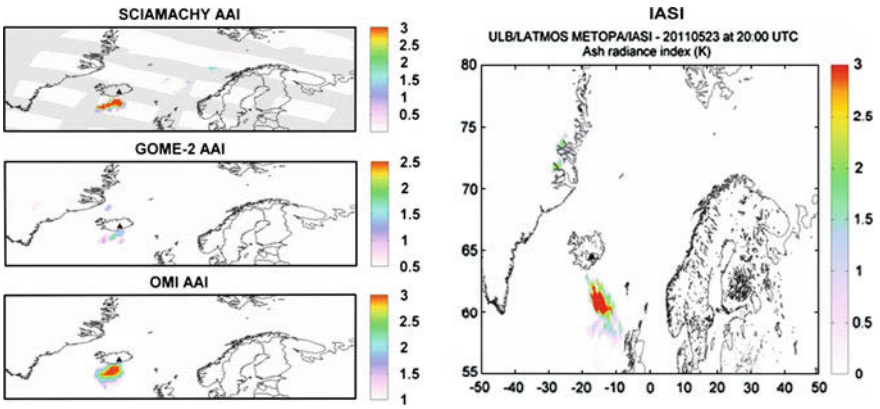

Fig. 16.3 Multi-orbit mosaic of Aerosol Ash Indexes from SCIAMACHY, GOME-2 and OMI (*daytime*) and IASI (*night time*) observations on May 23, 2011, two days after the eruption of Grímsvötn on May 21, 2011

(Indonesia), high SO_2 columns observed close to the volcano appeared to coincide with high SO_2 heights: retrieved plume height values were 16 ± 2 km (Fig. 16.2).

It should be noted that the peak altitude resulting from the retrieval process is an effective height. This means that lateral heterogeneity in the horizontal distribution of SO_2, or deviation from the parameterized plume shape are incorporated in the result. Further details on SO_2 retrieval from satellite UV sensors can be found in Nowlan et al. (2011), Rix et al. (2009, 2012), Valks et al. (2009), Van Geffen et al. (2007, 2008) and Yang et al. (2007, 2010) among others.

As a complement to ultraviolet sounding with GOME-2 and OMI, the retrieval of SO_2 is also feasible in the SO_2 absorption bands of thermal infrared, which allows for day-and-night measurement of VCs. There are several multispectral (MODIS, SEVIRI, e.g.) and hyperspectral sensors (AIRS, IASI, e.g.) theoretically suited to this purpose, at various levels of resolution and sensitivity: we exploit systematically the hyperspectral radiometer IASI (Clarisse et al. 2008, 2011). In the presence of an absorbing SO_2 layer, the measured radiance R can be written:

$$R_v = B_v\,(T_a)\,\tau + (1-\tau)\,B_v\,(T_l) \tag{16.10}$$

In (16.10) ν is the wavenumber, τ is the transmittance of the SO_2 plume, B_ν is the Planck function, T_l is the temperature of the plume and T_a is the total brightness temperature of the layers below.

The infrared hyperspectral retrieval by IASI, combines measured brightness temperature differences between baseline channels and wavenumbers (1371.75 and $1385\,\mathrm{cm}^{-1}$) in the strong SO_2 absorption $\nu 3$ band. However, because of competing water absorption, the vertical sensitivity to SO_2 is limited to atmospheric layers above 4–5 km. The conversion of measured signals into a SO_2 vertical column is

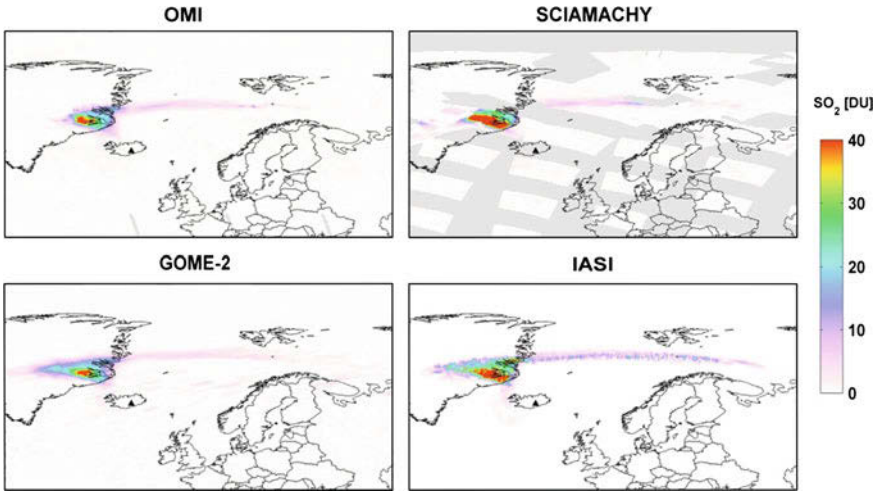

Fig. 16.4 SO_2 vertical column engendered by the eruption of Grímsvötn measured with polar orbiting payloads OMI, SCIAMACHY, GOME-2 and IASI on May 23, 2011. A plume altitude of 10 km is assumed for all estimates. SCIAMACHY ceased operations almost one year later, on April 8, 2012

performed by use of a look-up-table generated using elementary radiative transfer, and EUMETSAT operational pressure, temperature and humidity profiles.

The main features of the algorithm are a wide applicable total column range (four orders of magnitude, from 0.5 to 5000 DU), a low noise level and a low theoretical uncertainty (3–5 %). As in UV techniques, however, also in the infrared the main source of error is associated to the poor a-priori knowledge of the height of plumes. Consequently, the algorithm calculates the SO_2 columns for a set of pre-defined hypothetical altitude levels between 5 and 30 km. Errors vary from about 30 % for the lowest and highest altitudes, to about 5 % at the tropopause (Fig. 16.3). For further details the reader is referred to Clarisse et al. (2011).

16.4.2 Volcanic Sulfur Aerosol and Ash

Since SO_2 is reliably retrieved from satellite measurements, it is often used as a proxy for the presence of ash. However, some eruptions emit barely detectable amounts of SO_2 (e.g., Eyjafjallajökull in 2010), while others inject SO_2 and ash at different altitudes in the atmosphere, giving rise to a differentiation of the directions of transport (e.g., Grímsvötn in 2011: see Figs. 16.4 vs. 16.3). Unlike SO_2, the remote sensing of ash is hampered by the absence of narrow absorption bands in its spectral signature, which displays broad shape absorption.

Algorithms for quantitative ash retrieval (among others: Corradini et al. 2010; Gangale et al. 2010; Prata and Bernardo 2009; Prata and Prata 2012) must solve at once three geometrical and microphysical unknowns: the ash loading, the plume altitude and thickness, and the distribution of particle diameters. Such a severely under-determined problem does present constrained solutions if at least one of these parameters—in particular, plume height and thickness—are simultaneously available from independent observations: an event still sufficiently rare not to rely upon for real-time monitoring at a global scale. Therefore, given the strong operational, real-time orientation of EVOSS and SACS, we stuck to a qualitative routine information for the presence of ash in the atmosphere, in a combination of UV, Visible and Infrared observations to obtain global coverage several times daily.

For UV sensors GOME-2, OMI and the past SCIAMACHY, the Absorbing Aerosol Index (AAI) is a widely used product. The computation of AAI is based on a residual that separates the spectral contrast at two ultraviolet wavelengths (340 and 380 nm/354 and 388 nm) caused by absorbing aerosols, from that of other effects as molecular Rayleigh scattering, surface reflection, gaseous absorption and aerosol and cloud scattering (de Graaf et al. 2010; Herman et al. 1997; Tilstra et al. 2007). It reads:

$$AAI = -100 \cdot \left[\log_{10} \left(\frac{I_\lambda}{I_{\lambda,0}} \right)^{\text{meas}} - \log_{10} \left(\frac{I_\lambda}{I_{\lambda,0}} \right)^{\text{Ray}} \right] \tag{16.11}$$

where I_λ is the radiance at the top of the atmosphere at a wavelength λ. I^{meas} refers to a measured radiance of a real atmosphere with aerosols, as opposed to a calculated radiance for an aerosol-free atmosphere with only Rayleigh scattering and absorption by molecules and surface reflection and absorption (I^{Ray}).

AAI is not strictly selective for volcanic ash, as it is also triggered by other UV-absorbing aerosols, the most frequent observations of which arise from desert dust and biomass burning.

However, when a marked SO_2 plume is detected by means of any of the methods discussed above, the location and extent of a volcanic ash plume is generally made easier by the use of AAI.

In TIR, ash has a more marked and distinct spectral signature than in the UV wavelength range. Clarisse et al. (2010a, b) have demonstrated the possibility to retrieve qualitative and quantitative information on ash from IASI observations, by taking advantage of the numerous spectral channels of the sensor. However, the currently available IASI ash algorithm is an Ash Index based technique which exploits the brightness temperature difference of two well-chosen channels (1168 and 1231.5 cm^{-1}). This difference is very sensitive for all types of ash: however, although the IASI ash index is more selective than the UV AAIs for volcanic ash, it may also flag on other mineral dust.

An example of results of Aerosol Ash Indexes from the UV and IR sensors is shown in Fig. 16.3 for the eruption of Grímsvötn. All sensors clearly show an ash plume south of Iceland: however, if we turn to the simultaneous SO_2 observations shown

earlier in Fig. 16.4, we observe that the SO_2 plume was transported northwards. If all observations were carried out at the same time, the obvious explanation is that there was an altitude stratification between the SO_2 and the ash levels. As IASI-borne Ash Indexes (Fig. 16.3) are from night time observations carried out between 8 and 12 h after the measurement times of UV sensors (Fig. 16.4), another possible explanation is that ash was injected into the atmosphere at lower altitudes than SO_2, with different wind directions prevailing. Qualitative 'ground truth' observations confirm that the ash plume was transported southwards, towards Scotland, in that 12 h interval.

16.5 Case Studies of Multi-Technique Synergy

In the framework of the EVOSS project, EU and African Volcanoes, located within SEVIRI—MSG full disk, that underwent eruption from 2000 up to present day are monitored through analysis of SEVIRI data, allowing real time volcanic hot spot detection and computation of physical parameters (radiant flux and effusion rate), with information refreshment every 15 min. As of late 2012, the whole of volcanoes—nineteen—having erupted from 2004 in the Region of Interest are in the target of EVOSS. They are: Stromboli and Etna (Sicily, Italy), Hierro (Canary Islands, Spain), Jebel-al-Tair and Jebel Zubair (Yemen), Manda Hararo, Dalafilla, Dabbahu, Erta Ale and Nabro (Ethiopia), Mt.Cameroon (Cameroon), Nyiragongo and Nyamuragira (DR Congo), Ol Doinyo Lengai (Tanzania), Karthala (Comoros), Piton de la Fournaise (Réunion Island, France), Soufriere Hills (Montserrat, British Overseas Territory), Eyjafjallajökull and Grímsvötn (Iceland). They present major differences in: eruption styles and durations, distances from the centre of the SEVIRI-MSG full disk (pixel footprint between 9 km^2 at nadir and over 50 km^2 near the disk border), type and intensity of volcanic activities (effusive or explosive), thermal features dealt with (lava fountains, lava lake, lava flow, lava dome building), and magma temperatures (from ~1420 K at Piton de la Fournaise, to ~860 K in the natro-carbonatite lavas of Ol Doinyo Lengai).

16.5.1 The Reawakening of Nabro, Eritrea

Nabro (13.37°N, 41.70°E, 2218 m a.s.l.), one of the three volcanoes of the Bidu complex in the Danakil depression, marking the border between Eritrea and Ethiopia, erupted in the evening of the June 12, 2011, expelling enormous amounts of steam, SO_2 and ash in the atmosphere. Figure 16.5 shows the ash plume appearing at the onset of the eruption (20:30 UTC).

Right after the early detection, observation of the thermal source was hindered during about three days by a thick plume of ash, water vapor and SO_2.

Figure 16.6 displays the spatial distribution of the SO_2 columns measured by IASI on June 16, 2011 (daytime observations). For this event, IASI had a good

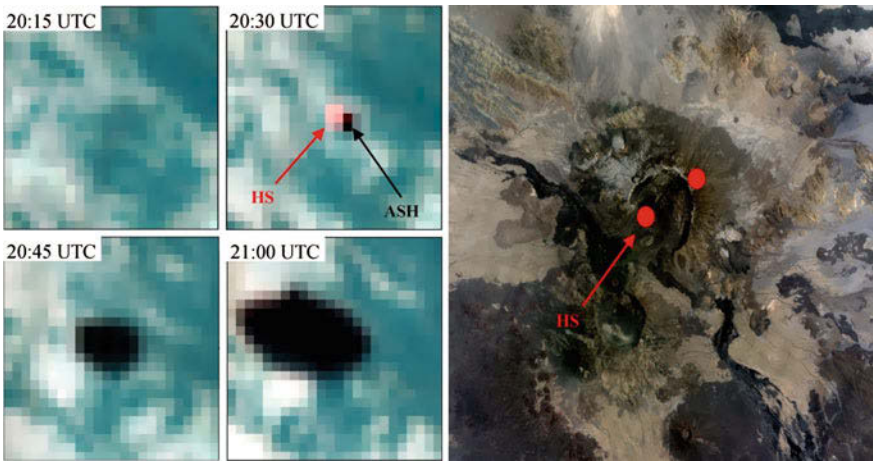

Fig. 16.5 *Left* SEVIRI observations with 15 min repeat, allowed detecting the onset of the eruption of the oversleeping volcano Nabro at 20:30 UTC on June 12, 2011 (in RGB false-colour composite with $R = MIR_{3.9}$, $G = TIR_{10.8}$, $B = TIR_{11.9}$) and the fast development of a major plume of steam, SO_2 and ash. *Right* The location of the centroids of the two hot-spot pixels (marked HS in the image *center-top*), overlain to a pre-eruption, image of Landsat 5-TM, allow locating the eruptive source within the Nabro caldera, and to amend an initial qualitative estimate set at the ca. 30 km distant volcano Dubbi, which last erupted in 1861

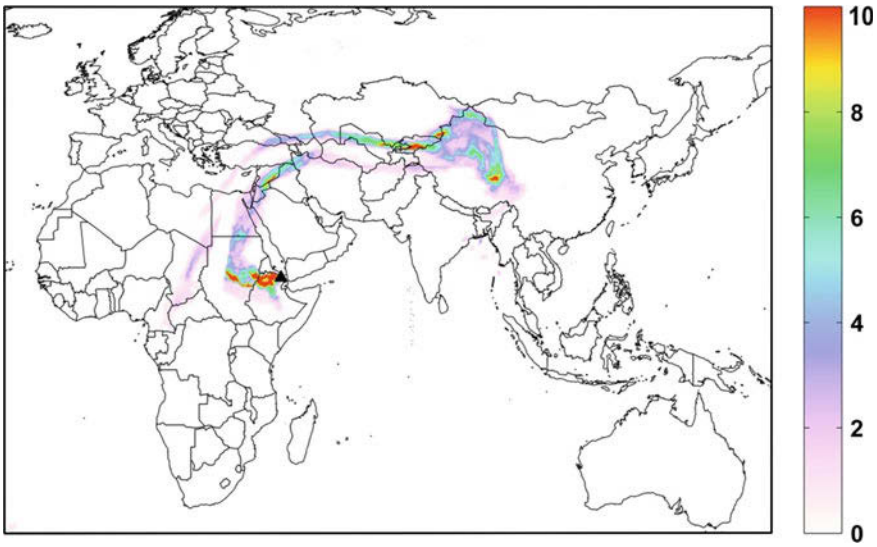

Fig. 16.6 SO_2 columns (DU) for a 13 km high plume from Nabro, Eritrea, are observed in this *mosaic* of daytime observations by the hyperspectral radiometer IASI, onboard METOP-A, on June 16, 2011

measurement sensitivity to SO_2 thanks to the high altitude of the plume. Compared to UV sensors, IASI has a superior spatial resolution and a better temporal resolution—twice daily instead of once. The pattern shown, integrates the SO_2 emissions and losses in the first three-and-half days of eruption.

The SO_2 plume reached tropopause altitudes (~15 km at these latitudes), and fast easterly jet winds spread the plume towards SE Asia.

All UV and IR sensors could still measure significant SO_2 concentrations several weeks after the onset of the eruption, which finished (from the remote-sensing standpoint) on July 17. A total SO_2 erupted mass of ~1.5 Mt was estimated by Clarisse et al. (2011).

Turning from global to local scales, Fig. 16.7 shows the very-high temporal resolution, synergistic merge of thermal Radiant Fluxes (method in Sect. 16.3.1) obtained over Nabro with SEVIRI, and maximum SO_2 columns (merge of results from separate processing of OMI, GOME-2, SCIAMACHY and IASI).

The maximum SO_2 column (313 DU) was measured on June 16 at 07:39 UTC by SCIAMACHY, whereas the maximum Radiant flux value (75 GW, Fig. 16.7) was measured by SEVIRI at 18:15 UTC, 13 h later.

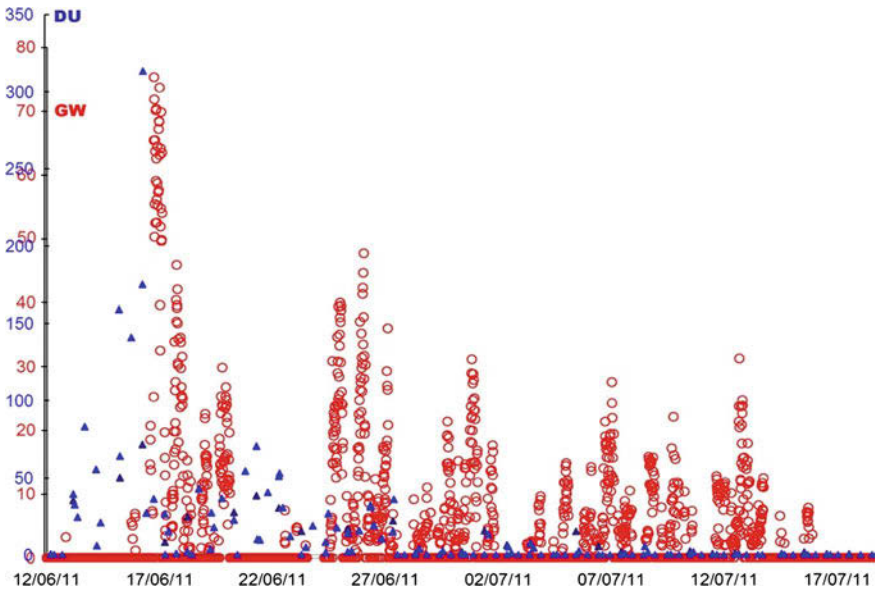

Fig. 16.7 Eruption of Nabro (Eritrea), June 12 to July 17, 2011. Outstanding values of radiant fluxes Q_R (*red scale*, in GW) and SO_2 vertical columns (*blue scale*, in DU) highlight the violent reawakening of Nabro after an hypothesized rest of 5,000 years. Involved payloads were the geostationary SEVIRI for Q_R (15 min revisit) and polar orbiting OMI, GOME-2, SCIAMACHY (all with circa daily revisit) and IASI (twice daily) for SO_2 vertical columns

16.5.2 The Eruption of Nyamuragira, Congo 2011–2012

Nyiragongo and Nyamuragira are known to be, together, one of the main sources of volcanic SO_2 worldwide.

The Nyamuragira summit caldera, which is not degassing in non-eruptive times, is located at a distance of about 14 km from Nyiragongo. The latter, hosts a permanent lava lake in its ca. 3,000 m high crater, which emits an average ∼3 GW, near-permanent radiant flux. Nyamuragira, erupted over 40 times in the last Century: between 1979 and 2005 its total SO_2 output per eruption—observed with the Total Ozone Mapping Spectrometer (TOMS)—was estimated at more than 0.8 Mt (Bluth and Carn 2008).

Almost two year after the last eruption of January 2–29, 2010, Nyamuragira started erupting on November 6, 2011 (18:45 UTC) with observed lava fountains reaching up to 300 m. The eruption lasted more than four months, coming to an end between March 6, 2012 (last evidence of high radiant fluxes on ground, from EVOSS) and March 15, 2012 (visual statement by the Volcano Observatory of Goma).

Figure 16.8 shows that at 17:30 UTC of November 6, 2011, only the radiant source associated to the permanent lava lake of Nyiragongo was detected (two hot-spot pixels across the crater area), for an overall, standard radiant flux of ∼3 GW (see Fig. 16.9). From 17:30 to 20:00 UTC, no hot-spots were visible in the whole area because of worsened cloud cover. At 20:15 UTC, conversely, the new lava flow led to measurable radiance in a set of three, L-shaped pixels shown in Fig. 16.8 right-top, 12 km east of Nyamuragira and about 15 km northeast of Nyiragongo. The SEVIRI pixel footprint in the area is ∼10 km^2; the radiant flux associated to the sum of the three pixels displayed an initial minimum of 12 GW.

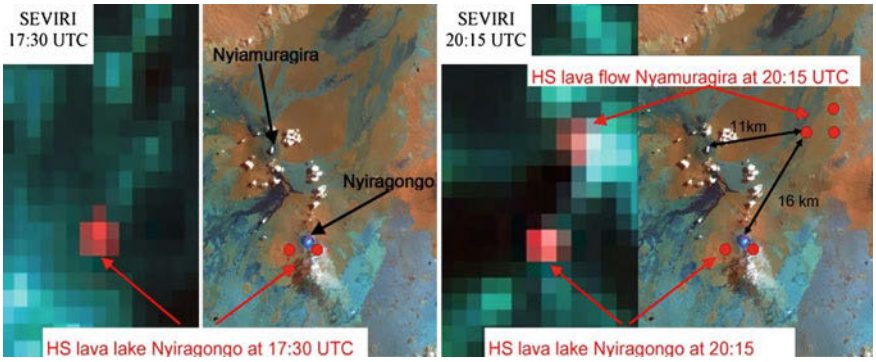

Fig. 16.8 Nyiragongo–Nyamuragira area, DR Congo: radiance change detection in time and space to constrain the onset of the 2011 eruption of Nyamuragira. In the *right half* of both images, hot-spots (HS) are located in a pre-eruption, high resolution Landsat 5-TM image of the area (the pixel footprint of SEVIRI in this area is ∼10 km^2, that of TM, $9 \cdot 10^{-4}$ km^2). *Left* Thermal situation at 17:30 UTC showing only the hot-spots associated to the Nyiragongo's permanent lava lake. *Right* Early detection of the new lava flow at Nyamuragira at 20:15 UTC

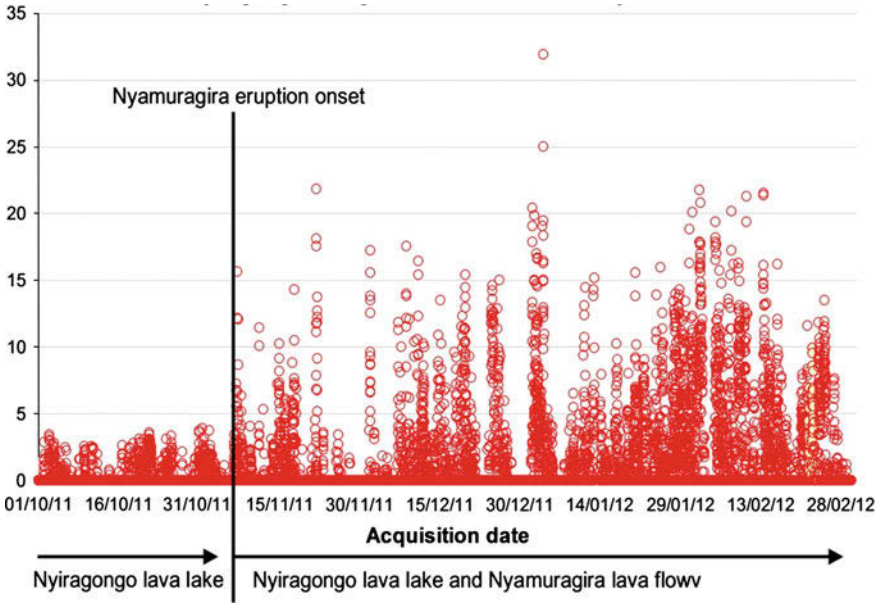

Fig. 16.9 Radiant flux Q_R (10^9 W) series across the onset of the eruption of Nyamuragira, Congo, started on November 6, 2011, and ended on March 15, 2012. Right-hand values integrate Q_R from both Nyiragongo (lava lake, $Q_{Rmax} \sim 4$ GW) and Nyamuragira (lava flow and fire fountains, up to ~32 GW)

Radiant fluxes (Fig. 16.9) computed for the whole area considering Nyiragongo and Nyamuragira as a whole—as usually done in ordinary operations when the only radiant source is at Nyiragongo—stays over 2–4 GW, which is the standard contribution of the lava lake in clear-sky conditions.

Radiant flux bursts regularly exceeding 10 GW, with an observed maximum of about 32 GW during the strong activity of early January—were associated with repeated episodes of long lasting, sustained lava fountains at the newly created vent at low altitudes. The strong degassing turned, once more, into an exceptional cover by a thick, near-stationary SO_2 cloud during almost two months, reported by the Volcano Observatory of Goma (see also Fig. 16.10).

From Figs. 16.10 and 16.11 it is clear that UV sensors OMI, SCIAMACHY and GOME-2 were best suited to the monitoring of the Nyamuragira event as they present good sensitivity to SO_2 at all altitudes.

Conversely, IASI was useful at the very beginning of the eruption, in presence of a SO_2 plume high in the troposphere: whereas after November 15 the plume stayed low (under ~500 mbar) and little SO_2 was detectable in infrared, with large errors.

We shall note further that—as expected—SO_2 vertical column estimates depend also on the spatial resolution of sensors, whose pixel footprints range today from slightly above 150 km^2 (OMI and IASI at nadir) and as much as over 3200 km^2 (GOME-2). This can influence the estimate of SO_2 masses and, consequently, the

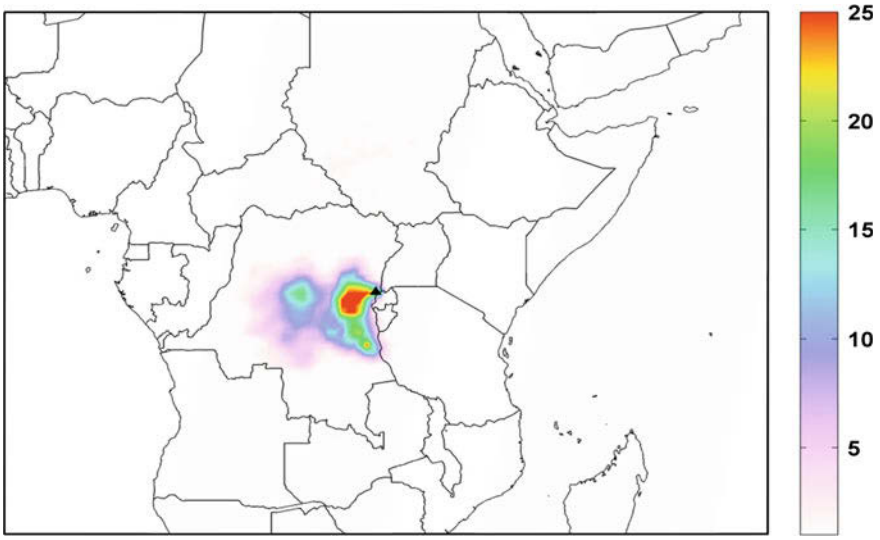

Fig. 16.10 SO_2 columns (DU) from GOME-2 on November 11, 2011, five days after the onset of the 2011–2012 eruption. Plume altitude: 6 km

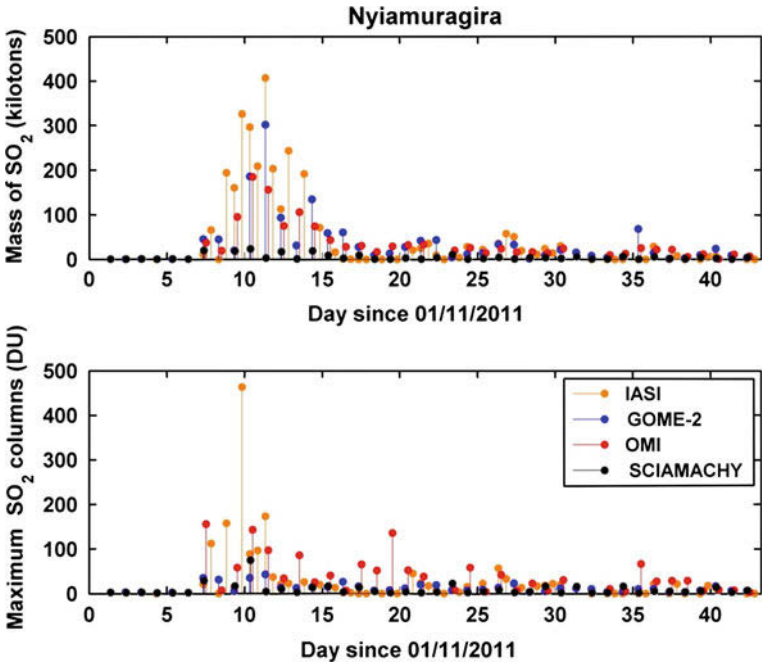

Fig. 16.11 Daily SO_2 burdens (*top*) and maximum vertical column (*bottom*) measured by GOME-2, OMI, SCIAMACHY and IASI over Central Africa (20°S–20°N, 10–50°E), November–December 2011. A middle tropospheric altitude (∼7 km) is assumed for the SO_2 vertical column calculation. A 3σ threshold is adopted for the UV datasets, with σ the standard deviation of daily SO_2 retrieved in background region

computation of mass rates and fluxes, which deserve a major role in volcanology for assessing the magmatic activity in the shallow magmatic plumbing system and above.

However, except for the values of SCIAMACHY (that are too low, due to the limited spatial coverage of the instrument), total SO_2 masses from GOME-2, OMI and IASI are in good agreement, with observed differences to be attributed to differences in the spatial coverage (position of the orbits) or to differences in measurement 'noise', for instance, clouds.

An attempt to carry out a rough estimate of daily SO_2 fluxes from the total SO_2 masses time series in Fig. 16.11 top, assuming ordinary SO_2 loss rates $k \approx 1\,day^{-}$ (Theys et al. 2012) returns about 1–1.5 Mt of SO_2 erupted by Nyamuragira in the first three months of eruption, from November 6, 2011 to January 31, 2012.

16.6 Conclusions

There are two potent reasons why a space-borne, real-time observing system can be of great use. The first reason comes from the fact that there are massive differences in the local on-ground observational capacity at different volcanoes. This varies from "everything" at a few State-of-the-Art observatories worldwide, to "nothing" in others. The stark reality is that most potentially dangerous volcanoes are not monitored, and it is not realistic to imagine this situation otherwise given the current resources of many nations faced with managing serious volcanic risk.

Clearly in the case where no volcano observatory or instrumental network exists, by definition, almost any volcanic event overwhelms the local observational capacity: as volcanic events of an unusually violent nature ramp up, however, instrumental capacity can be destroyed and even advanced observatories become progressively "blind" or even in exceptional cases themselves menaced. Between these extremes there is a whole spectrum of levels of on-site observing capacity which can never be designed to cope with all possibilities: hence, the problem of how to handle events that overwhelm that capacity is clearly posed.

This held true for Nabro, where no monitoring system of any type exists, and held true also for Nyamuragira, which is monitored by a volcano observatory which may easily be cutoff from actual unrests because of the huge extent of the area to observe, a generalized weakness of all telecommunication networks, and the objective complexity of anthropic and terrain components. The lack of monitoring facilities makes satellite observations unique, which means that no validation by quantitative "ground-truth" is expected. This is a strong point in favour of multi-payload multi-temporal observation, which is typically done in EVOSS with the pair SEVIRI-MODIS, and with the daily cluster GOME-OMI-IASI.

The second constraining point for structure and usefulness of a satellite observing system is that it is notoriously difficult to measure eruption fluxes from ground observing systems. Instrumental networks run by volcanic observatories are understandably designed primarily to identify precursor signals. These enable changes in

the system to be identified that even in the absence of a clearly adequate theoretical framework; can be used empirically to track changes until the onset of an event. Indeed, once lava and gas and/or ash begin to erupt at the surface, one of the key variables that can give access to how an event is evolving is the eruptive fluxes of those different materials. However, because neither the precise site of an eruption nor its impending magnitude can be known accurately in advance, no reliable or sufficiently flexible on-site solution has yet been devised to cope with the problem of monitoring all type of eruption fluxes.

The natural convergence of EVOSS' results shown above, synergistically obtained with as much as four different satellites for SO_2 detection and measurement (currently still released by SACS in the form of concentration) and with SEVIRI-MODIS for radiance driven estimates and 'running' validation of mass discharge rates, is conclusively more than promising. Prospectively, it points to the feasibility of systematically integrating in real-time lava and gas fluxes measured independently from each other at multiple sensors, using the thermal emission from cooling erupted material as a proxy for the amount of mass (essentially liquid magma) that is being erupted, and the flux information on SO_2 as a proxy for the overall amount of magmatic gases that have been erupted during the critical phases of major volcanic unrests anywhere on Earth.

Acknowledgments EVOSS (http://www.evoss.eu) "European Volcano Observatory Space Services" is a project funded in the frame of the European Commission FP7—GMES, with contract no. 242535 of the Research Executive Agency. SACS (http://sacs.aeronomie.be) "Support to Aviation Control Service" is a project of the European Space Agency ESA projects to support procedures of avoidance of volcanic ash based on satellite observations.

References

Bluth GJS, Carn SA (2008) Exceptional sulfur degassing from Nyamuragira volcano 1979–2005. Int J Remote Sens 29(22):6667–6685

Bovensmann H, Burrows JP, Buchwitz M, Frerick J, Noël S, Rozanov VV, Chance KV, Goede APH (1999) SCIAMACHY: Mission objectives and measurement modes. J Atmos Sci 56:127–150

Clarisse L, Coheur P-F, Prata AJ, Hurtmans D, Razavi A, Phulpin T, Hadji-Lazaro J, Clerbaux C (2008) Tracking and quantifying volcanic SO_2 with IASI, the September 2007 eruption at Jebel-at-Tair. Atmos Chem Phys 8:7723–7734

Clarisse L, Prata AJ, Lacour J-L, Hurtmans D, Clerbaux C (2010a) A correlation method for volcanic ash detection using hyperspectral infrared measurements. Geophys Res Lett 37:L19806. doi:10.1029/2010GL044828

Clarisse L, Hurtmans D, Prata AJ, Karagulian F, Clerbaux C, Mazière MD, Coheur P-F (2010b) Retrieving radius, concentration, optical depth and mass of different types of aerosols from high-resolution infrared nadir spectra. Appl Opt 49:3713–3722

Clarisse L, Hurtmans D, Clerbaux C, Hadji-Lazaro J, Ngadi Y, Coheur P-F (2012) Retrieval of sulfur dioxide from the infrared atmospheric sounding interferometer (IASI). Atmos Measur Technol 5:581–594. doi:10.5194/amt-5-581-2012

Clarisse L, R'Honi Y, Coheur P-F, Hurtmans D, Clerbaux C (2011b) Thermal infrared nadir observations of 24 atmospheric gases. Geophys Res Lett 38:L10802. doi:10.1029/2011GL047271

Clerbaux C, Boynard A, Clarisse L, George M, Hadji-Lazaro J, Herbin H, Hurtmans D, Pommier M, Razavi A, Turquety S, Wespes C, Coheur P-F (2009) Monitoring of atmospheric composition using the thermal infrared IASI/METOP sounder. Atmos Chem Phys 9:6041–6054

Corradini S, Merucci L, Prata AJ, Piscini A (2010) Volcanic ash and SO2 in the 2008 Kasatochi eruption: retrievals comparison from different IR satellite sensors. J Geophys Res 115:D00L21. doi:10.1029/2009JD013634 [printed 116(D2), 2011]

Crisp J, Baloga S (1990) A model for lava flows with two thermal components. J Geophys Res 95(B2):1255–1270

de Graaf M, Tuinder O, Tilstra G (2010) O3MSAF Algorithm Theoretical Basis Document for ARS, O3MSAF/KNMI/ATBD/002. Koninklijk Nederlands Meteorologisch Instituut (NL) 1:26

Dozier J (1981) A method for satellite identification of surface temperature fields of subpixel resolution. Remote Sens Environ 11:221–229

Ferretti A, Fumagalli A, Novali F, Prati C, Rocca F, Rucci A (2011) A new algorithm for processing Interferometric data-stacks: SqueeSAR. IEEE Trans Geosci Remote Sens. doi:10.1109/TGRS.2011.2124465

Flynn LP, Mouginis-Mark P (1992) Cooling rate of on active Hawaiian lava flow from night-time spectroradiometer measurements. Geophys Res Lett 19:1783–1786

Flynn LP, Mouginis-Mark PJ, Horton KA (1994) Distribution of thermal area an active lava flow field: Landsat observations of Kilauea, Hawaii, July 1991. Bull Volcanol 56:284–296

Gangale G, Prata AJ, Clarisse L (2010) The infrared spectral signature of volcanic ash determined from high-spectral resolution satellite measurements. Remote Sens Environ 114(2):414–425

Glaze L, Francis PW, Rothery DA (1989) Measuring thermal budget of active volcanoes by satellite remote sensing. Nature 338:144–146

Gottwald M, Bovensmann H (eds) (2011) SCIAMACHY: Exploring the changing Earth's atmosphere. Springer, New York. doi:10.1007/978-90-481-9896-2 [ISBN 978-90-481-9895-5]

Herman JR, Bhartia PK, Torres O, Hsu C, Seftor C, Celarier E (1997) Global distributions of UV-absorbing aerosols from Nimbus 7/TOMS data. J Geophys Res 102(D14):16911–16922. doi:10.1029/96JD03680

Hirn B, Di Bartola C, Ferrucci F (2008) Spaceborne monitoring 2000–2005 of the Pu'u'O'o-Kupaianaha (Hawaii) eruption by synergetic merge of multispectral payloads ASTER and MODIS. IEEE Trans Geosci Remote Sens 46(10):2848–2856

Hirn B, Di Bartola C, Ferrucci F (2009) Combined use of SEVIRI and MODIS for detecting, measuring and monitoring active lava flows at erupting volcanoes. IEEE Trans Geosci Remote Sens 47(8):2923–2930

Kaminski E, Tait S, Ferrucci F, Martet M, Hirn B, Husson P (2011) Estimation of ash injection in the atmosphere by basaltic volcanic plumes: the case of the Eyjafjallajökull 2010 eruption. J Geophys Res 116:B00C02. doi:10.1029/2011JB008297

Krotkov NA, Carn SA, Krueger AJ, Bhartia PK, Yang K (2006) Band residual difference algorithm for retrieval of SO_2 from the Aura ozone monitoring instrument. IEEE Trans Geosci Remote Sens 44(5):1259–1266. doi:10.1109/TGRS.2005.861932

Levelt PF, van den Oord GHJ, Dobber MR, Mälkki A, Visser H, de Vries J, Stammes P, Lundell J, Saari H (2006) The ozone monitoring instrument. IEEE Trans Geosci Remote Sens 44(5):1093–1101. doi:10.1109/TGRS.2006.872333

Matson M, Dozier J (1981) Identification of subresolution high temperature sources using a thermal infrared sensor. Photogram Eng Remote Sens 47:1311–1318

Nowlan CR, Liu X, Chance K, Cai Z, Kurosu TP, Lee C, Martin RV (2011) Retrievals of sulfur dioxide from the global ozone monitoring experiment 2 (GOME-2) using an optimal estimation approach: algorithm and initial validation. J Geophys Res 116:D18301. doi:10.1029/2011JD015808

Oppenheimer C (1991) Lava flow cooling estimated from Landsat Thematic Mapper infrared data: the Lonquimay Eruption (Chile, 1989). J Geophys Res 96:21865–21878

Oppenheimer C, Francis PW, Rothery DA, Carlton RWT, Glaze LS (1993a) Infrared image analysis of volcanic thermal features: Lascar Volcano, Chile, 1984–1992. J Geophys Res 98:4269–4286

Oppenheimer C, Rothery DA, Francis PW (1993b) Thermal distribution at fumarole fields: implication for infrared remote sensing of active volcanoes. J Volcanol Geoth Res 55:97–115
Pieri DC, Baloga SM (1986) Eruption rate, area, and length relationships for some Hawaiian lava flows. J Volcanol Geoth Res 30:29–45
Pieri DC, Glaze LS, Abrams MJ (1990) Thermal radiance observations of an active lava flow during the June 1984 eruption of Mt Etna. Geology 18:1018–1022
Prata AJ, Bernardo C (2009) Retrieval of volcanic ash particle size, mass and optical depth from a ground-based thermal infrared camera. J Volcanol Geoth Res 186:91–107
Prata AJ, Prata AT (2012) Eyjafjallajökull volcanic ash concentrations determined using spin enhanced visible and infrared imager measurements. J Geophys Res 117:D00U23. doi:10.1029/2011JD016800
Rix M, Valks P, Hao N, van Geffen J, Clerbaux C, Clarisse L, Coheur P-F, Loyola DG, Erbertseder T, Zimmer W, Emmadi S (2009) Satellite monitoring of volcanic sulfur dioxide emissions for early warning of volcanic hazards. IEEE J Sel Top Appl Earth Obs Remote Sens 2:196–206. doi:10.1109/JSTARS.2009.2031120 [ISSN: 1939-1404]
Rix M, Valks P, Hao N, Loyola DG, Schlager H, Huntrieser HH, Flemming J, Koehler U, Schumann U, Inness A (2012) Volcanic SO_2, BrO and plume height estimations using GOME-2 satellite measurements during the eruption of Eyjafjallajökull in May 2010. J Geophys Res 117:D00U19. doi:10.1029/2011JD016718
Rothery DA, Francis PW, Wood CA (1988) Volcano monitoring using short wavelength infrared data from satellites. J Geophys Res 93:7993–8008
Theys N, Campion R, Clarisse L, Brenot H, van Gent J, Dils B, Coheur P-F, Van Roozendael M, Hurtmans D, Clerbaux C, Corradini S, Merucci L, Tait S, Ferrucci F (2012) Volcanic SO_2 fluxes derived from satellite data: a survey using OMI, GOME-2, IASI and MODIS. Atmos Chem Phys Discuss 12(12):31349
Tilstra LG, de Graaf M, Aben I, Stammes P (2007) Analysis of 5 years of SCIAMACHY absorbing aerosol index data. In: Proceedings of the 2007 Envisat symposium, ESA Special Publication SP-636
Valks P, Loyola D, Hao N, Rix M, Slijkhuis S (2009) Algorithm theoretical basis document for GOME-2 total column products of ozone, minor trace gases and cloud properties (GDP 4.2 for O3MSAF OTO and NTO), O3MSAF, DLR/GOME-2/ATBD/01 rel.2009-01-28
Van Geffen J, Van Roozendael M, Di Nicolantonio W, Tampellini L, Valks P, Erbetseder T, Van der A R (2007) Monitoring of volcanic activity from satellite as part of GSE PROMOTE. In: Lacoste H, Ouwehand L (eds) Proceedings of the 2007 ENVISAT symposium, 23–27 April 2007, Montreux, Switzerland. ESA publication, Noordwijk, SP-636
Van Geffen J, Van Roozendael M, Rix M, Valks P (2008) Initial validation of GOME-2 GDP 4.2 SO_2 total columns (OTO/ SO_2)-ORR B, O3MSAF validation report, TN-IASB-GOME2-O3MSAF-SO2-01.1
Vergniolle S, Jaupart C (1986) Separated two-phase flow and basaltic eruptions. J Geophys Res 91(B12):12842–12860. doi:10.1029/JB091iB12p12842
Vergniolle S, Jaupart C (1990) Dynamics of degassing at Kilauea Volcano, Hawaii. J Geophys Res 95(B3):2793–2809. doi:10.1029/89JB03071 [ISSN: 0148-0227]
Yang K, Krotkov N, Krueger AJ, Carn S, Bhartia PK, Levelt P (2007) Retrieval of large volcanic SO_2 columns from the Aura ozone monitoring instrument (OMI): comparisons and limitations. J Geophys Res 112:D24S43. doi:10.1029/2007JD008825
Yang K, Liu X, Bhartia P, Krotkov N, Carn SA, Hughes E, Krueger AJ, Spurr R, Trahan S (2010) Direct retrieval of sulfur dioxide amount and altitude from spaceborne hyperspectral UV measurements: theory and application. J Geophys Res 115:D00L09. doi:10.1029/2010JD013982
Wright R, Flynn LP, Garbeil H, Harris AJL, Pilger E (2004) MODVOLC: Near-real-time thermal monitoring of global volcanism. J Volcanol Geoth Res 135:29–49

Chapter 17
Engineering Earthquake Early Warning via Regional Networks

I. Iervolino

Abstract Significant investments are undergoing internationally to develop earthquake early warning (EEW) systems. So far, reasonably, the most of the research in this field was driven by seismologists as the issues to determine essential feasibility of EEW were mainly related to the earthquake source. Many of them have been brilliantly solved, and the principles of this discipline are collected in the so-called *real-time seismology*. On the other hand, operating EEW systems rely on general-purpose intensity measures as proxies for the impending ground motion potential and suitable for population alert. In fact, to date, comparatively little attention was given to EEW by earthquake engineering, and design approaches for structure-specific EEW are mostly lacking. Applications to site-specific systems have not been extensively investigated and EEW convenience is not yet proven except a few pioneering cases, although the topic is certainly worthwhile. For example, in structure-specific EEW the determination of appropriate alarm thresholds is important when the false alarm may induce significant losses; similarly, economic appeal with respect to other risk mitigation strategies, as seismic upgrade, should be assessed. In the paper the least issues to be faced in the design of engineering applications of EEW are reviewed and some work done in this direction is discussed. The review presented intends to summarize the work of the author and co-workers in this field illustrating a possible *performance-based* approach for the design of structure-specific applications of EEW.

This invited paper is a shortened version of the review of the work of the author and related research group given in Iervolino (2011).

I. Iervolino (✉)
Dipartimento di Strutture per l'Ingegneria e l'Architettura, Università di Napoli Federico II,
Via Claudio, 21, 80125 Naples, Italy
e-mail: iunio.iervolino@unina.it

F. Wenzel and J. Zschau (eds.), *Early Warning for Geological Disasters*,
Advanced Technologies in Earth Sciences, DOI: 10.1007/978-3-642-12233-0_17,

17.1 Introduction

At a large scale, the basic elements of an earthquake early warning (EEW) system are seismic instruments (individual or multiple arranged in form of a network), a processing unit for the data measured by the sensors, and a transmission infrastructure spreading the alarm to the end users (Heaton 1985). This alarm may trigger security measures (manned or automated), which are expected to reduce the seismic risk in real-time; i.e., before the strong ground motion reaches the warned site. In fact, from the engineering point of view, an EEW system may be appealing for specific structures only if it is competitive cost-wise and/or if it allows to achieve some seismic performance traditional risk mitigation strategies cannot. EEW may be particularly useful in all those situations when some ongoing activity may be profitably interrupted, or posed in a safe mode, in the case of an earthquake to prevent losses (i.e., a *security action* is undertaken). This is the case for example, of facilities treating hazardous materials as nuclear power plants or gas distribution systems. In the first case, the reactor can be temporarily protected before the earthquake hits, in the second case distribution may be interrupted until it is verified that damages and releases potentially triggering fires and explosions did not occur. In these situations it is clear that the early warning, which is in principle only a piece of *information* regarding the earthquake, represents the input for a local protection system. Simpler, yet potentially effective, applications are related to manned operations as surgery in hospitals or the protection from injuries due to fall of non-structural elements in buildings. EEW information seems less suitable to reduce the risk directly related to structural damage (although some potential application may be conceived); in any case, it has to be proven that they are more convenient than more traditional seismic protection systems.

Two points, not usually faced by earthquake engineering, emerge then: (i) because effective engineering applications of EEW involve shutdown of valuable operations and the downtime is very costly for production facilities, unnecessary stops (*false alarms*) should be avoided as much as possible; (ii) development of EEW applications basically deals with the *best* engineering use of seismological information provided in *real-time* on the approaching earthquake. In fact, the basic design variables for EEW applied to a specific engineered system are:

- the estimated earthquake potential on the basis of the EEW information;
- the available time before the earthquake to strike (*lead-time*);
- the system *performance* (proxy for the loss) associated to the case the alarm is issued, which may also include the cost of false alarm and depends on the chosen security action.

In the following, the work of the author and co-workers regarding these issues will be reviewed. It will be discussed below how these three items are not independent each other and that the whole involves very large uncertainty.

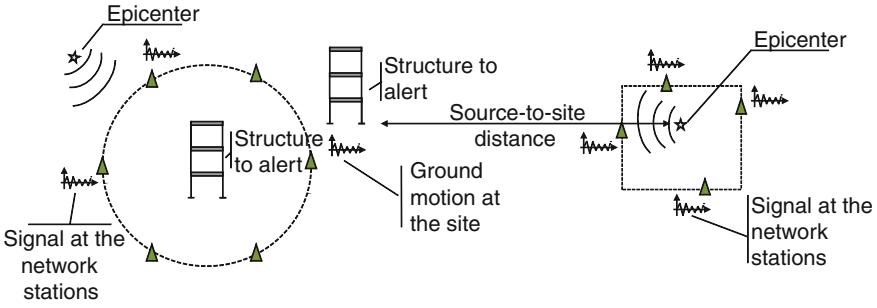

Fig. 17.1 Site-specific (*left*), and hybrid (*right*) EEW schemes; modified from Iervolino et al. (2006)

17.2 Estimating Ground Motion Potential in Real-Time

Conceptually, EEW systems are often identified by the configuration of the seismic network, as *regional* or *site-specific* (Kanamori 2005).

Site-specific systems are devoted to enhance in real-time the safety margin of critical systems as nuclear power plants, lifelines or transportation infrastructures by automated safety actions (e.g., Veneziano and Papadimitriou (1998) and Wieland et al. (2000)). The networks for specific EEW cover the surroundings of the system creating a kind of a fence for the seismic waves (Fig. 17.1, left). The location of the sensors depends on the time needed to activate the safety procedures before the arrival of the more energetic seismic phase at the site (or *lead-time*). In these *Seismic Alert Systems* (Wieland 2001) the alarm is typically issued when the S-phase ground motion at one or more sensors exceeds a given threshold and there is no attempt to estimate the source features as magnitude (M) and location because a local measure of the effects (i.e., the ground motion) is already available. In the *on-site* systems, the seismic sensors (one or more) are placed within the system to warn. In this case the ground damaging potential is typically estimated on the basis of the P-waves and the *lead-time* is given by the residual time for the damaging S-waves to arrive.

Regional EEWS' consist of wide seismic networks covering a portion of the area which is likely to be the source of earthquakes. Data from regional networks are traditionally used for long term seismic monitoring or to estimate, right after the event (i.e., in *near-real-time*), territorial distributions of ground shaking obtained via spatial interpolation of records (e.g., *Shakemap* (Wald et al. 1999)) for emergency management. Regional infrastructures are usually available in seismic regions and are operated by governmental authorities; this is why the most of the ongoing research is devoted to exploit these systems for real-time alert use (Fig. 17.1, right) as a few examples attest (e.g., Doi (2010)). In fact, the work presented in the following mostly refers to the feasibility and design of structure-specific alert (i.e., as in site-specific systems), starting from estimating the peak ground motion at the site, using the sole information from regional networks, which consists of the estimation of source features as M and location of the earthquake. This was referred to as *hybriding* the two EEW approaches (Iervolino et al. 2006).

17.2.1 Real-Time Probabilistic Seismic Hazard Analysis

In the framework of performance-based earthquake engineering or PBEE (Cornell and Krawinkler 2000) the earthquake potential, with respect to the performance demand for a structure, is estimated via the so-called probabilistic seismic hazard analysis or PSHA (Cornell 1968), which consists of the probability that a ground motion intensity measure (IM), likely to be a proxy for the destructive power of the earthquake, the peak ground acceleration (PGA) for example, is exceeded at the site of interest during the *service life* of the structure. This is done via Eq. (17.1), in which, referring for simplicity to a single earthquake source[1]: λ is the rate of occurrence of earthquakes on the source; $f(m)$ is the probability density function, or PDF, of M; $f(r)$ is the PDF of the source-to-site-distance (R); and $f(im|m,r)$is the PDF of IM given M and R (e.g., from a ground motion prediction equation or GMPE).

$$f(im) = \lambda \int_m \int_r f(im|m,r)\, f(m)\, f(r)\, dr dm \tag{17.1}$$

Because seismologists have recently developed several methods to estimate M and R in real-time while the event is still developing, for example from limited information of the P-waves, the PSHA approach can be adapted for earthquake early warning purposes. The so-called real-time PSHA or RTPSHA, introduced in Iervolino et al. (2006), tends to replace some of the terms in Eq. (17.1), with their real time counterparts.

It has been shown in Iervolino et al. (2007a) that if at a given time t from the earthquake's origin, the seismic network can provide a vector of measures informative for the magnitude, $\{\tau_1, \tau_2, \ldots, \tau_n\}$, then the PDF of M conditional to the measures, $f(m|\tau_1, \tau_2, ..., \tau_n)$, may be obtained via the Bayes theorem,[2] Eq. (17.2),

$$f(m|\tau_1, \tau_2, ..., \tau_n) = k \cdot e^{\left[2\cdot\mu_{\ln(\tau)}\cdot\left(\sum_{i=1}^{n} ln(\tau_i)\right) - n\cdot\mu^2_{\ln(\tau)}\right] / 2\cdot\sigma^2_{\ln(\tau)}} \cdot e^{-\beta m} \tag{17.2}$$

where β is a parameter depending on the Gutenberg-Richter relationship for the source and k is a constant. $\mu_{\ln(\tau)}$ and $\sigma_{\ln(\tau)}$ are the mean and standard deviation of the logs of the measure used to estimate M (e.g., from Allen and Kanamori (2003)). Note finally that the PDF of M in Eq. (17.2) depends on the real-time data only via n and $\sum_{i=1}^{n} \ln(\tau_i)$, which are related to the geometric mean, $\widehat{\tau} = \sqrt[n]{\prod_{i=1}^{n} \tau_i}$.

Regarding R, because of rapid earthquake localization procedures (e.g., Satriano et al. (2008)), a probabilistic estimate of the epicenter may also be available based

[1] In Eq. (17.1) it is assumed for simplicity that M and R are independent random variables, which may not be the general case.

[2] It is to mention that simpler approaches to estimation of M can be implemented in the RTPSHA although the Bayesian one has proven to be the most efficient one (Iervolino et al. 2009).

on the sequence according to which the stations trigger, $\{s_1, s_2, \ldots, s_n\}$. Thus, the real-time PDF of R, $f\,(r|s_1, s_2, ..., s_n)$, may replace $f\,(r)$ in Eq. (17.1). In fact, the PSHA hazard of Eq. (17.1), has its real-time adaption in Eq. (17.3). Because when the earthquake is already occurring the λ parameter does not apply, in principle, no further data are required to compute the PDF of the IM or, equivalently, the complementary cumulative distribution (or hazard curve) of IM at any site of interest. A simulation of RTPSHA for a magnitude 6 event is given in Fig. 17.2 referring to the *Irpinia Seismic Network* (ISNet, (Weber et al. 2007)) in Campania (southern Italy).

$$f\left(im|\underline{\tau}, \underline{s}\right) = \int_m \int_r f\,(im|m, r) f\,(m|\tau_1, \tau_2, \ldots, \tau_n)\, f\,(r|s_1, s_2, \ldots, s_n)\, dr dm \tag{17.3}$$

The figure shows that, because the knowledge level about the earthquake (i.e., M and R) increases as the seismic signals are processed by an increasing number of seismic sensors (i.e., n), the real-time hazard evolves with time. In Fig. 17.2 the panels (a), (b), and (c) show the number of stations of the network which have measured the parameter informative for the magnitude at three different instants form the earthquake origin time. In the (c) and (d) panels, the corresponding PDFs of M and R are given, while panel (e) shows the real-time hazard curves in which the IM considered is the PGA on stiff soil (computed using the GMPE of Sabetta and Pugliese (1996)). The three instants chosen correspond to when 2, 18 and 29 (the whole network) have recorded at least 4 s of the P-waves, which is the required time to estimate τ according to Allen and Kanamori (2003). For further details on the simulation the reader should refer to Iervolino et al. (2006), Iervolino et al. (2007a), and Iervolino et al. (2009).

Note finally that, the RTPSHA can be easily extended to estimate in real-time the response spectrum ordinates, this has been done in Convertito et al. (2008).

17.2.2 Decisional Rules, Alarm Thresholds and False Alarm Probabilities

An essential engineering issue in earthquake early warning is the *alarming decisional rule*, which should be based on the consequences of the decision of alarming or not and is remarkably dependent both on the information gathered on the earthquake and on the system to alarm.

If RTPSHA is the approach used in the early warning system, the knowledge level about the earthquake at a certain time is represented by the hazard curve computed at that instant. The alarming decisional rule should be established based on that. The simplest is to alarm if the expected value of the considered IM is larger than a threshold, Eq.[3] (17.4).

[3] Conditional dependencies are dropped from the equations for simplicity.

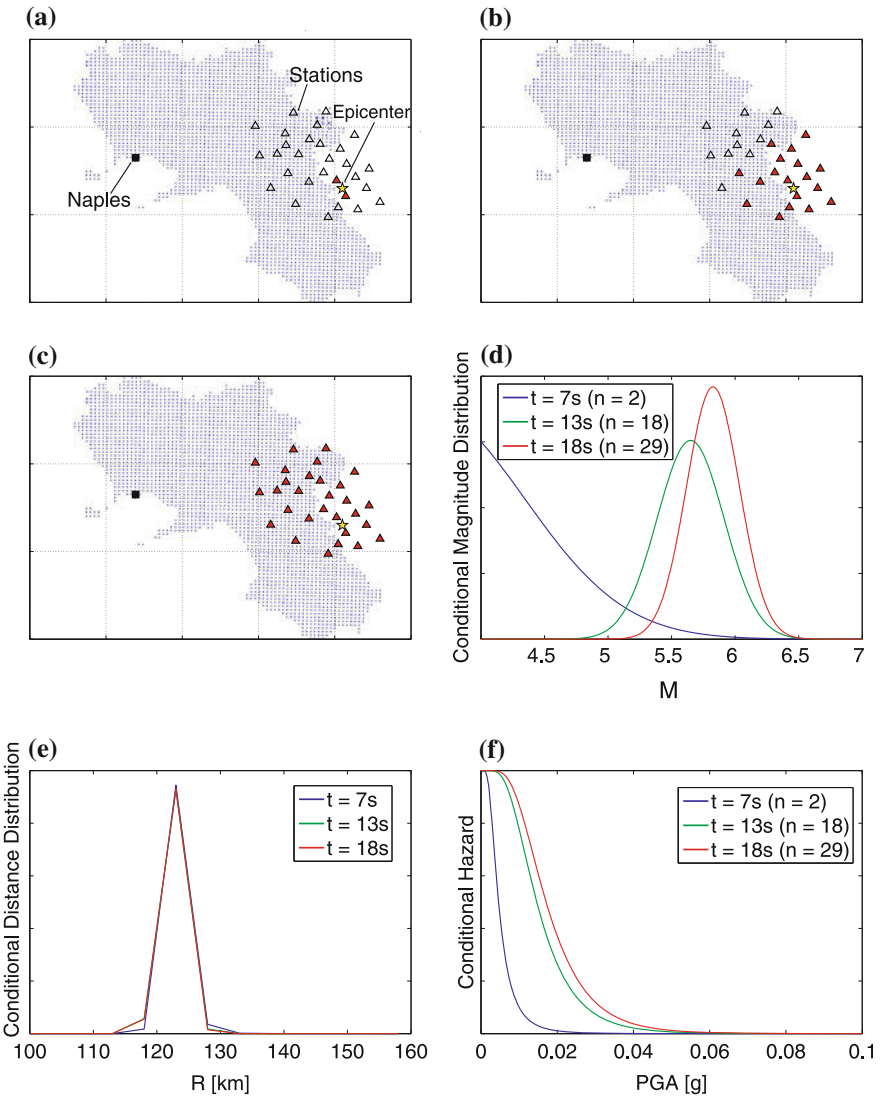

Fig. 17.2 **a–c** seismic stations which have measured the parameter informative for the magnitude of the earthquake (i.e., 4 s of the P-wave velocity signal (Allen and Kanamori 2003)) at three different instants during the earthquake; **d–f** are the M, R and PGA distributions computed at the same instants via the RTPSHA approach (modified from Iervolino et al. (2009))

$$E\left[IM\right] = \int_{-\infty}^{+\infty} im \;\; f\left(im\right) \;\; d\left(im\right) \geq im_c \tag{17.4}$$

The im_c threshold depends on the system to alarm. For example, if structural damage is the consequence, and the IM is the PGA, the PGA_c value should reflect the ground motion intensity above which damages for that specific structure are expected; e.g., the PGA value used for the design of the structure.

A more refined decisional rule, still based on the RTPSHA outcome, may be to alarm if the critical IM value has an *unacceptable* risk (represented by the probability value $\mathrm{Pr_c}$) of being exceeded in that earthquake, Eq. (17.5).

$$\Pr\left[IM > im_c\right] = 1 - \int_{-\infty}^{im_c} f\left(im\right) \;\; d\left(im\right) \geq \Pr_c \tag{17.5}$$

This latter approach to the EEW alarming decision is similar to the earthquake resistant design in codes worldwide, where the design is carried out for an IM value corresponding to a fixed probability of exceedance in the lifetime of the structure (e.g., 10 % in 50 years). In fact, Eq. (17.5) maybe seen as Eq. (17.6).

$$im\left(\Pr_c\right) < im_c \tag{17.6}$$

This means that, if PGA is the IM, the alarm has to be issued if the PGA, which in the real-time hazard curve has the critical probability of being exceeded, is larger than the critical PGA for the structure.

The two rules of Eqs. (17.4) and (17.5) are represented in Fig. 17.3a where, for the PDF of PGA derived from the hazard curve at $n = 29$ in Fig. 17.2, it is shown a case in which, for the specific im_c and Pr_c values, the alarm should be issued according to the first rule and should not according to the second one.

As discussed, the PDF of M may be seen as sole function of $\widehat{\tau} = \sqrt[n]{\prod_{i=1}^{n} \tau_i}$; moreover, as shown below, simply the modal value of R may adequately represent its PDF due to the negligible uncertainty involved in the earthquake location rapid estimation methods. Therefore, because the GMPE is a static piece (not depending on the real-time measures) of information, the RTPSHA integral may be computed offline for all possible values of the $\widehat{\tau}$ and R pair, and the result retrieved in real-time without the need for computing it. This is an attractive feature of the proposed approach for EEW purposes. As an example, in Table 17.1 the probabilities of exceedance are tabulated for the arbitrary PGA_c value of 0.017 g, using the GMPE of Sabetta and Pugliese (1996) and as a function of the two independent parameters required to compute the RTPSHA integral. Having them pre-computed allows to immediately check in real-time the decisional rule of Eq. (17.5).

Table 17.1 Exceedance probability for an arbitrary PGA_c value of 0.017 g as a function of the only two parameters required to compute the RTPSHA integral, showing offline computability

n = 18	Estimated source-to-site distance; i.e., modal value of the PDF of R (km)					
$\widehat{\tau}\,[s]$	50	70	90	110	130	150
0.2	0.0363	0.0053	0.0009	0.0002	0.0000	0.0000
0.4	0.0442	0.0069	0.0012	0.0003	0.0001	0.0000
0.6	0.1338	0.0351	.0098	0.0030	0.0010	0.0003
0.8	0.6085	0.3423	0.1795	0.0925	0.0479	0.0251
1.0	0.9240	0.7737	0.5949	0.4331	0.3055	0.2117
1.2	0.9912	0.9548	0.8814	0.7801	0.6669	0.5552
1.4	0.9990	0.9919	0.9700	0.9279	0.8661	0.7897
1.6	0.9998	0.9973	0.9875	0.9643	0.9245	0.8689
1.8	0.9999	0.9984	0.9917	0.9744	0.9425	0.8953
2.0	0.9999	0.9988	0.9933	0.9783	0.9499	0.9068

The decisional rule allows to define what false (FA) and missed (MA) alarms are; i.e., if the decision, whichever it is, results to be wrong. In the case of the rule of Eq. (17.5) these definitions become Eq. (17.7).

$$\begin{cases} MA: \{\Pr[IM > im_c] < \Pr_c \cap im > im_c\} \\ FA: \{\Pr[IM > im_c] > \Pr_c \cap im < im_c\} \end{cases} \tag{17.7}$$

In other words a MA [FA] occurs when the risk, that the critical IM level is going to be exceeded, is too low [high] to issue [to not issue] the alarm, while the actual IM occurring at the site is higher [lower] than im_c. Consequently, false and missed alarms probabilities, P_{FA} and P_{MA}, which are dependent on the time when the decision is supposed to be taken, may be computed; see Iervolino et al. (2006, 2009) for details. An example, referring to the simulation of Fig. 17.2 for some arbitrary PGA_c values and when $\Pr_c$ is equal to 0.2, is given in Fig. 17.3b. Two important result emerge

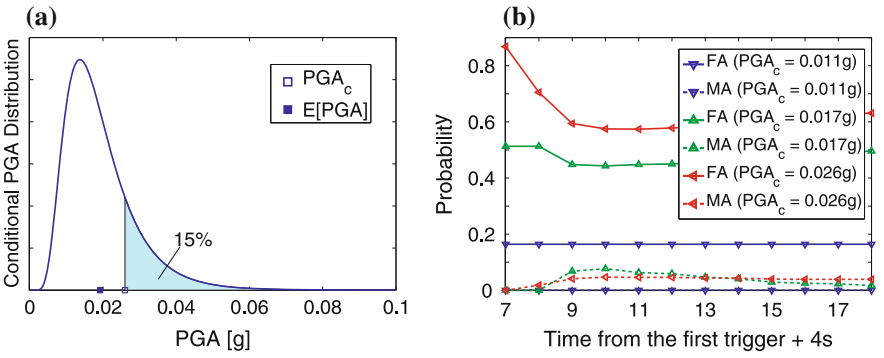

Fig. 17.3 Representation of decisional rules (**a**) and examples of false and missed alarm probabilities as a function of time for different IM values (**b**)

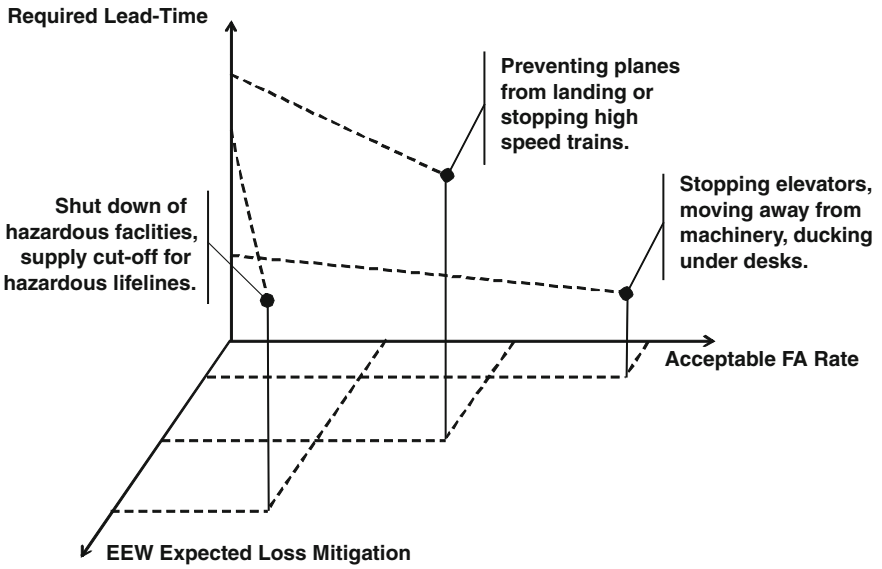

Fig. 17.4 Impact of missed/false alarms for categories of EEW applications; modified from Iervolino et al. (2007b)

from the plots: (1) after a certain t value the probabilities stabilize, this reflects the fact that after a certain instant the information about the real-time hazard does not change anymore (see following section); (2) there is a trade-off, that is, one can play with $\mathrm{Pr_c}$ and im_c to lower $\mathrm{P_{FA}}$, but this always implies that $\mathrm{P_{MA}}$ is going to increase, and vice-versa.

The careful evaluation of the false alarm (or *cry wolf*) probability is increasingly important as the cost associated to the alarm, or to the following security action, raises. In fact, in those cases when the alarm has neither costs nor undesired consequences, the optimal solution is to issue the alert whenever an earthquake event is detected by the EEW system. Conversely, if the alarm may cause costly downtime or affects large communities (e.g., in the case of emergency stop of power plants or lifelines' distribution networks) the alarm decision conditions have to be carefully evaluated to prevent, in the long run, the loss related to false alarms to be unacceptably large. In Fig. 17.4 simple scheme linking three important design variables of engineering earthquake early warning are shown for three different possible EEW applications (relative position with respect to the axes were arbitrarily given).

In the figure it is shown that there are security actions that require a limited lead-time and have a low impact, then a larger FA rate is accepted with respect to actions affecting a larger part of the community more costly, time consuming to operate and for which, then, false alarms are less tolerable (Goltz 2002).

It is to mention that decisional rules based on a ground motion IM thresholds, as those presented, have the advantage to be simple and requiring limited information of the structure to alert (i.e., those required to set im_c). However, the IM is only a proxy

for the loss associated to the earthquake hitting the structure. In fact, the alarming decision should be better taken comparing in real-time the expected losses consequent the decision to alarm or to not alarm, conditional on the available information about the impending earthquake. This has been investigated in Iervolino et al. (2007a) and is briefly discussed in the following.

17.2.3 ERGO: An Example of RTPSHA Terminal

The *EaRly warninG demo* (ERGO) was developed to test the potential of hybrid EEW based on RTPSHA. The system was developed by the staff of the *RISSC Lab* (www.rissclab.unina.it). ERGO processes in real-time the accelerometric data provided by a sub-net (6 stations) of ISNet and is installed in the main building of the school of engineering of the University of Naples Federico II, in Naples, which is the target site of the EEW. It is able to perform RTPSHA and eventually to issue an alarm in the case of potentially dangerous events occurring in the southern Appennines region. ERGO is composed of the following four panels (Fig. 17.5).

- *Real-time monitoring and event detection:* In this panel two kind of data are given: (a) the real-time accelerometric signals of the stations, shown on a two minutes time window; and (b) the portion of signal that, based on signal-to-noise ratio, determined the last trigger (i.e., event detection) of a specific station (on the left). Because it may be the case that local noise (e.g., veicular traffic) determines a station to trigger, the system declares an event (M larger than 3) only if at least three station trigger within the same 2 s time interval.
- *Estimation of earthquake parameters:* This panel activates when an event is declared. If this condition occurs, magnitude and location are estimated in real-

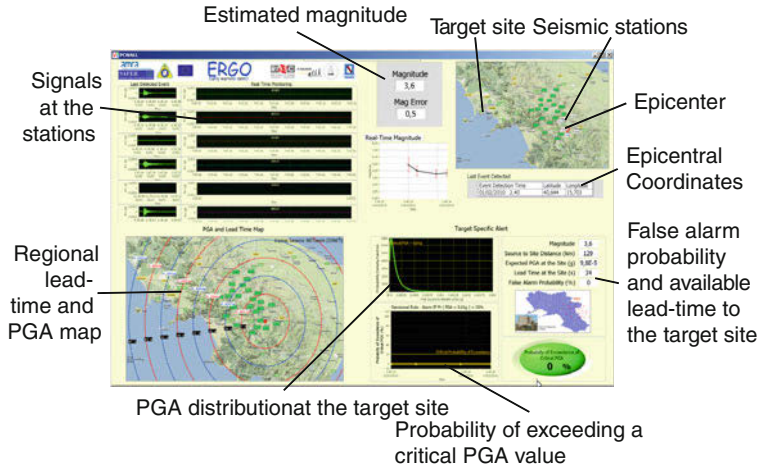

Fig. 17.5 ERGO, a RTPSHA-based early warning terminal

time as a function of evolving information from the first panel. Here the expected value of magnitude as a function of time and the associated standard error are given. Moreover, on a map where also the stations are located (rectangles), it shows the estimated epicenter (red circle), its geographical coordinates and the origin time.

- *Lead-time and peak-shaking map:* This panel shows the lead-time associated to S-waves for the propagating event in the whole region. As further information, on this panel the expected PGA on rock soil is given on the same map. As per the second panel, this one activates only if an event is declared from panel 1 and its input information come from panel 2.
- *RTPSHA and alarm issuance decision:* This panel performs RTPSHA for the site where the system is installed based on information on magnitude and distance from panel 2. In particular, it computes and shows real-time evolving PDFs of PGA at the site. Because a critical PGA value has been established (arbitrarily set equal to 0.01 g) the system is able to compute the risk this PGA is exceeded as a function of time. If such a risk exceeds 0.2, the alarm is issued and an otherwise green light turns to red, as per Eq. (17.5). This panel also gives, as summary information, the actual risk that the critical PGA value is exceeded along with the lead-time available and the false alarm probability.

Figure 17.5 refers to a real event detected and processed in real-time by ERGO on February 01 2010. The system estimated the event as an M 3.6, with an epicenter about 130 km far from the site. Because the event was a low-magnitude large-distance one, the risk the PGA_c could be exceeded was negligible and the alarm was, correctly, not issued. Finally, note that ERGO is a visual panel only for demonstration and testing purposes, but it may be virtually ready be connected to devices for real-time risk reduction actions.

17.2.4 Uncertainties in EEW Ground Motion Predictions and Information-Dependent Lead-Time

Three different sources of uncertainty affect the IM estimation according to Eq. (17.3), that is, those related to the estimation of M, R, and IM given M and R. Except for the PDF of IM given M and R, the uncertainty involved is time-dependent because the uncertain estimations of magnitude and distance are also time-dependent. A great deal of research has focused on the fine tuning of the estimation of M and related uncertainty; however in the RTPSHA ground motion prediction uncertainty, that on M is not the weak link. This is proven in Iervolino et al. (2009) from where Fig. 17.6a is taken. It shows, for the M 6 event simulated in Fig. 17.2 the coefficient of variation (CoV, the ratio of the standard deviation to the mean) of the PGA prediction is given as the time from the origin time of the earthquake and number of stations providing τ (the information about the source parameters of the impending earthquake) increase. This may be seen as a measure of the evolving uncertainty on EEW ground motion prediction, and it may be recognized to be significantly large (never below 0.45),

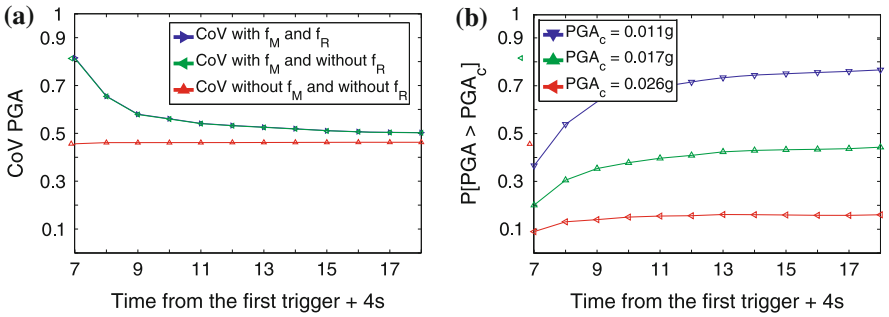

Fig. 17.6 Coefficient of variation of the IM PDFs when different uncertainties are considered (**a**), and dependence of IM estimations as a function of time (**b**); adapted from Iervolino et al. (2009)

at least in this example. This means that alarming decisions based on this approach may be taken in very uncertain conditions, and this is because of the IM given M and R (i.e., the GMPE). In fact, in the figure the CoV is computed, using Eq. (17.3) at any 1s step from the earthquake origin time, in the following cases:

- considering both PDFs of M and R;
- considering the PDF of M and only the modal value of the distance (R*) from Fig. 17.2d in place of its full PDF;
- neither the PDF of M nor of R, while using two statistics as the mode of R and the maximum likelihood value of magnitude ($\overline{\mathrm{M}}$).

Case (a) corresponds to fully apply the RTPSHA approach; in case (b) only the uncertainty on M reflects on the real-time PGA prediction; and in (3) neither uncertainty related to the estimation of M nor of R affect the estimation of PGA, and at any instant the real-time hazard is simply given by $f\,(im|m,r)$. In this latter case the uncertainty is only that of the GMPE computed for the specific $\left\{\overline{\mathrm{M}}, \mathrm{R}^*\right\}$ pair.

It clearly appears from the curves that the uncertainty of the distance is negligible with respect to the prediction of PGA because green and blue curves are overlapping, meaning that the CoV of PGA is almost the same with or without uncertainty on distance. Also the contribution of uncertainty of magnitude to the CoV of PGA is small if compared to that of the GMPE, except at the beginning when the estimation of M is not yet well constrained by several τ measurements. Unfortunately, the GMPE uncertainty, which largely dominates, is not dependent on the measures in the described RTPSHA approach. (Therefore, it seems that possible attempts reduce uncertainty in EEW ground motions predictions may only refer to random field modeling of spatial IM distribution, as discussed in Iervolino (2011)).

Because this time dependence of the M and R estimations, the prediction of IM becomes stable only after a number of stations have measured the early signal of the event. This is better shown in Fig. 17.6b where the estimation of the exceedance probability for three hypothetical PGA_c values, to be used in one of the decisional rules discussed, is given as a function of time (note that t equal to 7, 13 and 18 s correspond to Fig. 17.2a–c, respectively).

It appears that the probability of exceedance does not change after 10–13 s, independently of which PGA_c value is considered. In other words, after on average 11–18 stations of the ISNet have measured τ, the estimation of the critical PGA does not benefit much from further information. It may be concluded that there is a trade-off between the lead-time and the level of information based on which the alarm issuance is decided. Consequently, different lead-times may be computed for the Campania region, each of those corresponds to a different number of stations providing τ, for example 4, 18 and 29 representing three levels of information about the source of the earthquake: *poor*, *large*, and *full*, respectively (Fig. 17.7); see Iervolino et al. (2009) for details.

Because 18 stations is the minimum level of information to stabilize the uncertainty, the 18-station average lead-time map can be considered as the reference for the design of real-time risk reduction actions, some of which from Goltz (2002) are superimposed in Fig. 17.8.

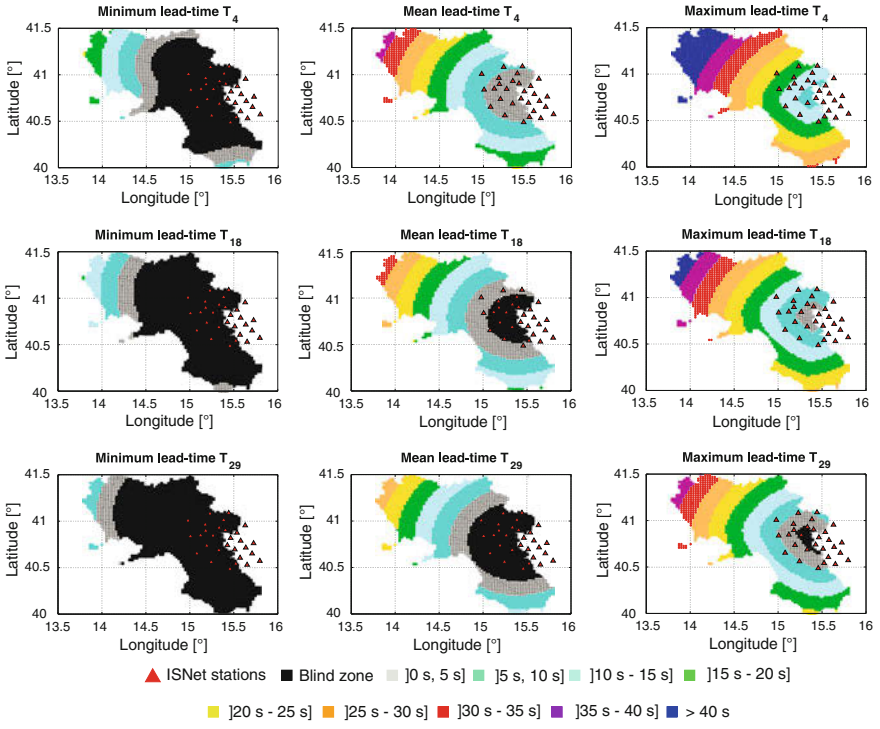

Fig. 17.7 Minimum, mean and maximum lead-time maps for random hypocenters when 4, 18 and 29 ISNet stations have provided information to estimate the magnitude

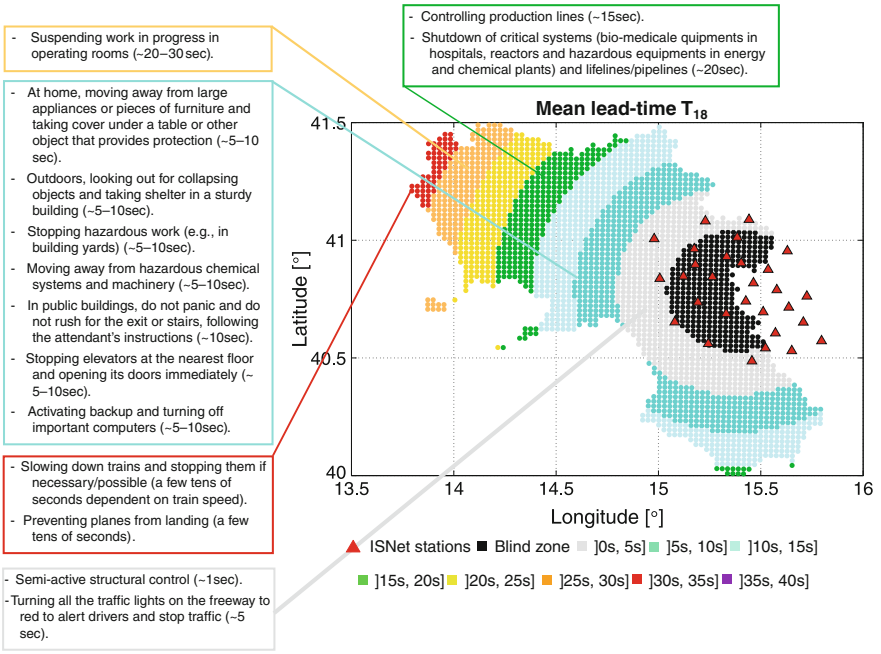

Fig. 17.8 Design lead-time map for the Campania region (southern Italy); modified from Iervolino et al. (2009)

17.3 Estimating Earthquake Consequences for Structures in Real-Time

The real-time prediction of a ground motion IM discussed so far, although the first step from real-time seismology to structural performance, is neither the best option to estimate the damage potential for a specific structure nor the more appropriate piece of information on the basis of which to decide whether to alarm. In fact, it is well known that the IM maybe only poorly correlated to the structural seismic response and that different damages occurring in a building (e.g., to structural components, to non-structural components, and to content) may require the estimation of more than one IM at the same time. In other words, if one is able to quantify the damages (i.e., the loss) specific for the structure of interest this is a sounder basis for the warning management. This structure-specific EEW design procedure was investigated in Iervolino et al. (2007a) where it was shown with respect to the issue of calibrating an alarm threshold which is *optimal* in the sense of minimizing the losses, including the false and missed alarm related costs. Such an approach is briefly reviewed in the following.

The performance-based seismic risk assessment of structures aiming to the estimation of the mean annual frequency of certain loss (L) may be adapted to the EEW

real-time case as done for the RTPSHA. In fact, for a structure provided of an EEW terminal such as ERGO, the expected loss may be computed in the case of warning issuance (W) and no alarm issuance ($\overline{W}$) as follows:

$$E^{W}\left[L|\underline{\tau},\underline{s}\right]=\int_{L}\int_{DM}\int_{EDP}\int_{IM} l\; f^{W}\left(l\left|\underline{dm}\right.\right)\; f\left(\underline{dm}\left|\underline{edp}\right.\right) \times f\left(\underline{edp}\left|\underline{im}\right.\right) f\left(\underline{im}\left|\underline{\tau},\underline{s}\right.\right) dL\; d\underline{DM}\; d\underline{EDP}\; d\underline{IM} \tag{17.8}$$

$$E^{\overline{W}}\left[L|\underline{\tau},\underline{s}\right]=\int_{L}\int_{DM}\int_{EDP}\int_{IM} l\; f^{\overline{W}}\left(l\left|\underline{dm}\right.\right)\; f\left(\underline{dm}\left|\underline{edp}\right.\right) \times f\left(\underline{edp}\left|\underline{im}\right.\right) f\left(\underline{im}\left|\underline{\tau},\underline{s}\right.\right) dL\; d\underline{DM}\; d\underline{EDP}\; d\underline{IM} \tag{17.9}$$

where the terms the two equations share are: $f\left(l\left|\underline{dm}\right.\right)$ which is the PDF of the loss given the vector of structural and non-structural damage measures $\left(\underline{DM}\right)$; $f\left(\underline{dm}|\underline{edp}\right)$ or the joint PDF of damages given the engineering demand parameters $\left(\underline{EDP}\right)$, proxy for the structural and non-structural response; $f\left(\underline{edp}|\underline{im}\right)$ or the joint PDF of the EDPs is generally conditional to a vector of ground motion intensity measures $\left(\underline{IM}\right)$; $f\left(\underline{im}\left|\underline{\tau},\underline{s}\right.\right)$ is the real-time hazard for the $\underline{IM}$ vector of interest (e.g., two IMs one related to structural response and one to non-structural response).

The two equations are different for the loss function term. In other words, it may be assumed that a security action, aimed at risk mitigation, is undertaken if the alarm is issued. For example, some critical system will shut down or people in a school building may duck under desks if the warning time is not sufficient to evacuate.[4] In fact, $f^{W}\left(l\left|\underline{dm}\right.\right)$ is the loss reflecting the risk reduction; and $f^{\overline{W}}\left(l\left|\underline{dm}\right.\right)$ is the loss function if no alarm is issued (no security action is undertaken).

In the case it is possible to compute, before the ground motion hits, the expected losses in case of warning or not, clearly one can take the optimal decision: to alarm if this reduces the expected losses and to not issue any warning otherwise, Eq. (17.10).

$$\begin{cases} to\ alarm\ if & E^{W}\left[L|\underline{\tau},\underline{s}\right] \le E^{\overline{W}}\left[L|\underline{\tau},\underline{s}\right] \\ to\ not\ alarm\ if & E^{W}\left[L|\underline{\tau},\underline{s}\right] > E^{\overline{W}}\left[L|\underline{\tau},\underline{s}\right] \end{cases} \tag{17.10}$$

The described approach was pursued for a simplified school building consisting of one classroom (Fig. 17.9), in which three kinds of losses were considered, the assumed occurrence of which is summarized in Table 17.2.

[4] More complex security measures may be related to the semi-active control of buildings; e.g. Iervolino et al. (2010) and Fujita et al. (2011).

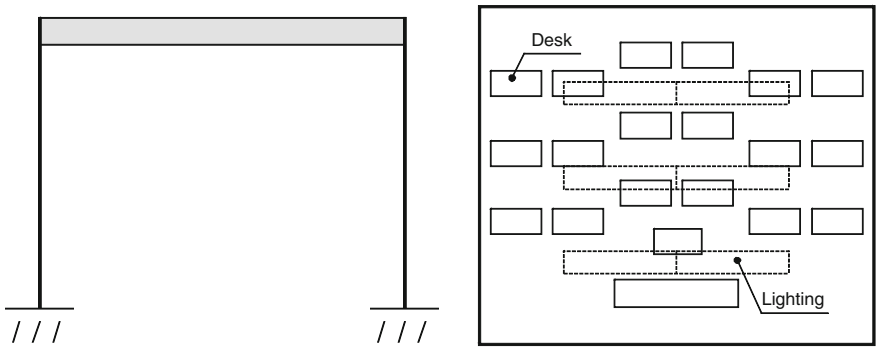

Fig. 17.9 Structural scheme for the school building (**left**), and classroom layout (**right**); modified from Iervolino et al. (2007a)

Table 17.2 Losses considered and occurrence cases

Loss	Structural collapse	Non-structural damage only	Neither structural nor non-structural damage
Costs due to casualties and injuries	*Occurs*	*May occur (in a reduced manner in the case of warning)*	*Does not occur*
Cost due to structural reparation and re-construction	*Occurs*	*Does not occur*	*Does not occur*
Costs related to downtime	*Occurs*	*Occurs*	*Occurs in the case of warning*

The costs of casualties and injuries were conventionally assigned in an approach similar to insurance premiums computation. The security action to be undertaken after the alarm issuance was supposed to be ducking of occupants under desks.

To reflect the undertaking of the security action in case of alarm, the loss function was generally reduced with respect to the non-issuance alarm case (Fig. 17.10a). All other terms shared by Eqs. (17.8) and (17.9) were computed via non-linear structural analyses.

With this approach $E^{W}\left[L\left|\hat{\tau}\right.\right]$ and $E^{\bar{W}}\left[L\left|\hat{\tau}\right.\right]$ were calculated for the example under exam considering the ISNet EEW system, for ten equally spaced $\hat{\tau}$ values in the range between 0.2 and 2 s and assuming $n = 29$; i.e., it is assumed that all stations of the ISNet have measured τ. Because it has been discussed that the localization method involves negligible uncertainty, the R value has been fixed to 110 km which is a possible distance of a building in Naples for an event having its epicentral location in the Irpinian region. In Fig. 17.10b the trends of the expected losses in the two cases are given, the black curve (dashed and solid) corresponds to the non-issuance of the alarm, the red one refers to the issuance. The intersection

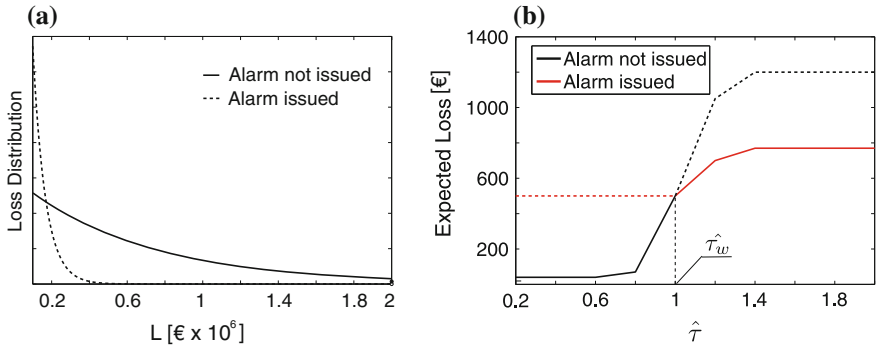

Fig. 17.10 Loss PDF when the alarm is not issued and when it is reduced because ducking under desks after the alarm is issued (**a**), and expected loss as a function of the measures used to estimate the magnitude in real-time with identified optimal alarm threshold (**b**); modified from Iervolino et al. (2007a)

of the two curves defines two $\hat{\tau}$ regions and the optimal alarm threshold $\left(\hat{\tau}_W\right)$; if the statistic of the measurements is below the intersection value the expected loss is lower if the warning is not issued, otherwise, if $\hat{\tau} > \hat{\tau}_W$, the optimal decision is to alarm because it minimizes the expected loss.

To determine the alarm threshold based on the expected loss allows to account for all actual costs related to the event striking and the alarm consequences probabilistically, and it is easy to recognize how this is an improvement with respect to synthesize all structural response, damages and consequences in the im_c threshold discussed above. Moreover, because the loss estimations accounts for false and missed alarms, the threshold is also optimal with respect to the MA and FA tradeoff.

17.4 Conclusions

In this paper a performance-based earthquake engineering framework to earthquake early warning was reviewed. The focus is the probabilistic prediction of the structural consequences or losses at a given site based on the information gathered during an earthquake by a seismic network able to process in real-time the recordings.

The first step was the early warning adaption of probabilistic seismic hazard analysis, which allows to predict in real-time any ground motion intensity measure for which a prediction equation is available. As a side results, an analytical form solution for the real-time estimation of magnitude, under some hypotheses, was found based on some fundamental results of real-time seismology. Subsequently, the alarm issuance based on strong motion intensity measures was faced. Possible decisional rules and consequent missed and false alarm probabilities were analyzed.

In the context of site-specific engineering ground motion predictions, it was shown that the GMPE is the largest source of uncertainty in EEW engineering ground motion

prediction with respect to real-time estimate of source parameters as magnitude and location. Similarly, it was show that because the information (the uncertainty) is time-dependent, the reference time after which the level of information does not increase significantly, while the earthquake has not yet reached all stations within the EEW network, may be identified in EEW systems. Therefore uncertainty-dependent lead-time should be considered as an additional design parameter for engineering EEW applications.

On the structural engineering counterpart, the structural performance and losses may be predicted in real-time, which allow: to evaluate the actual efficiency of security actions, to account explicitly for the cost of false alarms, and to take the alarming decision on a more rational basis for a specific structure; i.e., based on expected losses.

Finally, from this brief review of a possible design approach to structure-specific EEW it emerges that many important issues in engineering earthquake early warning still need to be addressed: first of all the effectiveness and economic convenience with respect to more traditional structural seismic risk mitigation technologies. However, these studies at least prove that EEW deserves attention from earthquake engineering as it is an opportunity to be investigated among advanced an cost-effective risk management approaches.

Acknowledgments The author would like to explicitly express his gratitude to coworkers who essentially contributed to the studies this paper reviews. Moreover, it is to mention that most of the research presented was developed within the funded research programs of AMRA (http://www.amracenter.com/) and the ReLUIS-DPC (http://www.reluis.it/) 2005–2008 project.

References

Allen RM, Kanamori H (2003) The potential for earthquake early warning in Southern California. Science 300(5620):786–789

Convertito V, Iervolino I, Manfredi G, Zollo A (2008) Prediction of response spectra via real-time earthquake measurements. Soil Dyn Earthq Eng 28(6):492–505

Cornell CA (1968) Engineering seismic risk analysis. Bull Seismol Soc Am 58(5):1583–1606

Cornell CA, Krawinkler H (2000) Progress and challenges in seismic performance assessment. PEER Center News 3(2):4p

Doi K (2010) The operation and performance of earthquake early warnings by the Japan meteorological agency. Soil Dyn Earthq Eng 31(2):119-126.

Fujita S, Minagawa K, Tanaka G, Shimosaka H (2011) Intelligent seismic isolation system using air bearings and earthquake early warning. Soil Dyn Earthq Eng 31(2):223–230

Goltz JD (2002) Introducing earthquake early warning in California: a summary of social science and public policy issues, report to OES and the operational areas. Governor's Office for Emergency Service, Pasadena, CA, US. http://www.cisn.org/docs/Goltz.TaskI-IV.Report.doc

Heaton TH (1985) A model for a seismic computerized alert network. Science 228(4702):87–90

Iervolino I (2011) Performance-based earthquake early warning. Soil Dyn Earthq Eng 31(2):209–222

Iervolino I, Convertito V, Giorgio M, Manfredi G, Zollo A (2006) Real time risk analysis for hybrid earthquake early warning systems. J Earthq Eng 10(6):867–885

Iervolino I, Giorgio M, Manfredi G (2007a) Expected loss-based alarm threshold set for earthquake early warning systems. Earthq Eng Struct Dyn 36(9):1151–1168

Iervolino I, Manfredi G, Cosenza E (2007b) Earthquake early warning and engineering application prospects. In: Gasparini P, Manfredi G, Zschau J (eds) Earthquake early warning. Springer, Berlin. ISBN 978-3-540-72240-3.

Iervolino I, Giorgio M, Galasso C, Manfredi G (2009) Uncertainty in early warning predictions of engineering ground motion parameters: what really matters? Geophys Res Lett 36:L00B06. doi:10.1029/2008GL036644.

Iervolino I, Galasso C, Manfredi G (2010) Preliminary investigation on integration of semi-active structural control and earthquake early warning. Early warning system for transport lines workshop, KIT Science Report, Karlsruhe, Germany, ISSN 1619–7399.

Kanamori H (2005) Real-time seismology and earthquake damage mitigation. Annu Rev Earth Planet Sci, 3:5.1-5.20.

Sabetta F, Pugliese A (1996) Estimation of response spectra and simulation of nonstationarity earthquake ground motion. Bull Seismol Soc Am 86(2):337–352

Satriano C, Lomax A, Zollo A (2008) Real-time evolutionary earthquake location for seismic early warning. Bull Seismol Soc Am 98(3):1482–1494

Veneziano D, Papadimitriou AG (1998) Optimization of the seismic early warning system for the Tohoku Shinkansen. In: Proceedings of 11th European conference on earthquake engineering, Paris, France.

Wald JD, Quitoriano V, Heaton TH, Kanamori H, Scrivner CW, Orden BC (1999) TriNet "ShakeMaps": rapid generation of peak ground motion and intensity maps for earthquake in Southern California. Earthq Spectra 15(3):537–555

Weber E, Convertito V, Iannaccone G, Zollo A, Bobbio A, Cantore L, Corciulo M, Di Crosta M, Elia L, Martino C, Romeo A, Satriano C (2007) An advanced seismic network in the southern Apennines (Italy) for seismicity investigations and experimentation with earthquake early warning. Seismol Res Lett 78(6):622–634

Wieland M (2001) Earthquake alarm, rapid response, and early warning systems: low cost systems for seismic risk reduction. Electrowatt Engineering Ltd., Zurich

Wieland M, Griesser M, Kuendig C (2000) Seismic early warning system for a nuclear power plant. In: Proceedings of 12th world conference on earthquake engineering, Auckland, New Zealand.

Chapter 18
Operational Earthquake Forecasting and Decision-Making

G. Woo and W. Marzocchi

Abstract Traditionally, seismic risk reduction is achieved only through a sound earthquake building code. Nonetheless, some recent seismic disasters have highlighted the need for enlarging the range of risk mitigation actions beyond that. In particular, the occurrence of a seismic sequence may increase the weekly probability of a large shock by orders of magnitude, although the absolute probability usually remains below 1/100. Here, we summarize the state of the art in short-term earthquake forecasting and discuss how these forecasts may be used to mitigate seismic risk in this time horizon. Because of the low probabilities and high false alarm rates of possible advisories, mandatory mitigation actions would not be an effective practical strategy to reduce risk. Alternatively, we propose some low cost strategies, such as increasing vigilance and preparedness, for using probabilistic forecasting to mitigate seismic risk. These are based on the 'nudging' principle of devolving decision-making down from civic authorities to the individual level.

18.1 Introduction

In an ideal world, all buildings would be properly constructed according to a modern regional earthquake building code, drafted to protect occupants from fatal injury, except for extreme levels of ground motion. Given that earthquake deaths are primarily caused by building damage, high quality earthquake engineering is the best defence against earthquake shaking.

The target of building improved earthquake-resistant structures is, and remains, imperative. Nonetheless, in the real world we face challenges that call for additional

G. Woo
Risk Management Solutions, London, UK

W. Marzocchi (✉)
Istituto Nazionale di Geofisica e Vulcanologia, Roma, Italy
e-mail: warner.marzocchi@ingv.it

F. Wenzel and J. Zschau (eds.), *Early Warning for Geological Disasters*,
Advanced Technologies in Earth Sciences, DOI: 10.1007/978-3-642-12233-0_18,

seismic risk reduction measures. In particular, many existing buildings have been constructed before the most recent building code update, or without adequate code compliance, and therefore would benefit from retrofitting to the seismic resistance level of new buildings. Yet, retrofitting requires a certain amount of time and it cannot be considered a reliable mitigation measure in a short-time window. Furthermore, the marginal cost of retrofitting, which may be as much as 30–50 % of the building value, is substantially greater than for new-build anti-seismic construction.

Moreover, building codes are generally based on probabilistic hazard maps, corresponding to a prescribed ground motion exceedance tolerance. As tragically illustrated in Christchurch, New Zealand, in February 2011, seismic strong ground motion levels may exceed the design basis of buildings and cause their collapse.

Rather than place the onus for seismic safety just on a reliable building code, scientists and decision makers have a humanitarian incentive and are under professional pressure to develop innovative seismic risk reduction strategies that use the best and most authoritative scientific information available. This is the principal goal of Operational Earthquake Forecasting (Jordan et al. 2011).

18.2 Operational Earthquake Forecasting

The term *Operational EarthquakeForecasting* (OEF hereafter) was proposed by the *International Commission on Earthquake Forecasting* for Italian Civil Protection (Jordan et al. 2011) nominated by the Italian government after the L'Aquila earthquake, 2009. This commission had two main tasks: (1) report on the current state of knowledge of short-term prediction and forecasting of tectonic earthquakes, and (2) indicate guidelines for utilization of possible forerunners of large earthquakes to drive civil protection actions, including the use of probabilistic seismic hazard analysis in the wake of a large earthquake.

The commission recommended the development of OEF, and of quantitative and transparent decision making protocols that encompass mitigation actions of different impact levels that might be implemented if certain probability thresholds are exceeded.

In essence, OEF comprises procedures for gathering and disseminating authoritative information about the time dependence of seismic hazards to help communities prepare for potentially destructive earthquakes (Jordan et al. 2011). This process involves two key activities: the continual updating of authoritative information about the future occurrence of potentially damaging earthquakes; and the officially sanctioned dissemination of this information to enhance earthquake preparedness in threatened communities.

The term *time dependence* signifies that the seismic hazard is not constant through time. This point deserves to be examined in detail. Traditionally, seismic risk is mitigated in the long-term through the definition of suitable building codes, i.e., the definition of appropriate rules for constructing buildings and infrastructure able to resist earthquake shaking, with limited damage. The primary scientific input in this

field is a seismic hazard map that specifies ground shaking at some probability of exceedance level during a time interval of typically 50 years.

Almost always, the earthquake occurrence process that underlies a hazard map is presumed to be time-independent (Cornell 1968), and the mean seismic hazard rate is expected to remain constant through time. This modeling is still common, and some authors have proposed extending the use of these hazard maps also to shorter time intervals (Mulargia 2012). Nonetheless, we know that the earthquake occurrence process has significant time variability in the seismic rate; such variations are much larger then would be anticipated with a pure time-independent process. The clearest of these variations is the time and space clustering of seismicity; an earthquake suddenly alters the dynamic conditions within fault systems that may lead to future nearby earthquakes.

These time variations are more evident in the short-term (days to weeks), in particular after a large shock. The use of time-dependent models based on earthquake clustering to track the evolution of aftershock sequences is becoming more and more popular (Gerstenberger et al. 2005; Marzocchi and Lombardi 2009; Reasenberg and Jones 1989). The short-term forecasting models so far proposed are of three types: the ETAS models (e.g. Ogata 1988, 1998; Zhuang et al. 2002) that have been used to forecast aftershocks after L'Aquila earthquake (Marzocchi and Lombardi 2009) and are the most popular; the Short Term Earthquake Probability, STEP, model (Gerstenberger et al. 2005); and the Agnew and Jones model (AJ; Agnew and Jones 1991). Another popular model is the one proposed by Reasenberg and Jones (1989) that may be considered as a simplified ETAS model. All of these models depend solely on the use of the seismic catalog. The AJ model uses also some constraint on the magnitude of the impending earthquakes taken from geology and paleoseismology.

The stochastic Epidemic-Type Aftershock Sequence (ETAS) model has been primarily used to forecast the evolution of an aftershock sequence. ETAS is based on simple physical components such as a tectonic seismic background that varies with space and a stationary Poisson distribution in time, with radially-symmetric triggering. The ETAS model is generically described by an equation of this form (Ogata 1988, 1998; Zhuang et al. 2002):

$$\lambda\left(\vec{x}, t, m\right) = \left[\gamma\mu\left(\vec{x}\right) + \sum_{t_i<t_0} f_1\left(M_i - M_{\min}\right) f_2\left(\vec{x} - \vec{X}_i\right) f_3\left(t - T_i\right)\right] g(m - M_{\min}) \tag{18.1}$$

where λ is the rate of events expected in the location $\vec{x}$, at the time t and of magnitude m. The first term represents the background varying with space (and not in time), and the summation takes into account the triggering effects of all previous earthquakes as a function of the distance, elapsed time and magnitude of the triggering event. The function $g\left(m - M_{\min}\right)$ is the frequency-magnitude law that is independent of space. In the most commonly used version, $f_1\left(M_i - M_{\min}\right)$ is the Utsu exponential scaling, $f_3\left(t - T_i\right)$ is the Omori-modified power-law scaling, $g\left(m - M_{\min}\right)$ is the exponential Gutenberg-Richter law, and $f_2\left(\vec{x} - \vec{X}_i\right)$ is a power-law spatial decay that may mimic the co-seismic stress transfer. Originally, all these functions were established empir-

ically looking at how aftershocks depend on the mainshock magnitude and decay in time and space; more recently, they have been physically justified.

Once $\lambda(\vec{x}, t, m)$ has been estimated, the probability of earthquakes in a specific time-space-magnitude window Ω is

$$P = 1 - \exp\left\{ - \iiint_{\Omega} \lambda(t, \vec{x}, m) dt d\vec{x} dm \right\} \tag{18.2}$$

Sometimes, the seismological output needs to be formulated in terms of ground shaking. In this case, the short-term models have to be implemented in conjunction with a ground motion prediction equation (GMPE). The choice of the most appropriate GMPE is far from trivial, and may depend on the model application. Here, we do not explore this important issue, but we remark that the choice of the GMPE may be difficult from a technical point of view, although it does not introduce any conceptual problems.

Jordan et al. (2011) emphasized the possibility of extending the use of clustering models also to track the evolution of a seismic sequence that may anticipate a large shock.

The occurrence of a seismic sequence with shocks felt by people raises concerns about the possibility to have large shocks in the short term. Although, most destructive earthquakes occur without being anticipated by such sequences (Marzocchi and Zhuang 2011; Reasenberg 1999), some of them are anticipated by more or less prolonged seismic sequences. Seismologists are not yet able to distinguish the features that characterize foreshock sequences with respect to seismic sequences that do not end with large earthquakes; nonetheless, it is clear that the occurrence of a seismic sequence increases the probability to have a large shock in the short-term.

To date, this kind of information has almost never been used to take practical mitigation actions like in L'Aquila earthquake 2009 (Marzocchi and Lombardi 2009) and the more recent Tohoku earthquake 2011 that was anticipated by a strong foreshock sequence that lasted few days (see below). There are several reasons for this. First, it is not helpful to talk about an increase of probability if we are not able to quantify it in a reliable way; there are many trivial probability increases where small earthquakes occur. But, as we will show later, this information can be of practical use within the framework of a quantitative assessment.

Secondly, the models so far proposed for short-term earthquake forecasting show that the occurrence of a seismic sequence may increase the probability with respect to the background as much as a thousand times, but the absolute probability still remains very low (usually below 1 %). These probabilities represent a formidable challenge for taking mitigation actions because it is obvious that in this low probability environment any warning would very likely be a false alarm.

For the sake of example, we report the case of the Tohoku earthquake. The map of the annual probability for 2011 of a $M \geq 8.5$ in Japan is reported in Fig. 18.1. This map has been extrapolated using the model submitted to CSEP (International Collaboratory for the Study of Earthquake Predictability) Japan and published by

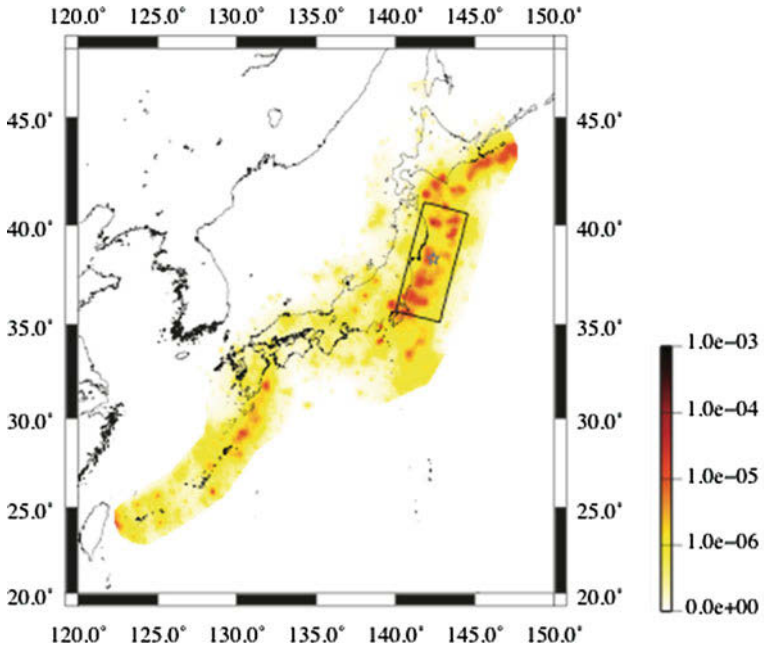

Fig. 18.1 Probability map for the period Jan.1–Dec.31 2011. The legend reports the annual probability map for a $M \geq 8.5$ earthquake in each cell of 0.1×0.1 degrees. The box is the fault of the Tohoku earthquake and the star is the epicenter

Lombardi and Marzocchi (2011). The annual probability for the area of the fault that slipped during the Tohoku earthquake was 0.64 % (about 0.21 % for $M \geq 9.0$).

A few days before the giant shock, a strong seismic sequence started with the strongest foreshock of M 7.2 that occurred on March 9. The weekly probability after the M 7.2 event increased, relative to the background probability, by a factor of 100 in a circular area around the epicenter with a radius of 100 km (see Fig. 18.2). In particular, the weekly probability calculated before the foreshock was 0.0012 %, whereas immediately afterwards it was raised to 0.12 %. If we consider a smaller circle around the epicenter of the M 7.2 event, the probability gain is much higher than 100, but the absolute weekly probability of a $M \geq 8.5$ is less than 0.12 %.

Another term in the OEF definition is worth noting: the scientific information has to be *authoritative*. This means that we should use forecasting models that are widely accepted and statistically tested. The statistical test of earthquake occurrence models is the primary objective of an international initiative named *Collaboratory for the Study of Earthquake Predictability*, CSEP (http://www.cseptesting.org; Jordan 2006). Specifically, the main purpose of the CSEP is to carry out scientific experiments to evaluate the reliability and skill of any forecasting/prediction model in different time windows (from 1 day to years). Reliability is the capability to produce forecasts/predictions compatible with the future seismicity; once a set of reliable

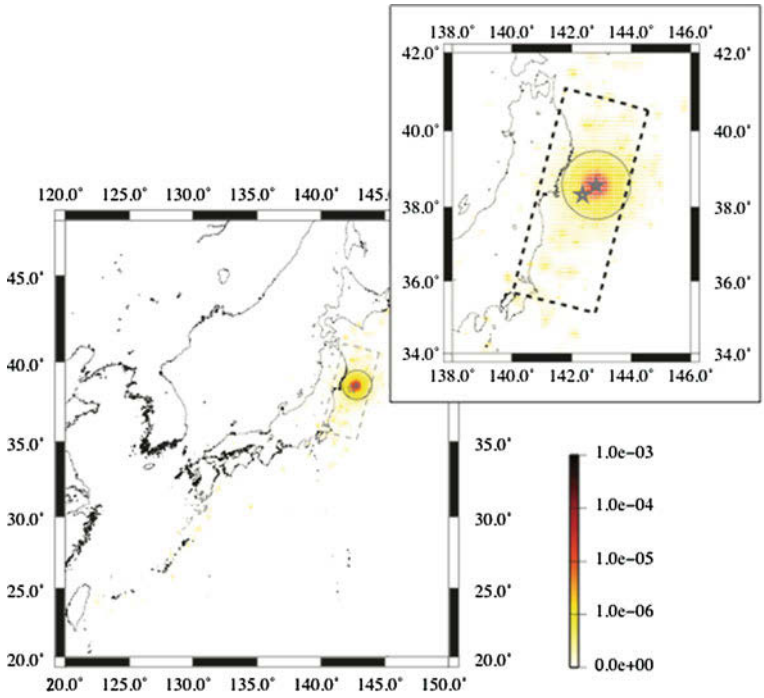

Fig. 18.2 Probability map for the period March 9– 16, 2011. The legend reports the weekly probability map for a $M \geq 8.5$ earthquake in each cell of 0.1 x 0.1 degrees. The box is the fault of the Tohoku earthquake; the circle is around the epicenter of the M 7.2 earthquake occurred on March 9; the star is the epicenter of the Tohoku earthquake

models is identified, the skill measures the relative precision of one specific model compared to the others. The best model is the reliable model with the highest skill.

Each experiment consists of comparing statistically the forecasts produced by the models and the real seismicity observed in a truly prospective way. CSEP can be considered the successor of the *Regional Earthquake Likelihood Model* (RELM) experiment (Schorlemmer and Gerstenberger 2007). While RELM was focusing on California, CSEP extends this focus to many other regions (New Zealand, Italy, Japan, part of China, and the whole world) as well as global testing centers (New Zealand, Europe, Japan, China). All testing regions are selected according to a high-level standard of seismic monitoring and to their capability to provide homogeneous and authoritative datasets required for the input of the models and for the testing phase. The coordinated international experiment has two main advantages: the evaluation process is supervised by an independent scientific international committee, not only by the modelers themselves, and the cross-evaluation of a model in different regions of the world can facilitate its evaluation in a much shorter period of time (Zechar et al. 2010).

The results of prospective tests are of fundamental importance to give an objective credibility to earthquake occurrence models, and, eventually, to merge all models in an average model (e.g. Marzocchi et al. 2012). The achievement of a consensus model is the main target of many important scientific initiatives like IPCC (Solomon et al. 2007), and long-term seismic hazard (Budnitz et al. 1997). This approach is probably the best solution to get an authoritative forecast whilst minimizing the unavoidable different opinions among scientists (Marzocchi and Zechar 2011). Last, but not least, an authoritative and timely information is the best approach to challenge possible mavericks who may lay claim to predicting earthquakes.

18.3 Decision-Making in a Low-Probability Environment

The rigorous scientific method of gathering evidence and seeking truth is resolutely upheld by the scientific community: scientists are generally reluctant to make premature statements about events over which there remains significant uncertainty. Decision-making is a different world: urgent decisions may have to be made irrespective of the state of uncertainty. One way of bridging the gap between seismologists and non-expert decision-makers is to use quantitative and formal techniques developed in operational research. Here we use the specific example of cost-benefit analysis.

18.3.1 Cost-Benefit Analysis

In the way that human beings deal with environmental threats, cost-benefit analysis is a key element. It has been said that evolution is Nature's way of doing cost-benefit analysis (Einhorn and Hogarth 1988). An evolutionary perspective redefines the assumptions many psychologists hold about what counts as rational. Our human ancestors needed to avoid getting killed, protect their families, and not succumb to diseases. The evolutionary pressure for survival has given modern Man a natural instinct to avoid environmental hazards. This survival instinct conforms well with a primitive cost-benefit analysis. People steer clear of dangerous animals just in case they are aggressive, and of sick humans, just in case of infectious disease contagion. Accidental deaths caused by animals are extremely low, because people heed warnings to avoid sharks, lions etc.

Since the ability to avoid hazards (predators, poisonous creatures, cliffs, etc.) would have been of significant evolutionary advantage to our ancestors, we should expect to find within the brain a cognitive system specialised for reasoning about hazards and precautions. This is the central idea in evolutionary psychology of hazard management theory (Atkinson and Wheeler 2003). Fiddick et al. (2000) characterize precaution rules as being of the form: if a valued entity is subjected to a hazard, then

taking an appropriate precaution lowers the risk of harm to an individual and his family.

Expressed in general quantitative terms in the context of operational earthquake forecasting (OEF), a particular personal risk mitigation action may be warranted if the cost C is less than the expected loss $p\,L$, where p is the probability of a dangerous earthquake, and L is a financial measure of the physical harm caused by the earthquake if evasive action is not taken (Marzocchi and Woo 2007, 2009).

Even allowing for progress in OEF, the probability value in the short-term (days to week) p is almost always very low, and hence most mitigation actions will actually turn out to be unnecessary. In the second half of the twentieth century, the type of mitigating action in the forefront of the minds of seismologists was large scale urban evacuation. Even a rudimentary cost-benefit analysis would rule out such a drastic response to any foreseeable type of operational earthquake forecast, because the p value is nowhere near high enough (van Stiphout et al. 2010).

The high number of expected false alarms suggests that mandatory mitigation actions imposed on society would not be the best solution since they can increase distrust of public officials and decision makers. A possible solution adopted in many fields is to provide different warnings to the public without imposing any specific mitigation action, instead nudging people to adopt their own mitigation strategy (see below). In the past, when facing low p values and high expected false alarm rates, consideration of less drastic responses than mass evacuation was generally dismissed on the grounds that public panic would ensue, which might lead to crush injuries, heart attacks and traffic accidents arising from the commotion and disorder.

The twenty-first century offers a very different environment for OEF. First, the world changed on 9/11. In common with earthquakes, terrorism is now also a low level global threat to life. In every airport in the world, passengers have to go through security before boarding a flight. Routinely, terrorism risk advisories are given to warn of potential attacks. But intelligence officers are no better at forecasting terrorist attacks than seismologists are at forecasting earthquakes (Woo 2011). The false alarm rate for such advisories is very high, nevertheless these advisories are considered worthwhile in encouraging public vigilance, and they do not cause mass panic.

A second development of this century significant for OEF is the widespread ownership of personal cell phones. Almost everyone in the industrialized world nowadays either owns a cell phone or has a close family member who owns one. In the future, advisory messages can be targeted at individuals, according to their geographical location, the construction of their home or place of work or worship, etc. Already text messages are sent to warn US residents of tornado and wildfire threats. Communication technology in the twentieth century did not permit such fine population segmentation of hazard warnings. Segmentation is important because mandatory actions for all would be unsuitable for many, who would understandably become distrustful of scientists.

18.3.2 Nudging Individual Decision-Making

The spectrum of possible hazard warnings is very broad, as is the diverse range of crisis situations. However well civic leaders choose the warnings they issue, people have to learn to make good decisions for themselves and their families in a crisis. In many awkward situations, an individual ultimately may have to be his or own decision-maker.

To answer the key public policy question how people can be helped to make good decisions for themselves, without a curtailment of freedom, a leading behavioural economist, Richard Thaler, teamed up with a law professor, Cass Sunstein, to write the highly influential book, *Nudge* (Thaler and Sunstein 2008). Nobody likes being pushed or shoved to do what is right for them—but being nudged is quite acceptable. Advocating a policy of libertarian paternalism, Thaler and Sunstein have suggested ways in which people can be 'nudged', rather than coerced or obligated, to make decisions that serve their own long-term interests. There are informed and unintrusive ways of achieving this goal. But it takes enterprise to find creative and viable solutions to the challenge of helping people to make good decisions for themselves. The primary tool for nudging people to make better decisions for themselves is education. Without needing to ban the sale of cigarettes or junk food, a government can encourage healthier lifestyles by educating the public about the risks of such consumption.

In the context of seismic safety, governments can do much to educate people about earthquake risks. Just as people should know if there is a cancer risk associated with any consumer product that is purchased (e.g. tobacco or some cheap processed food), or from aerosol emissions from industrial installations, people should know if their home, office, factory, school or church is in an active seismic zone, and whether it is collapse-prone, in the event of strong ground shaking. In the first instance, a simple indicator is just the style and date of earthquake construction—e.g. reinforced concrete structure, built to the 1970s Uniform Building Code. Already, the assignment of earthquake vulnerability to individual buildings is routine for earthquake insurance risk management. Modern technology is making this easier. The street level mapping capability of Google Earth facilitates this type of building-specific vulnerability classification.

It is crucial for the occupants of a building to have an awareness of its degree of earthquake vulnerability, in order to make an informed choice on action in the event of a hazard advisory. If it is not collapse-prone, then, as with windstorms, occupants may well be safer inside than outside, where they may be struck by debris. However, for occupants of on old unreinforced masonry construction, planning for an alternative place of shelter may be desirable.

Suppose that a building occupant is well informed about the seismic vulnerability of the building. An individual's response to an earthquake advisory, which may ultimately be tailored to building vulnerability, will then depend on personal circumstances, which is why an individual should optimally be his or her own decision-maker. Civil protection authorities may aspire to know the earthquake vulnerability

of each address, but could never know the urgency of the need for the occupant to be there at any given time. With privacy of personal information comes the responsibility of making personal safety decisions.

Furthermore, people differ in their level of risk aversion and their reluctance to take a gamble with their safety. This is tantamount to placing an especially high value on L. Accordingly, some people, e.g. parents with young children, may be willing to bear a higher cost to avoid the risk than others, e.g. single unattached men. Conversely, there are some risk-seeking individuals who would act as if they placed a comparatively low value on L. This may apply in particular to some reckless young students, and professionals, such as media journalists and photographers, who have become insensitive over time to high risk situations.

18.3.3 Low Cost Individual Actions

Mandatory actions imposed on society have to be based on sound quantitative cost benefit analysis, which is transparent to the public. In this way, any action can be justified at each step of the decision-making process. When each single person becomes responsible for taking actions, it is not anymore necessary to have written rules for any decision that we have to take in our private life. Nonetheless, it is clear that even in this case, weighing the pros and cons is expected to be advantageous.

As has been stated before, the probability value p for an OEF will always be low; usually very low. The essential cost-benefit inequality $C < pL$ would only be a call for action if C is low. The threshold cost for any individual would be dependent on personal risk aversion. There are numerous low cost actions that might be taken which would help to reduce the risk of harm coming to an individual in the event of an earthquake occurring. Just because most people may not be saved by an earthquake advisory does not diminish the value of saving even one life. This principle underlies the issuance of terrorism advisories. A selection of low cost options is listed.

(a) Vigilance
An individual who is vigilant and alert to danger will be able to react faster to an event, if one occurs. Terrorism advisories urge citizens to remain vigilant, and earthquake advisories should do the same. As with the terrorist threat, situation awareness is crucial for rapid reaction to ground shaking. Advisories can help to reduce cognitive bias of people who are slow at believing what is happening.

As a simple example of a low cost act of vigilance, suppose that a magnitude 4 earthquake occurs at night, and is felt quite strongly within a radius of 50 km. Those woken by the shaking would be advised to get dressed, and be alert just in case of further strong ground motion during the night. Even if the hazard probability gain associated with the magnitude 4 event occurrence may be small, the cost of extra vigilance is commensurately low.

(b) Preparedness

Every household and office should have an emergency kit in case disaster of any kind strikes. This kit should include food and water supplies, batteries, torch, breathing masks, first aid equipment, shovels, etc. Any hazard advisory should nudge citizens to ensure that they comply with this minimum level of preparedness.

Earthquake drills are known to save lives. If there has not been an earthquake drill in a region for more than a year, an earthquake hazard advisory would be a good opportunity to hold a public earthquake drill (Woo 2010).

On a practical level, engineering risk mitigation and retrofit are expensive (in contrast with new-build), and more importantly, time-consuming to undertake, but many low cost acts of preparedness are worthwhile to minimize injury, such as restraining objects from toppling off indoor shelves, or falling from outdoor parapets.

(c) Visitor options

Any visitor to an area for which a hazard advisory has been issued may choose to review his or her travel plans. If a trip is discretionary, and can be altered in date or destination, then the cost of plan substitution may be minimal. However, if there is some specific urgent personal or business reason for being in the hazard zone at the time of issuance of the hazard advisory, then this would need to be weighed carefully against the risk. In October 2010, the US State Department issued a terrorism advisory for US travellers to Europe. Some corporate travel plans were affected by this advisory, but most were not. It is right that every corporation should be free to decide for itself, in accordance with its own risk aversion.

(d) Resident options

In response to an OEF, a local resident living in a seismically vulnerable building may have available a range of alternatives which involve low additional cost, e.g. staying for a short while in a safer place with a neighbour, friend or family member, taking an early vacation away from home, or even staying outside in a tent or a car or caravan. For a short improvised stay of this kind, the cost should conform with the cost-benefit criterion, and be justifiable. However, whether it would be worth paying for a hotel on a nightly basis depends on the hazard level, and the resident's risk aversion.

Suppose that the weekly risk of a destructive earthquake is of the order of 0.1 %. (This is the approximate absolute risk arrived at above for the Tohoku foreshock analysis.) Assume that an occupant of a seismically highly vulnerable building has an even chance of being killed or seriously injured in the destructive earthquake through building collapse. Then the daily risk of being killed or seriously injured in an earthquake is of the order of $(1/1000) * (1/7) * (1/2) = 1/14000$ (1/7 reduces the probability from week to day, and 1/2 is the supposed even chance to be killed or seriously injured by the earthquake). This is a very significant degree of excess daily accidental risk: by comparison, the chance of a skydiver being killed in a jump is 1/100,000.

Suppose that, rather than taking advantage of the free hospitality of neighbours, friends or family, the occupant of a seismically vulnerable building decides to stay at an inexpensive budget hotel for €60 per night. Then $L = C/p$ is €840,000. This

figure is similar to that obtained for the willingness to pay to move someone away from Vesuvius red zone (Marzocchi and Woo 2009). If the occupant were rather risk averse, she would be advised to think about checking into a hotel.

Just because a seismic crisis may last for months does not negate the value of local residents reducing their hazard exposure for even a brief time window. If every family living in a vulnerable building within a hazard region were to manage to get away for a total of weeks over a crisis period of W weeks, the overall population exposure would be reduced by about A/W. It can be left to individuals to self-organize their own periods away from the hazard zone. Achieving 100 % reduction of exposure when a major earthquake occurs is nigh impossible. Assuming that a family might be able to spend a cumulative amount of two weeks away from a vulnerable home, spread over a number of time intervals within a crisis period of 6 months (i.e. 26 weeks), a reduction of $1/13 \sim 7\,\%$ is well possible, and is significantly better than zero.

This same argument applies to the occupancy of vulnerable public buildings. In Italy, the heritage of beautiful old churches leaves also a legacy of danger to congregations, in the event of severe earthquake shaking. During a seismic crisis, effort may be made to find alternative safer buildings for church services. Alternatively, if weather permits, there may be open-air services, or some curtailment of the weekly frequency of services. Hazard adjustment to church practices is nothing new: during the 2009 influenza pandemic, traditional communion practices changed to limit the oral transmission of infection. If, over a seismic crisis period of W weeks, services for A weeks are relocated or cancelled, the exposure reduction would be A/W, which is a saving achievable at comparatively low cost and inconvenience.

Being nudged to take a mitigating action gets harder as the period of disruption increases: a few days of inconvenience is acceptable; a week is tolerable; but two weeks may be hardship. Beyond two weeks, some civic compensation plan may have to be introduced, which will become more costly for the authorities as more people at risk are assisted.

Figure 18.3 charts the increasing marginal economic cost in reducing population exposure in seismically vulnerable buildings in zones for which an earthquake advisory is issued. Classical earthquake prediction was preoccupied with the tail of the curve: the grossly unaffordable economic cost of evacuating many thousands from a hazard zone. Through self-organization of the population, acting as their own decision-makers in response to an OEF with no official management or logistical assistance, quite a significant proportion of the population exposure might be reduced at a reasonable and affordable cost.

Further reductions would require more than nudging. Depending on the relative proportion of seismically vulnerable buildings, civic provision could be made to subsidize the cost of people staying away from their vulnerable homes, or to accommodate a modest proportion in designated earthquake-resistant shelters or hostels, or specially converted modern safe civic buildings. But this would be progressively more expensive and unaffordable, as indicated in Fig. 18.3.

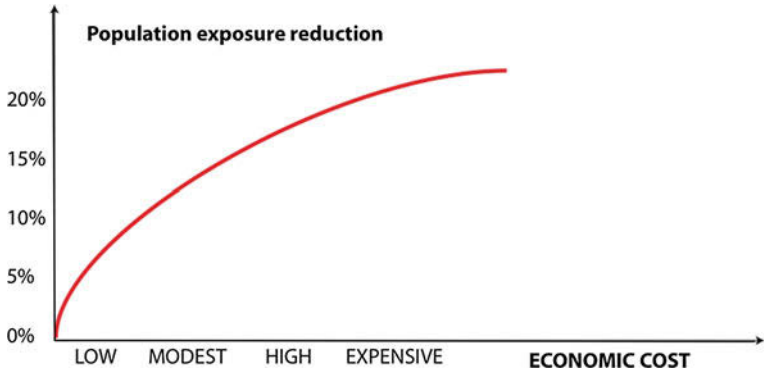

Fig. 18.3 Schematic graph indicating the marginally increasing economic cost associated with achieving a % reduction of population exposure in vulnerable buildings

18.4 Final Remarks

The verifiable record of lives saved through earthquake forecasting is almost non-existent. Realistically, evidence of an imminent earthquake will never be unambiguous enough to warrant the evacuation of even a small town. But for scientists and decision-makers, thinking should not stop there. First, it is only those in seismically vulnerable buildings who would be in serious danger from strong shaking. In future, it should become feasible for occupants to check online the vulnerability status of any building.

Secondly, some significant saving of human life is feasible through official nudging of low cost measures that individuals can choose themselves to adopt, according to their own circumstances and sense of risk aversion. For example, exposure can be reduced through the simple process of advising occupants of vulnerable buildings to take whatever opportunities arise for getting away to visit neighbours, friends, family etc. The smaller the proportion of vulnerable buildings, the easier it would be for the occupants of these buildings to be temporarily accommodated elsewhere.

Hardly anyone might be prepared to be away from home for the entire duration of a seismic crisis, so there is a degree of randomness in who might be saved by an earthquake advisory. The benefit is achieved at a community level. Already, with the present state-of-the-art level of OEF, earthquake advisories might be issued capable of reducing the community death toll of an earthquake disaster by a few per cent. This is a worthwhile start for scientists to save lives through operational earthquake forecasting. Progressively, this death toll percentage reduction factor could be increased to double figures. But as low cost options for hazard avoidance gradually become exhausted, the nudge limit will be reached—after a few weeks, a family may outstay its welcome away from home, and be impatient to return. The mortality reduction factor is then expected to saturate due to rising costs for civic authorities in subsidizing families for the expense of being away from home, or providing alternative safe accommodation.

Acknowledgments This work has been partially funded by the FP7 European project REAKT.

References

Agnew DC, Jones LM (1991) Prediction probabilities from foreshocks. J Geophys Res 96:11959–11971

Atkinson AP, Wheeler M (2003) Evolutionary psychology's grain problem and the cognitive neuroscience of reasoning. In: Over D (ed) Evolution and the psychology of thinking: the debate. Psychology Press, Hove

Budnitz RJ, Apostolakis G, Boore DM, Cluff LS, Coppersmith KJ, Cornell CA, Morris PA (1997) Senior Seismic Hazard Analysis Committee; recommendations for Probabilistic Seismic Hazard Analysis: guidance on uncertainty and use of experts, vol 1–2. U.S. Nuclear Regulatory Commission, U.S. Department of Energy, Electric Power Research Institute. NUREG/CR-6372, UCRL-ID-122160

Cornell CA (1968) Engineering seismic risk analysis. B Seismol Soc Am 58:1583–1606

Einhorn HJ, Hogarth RM (1988) Behavioral decision theory: processes of judgment and choice. In: Bell AD, Raiffa H, Tversky A (eds) Decision making. Cambridge University Press, Cambridge

Fiddick L, Cosmides L, Tooby J (2000) No interpretation without representation: the role of domain-specific representations and inferences in the Wason selection task. Cognition 77:1–79

Gerstenberger M, Wiemer S, Jones LM, Reasenberg PA (2005) Real-time forecasts of tomorrow's earthquakes in California. Nature 435:328–331

Jordan TH (2006) Earthquake predictability, brick by brick. Seismol Res Lett 77:3–6

Jordan TH, Chen Y-T, Gasparini P, Madariaga R, Main I, Marzocchi W, Papadopoulos G, Sobolev G, Yamaoka K, Zschau J (2011) Operational earthquake forecasting: State of knowledge and guidelines for implementation. Ann Geophys 54:315–391

Lombardi AM, Marzocchi W (2011) The Double branching model for earthquake forecast applied to the Japanese seismicity. Earth Planets Space 63:187–195

Marzocchi W, Woo G (2007) Probabilistic eruption forecasting and the call for an evacuation. Geophys Res Lett 34:L22310

Marzocchi W, Lombardi AM (2009) Real-time forecasting following a damaging earthquake. Geophys Res Lett 36:L21302

Marzocchi W, Woo G (2009) Principles of volcano risk metrics: theory and the case study of Mt. Vesuvius and Campi Flegrei (Italy). J Geophys Res 114:B03213

Marzocchi W, Zhuang J (2011) Statistics between mainshocks and foreshocks in Italy and Southern California. Geophys Res Lett 38:L09310

Marzocchi W, Zechar JD (2011) Earthquake forecasting and earthquake prediction: different approaches for obtaining the best model. Seismol Res Lett 82:442–448

Marzocchi W, Amato A, Akinci A, Chiarabba C, Lombardi AM, Pantosti D, Boschi E (2012) A ten-year earthquake occurrence model for Italy. Bull Seismol Soc Am 102:1195–1213

Mulargia F (2010) Opinion: extending the usefulness of seismic hazard studies. Seismol Res Lett 81:423–424

Ogata Y (1988) Statistical models for earthquake occurrences and residual analysis for point processes. J Am Stat Assoc 83:9–27

Ogata Y (1998) Space-time point-process models for earthquake occurrences. Ann Inst Stat Math 50:379–402

Reasenberg PA (1999) Foreshock occurrence rates before large earthquakes worldwide. Pure Appl Geophys 155:355–379

Reasenberg PA, Jones LM (1989) Earthquake hazard after a main-shock in California. Science 243:1173–1176

Schorlemmer D, Gerstenberger MC (2007) RELM testing center. Seismol Res Lett 78:30–36

Solomon S, Qin D, Manning M, Chen Z, Marquis M, Averyt KB, Tignor M, Miller HL (eds) (2007) Climate Change 2007: the physical science basis: contribution of working group I to the fourth assessment report of the Intergovernmental Panel on climate change. Cambridge University Press, Cambridge and New York

Thaler RH, Sunstein CR (2008) Nudge. Yale University Press, New Haven

van Stiphout T, Wiemer S, Marzocchi W (2010) When are mitigation actions warranted: the case of the 2009 L'Aquila earthquake. Geophys Res Lett 37:L06306

Woo G (2010) Operational earthquake forecasting and risk management. Seismol Res Lett 81:778–782

Woo G (2011) Calculating catastrophe. Imperial College Press, London

Zechar JD, Schorlemmer D, Liukis M, Yu J, Euchner F, Maechling PJ, Jordan TH (2010) The collaboratory for the study of earthquake predictability perspective on computational earthquake science. Concurr Comput Pract Exp 22:1836–1847

Zhuang J, Ogata Y, Vere-Jones D (2002) Stochastic declustering of space-time earthquake occurrences. J Am Stat Assoc 97:369–380

Chapter 19
How Useful is Early Warning and Can It Be Made More Effective?

M. Wyss, F. Wenzel and J. Daniell

Abstract The methods to detect the development of a large earthquake at an early time and to issue an appropriate warning have made great progress. Nevertheless, for population centers at risk, warnings can generally be issued only about 5–10 s before the strong shaking arrives. Systems and facilities that can benefit from a warning with such a short lead time include: Transportation systems, fire departments, medical facilities, schools, industrial plants, petroleum and gas pipelines, elevators, and power plants. However, for the population at home in vulnerable apartment buildings or at work in office buildings and factories that may not have been built following modern codes, the warning is too short for a person to reach a safe place. Although taking cover under a table can protect a person from falling objects, a structurally strong Earthquake Protection Unit (EPU) is required to save lives and limbs in a partially collapsing building. If a culture of earthquake awareness and the knowledge of early warning capabilities were developed, in which strong earthquakes closets could be bought in the lumber yard like tornado shelters, then the fine advances in earthquakes early warning could result in lives saved.

19.1 Introduction

In today's world of transmission of instant news from the ends of the globe to the television screen in millions of living rooms, people become increasingly aware of the great potential earthquakes have to create disasters. The numbers of fatalities in one event are counted in units of tens to hundreds of thousands, the injured may reach a million in future earthquakes with magnitudes exceeding M8 and located

M. Wyss (✉)
World Agency for Planetary Monitoring and Earthquake Risk Reduction, Geneva, Switzerland
e-mail: wyss.adh@gmail.com

F. Wenzel · J. Daniell
Geophysical Institute, Karlsruhe Institute for Technology, Karlsruhe, Germany

F. Wenzel and J. Zschau (eds.), *Early Warning for Geological Disasters*,
Advanced Technologies in Earth Sciences, DOI: 10.1007/978-3-642-12233-0_19,

below land, given that earthquakes with M $\leq$ 8 have injured many hundred thousand (Tangshan, M7.6, 1976, 700,000+, Sichuan M8.0, 2008, 375,000, Haiti, M7.0, 2010, 310,000; Daniell 2012; Daniell et al. 2011). The consumers of these startling news are perhaps shaken by the images of horror that invade their homes, but most of them don't think that they could be next, as they sip their coffee and listen to the announcer quote astronomical numbers of victims. Moved by the suffering they witness, many people donate money to help the survivors. If they knew that indeed they could be next, they certainly would invest ten to hundred times more to protect themselves, if a means to protect themselves were offered them.

Efforts to protect the population from disastrous earthquakes include attempts to develop methods to predict earthquakes, to construct new buildings such that they will resist strong ground shaking, and to retrofit existing weak buildings, so they are unlikely to collapse. Here we will briefly review these methods to reduce the earthquake risk and show that they are not very effective for the population at large.

Whereas this book is dedicated to detailing the technical advances, which have been and are being made in the field of earthquake early warning, some thought should be given to what degree early warning has been useful in disastrous earthquakes and how its effectiveness could be improved for protecting the population from collapsing buildings. Here we summarize examples of past experiences with earthquake early warning and we consider how effective Earthquake Protection Units (EPU) may become to allow families to make use of early warnings to save lives and limbs.

19.2 Earthquake Prediction So Far a Story of Failures

If the location, occurrence time, and the magnitude of earthquakes could be predicted accurately and reliable, the population could be made aware of the impending disaster and the risk could be reduced. Although some earthquakes have happened where and when they had been predicted no reliable method exists.

One of the reasons that it is so difficult to predict earthquakes is that their source volumes, at more than 5 km depth (mostly at 20 km), are inaccessible for direct observation. Another obstacle is the fact the stress level in the Earth's crust cannot be measured directly. Only changes of stress can be inferred by measuring deformations at the surface. Thus, it is not accurately known how close to the failure stress any part of the Earth's crust may be.

Locations of increased probability of large earthquakes can nevertheless be identified. The simplest method is an estimate of the accumulated strain (and thus amount of slip) stored along a plate boundary where the plate displacement is being monitored. Where the last release of strain (stress) has occurred hundred to a few hundred years ago, the possibly available slip amounts to several meters because the rate of plate motion is typically several centimeters per year. The occurrence dates and the amounts of slip can be determined approximately by excavating slip evidence for pre-historic earthquakes (e.g. Sieh 1984; Sietz et al. 1997; Clark et al. 2010). These paleoseismological efforts are only possible where fault traces are exposed on

land; under water they cannot be investigated. Where this information can be dug up, it becomes evident that the repeat intervals and the amounts of slip vary considerably along any single fault segment. In addition, the strain due to plate motions is relieved to an unknown amount along many plate boundaries by a-seismic creep, which renders the estimate of accumulated slip inaccurate.

In spite of these difficulties, the North Anatolian fault south of Istanbul (e.g. Stein et al. 1997; Kalkan et al. 2009) and the Himalayan plate boundary (e.g. Khattri 1999; Bilham et al. 2001; Bilham 2004) have been identified as locations where large earthquakes are bound to happen in most of the local population's lifetime. These are locations where early warning efforts can be useful, and that is why such efforts have been concentrated in Istanbul, for example Atakan et al. (2002), Fleming et al. (2009).

The M8 algorithm and its derivatives are methods to map Temporarily Increased Probabilities (TIPs) for large earthquakes, updated annually on the internet (http://www.mitp.ru/en/predictions/20110311.html). Although the authors have repeatedly been able to claim success (e.g. Kossobokov et al. 1999; Kossobokov 2012), the public as well as many seismologists are not aware of this warning method. For example, the New York Times and the Neue Zuercher Zeitung, among many newspapers, have published interviews in which seismologists asserted that the recent deadly earthquakes of May 20 and 29, 2012 in Emilia Romagna, Northern Italy, were surprises in a zone believed to be a-seismic, although a TIP warning, issued by Peresan et al. (2012) (http://www.ictp.trieste.it/www_users/sand/prediction/prediction.htm), was in effect for this region. The effectiveness of TIP warnings are reduced because they are perceived as vague due to their large radius (427–667 km), their large time window (3 years), and because they are mostly unknown to the public and experts.

19.3 Earthquake Engineering Solutions are Expensive and Marginally Implemented

The political will to protect the population is reflected by the fact that in the 1970s many countries introduced codes that require minimum quality construction practices, and in some countries the existing codes were upgraded to more stringent ones, during these years. One problem with this approach to reduce earthquake risk is that for a long time to come the majority of the population will continue to live in weak buildings constructed before the codes went into effect. The second problem is that in many countries the code is not enforced.

In countries where the building codes are enforced, such as for example the United States, Japan, and Taiwan the ratio of injured/fatalities is higher by about a factor of 10 than in developing countries. Using 1,400 fatal events with deaths to injury ratio from 1900–2012, where human development index at the time of the event is higher, it can be seen that the ratio of injuries to deaths is also higher (Fig. 19.1). Human Development index is the best measure of the development of a nation and is

a combination of life expectancy, education and GDP per capita. It is well correlated to building code enforcement.

This ratio can be taken as a measure of the ability of the built environment to resist strong shaking because in well constructed buildings few fatalities are to be deplored, while some occupants are injured in strong earthquakes.

Retrofitting poorly constructed buildings is almost never done because it is expensive. Private owners cannot be persuaded to spend money to prevent a disaster that they doubt will ever occur and governments in regions where weak buildings are at risk usually have other problems depleting their coffers and turn a blind eye to protecting their office workers from earthquakes which likely will not happen during their tenure in office.

Although there exist some spectacularly elegant means of detaching a building from the ground upon which it rests, such that it is not subjected to strong shaking by seismic waves, few people actually benefit from the engineering solution to the earthquake problem for the reasons given above.

19.4 Experience with Early Warning in Past Earthquakes

So far, little documentation exists regarding the value of Earthquake Early Warning Systems (EEWS) in disaster mitigation, specifically life-saving. There are only two systems in Mexico and Japan that actually issue alarms and where recent experience is available.

The Ometepec earthquake of Mexico (20th March 2012, 12:02 p.m. local time, magnitude of 7.4) occurred in the state of Oaxaca in South-Eastern Mexico. The earthquake was also strongly felt in Mexico City. The earthquake warning system (SAS) responded to this event and issued a warning about 60 s before the arrival of strong ground motion in Mexico City, such that the Metro system could stop operations and information on evacuation could be provided.

One Metro line sustained damage to rails, so that a chance for derailment existed. Stopping the trains because of the early warning was probably instrumental in avoiding a derailment. The fact that we cannot say for certain that lives have been saved in this case, and how many lives, highlights the problem that damage and losses are recordable, but avoided losses are very difficult to assess. The only fact we know is that no injuries were reported in the entire Metro system (EERI 2012).

The earthquake occurred during a Mexican Senate hearing, which was recorded by video. The meeting was, as shown in the video, interrupted by participants and immediately an orderly evacuation of the room took place (http://tremblingearth.wordpress.com/2012/03/31/mexico-city-earthquake-early-warning-it-works/).

The early warning system operated by the Japanese Meteorological Agency (JMA) since October 2007 issued so far more than a dozen alarms to the public. They are commonly issued by TV, radio, mobile phone services, and internet. The recent $M = 9.0$ Tohoku earthquake of March 11, 2011, posed a particular problem because the size of the expected earthquake consequences were updated for more than

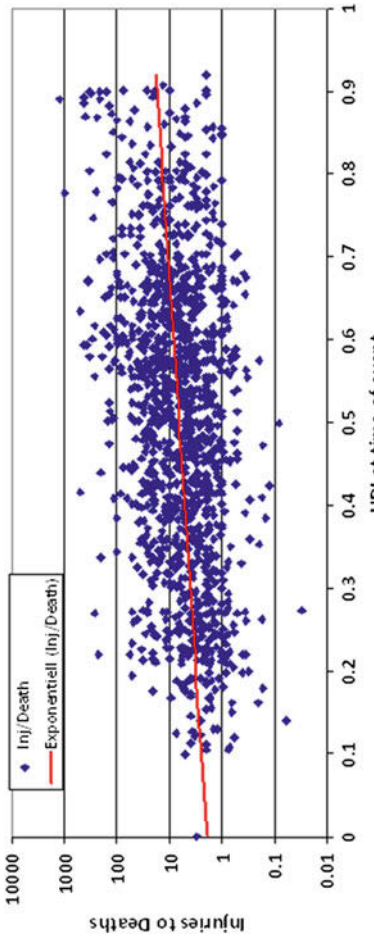

Fig. 19.1 CATDAT Damaging Earthquakes Database: 1,400 fatal events with an injured to fatalities ratio versus Human Development Index at time of event from 1900 to 2012

one hour, giving varying information on magnitudes and expected ground shaking (Cryanoski 2011). After 8.6 s of the first trigger at station OURI warning was provided estimating that an M = 7.2 earthquake had occurred, and forecasting the seismic intensity to be 5-lower (on the JMA scale) for the Central Mijagi prefecture, where Sendai City is located. The actual ground shaking in this area turned out to be intensity level 7 (the highest on the JMA scale).

Problems with the early warning for very large earthquakes have been identified earlier (Bose et al. 2009) as finite earthquake source models have to be used, but were not implemented during the Tohoku earthquake in the JMA procedure. The JMA system will be upgraded in the near future with additional instrumentation and methods (see Yamada 2012; this volume).

19.5 Early Warning Use for Protection Lifelines and Critical Facilities

Application of earthquake early warning for infrastructure systems has a long history in Japan. Instrumentation of bullet train lines, nowadays the Shinkansen lines, started in the 1970s and was completed for the Tokaido Shinkansen line in 1992 (Nakamura et al. 2007). The systems were upgraded after the Kobe, 1995, earthquake for a variety of other Shinkansen lines.

Applications for industrial production facilities have been demonstrated during the Kyoto 2009 Early Warning Conference. An outstanding example is presented by the protection of a semi-conductor protection facility which capitalises on the JMA signal but determines operational steps with ground motion records on the site of the plants.

An obvious application of EWS is the application to shutting down gas supplies or oil flow in pipelines. To avoid fires due to leakage of gas or oil from pipes that may brake due to shaking in an earthquake, a real-time safety control system, SUPREME, has been deployed and put into use for Tokyo Gas in 2005. SUPREME employs 3,800 intensity sensors and remote control devices to achieve quick gas supply shut off. It monitors the earthquake motion at a large number of sites on a real-time basis, interprets the data, and assesses gas pipe damage in order to decide whether or not the gas supply should be interrupted.

A similar installation was put in place in Taipei after the 1999 Chi Chi earthquake. It was successfully tested in a 2002 earthquake that generated higher ground motions in Taipei than the Chi Chi did (Shimizu et al. 2006). Several cities and companies in California and Europe have installed simpler systems with only a few sensors and a few valves that may be shut instantly when strong motions are detected.

19.5.1 Stopping of Elevators in High-Rise Buildings

Warnings not to use elevators in case of earthquakes or fires are standard displays encountered in hotels. In high rise buildings, trips on elevators take considerable time and therefore people are likely to become trapped, if strong shaking damages such a building. Thus, it is desirable to evacuate elevators and then stop them from taking on more passengers in case of strong shaking. For example, an elevator emergency management system based on EWS is installed in the 29 floors Kogakuin University building in downtown Tokyo. Trigger levels for P- and S-waves are used to stop the elevators at the nearest floor. Dependent on the degree of strong motion, the elevators resume operation after 60–90 s, or in case of strong motion, wait for inspection. The system worked well in over 20 earthquakes since installation (Kubo et al. 2008).

19.5.2 Evacuation of Schools

Although it is generally not recommended to run outside of buildings in a city in case of earthquakes because of falling debris, schools may be successfully evacuated because they are surrounded by open areas for recreation and sports. Also, in some earthquake prone regions, like in Lima, Peru, most schools have only two floors, which allows evacuation in 5–15 s.

Motosaka (2008) reports on school evacuation systems in Miyagi Province. Magnitude and hypocenter information is received from the JMA by a computer at the teacher's room. The computer estimates the countdown to the S-wave arrival and the expected seismic JMA intensity. Based on this information, the broadcasting system issues a warning voice message, audible in all parts of the compound. Voice/image warning information is also transmitted to a TV receiver in each classroom. The architecture of the school allows its evacuation in 15 s. Drills aimed at achieving rapid and orderly evacuation are performed several times per year. Demonstration tests at Nagamachi Elementary School in Sendai, started in 2004. A successful real-life test emerged during the June 14, 2008, Iwate-Miyagi Inland earthquake (M7.2).

19.5.3 Research for Implementing Additional Applications of EWS

Fujinawa and Noda (2007) and Fujinawa et al. (2008) developed a number of EWS applications for

- Fire departments,
- Medical facilities,
- Home electronics systems,
- Schools,

- Industrial plants,
- Liquid Petroleum and Gas pipelines,
- Outdoor activity systems,
- Building maintenance systems,
- Elevators, and
- Dams.

Their research was funded by the Ministry of Education, Culture, Sports, Science and Technology (http://www.bosai.go.jp/kenkyu/sokuji/index.htm).

Further applications that capitalize on dense accelerometer instrumentation in tunnels are reported from the new railway tunnel across the Bosporus (M. Erdik, personal communication).

19.6 Early Warning Use for Saving Lives and Reducing Injuries

In general, one could say that direct efforts to saving lives in residential buildings are currently not implemented. However, promises made by scientists regarding the potential of earthquake early warning are abundant. For instance, in Gasparini et al. (2007), the preface claims that 'this may be used to minimize property damage and loss of life in urban areas and to aid emergency response'. Contrary to these announcements, actual efforts to avoid fatalities and reduce injuries in residential-, office-, and industrial buildings are not visible, at the moment.

When we consider the potential to benefit from early warning for people in their homes and at work indoors, there are three categories; those who live too close to the rupturing fault and cannot be warned, those who live far enough from the fault where the ground motions are moderate enough so people do not need to be warned, and those who can benefit from early warnings, if they can get to a safe place within 5–10 s, once they receive a warning.

Wyss (2012) has listed 10 examples of large cities located in the vicinity of faults capable of magnitude 7+ earthquakes where the warning time might be in the range of 5–10 s, under favorable conditions. This lead-time is not enough for a person to get to safety unless there exists an EPU on each floor of a multistory building.

At the work place, such a unit could take the form of one room per floor, which is constructed in such a way that it will not collapse even if the rest of the building suffers greatly. In a vulnerable apartment building that may partially collapse in a strong earthquake, an earthquake closet, installed in a surplus bathroom or in a structurally strong corner of the apartment, could save the family that dashes into it after receiving an early warning.

The earthquake closet could be a crude construction put in place by the occupant of the apartment, it could be an engineered closet for sale in a lumber yard along with prefabricated saunas, or it could be specifically tailored by an expert to optimally fit the particular construction of the apartment building in question.

The probability gain for surviving or escape injury in a strong earthquake inside an earthquake closet depends on the ratio of the resistance to shaking by the closet to that of the apartment building. Wyss (2012) estimated that the probability gain may range typically from 1,000 to 10,000.

19.7 Discussion

Currently, the standard advice for self protection in an earthquake is to crawl under a table. This measure is effective against falling objects, but not in partially collapsing buildings. Thus we advocate that in education programs about seismic risk, the usefulness of earthquake closets in serious earthquake disasters be stressed along side with the recommendation to dash under a table, if nothing else is available.

It is fair to say that early earthquake warning can be useful to stop mass transportation system and dangerous processes in critical facilities (United Nations 2006), but it cannot be used for people to protect themselves, unless they are in the vicinity of an earthquake protection unit.

Tornado shelters in the form of strong closets are sold by several companies. The interest in individual protection from tornadoes is stronger than that in protection from earthquake consequences because tornadoes sweep over the same regions almost every year, whereas large earthquakes rupture the same fault segments only every several hundred years. Nevertheless, a family that has been informed that they live in a vulnerable building near a fault section that is likely to generate a damaging earthquakes within the lifetimes of some family members may very well be motivated to spend a few thousand Euros to increase their chances to survive more than a thousand fold.

Seat belts in cars were opposed and ridiculed by many, at the time they were introduced. Today, it is mandatory to wear them and no one doubts that they save lives and injuries. People needed to be educated to the danger and the usefulness of the device.

The motivation of owners of office buildings and industrial plants to build earthquake protection units is more difficult to generate. Perhaps litigation, or the threat of litigation, is the only way. It is certainly tragic and difficult to understand why countless industrial facilities collapsed in the minor earthquakes (M5.9 and M5.8) in northern Italy on May 20 and 29, when very few other buildings collapsed, except abandoned, old brick farms and barns. In these earthquakes, more people died in industrial plants than in homes, even though one of them occurred at night, when almost no one was at work, but everyone was sleeping at home.

The earthquake closet is a low cost means of reducing the earthquake risk and it has the advantage that false alarms may readily be tolerated because it is a small inconvenience to briefly pop into the unit, even if no disaster follows.

19.8 Conclusions

We conclude that the important advances in delivering early warnings before the strong shaking due to large earthquakes arrives have already been applied to stopping rapid transport systems and dangerous process in industrial facilities. In a next step, we need to work toward making these warnings useful for the population at home and at work. If we can develop a culture of early warning that includes education about the risk and the concept of the earthquake closet, then we would be on the way to an important realistic means of protecting a part of the population from being harmed in earthquakes.

Acknowledgments M. Wyss thanks the support of the JTI Foundation, based in Switzerland. J. Daniell thanks the General Sir John Monash Foundation of Australia for their generous support.

References

Atakan K, Ojeda A, Meghraoui M, Barka AA, Erdik M, Bodare A (2002) Seismic hazard in Istanbul following the 17 August 1999 Izmit and 12 November 1999 Duzce earthquakes. Bull Seismol Soc Am 92(1):466–482

Bilham R (2004) Historical studies of earthquakes in India. Ann Geophys 47(2):839–858

Bilham R, Gaur VK, Molnar P (2001) Himalayan seismic risk. Science 293:1442–1444

Bose M, Sokolov V, Wenzel F (2009) Shake map methodology for intermediate depth Vrancea (Romania): earthquakes. Earthq Spectra 25(3):497–514

Clark D, McPherson A, Collins C (2010). Mmax estimates for the Australian stable continental region (SCR) derived from palaeoseismicity data. Paper no. 5, Proceedings of the 2010 Australian earthquake engineering society conference. Perth, Western Australia

Cryanoski D (2011) Japan faces up to failure of its earthquake preparations. Systems for forecasting, early warning and tsunami protection all fell short on 11 March. Nature 471:556–557

Daniell JE (2003–2012) The CATDAT damaging earthquakes database. Searchable integrated historical global catastrophe database, digital database, updates v0.0 to latest update v5.108

Daniell JE, Khazai B, Wenzel F, Vervaeck A (2011) The CATDAT damaging earthquakes database. Nat Hazards Earth Syst Sci 11:2235–2251. doi:10.5194/nhess-11-2235-2011

EERI (2012) Newsletter, May, 46(5), 9

Fleming K, Picozzi M, Milkereit C, Kühnlenz F, Lichtblau B, Fischer J, Zulfikar C, Özel O (2009) The self-organizing seismic early warning information network (SOSEWIN). Seismol Res Lett 80(5):755–771

Fujinawa Y, Noda Y (2007) Research and development of earthquake early warning application systems for various users. BUTSURI-TANSA 60(5):375–386

Fujinawa Y, Rokugo Y, Noda Y, Mizui Y, Kobayashi M, Mizutani E (2008) Efforts of earthquake disaster mitigation using earthquake early warning in Japan. Paper S05–03-014, 14WCEE proceedings, pp 1–8.

Gasparini G, Manfredi G, Zschau J (eds) (2007) EWS–earthquake early warning systems. Springer, Berlin

Kalkan E, Gulkan P, Yilmaz N, Celebi M (2009) Reassessment of probabilistic seismic hazard in the Marmara region. Bull Seismol Soc Am 99(4):2127–2146. doi:10.1785/0120080285

Khattri KN (1999) Probabilities of occurrence of great earthquakes in the Himalaya. Proc Indian Acad Sci (Earth Planet Sci) 108:87–92

Kossobokov VG, Romashkova LL, Keilis-Borok VI, Healy JH (1999) Testing earthquake prediction algorithms: statistically significant advance prediction of the largest earthquakes in the Circum-Pacific, 1992–1997. Phys Earth Planet Inter 111(4):187–196

Kossobokov VG (2012) Earthquake prediction: 20 years of global experiment. Nat Hazards. doi:10.1007/s11069-012-0198-1. Published online 21 April 2012

Kubo T, Hisada Y, Horiuchi S, Yamamoto S (2008). Application of earthquake early warning system and real-time strong-motion monitoring—system to earthquake disaster mitigation of a high-rise building in Tokyo, Japan, Paper S10–058, 14WCEE Proceedings, pp 1–8

Motosaka M (2008) Application of earthquake early warning systems for disaster prevention in schools, 14WCEE, Proceedings

Nakamura J, Saita J (2007) The earthquake warning system: today and tomorrow. In: Gasperini G, Manfredi G, Zschau J (eds) EWS—earthquake early warning systems. Springer, Berlin

Peresan A, Kossobokov VG, Panza GF (2012) Operational earthquake forecast/prediction. Rend Fis Acc Lincei. doi:10.1007/s12210-012-0171-7. Published online 22 April 2012

Shimizu Y, Yamazaki F, Yasuda S, Towhata I, Suzuki T, Isoyama R, Ishida E, Suetomi I, Koganemaru K, Nakayama W (2006) Development of real-time control system for urban gas supply network. J Geotech Geoenviron Eng 132(2):237–249

Sieh KE (1984) Lateral offsets and revised dates of large prehistoric earthquakes at Pallett Creek, Southern California. J Geophys Res 89:7641–7670

Sietz G, Weldon R II, Biasi GP (1997) The Pitman canyon paleoseismic record: a re-evaluation of the southern San Andreas fault segmentation. J Geodyn 24(1–4):129–138

Stein R, Barka AA, Dieterich JH (1997) Progressive failure on the North Anatolian fault since 1939 by earthquake stress triggering. Geophys J Int 128(3):594–604

United Nations (2006) Global survey of early warning systems. Gaps and opportunities towards building a comprehensive global early warning system for all natural hazards. 46

Wyss M (2012) The earthquake closet: rendering early-warning useful. Nat Hazards 62(3):927–935